Joon Park

BIOCERAMICS

Properties, Characterizations, and Applications

Springer

Bioceramics

Joon Park

Bioceramics

Properties, Characterizations, and Applications

Springer

Joon Park
University of Iowa
Biomedical and Mechanical Engineering
Iowa City, IA 52242-1414
USA
joon-park@uiowa.edu

ISBN 978-0-387-09544-8 e-ISBN 978-0-387-09545-5

Library of Congress Control Number: 2008931285

© 2008 Springer Science+Business Media, LLC
All rights reserved. This work may not be translated or copied in whole or in part without the written permission of the publisher (Springer Science+Business Media, LLC, 233 Spring Street, New York, NY 10013, USA), except for brief excerpts in connection with reviews or scholarly analysis. Use in connection with any form of information storage and retrieval, electronic adaptation, computer software, or by similar or dissimilar methodology now known or hereafter developed is forbidden.
The use in this publication of trade names, trademarks, service marks, and similar terms, even if they are not identified as such, is not to be taken as an expression of opinion as to whether or not they are subject to proprietary rights.

Printed on acid-free paper.

9 8 7 6 5 4 3 2 1

springer.com

To my wife, Hyonsook (Danielle)

PREFACE

The writing of this book was begun in 1995. A course on "Ceramics and Glasses As Biomaterials (51:174)" was first offered during 1988 under the Department of Biomedical Engineering at the University of Iowa. It was largely based on my *Biomaterials Science and Engineering* (Plenum, 1984), especially Chapter 9, "Ceramic Implant Materials." Needless to say, there have been a multitude of significant new developments, notably with regard to cubic zirconia, diamond-like carbon, tissue engineering, and nanotechnology. The use of ceramics in tissue engineering is a logical extension of bioceramics, as bone and teeth are composed of ceramics and organic materials. The development of nanotechnology has unlimited potential for future applications. Already used as gemstones and in laser crystals, employment of bioceramics in sensory organ implants is promising. Their use means that cochlear implants can be made without electronic devices to feed sound waves to more than 20,000 nerve endings, as opposed to the 20 electrodes currently needed to stimulate the same number of nerves (see Example 11.3). One day we will manufacture a "direct-sensing" device made with ceramics and organic matter (e.g., collagen) that has piezoelectric properties. Similarly, electromagnetic wave-sensing ceramics or polymers can be developed for such "direct transfer" of energy in the eye or the ear and with other nerve signals.

The task of writing a textbook is difficult. One needs to cover all subjects in a balanced but adequate fashion. This author believes in mastering the basics and fundamentals first before advancing to other areas. It is therefore wise to study Chapters 2–5 before proceeding to Chapters 6–11, where specific bioceramics are presented and discussed. The final chapter (12) presents an amalgamation of all previous studies as applied to medicine and dentistry. The author has attempted to include as much related material as possible without overburdening the reader. Any errors of commission or omission that remain in spite of my and my copyeditor's utmost efforts are our responsibility alone.

The author is thankful to all the undergraduate and graduate students who took his course and helped in revising the book. My sincerest thanks go out to former and present PhD students D.N. Bingham, Jin C. Cho, Yoon H. Kang, Gilson Khang, Hyun S. Kim, Inae Hur, Jae H. Kim, Jeong K. Kim, NaJung Kim, Sung S. Kim, Young Kon Kim, Rong-Fu Kuo, Jin W. Lee, Tae-H. Lim, Kwideok Park, Sang Hyun Park, Young Il Park, Joseph A. Paulus, A. Suliman, and Seok-Jo Yang. Former students S.A Al-Husseini, J.C. Anderson, W. Barb, A. Berthusen, J.B. Bigelow, D. Black, G.J. Boys, J.A. Case, D.R. Clarke, J.P. Davies, M.F. DeMane, S.D. Ferguson, J.R. Frigstad, G.E. Gratzick, M.F. Grether, T. Hargens, R. Hart, D.E. Henrich, P.R. Iyer, J. Kuebler, Uyen Le, M.A. Looney, K. Markgraf, E.O. Martz, W.J. Whatley, J.M. Winterbottom, T.J. Wroblewski, and S.O. Young worked with me on various biomaterials research projects.

I am also indebted to Professor Merrill. L. Ebner of Boston University, who passed away on March 28, 2008, who introduced me to the materials field, and to Professors K.L. DeVries (Utah), W.O. Statton (Utah), and D.R. Uhlmann (MIT/Arizona), who taught me how to conduct research and to teach. Special thanks go to Professors S.R. Armstrong (Iowa), T.D. Brown (Iowa), E.Y.S. Chao (Johns Hopkins), Won W. Choi (Iowa), C.R. Clark (Iowa), F.W. Cooke (Clemson/Wichita State), E.A. Friis (Kansas), V.K. Goel (Toledo), N.M. Grosland (Iowa), V.J. Hetherington (Iowa/Ohio College of Podiatric Medicine), J.J. Callahan (Iowa), John C. Keller (Iowa), G.H. Kenner (Clemson/Utah), Gilson Khang (Chunbook National University), Jeong K. Kim (Inje University), Young Kon Kim (Inje University), Yong S. Kim (Catholic University), R.S. Lakes (Wisconsin), J.H. Lee (Dong-A University), Jae I. Ahn (Ajoo University), Tae-H. Lim (Iowa), Y.K. Liu (Iowa/University of Northern California), S.A. Loening (Iowa/Berlin), Sang Hyun Park (UCLA), A.K. Salem (Iowa), Whal Seo (Yonsei University), K.L. Shaull (Iowa), H.B. Skinner (UC Irvine), R.C. Tucker (Iowa), R.C. Turner (Clemson), A.F. von Recum (Clemson/Ohio State), J.N. Weinstein (Iowa/Dartmouth), D.G. Wilder (Iowa), and Seok-Jo Yang (Chungnam National University). Doctors Hae B. Lee (Korea Research Institute of Chemical Technology), Jae H. Kim (Pennsylvania), Jin W. Lee (BISCo), Kwideok Park (Korea Institute of Science & Technology), and Hong S. Shim (Carbomedics/Medtronics Inc.) deserve special thanks. Also, my sincere gratitude and respect go to Professor A.S. Hoffman (Washington), who introduced me to the bioengineering field, and Professor L.L. Hench (Florida/Imperial College of Science, Technology & Medicine, London), who introduced me to bioceramics when I started teaching in 1973 at the University of Illinois at Champagne-Urbana. I would also like to extend my respect and admiration to Professor H. Kawahara (Osaka Dental University), who has been the main promoter and researcher of ceramic (alumina) dental implants over the past four decades.

Messrs. Aaron Johnson and Tim Oliver of Springer have been a great help, not only with this book but also with *Biomaterials: An Introduction,* 3rd edition (Springer, 2007). I am grateful for their tireless dedication and professionalism.

This book would not be possible without the countless days and late evenings of work spent away from my most wonderful family: my wife Hyonsook, my daughters Misun and Na Jung, and my sons Yoon Ho and Yoon Il, to whom I am forever indebted.

Joon B. Park, PhD
Coralville, Iowa
May 2008

CONTENTS

Preface vii

1: Introduction

Problems 5
Definitions 7
References 8

2: Structure of Ceramics and Glasses

2.1. Atomic Bonding and Arrangement 12
2.2. Characterization of Microstructure 18
2.3. Quantitative Analysis of Single-Phase Microstructure 21
2.4. Microstructure Determination 22
Problems 24
Symbols/Definitions 25
References 27

3: Characterization of Ceramics and Glasses

3.1. Mechanical Properties 30
3.2. Strengthening of ceramics and Glasses 36
3.3. Weibull Statistics of Brittle Failure 38
3.4. Impact Strength, Hardness, Friction, and Wear Properties 43
3.5. Thermal Properties (Phase Changes) 47
3.6. Surface Properties 59
Problems 63
Symbols/Definitions 66
References 68

4: Glass Formation and Characterization

4.1. Glass Formation ... 70
4.2. Nucleation and Glass Formation ... 71
4.3. Strength of Glasses ... 72
4.4. Static Fatigue of Glasses ... 74
Problems ... 77
Symbols/Definitions ... 80
References ... 81

5: Hard Tissues: Structure, Properties, Healing, Remodeling, and Biocompatibility

5.1. Structure of Proteins ... 85
5.2. Structure–Property Relationships ... 90
5.3. Hard Tissue Healing and Remodeling ... 102
5.4. Biocompatibility ... 109
Problems ... 112
Symbols/Definitions ... 113
References ... 114

6: Aluminum Oxides (Alumina)

6.1. Source, Composition, and Structure ... 118
6.2. Mechanical Properties ... 120
6.3. Fatigue Properties and Service Life ... 124
6.4. Applications ... 128
6.5. Further Thoughts ... 132
Problems ... 133
Symbols/Definitions ... 136
References ... 138

7: Zirconium Oxides (Zirconia)

7.1. Source and Manufacturing of Zirconia ... 142
7.2. Structure and Properties of Zirconia ... 142
7.3. Long-Term Stability and Implant Design ... 149
7.4. Further Thoughts ... 161
Problems ... 162
Symbols/Definitions ... 163
References ... 165

8: Glass-Ceramics

8.1. Formation of Glass-Ceramics 168
8.2. Properties of Glass-Ceramics 170
8.3. Coatings and Composites 176
8.4. Further Thoughts 176
Problems 177
Definitions 178
References 179

9: Hydroxyapatite

9.1. Source, Composition, and Structure 184
9.2. Properties of Hydroxyapatite 191
9.3. Applications 192
9.4. Further Thoughts 197
Problems 197
Definitions 200
References 201

10: Carbons and Diamond-Like Carbon Coatings

10.1. Source and Structure of Carbons 206
10.2. Properties of Carbons 209
10.3. Manufacture of Carbon Implants 212
10.4. Diamond-Like Carbon (DLC) Coatings 214
10.5. Further Thoughts 221
Problems 221
Definitions 222
References 223

11: Sulfates and Titanates

11.1. Source, Composition, and Structure 228
11.2. Structure and Properties of Titanates 232
11.3. Applications 236
11.4. Further Thoughts 241
Problems 241
Symbols/Definitions 243
References 244

12: Composites, Tissue Substitutes, and Scaffolds

12.1. Fundamentals of Composite Theory 248
12.2. Applications of Composites 253
12.3. Composite Scaffolds 274
12.4. Fabrication of Bone Scaffolds 281
12.5. Biocompatibility of Composite Biomaterials 284
12.6. Further Thoughts 285
Problems 285
Symbols/Definitions 290
References 295

Appendices

Appendix I: Physical Constants and Conversions 303
Appendix II: SI Units 304
Appendix III: Common Prefixes 305
Appendix IV: Properties of Selected Elements 306

Bibliography 307

Name Index 327

Subject Index 339

1

INTRODUCTION

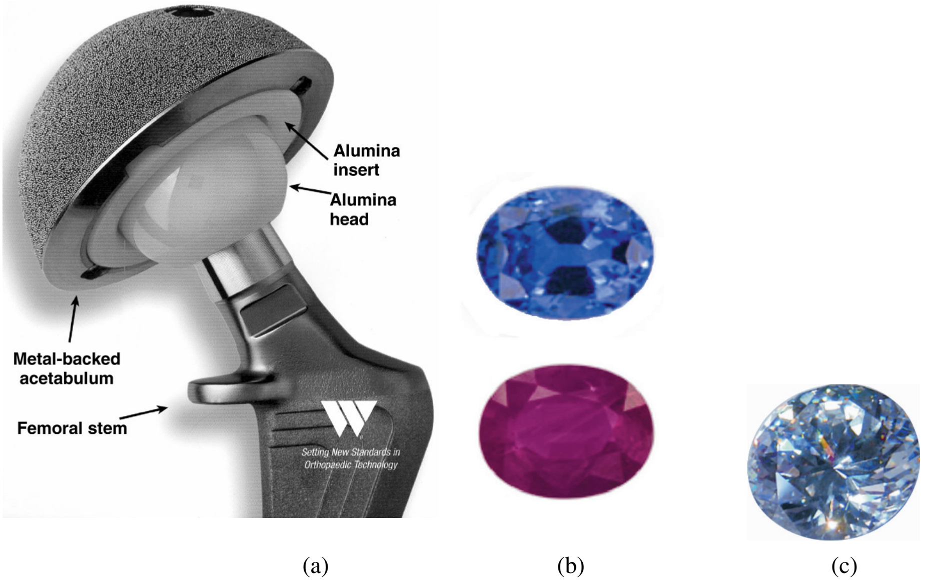
Alumina
insert
Alumina
head
Metal-backed
acetabulum
Femoral stem
Setting New Standards in
Orthopaedic Technology
(a)
(b)
(c)

(a) Use of alumina as bearing surfaces for a hip prosthesis. The metal (likely CoCr alloy, not specified) acetabular back is coated with Ti alloy beads to create porosity for tissue ingrowth fixation. Courtesy of Wright Medical Technology Inc., Arlington, TN. (b) Single-crystal alumina can be grown and cut as sapphire (top) and ruby (bottom) depending on the impurities (see Chapter 6). (c) Single-crystal cubic zirconia as a jewelry stone (see Chapter 7). Please refer to the color section to view this image in full color.

Ceramics are refractory polycrystalline compounds, usually inorganic, including silicates, metallic oxides, carbides, and various refractory hydrides, sulfides, and selenides [7]. Oxides such as Al_2O_3, ZrO_2, and SiO_2 contain metallic and nonmetallic elements while others are ionic salts: NaCl, CsCl, ZnS, etc. Covalently bonded ceramics are diamond and carbonaceous structures like graphite and pyrolyzed carbons. Important factors influencing the structure and property relationship of the ceramic materials are the *radius ratio* and the relative *electronegativity* between the positive and negative ions.

Ceramics and glasses have been given a lot of attention as candidates for implant materials since they possess some highly desirable characteristics for some applications, as shown in Figure 1.1. The main advantage is their inertness in aqueous conditions, and thus high biocompatibility. The ceramics we are going to study are limited to a few due to the limited knowledge on their effect on tissues (and vice versa) and the high cost of development. Another important aspect of ceramics and glasses is their brittleness and consequently very low strength in tension. Therefore, their use is mostly limited to compressive loading conditions, such as those in an acetabular cup or a femoral head of a total hip joint replacement. Some applications do not require high loading, including hydroxyapatite for artificial bone and barium sulfate ($BaSO_4$) for bone cement. Alumina, calcium phosphates, glass-ceramics, zirconia, and carbons are not extensively studied and are used infrequently. We will concentrate our efforts on studying these materials and some more experimental ceramics and glasses being developed and explored. It is emphasized that we have to know the *fundamentals* well enough to develop and use a new ceramic or glass. Therefore, we will try to understand the fundamentals first, then study the ceramics and glasses used currently, and then discuss new and future developments.

Ceramics (from the Greek *keramos,* meaning pottery or burnt stuff) are composed of inorganic and nonmetallic materials and include pottery, porcelain, refractory materials, clay products, abrasives, porcelain enamels, cements, glasses, nonmetallic magnetic materials, ferroelectrics, and manufactured single crystals.

Two ceramic processes are used in forming ceramic articles:

(1) Employment of lubricant and binder (liquid) with ceramic particles for shaping and subsequent firing.
(2) Materials are melted to form a liquid and are shaped during cooling and solidification.

The *raw materials* of silicates and aluminum silicates are O, Si, and Al, which comprise more than 90% of the earth's crust. Clay minerals are fine-particle hydrous aluminum silicates, of which kaolinite ($Al_2(Si_2O_5)(OH)_4$) is the most common. A similar compound is talc ($Mg_3(Si_2O_5)_2(OH)_2$). Anhydrous silica (SiO_2) and quartz are used to make glass products, glazes, enamels, refractory materials, abrasives, and white wares. Such nonsilicates as alumina processed from bauxite are used mainly for refractory materials. Many ceramics are made from chemically processed raw materials to obtain products with better qualities and properties (e.g., capacitors, resistors, and spark plug insulators) and also to make such single crystals as ruby and sapphire.

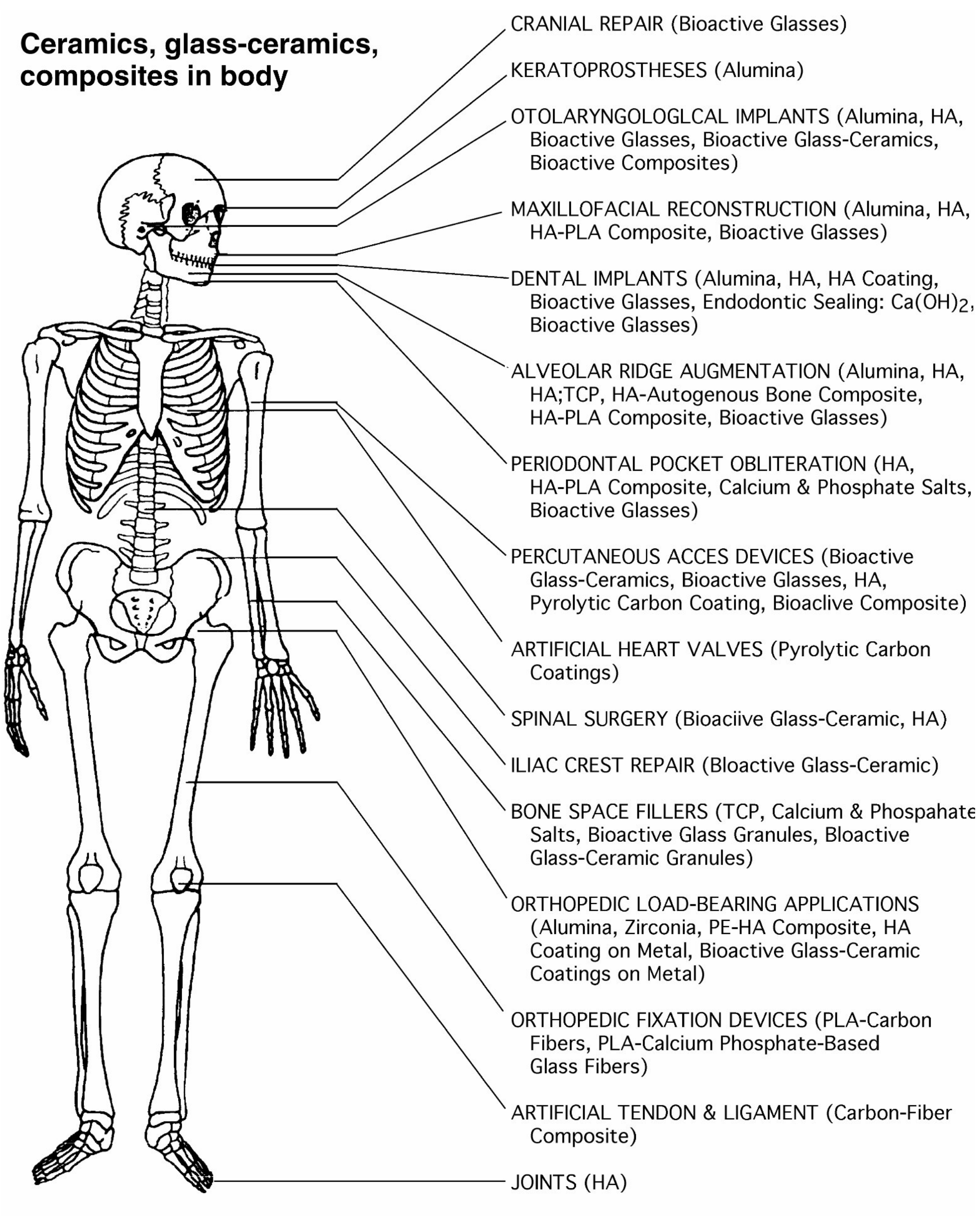
Ceramics, glass-ceramics, composites in body
CRANIAL REPAIR (Bioactive Glasses)
KERATOPROSTHESES (Alumina)
OTOLARYNGOLOGLCAL IMPLANTS (Alumina, HA, Bioactive Glasses, Bioactive Glass-Ceramics, Bioactive Composites)
MAXILLOFACIAL RECONSTRUCTION (Alumina, HA, HA-PLA Composite, Bioactive Glasses)
DENTAL IMPLANTS (Alumina, HA, HA Coating, Bioactive Glasses, Endodontic Sealing: $Ca(OH)_2$, Bioactive Glasses)
ALVEOLAR RIDGE AUGMENTATION (Alumina, HA, HA;TCP, HA-Autogenous Bone Composite, HA-PLA Composite, Bioactive Glasses)
PERIODONTAL POCKET OBLITERATION (HA, HA-PLA Composite, Calcium & Phosphate Salts, Bioactive Glasses)
PERCUTANEOUS ACCES DEVICES (Bioactive Glass-Ceramics, Bioactive Glasses, HA, Pyrolytic Carbon Coating, Bioaclive Composite)
ARTIFICIAL HEART VALVES (Pyrolytic Carbon Coatings)
SPINAL SURGERY (Bioaciive Glass-Ceramic, HA)
ILIAC CREST REPAIR (Bloactive Glass-Ceramic)
BONE SPACE FILLERS (TCP, Calcium & Phospahate Salts, Bioactive Glass Granules, Bloactive Glass-Ceramic Granules)
ORTHOPEDIC LOAD-BEARING APPLICATIONS (Alumina, Zirconia, PE-HA Composite, HA Coating on Metal, Bioactive Glass-Ceramic Coatings on Metal)
ORTHOPEDIC FIXATION DEVICES (PLA-Carbon Fibers, PLA-Calcium Phosphate-Based Glass Fibers)
ARTIFICIAL TENDON & LIGAMENT (Carbon-Fiber Composite)
JOINTS (HA)

Figure 1.1. Many uses of ceramics, glasses, and composites in the body. Adapted with permission from [4]. Copyright © 1993, World Scientific.

Forming and firing of ceramic products require proper selection of raw materials in terms of particle size and its distribution. For maximum packing and least shrinkage after firing, 70% coarse and 30% fine powders are mixed. Mixing is usually carried out in a ball mill for uniformity of properties and reaction during the firing process.

Mechanical die forming or sometimes extrusion through a die orifice can be used to produce a fixed cross-section. Drying involves removal of water and subsequent shrinkage of the product. Warping and even cracks may develop during the drying process due to local variations in water content. Dry pressing and hydrostatic molding can minimize the problems associated with drying. The blank (the "green") is fired first, then glazed and refired at low temperature. This process can be reversed in some cases, so that the "green" is glazed without firing. The firing temperature can range from 700 to 1800ºC.

Glass products are made in a high-temperature "viscous state" by blowing, pressing, drawing, rolling, and casting. The residual stresses built during the forming process can be relieved by annealing at high temperatures (400–500ºC).

Special processes can be used in making such glass-ceramics as those used for the bone-bonding Bioglass® and for coating pyrolytic carbon on an artificial heart valve disc by chemical vapor deposition (CVD). The fluidized bed deposition method can also be employed.

Single-crystal ceramics (e.g., aluminum oxide, garnet) can be made by the Czochralski process, where the crystal is slowly pulled from the melt. By adding powder on the surface of the liquid cap of a single-crystal boule we can achieve the same results (the Verneuil process).

Traditional ceramic products — such as silicates, clay ware, Portland cement, and soda-lime glasses — and structural clay products (e.g., brick and tile) are not suitable for making implants. New classes of ceramics, including pure oxides, Al_2O_3 and ZrO_2, and single-crystal Al_2O_3 are being used instead. Ceramic nitrides (e.g., silicon nitride, SiAlON) is a candidate for making implants. Cermets (ceramic metal composites made of mostly carbide- and aluminum oxide-bonded metals) have been used to make cutting tools, but they are not being considered for making implants. As mentioned above, glass-ceramics have found a use in making implants. Calcium sulfate ($CaSO_42H_2O$), popularly known as plaster of Paris, is being experimented with as a bone substitute

Some carbons have found use as implants in such blood-interfacing applications as heart valves. Due to their high specific strength as fibers and their biocompatibility, they are also being used as a reinforcing component for composite implant materials. Work is also being done to explore their use in such tensile loading applications as artificial tendon and ligament replacements. Although their black color can be a drawback in dental applications, their good biocompatibility and ease of fabrication are especially desirable qualities for implants. Table 1.1 summarizes typical properties of some ceramics and glasses.

Bioceramics can be classified according to their reactivity with living tissue, as *bioactive* or *bioinert.*

Those ceramics (e.g., calcium phosphates and glass-ceramics) designed to induce tissue reactions for bonding or those used to deliver drugs are usually bio(re)active. Most other ceramics are bioinert, including zirconia, alumina, sialon, and cermets.

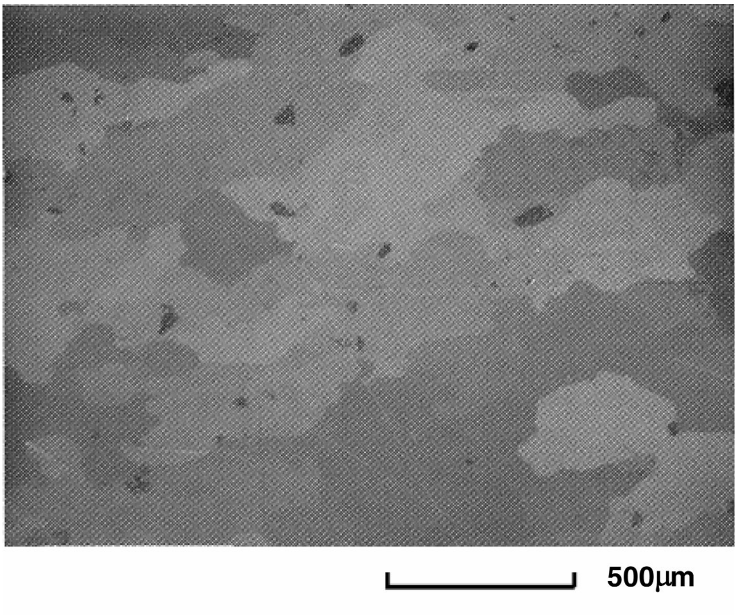

Figure 1.2. Microstructure of $BaTiO_3$–Sn composite under polarized light. $BaTiO_3$ appears as dark inclusions; the Sn matrix is light in shade. Modified with permission from [5]. Copyright ©2007, American Association for the Advancement of Science.

Special YAS (yttrium aluminosilicate) glass microspheres have been developed to deliver therapeutic radiation (β-rays) to an organ (liver) via arteries [3]. Some investigators have tried to use glass-ceramics for *hyperthermia* in bone cement formulation [8]. These ceramics can be utilized for extracorporeal treatment of prostate cancer using metallic (PdCo alloy) thermal seeds [10]. It would be interesting to apply the new concept of composite materials, which can result in a "viscoelastic" stiffness greater than that of the diamond. The composite is made of TiO_3 and tin, and its microstructure is shown in Figure 1.2 [5]. Obviously, the use of tin might result in less desirable biocompatibility and could be replaced by other (noble) metals. The reader is directed to more fundamental studies on bioceramics, including chapters 6, 8, and 9 in the author's book on biomaterials [2,6,9].

PROBLEMS

1.1. Calculate the maximum theoretical packing efficiency of two spherical particles of alumina with mean diameters of r and R of equal density. What would be the resulting overall packing efficiency?

1.2. Define biocompatibility.

Table 1.1. Typical Properties of Some Ceramics and Glasses

Materials	Specific gravity (g/cm^3)	Young's modulus (GPa)	Compressive strength (MPa)	Modulus of rupture (MPa)	Weibull exponent (*m*)	Time exponent (*n*)
Alumina (Al_2O_3)	3.9	380	3000	300–400	10	10
Zirconia (ZrO_2)	5.6	200	2000	200–500	10–21	10
Glass-ceramic (Bioglass®)	~2.8	~100	~1000	~100	~10	10
Hydroxyapatite $Ca_{10}(PO_4)_6(OH)_2$	3.15	100~200	~1000	<100	~10	10
Barium titanate ($BaTiO_3$)	6.02	~50	486	–	–	–
Quartz (SiO_2)	2.65	310	–	–	–	–
Diamond	3.52	1050	5000	–	–	–
Graphite	1.6~2.1	10	20	10	–	–
Soda lime glass	2.48	74	1000	50	10	10
Borosilicate glass	2.23	65	1200	55	10	10
Porcelain	2.3-2.5	70	350	45	10	–
Silicon carbide	3.2	410	2000	200–500	10	40
Silicon nitride	3.2	310	1200	300–850	–	40
Sialons	3.2	300	2000	500–830	15	10
Concrete	2.4	30–50	50	7	12	40
Polystyrene[b]	1.05	2.8	–	–	–	–
Polymethyl methacrylate[b]	1.2	3.5	–	–	–	–

[a] Organic glass.

Adapted in part with permission from [1]. Copyright © 1986, Pergamon.

1.3. List the names of ceramic materials used in medicine and dentistry, such as plaster of Paris, porcelain artificial teeth, etc.

1.4. Discuss the economic implications of “class-action” versus “individual” litigation related to an implant, such as a spinal disc fusion device, for the (a) manufacturer, (b) the consumer, and (c) attorneys.

1.5. What would be the major factors influencing tissue behavior when in contact with ceramic materials? Be specific.

1.6. The FDA (Food and Drug Administration) plays a major role in bringing an innovative medical and dental product to the market. Discuss the pros and cons of their role for consumers and manufacturers.

1.7. Would it be advantageous to coat the surface of intraocular lenses (IOLs) with an amorphous diamond (DLC, diamond-like carbon)?

Table 1.1. cont'd

Fracture toughness (MPa·m$^{1/2}$)	Melting (softening) temperature (°C)	Specific heat (J/kg/K)	Thermal conductivity (W/m/K) $\times 10^{-6}$	Thermal expansion coefficient (/K) $\times$ 10^{-6}	Thermal shock resistance (K)
3–5	2323 (1470)	795	25.6	8.5	150
4–12	2843	670	1.5	8	500
~3	–	–	–	–	–
~3	–	–	–	–	–
–	1625	–	–	–	–
–	–	–	0.012	–	–
–	>4000	510	70	1.2	1000
–	–	120	–	–	–
0.7	1000	990	1	8.5	84
0.8	1100	800	1	4.0	280
1.0	1400	800	1	3	220
–	3110	1422	84	4.3	300
4	2173	627	17	3.2	500
5	–	710	20–25	3.2	510
0.2	–	–	2	10–14	<50
–	–	95 (T_g)	0.00008	63	–
–	–	135~140 (T_g)	0.0002	90	–

1.8. Surgical scissors and knives can be coated with DLC. Suggest at least one method for testing their effectiveness.

1.9. Suggest ways of using nanotechnology in medicine and dentistry using ceramics as raw materials.

1.10. One day some people may try to use cells to build implants. Discuss the possibility of the contributions of ceramics to such a process.

DEFINITIONS

Anhydrous silica (SiO_2): A network-forming oxide used in the production of a number of bioglasses (e.g., Bioglass® 45S5, Ceravital®, Biovert®).

Barium titanate–tin ($BaTiO_3$–Sn) composite: A ceramic–metal (viscoelastic) composite with a viscoelastic modulus higher than that of diamond.

Cermet: A large-particle metal–ceramics composite, most commonly cemented carbide, titanium carbide, or tungsten carbide, used extensively in cutting tools for hardened steels.

Chemical vapor deposition (CVD): High-temperature process by which materials are deposited or coated for corrosion resistance and strength using a reactive gas atmosphere that decomposes at high temperatures and recombines to form the coating.

Czochralski process: A process by which crystal growth is obtained through a seed crystal being lowered into a melted doped semimetal or ceramic and raised back at a particular rate to control crystal growth.

Electronegativity: The potential of an atom to attract electrons, especially in the context of forming a chemical bond.

Fluidized bed process: Hydrocarbons are mixed with carrier gas, then fed into a furnace (bed) for pyrolyzation to coat an implant (artificial heart valve).

Glass-ceramics: Polycrystalline ceramics made by controlled crystallization of glasses, such as Bioglass® and Ceravital®. Some are formulated to have the ability to form chemical bonds with hard and soft tissues.

Hyperthermia: The condition of having a body temperature greatly above normal. Local hyperthermia (40~65°C) can be created by using ceramic or metal alloy interstitial seeds, which in turn can be excited by placing a Helmholtz coil extracorporeally and radio-frequency (rf) modulation. This technique has been explored in treating prostate cancer or BPH (benign prostate hyperplasia).

Kaolinite ($Al_2(Si_2O_5)(OH)_4$): One of the most common clay minerals, with a two-layer silicate sheet structure that is repeated and stacked parallel to each other, forming small flat hexagonal plates.

Pd–Co alloy: Metal alloy used to make thermal seeds for hyperthermic treatment of prostate cancer. Palladium is not ferromagnetic, but is used for its excellent biocompatibility, and addition of up to 97.5% Pd will lower the Curie temperature of cobalt to 50–65°C.

Quartz: A brilliant hexagonally crystalline mineral, SiO_2, occurring in abundance, mostly in a colorless, transparent form but also in a colored form, used as a gemstone.

Radius ratio: Ratio between the radius of a smaller atom or ion to that of larger ones, into which the smaller are fitted, based on geometric considerations.

Silicon nitrides (Si_3N_4): Non-oxide network solid ceramic that is hard, lightweight, and heat and creep resistant with high corrosion resistance.

Talc ($Mg_3(Si_2O_5)_2(OH)_2$): A very soft (Mohs hardness 1), usually massive and foliated mineral, magnesium silicate, with a greasy feel, used to make talcum powder, lubricants, etc.

Verneuil process: A flame fusion technique for production of gems and other crystals. The method involves melting powdered material, and allowing drops of melt fall onto a growing "boule" crystal that is lowered as it grows.

YAS (yttrium aluminosilicate) glass: A special glass made to deliver radiation (β-rays) to a cancerous liver via hepatic arteries.

REFERENCES

1. Ashby MF, Jones DR. 1985. *Engineering materials 2: an introduction to microstructures, processing and design*, pp. 147–152, Oxford: Pergamon.
2. ASM. 1987. *Engineered materials handbook*, Vol. 4: *Ceramics and glasses*. Metal Park, OH: ASM International.
3. Day DE, Day TE. 1993. Radiotherapy glasses. In *An introduction to bioceramics*, pp. 305–317. Ed LL Hench, J Wilson. Singapore: World Scientific.

4. Hench LL, Wilson J, eds. 1993. *An Introduction to bioceramics*, pp. 1–24. Singapore: World Scientific.
5. Jaglinski T, Kochman D, Stone D, Lakes RS. 2007. Composite materials with viscoelastic stiffness greater than diamond. *Science* **315**:620–622.
6. Jones JJ. 2006. Biomaterials: bioceramics. In *Encyclopedia of medical devices and instrumentation*, pp. 283–296. Ed JG Webster. Hoboken, NJ: Wiley.
7. Kingery WD, Bowen HK, Uhlmann DR. 1976. *Introduction to ceramics*, 2nd ed, pp. 3–20. New York: Wiley.
8. Ohura K, Nakamura T, Yamamuro T, Ebisawa Y, Kokubo Y, Oka M. 1991. A heat-generating bioactive glass-ceramic for hyperthermia. *J Appl Biomed* **2**:153–159.
9. Park JB, Lakes RS. 2007. *Biomaterials: an introduction*, 3rd ed. New York: Springer.
10. Paulus JA, Richardson JS, Tucker RD, Park JB. 1996. Evaluation of inductively heated ferromagnetic alloy implants for therapeutic interstitial hyperthermia. *IEEE Trans Biomed Eng* **43**:406–413.

2

STRUCTURE OF CERAMICS AND GLASSES

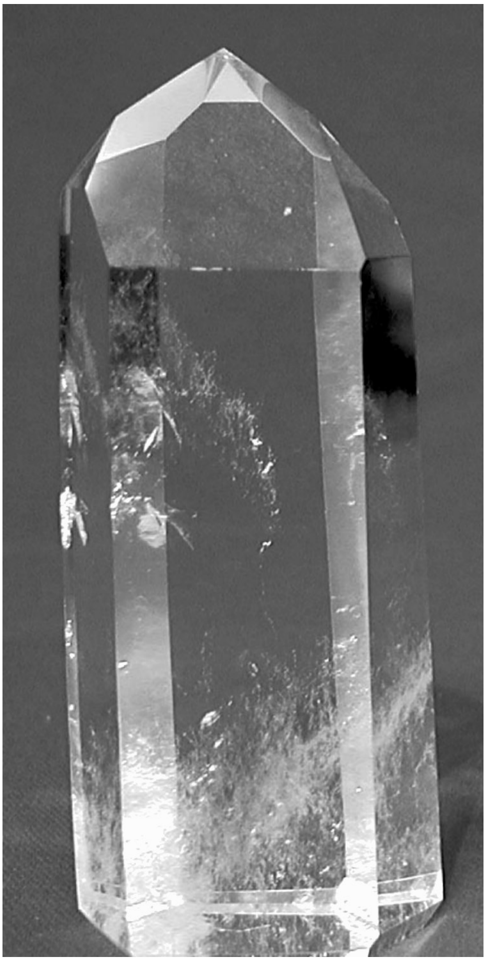

Quartz is the second most common mineral (after feldspar) in the earth's crust. The silica (SiO_2) tetrahedron is a basic molecular building block. It has a Mohs scale hardness of 7 and a density of 2.65 g/cm^3. Large industrial crystals can be grown using a furnace with a controlled rate of solidification. These are cut and used in watch movements, telephone receivers, etc.

2.1. ATOMIC BONDING AND ARRANGEMENT

When (neutral) atoms such as sodium (metal) and chlorine (nonmetal) are ionized, the sodium loses an electron and the chlorine gains an electron:

$$\mathrm{Na} \Leftrightarrow \mathrm{Na}^+ + \mathrm{e}^-, \quad \mathrm{e}^- + \mathrm{Cl} \Leftrightarrow \mathrm{Cl}^-. \tag{2.1}$$

Thus, the sodium and chlorine are able to make up an "ionic compound" by the strong attraction of the positive and negative ions. The negatively charged ions are much larger than the positively charged ones (see Table 2.1) due to the gain and loss of valence electrons. The radius of an ion varies according to the coordination number (CN): the higher the CN, the larger the radius. For example, an oxygen ion (O^{2-}) has a radius of 1.28, 1.40, and 1.44 Å for CNs of 4, 6, and 8, respectively.

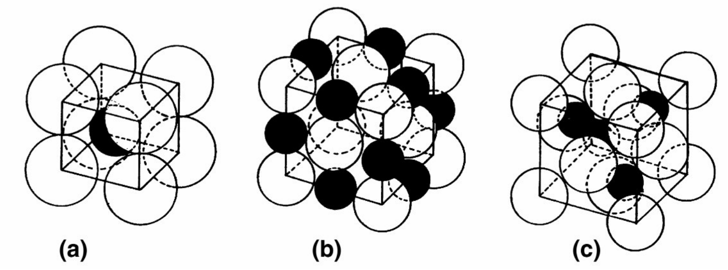

Figure 2.1. AX structures of ceramics: (a) CsCl; (b) NaCl; (c) ZnS. The dark spheres represent positive ions (A^+) and the circled ones represent negative ions (X^-).

Ceramics can be classified according to their structural compounds, of which A_mX_n is an example (A represents a metal and X a nonmetal element; and m and n are integers). The simplest case of this system is the AX structure ($m = n = 1$), of which there are three types (Fig. 2.1). CsCl has a *simple cubic* structure, as shown in Figure 2.1a. One must not confuse this with the *body-centered cubic* (bcc) structure, which would have the *same* ion or atom occupying the center (body) of the unit cell. CsBr and CsI have the same CsCl structure. The NaCl has a *face-centered cubic* (fcc) structure, where the positive (Na^+) and negative (Cl^-) ions are surrounded by 6 opposite ions (CN = 6). This is called a *rock salt structure*; MgO, CaO, SrO, BaO, CdO, MnO, FeO, CoO, and NiO belong to the same group.

The difference between these structures is due to the relative size of the ions (*minimum radius ratio*). If the positive and negative ions are about the same size ($r_A/R_X > 0.732$), the structure becomes a simple cubic (CsCl) structure. The face-centered cubic structure arises if the relative size of the ions is quite different since the positive ions can be fitted in the *tetragonal* or *octagonal* spaces created among larger negative ions. These are summarized in Table 2.2. The aluminum and chromium oxide have an A_2X_3 type structure. The O^{2-} ions form a *hexagonal close-packed* (hcp) structure, while the positive ions (Al^{3+}, Cr^{3+}) fill in 2/3 of the *octahedral* sites, leaving a third of them vacant.

Table 2.1. Atomic and Ionic Radii of Some Elements (units in Å)

Group I			Group II			Group IV			Group VI		
Element	Atomic radius	Ionic radius	Element	Atomic radius	Ionic radius	Element	Atomic radius	Ionic radius	Element	Atomic radius	Ionic radius
Li^+	1.52	0.68	Be^{2+}	1.11	0.31	O^{2-}	0.74	1.40	F^-	0.71	1.36
Na^+	1.86	0.95	Mg^{2+}	1.60	0.65	S^{2-}	1.02	1.84	Cl^-	0.99	1.81
K^+	2.27	1.33	Ca^{2+}	1.97	0.99	Se^{2-}	1.16	1.98	Br^-	1.14	1.95

Table 2.2. Selected A_mX_n Structures

Prototype compound	Lattice of A (or X)	CN of A (or X) sites	Available sites filled	Minimum r_A/R_X	Other compounds
CsCl	Simple cubic	8	All	0.732	CsI
NaCl	fcc	6	All	0.414	MgP, MnS, LiF
ZnS	fcc	4	1/2	0.225	β-SiC, CdS, AlP
Al_2O_3	hcp	6	2/3	0.414	Cr_2O_3, Fe_2O_3

Cubic zirconia (ZrO_2) has an fcc packing of the Zr^{4+} ions and O^{2-} ions occupying the octahedral sites. Due to charge balance, two O^{2-} ions will balance one Zr^{4+} ion; therefore, half the available tetrahedral sites in the unit cell will be occupied by O^{2-} ions. Similarly, the MgO can be said to have O^{2-} ions occupying all available octahedral sites in the unit cell structure. There are one octahedral and two tetrahedral sites per atom in face-centered cubic and hexagonal close-packed structures, which represent the most close-packed structure (see Fig. 2.2). The unit cell structure of cubic zirconia and alumina are shown in Figure 2.3. Aluminum ions (Al^{3+}) occupy 2/3 of the available octahedral sites of the hcp structure due to the valence electron balance with oxygen ion (O^{2-}), as mentioned. The Fe_2O_3, Cr_2O_3, Ti_2O_3, V_2O_3, and Ga_2O_3 belong to the same group.

Some ceramics have *covalent bonds* as their primary chemical bonding force, e.g., diamond and silica. The diamond structure is shown in Figure 2.4a, where one can see a tetrahedron of carbons. Also, one can discern the fcc structure, in which the carbon atoms occupy half the tetrahedral sites available. Silicon carbide (SiC) has a similar structure, in which the Si atoms occupy half the tetrahedral sites available, as shown in Figure 2.4b. Silica structure can be understood similarly as having the SiO_4 *tetrahedron* on each Si site, as shown in Figure 2.4c. These structures are not close-packed structures since the CNs are not 12 but 4; therefore, their densities are low. However, the SiC is a very hard ceramic and is used as an abrasive, similar to diamond.

Silicate glasses are based on the silica (SiO_2) tetrahedron, which can be linked together into a two- or three-dimensional network structure, as shown in Figure 2.5.

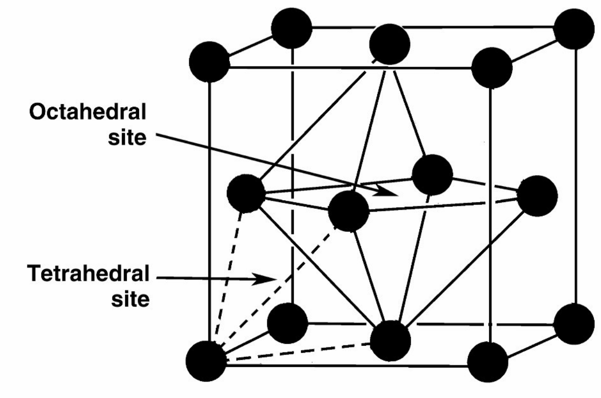

Figure 2.2. Unit cell representation of close packing of fcc. There are 4 octahedral and 8 tetrahedral sites in the unit cell. The hcp structure has a close packed structure, with the same number of octahedral and tetrahedral sites in the unit cell.

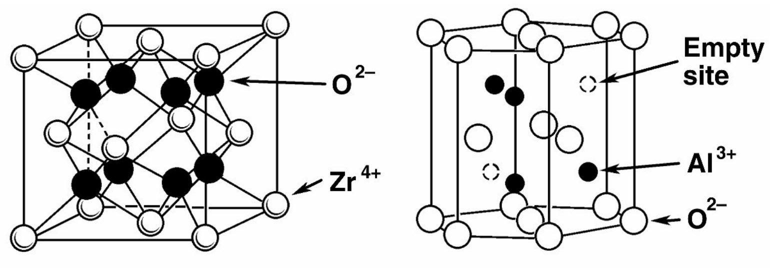

Figure 2.3. Unit cell representation of (a) cubic zirconia and (b) alumina.

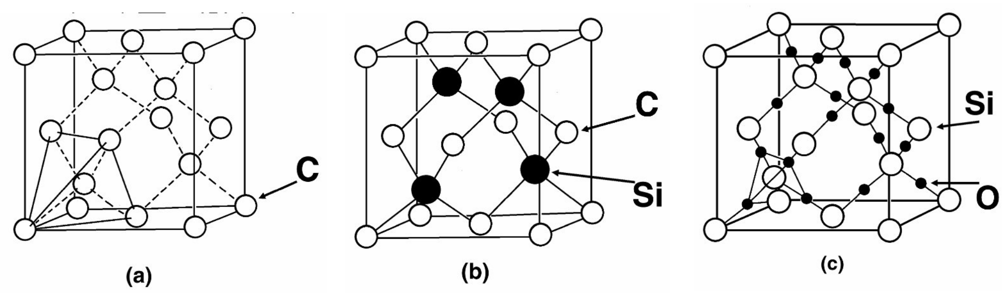

Figure 2.4. Unit cell representation of covalently bonded ceramics: (a) diamond, (b) SiC, and (c) cubic silica.

When the Si–4O tetrahedron forms a three-dimensional network and is arranged in a coordinated manner, it takes on a crystalline structure, as shown in Figure 2.6a, but it can be distorted, resulting in amorphous silica glass, as shown in Figure 2.6b. The silica glass has a very high glass transition temperature (T_g); therefore, network-

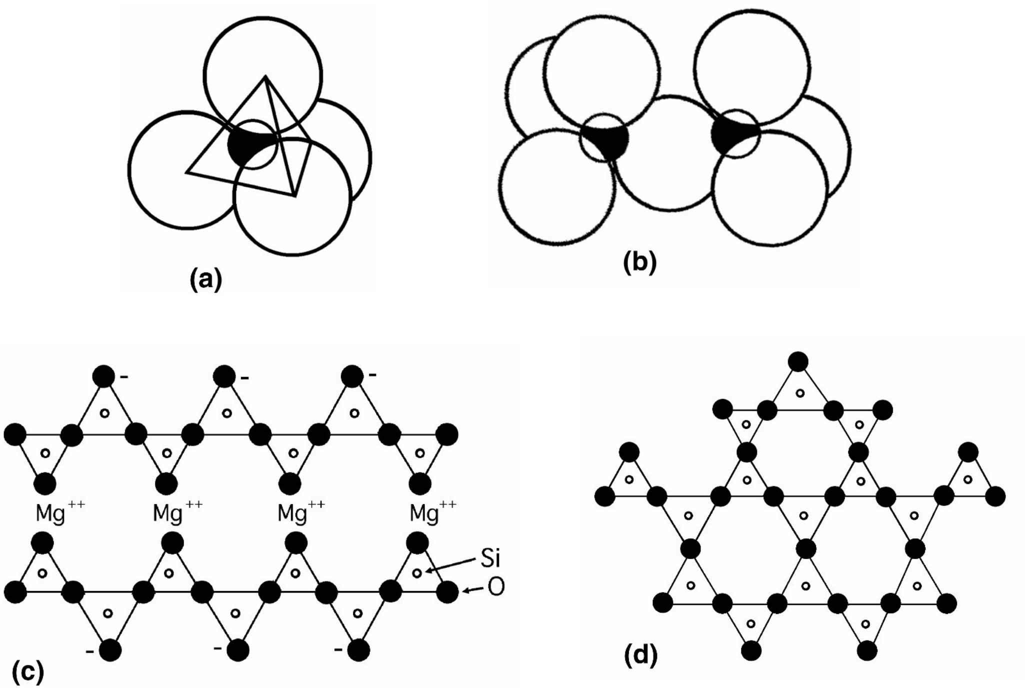

Figure 2.5. Silicate structures: (a) SiO_4 tetrahedron; (b) two SiO_4 tetrahedra with a bridging oxygen; (c) chain silicates with metal ion (Mg^{2+}) links; (d) a silicate sheet.

modifying chemicals such as Na_2O and CaO are added to lower T_g, as shown in Figure 2.6c, thus lowering the cost of processing the glass.

Similar to metals, two or more ceramics can be melted and solidified to make alloys (solid solutions) (see Fig. 2.7). The SiO_2 and Al_2O_3 will form an intermediate compound, *mullite* ($3Al_2O_3{\cdot}SiO_2$). The high-temperature form of pure SiO_2 is called *cristobalite* and the low temperature form *tridymite*. Other oxides can be solid solutionized to obtain higher-density and more fracture-resistant ceramic compounds. The same *phase rule* can be applied to ceramic materials as those applied to metals.

Example 2.1

Calculate the densities of diamond and NaCl.

Answer:

a. Diamond has a crystalline structure (Fig. 2.4a) in which 8 carbon atoms per unit cell exist and the unit cell volume is a^3.

Density:

$$\frac{\text{mass}}{\text{unit cell}} = \left(\frac{8 \text{ atoms}}{\text{unit cell}}\right)\left(\frac{12 \text{ g}}{\text{mole}}\right)\left(\frac{\text{mole}}{6\times 10^{23}\,\text{atoms}}\right) = 1.59\times 10^{-22}\,\text{g/unit cell},$$

$$\frac{\text{volume}}{\text{unit cell}} = a^3 = \left(\frac{4 \text{ atoms} \times 0.154 \text{ nm}}{\sqrt{3}}\right)^3 = 4.5 \times 10^{-23}\,\text{cm}^3/\text{unit cell},$$

$$\text{Density} = \frac{1.59 \times 10^{-22}\,\text{g/unit cell}}{4.5 \times 10^{-23}\,\text{cm}^3/\text{unit cell}} = \underline{3.53\ \text{g/cm}^3},$$

which is close to the reported value of 3.51 g/cm^3 (*Physics and Chemistry Handbook*, 49th ed, Cleveland: CRC Press, 1968).

b. The crystal structure of NaCl is fcc (face centered cubic), therefore the density can be calculated,

$$\frac{\text{mass}}{\text{unit cell}} = \left(\frac{4(\text{Na}^+ + \text{Cl}^-)}{\text{unit cell}}\right)\left(\frac{58.44\text{ g}}{\text{mole}}\right)\left(\frac{\text{mole}}{6 \times 10^{23}(\text{Na}^+ + \text{Cl}^-)}\right) = 3.896 \times 10^{-22}\ \text{g/unit cell},$$

$$\frac{\text{volume}}{\text{unit cell}} = a^3 = \left[2(r_{\text{Na}^+} + r_{\text{Cl}^-})\right]^3 = \left[2(0.097 + 0.181)\text{ nm}\right]^3 / \text{unit cell}$$

$$= 1.72 \times 10^{-22}\ \text{cm}^3/\text{unit cell},$$

$$\text{Density} = \frac{3.896 \times 10^{-22}\,\text{g/unit cell}}{1.72 \times 10^{-23}\,\text{cm}^3/\text{unit cell}} = \underline{2.265\ \text{g/cm}^3},$$

which is close to the reported value of 2.165 g/cc; T_m = 801°C, T_b = 1413°C, m.w. = 58.44 amu (from *Physics and Chemistry Handbook*).

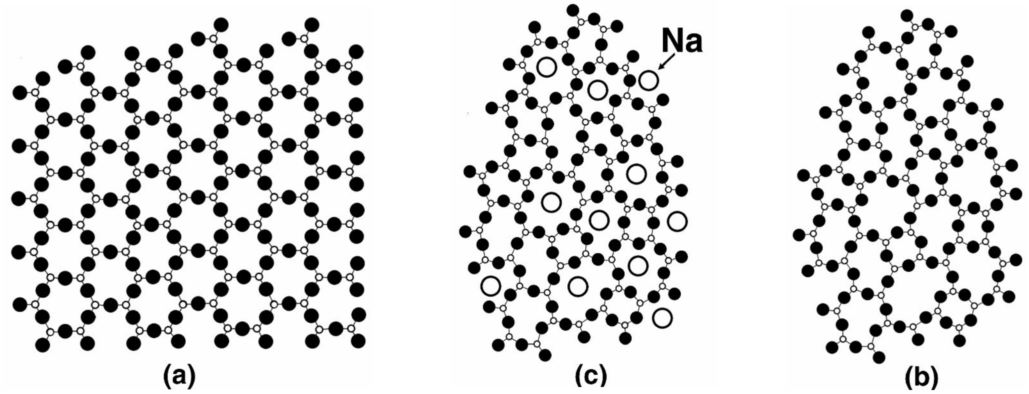

Figure 2.6. Glass structures: (a) coordinated network structure of crystalline silica; (b) uncoordinated random network structure of amorphous glass of silica; (c) network-modified glass structure lowering its T_g considerably.

Example 2.2

Give descriptions or steps to make 99.99% pure alumina from 99% pure alumina by using the phase diagram in Figure 2.7.

Answer:

Purification of any materials can be accomplished by using the phase separation phenomenon since each phase will contain a different amount of the original composition. The following steps can therefore yield a purer material:

1. Heat the 99% alumina above the liquidus line (>2,050°C)
2. Cool below the liquidus line
3. Throw away the liquid
4. Reheat the remaining solid above the liquidus line
5. Cool below the liquidus line
6. Throw away the liquid

These steps can be repeated until the desirable purity is attained. The material is then cooled to room temperature.

Similar results can be obtained if one uses a "zone melting and solidification" process in which cylindrical solids are melted and solidified in one direction slowly (to achieve thermal equilibrium). Finally, the "impure liquid" will be accumulated. The process can be repeated as many times as is necessary to reach the desired purity.

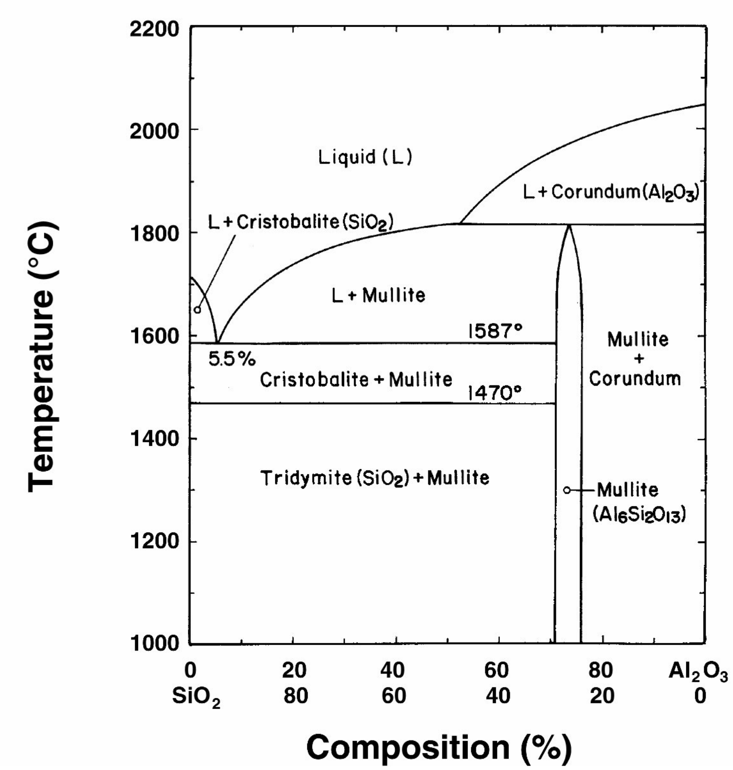

Figure 2.7. Phase diagram of SiO_2–Al_2O_3. Modified with permission from [1]. Copyright © 1976, Wiley.

2.2. CHARACTERIZATION OF MICROSTRUCTURE

The physical properties of ceramics depend on their microstructure, which can be characterized in terms of the number and types of phases present, the relative amount of each, and the size, shape, and orientation of each phase. Microstructures can usually be studied by thin sectioning (15–30 μm) on a diamond or silicon carbide-dressed wafer saw and polishing by a graded series of sandpaper. The final polishing involves using alumina or diamond paste on a wheel. The thin sections can be observed under a plain or polarized light microscope. A reflected light microscope can be used if the specimen is mounted on a polymer resin and only one side is polished. Optical microscopy can magnify an object up to 1,500 times due to the large wavelength of light ($\lambda \sim 10^{-6}$ m), but scanning and transmission electron microscopy (SEM and TEM) can theoretically magnify an object more than 1,000,000 times ($\lambda \sim 10^{-12}$ m). In addition, elemental analysis can be made with an SEM electron microprobe and electron diffraction can be undertaken using TEM, which give a better understanding of microstructure.

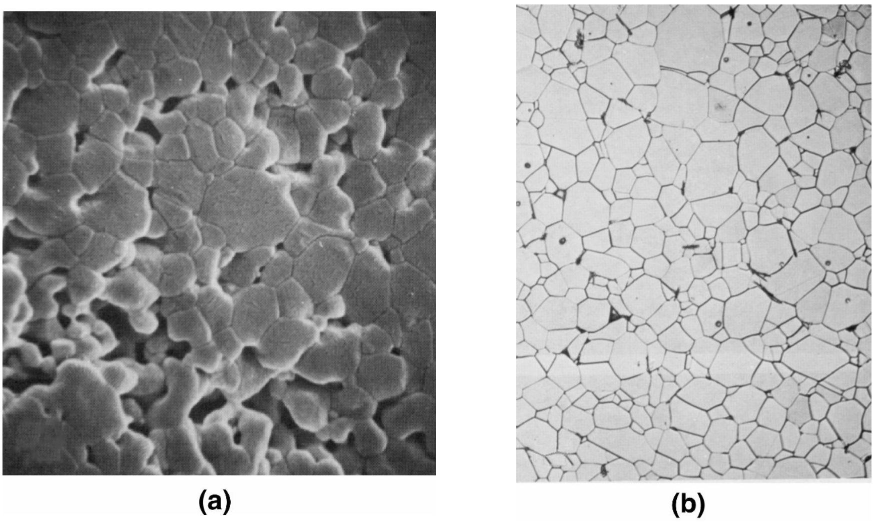
(a) (b)

Figure 2.8. SEM (a) and optical microscopic pictures of Lucalox® alumina. Note the large pores in the SEM image (5,000×) and the very small pores in optical microscopic picture (500×). Reprinted with permission from [1]. Copyright © 1976, Wiley.

The most important property of brittle materials such as ceramics and glasses is their *porosity*. Porosity has a tremendous influence on the physical properties of brittle materials since it greatly increases and intensifies stress. In addition, it is difficult to avoid formation of pores during processing of materials. The nonyielding nature of brittle materials is the main reason for the increased stress. The microstructure of polycrystalline alumina is shown in Figure 2.8.

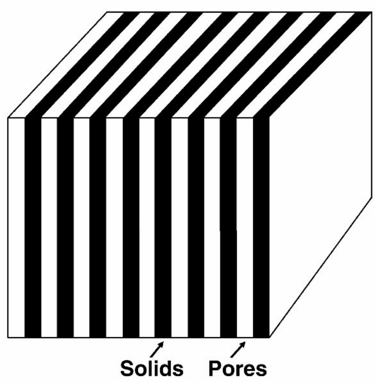

Figure 2.9. Representation of two phase materials in slabs. Reprinted with permission from [1]. Copyright © 1976, Wiley.

If we idealize the pores, as shown in Figure 2.9, where there is a series of pores and solid slabs, then electrical or thermal conductivity can be expressed in the parallel direction according to the Voigt model as

$$K_t = v_s K_s + v_p K_p \, , \tag{2.2}$$

and in series according to the Reuss model as

$$\frac{1}{K_1} = \frac{v_s}{K_s} + \frac{v_p}{v_p} \, . \tag{2.3}$$

Equations (2.2) and (2.3) are plotted in Figure 2.10.

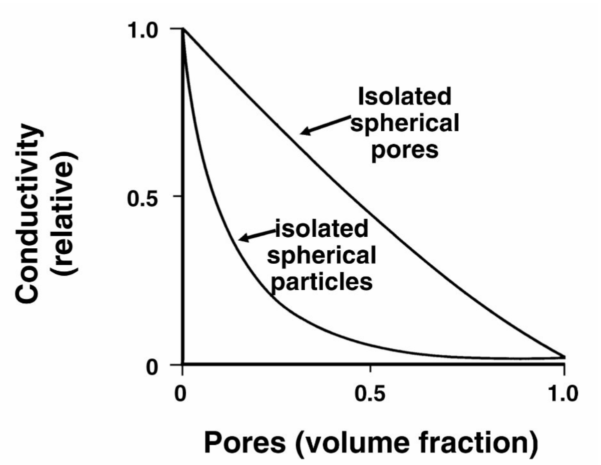

Figure 2.10. Thermal conductivity of Voigt and Reuss models, representing an isolated spherical pore and a matrix, respectively. Reprinted with permission from [1]. Copyright © 1976, Wiley.

The strength of ceramics and other materials — e.g., some ductile materials such as metals and some polymers like polymethylmethacrylate (PMMA) — depends on porosity as follows:

$$\sigma = \sigma_0 e^{-np}, \tag{2.4}$$

where σ_0 is the pore free strength, p is the volume fraction of porosity, and n is an integer (n = 4~7). Figure 2.11 depicts strength versus porosity plotted for two different materials: plaster of Paris and stainless steel.

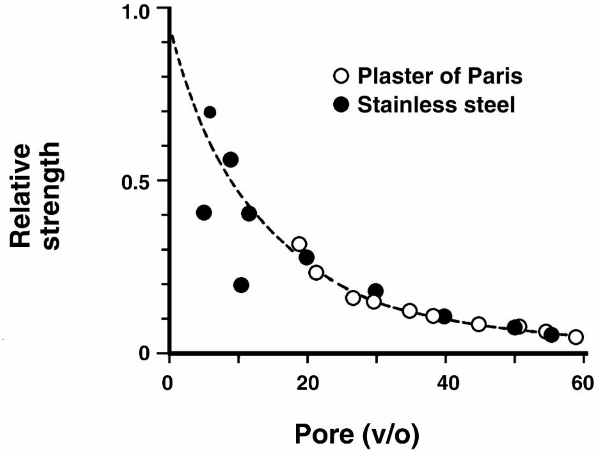

Figure 2.11. Plot of porosity versus strength of stainless steel and plaster of Paris. Reprinted with permission from [1]. Copyright © 1976, Wiley.

Pores connected to the surface are termed *open pores*; all others are *closed pores*. Total porosity includes open and closed pores, while *apparent porosity* includes only open pores. Open pores can be nearly eliminated if porosity decreases below 5%.

The fraction of porosity, f_P, is related to the density of a material as

$$f_P = \frac{\rho_t - \rho_b}{\rho_t} = 1 - \frac{\rho_b}{\rho_t}, \tag{2.5}$$

where ρ_t is the true density, and ρ_b is the bulk density, which is the total weight per unit volume, including pores.

Example 2.3

Calculate the relative conductivity of a material with 1 and 50% porosity for isolated particles using Eqs. (2.2) and (2.3).

Answer:

From Eq. (2.3), for 1% porosity, $K_t = 0.99K_s + 0.01K_p$, and assume that $K_s = 10K_p$; therefore, $\underline{K_t = 0.991K_s}$. For 50%, porosity $K_t = 0.5K_s + 0.5K_p$; thus, $\underline{K_t = 0.55K_s}$.

From Eq. (2.4), for 1% porosity, $K_t^{-1} = 0.99K_s^{-1} + 0.01K_p^{-1}$; therefore, $\underline{K_t = 0.917K_s}$. For 50% porosity, $K_t^{-1} = 0.5K_s^{-1} + 0.5K_p^{-1}$, and thus, $\underline{K_t = 0.182K_s}$.

2.3. QUANTITATIVE ANALYSIS OF SINGLE-PHASE MICROSTRUCTURE [1]

Two-dimensional structure can be studied by statistical analysis assuming a random distribution of phases, which can be expressed as

$$f_V^\alpha = f_A^\alpha = f_L^\alpha = f_P^\alpha\,, \tag{2.6}$$

where *V*, *A*, *L*, and *P* are subscripts that represent volume, area, linear, and point, respectively. In other words, Eq. (2.6) can be written as

$$V_V = A_A = L_L = P_P\,, \tag{2.7}$$

where V_V is the volume fraction, A_A is area fraction, etc.

The surface area per unit volume can be expressed as

$$S_V = \frac{4}{\pi} L_A = 2P_L\,, \tag{2.8}$$

where L_A is the length fraction of linear elements per unit area, and P_L is the number of points intersected per unit line length. One can then derive the following relationships:

$$L_V = 2P_A \tag{2.9}$$

and

$$P_V = \frac{1}{2} L_V S_V = 2P_A P_L\,. \tag{2.10}$$

The structural constituents (e.g., plates, rods, and spheres) can be represented by the mean intercept length ($\bar{L}$):

$$\bar{L} = \frac{L_L}{N_L}\,, \tag{2.11}$$

where L_L is the length fraction and N_L the number of intersections per unit length of test line. The spherical particles can be related to the mean intercept length as follows:

$$\bar{L} = \frac{4}{3} r\,; \tag{2.12}$$

for rods,

$$\bar{L} = 2r\,; \tag{2.13}$$

and for plates,

$$\bar{L} = 2t\,, \tag{2.14}$$

where r and t are the radius of the spheres and rods and the thickness of plates, respectively.

The mean free distance between particles ($\bar{l}$) can be expressed as

$$\bar{l} = \frac{1 - V_V}{N_L}\,, \tag{2.15}$$

and is related to the mean intercept length as

$$\bar{l} = \frac{\bar{L}(1 - V_V)}{N_L}\,, \tag{2.16}$$

and if the mean distance between particle centers ($\bar{d}$)can be written as

$$\bar{d} = \frac{1}{N_L}\,, \tag{2.17}$$

then

$$\bar{L} = \bar{d} = \bar{l} \tag{2.18}$$

2.4. MICROSTRUCTURE DETERMINATION [2]

When a single- or multicomponent material solidifies from a liquid, it forms either a single-crystal or polycrystalline solid that is composed of many grains. Each grain is a single crystal; if only one phase is present, all grains have the same crystal structure. However, grains may have different orientations and sizes. The size of grains can vary considerably: from submicrometers to several millimeters.

The most important grain features of a single-phase microstructure are size, shape, and orientation, as shown in Figure 2.12. All three of these factors influence the properties of solids. Grain size is often expressed as an average "diameter" within a two-dimensional section. This indicates the order of magnitude but leaves much to be desired, since (a) the grains are not spherical, and (b) a two-dimensional section does not represent the full "diameter" of each grain. Improved measurement techniques (e.g., SEM) are needed to compensate for these deficiencies.

A widely used grain size index is one published by the American Society for Testing and Materials (ASTM). An index n is related to the number of grains per square inch, N, at a linear magnification of 100× as

$$N = 2^{n-1} \tag{2.19}$$

(see Table 2.3).

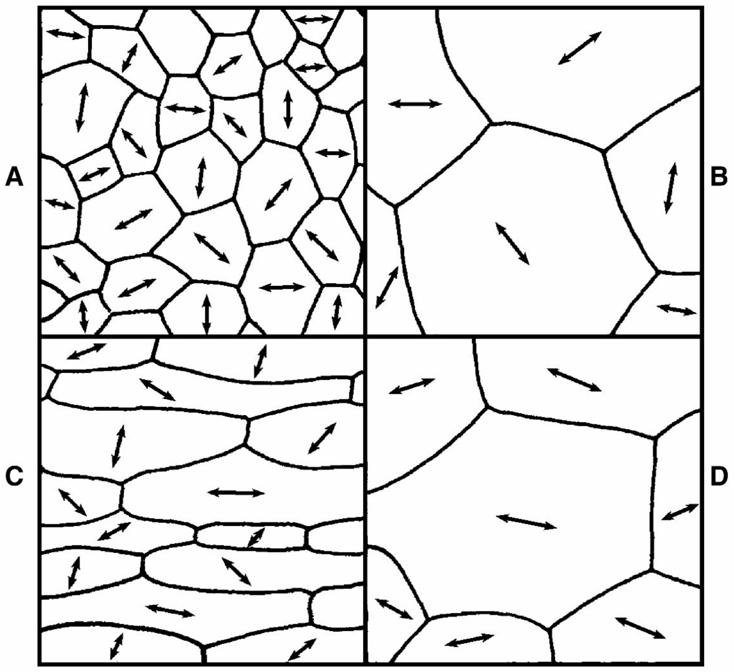

Figure 2.12. Microstructural variables of single-phase metals (from top left, clockwise: A vs. B, grain size; A vs. C, grain shape; B vs. D, preferred orientation. Reprinted with permission from [2]. Copyright © 1970, Addison-Wesley.

Table 2.3. Grain Size Ranges (ASTM) ($N = 2^{n-1}$)

Grain size number	Grain size/in^2 at 100× (linear)	
	Mean	Range
$n = 1$	$N = 1$	–
2	2	1.5–3
3	4	3–6
4	8	6–12
5	16	12–24
6	32	24–48
7	64	48–96
8	128	96–192

If shape assumptions are made, the number of grains can be calculated from the grain boundary areas derived from Eq. (2.8). By geometric analysis,

$$N_V = (S_V / F)^3 , \tag{2.20}$$

where N_V is the number of grains per unit volume, and S_V is the grain boundary area per unit volume. The shape factor, F, is 3 for assumed cubic grains, but more nearly 2.7 for the equiaxed noncubic grains commonly encountered in isotropic microstructures.

Example 2.4

Calculate the grain size of the Lucalox® shown in Figure 2.8 (500× magnification).

Answer:

The number of grains in the micrograph is about 320, and the area is 3.25” × 2.5” at 500×. Therefore, 320/8.125 in^2; hence, 39.385 grains/in^2 at 500×. At 100×, 985 grains/in^2, and from Eq. (2.19), $N = 2^{n-1}$, where N is 985. Therefore, $985 = 2^{n-1}$, and $\underline{n = 11}$. These grains are extremely small (smaller than the wavelength of light), making the material translucent, so that it can be used as a mercury lamp housing since it can also resist high temperatures.

Example 2.5

Calculate the surface area of the grains in of the previous example. Assume the grains are cubes.

Answer:

Since there are 985 grains/in^2 at 100×, the grain distribution is 9.85×10^6/in^2. Thus, the number of grains is 3.13×10^3 grains/in, which yields 3.1×10^{10} grains/in^3. The surface area of each grain is $6(1/3.13 \times 10^3)^2$/in^2; therefore, the total boundary area would be half that value, since two grains can constitute one boundary area; therefore,

$$\text{Total boundary area} = 1/2 \times 6(1/3.13 \times 10^3)^2 \text{ in}^2 \times (3.13 \times 10^3/\text{in})^3$$
$$= \underline{9.39 \times 10^3 \text{ in}^2/\text{in}^3}.$$

The large boundary area would make the material stronger, with a large amount of stored surface energy, which would result in deflection of cracks along the grain boundaries during crack propagation.

PROBLEMS

2.1. Calculate the number of atoms present per cm^3 for cubic zirconia (ZrO_2), which has a density of 6.2 g/cm^3.

2.2. Calculate the minimum radius ratios of a unit cell with CN = 6, 8.

2.3. Plot Eqs. (2.2) and (2.3).

2.4. Calculate the strength of alumina ceramics that have 1 and 5% porosity by volume. Provide your assumptions.

2.5. For 50%SiO_2 and 50%Al_2O_3 alloy, using the phase diagram in Figure 2.7:
   a. What phase(s) exist at 1600°C, 1500°C, and room temperature?
   b. What is the composition of each phase?
   c. What is the relative amount of each phase in the fractions?

2.6. Calculate the exact percentage of SiO_2 and Al_2O_3 for the mullite ($Al_6Si_2O_{13}$) from the phase diagram in Figure 2.7.

2.7. Determine the grain size of alumina from the optical micrograph of Figure 2.8.

2.8. Determine the relationship between relative strength and porosity (pore volume) in Figure 2.11.

2.9. Use this optical microstructure of Japanese hard porcelain depicted (100×) (reprinted with permission from [1], copyright © 1976, Wiley) to answer the following questions.

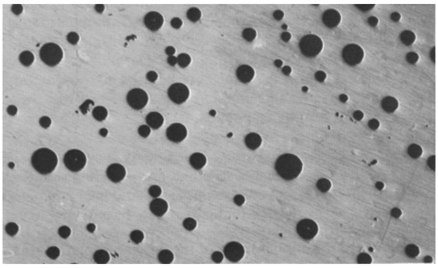

   a. Calculate the mean pore diameter.
   b. Calculate the mean distance between pores.
   c. Calculate the fraction of pores.

SYMBOLS/DEFINITIONS

Roman Letters

f: fraction of a phase.

f_P: fraction of porosity.

$\bar{d}$: mean distance between particle centers.

$\bar{l}$: mean free distance between particles .

$\bar{L}$: mean intercept length.

A: area.

L: line.

N: number of intersections.

P: point.

P_V: volume fraction of porosity.
r: radius of spherical particle.
S: surface area.
t: thickness of plate.
V: volume.

Greek Letters

κ: thermal conductivity.
ν: volume fraction
σ: strength.
ρ_t: true density.
ρ_t: bulk density.

Definitions

Apparent porosity: Ratio of the open pore space of a body to its bulk volume, expressed as

$$p = \frac{(w_s - w_f)}{V},$$

where w_s is the weight of the water-saturated specimen in (g), w_f is the weight of the original specimen (g), and v is the volume of the specimen (cm^3).

Bulk density: Ratio of the weight of an abject or material to its total volume, including the pore space.

Closed pores: Pores or small bubbles entrapped in a ceramic body that are not connected to the exterior of the body, calculated as

$$p_c = \frac{w_d}{\rho_a} - \frac{w_d}{\rho_t},$$

in which p_c is the volume of sealed or closed pores, w_d is the dry weight of the specimen, ρ_a is the apparent density, and ρ_t is the true density of the specimen.

Coordination number (CN): Number of atoms or ions touching an adjacent atom or ion.

Cristobalite: A crystalline allotropic type of silica formed by inversion of quartz at 1470°C; T_m = 1713°C. It is a major component of silica refractory, and is also used in investment casting of metals. Sometimes present in siliceous ceramic bodies.

Face-centered cubic (fcc) structure: A crystal structure found in some common elemental metals. Within the cubic unit cell atoms are located at all corner and face-centered positions.

Glass transition temperature (T_g): The temperature at which, upon cooling, a noncrystalline ceramic or glass transforms from a supercooled liquid to a rigid glass-like solid.

Hexagonal close-packed structure (hcp): A crystal structure found in some metals, where the hcp unit cell is of hexagonal geometry and is generated by stacking of close-packed planes of atoms.

Mean free distance between particles ($\bar{l}$): Average distance between particles or pores.

Mean free distance between particle centers ($\bar{d}$): Average distance between the centers of particles or pores.

Mean intercept length ($\bar{L}$): Defined as L_L/N_L, where L_L is the length fraction and N_L is the number of intersections per unit length of the test line.

Minimum radius ratio (*r*/*R*): Ratio between the radius of a smaller atom to be fitted into the space among larger atoms, based on geometric considerations.

Mullite: With m.w. 425.9; T_m = 1810°C; T_g = 1650°C. Resistant to corrosion and heat; used as a refractory in high-temperature applications and as a strength-producing ingredient in stoneware and porcelain.

Octahedral site: The void space among close-packed hard-sphere atoms or ions for which there are six nearest neighbors. An octahedron (double pyramid) is circumscribed by lines constructed from centers of adjacent spheres.

Open pores: The pores of a solid body that may be penetrated by a liquid or gaseous substance outside the external surface of the body.

Phase rule: $P + V = C + E$, where P is the number of phases at thermal equilibrium, V is the number of variances, C is the number of components, and E is the number of environmental variables (e.g., pressure, temperature).

Polymethylmethacrylate (PMMA): An acrylic linear polymer having excellent resistance to the environment, including tissues, and allows excellent transmission of light. It is used for making bone cement and contact lenses.

Reuss model: A mathematical model where the properties of a series of phases are represented by Eq. (2.3).

Simple cubic structure (CsCl): AX structure of ceramic crystals, where A is a metal and X nonmetal; forms a simple cubic structure resembling bcc.

Tetrahedron: Geometric structure where one atom or sphere is surrounded by four nearest neighbors.

Tridymite: A high-temperature polymorph of SiO_2: m.w. = 60.1; density 2.28–2.3 g/cm^3; hardness (Mohs) = 7. Used in ceramic bodies to improve thermal shock resistance and minimize crazing.

True density: The weight of a unit volume of a substance excluding its pore volume and interparticle voids, when measured under standard or specified conditions.

Voigt model: A mathematical model where the properties of a series of phases are represented by Eq. (2.2).

REFERENCES

1. Kingery WD, Bowen HK, Uhlmann DR. 1976. *Introduction to ceramics*, 2nd ed, pp. 3–20. New York: Wiley.
2. Van Vlack LH. 1970. *Materials science for engineers*. Reading, MA: Addison-Wesley.

3

CHARACTERIZATION OF CERAMICS AND GLASSES

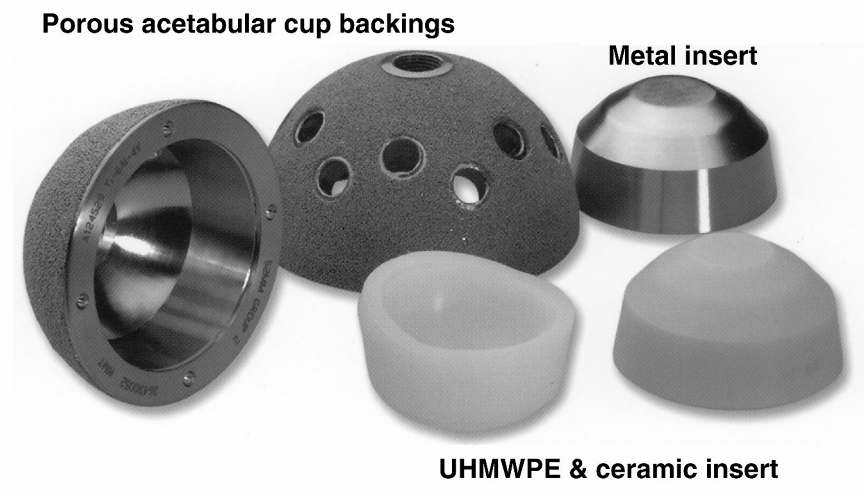
Porous acetabular cup backings
Metal insert
UHMWPE & ceramic insert

Ceramic (alumina), polymer [UHMWPE (ultrahigh-molecular-weight polyethylene)] and metal (CoCr alloy) acetabular cup inserts of hip joint prosthesis. Clinical performance of various designs and materials is largely not known due to a lack of data in the United States. In Scandinavian countries data are collected due to a mandatory reporting system. Only through their system of reports can we evaluate the clinical performance of "all" implants. Modified with permission from [10]. Copyright © 2005, Lippincott Williams & Wilkins.

The physical and chemical characterizations or properties required of ceramics and glasses for medical applications vary widely according to the particular application. Moreover, due to our limited understanding of tissue–material interactions, it is difficult — if not impossible — to transpose the values of the physicochemical properties of materials directly into in-vivo performance. Nonetheless, this should not prevent us from a thorough investigation and understanding of the characteristics of materials in vitro before using them as implants. On the contrary, the study of implant materials must begin with a basic understanding of the behavior of materials under various conditions. In this chapter we will limit our study to some basic characterizations.

Two major characteristics of brittle fracture are: (1) the fracture strength is far below the theoretical value, and (2) it is more difficult to precisely predict failure strength in ceramics than in metals and polymers.

The latter fact is the main reason why ceramics and glasses are not used extensively for implants despite their excellent tissue compatibility. However, if one uses a proper method of predicting failure such as statistical means, and design the implant properly avoiding (tensile) stress-raisers, then these materials can be utilized even for "load-bearing" implants. An excellent overview of the structural properties of biomaterials testing can be found elsewhere [19].

3.1. MECHANICAL PROPERTIES

Young's modulus is calculated from the slope of the stress and strain curves. Most brittle, isotropic, and homogeneous materials obey Hooke's law:

$$\sigma = E\varepsilon, \tag{3.1}$$

where σ is the stress force per unit cross-sectional area (F/A_0), ε is the strain, which is equal to $\Delta l/l_0$, and E is termed the *elastic modulus* or *Young's modulus*. If one uses the true cross-sectional area of the deforming specimen, then true stress can be calculated. Sometimes the stretch ratio (l/l_0) is used instead of the strain to express deformation. It can be shown further that Young's modulus is related to the *shear* (G) and *bulk* (K) moduli for an isotropic material through Poisson's ratio ($\nu = -\varepsilon_x/\varepsilon_z = -\varepsilon_x/\varepsilon_z$ for a cubic specimen):

$$G = \frac{E}{2(1+\nu)}, \tag{3.2}$$

$$K = \frac{E}{3(1-2\nu)}. \tag{3.3}$$

Table 3.1 lists the elastic modulus for various ceramics and glasses along with Poisson's ratio, density, and specific modulus, which is defined as modulus per unit density. The table demonstrates that the alumina and carbides give the highest specific modulus. Steels and other metal alloys are about 20 to 30 GPa cm^3/g, which is a lot lower than alumina or carbides.

Table 3.1. Moduli, Poisson's Ratio, Density, and Specific Modulus for Some Ceramics and Glasses

Material	Elastic modulus, E (GPa)	Shear modulus G (GPa)	Poisson's ratio, ν	Density (g/m^3)	Specific modulus (GPa·cm^3/g)
Alumina (Al_2O_3)	390	154[a]	0.27	3.9	100
Magnesia (MgO)	207	76[a]	0.36	3.58	58
Spinel ($MgAl_2O_4$)	284	–	–	3.55	80
Zirconia (ZrO_2), cubic	152	58[a]	0.32	5.56	27
Soda-lime glass	69	22	0.23	2.48	28
Borosilicate glass	62	26[a]	0.20	2.23	28
Fused silica (SiO_2)	75	32[a]	0.16	2.2	34
Silicon carbide (SiC)	414	174[a]	0.19	3.22	120
Silicon nitride (Si_3N_4)	304	123[a]	0.24	3.44	88
Titanium carbide (TiC)	462	–	–	4.92	94
Cement, portland	45	–	–	2.4	19

[a] Estimated using Eq. (3.2).

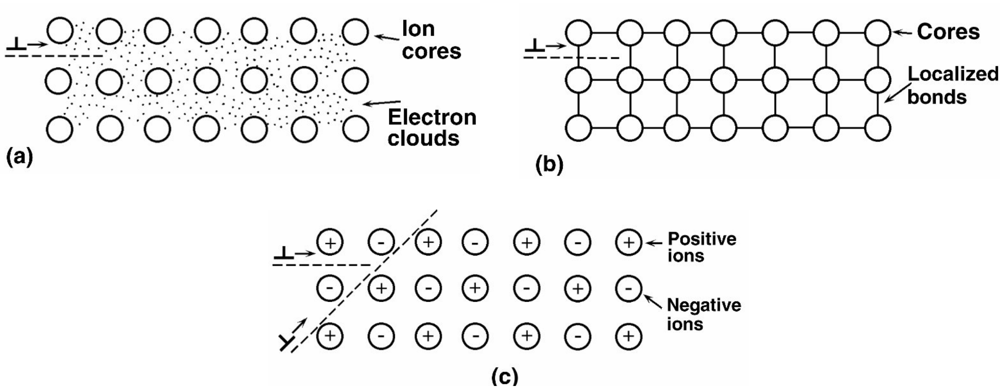

Figure 3.1. Schematic representation of the dislocation motion in (a) metallic, (b) covalent, and (c) ionic bonded structure.

The reason for their brittleness is the atomic or molecular bonding characteristics, since the ionic and covalent bonds are quite localized, unlike metallic bonds, as shown in Figure 3.1. The *dislocations* can move through the metallic bonds with the least resistance since the (re)location of positive ions can be arranged without much resistance from neighboring ions — unlike ionic bonds, where the positive ions have to be surrounded by negative ions, thus limiting the number of possible locations. In other words, the ionic bonds have fewer *slip systems* than the metallic bonds. Covalent bonds are also highly directional, and the bonds have to be broken and reformed, which limits the motion of dislocations, making materials like diamond and carbides brittle.

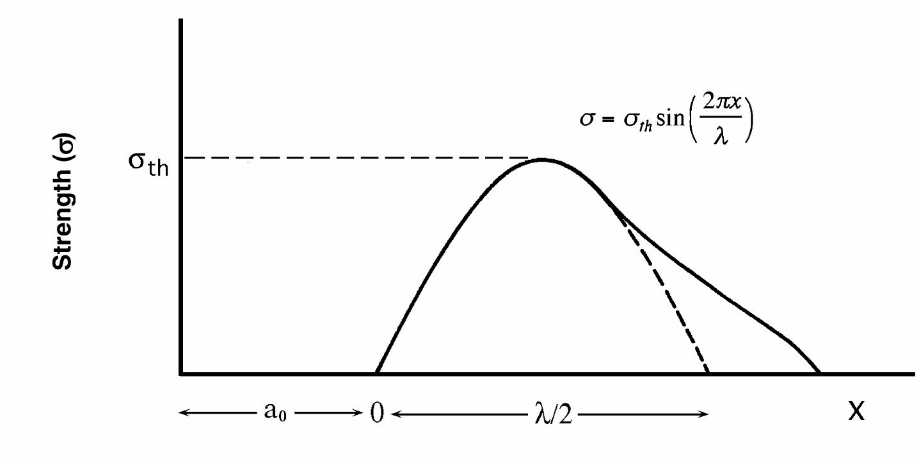

Figure 3.2. Schematic representation of force versus interatomic separation.

The theoretical strength of a material can be considered as the stress required to break it into two parts, with the separation taking place simultaneously along the cross-section. The force of cohesion between two planes of atoms varies with their separation, as depicted in Figure 3.2.

Part of the strength curve can be approximated by

$$\sigma = \sigma_{th} \sin\left(\frac{2\pi x}{\lambda}\right). \tag{3.4}$$

The work per unit area to separate the two planes of atoms is expressed as

$$\frac{\text{Work}}{\text{Area}} = \int_0^{\lambda/2} \sigma_{th} \sin\left(\frac{2\pi x}{\lambda}\right) dx, \tag{3.5}$$

and then one can obtain

$$\frac{\text{Work}}{\text{Area}} = \sigma_{th} \frac{\lambda}{\pi}. \tag{3.6}$$

Since separation of planes of atoms creates two new surfaces with surface energy γ,

$$\sigma_{th} = \frac{2\pi\gamma}{\lambda}. \tag{3.7}$$

For the initial part of the curve near equilibrium spacing a_0,

$$\sigma = E\frac{x}{a_0}, \tag{3.8}$$

where E is Young's modulus. For small values of x, from Eq. (3.4),

$$\frac{d\sigma}{dx} = \frac{2\pi}{\lambda}\sigma_{th}\cos\left(\frac{2\pi x}{\lambda}\right) \approx \frac{2\pi}{\lambda}\sigma_{th}. \tag{3.9}$$

From Eqs. (3.7) and (3.8), one can get the following relationship:

$$\sigma_{th} = \sqrt{\frac{E\gamma}{a_0}}. \tag{3.10}$$

Example 3.1

Calculate the theoretical strength of diamond assuming a_0 to be about the diameter of carbon and the surface energy about 2000 dynes/cm.

Answer:

From Table 1.1, diamond has a Young's modulus of 1050 GPa; therefore, using Eq. (3.10),

$$\sigma_{th} = \left(\frac{\left(1050 \times 10^{9}\ \frac{\mathrm{N}}{\mathrm{m}^2}\right)\left(2000 \times 10^{-3}\ \frac{\mathrm{N}}{\mathrm{m}}\right)}{0.077 \times 10^{-9}\ \mathrm{m}} \right)^{1/2}$$

$$\approx \underline{165\ \mathrm{GPa}}.$$

This value far exceeds the compressive strength given for diamond in Table 1.1, but it is close to the theoretical values given in Table 3.2. Mainly due to the flaws in the actual material, it becomes a lot weaker, as we will discuss later.

The theoretical strength of materials can be expressed in terms of Young's modulus:

$$\sigma_{th} = \frac{E}{5} \sim \frac{E}{10} \quad \text{if } \lambda \approx \alpha_0. \tag{3.11}$$

For ceramics like alumina its strength is about 1/100 and for glasses about 1/1000.

It is also interesting to note that we can express the shear modulus and shear strength in relation to tensile or compressive strength and modulus as follows:

$$\frac{\sigma_{\max}}{E} \approx 0.1 \approx \frac{\tau_{\max}}{G}, \tag{3.12}$$

For all materials $\sigma_{\max}$ is greater than $\tau_{\max}$ since it is easier to shear than cleave a plane. Also, the $\sigma_{\max}/\tau_{\max}$ ratio can be used as an indicator of whether a material will behave in a ductile or brittle fashion:

$$\text{ductile: } \frac{\sigma_{\max}}{\tau_{\max}} \geq 10, \tag{3.13}$$

and

$$\text{brittle: } \frac{\sigma_{\text{max}}}{\tau_{\text{max}}} \approx 1\,. \tag{3.14}$$

Therefore, metals such as copper will always behave in a ductile fashion, while silicon, diamond, Al_2O_3, and NaCl will always be brittle (cf. Table 3.1). Such *transition metals* as tungsten and iron, which have bcc crystal structures, often fail in a brittle manner at low temperatures or if they contain impurities. However, they fail in a ductile fashion if they are in pure crystalline form or at above transition temperatures.

Table 3.2. Theoretical Strengths of Various Materials

Material	Young's modulus, E (GPa)	σ_{max} (GPa)	σ_{max}/E	Shear modulus G (GPa)	τ_{max} (MPa)	τ_{max}/G	$\tau_{\text{max}}\sigma_{\text{max}}$	Behavior
Graphite	10	1.4	0.14	2.3	0.12	0.05	12	B
Silicon	190	32	0.17	57	13.7	0.24	2.3	B
Diamond	1200	205	0.17	505	121	0.24	1.7	B
Al_2O_3	460	46	0.10	147	17	0.12	2.7	B
NaCl	44	4.3	0.10	24	2.8	0.12	1.5	B
Silver	120	24	0.20	20	0.8	0.04	30	D
Gold	190	40	0.21	31	1.2	0.04	36	D
Copper	190	40	0.21	31	1.2	0.04	33	D
Tungsten	400	86	0.22	150	16.5	0.11	5.5	B/D
Iron	210	46	0.22	60	6.6	0.11	7.0	B/D
Silica(glass)	75	16	0.21	–	–	–	–	B
Polyethylene	240 (theor.)	33	0.14	–	–	–	–	D

B = Brittle, D = Ductile, B/D = Transitional.

Reprinted with permission from [7]. Copyright © 1977, Longmans.

Some materials can be made to approach their theoretical strengths; for example, extremely fine glass fibers freshly drawn from the melt. However, if the fibers are exposed to the atmosphere even for a short period of time, their strength decreases greatly. This indicates that fiber strength is highly dependent on surface condition. Metal whiskers show an increase in strength with a decrease in diameter, indicating that a decreased number of dislocations in smaller-diameter whiskers results in greater strength. These experimental results indicate that the difference between theoretical and observed strength is due to structural irregularities and surface conditions.

Griffith, Orowan, and Irwin approached the strength of brittle materials in *tension* based on earlier assumptions by Griffith [6];

1. Stress is concentrated around the crack tip, and
2. Crack initiation is made by the sequential separation of surfaces.

For an elliptic crack with length 2c inside a thin plate with unit thickness, the energy to fracture becomes the energy to create two new surfaces:

$$\frac{d}{dc}\left(\frac{\pi c^2\sigma^2}{E}\right)=\frac{d}{dc}\left(4\gamma c\right). \tag{3.15}$$

Therefore,

$$\sigma_f=\left(\frac{2E\gamma}{\pi c}\right)^{1/2}\approx\left(\frac{E\gamma}{c}\right)^{1/2}. \tag{3.16}$$

It is noted that one has to double the energy under the stress–strain curve for brittle materials to come to a conclusion similar to that of Eq. (3.10).

Inglis [8] showed that elliptic flaws produce maximum stress in the vicinity of the crack tip (σ_m):

$$\sigma_m=2\sigma\left(\frac{c}{\rho}\right)^{1/2}, \tag{3.17}$$

where ρ is the crack tip radius. The crack will propagate if

$$\sigma_m\geq\sigma_{th}. \tag{3.18}$$

Orowan [16] noted that the minimum radius of curvature at the crack tip is of the same order of magnitude as the *interatomic spacing*, a_0. If ρ in Eq. (3.17) can be replaced by a_0, then

$$\sigma_f=\left(\frac{E\gamma}{4c}\right)^{1/2}. \tag{3.19}$$

For partially ductile materials,

$$\sigma_f=\left(\frac{E(\gamma+\gamma_p)}{c}\right)^{1/2}, \tag{3.20}$$

where γ_p is the *plastic work* to fracture per unit area. Note also that $\gamma_p >> \gamma$.

Toughness is defined as the amount of energy required to produce failure and can be expressed in terms of stress and strain:

$$\text{Toughness (energy)}=\int_{\varepsilon_0}^{\varepsilon_f}\sigma d\varepsilon=\int_{l_0}^{l_f}\sigma\frac{dl}{l}. \tag{3.21}$$

Expressed another way, toughness is the summation of (true) stress times the distance over which it acts (strain), taken in small increments. The area under the stress–strain curve provides a simple method for estimating toughness.

The fracture toughness of ceramics is usually low and, due to brittleness (no yielding), the largest-sized microcrack determines its strength. If the size of the crack is *2c*, then from Eq. (3.16),

$$\sigma_f = \frac{K_{IC}}{\sqrt{\pi c}}, \tag{3.22}$$

where K_{IC} is the crack initiation stress. Table 3.3 gives K_{IC} and the yield strength of various materials for comparison. High-performance ceramics like alumina have high K_{IC} values, far smaller than metal alloys. Glasses and other structural ceramics have much lower values. The compressive strength of ceramics and glasses are much higher (15 times) than the tensile strength due to the fact that the cracks in compression propagate solidly and twist out of their original location to propagate parallel to the compression axis.

Table 3.3. Fracture Toughness and Yield Strength of Various Materials

Materials	K_{IC} (MPa $\sqrt{m}$)	Yield strength (MPa)
Ti6Al4V	44–66	910
Alumina	3–5	NA
Soda-lime glass	0.7–0.8	NA
Concrete	0.2–1.4	NA
PMMA[a]	2.2	62.1

[a] Polymethylmethacrylate polymer. Fracture toughness values are obtained in a plain strain condition.
NA= not applicable.
Reprinted with permission from [4]. Copyright © 1994, Wiley.

Example 3.2

Estimate the fracture strength of an alumina, which has an 11-μm crack length. The K_{IC} is about $4\ \text{MPa}\sqrt{\text{m}}$.

Answer:

Using Equation (3.22),

$$\sigma_f = \frac{K_{IC}}{\sqrt{\pi c}}$$

$$= 4\ \text{MPa} \cdot \text{m}^{1/2} (\pi \times 11\ \mu\text{m})^{-1/2}$$

$$= \underline{680\ \text{MPa}}.$$

This estimate is much higher than the value given in Table 1.1.

3.2. STRENGTHENING OF CERAMICS AND GLASSES

The lack of slip systems in ceramics and glasses prevents dislocation motion and generation, resulting in a material that is hard and brittle, as mentioned earlier. This is partly because of the ionic nature of the bonding of oxides and covalent bonding of Si and C (Fig. 2.4). Slip can occur only in diagonal directions (not horizontally) due to repulsion of like-charged ions, as shown in Figure 3.1. In glasses brittleness is caused by a *lack of plastic deformation* exhibited by the three-dimensional network structure (Fig. 2.6).

Some ionic crystals will behave differently, however, if tested under certain conditions. For example, NaCl crystals in water are ductile, but this quality is lost if testing is done in air for a prolonged time. It is believed that variations in moisture content cause precipitates to form on the crystal surface by local dissolution and subsequent reprecipitation, which originates fracture. The strength of brittle materials is lower in tension than in compression, as mentioned earlier. These experimental observations led Griffith and others to investigate the relationship between strength and microflaws in brittle materials, as studied in the previous section.

Elimination of Griffith flaws is one method used to increase the strength of brittle materials. *Chemical etching* can round the crack tips, thus reducing the stress concentration. Hydrofluoric (HF) acid is frequently used because it dissolves silicates rapidly. *Fire polishing* removes surface flaws by heating the material just above its glass transition temperature (T_g) so that it can flow to close cracks or smooth crack tips [6].

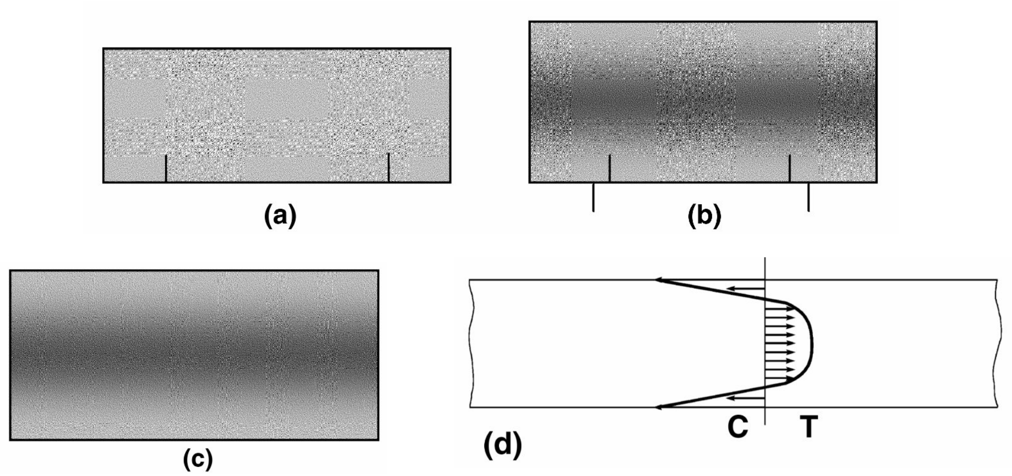

Figure 3.3. Development of surface compression in tempered glass: (a) hot state; (b) quenched state, surface cooled; (c) cooled state; (d) cross-sectional view of the stress distribution; arrows in (d) indicate compression (←) and tension (→). Modified with permission from [22]. Copyright 1970, Addison-Wesley.

A ceramic material's ability to withstand tensile stress can be improved by making surface layers compressive relative to the interior, since applied force should overcome compressive force before tensile force can take over. Surface compression can be introduced by *ion exchange*, *quenching*, and *surface crystallization*. The development of surface compression by thermal quenching is shown in Figure 3.3. Ion exchange can be accomplished by diffusion or electrical-migration techniques. Principally, larger ions are exchanged with smaller ions (e.g., K^+ for Na^+), making the surface compressive due to lattice straining. Use of electric fields can be advantageous since foreign ions can be introduced at the surface at a lower temperature than is possible with the diffusion process alone.

Glass-ceramics can be surface crystallized by changing the molar or specific volume of surface layers. Similar results can be achieved by rapid cooling (quenching), as the interior of the glass or ceramic tends to shrink but is restrained by the rigid surface layer cooled by quenching, rendering the surface in compression and the interior in tension.

Table 3.4. Various Strengthening Methods for Brittle Materials

Treatment	Maximum strengthening	Examples
Chemical etching	30×	Soda lime, borosilicate, silica glass
Fire-polishing	200×	Fused silica
Ion exchange	20×	Sodium aluminosilicate glass with potassium nitrate
Quenching	6×	Alkali silicate glass
Ion exchange and surface crystallization	22×	Lithium–sodium–aluminosilicate glass
Surface crystallization	17×	Lithium–aluminosilicate glass
Second-phase particles	2×	Borosilicate glass with alumina

Reprinted with permission from [5]. Copyright © 1973, Wiley.

Addition of a *second crystalline phase* can increase the strength by forming second-phase particles, which can pin the propagating cracks. Table 3.4 gives a summary of the strengthening of brittle materials, and Table 3.5 compares the effects of strengthening on ceramics and glasses.

Ceramics and glasses are used effectively for making composite materials due to their high modulus and strength. Matrix materials are usually more ductile materials, such as polymers and metals. The properties of fibers and wires used to make composites are given in Table 3.6. See Chapter 12 for more details on composites.

3.3. WEIBULL STATISTICS OF BRITTLE FAILURE [1]

As mentioned earlier, the strength of brittle materials depends on the size of flaws distributed throughout the material. According to Griffith's theory of fracture in tension, the largest flaw or crack will contribute the most to the failure of a material. Strength also depends on the volume of a specimen since flaw size is limited to the size of the specimen's cross-section. Therefore, the smaller the specimen (e.g., fibers), the higher the fracture strength. A statistical distribution is used to account for the test results and

Table 3.5. Properties of Various Glasses and Alumina

Material and conditions	Particle or fiber diameter (μm)	Density (g/cm^3)	Young's modulus E (GPa)	Tensile strength, σ_f (MPa)	$\sigma_f/\sigma_{\max}$
Bulk soda glass, off the shelf	$>10^4$	2.5	70	7~140	1/1000
Ordinary-quality glass fiber (E glass)	10	2.5	70	1500~2000	1/10
E rods, etched in HF to remove all surface defects	10	2.5	70	2800	1/6
E glass fiber prepared under exacting conditions	5–50	2.5	70	3700	1/4
S glass fiber	10	2.6	84	4550	1/3
Silica fiber, tested in air	50	2.2	75	5600	1/3
SiO_2 fiber, tested in vacuum	50	2.2	75	7000	1/2
Sintered Al_2O_3 (bulk polycrystalline body)	$>10^4$	3.85–3.92	350	280	1/200
Fully dense Al_2O_3 (bulk polycrystalline body)	10^4	3.98	370	700	1/60
Polycrystalline fiber	100	3.15	400	2000	1/25
Single crystal Al_2O_3 rod, surface ground	10	3.98	370	500	1/100
Single crystal rod, Al_2O_3 flame-polished surface free of defects	10	3.98	400	5000	1/9
Whisker, Al_2O_3	10	3.98	490	7000	1/7
Whisker, Al_2O_3	1	3.98	490	21000	1/2

Reprinted with permission from [7]. Copyright © 1977, Longmans.

to predict the probability of failure under certain conditions. A Weibull [23,24] distribution can be used instead of a traditional safety factor, which cannot be accurately obtained for brittle materials. The survival probability of a Weibull distribution can be written as

$$P_S(V_0) = \exp\left[-\left(\frac{\sigma}{\sigma_0}\right)^m\right], \tag{3.23}$$

where σ_0 and m are constants; m is called the Weibull modulus, which varies between 5 and 25 for brittle materials, and can be greater than 100 for steels, indicating that steel can be characterized by a single strength value with very little variation from the mean, as shown in Figure 3.3. Equation (3.23) can be written as

$$\ln\left[\ln\left(\frac{1}{P_S(V_0)}\right)\right] = m\ln\left(\frac{\sigma}{\sigma_0}\right). \tag{3.24}$$

Table 3.6. Properties of Fibers Used for Composite Materials

Class Material	strength (GPa)	Tensile modulus (GPa)	Young's Density (g/cm^3)	T_m (ºC)
Whisker				
Graphite	20.7	675.7	2.2	3000
Al_2O_3	15.2	524.0	4.0	2050
Iron	12.4	193.1	7.8	1540
Si_3N_4	13.8	379.2	3.1	1900
SiC	20.7	689.5	3.2	2600
Boron	–	441.3	2.3	2300
Glass, ceramic, polymer, fibers				
Drawn silica	5.9	72.4	2.5	1700
Boron glass	2.4	379.2	2.3	–
High-tenacity nylon 66	0.8	4.8	1.1	265
Metal wire				
Carbon steel	3.9	206.9	7.8	1500
Molybdenum	2.1	365.4	10.3	2610
Tungsten	2.9	344.8	19.3	3380

Reprinted with permission from [12]. Copyright © 1966, Addison-Wesley.

Figure 3.4 can be replotted by using Eq. (3.24), as shown in Figure 3.5, where the curves become straight. Note that the probability of survival or failure depends on the stress level, as well as on its volume. If the survival probability of one specimen is $P_S(V_0)$, then the probability of survival of n specimens is $[P_S(V_0)]^n$. If n specimens are aggregated to give a single specimen to test, then $V = nV_0$, and the survival probability can be written as

$$P_S(V) = \left[P_S(V_0)\right]^n = \left[P_S(V_0)\right]^{V/V_0}. \tag{3.25}$$

Therefore,

$$\ln\left[P_S(V)\right] = \frac{V}{V_0}\ln\left[P_S(V_0)\right], \tag{3.26}$$

or

$$P_S(V) = \exp\left\{\frac{V}{V_0}\ln\left[P_S(V_0)\right]\right\}. \tag{3.27}$$

From Eq. (3.23),

$$\ln\left[P_S(V_0)\right] = \left(\frac{\sigma}{\sigma_0}\right). \tag{3.28}$$

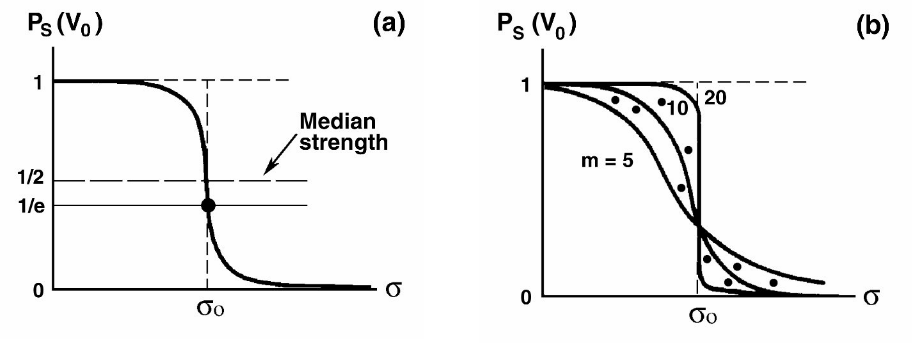

Figure 3.4. Plot of survival probability versus proof test stress; (a) Weibull distribution function; (b) dependency of the function on the modulus *m*. Reprinted with permission from [1]. Copyright © 1986, Pergamon.

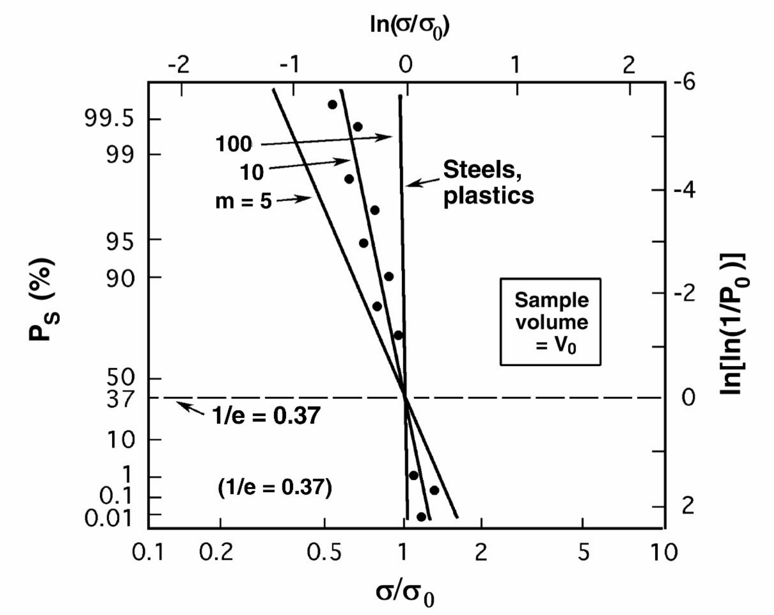

Figure 3.5. Plot of Eq. (3.24) for constant-volume specimens. Reprinted with permission from [1]. Copyright © 1986, Pergamon.

From Eqs. (3.28) and (3.27) one can obtain

$$P_S(V) = \exp\left\{-\frac{V}{V_0}\left(\frac{\sigma}{\sigma_0}\right)^m\right\}, \tag{3.29}$$

or

$$\ln\left[P_s(V)\right] = -\frac{V}{V_0}\left(\frac{\sigma}{\sigma_0}\right)^m . \tag{3.30}$$

Equation (3.30) indicates that strength depends on the level of *stress* and the *volum*e of a specimen.

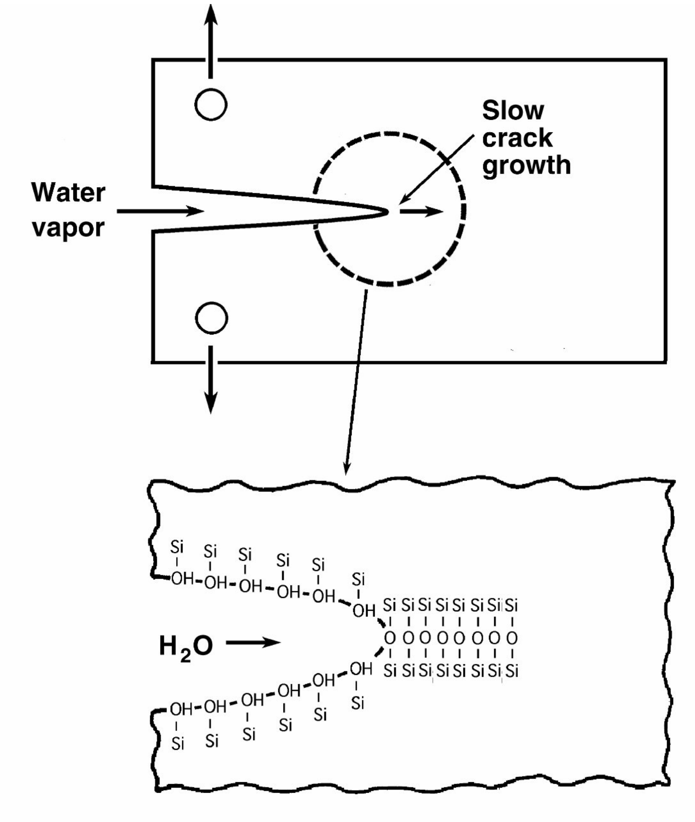

Figure 3.6. Time-dependent failure model due to slow crack growth accelerated by corrosion. Reprinted with permission from [1]. Copyright © 1986, Pergamon.

When a material is subjected to a constant or repeated load below its fracture stress, it can fail (*fatigue fracture*) after some time by slow crack growth (Fig. 3.6). The relationship among time of failure (t_f), failure stress (σ_f), and time t that a specimen endures stress σ can be written as

$$\left(\frac{\sigma}{\sigma_f}\right)^n = \frac{t_f}{t}, \tag{3.31}$$

where n is a constant (time exponent), which varies between 10 and 40 for most oxide ceramics, as given in Table 1.1. Its value can be as large as 100.

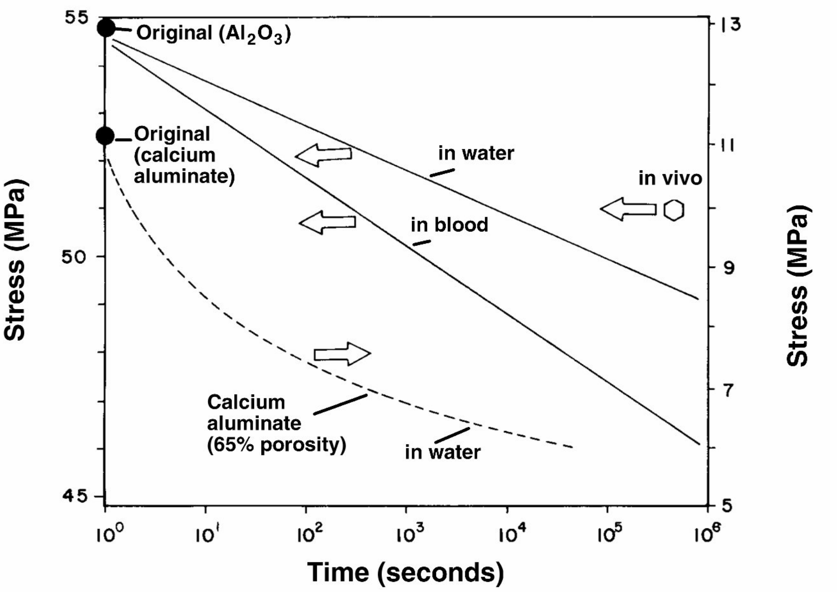

Figure 3.7. Effect of water and blood on the strength of ceramics under static loading. Reprinted with permission from [18]. Copyright © 1973, Wiley.

Fatigue can also be induced by dynamic (cyclic) *load*, and is usually plotted as stress versus log time or log cycles (N), as depicted in Figure 3.7. The time or number of cycles before failure depends on the magnitude and type of load, the test environment, and the temperature.

Fatigue tests in a simulated body environment will give a better evaluation of a material since materials placed in the body undergo loading and unloading cycles. However, it is impossible to simulate the complicated loading and unloading conditions an implant undergoes in vivo. Nevertheless, a fatigue test is useful for comparing the performance of various implants under given test conditions.

3.4. IMPACT STRENGTH, HARDNESS, FRICTION, AND WEAR PROPERTIES

Like toughness, *impact strength* is the amount of energy that can be absorbed by a material when an impact force is applied. Impact strength can be measured by subjecting a specimen to impact by a swinging pendulum. The amplitude change of the swing of the pendulum is a measure of the energy absorbed by the specimen. From this the impact strength or energy can be calculated. An impact test usually requires a large number of samples because there is a large amount of variation in the results. Ceramics and glasses have relatively low impact strengths, which vary widely.

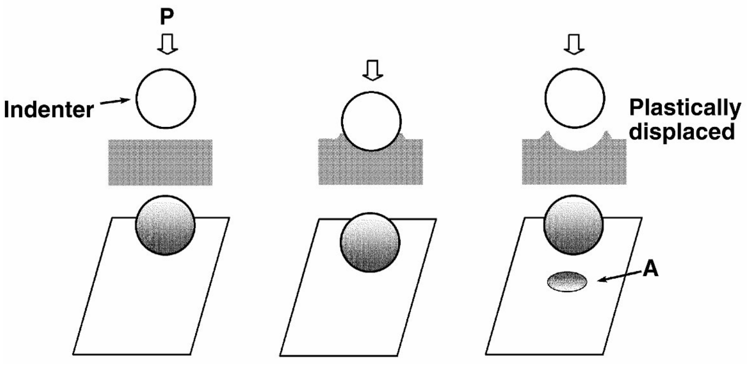

Figure 3.8. Schematic representation of a hardness test. The hardness is defined as *P*/*A* (= stress).

Hardness is a measure of plastic deformation and is defined as the force per unit area of indentation or penetration, and thus has the dimensions of stress, as schematized in Figure 3.8. The stress values obtained by the hardness test is 2.5 to 3 times higher than the tensile stress for a ductile material due to impingement of the elastic material surrounding the plastic indentation that restricts free expansion of the indented region. Frequently used in hardness tests are the Brinell hardness number, and the Vickers, Knoop test, and Rockwell tests. They differ from each other mainly in their indenter material, its configuration, and the applied load. For example, the Brinell hardness number (BHN) is obtained by using a 10-mm-in-diameter steel or tungsten carbide sphere that is pressed into the flat surface of a test specimen under a load of 300 or 3000 kg (29.42 kN) for 30 s. The Vickers test utilizes a pyramidal indenter made of diamond and a low load (1.18 kN). The values of different hardness scales for various materials are given in Figure 3.9. It is rather difficult to use a traditional hardness test for ceramics and glasses due to their nonyielding nature (no plastic deformation).

The wear properties of an implant material are important, especially for various joint replacements. Wear cannot be discussed without some understanding of the friction between two materials. When two solid materials contact, they touch only at the tips of their highest asperities. Therefore, the real contact area is much smaller than the apparent surface area. It has been found that the true area of contact increases with applied load (P) for ductile materials but not for elastic materials like rubber and diamond. Ductile materials can be pressure welded due to formation of plastic junctions, as shown in Figure 3.10. The plastic junctions are the main source of adhesive friction when two materials are sliding over each other with or without lubricating film. Resistance to the shear failure of a plastic junction results in a frictional force. Therefore, the sliding force F will be simply proportional to the shear yield strength, k, of the junctions and the contact area A:

$$F = Ak\,. \tag{3.32}$$

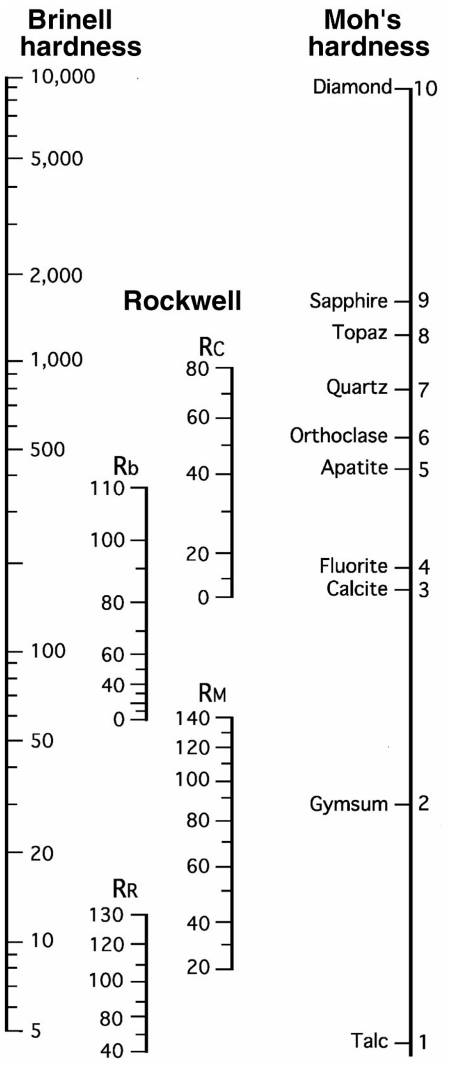
Brinell hardness
10,000
5,000
2,000
1,000
500
100
50
20
10
5
Rockwell
RC
80
60
40
20
0
Rb
110
100
80
60
40
0
RM
140
120
100
80
60
40
20
RR
130
120
100
80
40
Moh's hardness
Diamond
10
Sapphire
9
Topaz
8
Quartz
7
Orthoclase
6
Apatite
5
Fluorite
4
Calcite
3
Gymsum
2
Talc
1

Figure 3.9. Comparison of hardness scales. Reprinted with permission from [3]. Copyright © 1965, Wiley Interscience.

Since for ductile materials the area of contact increases with P,

$$P = HA\,, \tag{3.33}$$

where H is the penetration hardness or yield pressure. If we combine Eqs. (3.32) and (3.33), the coefficient of sliding friction, μ, can be obtained:

$$\mu = \frac{F}{P} = \frac{k}{H}\,. \tag{3.34}$$

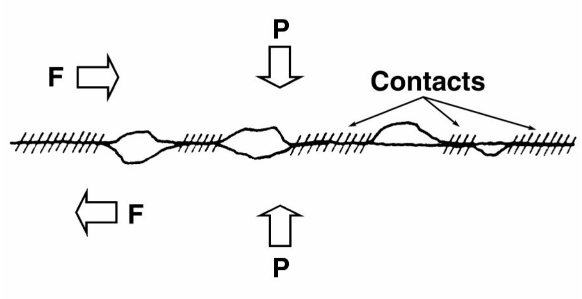

Figure 3.10. Plastic junctions are formed when ductile materials are pressed together between asperities.

This equation implies that the friction coefficient is merely a ratio of two plastic strength parameters of the weaker material and is independent of the contact area, load, and sliding speed, including surface roughness, and geometry. Wear results from removal and relocation via contact between two materials.

Wear is obviously very important for selection of implant materials, especially for joint prostheses. There are several different types of wear.

Corrosive wear is due to chemical activity on one or both of the sliding materials. The sliding action removes the product of corrosion that would protect the surface from further attack, resulting in faster corrosion. *Surface fatigue wear* is due to the formation of surface or subsurface cracks followed by breaking off of large chunks under repeated loading and sliding cycles.

Adhesive wear is a process in which particles are pulled off from one surface and adhere to the other during sliding. At a later time the particles may be loosened or lost. This kind of wear can be minimized if the surfaces are smooth and hard particles are kept off the sliding surfaces (a small number of hard particles also come off from the hard surfaces). This type of wear is the most important process in implant materials and can be analyzed more easily than any other type of wear mentioned previously.

The volume of wear, ΔV, is proportional to the applied load, P, across the two surfaces, and to the sliding distances, Δl, and is inversely proportional to the hardness of the softer material, H; therefore,

$$\frac{\Delta V}{\Delta l} = \frac{KP}{3H}, \tag{3.35}$$

where K is the *wear constant.* Table 3.7 gives some wear constants for various sliding combinations.

When *lubrication* is present between two contacting surfaces, the friction and wear properties change drastically. In most implant applications there is some type of lubricant present, so it is important to understand the lubrication process. Generally, there are two types of lubrication. *Fluid lubrication* can be achieved by a film of some

Table 3.7. Wear Constant of Various Sliding Combinations

Combination	K ($\times 10^{-3}$) of first material[a]
Zinc on zinc	160
Copper on copper	32
Stainless steel on stainless steel	21
Copper on low-carbon steel	1.5
Low-carbon steel on copper	0.5
Bakelite on bakelite	0.02

[a] $K = (\Delta V/\Delta T)(P/[3H])$.

Reprinted with permission from [12]. Copyright © 1966, Addison-Wesley, Reading, Mass (1966).

liquid or gas thick enough to completely separate two solid surfaces. This type of lubrication is mainly dependent on the properties of the lubricating fluids and is achieved more easily at high sliding surface speed. *Boundary lubrication* is achieved when a very thin film of lubricant or a softer material is introduced between two harder materials. The lubricant can reduce the direct contact of two sliding surfaces drastically, thus reducing friction and wear. This type of lubrication is more important for artificial joints.

3.5. THERMAL PROPERTIES (PHASE CHANGES)

The properties of a material depend on its phase. A *phase* is defined as a physically distinct region of matter with characteristic atomic (molecular) structure and properties. The phase changes with such thermodynamic variables as temperature, pressure, and composition. The various phases of a material are, in principle, separable mechanically. Basic thermodynamic principles will be applied to understand some simple phase changes occurring in ceramics and glasses.

3.5.1. Single-Component Systems: Allotropy

Changes in phase are most familiar in water, as shown in Figure 3.11. Each phase (vapor, liquid, and solid) is stable for a given pressure and temperature, that is, it is in thermodynamic equilibrium. Since two variables determine the phase, it is in *bivariant* equilibrium. Three phases exist at one point for a particular temperature (0.0075°C) and pressure (4.58 mm Hg); hence, it is called an *invariant* point. If two phases are present (ice and water at 0°C, water and steam at 100°C, both at 1 atm), the equilibrium becomes *univariant*, so that only either temperature or pressure can be varied. The lines dividing the three phases represent the univariant equilibrium states.

Some elements or compounds can exhibit two or more phases in the solid state. The process of temperature-induced phase change is called allotropic (or *polymorphic*) phase transformation. A good example is zirconia (ZrO_2), which exhibits three crystal structures (see Figure 3.12). It is noted that the monoclinic structure is least dense and increases its volume by cooling. This results in breakage (cracking); thus, partial stabilization of the cubic phase with other oxides is required (see Chapter 8).

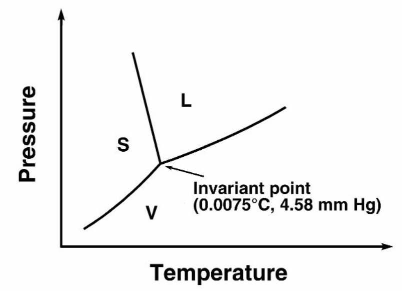
Pressure
L
S
V
Invariant point
(0.0075°C, 4.58 mm Hg)
Temperature

Figure 3.11. P–T phase diagram of water.

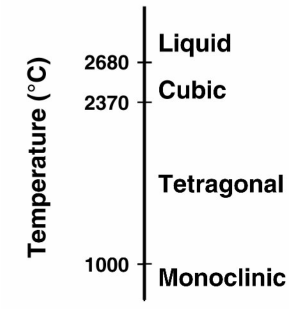
Temperature (°C)
2680
2370
1000
Liquid
Cubic
Tetragonal
Monoclinic

Figure 3.12. Phase diagram of zirconia at 1 atm.

The phase changes can be explained in terms of their temperature dependence of the free energies, as shown in Figure 3.13. The Gibbs free energy (*G*) is defined in relation to the enthalpy (*H*) and entropy (*S*) as

$$G = H - TS\,. \tag{3.36}$$

The entropy can be expressed as

$$dS = \frac{dq_{\text{rev}}}{T} = \left(\frac{C_p}{T}\right) dT\,, \tag{3.37}$$

where the heat capacity at constant pressure is

$$Cp = \left(\frac{\partial H}{\partial T}\right)_p = \left(\frac{dq}{dT}\right)_p\,. \tag{3.38}$$

Differentiating Eq. (3.36) and substituting (3.37) and (3.38) at a constant pressure yields

$$dG = -SdT\,. \tag{3.39}$$

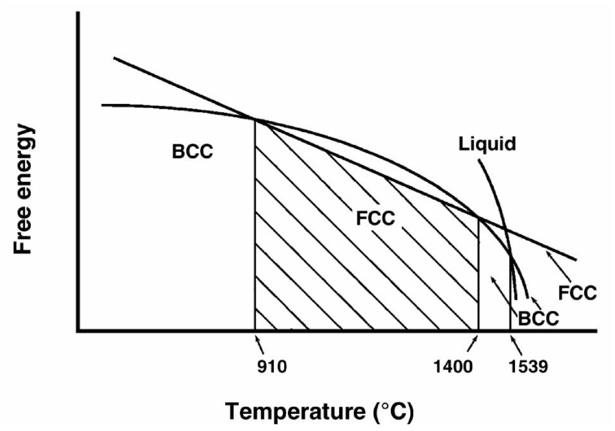

Figure 3.13. Schematic illustration of the free energy variations with temperature for iron phases.

Hence, the free energy at any temperature T can be given as

$$G = G_0 = \int_0^T S dT \, , \tag{3.40}$$

where G_0 is the free energy at 0°K. From Eq. (3.37), entropy at T (°K) is

$$S(T) = \int_0^T \left(\frac{C_p}{T} \right) dT \, . \tag{3.41}$$

Therefore, the temperature dependence of the free energy is given by

$$G = G_0 - \int_0^T \int_0^T \left(\frac{C_p}{T} \right) dT \, dT \, . \tag{3.42}$$

Equation (3.42) gives the forms of curves as shown in Figure 3.13, and the relative phases at any given temperature can be determined by the relative specific heats of the different structures.

3.5.2. Composition and Phase Stability

The same thermodynamic laws can be applied to mixing two or more components. When mixed into a single homogeneous solution between two miscible components, it is said to be an *irreversible process*. Therefore, mixing always increases the *entropy* and will be maximal near a 50–50 composition. An increase in the entropy of mixing, S_{mix}, causes a decrease in free energy, which leads to greater mixing. The entropy of mixing can be deduced from a statistical definition of entropy by considering reversible isothermal expansion of an *ideal gas*:

$$\Delta S = k \ln W \,, \tag{3.43}$$

where k is Boltzmann's constant, and W is the relative probability of two states or the increase in randomness occurring during change. Table 3.8 gives the entropy of some common substances. Generally, more rigid materials exhibit higher entropy.

Table 3.8. Entropies of Some Common Substances

Substance	Entropy @25°C × 10^{-24}J/°K per atom or molecule
Diamond	4.2
Iron	45
Platinum	69
Alumina (corundum)	85
Lead	108
Water	116
Mercury	128
Laughing gas (N_2O)	368

Reprinted with permission from [7]. Copyright © 1977, Longmans.

For a two-component system, we have to calculate the number of ways to arrange atoms A and B in a crystalline state. If we are to arrange atoms on vacant lattice sites, we can insert the first A atoms on any of the N sites, the second atom can be put on any of the remaining N – 1 sites, and so on. Since A atoms are not distinguishable from one another, the number of ways of arranging N atoms is given as follows:

$$W_{AB} = \frac{N!}{n!(N-1)!} \,, \tag{3.44}$$

where n is the number of A atoms. Therefore, the entropy of mixing becomes

$$S_{\text{mix}} = k\left[\ln \frac{N!}{n!(N-n)!}\right]. \tag{3.45}$$

Using Stirling's approximation ($\ln N! = N \ln N - N$), Eq. (3.45) can be rearranged to

$$S_{\text{mix}} = k\left[N \ln N - n \ln n - (N-n)\ln(N-n)\right]. \tag{3.46}$$

Since $C_A = n/N$ and $C_B = 1 - C_A = (N - n)/N$,

$$S_{\text{mix}} = -Nk(C_A \ln C_A + C_B \ln C_B)\,. \tag{3.47}$$

S_{mix} is positive since C_A and C_B are less than unity and are maximum at 50%, as shown in Figure 3.14.

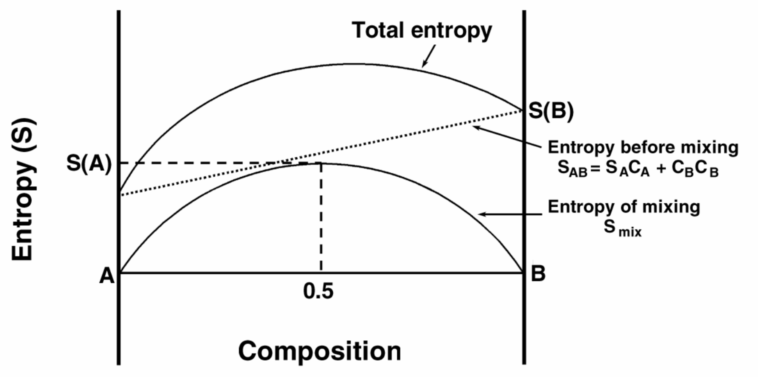
Total entropy
S(B)
Entropy before mixing
S_AB = S_A C_A + C_B C_B
Entropy of mixing
S mix
Entropy (S)
S(A)
A
B
0.5
Composition

Figure 3.14. Schematic illustration of the entropy of mixing.

Another contribution to the free energy, enthalpy or internal energy, will determine the mixing tendency. If there is an atomic size mismatch, then enthalpy will increase by increasing the stored elastic strain energy. However, in some cases this increase is offset by having the energy of the *A–B* bond be less than the energy of the *A–A* or *B–B* bonds. This results in a lower overall internal energy by mixing *A* and *B*. The reverse may be true in some cases, where there is a large distortional strain energy and a larger *A–B* bonding energy, resulting in an increase in the internal energy of mixing (Fig. 3.15). If both entropic (Fig. 3.14) and enthalpic or internal energies (Fig. 3.15) are added according to compositional variations, we will have a curve representing the free energy of mixing as shown in Figure 3.16. If E_{mix} is either zero (ideal solution) or a negative deviation from zero, the free energy of mixing is always lower than before mixing, which fosters mixing. On the other hand, if E_{mix} is positive, then

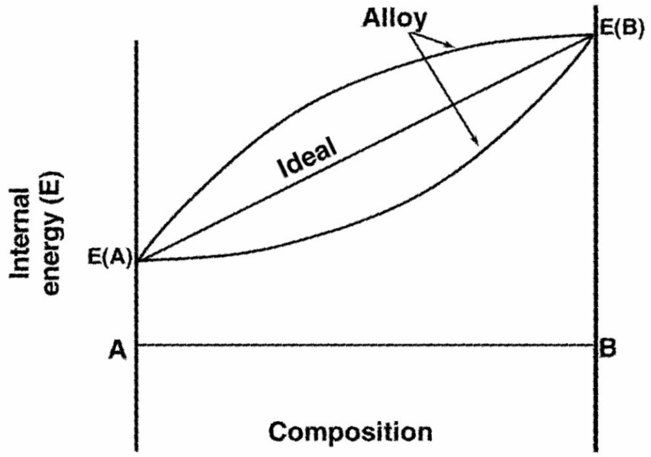
Alloy
E(B)
Ideal
Internal energy (E)
E(A)
A
B
Composition

Figure 3.15. Variation of internal energy with composition in a two-component system.

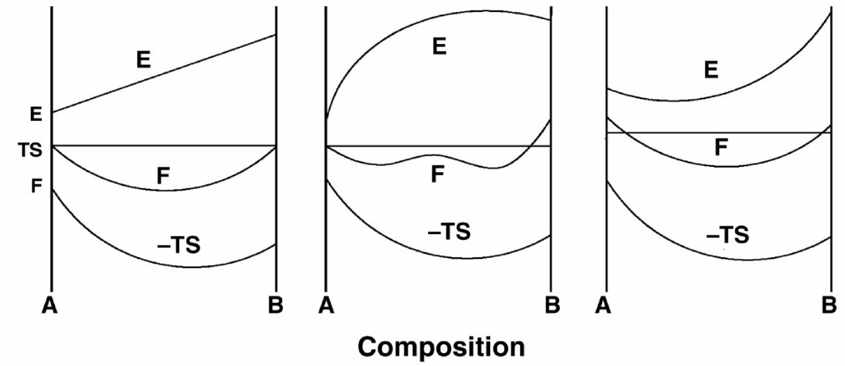

Figure 3.16. Variation of internal, entropic, and free energy with composition in a two-component system.

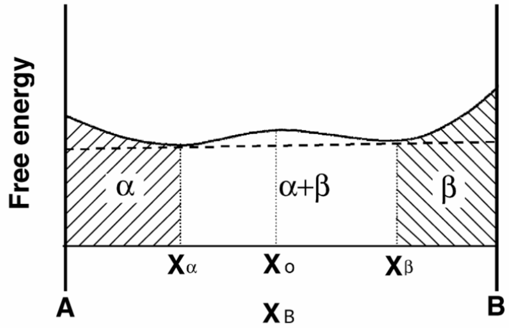

Figure 3.17. Free energy diagram for a two-component system showing phase separation into two terminal solutions: α and β.

the free energy of mixing curve will have two minima. This is because the initial rate of increase of S_{mix} is usually so great that $-TS_{mix}$ outweighs the contribution of E_{mix}; thus, the resultant free energy will usually decrease upon mixing.

To find a stable arrangement for any given composition X, we need to consider the lowest possible total free energy, as shown in Figure 3.17. Since the free energy of mixing of composition X_0 is greater than that of compositions X_α and X_β, it will split up into a mixture of α and β phases. The relative amount of α and β phases for the given composition X_0 and temperature can be calculated using a *lever rule*:

$$\frac{\alpha}{\alpha+\beta}=\frac{X_0-X_\alpha}{X_\beta-X_\alpha};\quad \frac{\beta}{\alpha+\beta}=1-\frac{\alpha}{\alpha+\beta}=\frac{X_0-X_\beta}{X_\beta-X_\alpha}. \tag{3.48}$$

The stable phase equilibrium diagram can be constructed by a similar method as for allotropic phase transformation if the free energy-versus-composition curves for the various phases are known at various temperatures, as shown in Figure 3.18. At each

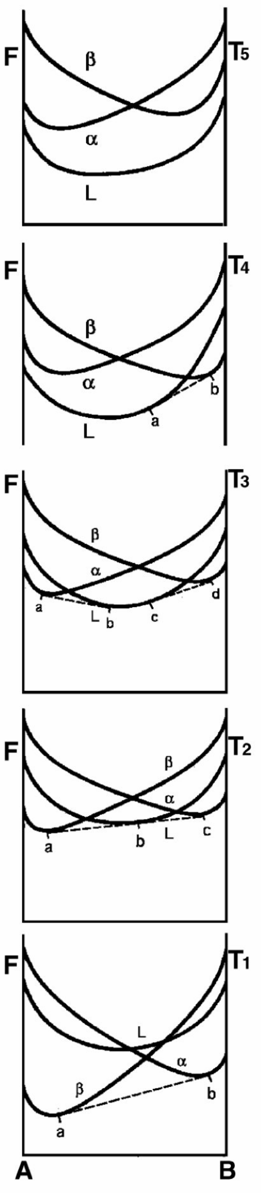

Figure 3.18. Schematic illustration of free energy and temperature versus composition.

temperature the appropriate tangents are drawn to the free energy curves, as in Figure 3.17. The points of tangency mark the constant composition of the two phases in the two-phase regions and the boundaries between the two- and single-phase regions. It is interesting to note that at T_2 a single line touches all three free energy curves at their minimum in which all three phases coexist, and a *eutectic reaction* results:

$$L \Leftrightarrow \alpha + \beta \,. \tag{3.49}$$

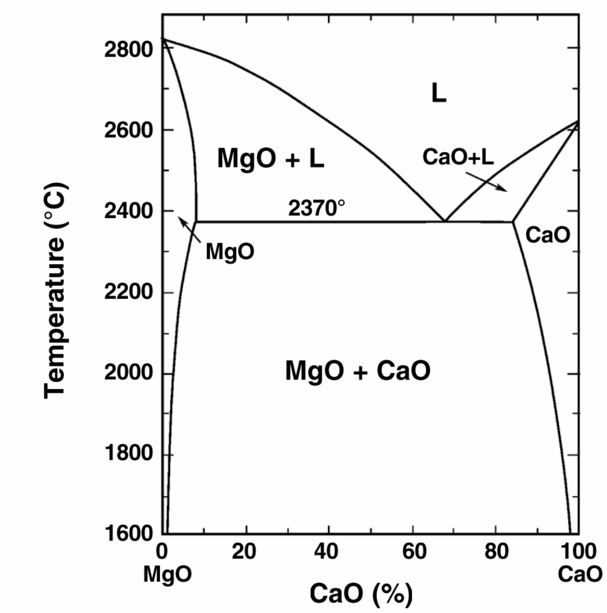

Figure 3.19. MgO–CaO phase diagram.

The eutectic reaction only occurs at a fixed temperature T_2; therefore, it is an invariant point for the binary system. For a C-component P-phase system, it will have a total of $CP + 2$ variables, the 2 variables being temperature and pressure. The number of independent variables at a constant pressure (1 atm) is given by

$$V = C - P + 1\,. \tag{3.50}$$

For a two-component system, $V = 3 - P$; therefore, the three-phase equilibria are invariant, two-phase equilibria have one variable, and one-phase equilibrium has two variables, T and C. A binary phase diagram of the MgO–CaO system is shown in Figure 3.19. It is important to remember that this phase diagram is determined under (closed) thermodynamic equilibrium states of phases for a given temperature, pressure (1 atm), and composition. It does not give information on how fast the system will approach equilibrium nor on the structural distribution of the phases present. The reaction rate depends on the mechanism of phase changes while the distribution of phases depends on the surface energy and the strain energy of the phase transformation.

3.5.3. Mechanism of Phase Changes

There are two types of phase changes in solids; one is diffusion-controlled nucleation and growth and the other diffusionless transformation. The best example of the latter is the *martensitic* phase transformation of steel, in which a bcc structure changes into a body-centered tetragonal (bct) one by shearing and distorting the lattice structure in the presence of excess carbon atoms. The majority of transformations, however, occurs by the nucleation and growth of a new phase within the old phase. Shape memory alloys (e.g., Nitonol®) also change phase by the diffusionless process. Another martensitic phase transformation can be seen in $BaTiO_3$ ceramic, a piezoelectric ceramic that can change phase by pressure or heat (above 120°C, cubic; below, tetragonal).

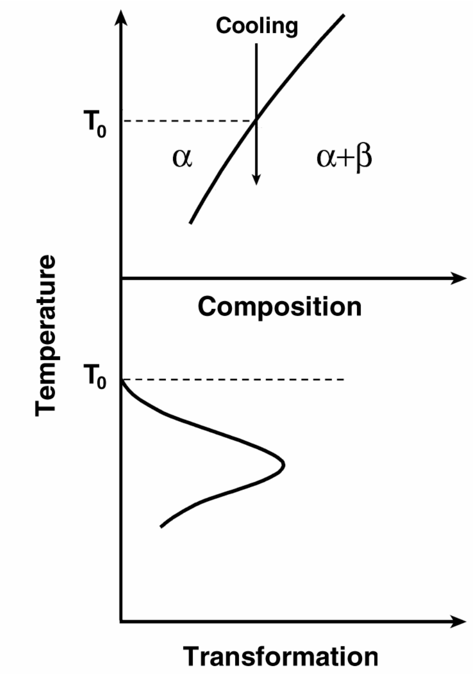

Figure 3.20. Schematic illustration of the rate of phase transformation from α to α + β.

The formation of the second (β) phase starts by nucleating small regions of the α phase, as shown in Figure 3.20. This phase diagram indicates that the new phase is thermodynamically stable in the old phase α, which is no longer in a thermodynamically favorable state due to decreased temperature. The transformation from α to β does not occur instantaneously because in order to precipitate the new crystals from the old it is necessary for atoms to diffuse over long distances. Therefore, when cooling through the equilibrium transformation temperature T_0, there will be a gradual change of phase, depending on the degree of undercooling. There will be competing forces (energy) that will control the degree of transformation for a given temperature. The total free energy change accompanying the formation of the new β phase, ΔF, is contributed by the surface and volume free energy changes:

$$\Delta F = \Delta F_s - \Delta F_v , \tag{3.51}$$

where $+\Delta F_S$ opposes the new phase formation and $-\Delta F_V$ favors it. ΔF_S and ΔF_V are also proportional to the surface area and volume of the new phase nucleating out of the old one. Therefore, if we assume the nucleus has diameter r, then

$$\Delta F = Ar^3 + Br^2 . \tag{3.52}$$

When Eq. (3.52) is plotted, as shown in Figure 3.21, there is a critical size of the nucleus, r^*, associated with nucleation energy ΔF. When the nucleus becomes larger than r^*, it will grow larger, and when smaller than r^* it will disappear.

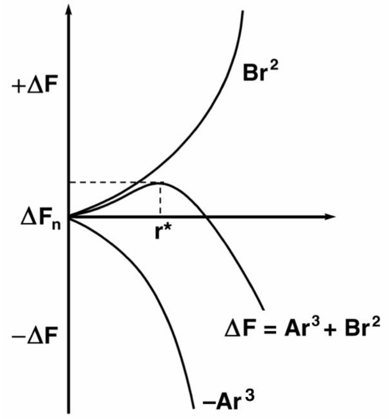

Figure 3.21. Free energy changes with the size of the new phase formed by homogeneous nucleation.

The probability of forming a stable nucleus ($r > r^*$) is given by

$$\text{probability} = \text{constant} \times e^{\left(-\frac{\Delta F_n^*}{RT}\right)} . \tag{3.53}$$

Since the nucleation requires diffusion of atoms (see the next section) to overcome the diffusion activation energy, the rate of (homogeneous) nucleation will be

$$\frac{dn}{dt} = \text{constant} \times \exp\left[-\frac{\left(\Delta F_d + \Delta F_n\right)}{kT}\right], \tag{3.54}$$

where n is the number of nuclei formed. At high temperatures near the phase transition temperature, ΔF_n is very large, and hence $\exp(-\Delta F_n/kT)$ and dn/dt are small. As the temperature decreases, diffusion of atoms to the nuclei becomes slow and ΔF_n is still large, so that dn/dt depends largely on $\exp(-\Delta F_d/kT)$. Therefore, the rate of nucleation decreases again due to slow diffusion. Figure 3.22 shows that there is a maximum rate of nucleation where the $\exp(-\Delta F_n/kT)$ and $\exp(-\Delta F_d/kT)$ curves meet.

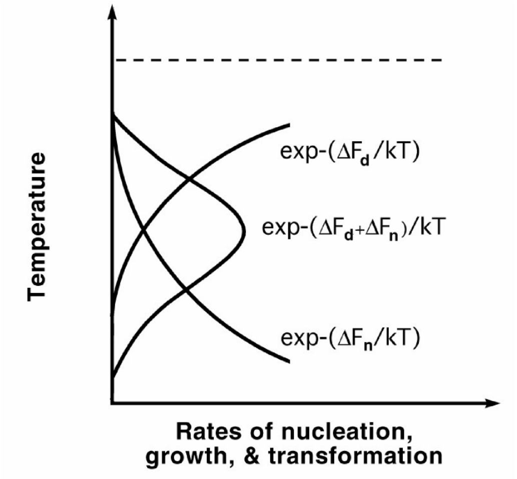

Figure 3.22. Temperature versus nucleation rate.

The main problem of applying the homogeneous nucleation theory is that it does not apply to a real material system since the free energy of nucleation for the homogeneous process is much higher than the heterogeneous route, since

$$F^* \text{ (homogeneous)} > F^* \text{ (heterogeneous)}. \tag{3.55}$$

The *thermal shock resistance* of ceramics can be understood through the *thermal expansion coefficient*, α, which is the change in length per unit length of a sample caused by change in temperature. Therefore, the maximum temperature change a material can undergo before fracture can be expressed as

$$\Delta T = \frac{\sigma_{TS}}{E\alpha}. \tag{3.56}$$

Values for ΔT are given in Table 1.1.

Example 3.3

A cubic zirconia is made by adding 8 mol% CaO. From the phase diagram given in Figure 3.15, answer the following: (a) Estimate the lowest temperature at which the cubic structure can exist. (b) What phases exist at 1250°C? (c) What are the compositions of each phase? (d) What are the relative amounts of each phase? (e) Determine the wt% of 8 mol% of CaO of the cubic zirconia.

Answer:

a. About 1800°C.
b. Tetragonal and cubic phase.
c. Tetragonal: 6 m/o CaO and 94 m/o ZrO_2,
d. Tetragonal and cubic phase.

e. Tetragonal: 6 m/o CaO and 94 m/o ZrO_2, cubic: 15 m/o CaO and 85 m/o ZrO_2:

$$\frac{T}{T+C}=\frac{15-8}{15-6}=\frac{7}{9}=\underline{0.78\ (78\%)},$$

$$C=1-0.78=\underline{0.22\ (22\%)}.$$

$$\frac{\mathrm{CaO}\times 0.08}{\mathrm{CaO}\times 0.08+\mathrm{ZrO_2}\times 0.92}=\frac{(40+16)\times 0.08}{[(40+16)\times 0.08+(91+16\times 2)\times 0.92]}=$$

$$\frac{4.48}{4.48+113.16}=\underline{0.0038\ (3.8\%)}.$$

Example 3.4

For the 50%SiO_2/50%Al_2O_3 compound and the phase diagram given in Figure 2.7:

a. What phase(s) exist at 1600ºC, 1500ºC, and room temperature?
b. What is the compositions of each phase?
c. What is the relative amount of each phase in fractions?

Answer:

a.

Temperature (ºC)	Phases present
1,600	Liquid + mullite
1,500	Cristobalite + mullite
Room	Tridymite + mullite

b. At 1,600ºC

L: 94.4% SiO_2, 5.6% Al_2O_3
M: 33% SiO_2, 67% Al_2O_3

At 1,500ºC

M: 33% SiO_2, 67% Al_2O_3
C: 100% SiO_2, 0% Al_2O_3

Room temperature

M: 33% SiO_2, 67% Al_2O_3
T: 100% SiO2

0% Al_2O_3

c. To determine relative amount of each phase one could use the “lever rule,”

At 1,600ºC:

$$\frac{L}{M+L}=\frac{C_0-C_m}{C_l-C_m}=\frac{50-67}{10-67}=\ 0.3\ \text{(30\% liquid : 70\% mullite).}$$

At 1,500ºC:

$$\frac{M}{M+L}=\frac{C_0-C_l}{C_m-C_l}=\frac{50-1}{67-1}=\ 0.742\ \text{(74.2\% mullite : 25.8\% cristoballite).}$$

At room temperature:

$$\frac{M}{M+L}=\frac{C_0-C_l}{C_m-C_l}=\frac{50-1}{67-1}=\ 0.742\ \text{(74.2\% mullite : 25.8\% cristoballite).}$$

Example 3.5

Estimate the thermal shock resistance, ΔT, for the ceramics listed in Table 1.1. Use the data for Young's modulus E, modulus of rupture σ_r, and thermal coefficient of expansion α. Compare with the results given in the same table. Assume the tensile strength can be approximated by the modulus of rupture.

Answer:

For soda lime glass:

$$\Delta T = \frac{\sigma_{t.s.}}{E\alpha} = \frac{50 \text{ MPa}}{74 \text{ GPa} \times 8.5 \times 10^{-6}} = 79.49\text{K} \ \text{(cf. 84K)}.$$

3.6. SURFACE PROPERTIES

The surface properties of a material are related to its fracture strength and its susceptibility to corrosion. In addition, tissue reaction to the ceramics and polymers is strongly related to surface properties [11]. As we have seen in Eqs. (3.10) and (3.19), the surface (free) energy and Young's modulus are intrinsic properties of a material, and, depending on crack opening or propagation direction in a crystal, the strength can be somewhat changed. The smaller the lattice spacing, the higher the strength it will exhibit. It is estimated that the maximum tensile strain (σ/E) of a perfect lattice is about 0.1; therefore, the surface energy of Eq. (3.10) can be written as

$$\gamma_0 = \frac{E\alpha}{125}. \tag{3.57}$$

In the case of alumina, Young's modulus is 380 GPa and a_0 is about 4 Å, which gives a γ_0 value of 1.2 J/m^2, which agrees well with the experimental data given in Table 3.7.

The surface free energy can be estimated by means other than the cleavage of crystals, for example, by measuring sublimation energy. An approximate relationship was given by Bruce [3]:

$$\gamma_0 = \gamma_0^* - CT, \tag{3.58}$$

where γ_0^* is the surface energy at 0°K, C is a constant, and T is absolute temperature. Equation (3.58) is applied to single crystals better since the polycrystalline ceramics have grain boundaries and pores, which tend to increase the surface energy to much higher values (up to 10 to 50 J/m^2). Therefore, if the grain size is increased, the effective surface energy decreases, as shown in Figure 3.23.

It is interesting that the influence of grain size on the tensile strength of polycrystalline ceramics can be expressed as

$$\sigma = Kd^{-1/3}, \tag{3.59}$$

where d is grain size. Figure 3.24 shows the relationship between strength and grain size.

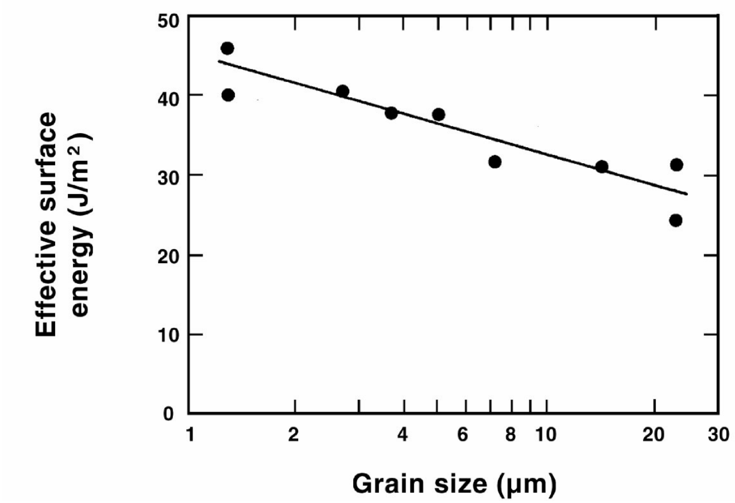

Figure 3.23. Variation of the surface energy with grain size for alumina. Reprinted with permission from [20]. Copyright © 1974, Plenum.

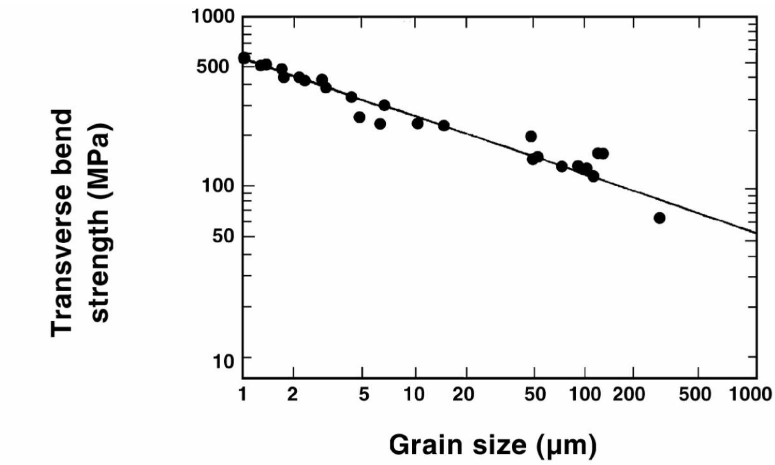

Figure 3.24. Variation of bending strength with grain size for alumina. Reprinted with permission from [21]. Copyright © 1963, The American Ceramic Society.

Surface tension is a direct result of the atomic or molecular force imbalance at two phases, as shown in Figure 3.25. A molecule at the surface is attracted toward the interior, which is surrounded by a uniform average field of neighboring molecules. Therefore, the surface has a higher free energy than the bulk and tends to contract to minimize its area. The extra surface free energy can be expressed by

$$dG = dw - \gamma dA, \tag{3.60}$$

where A is surface area, w is work, and γ is surface tension.

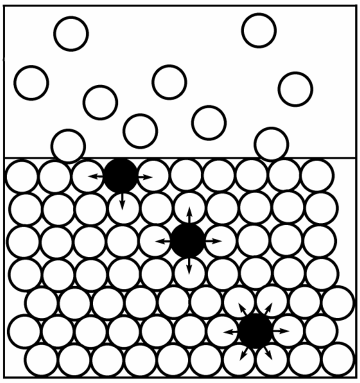

Figure 3.25. A two-dimensional representation of a liquid–vapor interface.

The surface tensions of some substances are given in Table 3.9. The conventional unit for surface tension is dynes per centimeter, and for surface energy ergs per square centimeter, but both units are exactly the same since 1 erg is equal to 1 dyne-cm. The SI (International System) unit N/m is equal to J/m^2 or 1000 dynes/cm.

Table 3.9. Surface Free Energy of Single Crystal Ceramics

Material	Maximum energy plane	Average surface free energy (γ_a)	γ_a at 20°C	γ_a at 1500°C
MgO	[100]	2600 – 0.476T	2460	1756
β-SiC	[110]	3000 – 0.546T	2840	2030
SiO_2	[110]	925 – 0.193T	870	580
TiO_2	[110]	800 – 0.167T	750	500
Al_2O_3	$\{10\bar{1}4\}$	1200 – 0.232T	1130	790
Cr_2O_3	$\{10\bar{1}4\}$	925 – 0.200T	870	570

Reprinted with permission from [3]. Copyright © 1965, Academic Press.

If a liquid is dropped on a flat solid surface, the liquid drops will spread out or form a spherical bubble, as shown in Figure 3.26. At equilibrium the surface tension among the three phases in the solid plane should be zero because the liquid is free to move until force equilibrium is established; therefore,

$$\gamma_{GS} - \gamma_{LS} - \gamma_{GL} \cos\theta = 0, \tag{3.61}$$

and hence

$$\gamma_{GS} = \gamma_{LS} + \gamma_{GL} \cos\theta. \tag{3.62}$$

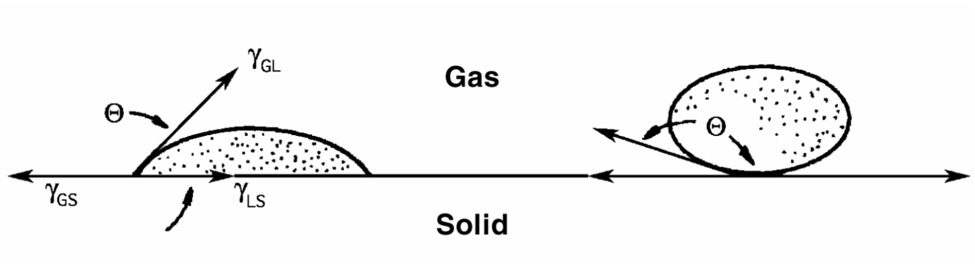

Figure 3.26. Wetting and nonwetting of a liquid on the flat surface of a solid. Note the contact angle Θ.

Table 3.10. Surface Tension of Some Substances

Substance	Temp (°C)	Surface tension Dynes/cm	N/m[a]
Isopentane	20	13.72	0.014
n-Hexane	20	18.43	0.018
Ethyl mercaptan	20	21.82	0.022
Benzene	20	28.86	0.029
Carbon tetrachloride	20	26.66	0.027
Water	20	72.75	0.073
Silver	970	800.00	0.800
Gold	1070	1000.00	1.000
Copper	1130	1100.00	1.100
NaF	1010	200.00	0.200
NaCl	1000	98.00	0.098
NaBr	1000	88.00	0.088

[a] 1 N/m = 1 J/m^2 = 1000 dynes/cm or ergs/cm^2.

Reprinted with permission from [13]. Copyright © 1962, Prentice-Hall.

The angle θ is called a contact angle, and the wetting characteristics for a given liquid and solid can be generalized as

$$\begin{gathered} \theta = 0 \quad \text{(complete wetting)}, \\ 0 < \theta < 90^\circ \quad \text{(partial wetting)}, \\ \theta > 90^\circ \quad \text{(nonwetting)}. \end{gathered} \tag{3.63}$$

Note that Eq. (3.40) only gives ratios rather than absolute values of the surface tension. However, the contact angle method can be used to measure the critical surface tension of a given liquid and a given solid, which has a value close to that of the intrinsic surface tension. A series of homologous liquids is used to measure contact angles with the solid, and these angles can be plotted in a Zisman plot (see Fig. 3.27). The surface tension values obtained by this method are in good agreement with results obtained by other methods (see Table 3.10).

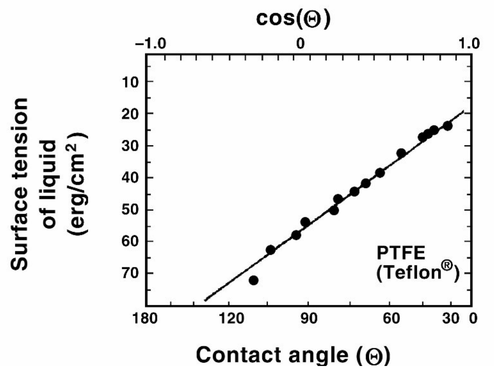

Figure 3.27. A Zisman plot of Teflon®. The contact angles of Teflon® with each of a series of pure liquids are presented. Reprinted with permission from [2]. Copyright © 1980, NIH.

PROBLEMS

3.1. A series of glass rods of circular cross-section (0.25-inch diameter) fractured at an average stress of 15,000 psi when bent. Assuming the modulus of elasticity is 10^7 psi, Poisson's ratio 0.3, and the surface tension 300 dynes/cm:

a. Calculate the average depth of the Griffith flaw.

b. It is desirable to coat this rod with another glass with a different coefficient of thermal expansion but with essentially the same physical properties in order to double the average strength of the rods. Should the new glass have a higher or lower coefficient than the parent rod?

3.2. The modulus of elasticity of polycrystalline Al_2O_3, is 6×10^7 psi, and the surface energy is assumed to be about 1000 dynes/cm. The fracture stress for sintered alumina varies from 20,000 psi for alumina of 100-μm grain size to 50,000 psi for 5-μm grain size. Show whether or not the Griffith flaw could be the grain boundary.

3.3. A set of samples of Al_2O_3 doped with Cr_2O_3 indicated that Cr_2O_3 did not affect strength but that porosity did, although there is some scatter in the data as given.

Cr_2O_3, wt%	% theoretical density	Number of bars broken	Average modulus of rupture (ksi)
1.0	97.7	24	33.4
2.0	92.4	25	29.5
5.0	94.8	19	31.0
10.0	93.6	32	27.9
20.0	87.5	32	24.0
50.0	58.1	23	9.5

a. Predict the strength of sintered Al_2O_3 with no porosity.
b. What would be your prediction concerning modulus of elasticity for these samples; that is, how would this measurement vary from sample to sample?
c. What can be said about the sphericity of pores?
d. Compare the modulus of rupture and the compressive modulus of alumina. Why are the values widely different?

3.4. A polyphase ceramic sample consists of *N* phases. The following is given: W_i = weight fraction of *i*th phase ($i = 1, 2, ..., N$), r_i = true density of the *i*th phase ($i = 1, 2, ..., N$). Prove the following equation:

$$\left[\sum W_i r_i^{-1}\right]^{-1}.$$

3.5. Estimate the thermal shock resistance, ΔT, for the ceramics listed in Table 1.1. Use the data for Young's modulus E and thermal expansion coefficient α. Compare with the results given in the same table.

3.6. From the following SiO_2–Al_2O_3 phase diagram, answer:

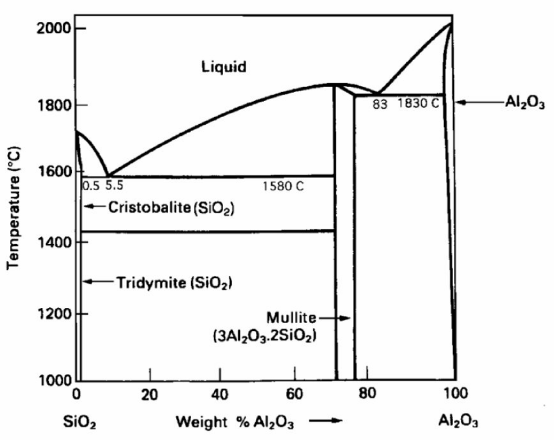

a. Give the eutectic reactions for the system. Specify the temperatures, compositions, and phases involved.
b. What phase(s) exist at 1700°C, 1500°C, and room temperature for the lower-temperature eutectic composition?
c. What are the compositions of each phase at 1500°C temperature for the lower-temperature eutectic composition?
d. Determine the exact weight% of Al_2O_3 for mullite, which has a composition of $3Al_2O_3{\cdot}2SiO_2$ [Al, 27 amu; Si, 28 amu; O,16 amu].
e. What is the relative amount of each phase in fractions at 1500°C for the lower-temperature eutectic reactions?
f. Give descriptions of the steps to make 99% pure alumina from 96% pure alumina.

3.7. From the data given for alumina ceramic, answer the following:

Properties	As-received	Glazed & quenched
Strength, σ (MPa)	140	210
Poisson's ratio (ν)	0.25	0.3
Linear expansion coefficient α ($\times 10^{-7}$/°C)	60	50
Modulus E (GPa)	200	200

a. Estimate the amount of thermal shock (ΔT) needed to fracture an as-received sample? Hint:

$$\Delta T = \frac{\varepsilon(1-\nu)}{\alpha} = \frac{\sigma(1-\nu)}{E\alpha}.$$

b. Estimate K_{IC} for the as-received sample if the largest flaw depth was 5 μm. Hint:

$$\gamma = 1 \text{ N/m}, \quad \sigma = \sqrt{\frac{2\gamma E}{\pi c}},$$

c. Calculate the crack tip radius of the as-received sample. Hint:

$$\rho = \frac{8\gamma E}{\sigma_f^2}.$$

d. Why do glazing and quenching improve the strength of alumina?

3.8. Alumina was coated with Bioglass® and measured for its static fatigue properties and plotted as given:

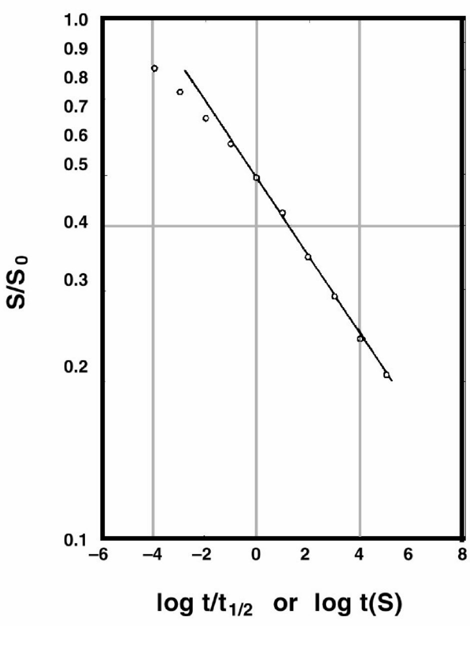

a. Assuming you can estimate the result by a straight line, estimate the slope n from the relationship log $t/t_{1/2} = n$ log $S/S_N + C$, where C is a constant (stress in units of psi, time in seconds).
b. Estimate the time for proof-testing the Bioglass®-coated alumina glass at 15,000 psi if the alumina is to support 5000 psi for 10^7 sec.
c. Briefly state the theory of static fatigue proposed by Hillig and Charles for glass failure.

SYMBOLS/DEFINITIONS

Greek Letters

θ: contact angle.
σ: stress.
ε: strain.
ν: Poisson's ratio.
λ: wavelength.
γ: surface energy.
ρ: rack tip radius or density.
γ_p: surface energy.
μ: friction coefficient.
ΔT: thermal shock resistance.

Roman Letters

E: Young's modulus.
G: shear modulus.
K: bulk modulus.
a_0: lattice space.
c: crack length.
K_{IC}: crack initiation stress,
P_S: survival probability of a Weibull distribution.
m: Weibull modulus.
V: volume.
t_f: time to failure,
n: time exponent constant.
F: sliding force.
A: area.
k: yield shear strength.
H: hardness,
K: wear constant.
C: constant.
T: temperature.

d: grain diameter.

G: Gibbs free energy.

w: work.

Definitions

Bulk modulus: Stiffness of a material, defined as change per unit volume by applied pressure.

Dislocation: A line of imperfection that can be viewed as the boundary between a region of internal surface over which slip has taken place and another region over which no slip has taken place. Edge and screw dislocations can operate on crystals.

Fire polishing: A thermal process applied to brittle materials such as glasses and ceramics to increase their strength by decreasing crack size and annealing the built-in surface strains.

Griffith theory: Early developed theory of the fracture of brittle materials relating the intrinsic properties (modulus, surface energy) and extrinsic properties — mainly crack size — to predict its tensile strength.

Hooke's law: Linear relationship between stress and strain via elastic modulus.

Impact strength: Strength of a material measured at high speed of load (force) application.

Ionic bond: Bond formed between ionic atoms or molecules such as salt (NaCl).

Metallic bond: Positive ions share valence electrons freely (a "sea" or "cloud" of electrons), thus forming much less directional bonds compared to covalent bonds.

Plastic deformation: When a material is deformed beyond elastic limits (the yield point), it undergoes plastic deformation. Metals and plastics show this behavior, while ceramics and glasses only show this behavior at high temperatures or in near-solution state.

Poisson's ratio: Ratio of strain in the orthogonal direction due to stress. Ceramics and glasses have a low Poisson's ratio (0.15–0.25), while metals and plastics have higher values (>0.3). Water has a value near 0.5, making it incompressible.

Quenching: Thermal process of lowering temperature suddenly, thus preserving the state (phase) of a material. This process is nonequilibrium, so that the state will go to equilibrium above 0°K. Some quenched materials such as glasses will go to equilibrium rather slowly.

Shear modulus: Ratio between shear stress and shear strain: usually a much lower value than the tensile or compressive modulus (~1/3, depending on Poisson's ratio).

Slip system: Number of slip directions and planes operating for a given (crystal) structure.

Surface crystallization: In order to increase the strength of a brittle (amorphous) material, its surface is crystallized to impose compressive stress or strain on the surface relative to the interior. This unbalanced energy state will increase its strength (higher energy state).

Surface energy: Excessive surface energy created by less tightly bound surface atoms and molecules.

Toughness: Energy of a material absorbed before fracture. Such materials as metals and some plastics have high toughness, while most ceramics and glasses have very low toughness values.

Weibull distribution: Unlike a normal distribution, the statistical function of material strength shows a rather different distribution (function). Proposed by Waloddi Weibull in 1939.

Whisker: A single crystal of a material in the form of a filament without dislocations. These materials can approach theoretical strength since no dislocations and defects are present.

Young's modulus: Stiffness of material defined as the change in stress per unit strain.

REFERENCES

1. Ashby MF, Jones DR. 1986. *Engineering materials 2: an introduction to microstructures, processing and design*, pp. 147–152, Oxford: Pergamon.
2. Baier R. 1980. Guidelines for physicochemical characterization of biomaterials. In *Devices and technology branch, National Heart, Lung and Blood Institute*, pp. 97–104. Washington, DC: NIH Publication.
3. Bruce RH. 1965. Science of ceramics. *Sci Ceram* **2**:359–381.
4. Callister JWD. 1994. *Materials science and engineering: an introduction*, 3rd ed. New York: Wiley.
5. Doremus RH. 1973. *Glass science*. New York: Wiley.
6. Griffith A. 1920. The phenomena of rupture and flow in solids. *Philos Trans Roy Soc London Ser A* **221**:163–198.
7. Harris B, Bunsell A. 1977. *Structure and properties of engineering materials*. London: Longmans.
8. Inglis C. 1913. Stress in a plate due to the pressure of cracks and sharp corners. *Trans Inst Naval Arch* **55**:219–230.
9. Kitsugi T, Yamamuro T, Nakamura T, Kokubo T, Takagi M, Shibuya T, Takeuchi H, Ono M. 1987. Bonding behavior between two bioactive ceramics. *J Biomed Mater Res* **21**:1109–1123.
10. Malchau H, Garellick G, Eisler T, Karrholm J, Herberts P. 2005. The Swedish hip registry, increasing the sensitivity by patient outcome data. *Clin Orthop Relat Res* **441**:19–29.
11. McArthur SL. 2006. Surface properties of biomaterials. In *Encyclopedia of medical devices and instrumentation*, pp. 342–354. Ed JG Webster. Hoboken, NJ: Wiley.
12. McClintock F, Argon A. 1966. *Mechanical behavior of materials*. Reading, MA: Addison-Wesley.
13. Moore WJ. 1962. *Physical chemistry*, 3rd ed. Englewood Cliffs, NJ: Prentice-Hall.
14. Nakamura T, Yamamuro T. 1993. Development of a bioactive ceramic, A-W glass-ceramic. In *Bioceramics*, Vol. 6, pp. 105–110. Ed P Ducheyne, D Christiansen. Oxford: Pergamon/Elsevier Science.
15. Oosterbos CJM, Rahmy AIA, Tonino AJ, Witpeerd W. 2004. High survival rate of hydroxyapatite-coated hip prostheses: 100 consecutive hips followed for 10 years. *Acta Orthop Scand* **75**:127–133.
16. Orowan E. 1934. Die mechanischen Festigkeitseigenschaften und die Realstruktur der Kristalle. *Z Kristallogr* **A89**:327–343.
17. Park JB, Kelley BJ, von Recum AF, Kenner GH, Coffeen WW, Grether MF. 1981. Piezoelectric ceramic implants: in vivo results. *J Biomed Mater Res* **15**:103–110.
18. Schnittgrund G, Kenner G, Brown S. 1973. In vivo and in vitro changes in strength of orthopedic calcium aluminate. *J Biomed Mater Res Symp* **4**:435–452.
19. Shi D. 2006. Testing and structural properties of biomaterials. In *Encyclopedia of medical devices and instrumentation*, pp. 354–365. Ed JG Webster. Hoboken, NJ: Wiley.
20. Simpson LA. 1974. Microstructural considerations for the application of fracture mechanics techniques. In *Fracture mechanics of ceramics*, pp. 567–577. Ed RC Bradt, DPH Hasselman, FF Lange. New York: Plenum.
21. Spraggs M, Vasilos T. 1963. Effect of grain size on transverse bend strength of alumina and magnesia. *J Am Ceram Soc* **46**:224–228.
22. Van Vlack LH. 1970. *Materials science for engineers*. Reading, MA: Addison-Wesley.
23. Weibull WA. 1939. Statistical theory of the strength of materials. *Proc Roy Swedish Inst Eng Res* **151**:1–45.
24. Weibull W. 1951. A statistical distribution function of wide applicability. *J Appl Mech* **18**:293–297.

4

GLASS FORMATION AND CHARACTERIZATION

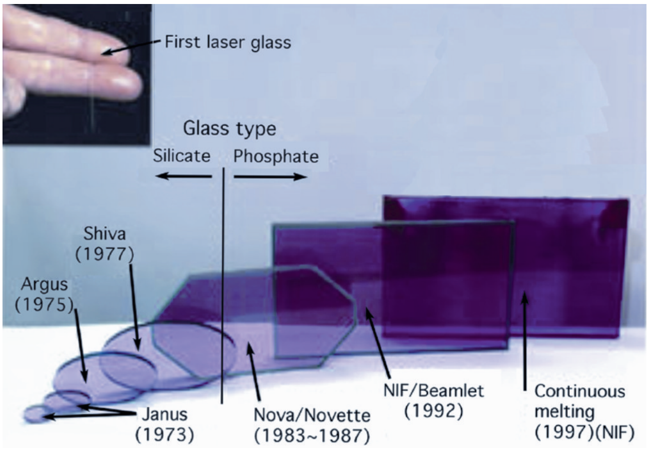
First laser glass
Glass type
Silicate
Phosphate
Shiva
(1977)
Argus
(1975)
Janus
(1973)
Nova/Novette
(1983~1987)
NIF/Beamlet
(1992)
Continuous
melting
(1997)(NIF)

(A) Egyptian glass beads (ca. 3,000–2,500 BCE. Modified with permission from [5]. Copyright © 1994, Dorling Kindersley. (B) The types and uses of glass for scientific and technical purposes are myriad, and range from applications involving the smallest of devices, such as DNA microarrays, to football field-sized, enormously powerful neodymium-doped glass lasers used in laser fusion. Modified with permission from http://en.wikipedia.org/wiki/Glass. Please refer to the color section to view this image in full color.

In this chapter we will discuss some fundamentals of glass formation and the characteristics of glasses relevant to our interests, as implant materials application. This chapter is largely based on *Glass Science* by Doremus [4].

4.1. GLASS FORMATION

Glass is defined as an amorphous solid that has no long-range order (<10 Å), is rigid, and has a viscosity greater than 10^{13} Poise. Others have defined glass as a material formed by cooling from a liquid state without experiencing a change in specific volume, which becomes more or less rigid with increased viscosity [4]. The ASTM defines glass as "an inorganic product of fusion, which has been cooled to a rigid condition without crystallization." Some glasses can be made without cooling by evaporating water from a liquid solution (i.e., sodium silicate). Glasses can also be made from organic material [e.g., Plexiglas®, polymethylmethacrylate (PMMA), polystyrene (PS)]. Glasses sometimes contains crystals as small as 100 Å in size, making them hard to detect. Table 4.1 lists some materials that can be made into glass. Oxides such as B_2O_3, SiO_2, GeO_2, P_2O_3, As_2O_3, Sb_2O_3, In_2O_3, Tl_2O_3, SnO_2, PbO_2, and SeO_2, ionic glasses such as halides, nitrides, sulfides, and carbonates, and organic compounds such as methanol, ethanol, and PMMA can form glasses.

Table 4.1. Some Glasses Formed from Liquid by Quenching

Category	Examples
Elements	S, Se, P
Oxides	B_2O_3, SiO_2, GeO_2, P_2O_3, As_2O_3, Sb_2O_3, In_2O_3, Tl_2O_3, SnO_2, PbO_2, SeO_2,
Sulfides	As_2S_3, Sb_2S_3
Carbonates	K_2CO_3–$MgCO_3$
Polymers	PMMA[a], PS[b], PVC[c]
Metallic alloys by "sprat cooling"	Au_4Si, Pd_4Si

[a] Polymethylmethacrylate.
[b] Polystyrene.
[c] Polyvinylchloride.
Modified with permission from [4]. Copyright © 1973, Wiley.

Thermodynamically the crystalline state is more stable; therefore, the glass state tends to change to crystalline if enough thermal energy is supplied over long periods of time, even at low temperatures, or vice versa. Therefore, the rate of crystallization is directly related to the rate of glass formation. The crystallization rate is plotted against temperature in Figure 4.1 for cristobalite (SiO_2). The maximum rate of crystallization is 10^{-4} cm/s, which translates into 10 milliseconds (ms), and prevents growth of crystals larger than 100 Å. This time is too short to form glasses other than silica glass. It is proposed that the *rate of crystallization* can be expressed as

$$\nu = \frac{H_f(T_m - T)}{3\pi a^2 \eta T_m}, \tag{4.1}$$

where H_f is the heat of fusion at the melting temperature, a is the lattice spacing, and η is the viscosity of the liquid. Equation (4.1) indicates that high viscosity at near T_m will result in a low rate of crystallization, making glass formation easier. Table 4.2 lists some measured values of the crystallization velocities of glass-forming liquids.

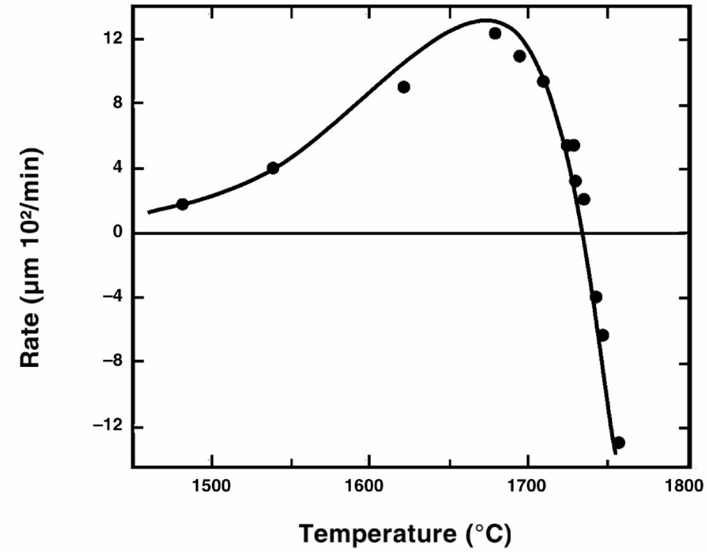

Figure 4.1. Rate of crystallization of cristobalite from fused silica vs. temperature. Reprinted with permission from [4]. Copyright © 1973, Wiley.

4.2. NUCLEATION AND GLASS FORMATION

The rate of homogeneous nucleation of a crystal from a liquid can be expressed as

$$\frac{dN}{dt}(=\dot{N}) = K \exp\left(\frac{E^*}{RT}\right), \tag{4.2}$$

where K is a coefficient and E^* is the energy needed to form a critical nucleus, which can be obtained from the following equation:

$$E^* = -\frac{16\pi\gamma^3 V^2 T_m^2}{3H_f^2 \Delta T^2}, \tag{4.3}$$

where V is the molar volume of the liquid, and $\Delta T = T - T_m$. The rate of nucleation may also be limited by transport of molecules to the nuclei. Uhlmann suggested that viscosity and rate of viscosity decrease with temperature are important determinants of nucleation rate [6].

Table 4.2. Rate of Crystallization and Viscosity of Glass Forming Liquids

Material	T_m (°C)	Maximum velocity (cm/s)	Temperature at max. velocity (°C)	Log viscosity at T_m (P)
SiO_2	1734	2.2×10^{-7}	1674	7.36
GeO_2	1116	4.2×10^{-6}	1020	5.5
P_2O_5	580	1.5×10^{-7}	561	6.7
Na_2O–$2SiO_2$	878	1.5×10^{-4}	762	3.8
PbO–$2B_2O_5$	774	1.9×10^{-4}	705	1.0
Glycerol	18.3	1.8×10^{-4}	–6.7	1.0

Reprinted with permission from [4]. Copyright © 1973, Wiley.

A low melting temperature with an asymmetric molecular structure will generally form glasses easier. Therefore, glasses with lower T_m and ones with T_m closer to T_g will form glasses.

For oxides, the most favorable substrate for glass formation is a substance that will form extended three-dimensional aperiodic networks with an energy content comparable to that of the crystal network. Specifically,

1. An oxygen atom is linked to not more than two glass-forming atoms.
2. The coordination number (CN) of the glass-forming atoms is small.
3. The oxygen polyhedra share corners with each other, not edges or faces.
4. The polyhedra are linked in a three-dimensional network.

According to this rule. AO_2 and A_2O_5 [A: metal atom] satisfy these rules if the O atoms form tetrahedra around each A; A_2O_3 satisfies rules 1, 3, and 4 if the oxygen atoms form triangular bonds around each A; A_2O and AO do not satisfy the rules in any manner.

The three-dimensional network normally results in high viscosity, which in turn causes a low rate of crystallization, which favors glass formation. Another characteristic of glass formers is the high bonding energy between O and A atoms (>80 kcal/mol), although the heat of fusion is lower than for other similar materials. The low heat of fusion causes a lower nucleation rate and crystal growth, thus facilitating glass formation.

4.3. STRENGTH OF GLASSES

The Griffith theory of fracture can be used for brittle materials with flaws. Similar analysis can be applied to glasses; indeed, the Griffith theory was first developed using glass as the experimental specimen. Table 4.3 gives some properties used to calculate the theoretical strength of silica glass (e.g., surface energy), Young's modulus, and Si–O bond distance.

Table 4.3. Properties of Silica Glass

Characteristics	Values
Si–C bond energy	106 kcal/mol
Bond density	7.9×10^{14} molecules/cm^2 [= 1.3×10^{-5} moles/m^2]
Surface energy	2.9 N/m [= J/m^2]
Young's modulus	72 GPa
Bond distance	1.62 Å
Theoretical strength	18 GPa
Measured strengths	13.5 GPa @ –196ºC 14.7 GPa @ –269ºC

Reprinted with permission from [4]. Copyright © 1973, Wiley.

Example 4.1

Calculate the theoretical strength of the silicate glass using values given in Table 4.3.

Answer:

From Eq. (3.10),

$$\sigma_{th} = \sqrt{\frac{E\gamma}{a_0}} .$$

The bond distance is estimated to be 1/4 of the lattice spacing, a_0.

$$\sigma_{th} = \frac{\left(7.2\times10^{10}\ \frac{\mathrm{N}}{\mathrm{m}^2}\right)\ \left(2.9\ \frac{\mathrm{N}}{\mathrm{m}}\right)}{4\times1.62\times10^{-10}\ \mathrm{m}} .$$

$$\sigma_{th} = \underline{18\ \mathrm{GPa}}.$$

This value is close to the measured value of 14.7 GPa at –269ºC given in Table 4.4.

As mentioned earlier, the fracture strength of a brittle material depends on the size of the flaw or crack in the test specimen. One such measurement on glass is given in Table 4.4. Equation (3.16) can be rewritten as

$$\sigma_f \sqrt{c} = \sqrt{E\gamma} , \tag{4.4}$$

and $\sqrt{E\gamma}$ is constant regardless of crack size c. Table 4.4 shows the results when $\sqrt{E\gamma}$ values do not change with c.

Table 4.4. Fracture Strength of Glass with Varying Crack Size

Crack length, $2c$ (m)	Fracture stress, σ_f (MPa)	$\sigma_f\sqrt{c} = E\sqrt{\gamma}$ (MPa $\sqrt{m}$)
0.0038	5.96	0.37
0.0069	4.30	0.36
0.0137	3.32	0.39
0.0226	2.52	0.38

1 psi = 6895 Pa.
Reprinted with permission from [4]. Copyright © 1973, Wiley.

4.4. STATIC FATIGUE OF GLASSES

As with any other materials, glasses undergo deterioration of strength under static and dynamic loading conditions. Static properties can be measured by making three (or four)-point-bend tests in which a constant load is applied and the time is monitored automatically until the specimen fractures. In order to shorten the experimental time, higher stress and temperatures or more hostile environments to the specimens (such as body serum) can be applied throughout the test. One set of static test results with glasses are given in Table 4.5 and plotted in Figure 4.2, where specimen surface preparation is varied. The fracture strength of the glass slide in liquid nitrogen is given as σ_N, and the average failure time at $\sigma/\sigma_N = 1/2$ is $t_{1/2}$. As can be seen from the figure, σ/σ_N varies almost linearly with log $t_{1/2}$, regardless of the type of surface treatment, and both have very similar curves. If one can shift the curves, they would form a master curve analogous to the WLF equation for the time and temperature dependence of the relaxation modulus in glassy polymers. The shift factors in this case would be surface crack size and their distribution.

Table 4.5. Effect of Different Abrasions on the Mechanical Properties of Slide Glass

Abrasion	σ_N (MPa)	$t_{1/2}$ (sec)
a. Severe grit blast	93.8	2.9
b. Mild grit blast, emery cloth, perpendicular to stress	85.5	8.8
d. 600 grit	134.5	0.0043
e. 320 grit	95.2	0.039
f. 150 grit, parallel to stress	69.6	0.56
c. 150 grit	164.8	0.14

Reprinted with permission from [4]. Copyright © 1973, Wiley.

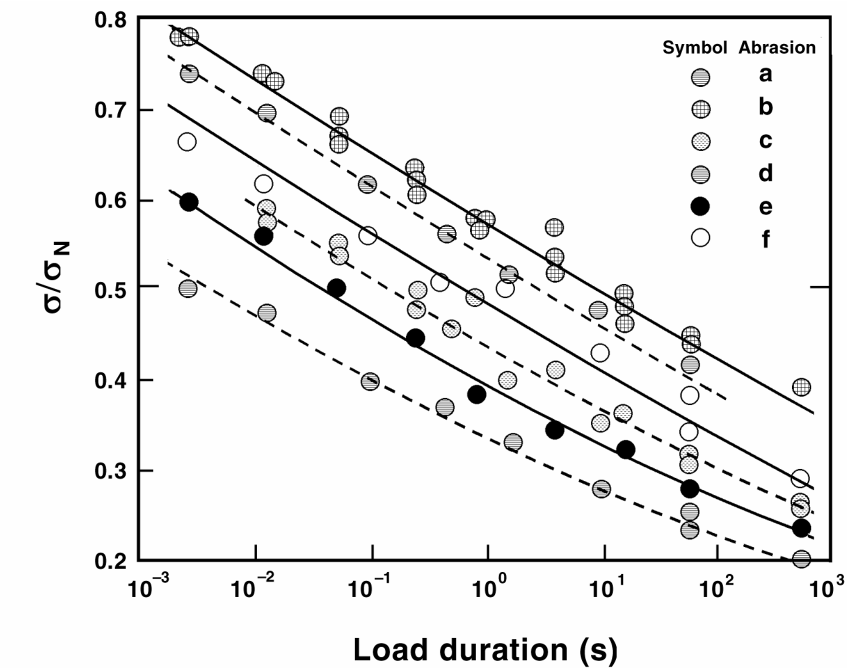

Figure 4.2. Plot of σ/σ_N vs. log $t_{1/2}$ for soda-lime glass slide. Reprinted with permission from [4]. Copyright © 1973, Wiley.

The fraction of specimens that fails at time t can be expressed as a Gaussian distribution:

$$F = \frac{1}{2}\left\{1 + \operatorname{erf}\left[h \log\left(\frac{t_{1/2}}{t}\right)\right]\right\}, \tag{4.5}$$

where $t_{1/2}$ is the time at $F = ½$, and h is a measure of the spread of the distribution. Figure 4.3 shows the distribution of Eq. (4.5) with $h = 0.7$ and experimental data for FN borosilicate glass (Corning 7052: 66% SiO_2, 24% B_2O_3, 3% Al_2O_3, 4% Na_2O, 3% K_2O). As can be seen, there is some disagreement for the short initial time periods (various experiments have yielded different results) but good agreement for longer time periods.

Example 4.2

A bioengineer is trying to improve the mechanical properties of UI-Ceram, which is made of sapphire (Al_2O_3). The Young's modulus (400 GPa), Poisson's ratio (0.3), and density (3.9 g/cm^3) are comparable to those of other alumina ceramics. The bioengineer measured strength and made the following recordings for the control and the UI-Ceram.

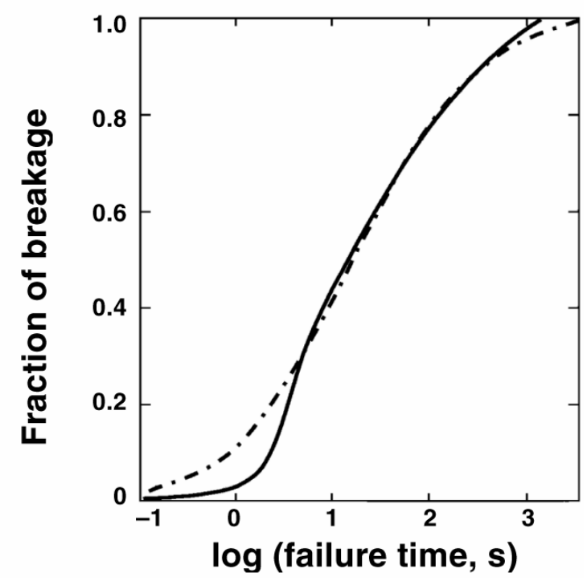

Figure 4.3. Distribution of log failure times for Eq. (4.5) with h = 0.7 and experimental data with FN borosilicate glass. Reprinted with permission from [4]. Copyright © 1973, Wiley.

Stress level (MPa)	Number of broken specimens	
	Control	New-Ceram
100 (95~105)	1	0
110 (105~115)	2	1
120 (115~125)	4	3
130 (125~135)	9	6
140 (135~145)	4	9
150 (145~155)	0	1

1. Calculate the average strength for the control and UI-Ceram.
2. Calculate the percent increase in strength by the treatment.
3. Calculate the largest Griffith crack length *inside* the specimen for the control alumina by assuming an elliptically shaped crack and that the surface energy is 0.1 N/m.
4. Calculate the thermal shock resistance (ΔT) of UI-Ceram that has a linear thermal expansion coefficient of 8.5×10^{-6}/K. Is your answer reasonable?
5. Which one would be more likely to break at a given thermal shock: 1 mm or 10 mm thick UI-Ceram? Why?

6. The bioengineer found that strength was higher for the smaller- rather than the large-grained UI-Ceram. Why?
7. Plot the cumulative probability of failure (CPF) vs. fracture (rupture) strength.

Answer:

1. Control, 126.5 MPa; UI-Ceram, 133 MPa.
2. % change = (133 – 126.5)/126.5 = 5.14% increase.
3. $c=\frac{2\gamma E}{\pi\sigma_f^{\,2}}=\frac{2\times0.1\text{N}/\text{m}\times400\times10^9\text{N/m}^2}{\pi\times(126.5\times10^6)^2(\text{N/m}^2)^2}=1.6\times10^{-6}\text{m}=1.6\ \mu\text{m}$. $2c = 3.2\ \mu\text{m}$ for an inside crack.
4. $\Delta T=\frac{\sigma_f(1-\nu)}{E\alpha}=\frac{133\text{ MPa}\times(1-0.3)}{400\text{ GPa}\times8.5\times10^{-6}/K}=$ $\underline{27.4\text{ K}}$. This value is somewhat low, but reasonable. It would be unlikely that the thermal shock would be a problem in vivo since the temperature remains constant.
5. A 10 mm thick implant, since the chances of containing larger cracks are higher for a thick specimen. A thicker implant will take longer to reach thermal equilibrium.
6. The implant with a smaller grain size is stronger due to increased surface area and smaller crack size.
7. Try this on your own.

PROBLEMS

4.1. When a brittle material of volume V is subjected to a uniform tensile stress, σ, we can write

$$P_S(V)=\exp\left[-\frac{V}{V_0}\left(\frac{\sigma}{\sigma_0}\right)^m\right],$$

where $P_S(V)$ is the probability that the material will survive unbroken, and V_0, σ_0, and m are constants.

If, instead of being constant throughout the material, the tensile stress varies with position, the survival probability becomes

$$P_S(V)=\exp\left[-\frac{1}{\sigma_0^m V_0}\int_V \sigma^m dV\right].$$

Modulus-of-rupture tests were carried out on uniform beams of silicon nitride, as shown in (a) below. 50% of the beams broke at the moment of or before maximum tensile stress σ_r reached 500 MPa. An identical specimen is to be used in a situation where it is loaded in tension along its length, as shown in (b) below.

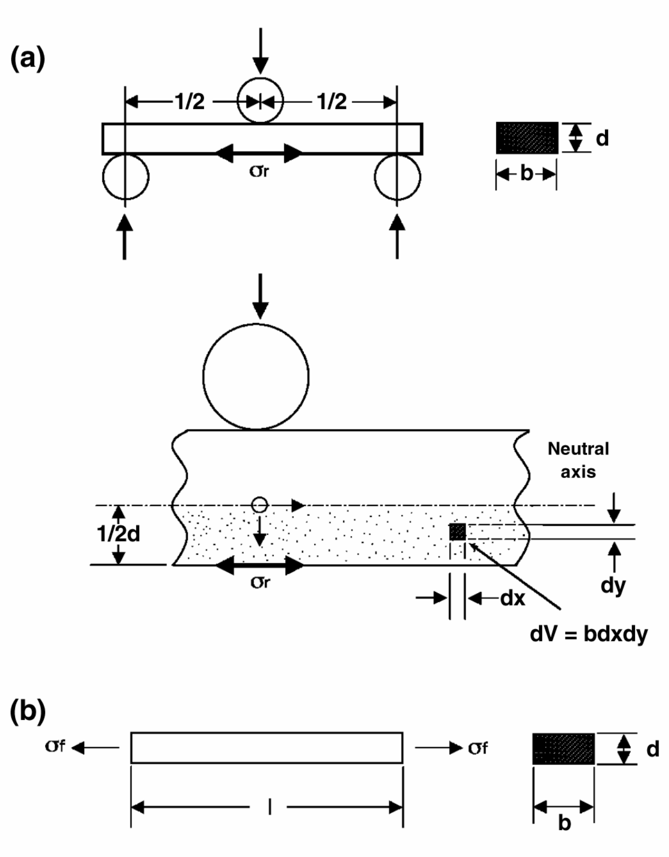

Calculate the tensile stress σ that gives a 50% chance of breaking this specimen. You may assume that $m = 10$ for silicon nitride (Problem 18.2 of [1]).

[Hints for use with modulus-of-rupture test: (a) you should only integrate $\sigma^m dV$ over the lower half of the beam (why?); (b) you may assume that the tensile stress at a general position (x,y) is given by

$$\sigma_r = \frac{y}{\frac{d}{2}}\left[\frac{\left(\frac{l}{2}-x\right)}{\frac{l}{2}}\right].$$

4.2. (See diagrams in Problem 4.1 for notation.) Modulus-of-rupture tests were done on samples of enhanced glass-ceramic with dimensions $l = 100$ mm, $b = d = 10$ mm. The median value of σ_r (i.e., σ_r for $P_S = 0.5$) was 300 MPa. The glass-ceramic is to be used for components with dimensions $l = 50$ mm, $b = d = 5$ mm loaded in simple tension along their length. Calculate the tensile stress that will give a probability of failure, P_f, of 10^{-6}. Assume that $m = 10$.

[Hint: for $m = 10$, $\sigma_{TS} = \sigma_r / 1.73$]

4.3. From the data given for alumina ceramic, answer.

Properties	As-received	Glazed & quenched (1500°C, silicone oil)
σ_f (psi)	40,000	61,000
ν	0.25	0.3 (glaze)
α ($\times 10^{-7}$/°C)	65	53 (glaze)
E (GPa)	390	390

a. Estimate the amount of thermal shock (ΔT) needed to fracture as-received and glazed and quenched samples.
b. Would you expect a higher ΔT if the as-received sample was flame polished on the surface? Why? Why not?
c. Estimate K_{IC} for the as-received and glazed & quenched samples if the largest flaw depths was 1 mm.
d. Can you use the same K_{IC} value obtained for single-crystal sapphire to estimate flaw depth for the polycystalline alumina? Give reasons.

4.4. Griffith measured the fracture strength of glass after introducing different-sized flaws, as given.
a. Calculate the crack tip radius.
b. Prove that the theoretical strength of the glass depends on $1/\sqrt{c}$.

Crack length	Fracture strength (psi)
0.15	864
0.29	623
0.54	482
0.89	366

4.5. a. Integrate to obtain the fraction (F) of samples that break below certain loads:

$$F = \frac{1}{2}\left[1 + \operatorname{erf} h(S - S_m)\right].$$

b. Plot F vs. S; assume S_m is arbitrary.

4.6. One constructs intraocular lenses (IOLs) from PMMA glass and Pyrex® glass (fused silica). Give the advantages and disadvantages in terms of their mechanical and surface property, density, manufacturability, functionality, and biocompatibility.

4.7. A golf driver with a liquid metal head is supposed to be amorphous (noncrystalline). What would be the advantages if one used liquid metal for the femoral stem in a total hip joint replacement?

4.8. Explain the reason(s) why some crystalline structures (such as diamond and alumina) is transparent, while others (e.g., crystalline gold) are not? Why are some glasses (e.g., soda-lime glass) transparent, and some (liquid metal) not?

SYMBOLS/DEFINITIONS

Greek Letters

γ: surface energy.
η: viscosity.
ν: rate of crystallization.

Roman Letters

$\dot{N}$: homogeneous nucleation rate.
a: lattice space.
E^* : activation energy of nucleation.
erf: error function.
F: Gaussian distributuion function.
h: spread of Gaussian distribution.
H_f: heat of fusion.
k: constant.
R: gas constant.
T_m: melting temperature.
ΔT: degree of supercooling.
V: molar volume.

Definitions

ASTM: American Society for Testing and Materials.

Coordination number (CN): Number of direct contact atoms or ions in a unit cell of a crystal structure.

Gaussian distribution: A family of distributions of the same general form, differing in their location and scale parameters: the mean ("average") and standard deviation ("variability"), respectively. The standard normal distribution is the normal distribution with a mean of 0 and a variance of 1. It is often called a bell curve because the graph of its probability density resembles a bell. Named after Carl Friedrich Gauss, who published his work in 1801 [2].

Master curve: Often used to plot relaxation modulus curves over decades on a semi-log graph to obtain the whole spectrum of relaxation. See WLF equation.

Neodymium-doped glass: Used extensively as laser and waveguide glass (soda-lime-silicate-glass containing 2% Nd_2O_3 by weight). Can be made into a glass-ceramic.

PMMA: Polymethylmethacrylate. Noncrystalline, clear, hard polymer used to make synthetic window glass, hard contact lens, bone cement, etc.

Poise: Unit of viscosity, 1 P = 1 Pa·s.

PS: Polystyrene. Noncrystalline, clear, hard, and brittle polymer used to make toys and other inexpensive articles.

Viscosity: Internal friction of a fluid that makes it resist flowing past a solid surface or other layers of a fluid.

WLF equation: Williams, Wendel, and Ferry proposed that the time–temperature behavior of amorphous materials (polymers) can be expressed as

$$\log a_T = \frac{-17.44(T - T_g)}{51.6 + (T - T_g)},$$

where a_T is a shift factor and T_g is the glass transition temperature. The rheological behavior (e.g., stress relaxation) can be obtained over decades if one can get the relaxation data at various temperatures and then plot the shift factors. This may not apply to inorganic glasses since the relaxation behavior may not be similar to that of long-chain molecules (e.g., glassy polymers) [3].

REFERENCES

1. Ashby MF, Jones DR. 1986. *Engineering materials 2: an introduction to microstructures, processing and design*, pp. 147–152, Oxford: Pergamon.
2. Bell ET. 1986. The prince of mathematicians: Gauss. In *Men of mathematics: the lives and achievements of the great mathematicians from Zeno to Poincaré*, pp. 218–269. New York: Simon and Schuster.
3. Billmeyer Jr FW. 1984. *Textbook of polymer science*. New York: Wiley.
4. Doremus RH. 1973. *Glass science*. New York: Wiley.
5. Platt R. 1994. *Smithsonian visual timeline of inventions*. New York: Dorling Kindersley.
6. Uhlman DR. 1972. A kinetic treatment of glass formation. *J Noncryst Solids* **7**:337–348.

5

HARD TISSUES: STRUCTURE, PROPERTIES, HEALING, REMODELING, AND BIOCOMPATIBILITY

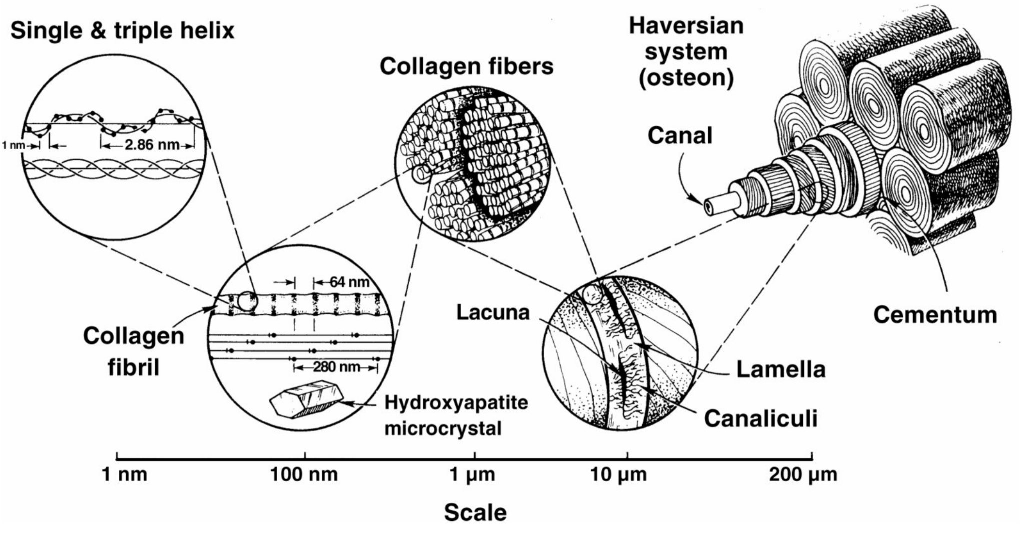
Single & triple helix
1 nm
2.86 nm
Collagen fibers
Haversian system (osteon)
Canal
Collagen fibril
64 nm
280 nm
Hydroxyapatite microcrystal
Lacuna
Lamella
Canaliculi
Cementum
1 nm
100 nm
1 μm
10 μm
200 μm
Scale

Hierarchical structure of compact bone. Modified with permission from [21]. Copyright © 1993, American Association for the Advancement of Science.

In this chapter we study the structure–property relationship of hard tissues, since ceramics and glasses are mainly used to replace or augment hard tissues. In addition, hard tissues contain a mineral phase that is similar to hydroxyapatite ceramic (Table 5.1). We will study basic organization and macrostructure and relate them to properties. Structurally, biological tissues consist of a vast network of intertwining fibers with ground substances made up mostly of polysaccharides and immersed in a pool of ionic fluid. Attached to the fibers are cells whose function is nutrition and regeneration of living tissues (fibers and ground substances). The ground substances have a definite structural organization and are not completely analogous to solute suspended in a solution. Physically, ground substances behave as glue, lubricant, and shock absorber in various tissues.

Table 5.1. Distribution of Various Tissues and Physiological Conditions of Western Man

Muscle 43%, bone 30%, skin 7%, blood 7.2%

Organs: spleen (0.2%), heart (0.4%), kidneys (0.5%), lungs (1.0%), liver (2%), brain (2.3%), viscera (5.6%)

Water 60%, solids 40%

Average body weight: 70 kg (155 lb)

Medium height: 1.8 m (5.91 ft)

Basic metabolic rate 68 kcal/hr

pH: gastric contents (1.0), urine (4.5–6.0), intracellular fluid (6.8), blood (7.15–7.35)

P_{O_2} (mm Hg): interstitial (2–40), venous (40), arterial (100), atmospheric (160)

P_{CO_2} (mm Hg): alveolar (40)

Reprinted with permission from [1]. Copyright © 1981, Marcel Dekker.

The structure and properties of a given biological material depend on the chemical and physical nature of its components, their relative amounts, and the interactions among them. For example, neural tissues consist almost entirely of cells, whereas bone is composed of collagen fibers and calcium phosphate minerals, with minute quantities of cells and ground substances as glue.

An understanding of the exact roles played by a tissue and its interrelationship with the function of the entire living organism is essential if one is to use biomaterials intelligently. Thus, to design a hip joint prosthesis one has to understand not only the adjoining bone structure–property relationship itself but also the relative functions of the prosthesis and the bone. This chapter is based in part on Chapter 9 of [26]. An excellent summary on the subject can also be found in [22].

5.1. STRUCTURE OF PROTEINS

The organic phase of hard tissues is mostly made of collagen, one form of protein. Polysaccharides act as the cementing medium between osteons.

5.1.1. Proteins

Similar to polymeric materials, proteins are made of monomers called amino acids:

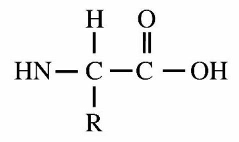

$$HN-\overset{\displaystyle H}{\underset{\displaystyle R}{C}}-\overset{\displaystyle O}{\overset{\|}{C}}-OH \qquad (5.1)$$

Peptides, in turn, are polyamides formed by step-reaction polymerization between the amino and carboxyl groups of amino acids, whose basic chemical formula can be represented as

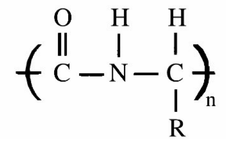

$$\left(\overset{\displaystyle O}{\overset{\|}{C}}-\overset{\displaystyle H}{\overset{|}{N}}-\overset{\displaystyle H}{\underset{\displaystyle R}{C}} \right)_n \qquad (5.2)$$

where R is a side group. Hydrogen is the smallest side group, the addition of which forms glycine. The geometry of a peptide with a hypothetical flat sheet structure is shown in Figure 5.1a. The structure has a repeating distance of 0.72 nm, so that the

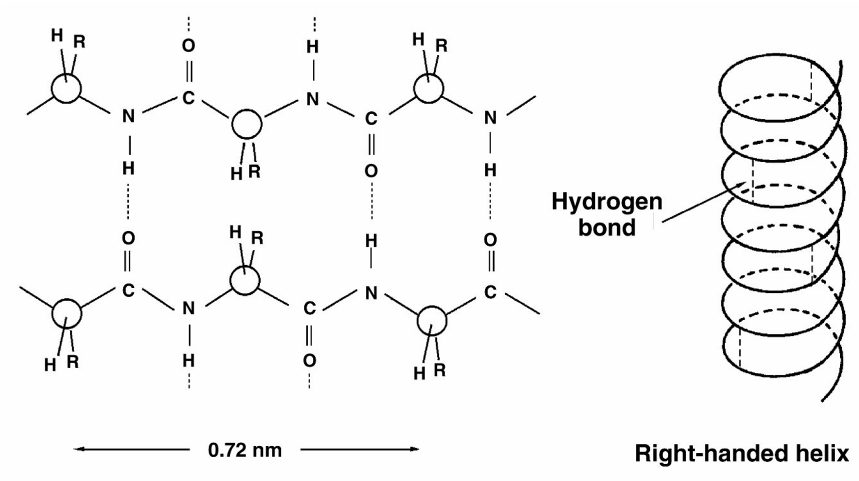

Figure 5.1. (a) Hypothetical flat sheet structure of a protein. (b) Helical arrangement of a protein chain.

Table 5.2. Amino Acids

	R	Abbreviation	T_m (°C)	Isoelectric point
Glycine	H	Gly	292	5.97
Alanine	CH_3	Ala	297	6.02
Valine*	$CH(CH_3)_2$	Val	315	5.97
Leucine*	$CH_2CH(CH_3)_2$	Leu	337	5.98
Serine	CH_2OH	Ser	228	5.68
Threonine	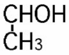 $\underset{CH_3}{CHOH}$	Thr	253	5.60
Aspartic acid	$CH_3\text{-}COOH$	Asp	269	2.98
Glutamic acid	$CH\text{-}CH_2COOH$	Glu	247	3.22
Tyrosine	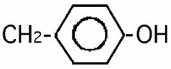	Tyr	347	5.67
Lysine*	$(CO_2)_4NH_2$	Lys	224	9.74
Arginine*	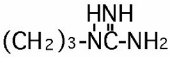 $(CH_2)_3\text{-}\overset{H}{N}\text{-}\overset{NH}{C}\text{-}NH_2$	Arg	230-244	10.76
Histidine*	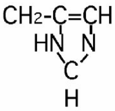	His	227	7.59
Proline (immino acid)	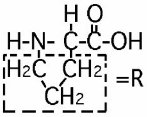	Pro	220	6.30
Hydroxyproline (immino acid)	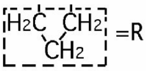	Hypro	270	6.33
Cysteine	CH_2SH	Cys	-	5.02
Methionine*	$CH_2CH_2SCH_3$	Met	283	5.06
Cystine	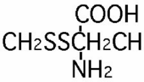 $CH_2SS\underset{NH_2}{\overset{COOH}{C}}H_2CH$		258	5.06
Tryptophan*	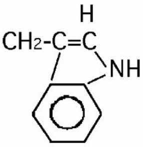	Trp	283	5.88
Phenylalanine*	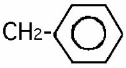	Phe	283	5.48

[a] Basic formula:

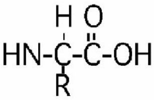

$$HN\text{-}\underset{R}{\overset{H}{C}}\text{-}\overset{O}{C}\text{-}OH$$

* Essential amino acid

side groups (R) are crowded. This crowding makes a flat structure impossible, except for H side groups (i.e., polyglycine). If the side groups are larger, the resulting structure is an α–helix where the H bonds occur between different parts of the same chain and hold the helix together, as shown in Figure 5.lb. Table 5.2 lists the naturally occurring amino acids.

5.1.1a. Collagen

One of the basic constituents of protein is collagen, which has the general amino acid sequence –Gly–Pro–Hyp–Gly–X– (X = any amino acid) arranged in a triple α-helix. It has a high proportion of proline and hydroxyproline, as given in Table 5.3. Since the presence of hydroxyproline is unique to collagen, determination of the collagen content in a given tissue is readily done by assaying the hydroxyproline (elastin is in minute amounts).

Table 5.3. Amino Acid Content of Collagen

Amino acids	Content (mol/l00 mol amino acids)
Gly	31,4–33.8
Pro	11.7–13.8
Hvp	9.4–10.2
Acidic polar amino acids (Asp, Glu, Asp)	11.5–12.5
Basic polar amino acids (Lys, Arg, His)	8.5–8.9
Other amino acids	Residue

Reprinted with permission from [4]. Copyright © 1967, Butterworths.

Three left-handed-helical peptide chains are coiled together to give a right-handed coiled helix with a periodicity of 2.86 nm. This *triple superhelix* is the molecular basis of *tropo(pro)collagen*, the precursor of collagen. The three chains are held together strongly by H bonds between glycine residues and between hydroxyl (OH) groups of hydroxyproline. In addition, there are crosslinks via lysine among the helices (see Figure 5.2).

The primary factors stabilizing collagen molecules are invariably related to the interactions among α-helices. These factors include H bonding between C=O and NH groups, ionic bonding between the side groups of polar amino acids, and interchain crosslinks. One of the secondary factors affecting the stability of collagen is *steric rigidity*, which is related to a high pyrolidine content.

The collagen fibrils (diameter 20~40 nm) form fiber bundles of diameter 0.2~1.2 µm. Figure 5.3 shows scanning and transmission electron micrographs of collagen fibrils in bone, tendon, and skin. Note the straightness of tendon collagen fibrils compared to those of the skin fibrils.

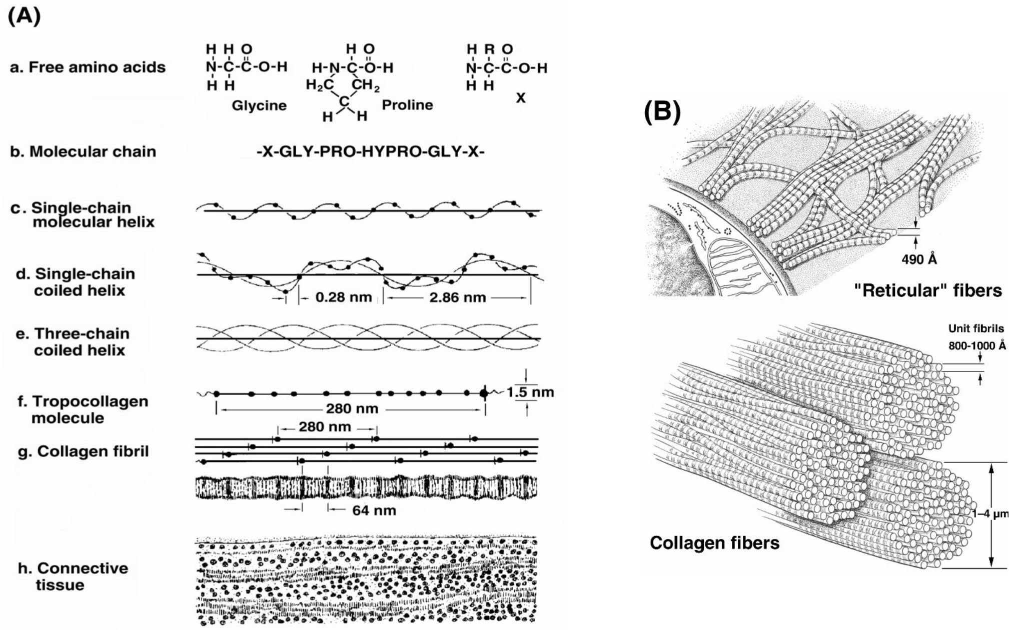
(A)
a. Free amino acids
H H O N-C-C-O-H H H
Glycine
H O H-N-C-O-H H2C CH2 C H H
Proline
H R O N-C-C-O-H H H
X
b. Molecular chain
-X-GLY-PRO-HYPRO-GLY-X-
c. Single-chain molecular helix
d. Single-chain coiled helix
0.28 nm
2.86 nm
e. Three-chain coiled helix
f. Tropocollagen molecule
280 nm
1.5 nm
g. Collagen fibril
280 nm
64 nm
h. Connective tissue
(B)
490 Å
"Reticular" fibers
Unit fibrils 800-1000 Å
1–4 μm
Collagen fibers

Figure 5.2. (A) Diagram depicting the formation of collagen, which can be visualized as taking place in seven steps. The starting materials (a) are amino acids, of which two are shown and the sidechain of any others is indicated by R in amino acid X. (b) The amino acids are linked together to form a molecular chain. (c) This then coils into a left-handed helix (d, e). Three such chains then intertwine in a triple-stranded helix, which constitutes the tropocollagen molecule (f). Many tropocollagen molecules become aligned in staggered fashion, overlapping by a quarter of their length to form a cross-striated collagen fibril (g) [Reprinted with permission from [13]. Copyright © 1961, Scientific American.]. (B) Diagram showing that the "reticular fibers" associated with the basal lamina of an epithelial cell (above) and the "collagen fibers" of the connective tissue in general (below) are both composed of unit fibrils of collagen. Those of the reticulum are somewhat smaller and interwoven in loose networks instead of in larger bundles. [Reprinted with permission from [2]. Copyright © 1968, Saunders.] See also the cover illustration of this chapter for the hierarchal structure of bone.

The side groups of amino acids are highly nonpolar and hence hydrophobic; therefore, the chains avoid contact with water molecules and seek the greatest number of contacts with nonpolar chains of amino acids. If we destroy the hydrophobic contact by means of a solution (e.g., urea), the characteristic structure is lost, resulting in such microscopic changes as shrinkage of collagen fibers. The same effect can be achieved by simply warming collagen fibers. Another factor affecting the stability of collagen is incorporation of water molecules into the intra- and interchain structure. If the water content is lowered, structural stability is decreased. If dehydrated completely (lyophilized), solubility also decreases (so called in-vitro aging of collagen).

It is known that acid mucopolysaccharides also affect the stability of collagen fibers by mutual interactions that form mucopolysaccharide–protein complexes. It is believed that the water molecules affect the polar region of the chains, making the dried collagen more disoriented than that in the wet state.

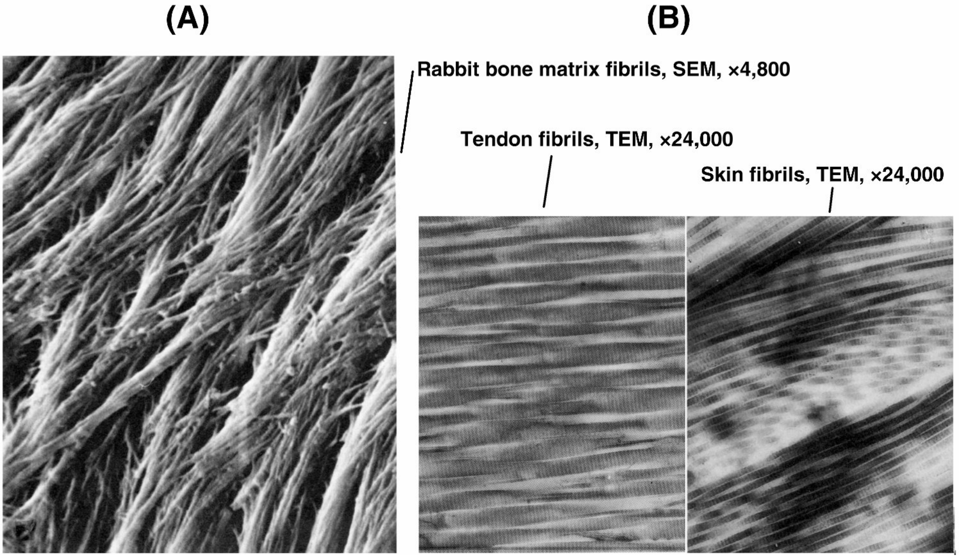
(A)
(B)
Rabbit bone matrix fibrils, SEM, ×4,800
Tendon fibrils, TEM, ×24,000
Skin fibrils, TEM, ×24,000

Figure 5.3. (A) Scanning electron micrograph of the surface of an adult rabbit bone matrix, showing how the collagen fibrils branch and interconnect in an intricate, woven pattern (4800×). Reprinted with permission from [29]. Copyright © 1980, Lippincott. (B) Transmission electron micrographs of (a) parallel collagen fibrils in a tendon and (b) a meshwork of fibrils in skin (24,000×). Reprinted with permission from [12]. Copyright © 1981, Springer-Verlag.

5.1.1b. Elastin

Elastin is another structural protein found in relatively large amounts in such elastic tissues as ligament, aortic wall, and skin. We will not elaborate more on this subject since hard tissues do not contain elastin in any significant amount.

5.1.2. Polysaccharides

Polysaccharides exist in tissues as a highly viscous material that interacts readily with proteins, including collagen, resulting in mucopolysaccharide–protein complexes called glycosaminoglycans or proteoglycans. These molecules readily bind both water and cations. They also exist at physiological concentrations not as viscous solids but as viscoelastic gels. All of these polysaccharides consist of disaccharide units polymerized into unbranched macromolecules. One of the polysaccharides is found in synovial fluid, which acts as a lubricant between joint surfaces. Some polysaccharides act as glue or cement between the lamellae of collagen and mineral in osteons

5.2. STRUCTURE–PROPERTY RELATIONSHIPS

The main objective of studying the structure–property relationships of tissues is to improve the performance of implants. One should therefore always examine the type of physiological functions carried out by the tissues or organs under study in vivo and how to best reproduce the functions (properties) with as few parameters as possible.

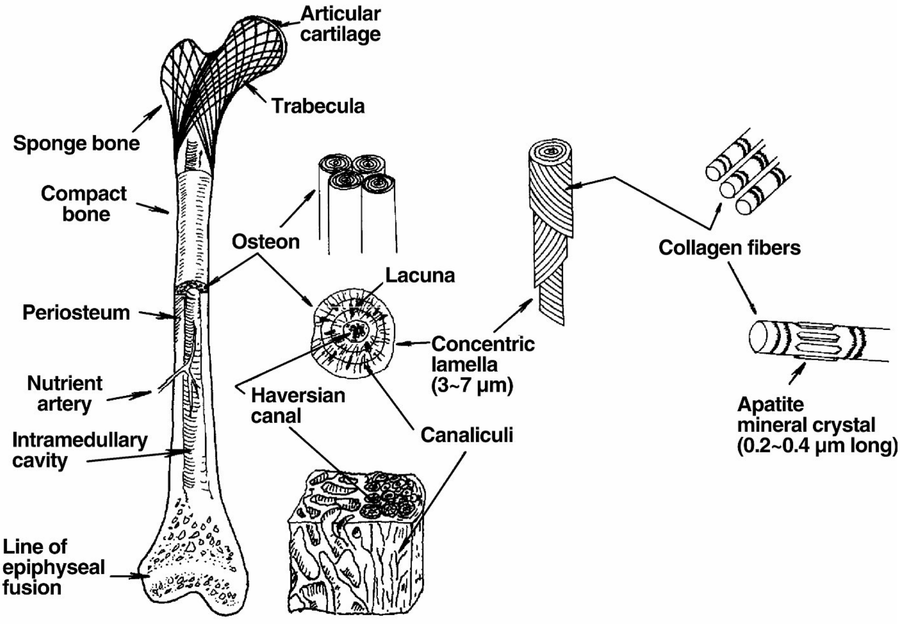
Articular cartilage
Trabecula
Sponge bone
Compact bone
Osteon
Lacuna
Periosteum
Concentric lamella (3~7 μm)
Nutrient artery
Haversian canal
Canaliculi
Intramedullary cavity
Line of epiphyseal fusion
Collagen fibers
Apatite mineral crystal (0.2~0.4 μm long)

Figure 5.4. Organization of a typical bone. Reprinted with permission from [20]. Copyright © 1963, Saunders.

5.2.1. Composition and Structure

Bone and teeth are mineralized tissues whose primary function is "load carrying and load transmission." Teeth are in more extraordinary physiological circumstances since their function is carried out in direct contact with ex-vivo substances, while the functions of bone are carried out inside the body in conjunction with muscles and tendons. A schematic anatomical view of a long bone is depicted in Figure 5.4.

Wet cortical bone is composed of a 22 weight percent (w/o) organic matrix, of which 90~96 w/o is collagen, and the rest mineral (69 w/o) and water (9 w/o) (see Fig. 5.5). The major subphase of the mineral consists of submicroscopic crystals of an apatite of calcium and phosphate, resembling the crystal structure of hydroxyapatite $[Ca_{10}(PO_4)_6(OH)_2]$. There are other mineral ions [e.g., citrate ($C_6H_5O_7^{-4}$), carbonate (CO_3^{-2}), fluoride (F^-), and hydroxyl ions (OH^-)] that may cause some other subtle differences in the microstructural features of bone. Apatite crystals are formed as slender needles, 20–40 nm in length by 1.5~3 nm in thickness, in the collagen fiber matrix, as shown in Figure 5.6. These mineral-containing fibrils are arranged into lamellar sheets (3–7 μm thick) that run helically with respect to the long axis of the cylindrical osteons (sometimes called Haversian systems). The osteon is made up of 4 to 20 lamellae, which are arranged in concentric rings around the Haversian canal. Between these

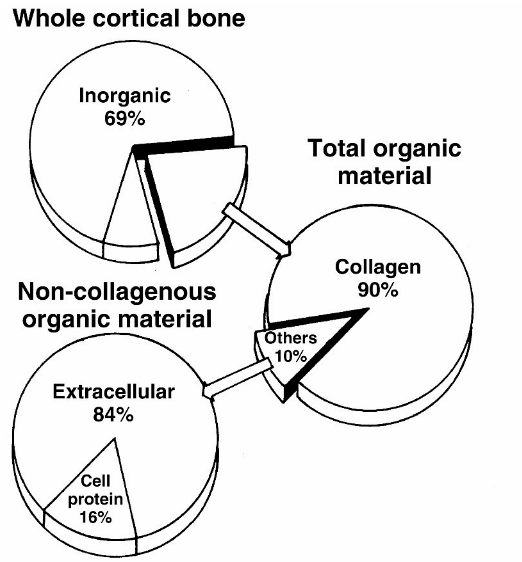

Figure 5.5. Distribution by weight of the constituents of whole cortical bone to illustrate the proportion of cell protein in organic material. Reprinted with permission from [29]. Copyright © 1980, Lippincott.

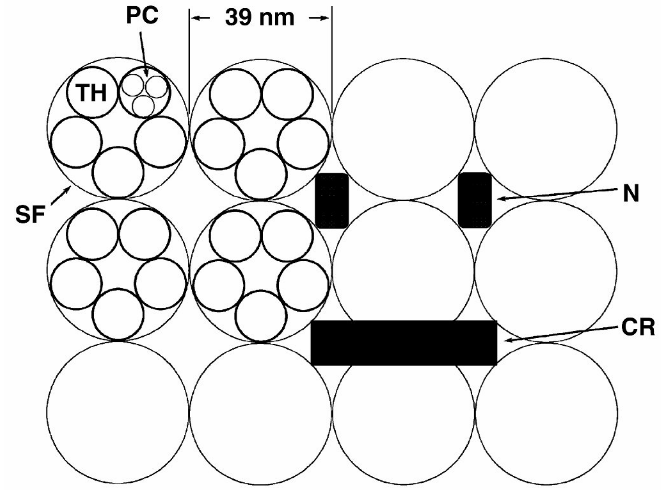

Figure 5.6. Diagrammatic cross-section through a model of the tetragonal arrangement of subfibrils in collagen fiber, according to Miller and Perry. On the left is shown the elements of the collagen structure; on the right calcium phosphate nuclei (N) and crystals (CR), which may develop in the fiber. SF, subfibrils; TH, triple helix; PC, protein chain; H, hole region between the subfibrils. Reprinted with permission from [17]. Copyright © 1974, Springer-Verlag.

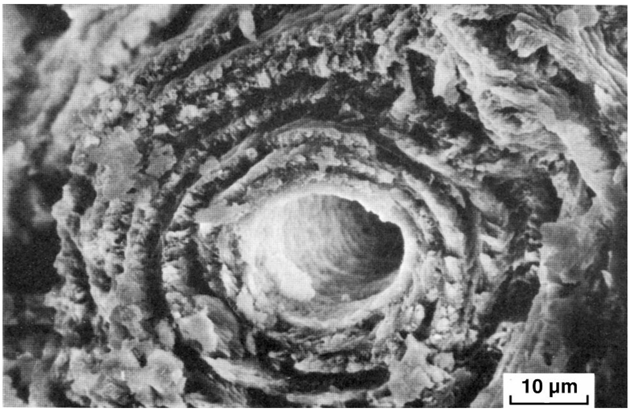

Figure 5.7. Scanning electron micrograph showing the mineral portion of osteon lamillae. The organic phase has been removed using ethylenediamine in a soxhlet apparatus. Reprinted with permission from [27]. Copyright © 1978, Academic Press.

osteons the interstitial systems are sharply divided by the cementing line. The metabolic substances can be transported by the intercommunicating systems of *canaliculi, lacunae,* and *Volkmann's canals,* which are connected with the Haversian canal and marrow cavity. These various interconnecting systems are filled with body fluids, and their volume can be as high as 18.9 ± 0.45% according to one estimate for beef compact bone [9]. The external and internal surfaces of the bone are called the *periosteum* and *endosteum,* respectively, and both have osteogenic properties.

It is interesting to note that the mineral phase is not a discrete aggregation of calcium phosphate mineral crystals. Rather, it is made up of a continuous phase (as evidenced in Fig. 5.7), and complete removal of the organic phase of the bone still gives very good strength.

Long bones like the femur are usually made of cancellous (or spongy) and compact bone. The spongy bone consists of three-dimensional branches or bony trabeculae interspersed by the bone marrow. More spongy bone is present in the epiphyses of long bone, whereas compact bone is the major form present in the diaphysis of the bone (see Fig. 5.4). More detailed structures of compact bones are shown in Figure 5.8. Figure 5.9 shows a diagram of the direction of the fibrils in successive lamellae of a Haversian system. Note the alternating pattern of reinforcement of the fibers around the lumen of the Haversian system.

There are two types of teeth — *deciduous* or primary and *permanent* — of which the latter is more important for us in terms of biomaterials. All teeth have two main portions — the crown and the root — demarcated by the gingiva (gum). The root is placed in a socket called the alveolus in the maxillary (upper) or mandibular (lower) bones. A sagittal cross-section of a permanent tooth is shown in Figure 5.10 to illustrate various structural features. Figure 5.11 shows a portion of ground cross-section of crown of a human cuspid and the dentinoenamel junction of the tooth of a man. The enamel prisms appear as fine, wavy striations.

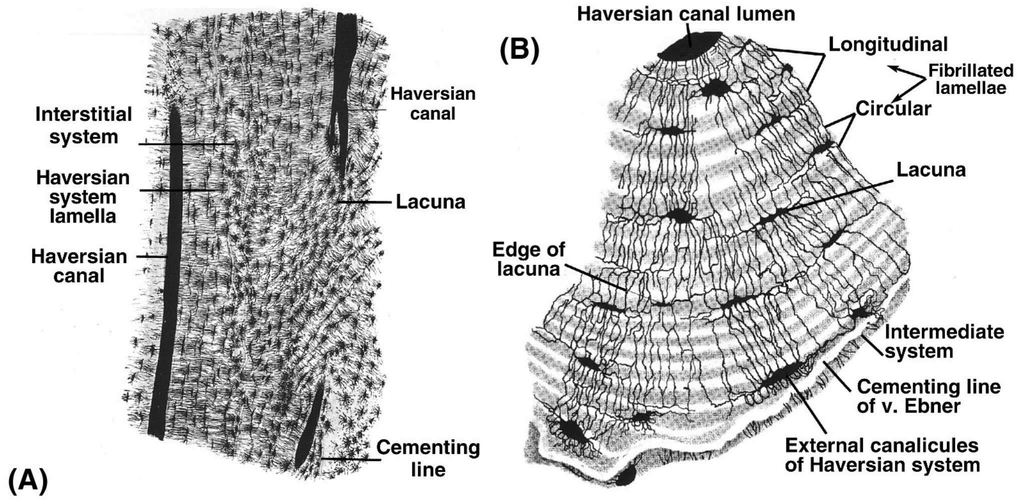
(A)
Interstitial system
Haversian system lamella
Haversian canal
Haversian canal
Lacuna
Cementing line
(B)
Haversian canal lumen
Longitudinal
Fibrillated lamellae
Circular
Lacuna
Edge of lacuna
Intermediate system
Cementing line of v. Ebner
External canalicules of Haversian system

Figure 5.8. More detailed structure of compact bone: (A) portion of a longitudinal ground section of the ulna of man (160×); (B) sector of a cross-section of a Haversian system of a human hip bone (520×). Modified with permission from [2]. Copyright © 1968, Saunders.

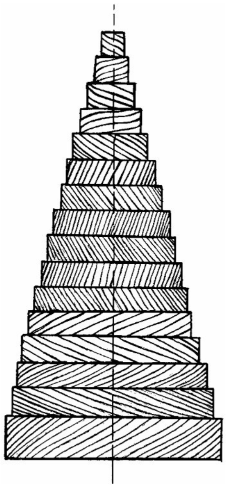

Figure 5.9. Diagram of the direction of the fibrils in successive lamellae of a Haversian system. Reprinted with permission from [2]. Copyright © 1968, Saunders.

Figure 5.12 shows the ultrastructure of the slightly oblique section of undecalcified calf enamel, showing the rough ovoid enamel prism and the interprismatic substance. Note the remarkable orientation of the apatite crystals within the individual prisms, and the different orientations of the crystals in the interprismatic substances. The clear areas define the prisms. The long axis of the crystals (the corresponding C-axis of the apatite crystal lattice) is relatively parallel to the long axis of the prisms. The crystals in the interprismatic area have a distinctly different orientation.

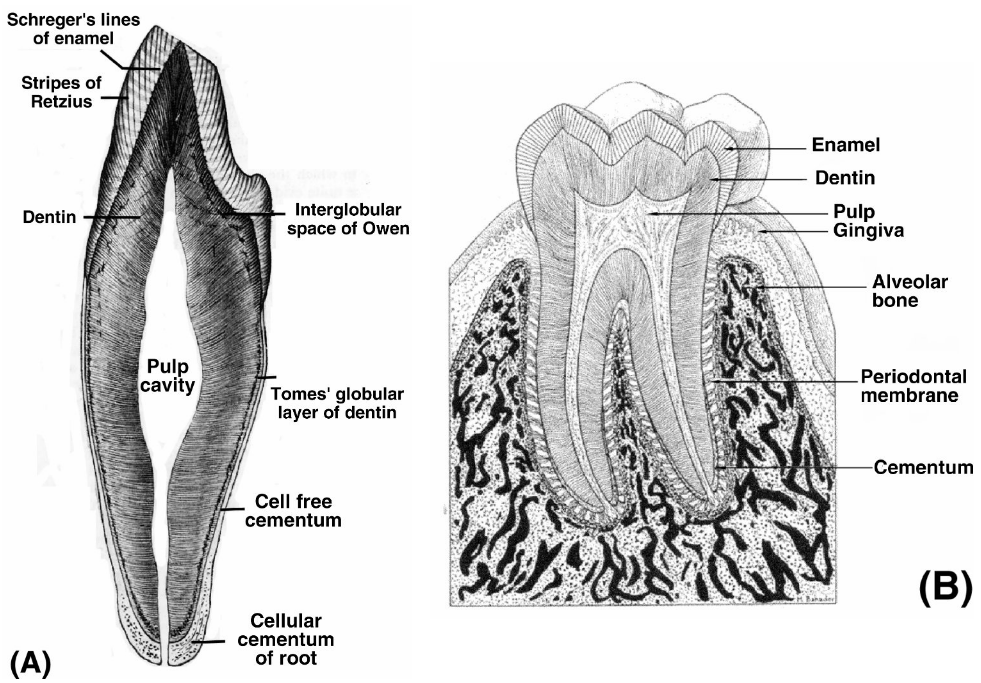
Schreger's lines of enamel
Stripes of Retzius
Dentin
Interglobular space of Owen
Pulp cavity
Tomes' globular layer of dentin
Cell free cementum
Cellular cementum of root
(A)
Enamel
Dentin
Pulp
Gingiva
Alveolar bone
Periodontal membrane
Cementum
(B)

Figure 5.10. (A) Schematic diagram of a longitudinal ground section of human cusp. The top of the crown has been ablated. (B) Diagram of saggital section of human lower first permanent molar. Modified with permission from [2]. Copyright © 1968, Saunders.

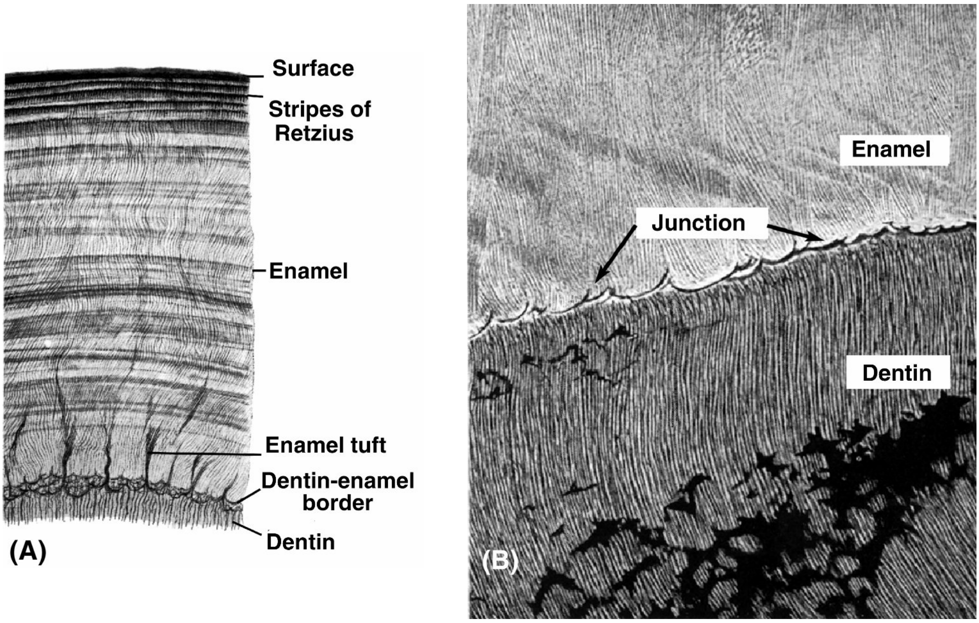
Surface
Stripes of Retzius
Enamel
Enamel tuft
Dentin-enamel border
Dentin
(A)
Enamel
Junction
Dentin
(B)

Figure 5.11. (A) Portion of ground cross-section of the crown of a human cuspid. (B) Dentino-enamel junction of the tooth of a man (ground section). The enamel prisms appear as a fine, wavy striation. The interglobular spaces in the dentin are black (air filled). Between these lacunae are the dentinal tubules. Both 80×. Reprinted with permission from [2]. Copyright © 1968, Saunders.

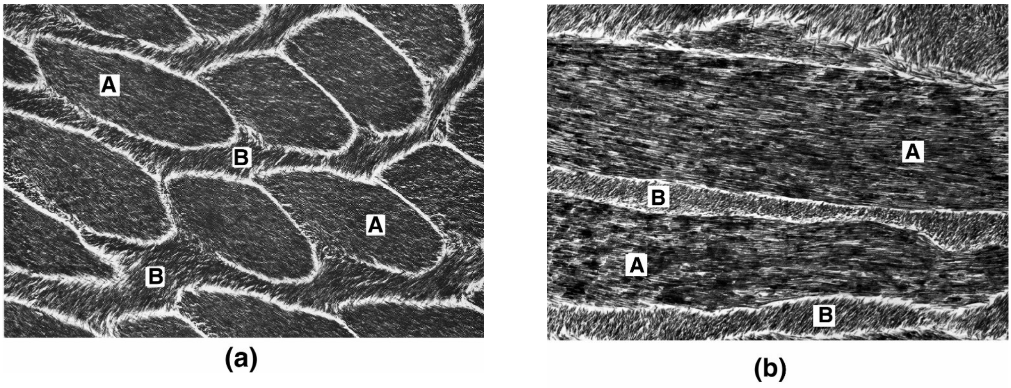

Figure 5.12. Electron micrographs of undecalcified bovine embryonic dental enamel. (a) EM of undecalcified bovine embryonic dental enamel showing two of the prisms (A) in predominantly longitudinal section. The long axis of the crystals (corresponding *c*-axis of the apatite crystal lattice) is relatively parallel to the long axis of the prisms. The crystals in the interprismatic area (B) have a distinctly different orientation. Osmium fixation, 25,000×. Courtesy F.J. Daniel and M.J. Glimcher. (b) Higher magnification of an area of bovine dental enamel similar to that shown in (a), showing longitudinally oriented prismatic crystals (A) with the interprismatic crystals (B) oriented approximately 30º in the direction of the crystals within the prism. Osmium fixation, 100,000×. Courtesy F.J. Daniel and M.J. Glimcher.) Reprinted with permission from [2]. Copyright © 1968, Saunders.

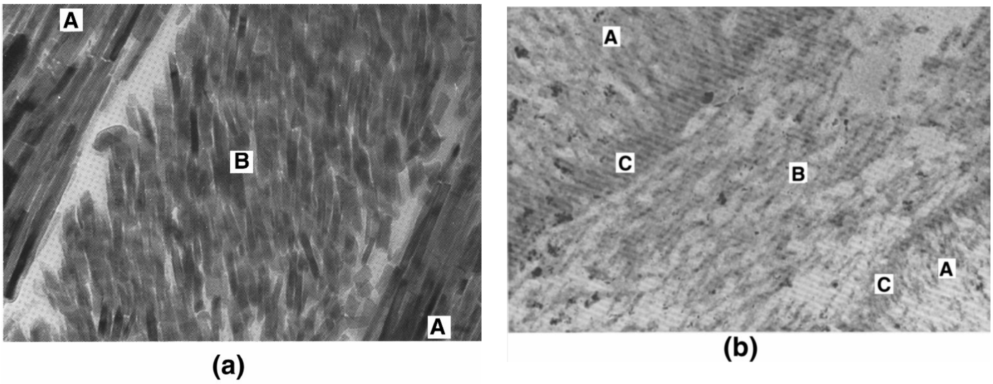

Figure 5.13. More detailed morphology of the enamel ultra-structure. (a) Oblique section of *decalcified* bovine dental enamel. This was prepared by sectioning calcified enamel, which was then decalcified on a grid with phosphotungstic acid and a chelating agent (ethylene-diaminetetraacetic acid). This procedure preserves the orientation of the organic matrix in relation to that of the crystals, as seen in the electron microscope before decalcification. The orientation of' the enamel protein filaments easily distinguishes the prisms (A) and the interprismatic area (B). Courtesy F.J. Daniel and M.J. Glimcher. (b) The inorganic crystals were similarly oriented. The borders (C) surrounding enamel prism sites have a relatively heavy concentration of organic matrix, corresponding to the clear areas seen in fully calcified sections. The micrographs show that the organic material and the inorganic constituents are similarly oriented, much like the apatite crystals and collagen in bone. Osmium fixation, 100,000×. Courtesy F.J. Daniel and M.J. Glimcher. Reprinted with permission from [2]. Copyright © 1968, Saunders.

Figure 5.13 gives a more detailed morphology of the enamel ultrastructure, obtained from an oblique section of *decalcified* bovine dental enamel. The orientation of' the enamel protein filaments easily distinguishes the prisms and the interprismatic area. The inorganic crystals are similarly oriented. The borders surrounding site enamel prisms have a relatively heavy concentration of organic matrix, corresponding to the clear areas seen in the fully calcified sections. The micrographs also show that the organic material and the inorganic constituents are similarly oriented, much like the apatite crystals and collagen in bone.

Enamel is the hardest substance found in the body and consists almost entirely of calcium phosphate salts (97%) in the form of relatively larger apatite crystals. Enamel does re-grow to replace ground-away portions during mastication, but very slowly.

The *dentin* is another mineralized tissue whose distribution of organic matrix and mineral is similar to that of regular compact bone. Consequently, it has similar physical properties. The collagen matrix of dentin might have a somewhat different molecular structure than that of normal bone, that is, being more crosslinked than that found in other tissues, resulting in less swelling. Dentinal tubules (3–5 μm in diameter) radiate from the pulp cavity toward the periphery and penetrate every part of the dentin. Collagen fibrils (2–4 μm in diameter) fill the dentinal tubules in the longitudinal direction, and the interface is cemented by a protein–polysaccharide complex.

The *cementum* covers most of the root of the tooth with coarsely fibrillated bone substance but is devoid of canaliculi, Haversian systems, and blood vessels. The pulp occupies the cavity and contains thin collagenous fibers running in all directions and not aggregated into bundles. The ground substance, nerve cells, blood vessels, etc., are also contained in the pulp. The *periodontal membrane* anchors the root firmly into the alveolar bone and is made up mostly of collagenous fibers plus glycoproteins (protein–polysaccharide complex).

Example 5.1

Calculate the volume percent (%) of bone for the organic (mostly collagen) and mineral (hydroxyapatite).

Answer:

Based on 100 g of bone, 69% inorganic (hydroxyapatite), 31% organic (mostly collagen),

$$V_{\text{inorg}} = \frac{100\ \text{g}}{3.2\ \text{g/cm}^3} = 31.25\ \text{cm}^3,\quad V_{\text{org}} = \frac{31\ \text{g}}{1.0\ \text{g/cm}^3} = 31\ \text{cm}^3;$$

therefore,

$$\frac{31.25}{31.25+31} = \underline{0.50\ (50\%)}.$$

There are almost equal volumes of inorganic and organic substances in cortical bone.

5.2.2. Mechanical Properties

As with most other biological materials, the mechanical properties of bone and teeth depend largely on humidity, the mode of applied load (compressive or tensile, rate of loading, etc.), and the direction of the applied load with respect to the specimen. Therefore, one usually studies the effect of the above-mentioned factors and correlates the results with structural features. For brevity of our discussion here, we will follow the same practice. Table 5.4 gives the mechanical properties of various bones.

Table 5.4. Properties of Bone

Types of bone	Direction of test	Modulus of elasticity (GPa)	Tensile strength (MPa)	Compressive strength (MPa)
Leg bones	Longitudinal			
	Femur	17.2	121	167
	Tibia	18.1	140	159
	Fibula	18.6	146	123
Arm bones	Longitudinal			
	Humerus	17.2	130	132
	Radius	18.6	149	114
	Ulna	18.0	148	117
Vertebrae	Longitudinal			
	Cervical	0.23	3.1	10
	Lumbar	0.16	3.7	5
	Spongy bone	0.09	1.2	1.9
Skull	Tangential	–	25	–
	Radial	–	–	97

Reprinted with permission from [33]. Copyright © 1970, Williams & Wilkins.

The effect of *drying* bone can be easily seen from Figure 5.14, where the dry sample shows a higher modulus of elasticity and compressive strength but lower toughness, fracture strength, and strain. Thus, wet bone, whose characteristics are similar to those of bone in vivo, can absorb more energy and elongate more before fracture, and has far greater toughness.

The effect of *anisotropy* is expected since the osteons are longitudinally arranged and the load is borne in that direction, as shown in Table 5.5. It is obvious that Young's modulus and the tensile and compressive strengths in the longitudinal direction are much higher than those in the radial or tangential directions. The tangential and radial directions differ little in terms of mechanical properties.

The effect of the *rate of loading* on the bone is shown in Figure 5.15, and the data are summarized in Table 5.6. As can be seen, Young's modulus, ultimate compressive, and yield strength increase with increased rate of loading. However, the failure strain and the fracture toughness of the bone reach a maximum and then decrease. This implies that there is a critical rate of loading.

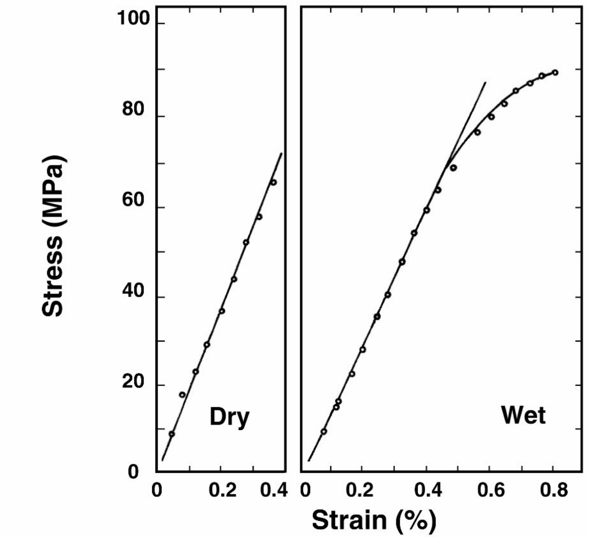

Figure 5.14. Effect of drying on the behavior of human compact bone. Reprinted with permission from [10]. Copyright © 1952, Excerpta Medica.

Table 5.5. Ratios of Properties Measured Parallel to and across the Grain of Human Bone

Young's modulus		Tensile strength		Compressive strength			
L/R	L/T	L/R	L/T	L/R	L/T	Remark	Reference
1.92	1.92			1.54	1.61	DF	[8]
2.33	2.08			1.12	1.22	WF	[7]
		12.5	12.5			DT	
		9.8	9.8			WT	

Abbreviations: L = longitudinal; R = radial; T = tangential direction; D = dry; W = wet; F = femur; T = tibia.

The effect of *mineral content* on the mechanical properties is given in Table 5.7. More mineralized bone has a higher modulus of elasticity and bending strength but lower toughness, illustrating once again that the organic phase of the bone exhibits the energy absorption capacities by straining or yielding to the applied load.

5.2.3. Modeling of Mechanical Properties of Bone

As mentioned earlier, bone is a composite material. Many researchers have proposed a composite model based on two components: the mineral and organic phases. If one

Table 5.6. Summary of Data from Compression Tests of Human Compact Bone at Various Rates of Strain

Strain rate (1/s)	Ultimate compressive strength ($\times 10^3$ psi)	Energy absorption capacity (in·lb/in^3)	Elastic modulus ($\times 10^6$ psi)	Maximum strain to failure (%)
0.001	21.8	270	2.2	1.65
0.01	26	310	2.5	1.75
0.1	29	340	2.6	1.8
1	32	350	3.2	1.78
300	40.5	300	4.3	1.10
1500	46	260	5.9	0.95

1 psi = 6895 Pa

Reprinted with permission from [24]. Copyright © 1966, American Physiological Society.

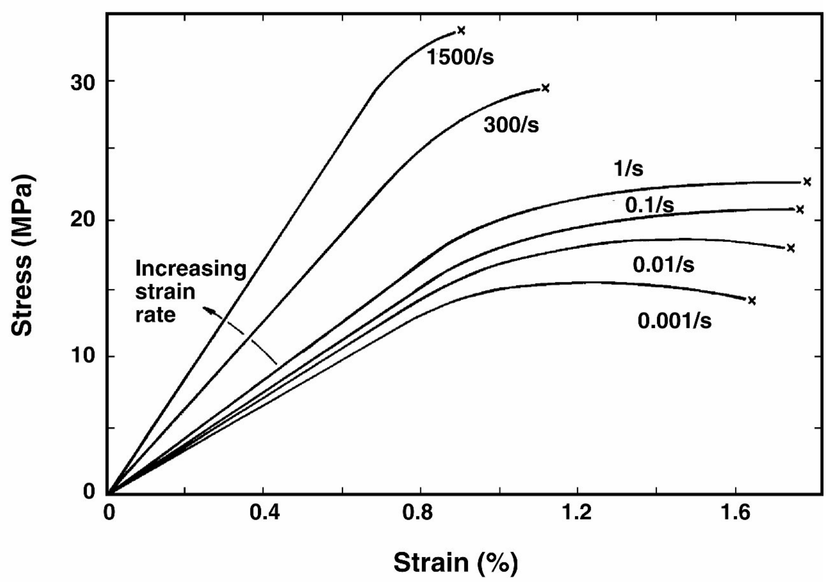

Figure 5.15. Strength as a function of strain and strain rate for human compact bone. Reprinted with permission from [24]. Copyright © 1966, American Physiological Society.

assumes that the load is independently borne by the two components (collagen and mineral, hydroxyapatite), then the total load (P_t) is borne by mineral (P_m) and collagen (P_c):

$$P_t = P_m + P_c. \tag{5.3}$$

Since $\sigma = P/A = E\varepsilon$, thus,

$$P_c = A_c \times E_c \times \varepsilon_c, \tag{5.4}$$

where A, E, and ε are the area, modulus, and strain, respectively. The strain of collagen can be assumed to be equal to that of mineral, that is, $\varepsilon_c = \varepsilon_m$; and thus,

$$P_c = P_m \frac{A_c E_c}{A_m E_m}; \tag{5.5}$$

therefore,

$$P_m = \frac{P_t A_m E_m}{A_m E_m + A_c E_c}. \tag{5.6}$$

Table 5.7. Properties of Three Different Bones with Varying Mineral Contents

Type of bone	Work of fracture (J/m^2)	Bending strength (MPa)	Young's modulus (GPa)	Mineral content (%)	Density (g/cm^3)
Deer antler	6190	179	7.4	59.3	1.86
Cow femur	1710	247	13.5	66.7	2.06
Whale tympanic bulla	200	33	31.3	86.4	2.47

Reprinted with permission from [6]. Copyright © 1981, American Society of Mechanical Engineers.

Example 5.2

Calculate the percent load borne by the mineral phase of cortical bone.

Answer:

Based on a load of 1000 N acting on a cross-sectional area of 10 mm^2 bone, σ_t = 100 MPa. Since the modulus of elasticity of collagen and bone are about 0.1 and 17 GPa, respectively, and the volume fraction of each component is about the same (see Ex. 5.1), the percentage of load borne by the collagen and mineral phase becomes 0.6 and 99.4%, respectively. This indicates that most of the load is carried out by the mineral phase at a normal loading condition. Actually, the strength of the demineralized bone is about 5% of intact bone.

If we express Eq. (5.3) in terms of Young's modulus, it becomes a Voigt model:

$$E_t = E_m V_m + E_c V_c, \tag{5.7}$$

where V is the volume fraction. The above equation is valid if we assume the fibers to be oriented parallel to the direction of loading. However, if the fibers are arranged in the perpendicular direction, one can derive the Reuss model as the following equation:

$$\frac{1}{E_t} = \frac{V_m}{E_m} + \frac{V_c}{E_c}. \tag{5.8}$$

Since not all collagen fibers are exactly oriented in the same direction, one can propose another model:

$$\frac{1}{E_t} = \frac{x}{E_m V_m + E_c V_c} + (1-x)\left(\frac{V_m}{E_m} + \frac{V_c}{E_c}\right), \tag{5.9}$$

where x is that portion of bone that conforms to the parallel direction and $(1 - x)$ that which is perpendicular.

Another interesting view of the properties of bone is the porosity model in which the strength varies according to the following equation [27]:

$$\sigma = \sigma_0 e^{(-nV)}, \tag{5.10}$$

where V is the fraction of the volume that is porous, and n is in the range of 4~7. The elastic modulus also can be expressed as

$$E = E_0(1 - 1.9V + 0.9V^2). \tag{5.11}$$

It is estimated that 18.9 ± 0.45% porosity can exist in compact beef bone due to the various canals in bone, as mentioned previously, and one can arrive at similar values for tensile strength and modulus, as reported in the literature, by employing Eqs. (5.10) and (5.11).

The rheological properties of bone naturally lend themselves to viscoelastic representation, one of which is shown in Figure 5.16. The differential equation for the three-element model can be used to describe the viscoelastic response of bone [25].

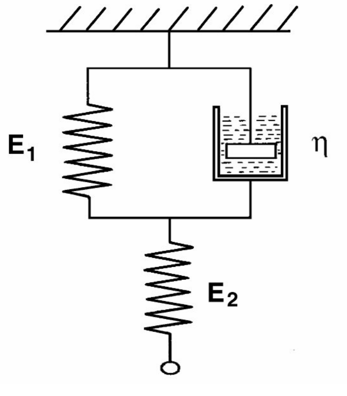

Figure 5.16. Three-element viscoelastic model of bone.

Before going on to the next section, some of the physical properties of teeth are given in Table 5.8. As can be expected, strength is highest for enamel, and dentin is intermediate between bone and enamel. Thermal expansion and conductivity are higher for enamel than for dentin.

Table 5.8. Physical Properties of Teeth

Material	Density (g/ml)	Modulus of elasticity (GPa)	Compressive strength (MPa)	Coefficient of thermal expansion (/°C)	Thermal conductivity (W/m°K)
Enamel	2.2	48	241	11.4×10^{-6}	0.82
Dentin	1.9	13.8	138	8.3×10^{-6}	0.59

Example 5.3

Cortical bone is about 19% porous (Haversian and Volkmann's canal, canaliculi, etc.). Calculate the modulus of elasticity. Assume the pore-free modulus is equal to that of solid hydroxyapatite (Table 10.3).

Answer:

The modulus of solid hydroxyapatite is 120 GPa, so that

$$E = 120 \text{ GPa } (1 - 1.9 \times 0.19 + 0.9 \times 0.19^2 = 120 \times 0.39 = \underline{47 \text{ GPa.}}$$

This value is more than twice the modulus of bone, indicating that the pore-free modulus is far less than that for solid hydroxyapatite. Indeed, the apatites are crystallized onto the collagen fibrils as discrete crystals, not as a large continuous mass.

5.3. HARD TISSUE HEALING AND REMODELING

Bone healing or repair is regenerative rather than simple, as it is skin repair. The only other tissue that regenerates in humans is the liver. Nevertheless, the extent of regeneration is limited. The events following injury are complex, and all the factors involved with repair are complicated. We will examine some factors essential to understanding how to use materials and design devices to help wounds heal faster without unwanted effects.

5.3.1. Wound Healing Process of Hard Tissues

A histomorphological description of wound (fracture) healing events is given in Figure 5.17. The cellular events following fracture of bone are illustrated in Figure 5.18. A hematoma forms after inflammation in the initial stages, followed by demolition of nonvital debris, granulation tissue proliferation, callus formation, transformation of

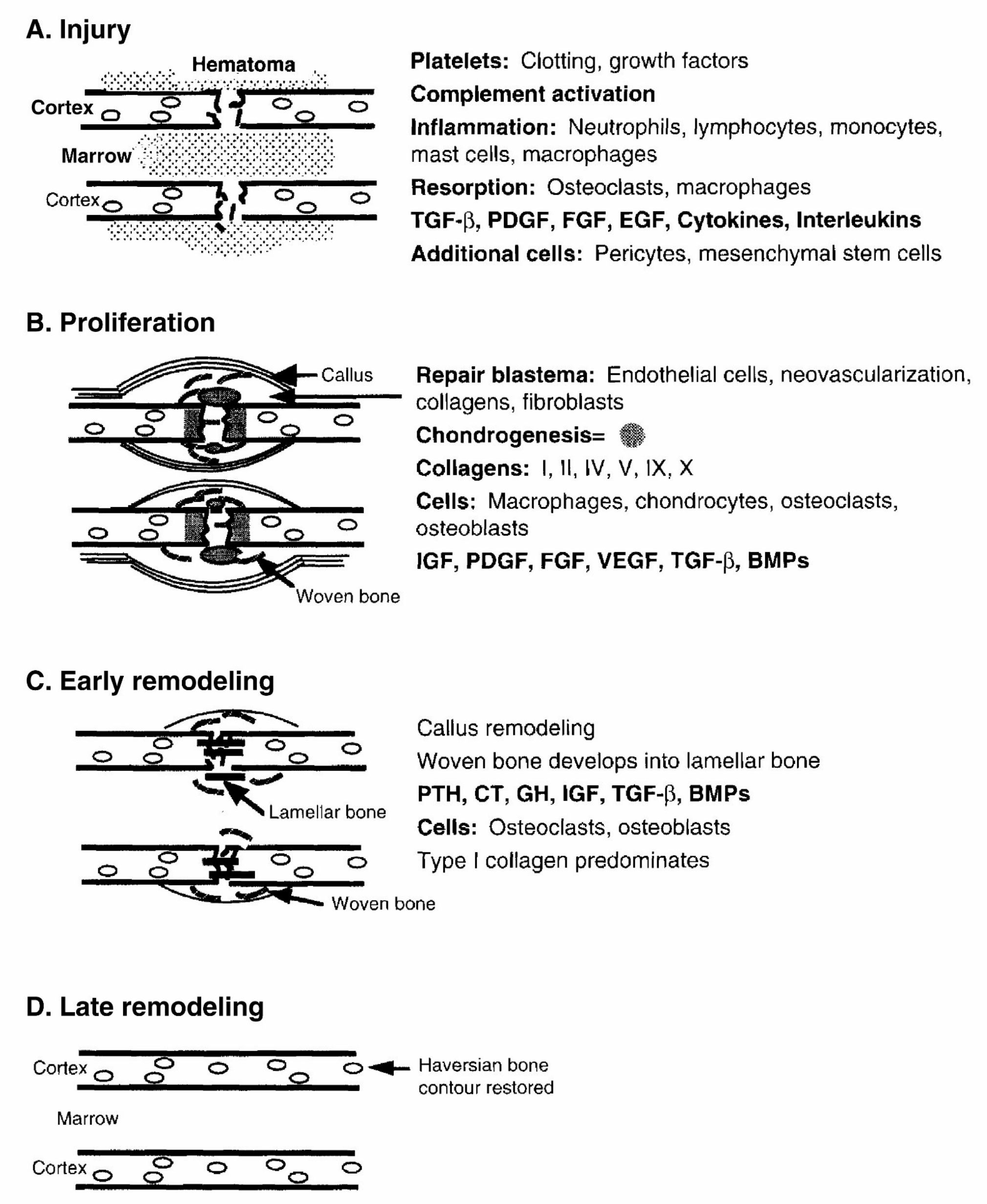
A. Injury
Hematoma
Cortex
Marrow
Cortex
Platelets: Clotting, growth factors
Complement activation
Inflammation: Neutrophils, lymphocytes, monocytes, mast cells, macrophages
Resorption: Osteoclasts, macrophages
TGF-β, PDGF, FGF, EGF, Cytokines, Interleukins
Additional cells: Pericytes, mesenchymal stem cells
B. Proliferation
Callus
Woven bone
Repair blastema: Endothelial cells, neovascularization, collagens, fibroblasts
Chondrogenesis= ●
Collagens: I, II, IV, V, IX, X
Cells: Macrophages, chondrocytes, osteoclasts, osteoblasts
IGF, PDGF, FGF, VEGF, TGF-β, BMPs
C. Early remodeling
Lamellar bone
Woven bone
Callus remodeling
Woven bone develops into lamellar bone
PTH, CT, GH, IGF, TGF-β, BMPs
Cells: Osteoclasts, osteoblasts
Type I collagen predominates
D. Late remodeling
Cortex
Marrow
Cortex
Haversian bone contour restored

Figure 5.17. Sequence of events following bone fracture. Reprinted with permission from [18]. Copyright © 1999, Quintessence Publishing.

woven bone to lamellar (compact) bone, and, finally, remodeling of the bone. When a bone is fractured, many blood vessels (including those in adjacent soft tissues) hemorrhage and form a blood clot (hematoma) around the fracture site. Shortly after fracture, the fibroblasts in the outer layer of the periosteum and the osteogenic cells in the inner layer of the periosteum migrate and proliferate toward the site of injury. These cells lay down a fibrous collagen matrix called a *callus*. Osteoblasts evolved from the osteogenic cells near the bone surfaces start to calcify the callus into trabeculae, which are the structural elements of spongy bone. The osteogenic cells migrating further away from an established blood supply become chondroblasts, which lay down cartilage. Thus, after 2–4 weeks the periosteal callus is made up of three parts, as shown in Figure 5.19.

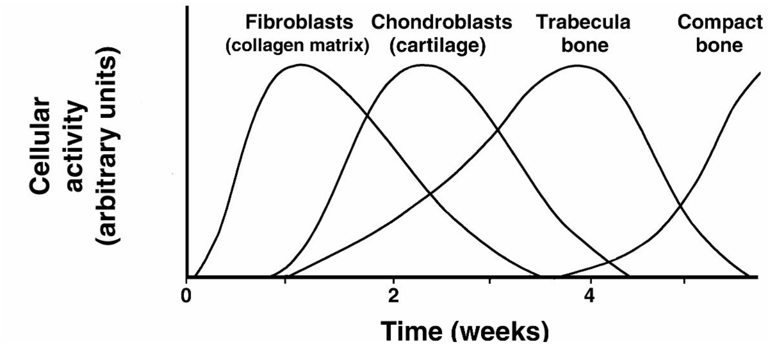

Figure 5.18. Sequence of events followed by bone fracture. Reprinted with permission from [15]. Copyright © 1975, Wiley Interscience.

Simultaneous with external callus formation, a similar repair process occurs in the marrow cavity. Since there is an abundant supply of blood, the cavity turns into callus rather fast and becomes fibrous or spongy bone. New trabeculae develop at the fracture site by appositional growth, and the spongy bone turns into compact bone. This maturation process begins after about 4 weeks.

Along the repair of a fracture, many biological processors join in to help in healing. Some important proteins, including bone morphogenetic proteins (BMPs), associated with fracture repair are given in Figures 5.20 and 21. Figure 5.20 shows BMP's amino acid sequence. The horizontal line length corresponds to the number of differences between the proteins or groups of proteins, and shorter lines indicate that the molecules are more closely related in the amino acid sequence. For example, BMP-2 and BMP-4 have very few amino acid differences, whereas BMP-2 and TGF-β have many [32]. Figures 5.21 shows the amino acid sequence of the TGF superfamily [32].

Some other interesting observations have been made on the healing of bone fractures in relation to synthesis of polysaccharides and collagen. It is believed that the amount of collagen and polysaccharides is closely related to the cellular events following fracture. When the amount of collagen starts to increase, this marks the onset of the *remodeling process*, which occurs after about 1 week. Another interesting observation is the electrical potential (or biopotential) measured in the long bone before and after fracture (see Fig. 5.22). The large electronegativity in the vicinity of fracture

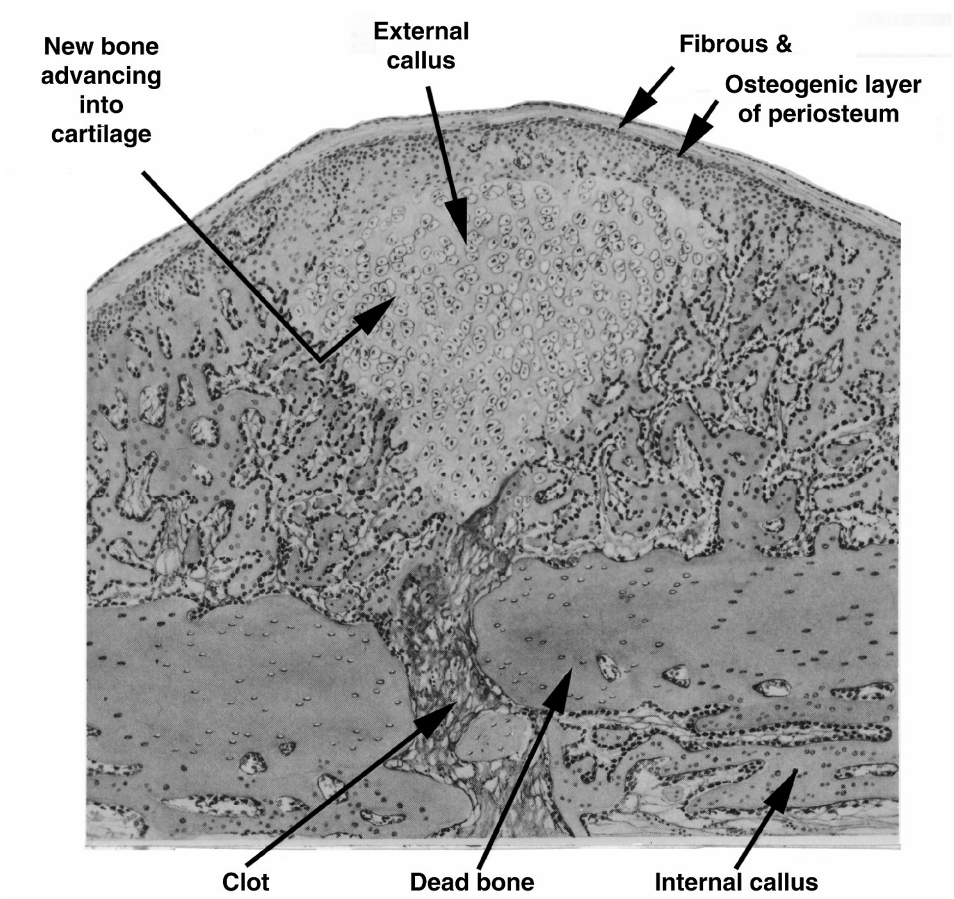
New bone advancing into cartilage
External callus
Fibrous &
Osteogenic layer of periosteum
Clot
Dead bone
Internal callus

Figure 5.19. Drawing of a longitudinal section of the fractured rib of a rabbit after two weeks, H&E stain. Reprinted with permission from [14]. Copyright © 1971, Academic Press.

marks the presence of increased cellular activity in the tissues. Thus, there is maximum negative potential in the epiphysis in normal bone since this zone is more active (the growth plate is in the epiphysis).

5.3.2. Bone Remodeling

Understanding the process of bone remodeling is of paramount importance in implant design and materials selection. This can be illustrated easily by the fact that a bone plate that is too stiff results in thinning of the cortical bone underneath it after the fracture heals due to the "stress shielding" effect [31]. This concept of *functional adaptation* of bone was first introduced by Wolff as the "law of bone transformation" in the 1870s, in which he emphasized that remodeling of cancellous bone structure follows mathematical rules corresponding to the principal stress trajectories, as shown in Figure 5.23 [30].

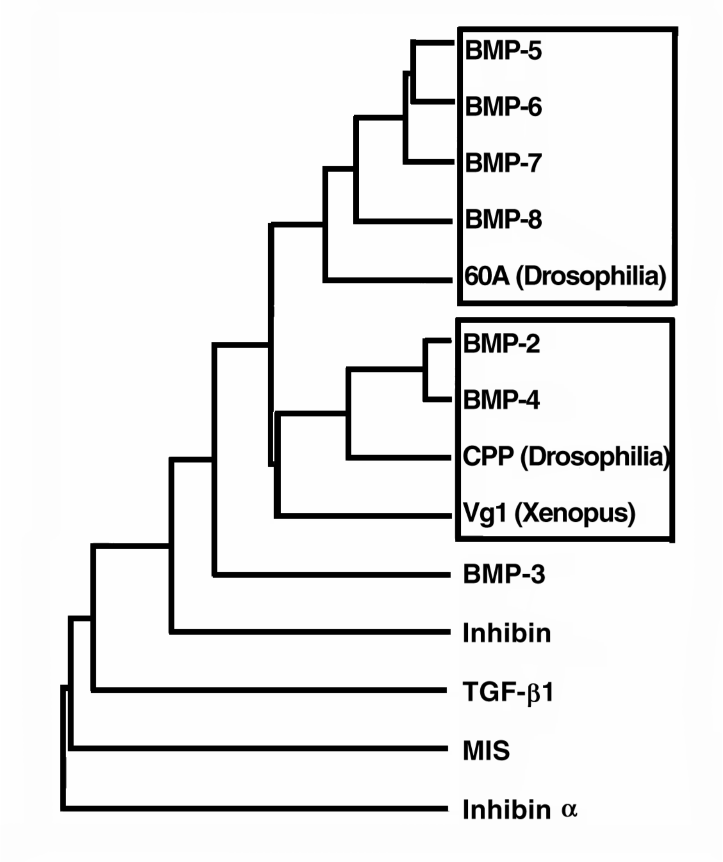

Figure 5.20. Amino acid sequence relationship between bone morphogenetic protein (BMP) molecules identified in osteoinductive extracts derived from bone, as well as representative other members of the TGF superfamily. This illustration was generated using a Genetics Computer Group software program, PileUp, utilizing amino acid sequences from the first conserved cysteine residue in the mature part of the human molecules to the carboxy terminus. The length of the horizontal lines corresponds to the number of differences between the proteins or groups of proteins; i.e,, shorter lines indicate that the molecules are more closely related in terms of amino acid sequence. For example, BMP-2 and BMP-4 have very few amino acid differences, whereas BMP-2 and TGF-β have many. Reprinted with permission from [32]. Copyright © 1999, Quintessence Publishing.

The exact mechanism of bone remodeling (micro- as well as macro-remodeling) is as yet incompletely understood, though there are several proposed theories. One is the *piezoelectricit*y, in which bone modifies its structure by sensing the mechanical stresses generated by dynamic loading and unloading cycles in vivo, which in turn generate the electricity that triggers remodeling activities. The piezoelectric properties of bone were first discovered by Fukuda and Yasuda in the late 1950s and later independently verified by Bassett, Brighton, and coworkers. In fact, the original study by Fukuda and Yasuda led to experiments on "electric callus" formation by applying electricity. Stimulation by a negative electrode produced a callus with a charge similar to that obtained when bone is bent. Using a microelectrode, one can show that the generation of electricity in bone is much more complicated than originally thought; it has also uncovered the existence of *strain-generated potentials* (SGPs), as depicted in Figure 5.24. We can see that there are large, nonlinear electric fields near the Haversian canal. This field is radial and is 30 to 1000 times larger than the average electric field determined from simultaneous macroscopic measurements. "Electric callus" formation by direct (electrical) or indirect (oscillating magnetic field) has been used to successfully overcome nonunion of long bones [3,23].

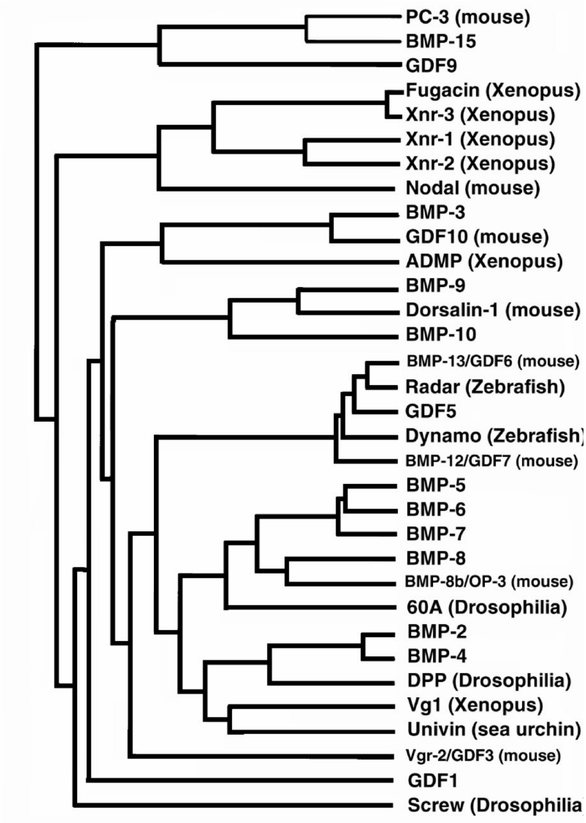
PC-3 (mouse)
BMP-15
GDF9
Fugacin (Xenopus)
Xnr-3 (Xenopus)
Xnr-1 (Xenopus)
Xnr-2 (Xenopus)
Nodal (mouse)
BMP-3
GDF10 (mouse)
ADMP (Xenopus)
BMP-9
Dorsalin-1 (mouse)
BMP-10
BMP-13/GDF6 (mouse)
Radar (Zebrafish)
GDF5
Dynamo (Zebrafish
BMP-12/GDF7 (mouse)
BMP-5
BMP-6
BMP-7
BMP-8
BMP-8b/OP-3 (mouse)
60A (Drosophilia)
BMP-2
BMP-4
DPP (Drosophilia)
Vg1 (Xenopus)
Univin (sea urchin)
Vgr-2/GDF3 (mouse)
GDF1
Screw (Drosophilia

Figure 5.21. Amino acid sequence relationships between members of the TGF superfamily. All sequences are human unless otherwise indicated. BMP, bone morphogenetic protein; GDF, growth and differentiation. Reprinted with permission from [32]. Copyright © 1999, Quintessence Publishing.

Streaming potentials of positive and negative ions in the tissue fluids are thought to be more important factors corresponding to electrical potentials in vivo than the piezoelectric properties of bone [9]. It is conceivable that more rigorous exercise will lead to higher kinetic activities of ions, which will induce higher streaming potentials,

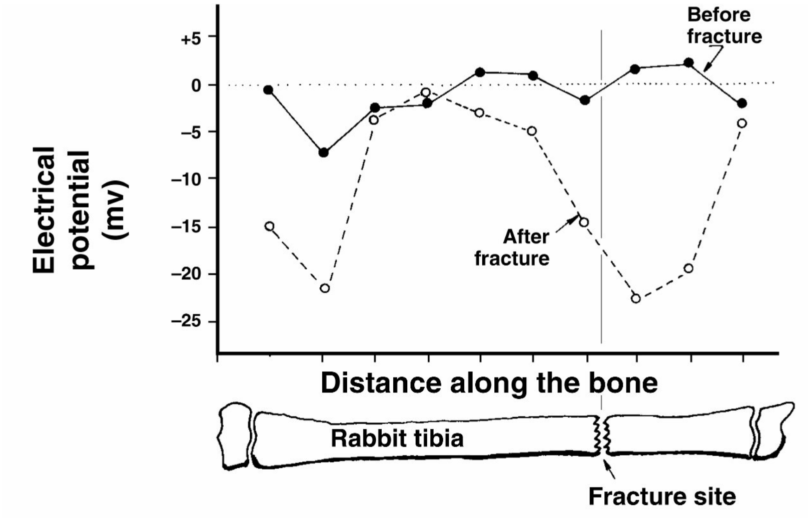

Figure 5.22. Skin surface of rabbit limb before and after fracture. Note that the fracture site has an increased electronegative potential. Reprinted with permission from [11]. Copyright © 1966, Journal of Bone and Joint Surgery.

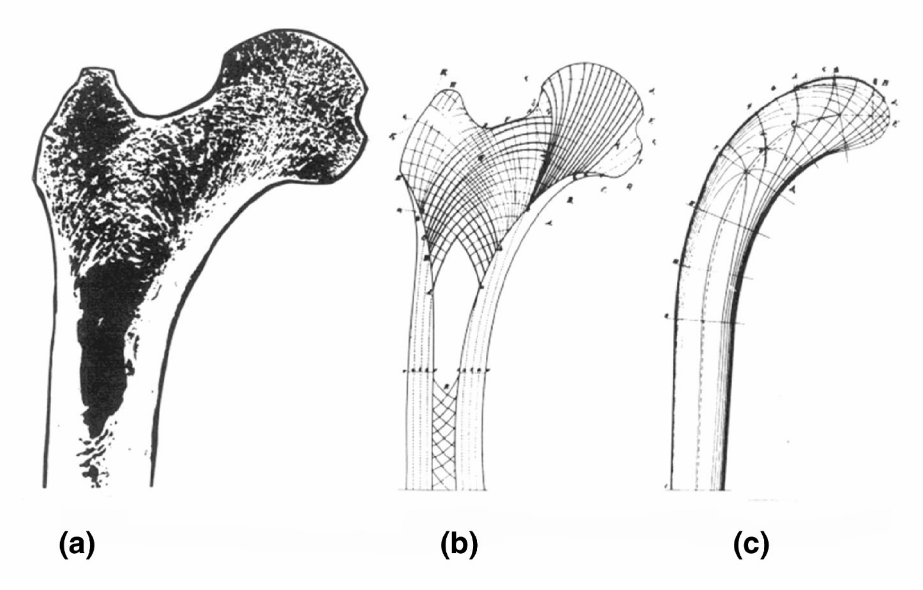

Figure 5.23. Frontal section through the proximal end of the femur (a); line drawing of the cancellous structure (b); Culmann's crane (c). Reprinted with permission from [30]. Copyright © 1892, Hirchwild.

which will in turn signal more bone mineral deposition. The exact mechanism, however, cannot be pinpointed by this theory. The remodeling process can be mediated by biomechanical activities of enzymes and other chemical species such as amino acids and minerals, as shown in Figure 5.25.

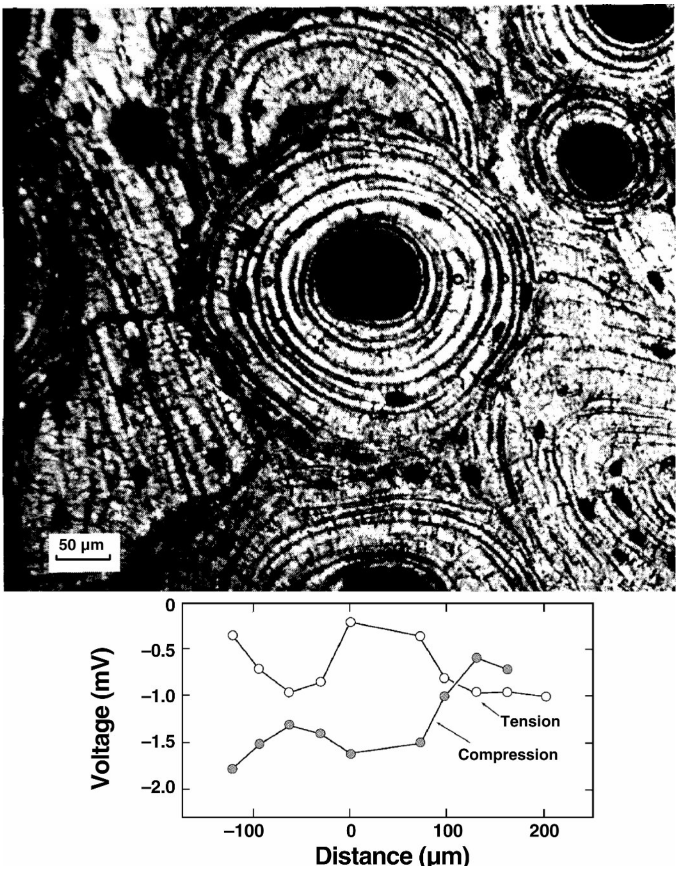

Figure 5.24. Tension and compression data for a human osteon. Reprinted with permission from [28]. Copyright © 1979, Wiley.

Bone remodeling can be separated into two categories; surface and internal remodeling [5]. Surface remodeling is the resorption and deposition of bone material on the external surfaces of bone (periosteal surfaces), while internal remodeling is reinforcement and resorption in the endosteal surfaces, resulting in changes in the bulk density of the bone. In cancellous bone, this latter process can be accomplished by increasing the thickness of each trabecula. In cortical bone, internal remodeling occurs by changing the diameter of the lumina of the osteons and by totally replacing osteons (osteoporosis).

5.4. BIOCOMPATIBILITY

In this section we discuss the biocompatibility of ceramics and glasses. However, some are used as cardiovascular devices such as the carbon heart valve disc, in which

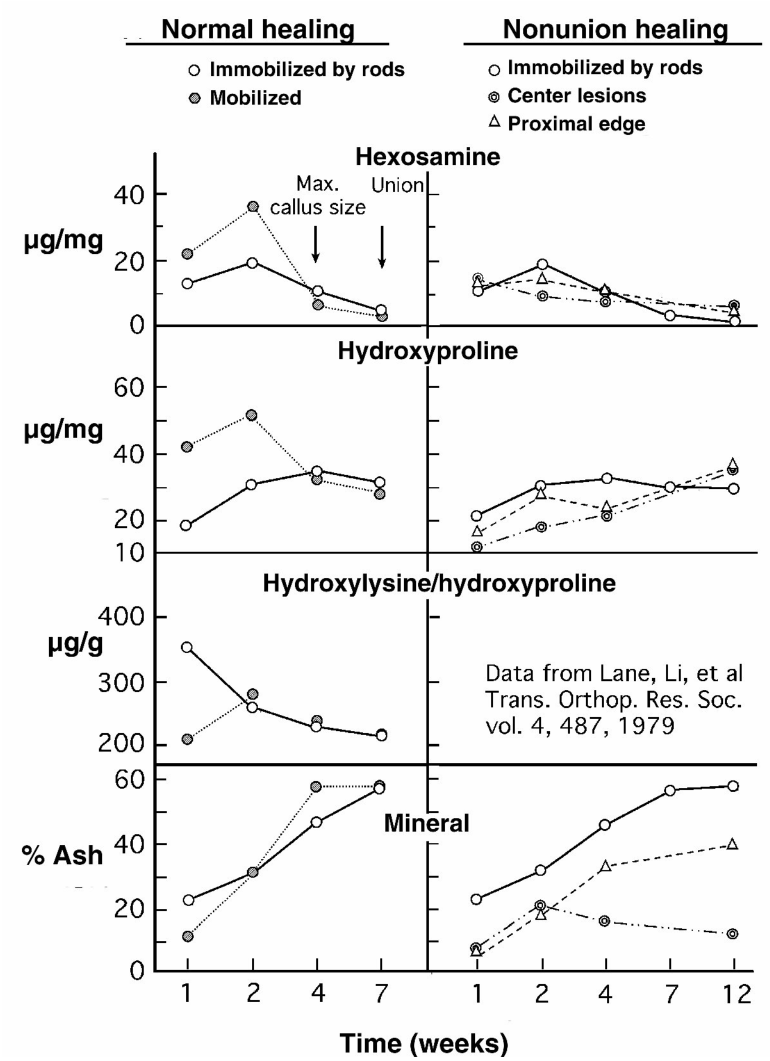

Figure 5.25. An overview of metabolic interrelationships within the callus. Reprinted with permission from [19]. Copyright © 1975, Lippincott Williams & Wilkins.

case we have to involve blood compatibility. Biocompatibility is the interaction of materials and tissues in vivo. The body environment will have a great effect on the surface, mechanical, and chemical properties of the material, and the immunologic, carcinogenic, and allergenic reactions of the tissue. Table 5.9 offers broad guidelines for assessment of biocompatibility. Figure 5.26 gives a schematic illustration of biocompatibility.

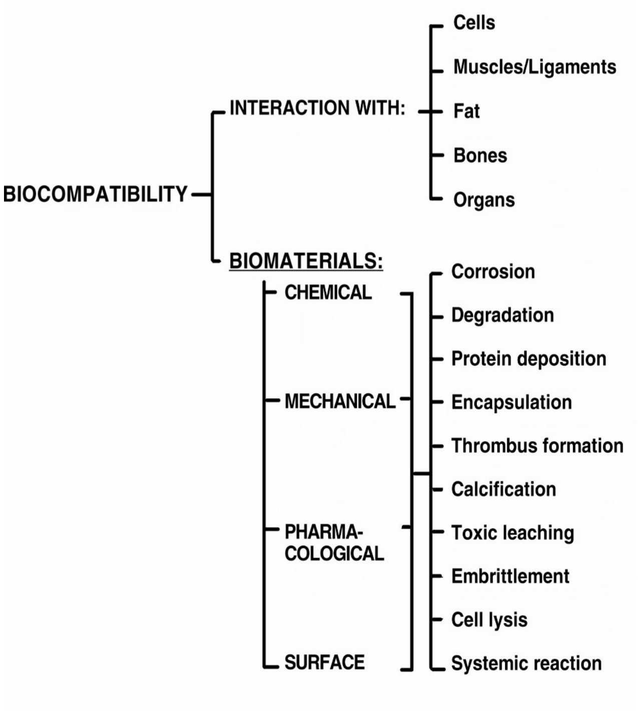
BIOCOMPATIBILITY
INTERACTION WITH:
Cells
Muscles/Ligaments
Fat
Bones
Organs
BIOMATERIALS:
CHEMICAL
MECHANICAL
PHARMA-COLOGICAL
SURFACE
Corrosion
Degradation
Protein deposition
Encapsulation
Thrombus formation
Calcification
Toxic leaching
Embrittlement
Cell lysis
Systemic reaction

Figure 5.26. Schematic illustration of biocompatibility. Modified with permission from [16]. Copyright © 1998, Wiley.

Table 5.9. Biocompatibility Assessment Guidelines

A. Data required to assess suitability
   1. Material characterization. Identify the chemical structure of a material and any potential toxicological hazards. Residue levels. Degradation products. Cumulative effects of each process.
   2. Information on prior use. Documented proof of prior use, which would indicate the suitability of a material.
   3. Toxicological data. Results of biological tests that would aid in assessing potential reactions (adverse or otherwise) during clinical use.

B. Supporting documents
   1. Details of application: shape, size, etc.
   2. Chemical breakdown of all materials involved in the product.
   3. A review of all toxicity data on those materials in direct contact with body tissues.
   4. Prior use and details of effects.
   5. Toxicity tests [FDA or ISO (International Standard Organization) guidelines]
   6. Final assessment of all information, including toxicological significance.

FDA internet address: http://www.fda.gov/cdrh/index.html. The CDRH (Center for Devices and Radiological Health) of the FDA administers medical devices.
Adapted with permission from [16]. Copyright © 1998, Wiley.

PROBLEMS

5.1. Calculate x in Eq. (5.9) for bone with a Young's modulus of 17 GPa by assuming

$$V_m = V_c, \quad E_m = 100 \text{ GPa}, \quad E_c = 0.1 \text{ GPa}.$$

5.2. If a bone has a porosity of 18.9%, what is its modulus of elasticity if the modulus without pores is the same as that of hydroxyapatite?

5.3. The viscoelastic properties of compact bone have been described by using the three-element model shown in Figure 5-16.

a. Derive differential equations for the model. Assume the spring and dashpot follow ideal elastic and viscous behavior, respectively.

b. Solve the differential equation for stress (σ) for a stress-relaxation behavior of the model.

c. What are the shortcomings of the model? Compare with the behavior of bone in vivo and the model.

5.4. Estimate the strength of a compact bone using the Griffith theory of fracture. Compare with known values.

5.5. Plot E_t versus V_m using the Voigt and Reuss models and assuming $E_m/E_c = 100$. At $V_m = 50\%$, what are the modulus values according to the Voigt and Reuss models?

5.6. There are many "bone substitutes" on the market. List an ideal bone substitute and propose your own. See Chapter 9 for additional reading on this subject.

5.7. Bone is similar to such soft tissue as skin, in that the organic part of the bone has similar constituents (e.g., collagen and polysaccharide). Would it be advantageous to use demineralized bone as a soft tissue substitute? Give your rationale and methods.

5.8. Design an experiment to prove or disprove the effect of BMPs on bone fracture healing.

5.9. Such alternative medicine as acupuncture can an effective in some diseases. Can one use ceramic- or glass-coated needles? How would you prove its efficacy?

5.10. Read Hohling HJ, Barckhaus RH, Krefting ER, Althoff J, Quint P. 1990. Collagen mineralization: aspects of the structural relationship between collagen and apatite crystallites. In *Ultrastructure of skeletal tissues: bone and cartilage in health and disease*, pp. 41–62. Ed E Bonucci, PM Morra. Boston: Kluwer Academic Publishers.

5.11. Read Chapters 9 and 10 in Park JB, Lakes RS. 2007. *Biomaterials: an introduction*, 3rd ed. New York: Springer.

SYMBOLS/DEFINITIONS

Greek Letters

ε: strain.
ρ: density.
σ: stress.

Roman Letters

A: area.
E: Young's modulus, a measure of stiffness.
P: load (force) or pressure (force per area).
V: volume (fraction).
w/o: weight percent.

Definitions

Canaliculi: Small channels (~0.3 mm in diameter) radiating from the lacunae in bone tissue.

Cementum: Calcified tissue of mesodermal origin covering the root of a tooth.

Crown: A crown-shaped structure, especially the exposed or enamel-covered portion of a tooth. It is largely (97%) made of hydroxyapatite mineral. An artificial replacement of the exposed surface or the upper part of a tooth is also called a crown.

Dentin: The chief substance of a tooth, forming the body, neck, and roots, covered by enamel on the exposed part of the tooth and by cementum at the root. It is similar in composition and properties (but not structure) to compact bone.

Elastin: One of the proteins in connective tissue. It is highly stable at high temperatures and in chemicals. It also has rubber-like properties, hence its nickname “tissue rubber.”

Fibroblast growth factor (FGF): Basic FGF (bFGF) is a chemoattractant and mitogen for chondrocytes and is a key regulator in terminal differentiation of growth plate chondrocytes.

Glutamic acid (Glu): One of the essential amino acids occurring much more commonly in collagen than in elastin.

Glycine (Gly): One of the amino acids having the simplest structure.

Haversian system: Same as osteon.

Hydroxyapatite: Mineral component of bone and teeth. It is a type of calcium phosphate, with composition $Ca_{10}(PO_4)_6(OH)_2$.

Hydroxyproline (Hypro): One of the amino acids commonly occurring in collagen molecules.

Insulin-like growth factor (IGF): Cell mitogen that promotes cartilage matrix synthesis.

Lacuna: A pore (~10 × 15 × 25 μm) in Haversian bone; lacunae often contain osteocytes (bone cells).

Mixture rule: The properties of a material made up of many materials depend linearly on the relative amount of each material.

Osteons: Large fiber-like structure (150~250 μm in diameter) in compact bone. Concentric layers or lamellae surround a central channel or Haversian canal, which contains a small blood vessel. Each lamella contains smaller fibers. Osteons, also called Haversian systems, are separated by cement lines.

Piezoelectricity: Electric polarization resulting from mechanical stress upon a material; conversely, deformation resulting from an imposed electric field.

Platelet-derived growth factor (PDGF): Released from platelet α granules, a potent mitogen, especially for fibroblasts. Associated with increases in type I collagen and modulation of local blood flow, PDGF has a significant positive role in wound healing.

Polysaccharides: Polymerized sugar molecules found in tissues as lubricant (synovial fluid), cement (between osteons, tooth root attachment), or complexed with proteins (e.g., glycoproteins, mucopolysaccharides).

Pulp: Richly vascularized and innervated connective tissue inside a tooth.

Proline (Pro): One of the amino acids commonly occurring in collagen molecules.

Reuss model: Modeling the properties of a material assuming an inverse volume fraction of each component.

Tropocollagen: Precursor of collagen. Has a right-handed superhelical coil structure, which is in turn made up of three left-handed helical peptide chains.

Volkmann's canal: Vascular channels in compact bone that are not surrounded by concentric lamellae, as are Haversian canals.

Voigt model: Modeling properties of a material assuming an additive volume fraction of each component.

REFERENCES

1. Black J. 1981. *Biological performance of materials: fundamentals of biocompatibility*. New York: Marcel Dekker.
2. Bloom W, Fawcett DW. 1968. *A Textbook of Histology*, 9th ed. Philadelphia: Saunders.
3. Brighton C, Friedenberg Z, Black J. 1979. Evaluation of the use of constant direct current in treatment of nonunion. In *Electrical properties of bone and cartilage*, pp. 519–545, Ed C Brighton, J Black, S Pollack. New York: Grune & Stratton.
4. Chvapil M. 1967. *Physiology of connective tissue*. London: Butterworths.
5. Cowin S. 1981. *Mechanical properties of bone*. New York: ASME.
6. Currey JD. 1981. What is bone for? property–function relationships in bone. In *Mechanical properties of bone*, pp. 13–26. Ed SC Cowin. New York: ASME.
7. Dempster WT, Coleman RF. 1961. Tensile strength of bone along and across the grain. *J Appl Physiol* **16**:355.
8. Dempster WT, Liddicoat RT. 1952. Compact bone as a nonisotropic material. *Am J Anat* **91**:331–362.
9. Eriksson C. 1974. Streaming potentials and other water-dependent effects in mineralized tissue. *Ann NY Acad Sci* **238**:321–338.
10. Evans FG, Lebow M. 1952. The strength of human compact bone as revealed by engineering technics. *Am J Surg* **83**:326–331.
11. Friedenberg Z, Brighton C. 1966. Bioelectric potential in bone. *J Bone Joint Surg* **48A**:915–923.

12. Fung YC. 1981. *Biomechanics: mechanical properties of living tissues*. Berlin: Springer-Verlag.
13. Gross J. 1961. Collagen. *Sci Am* **204**:121–130.
14. Ham A, Harris W. 1971. Repair and transplantation of bone. In *The biochemistry and physiology of bone*, pp. 337–399. Ed G Bourne. New York: Academic Press.
15. Hench L, Ethridge E. 1975. Biomaterials: the interfacial problem. *Adv Biomed Eng* **5**:35–150.
16. Hill D. 1998. *Design engineering of biomaterials for medical devices*. New York: Wiley.
17. Hohling H, Ashton B, Koster H. 1974. Quantitative electron microscope investigation of mineral nucleation in collagen. *Cell Tissue Res* **148**:11–26.
18. Hollinger JO, Buck DC, Bruder SP. 1999. Biology of bone healing: its impact on clinical therapy. In *Tissue engineering: applications in maxillofacial surgery and periodontics*, pp. 17–53. Ed SF Lynch, RJ Genco, RE Marx. Chicago: Quintessence.
19. Ketenjian A, Arsenis C. 1975. Morphological and biochemical studies during differentiation and calcification of fracture callus cartilage. *Clin Orthop Relat Res* **107**:266–273.
20. King BG, Showers MJ. 1963. *Human anatomy and physiology*. Philadelphia: Saunders.
21. Lakes RS. 1993. Materials with structural hierarchy. *Nature* **361**:511–515.
22. Lakes RS. 2006. Properties of bone and teeth. In *Encyclopedia of medical devices and instrumentation*, pp. 523–540. Ed JG Webster. Hoboken, NJ: Wiley.
23. Liboff AB. 2006. Electrical treatment of bone-united fracture and spinal fusion. In *Encyclopedia of medical devices and instrumentation*, pp. 558–571. Ed JG Webster. Hoboken, NJ: Wiley.
24. McElhaney J. 1966. Dynamic response of bone and muscle tissue. *J Appl Physiol* **21**:1231–1236.
25. Park JB. 1984. *Biomaterials science and engineering*. New York: Plenum.
26. Park JB, Lakes RS. 2007. *Biomaterials: an introduction*, 3rd ed. New York: Springer.
27. Piekarski K. 1978. Structure, properties and rheology of bone. In *Orthopaedic mechanics: procedures and devices*. Ed D Ghista, R Roaf. New York: Academic Press.
28. Starkebaum W, Pollack S, Korostoff E. 1979. Microelectric studies of stress-generated potential in four-point bending of bone. *J Biomed Mater Res* **3**:729–751.
29. Triffit JT. 1980. The organic matrix of bone tissue. In *Fundamental and clinical bone physiology*, pp. 45–82. Ed MR Urist. Philadelphia: Lippincott.
30. Wolff J. 1892. *Das Gesetz der Transformation der Krochen*. Berlin: Hirchwild.
31. Woo S-Y, Akeson W, Coutts R, Rutherford L, Doty D, Jemmott G, Amiel D. 1976. A comparison of cortical bone atrophy secondary to fixation with plates with large differences in bending stiffness. *J Bone Joint Surg* **58A**:190–195.
32. Wozney JM. 1999. Biology and clinical application of rhBMP-2. In *Tissue engineering: application in maxillofacial surgery and periodontics*, pp. 103–123. Ed SE Lynch, RJ Genco, RE Marx. Chicago: Quintessence.
33. Yamada H. 1970. *Strength of biological materials*. Baltimore: Williams & Wilkins.

6

ALUMINUM OXIDES (ALUMINA)

Many-colored alumina single crystals. These can be grown artificially. Polycrystalline alumina has been used for many years as spark plug insulators, high-voltage insulators, and implants. See Figures 6.11 and 6.15. Reprinted with permission from http://en.wikipedia.org/wiki/Image:Sapphire01.jpg. Please refer to the color section to view this image in full color.

Aluminum oxides have been used in industry as, for example, cutting tools, spark plug insulators, and sodium vapor lamp housings due to their excellent mechanical, electrical, chemical, and thermal properties [8]. Aluminum oxides have been investigated since 1907, when a patent was issued for refining alumina ceramic. However, commercialization of products came along much later in the 1920s and 30s, at which time high-temperature furnace materials were manufactured and sintering of alumina powder with some addition of MgO as an aid was developed.

Essentially pure alumina (>99.5%) has been utilized since the early 1970s as an implant material, especially for artificial joint prostheses (mostly hip) and teeth because of its excellent compatibility with tissues and its good mechanical properties (particularly friction and wear) [8]. However, it has a much lower tensile strength than compressive strength due to its brittleness (i.e., it cannot undergo plastic deformation like metals and plastics, as mentioned in §3.1). These characteristics limit its use to compressive loading applications.

Most alumina used for implant fabrication is either a polycrystalline solid of high density and purity or an artificially grown colorless single crystal similar to sapphire or ruby.

Table 6.1. Chemical Composition, Grain Size, and Density of Alumina

	Calcined, A-14	Tabular, T-60	ISO6474[b]	Biolox®[c]
Al_2O_3	99.6	99.5+	99.5+	99.7+
SiO_2 + alkali oxides[a]	0.12	0.06	–	–
SiO_2	–	–	<0.01	<0.01
Fe_2O_3	0.03	0.06	–	<0.015
Na_2O	0.04	0.20	<0.01	<0.01
CaO	–	–	–	<0.01
Grain size (μm)	–	–	<4.5	3
Density (g/ml)	3.8–3.9	3.65–3.8	>3.94	>3.95

[a] ASTM F603 specifies that combined SiO_2 alkali oxides should be less than 0.1% for surgical and dental implant application.

[b] After the 1981 issue. Also, combined $SiO_2 + Fe_2O_3 + Na_2O + CaO < 0.1\%$.

[c] Product of Feldmuhle (Plochingen, Germany).

Reprinted with permission from [13]. Copyright © 1970, American Ceramic Society.

6.1. SOURCE, COMPOSITION, AND STRUCTURE

Bauxite (hydrated aluminum oxide) and native corundum (aluminum oxide mineral) are the main sources of high-purity alumina. The most common refining process is the Bayer process, which yields α-alumina [12]. The Bayer process involves dissolution of crushed bauxite in sodium hydroxide (NaOH) solution under pressure at high temperatures (up to 300°C) to form a supersaturated sodium aluminate solution. The hydrated aluminum oxide is precipitated by seeding or as a metastable bayerite on reduction of the pH by carbon dioxide. Washing and dehydrating the precipitate at 1000~1200°C turns it into a low-temperature form of "calcined" alumina. Various other refining processes have been developed depending on the source of the raw materials [12]. Commercially available pure alumina typically contain 99.5—99.6% $A1_2O_3$, 0.06–0.12% SiO_2, 0.03–0.06% Fe_2O_3, and 0.04–0.20% Na_2O, and have a density of 3.65–3.9 g/cm^3, as given in Table 6.1. It is also possible to obtain 99.9% pure alumina prepared from ammonium alum. However, for implant work, the American Society for Testing and Materials (ASTM) specifies only 99.5% pure alumina, with less than 0. 1% of combined SiO_2 and alkali oxides (mostly Na_2O).

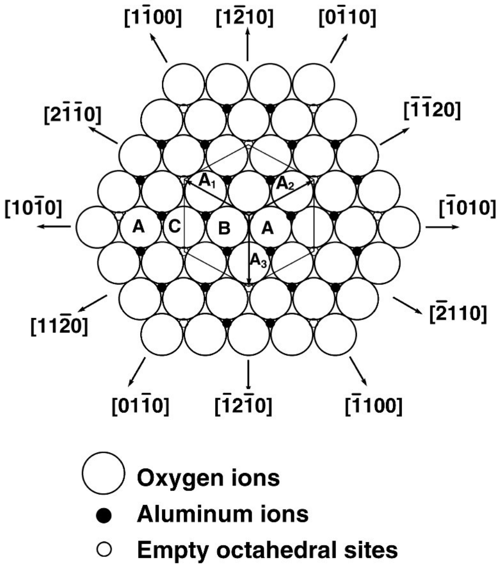

Figure 6.1. Basal plane of alumina crystal structure. Basal plane directions and hexagonal cell vectors are indicated. Reprinted with permission from [8]. Copyright © 1984, Springer-Verlag.

The crystal structure of α-alumina is hexagonal close packed (a = 0.4758 and c = 1.299 nm) and belongs to space group D_3^6d. The packing of Al and O in the basal plane of the hexagonal close-packed structure is shown in Figure 6.1. As noted in Table 2.2, a third of the available octahedral sites are vacant in the Al_2O_3 structure, so that three different types of cation layers exist. The coordination numbers for the Al^{3+} and O^{2-} are 6 and 4, and their radii are 0.053 and 0.138 nm, respectively.

Single crystals of alumina have been used successfully to make implants [14]. These are made by feeding fine alumina powders onto the surface of a seed crystal heated in an electric arc or oxyhydrogen flame, and then slowly withdrawing the crystal from the heat source as the fused powders build up. Alumina crystals up to 10 cm in diameter have been grown by this method. Pure single-crystal rubies can be used as watch crystal. Some can be colored by adding Cr_2O_3 (0.05%), which turns them pink, and they then can be used to fabricate lasers with a wavelength of 694 nm. An additional 0.5% Cr_2O_3 will make crystals that can be used in 701- and 704-nm laser crystals. Other metal ions (Ti^{3+}, Fe^{3+}) can be used to make blue sapphires.

Table 6.2. Mechanical Properties of Alumina

Properties and materials	Values
Bending strength (modulus of rupture, MPa)	
Sapphire	496–703
Ruby	345
Polycrystalline	241–482
Compressive strength (MPa)	
Sapphire	3055–3413
Polycrystalline	2069–3861
Tensile strength (MPa)	
Single crystal	490
Filaments	
Coated	1448
Uncoated	483
Polycrystalline	259
Modulus of elasticity (GPa)	
Single crystal	362.7
Polycrystalline	408.9
Poisson's ratio	
Sapphire	0.257
Polycrystalline	0.32

All measurements made at 25°C.

Reprinted with permission from [13]. Copyright © 1970, American Ceramic Society.

Example 6.1

Calculate the theoretical density of single-crystal alumina.

Answer:

Since the density is given as

$$\text{Density }(\rho) = \frac{\text{mass}}{\text{volume}} = \frac{4\sqrt{3}\text{ molecular weight}}{a_0^2 c_0\text{ Avogadro's number}},$$

then

$$\rho = \frac{4\sqrt{3}(27\times 2 + 16\times 3)\text{ gmol}^{-1}}{0.4758^2 \times 1.299\times 10^{-27}\text{nm}^3\ 6.02\times 10^{23}\text{mol}^{-1}} = \underline{3.99\text{ g/cm}^3}.$$

6.2. MECHANICAL PROPERTIES

As with all other brittle materials, the mechanical properties of polycrystalline alumina depend largely on grain size, grain distribution, and porosity. For example, the bend strength (σ_b) of a polycrystalline alumina with constant grain size can be expressed, similar to Eq. (5.10), as

$$\sigma_b = \sigma_0 e^{(-nP)}, \tag{6.1}$$

where σ_0 is the bend strength at zero porosity, n is a constant, and P is the porosity. The zero-porosity strength can be obtained by Eq. (3.57) and Figure 3.24. The relationship between grain size and porosity for fully dense alumina is given in Figure 6.2. Large experimental scatter can be observed, indicating the difficulty of this type of measurement.

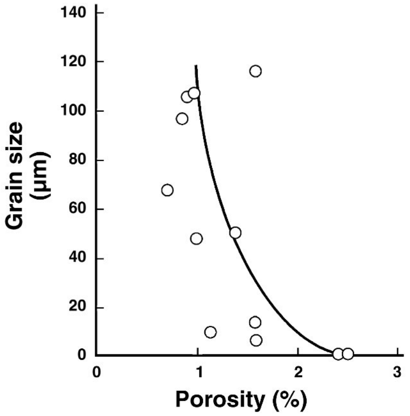

Figure 6.2. Grain size versus porosity of highly pure (99.9+%) fully dense alumina. Reprinted with permission from [27]. Copyright © 1963, American Ceramic Society.

When the porosity is below 2%, the grains become much larger, which according to Eq. (3.59) will decrease its strength. The size of the grains can be kept below 2 µm by adding 0.1% MgO. The typical microstructure of high-density alumina used for implants is shown in Figure 6.3. The addition of MgO will make the alumina almost translucent, so that it can even be used for housing sodium vapor lamps (Lucalox®). This type of alumina has not been used for implants. Table 6.2 gives the mechanical properties of typical implant alumina.

Alumina in general has a hardness of 20~30 GPa and a Mohs hardness of 9. The high hardness is accompanied by low friction and wear, which are major advantages in using alumina as a joint-replacement material, in spite of its brittleness. Table 6.3 gives the tribological properties of alumina. The long-term tribological properties of dense alumina are more favorable than those of other materials, as the coefficients of friction, wear volume, and surface roughness of alumina–alumina couples decrease with time, as shown in Figure 6.4. These properties derive from the fact that water and long-chain carboxylic acids are preferentially chemisorbed onto alumina surfaces, even at low water vapor concentrations (see Table 6.4). as proposed in Figure 6.5.

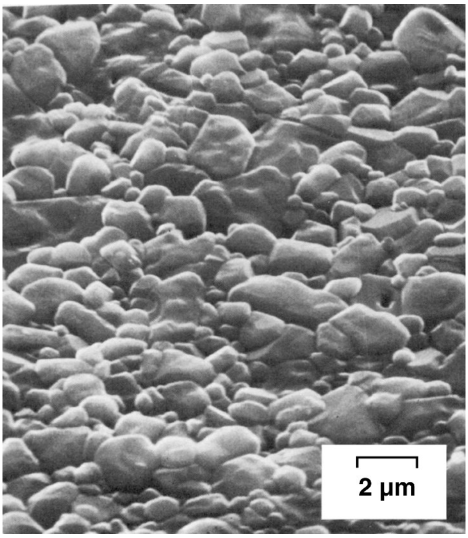

Figure 6.3. Microstructure of high-density alumina used for implants (100×). Reprinted with permission from [8]. Copyright © 1984, Springer-Verlag.

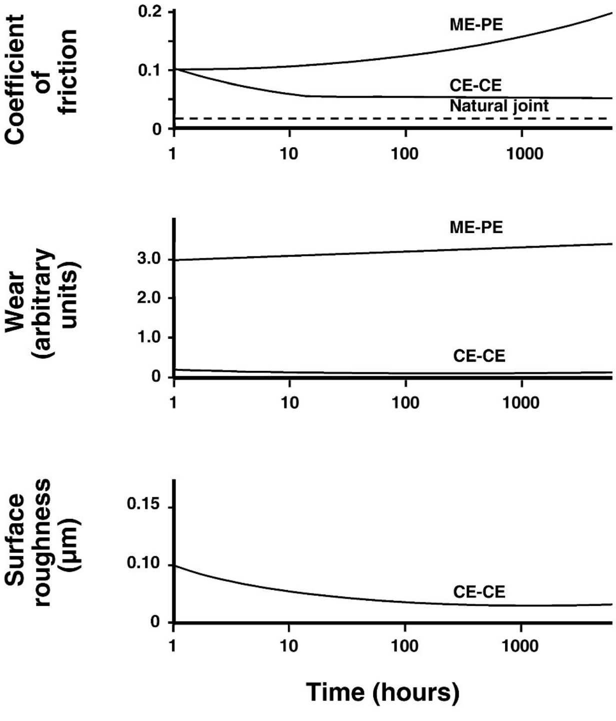

Figure 6.4. Tribological behavior of alumina: (a) friction, (b) wear, and (c) surface roughness [7]. Reprinted with permission from [7]. Copyright © 1980, Wiley.

Table 6.3. Tribological Properties of Alumina

Properties	Value	Test condition
Coefficient of friction		
Alumina–alumina	0.71	Dry
	0.09	Water
Alumina–UHMWPE	0.16	Dry
	0.05	Water
Wear rate (mg per 20 h)		
Alumina on alumina	0.10	Dry
UHMWPE on alumina	0.10	Dry

Reprinted with permission from [27]. Copyright ©1977, Wiley.

Table 6.4. Wear and Friction of High-Density Alumina at Various Relative Water Vapor Pressures

Relative water vapor pressure P/P_0	Wear (10^{-4} mm^{3}m^{-1})	Coefficient of friction
2.5×10^{-7}	139	0.50
4.0×10^{-3}	70	0.50
4.0×10^{-2}	3	0.40
7.0×10^{-1}	2	0.20
9.5×10^{-1}	–	0.03

Monomolecular coverage occurs when $P/P_0 = 10^{-2}$.
Reprinted with permission from [9]. Copyright © 1984, Springer-Verlag.

Example 6.2

Determine the average grain size and grain size number for the alumina microstructure depicted in Figure 6.3. Also, estimate the transverse bend strength of the alumina based on grain size from Figure 3.24.

Answer:

The number of grains per 10 cm of linear scale is about 20; therefore, the average size is 0.5 cm, which translates into 5 μm since it was magnified 1000×. The grain size index is standardized by the ASTM according to the equation $N = 2^{n-1}$, where n is the grain size number, and N is the number of grains per square inch at a linear magnification of 100×. Therefore, if one puts a one-square-inch grid on the picture randomly, one would obtain about 30 grains. However, this picture is magnified 1000× instead of 100×, and the number of grains per square inch is 3000. Therefore, $3000 = 2^{n-1}$, and $n = 12.55$. The grain size number is close to 13. According to Figure 3.24, the transverse bend strength of 5-μm grain size is about 300 MPa, which is higher than the tensile strength given in Table 6.2 for alumina.

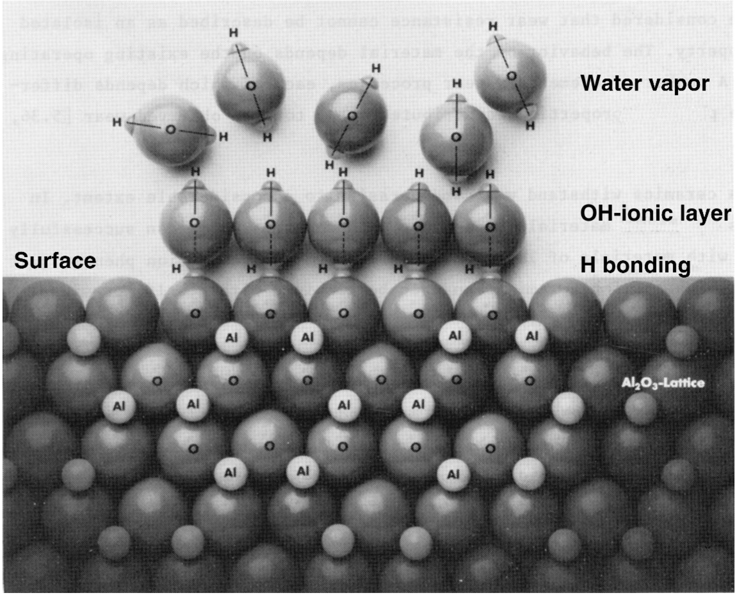

Figure 6.5. Adsorption behavior of an alumina ceramic surface. Reprinted with permission from [8]. Copyright © 1984, Springer-Verlag.

6.3. FATIGUE PROPERTIES AND SERVICE LIFE

It is of great interest whether inert ceramics such as alumina can be fatigued in either dynamic or static conditions. In one study it was shown that the fatigue strength of alumina decreases with the presence of water above critical stress [10]. This decrease in fatigue strength is due to delayed crack growth, which is accelerated by the water molecules. However, another study showed that reduced strength results if water absorption is observed by scanning electron microscopy of the broken specimens, but they did not detect any decrease in strength for samples that showed no watermarks on the fractured surface (Figure 6.6). It was suggested that the presence of minor amounts of silica in one lot may have contributed to the permeation of water molecules, which is detrimental to strength [15]. It is not clear whether the same static fatigue mechanism operates in single-crystal alumina. It is, however, reasonable to assume that the same static fatigue will occur if the crystals contain flaws or impurities, which will act as sources of crack initiation instead of grain boundaries for the polycrystalline alumina and cause the crack to grow under stress.

The *impact fatigue* property of alumina is important for application of such load-bearing implants as joint replacements. This is similar to dynamic fatigue except that the load is applied by impact, e.g., by a pendulum. One such test result is shown in Figure 6.7, which is similar to a Wohler graph of stress versus number of cycles. The

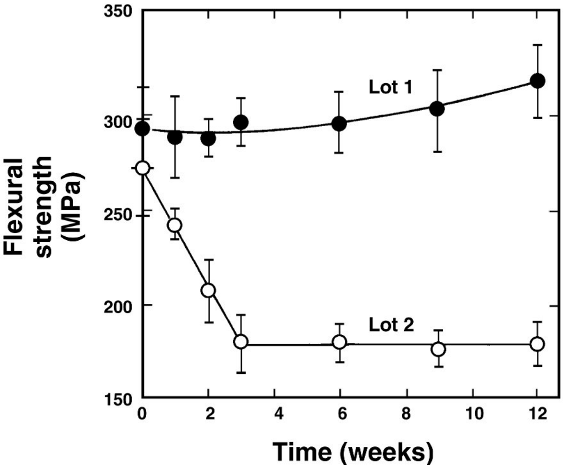

Figure 6.6. Flexural strength of dense alumina rods after aging under stress in Ringer's solution. Reprinted with permission from [15]. Copyright © 1978, Wiley.

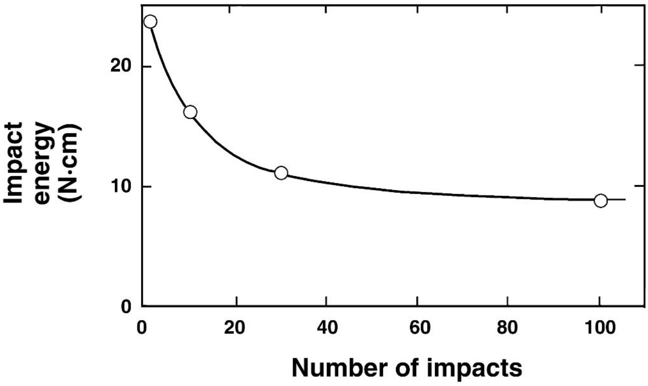

Figure 6.7. Impact fatigue strength of alumina measured by a pendulum test. Reprinted with permission from [7]. Copyright © 1980, Wiley.

failure on each specimen was judged by appearance of the first crack. Obviously, the test cannot detect internal cracks or microcracks, which are beyond the capability of observation instruments like optical microscopes. This is why it is quite difficult to predict the fatigue life of ceramic materials like alumina in dynamic conditions.

Some have used probability theory to understand the static- and dynamic-fatigue behavior of polycrystalline alumina [4]. The cumulative probability of failure under stress for a constant surface area is given by

$$F = 1 - \exp\left[-\left(\frac{\log t - \log t_u}{L_0}\right)^m A\right], \tag{6.2}$$

where t is the time to failure, t_u is the lower bound of the time to failure, L_0 is a scale parameter, A is the surface area under stress, and m is the Weibull modulus. Figure 6.8 shows the results of static and dynamic fatigue tests of alumina at room temperature, from which two observations can be made: (1) the environmental has a drastic effect on fatigue life, which is again due to stress corrosion with water vapor, and (2) the resistance of a polycrystalline alumina ceramic to cyclic loading is lower than static loading at room temperature, which may be significant in implant design.

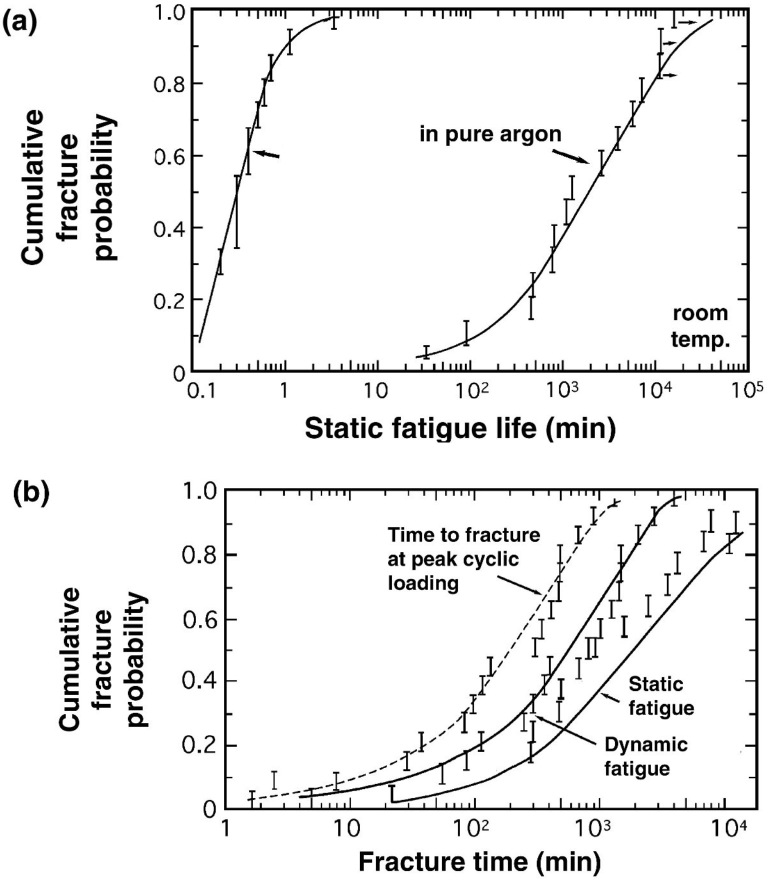

Figure 6.8. (a) Time to fracture under static loading versus fracture probability in air and (50% RH) in pure argon at room temperature. (b) Cumulative fracture probability versus fracture time for static and dynamic fatigue tests at room temperature. Reprinted with permission from [4]. Copyright © 1974, Plenum.

Some have predicted the fatigue life of alumina and Bioglass® (glass-ceramic, see §8.3) coated alumina based on fracture mechanics theory, which is based on the assumption that fatigue is controlled by the slow crack growth of preexisting flaws [23]. Generally, the strength distribution of ceramics in an inert atmosphere (σ_i) can be correlated to the probability of failure (F) by the Weibull relationship, which according to Trantina [29] is similar to Eq. (6.2):

$$\ln\ln\left(\frac{1}{1-F}\right) = \mathrm{min}\left(\frac{\sigma_i}{\sigma_0}\right), \tag{6.3}$$

where m and σ_0 are constants. Figure 6.9 shows a good fit for Bioglass®-coated alumina tested in a tris buffer solution and liquid nitrogen [23].

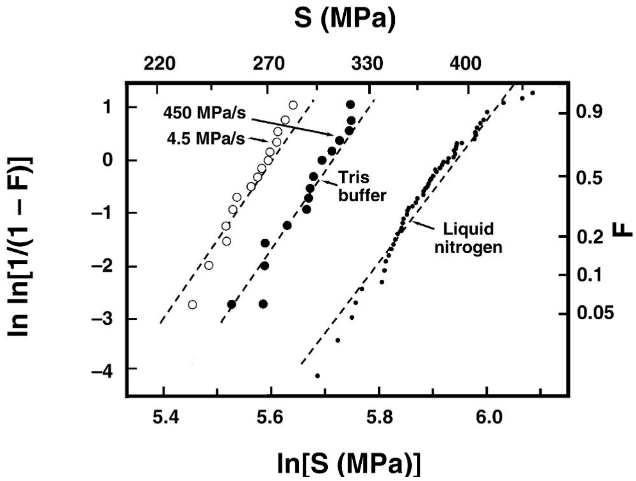

Figure 6.9. Plot of ln ln(1/1 – F) versus ln σ for Bioglass®-coated alumina in a trishydroxyamino methane buffer solution and liquid nitrogen. Reprinted with permission from [23]. Copyright © 1979, Wiley.

A minimum service life, $t_{\min}$, can be predicted if each sample is subjected to testing at stresses greater than those expected during service:

$$t_{\min} = B\sigma_P^{N-2}\sigma_a^{-N}, \tag{6.4}$$

where σ_P is the proof-test stress, σ_a is the applied stress, and B and N are constants. Rearranging Eq. (6.4) yields

$$t_{\min}\sigma_a^2 = B\left(\frac{\sigma_P}{\sigma_a}\right)^{N-2}, \tag{6.5}$$

which results in a straight line if log $t_m\sigma_a^2$ is plotted against log(σ_P/σ_a), with a slope of $N - 2$ and an intercept equal to B (see Fig. 6.10).

Example 6.3

Calculate the proof-test stress of an alumina ceramic implant for a minimum lifetime of 50 years under constant applied stress of normal body weight (700 N). Assume a cross-sectional area of 2 cm^2 and that the dynamic loading can be 10 times the static loading.

Answer:

The stress on the alumina implant is [(700 N)/(2 cm^2)] = 3.5 MPa. If we assume dynamic loading, the maximum stress would be 35 MPa. Therefore,

$$\log t_{\min}\sigma_a = \log[50 \text{ yr} \times 365 \text{ days/yr} \times 24 \text{ hr/day} \times 60 \text{ min/hr} \times 60 \text{ s/min} \times 35 \text{ MPa}]$$

$$= 10.74.$$

From Figure 6.7, σ_p/σ_a = 2.35 in Ringer's solution; therefore, σ_p = 82.25 MPa. This value should be increased considerably due to the more hostile environment of the body.

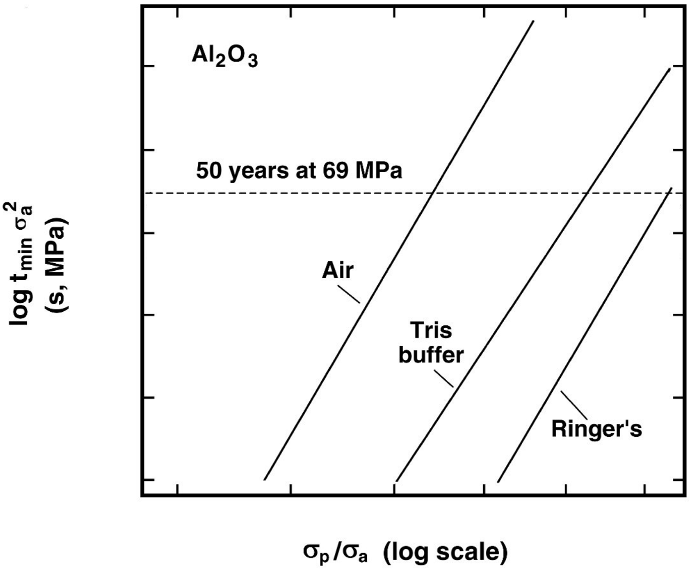

Figure 6.10. Plot of Eq. (6.4) for alumina after prooftesting. N = 43.85; log B = 3.256, m = 13.21, and σ_0 = 55,728 (psi). Reprinted with permission from [23]. Copyright © 1979, Wiley.

6.4. APPLICATIONS

In biomedical applications, alumina has considerable advantages over other materials because of its inertness, which offers excellent biocompatibility and nonsensitization of tissues. In addition, its excellent wear and friction properties in vivo make it suitable for artificial joint surfaces. Its compressive strength being higher than its tensile strength makes it better suited for compressive loading, as in artificial joints and teeth.

6.4.1. Joint Replacements

As mentioned earlier, one of the most important aspects of brittle materials is the reliability or predictability of in-service performance. The distribution of microcracks in the material and the dependence of mechanical properties on the Griffith flaws make it essential to proof-test the implants, as mentioned in §6.3. Some have addressed the design criteria of ceramic-metallic hip joints based on strength analysis, proof-testing, and structural testing [16], where the femoral head sphere was made of alumina ceramic and the stem of CoCrMo alloy. The acetabular cup was made of ultra-high-molecular-weight polyethylene (UHMWPE), as shown in Figure 6.11.

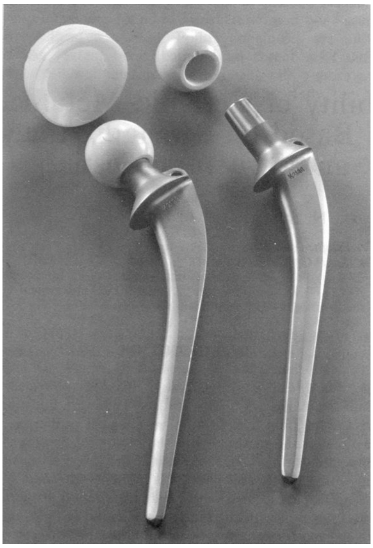

Figure 6.11. Total hip joint implant with alumina ceramic head sphere, metal stem, and UHMW polyethylene cup. Reprinted with permission from [16]. Copyright © 1980, Wiley.

The effect of size (or volume, see §3.3) and fracture toughness, K_{IC}, which is the intrinsic material property, is illustrated in Figure 6.12. The critical stress of fracture, σ_c, is given as

$$\sigma_c = \frac{K_{IC}}{Y\sqrt{a}}, \tag{6.6}$$

where a is crack size and Y is a geometric factor. Equation (6.6) is similar to Eq. (3.22). The combined effect of K_{IC} and $V_{\text{effective}}$ is quite drastic in terms of strength due to the statistical nature of the distribution of the largest-sized Griffith flaws.

The issue of reliability of the ceramic head makes proof-testing very important, as studied in a previous section and as shown in Figure 6.13. If every implant is proof-tested at a stress much higher than the actual stress the implant is subjected to in vivo,

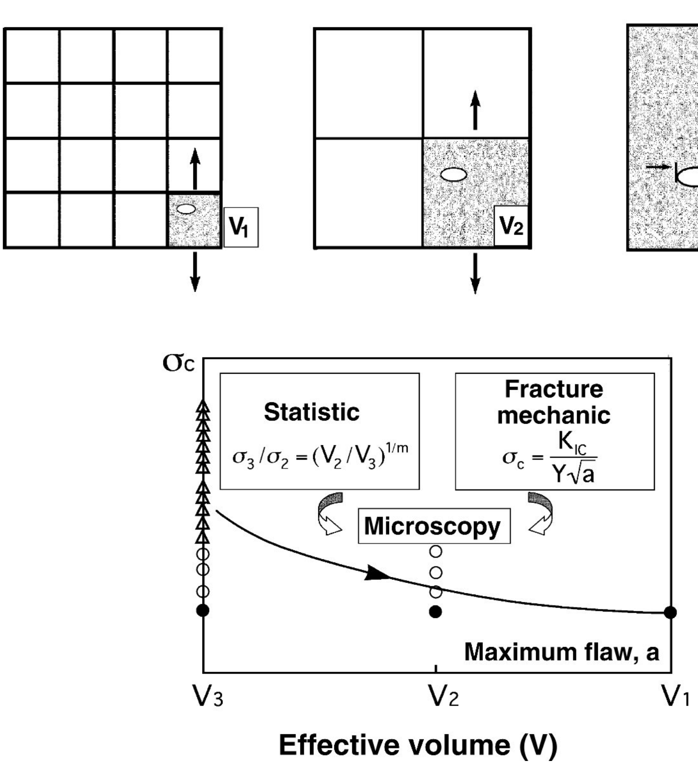

Figure 6.12. The K_{IC} and V_{eff} model of alumina ceramic. Reprinted with permission from [16]. Copyright © 1980, Wiley.

the surviving specimens can be assured of a certain lifetime. The same should be true of the whole structure of the joint, i.e., the stem, ceramic head, and acetabular cup. Therefore, one has to subject the whole structure to the same type of proof-testing, which is much more difficult to accomplish due to the many contributing factors involved. One such test result is shown in Figure 6.14, where the test load was a sinusoidal cyclic load between 1000 and 9000 N (body load = 700 N) at 37 Hz (very high) that lasted for between 10^6 and 10^7 cycles. If the specimen lasted more than 5×10^6 cycles under the given conditions, the structure was proof-tested to last longer than the normal service life. One has to be careful interpreting such results since the body environment is much more hostile than the Ringer's solution in which the structure was tested, and also an accelerated test sometimes underestimates the actual dynamic fatigue life. Other problems related to the reliability of the implant is implant fixation and aseptic loosening [21]. Yet other problems include tissue reaction to wear particulates, infection, ectopic bone formation, and pain. Nevertheless, the femoral head spheres have been used widely since 1974, mostly outside of the United States. One report estimated that more than 2 million were used by 1994 [31].

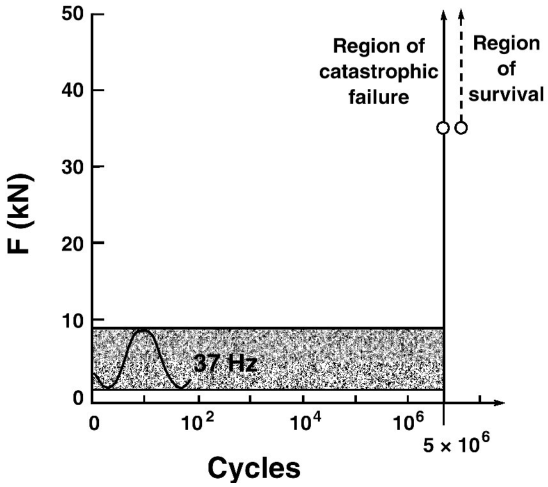

Figure 6.13. Results of dynamic testing of a total hip joint structure. Reprinted with permission from [16]. Copyright © 1980, Wiley.

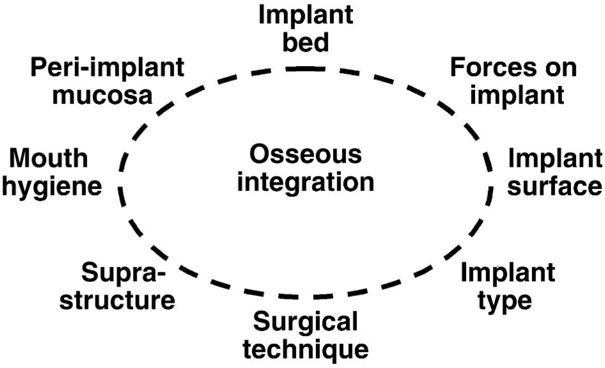
Implant bed
Peri-implant mucosa
Forces on implant
Mouth hygiene
Osseous integration
Implant surface
Supra-structure
Implant type
Surgical technique

Figure 6.14. Factors affecting the outcome of dental implants. Reprinted with permission from [30]. Copyright © 1989, Elsevier.

The use of alumina ceramics in other joints (e.g., the knee) has been attempted but has not gained much popularity [11]. This is due to the much larger range of motion (ROM) in the knee than in the hip, as well as the much smaller surface contact area and greater incongruency. Again, fixation is much more difficult in the hip than in the knee joint.

6.4.2. Dental Implants

As with joint implants, the most difficult problem in this area is implant fixation. The factors affecting the success of dental implants are depicted in Figure 6.14. This has led to many attempts to make dental root implants with an increased surface area. Root surfaces can be coated with bone-integrating or bonding materials (see Fig. 12.19).

Attempts have been made to fix alumina implants by rendering their surfaces porous or grooved in which to allow tissues to grow, as shown within the dental root shown in Figure 12.18. Many investigations of this type have been conducted in order to understand the mode and kinetics of tissue ingrowth into porous implant materials. This type of (bone) cement-free direct fixation in total artificial hip prostheses has been tried, but so far only the acetabular cup with a porous metal-back component has been stabilized. More discussion on the ankylosis or osseo (osteo) integration with bone can be found in §12.2.3.

6.5. FURTHER THOUGHTS

Alumina has been used for a long time to fabricate orthopedic and dental implants [24]. Newer studies on using alumina ceramics for pairing alumina–alumina [2,13,20,25] and alumina–zirconia [17,18] have shown an interesting approach to the friction and wear problems encountered with other materials, metals, and polymers, although these approaches are not new [2,19,22]. It would be desirable to prevent the catastrophic failure of ceramics and glasses by developing new methods of detecting the growth of microcracks and preventing them from growing [6]. Other issues such as porosity and impurities can be overcome by careful quality control during manufacture [1].

The use of ceramics for crowns in dental implants has been around for many years. Their popularity has been due to their strength and aesthetics, despite their brittleness and the expense involved. The retentive strength of ceramic crowns using different luting agents is another issue [9]. In this and other similar applications, the softer zirconium oxide (Chapter 7) may be better suited. Zirconia, however, undergoes phase transformation in vivo, which lowers its mechanical properties more than originally predicted. Alumina has been used as dental roots in polycrystalline (Synthodont®) or single-crystal [28] form. However, Ti-based alloys are used more prevalently for such applications due to the perception that they integrate better with alveolar or maxillary bone (osseointegration) [3]. The reasons for such behavior at the interface of bone and Ti alloys are not clear. Such behavior has not been reported in orthopedics. Instead, a thin layer of collagen membrane separates them. All other conditions being equal, the thickness of the membrane depends largely on the motion of implants relative to tissue.

PROBLEMS

6.1. Calculate the theoretical density of single-crystal alumina.

6.2. Determine the average size and grain size number for the alumina microstructure shown in Figure 2.8. Also, estimate the transverse bend strength of the alumina based on the grain size from Figure 3.24.

Hint: The grain size index is standardized by the ASTM according to $N = 2^{n-1}$, where n is the grain size number and N is the number of grains per square inch at a linear magnification of 100×.

6.3. Calculate the proof-test stress of an alumina ceramic implant for a minimum lifetime of 50 years under constant applied stress of normal body weight (700 N). Assume a cross-sectional area of 2 cm^2, and the dynamic loading can be 10 times static loading.

6.4. Alumina was measured for its static fatigue properties and plotted as follows:

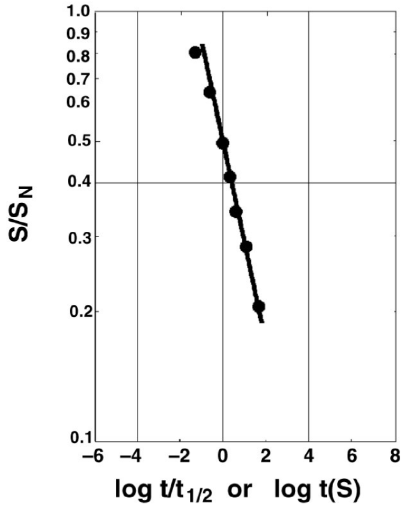

a. Assuming you can estimate the result by a straight line drawn according to log $t = -n \log s + c$, estimate n.
b. Estimate the time for proof-testing soda lime glass for 10,000 psi if the glass is to support 3000 psi for 10^6 sec.
c. Briefly state the theory of static fatigue proposed by Hillig and Charles.
d. Would you expect to improve static fatigue properties if the surface is treated by fire-polishing? Why?

6.5. From the following phase diagram of SiO_2–Al_2O_3, for a 50–50 (mol%) solid solution, answer:

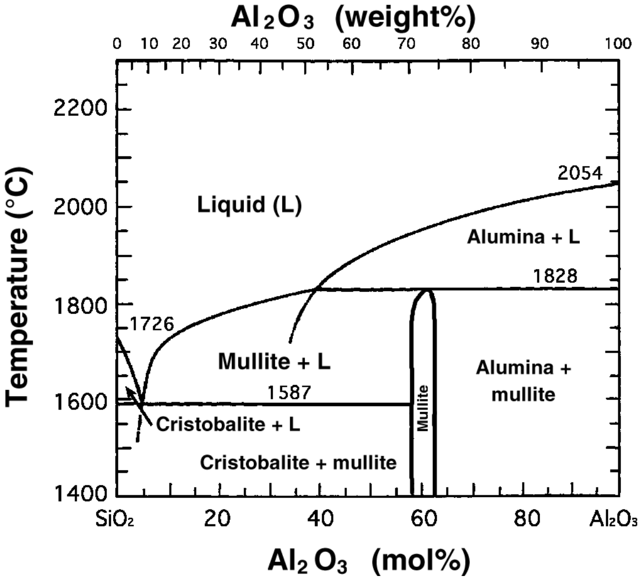

a. What phase(s) exist at 1600 and 1500°C?
b. What are the compositions of each phase at 1600°C?
c. What are the percentages of each phase at 1600°C?
d. List the eutectic reaction(s) for the system.

6.6. Which of the following parameters can affect the strength of sintered alumina? Write yes if the parameter can increase strength and no if it cannot.
a. Increased viscosity of quenching media.
b. Increased quenching temperature.
c. Applying glazes.
d. Increased diameter of the specimen.
e. What other factors can you suggest that would strengthen sintered alumina?

6.7. A series of alumina rods of circular cross-section (0.25-inch diameter) fractured at an average stress of 20,000 psi when bent. Assume that the modulus of elasticity is 10^7 psi, a Poisson's ratio of 0.3, and a surface tension of 300 dynes/cm, and $\sigma_f = \sqrt{E\gamma / c}$ (1 psi = 6895 Pa, 1 dyne = 10^{-5} N).
a. Calculate the average depth of the Griffith flaw.
b. Calculate the crack tip radius, ρ ($= 8\gamma E/\sigma_t^2$), assume $\sigma_t = E/50$.
c. It is desired to coat this rod with another glass with a different coefficient of thermal expansion but with essentially the same physical properties in order to double the average strength of the rods. Should the new glass have a higher or lower coefficient than the parent rod?

6.8. From the data given for alumina ceramic, answer the following:

Properties	As received	Glazed & quenched (1500°C, silicone oil)
σ_f (psi)	50,000	80,000
ν	0.25	0.3 (glaze)
α ($\times 10^{-7}$ °C)	65	53 (glaze)
E (GPa)	390	390

a. Estimate the amount of thermal shock (ΔT) needed to fracture an as-received sample: $\sigma_f = E\alpha\Delta T/(1-\nu)$.

b. Would you expect a higher ΔT if the as-received sample was flame polished on the surface? Explain.

c. Estimate K_{IC} for the as-received sample if the largest flaw depths are 1 μm: $K_{IC} = \sqrt{2\gamma E/(1-\nu^2)}$; assume that $\gamma = \sigma_f^2\rho/8E$.

d. Can you use the same K_{IC} value obtained for the single-crystal sapphire to estimate flaw depth for the crystalline alumina? State your reasons.

6.9. Express the relationship between transverse bend strength and grain size given in the following illustration:

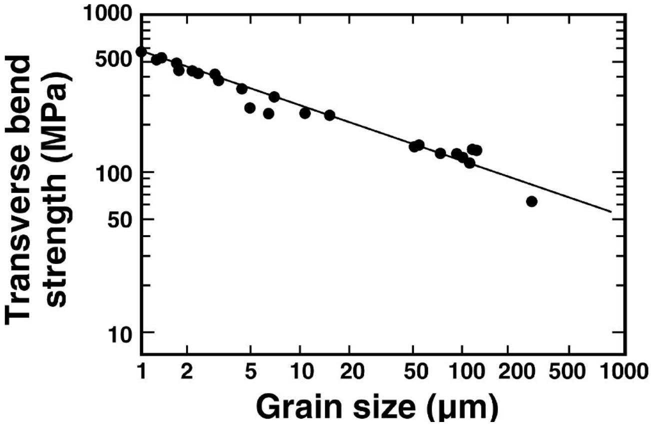

6.10. The relationship between the modulus of rupture and porosity of alumina is given [5].

a. Obtain a relationship similar to Eq. (6.1).

b. Plot the same curve for log porosity versus modulus of rupture.

c. What conclusions can you draw?

d. Can you use the relationship between porosity and grain size of Figure 6.2 to relate the two variables (porosity and grain size) to modulus?

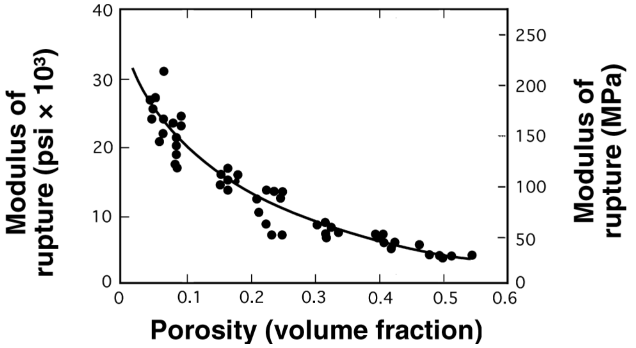

6.11. Can you make a heart valve disc from alumina? Give the requirements for the disc and describe the design in detail for a "ruby/sapphire heart valve."

6.12. Read the following and list two or more shortcomings of Maier's method of evaluating the ceramic.

a. Hulbert SF, Klawitter JJ. 1976. Ceramics as a new approach to the improvement of artificial joints. In *Advances in artificial hip and knee joint technology*, Engineering in Medicine Vol. 2, pp. 287–293. Ed M Schaldach, D Hohmann. Berlin: Springer-Verlag.

b. Maier HR, Stark N, Krauth A. 1980. Reliability of ceramic-metallic hip joints based on strength analysis, proof, and structural testing, In *Mechanical properties of biomaterials*, pp. 177–194. Ed GW Hastings, DF Williams. New York: Wiley.

SYMBOLS/DEFINITIONS

Greek Letters

σ_0: bend strength without porosity.

σ_a: applied stress.

σ_b: bend strength.

σ_c: critical stress of fracture.

σ_i: strength in an inert atmosphere.

σ_P: proof stress.

Roman Letters

A: area.

a: crack size.

b: constant.

F: probability of failure.
K_{IC}: critical crack initiation stress.
m: Weibull constant.
N: constant.
p: porosity.
t: time to failure.
Y: geometric factor of crack initiation.

Definitions

D_3^6d **space group**: Notation for the crystallographic representation of one of the hexagonal close-packed structures.

Ammonium alum [$Al_2(SO_4)_3(NH_4)SO_4 24H_2O$ or $AlNH_4(SO_4)_2 12H_2O$]: Double sulfate of a monovalent metal or radical (sodium, potassium, or ammonium) with a trivalent metal (aluminum, iron, or chromium) used to increase the set of porcelain-enamel ground coats and acid-resisting cover coats.

Bauxite: A claylike ore, mainly hydrated aluminum oxide, from which aluminum is obtained. Density, 2.45–3.25 g/cm^3.

Bayerite: Aluminum trioxide that has the property of being dehydrated at 300ºC to give aluminum oxide. Intermediate product of the Bayer process.

Bayer process: A high-temperature purification process applied to bauxite ore after being dissolved in a hot sodium hydroxide solution.

Bioglass®: A glass-ceramic using phosphorous pentoxide (P_2O_5) as seeding material for tissue (especially hard tissue) formation at the interface by slowly dissolving its surface.

Calcine: Dehydration process of hydrated ceramics at elevated temperature.

Carboxylic acid: An organic acid containing one or more carboxyl group [COOH].

Chemisorption: The binding of an absorbate to the surface of a solid by forces exhibiting energy levels approximating those of a chemical bond.

Fracture toughness: Amount of energy absorbed by a material before fracture or failure.

Griffith flaws: Microcracks contributing crack propagation without plastic deformation, as in brittle materials like ceramics.

Impact fatigue: Fatigue of materials by repeated impact loading.

Incongruency: Misalignment between two (joint) interfaces caused by a large range of motion and a small-sized surface contact.

Laser: Acronym for “light amplification by stimulated emission of radiation.” A device containing a substance (e.g., a ruby), the majority of whose atoms or molecules can be put into an excited energy state in an intense, narrow, and coherent beam.

Lucalox® (General Electric): A commercial alumina with very small grains for making it translucent and high strength. Used for sodium light housing.

Mohs number: Hardness scale for ceramics and glasses: diamond is 10, alumina 9, quartz 7, gypsum 2, and talc 1.

Ringer’s solution: A solution of chlorides, sodium, potassium, and calcium in purified water that has the same osmotic pressure as that found in blood or tissue.

Sintering: Bonding of solid powders at elevated temperature and pressure for faster and better bonding without melting.

Sodium hydroxide (NaOH): A white deliquescent substance in the form of a powder, flakes, sticks, etc., which has a strong caustic base.

Weibull relationship: Relationship between the probability of survival or failure under stress of brittle materials.

Wohler graph: Graph of stress versus number of cycles to failure.

REFERENCES

1. Barralet JE, Gaunt T, Wright AJ, Gibson IR, Knowles JC. 2002. Effect of porosity reduction by compaction on compressive strength and microstructure of calcium phosphate cement. *J Biomed Mater Res* **63**:1–9.
2. Bizot P, Nizard R, Lerouge S, Prudhommeaux F, Sedel L. 2000. Ceramic/ceramic total hip arthroplasty. *J Orthop Sci* **5**:622–627.
3. Brånemark P-I, Hansson BO, Adell R, Breine U, Lidstrom J, Hallen O, Ohman A. 1977. *Osseous integrated implants in the treatment of the edentulous jaw, experience from a 10-year period*. Stockholm: Almqvist & Wiksell International.
4. Chen C, Knapp W. 1974. Fatigue fracture of a alumina ceramic at several temperatures. In *Fracture mechanics of ceramics*, pp. 691–707. Ed RC Bradt, DPH Hasselman, FF Lange. New York: Plenum.
5. Coble RL, Kingery WD. 1956. Effect of porosity on physical properties of sintered alumina. *J Am Ceram Soc* **39**:377–385.
6. De Aza AH, Chevalier J, Fantozzi G, Schehl M, Torrecillas R. 2002. Crack growth resistance of alumina, zirconia and zirconia toughened alumina ceramics for joint prostheses. *Biomaterials* **23**:937–945.
7. Dorre E, Dawihl W. 1980. Ceramic hip endoprostheses. In *Mechanical properties of biomaterials*, pp. 113–127. Ed GW Hastings, DF Williams. New York: Wiley.
8. Dorre E, Hubner H. 1984. *Alumina*. Berlin: Springer-Verlag.
9. Ernst CP, Cohen U, Stender E, Willershausen B. 2005. In vitro retentive strength of zirconium oxide ceramic crowns using different luting agents. *J Prosthet Dent* **93**:551–558.
10. Frakes J, Brown S, Kenner G. 1974. Delayed failure and aging of porous alumina in water and physiological medium. *Am Ceram Soc Bull* **53**:193–197.
11. Geduldig D, Lade R, Prussner P, Willert H-G, Zichner L, Dorre E. 1976. Experimental investigations of dense alumina ceramic for hip and knee joint replacements. In *Advances in artificial hip and knee joint technology*, *Engineering in medicine*, Vol. 2, pp. 434–445. Ed M Schaldach, D Hohmann. Berlin: Springer-Verlag.
12. Gitzen WH. 1970. *Alumina as a ceramic material*. Columbus, OH: American Ceramic Society.
13. Hannouche D, Hamadouche M, Nizard R, Bizot P, Meunier A, Sedel L. 2005. Ceramics in total hip replacement. *Clin Orthop Relat Res* **430**:62–71.
14. Kawahara H, Hirabayashi M, Shikita T. 1980. Single crystal alumina for dental implants and bone screws. *J Biomed Mater Res* **14**:597–606.
15. Krainess F, Knapp W. 1978. Strength of a dense alumina ceramic after aging in vitro. *J Biomed Mater Res* **12**:241–246.
16. Maier HR, Stark N, Krauth A. 1980. Reliability of ceramic–metallic hip joints based on strength analysis, proof, and structural testing. In *Mechanical properties of biomaterials*, pp. 177–194. Ed GW Hastings, DF Williams. New York: Wiley.
17. Marti A. 2000. Inert bioceramics (Al_2O_3, ZrO_2) for medical application. *Injury* (Suppl) **4**:33–36.
18. Morita Y, Nakata K, Kim YH, Sekino T, Niihara K, Ikeuchi K. 2004. Wear properties of alumina/zirconia composite ceramics for joint prostheses measured with an end-face apparatus. *Biomed Mater Eng* **14**:263–270.
19. Murphy S. 2002. Alumina ceramic–ceramic bearings in THA: the new gold standard. *Orthopedics* **25**:2–3.

20. Nizard R, Sedel L, Hannouche D, Hamadouche M, Bizot P. 2005. Alumina pairing in total hip replacement. *J Bone Joint Surg Br* **87**:755–758.
21. Park JB. 1992. Orthopedic prosthesis fixation. *Ann Biomed Eng* **20**(1):583–594.
22. Rieker C, Konrad R, Schon R. 2001. In vitro comparison of the two hard-hard articulations for total hip replacements. *J Eng Med* **215**:153–160.
23. Ritter Jr J, Greenspan D, Palmer R, Hench L. 1979. Use of fracture of an alumina and Bioglass-coated alumina. *J Biomed Mater Res* **13**:251–263.
24. Sedel L. 1992. Symposium: alumina ceramic arthroplasty. *Clin Orthop Relat Res* **282**:2–94.
25. Sedel L. 2000. Evolution of alumina-on-alumina implants: a review. *Clin Orthop Relat Res* **379**:48–454.
26. Semlitsch M, Lehmann M, Weber H, Dorre E, Willert H-G. 1977. New prospects for a prolonged functional lifespan of artificial hip joints by using the material combination polyethylene/aluminum oxide ceramic/metal. *J Biomed Mater Res* **11**:537–552.
27. Spraggs M, Vasilos T. 1963. Effect of grain size on transverse bend strength of alumina and magnesia. *J Am Ceram Soc* **46**:224–228.
28. Tamura J, Kawanabe K, Yamamuro T, Nakamura T, Kokubo T, Yoshihara S, Shibuya T. 1993. Bioactive bone cement: effect of amount of glass powder on its bioactivity and mechanical properties. In *Bioceramics*, Vol. 6, pp. 463–468. Ed P Ducheyne D Christiansen. Oxford: Pergamon/Elsevier Science.
29. Trantina C. 1977. Brittle fracture and subcritical crack growth in a ceramic structure. In *Fracture*, pp. 921–927. Ed D Taplin. Waterloo, Canada: University of Waterloo.
30. Watzek G, Watejka M, Lill W, Mailath G. 1989. Efficiency of different clinical procedures regarding optimal implant integration. In *Oral implantology and biomaterials*, pp. 287–293. Ed H Kawhara. Amsterdam: Elsevier.
31. Willmann G. 1994. Medical-grade alumina during the past two decades. In *Bioceramics*, Vol. 7, pp. 359–363. Ed OH Andersson, R-P Happonen, A Yli-Urpo. Oxford: Pergamon.

7

ZIRCONIUM OXIDES (ZIRCONIA)

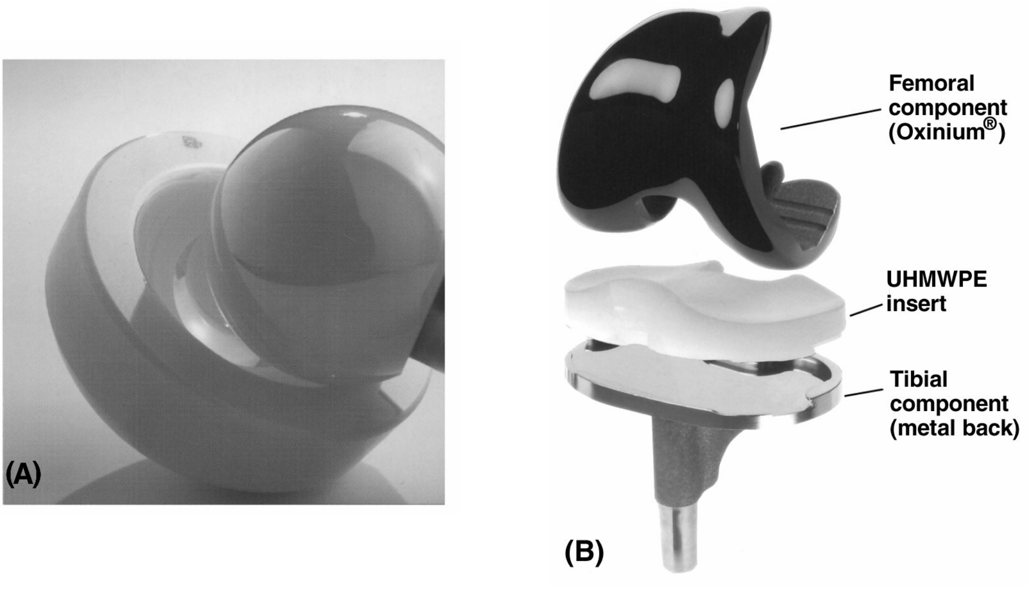
(A)
Femoral component (Oxinium®)
UHMWPE insert
Tibial component (metal back)
(B)

(a) Zirconia-based acetabular cup and femoral head with metal stem. Courtesy of Norton Advanced Ceramics, Export, PA. (b) Newly developed zirconium–niobium alloy for the femoral component of a knee joint prosthesis. The heavily oxidized surface acts as zirconia ceramic (ZrO_2) for good wear and friction. Modified with permission from a brochure published by Smith & Nephew Inc., Memphis, Tennessee.

Zirconium oxides (zirconia) have been used for the purpose of fabricating implants. Some are called “fake diamond” or “cubic zirconia” since some zirconia single crystals can be of gem grade and made into jewels. Some of their mechanical properties are as good or better than those of alumina ceramics. They are highly biocompatible, like other ceramics, and can be made into such large implants as the femoral head of a hip joint replacement. Some of their drawbacks include the fact that they exhibit high density, low hardness, and phase transformations under stress in aqueous conditions, thus degrading their mechanical properties.

It is noteworthy that zirconium–niobium metal can be used as an articulating material for joint implants. In bulk behavior this material is very similar to *metallic* zirconium.

7.1. SOURCE AND MANUFACTURING OF ZIRCONIA

Zirconium (Zr) belongs to the same subgroup as titanium in the periodic table and shows similar chemical properties. Zircon ($ZrSiO_4$) is the most commercially important zirconium mineral and is found mostly in the mineral baddeleyite. Zircon is a gold-colored silicate of zirconium, a mineral found in igneous and sedimentary rock and occurring in tetragonal crystals colored of many colors. The transparent varieties are usually deposited in beach sand, and are used as gems. Zircon is first chlorinated to form $ZrCl_4$ in a fluidized bed reactor in the presence of petroleum coke. A second chlorination is required for high-quality zirconium. Zirconium is precipitated with either hydroxides or sulfates, and then calcined to its oxide [36].

Zirconia is partially stabilized above 1700ºC in the cubic phase, which results in large grain sizes (50–70 μm). When cooled, phase transformation takes place and tetragonal precipitates can be formed in the cubic matrix. The combined cubic and tetragonal phase results in a stronger material due to closure of cracks by expansion of the precipitates.

7.2. STRUCTURE AND PROPERTIES OF ZIRCONIA

Zirconia undergoes an allotropic phase transition from monoclinic ($a \neq b \neq c$, $\alpha \neq \gamma = 90° \neq \beta$) to tetragonal ($a = b \neq c$, $\alpha = \gamma = \beta = 90°$) at 1000~1200ºC, and from tetragonal to cubic ($a = b = c$, $\alpha = \gamma = \beta = 90°$) at 2370ºC (see Fig. 3.12). The cubic-to-monoclinic and tetragonal phase transition is diffusionless and accompanies a volume expansion of about 7%. The cubic structure of zirconia belongs to the group of fluorite (CaF_2) structures, as shown in Figure 7.1. The crystallographic parameters of the unit cell structures are given in Table 7.1. The partial phase diagram of ZrO_2–CaO is shown in Figure 7.2. The CaO acts as a stabilizing oxide, where C_{ss} is the cubic solid solution, termed fully stabilized zirconia, which is resistant to most molten metals and thus used to make crucibles. Partially stabilized zirconia (PSZ) results in a two-phase region [$T_{ss} + C_{ss}$]. These materials have enhanced mechanical properties, as mentioned

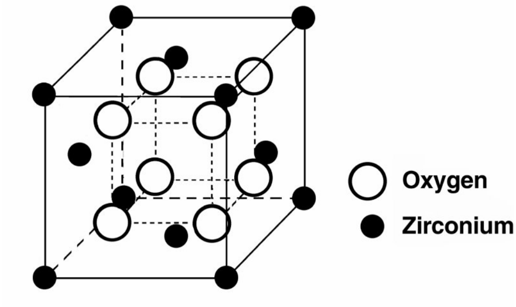

Figure 7.1. Cubic structure of zirconia, which is classified as a fluorite structure. Modified with permission from [22]. Copyright © 1976, Wiley.

Table 7.1. Physical Properties of Zirconia

Property	Values
Polymorphism[a,b]	
Monoclinic → tetragonal	1273–1473 (K)
Tetragonal → cubic	2643 (K)
Cubic → liquid	2953 (K)
Crystallography	
Monoclinic	
a	5.1454 Å
b	5.2075 Å
c	5.3107 Å
β	99°14'
Space group	$P2_1/c$
Tetragonal	
a	3.64 Å[c]
c	5.27 Å
Space group	$P4_2/nmc$
Cubic	
a	5.065 Å
Space group	Fm3m
Density (g/cm^3)	
Monoclinic	5.68
Tetragonal	5.86[a]
Cubic	6.29[b]
Thermal expansion coefficient[c] ($10^{-6}/K$)	
Monoclinic	7
Tetragonal	12
Heat of formation[c] (kJ/mol)	–1,096.73
Boiling point (K)	4,549
Thermal conductivity (W /m/K)	
at 100°C	1.675
at 1300°C	2.094
Mohs hardness	6.5
Refractive index	2.15

[a] See Problem 7.2.

[b] Calculated value (see Example 7.1).

Reprinted with permission from [14]. Copyright © 1993, Pergamon.

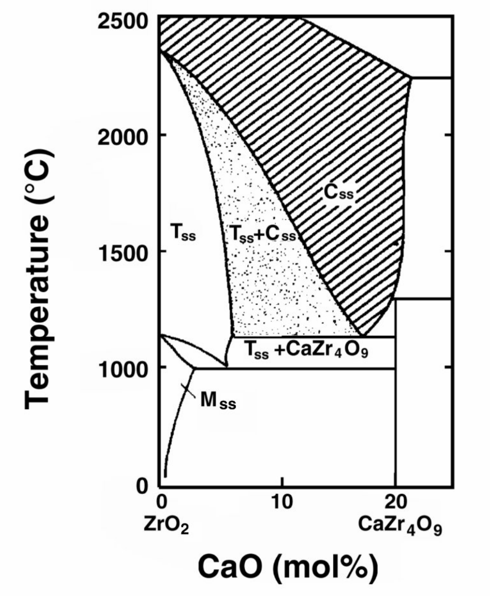

Figure 7.2. Partial phase diagram of ZrO_2–CaO. C_{ss} = cubic, T_{ss} = tetragonal, and M_{ss} = monoclinic solid solution phase. Reprinted with permission from [14]. Copyright © 1986, MIT Press.

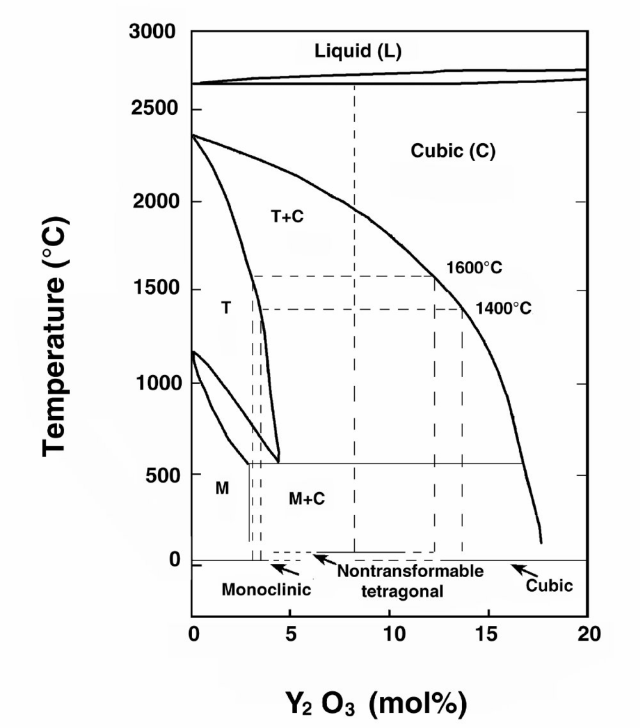

Figure 7.3. Phase diagram of ZrO_2–Y_2O_3. Reprinted with permission from [3]. Copyright © 1993, Pergamon.

earlier. Another oxide commonly used to stabilize cubic zirconia is yttrium oxide (Y_2O_3), as shown in Figure 7.3. It is critical that the precipitates of the tetragonal phase remain small (<0.2 μm) in the cubic zirconia matrix to enhance its mechanical properties. If the tetragonal precipitates become large, a monoclinic transform takes place, causing cracks in the material [14]. To control this phase transformation MgO is used along with the Y_2O_3 during the sintering and aging process. Figure 7.4 shows the microstructures of yttrium- and magnesium-stabilized zirconia. The tetragonal precipitates strengthen the structure of cubic the zirconia matrix due to the volume difference during the phase transformation.

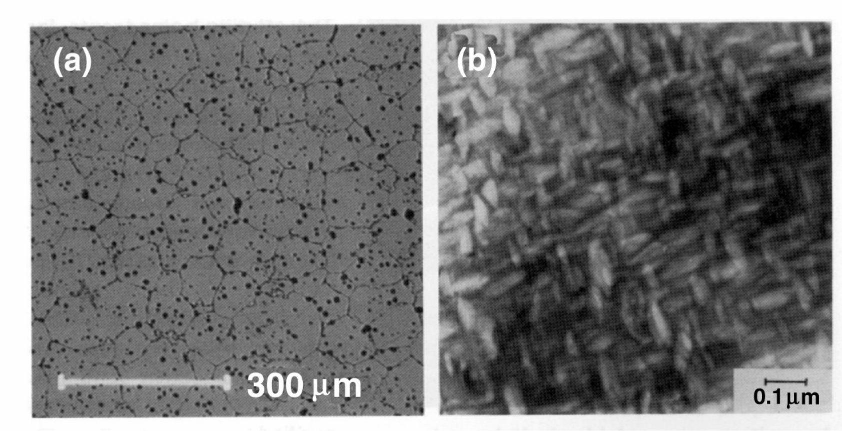

Figure 7.4. Yttria- and magnesium-stabilized zirconia (a) and tetragonal precipitates in the cubic matrix grains (b). Reprinted with permission from [3]. Copyright © 1993, Pergamon.

The properties of various zirconia are summarized in Table 7.2. The strength of the partially stabilized zirconia with yttrium oxide (Y–TZP) showed the highest flexural strength and fracture toughness. However, the Weibull modulus was lower than the yttrium magnesium oxide-stabilized zirconia (Y–Mg–PSZ). It is also interesting that the increased fracture toughness is due to a phase transformation caused by cessation of crack propagation, as shown in Figure 7.5. Small particles of partially stabilized ZrO_2 are dispersed in the matrix material, which could be zirconia itself. The partial stabilization enables retention of the metastable tetragonal structure at ambient temperature. During crack propagation the tetragonal particles in the crack tip region undergo a phase transformation, increasing their volume, which sets up a compressive field surrounding the particles and shuts crack openings, resulting in a stronger material, similar to formation of tetragonal grains from cubic structures.

Yttrium-stabilized zirconia has been used to fabricate the femoral head of total hip joint prostheses (see the illustration at the opening of this chapter) and has two advantages over alumina [6]. One is the finer grain size and well-controlled microstructure with minimum residual porosity, resulting in a better tribological material than with

Table 7.2. Properties of Various Zirconia

Properties	CSZ	Y–Mg–PSZ	Y–TZP
Young's modulus (GPa)	210	210	210
Flexural strength (MPa)	200	600	950
Hardness (Vickers, HV0.5)	1250	1250	1250
Fracture toughness ($\text{MPa}\cdot\text{m}^{1/2}$)	–	5.8	10.5
Weibull modulus	8	25	18
Density	6.1	5.85	6

CSZ, cubic stabilized zirconia; Y–Mg–PSZ, yttrium magnesium oxide stabilized zirconia. Y–TZP, partially stabilized zirconia with yttrium oxide.
Reprinted with permission from [3]. Copyright ©1993, Pergamon.

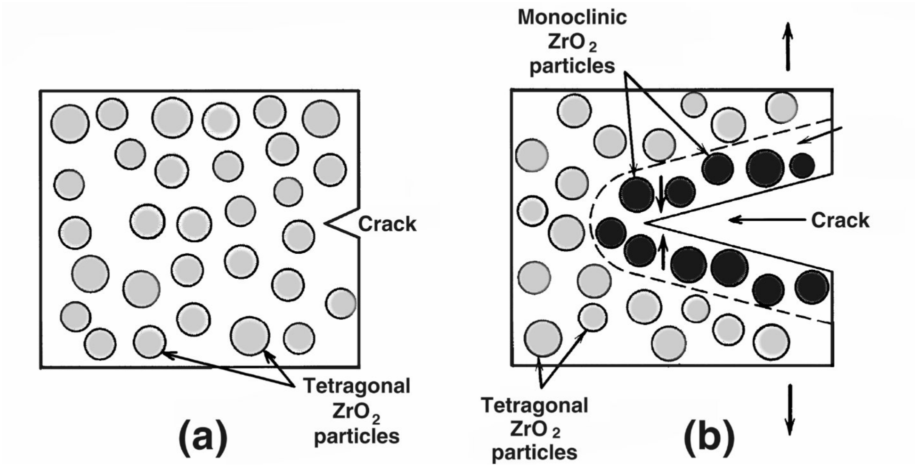
Crack
Tetragonal ZrO_2 particles
(a)
Monoclinic ZrO_2 particles
Crack
Tetragonal ZrO_2 particles
(b)

Figure 7.5. Schematic representation of the toughening of zirconia with partially stabilized zirconia; (a) crack before phase transformation, (b) crack arrestment due to phase transformation of the dispersed PSZ particles. Reprinted with permission from [7]. Copyright © 1994, Wiley.

alumina. The other is higher fracture strength and toughness due to the phase transformation toughening process. The long fatigue life of the zirconia can be related to the slow crack growth (SCG), which can be described as

$$v = AK_I^n , \tag{7.1}$$

where v is the crack velocity, K_I is the stress intensity factor, and A and n are constants. Figure 7.6 shows the results of SCG measurement on Y–TSZ using double torsion in air and Ringer's solution [6]. The results tested in air showed the classical three different stages of crack propagation, while the test done in Ringer's solution only showed the first stage of SCG, similar to other ceramics tested in water. A prediction of the life of the implant can be made from the initial stage of SCG; therefore,

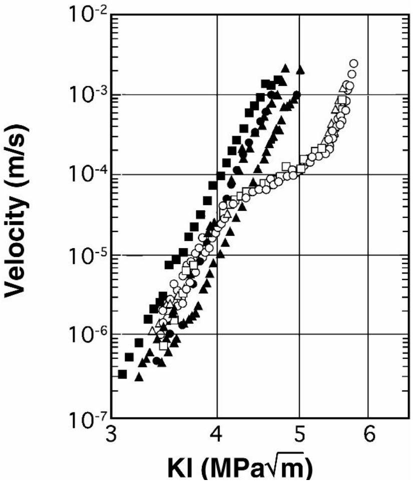

Figure 7.6. Slow crack propagation of Y-PSZ zirconia in air and in Ringer's solution (filled symbols). Reprinted with permission from [6]. Copyright © 1993, Pergamon.

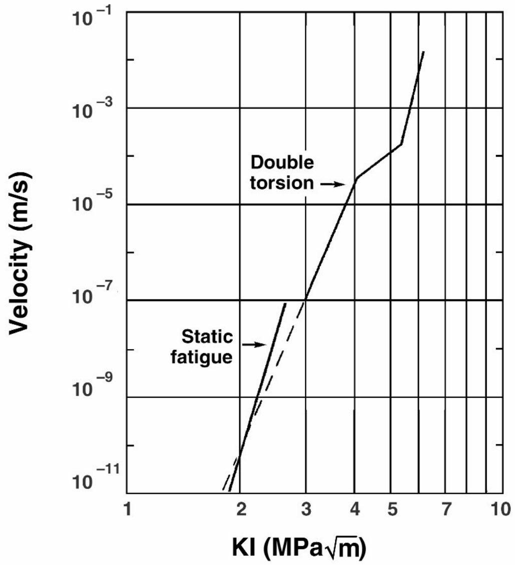

Figure 7.7. Static and dynamic fatigue tests of zirconia. The dashed line represents extrapolation. Reprinted with permission from [6]. Copyright © 1993, Pergamon.

the results from the tests done in air can be used for prediction of the life of implants [6]. It is also important to note that the crack propagation is a low-velocity event, so that four-point double-torsion bending tests cannot be employed. Statistical analysis was utilized to obtain the results shown in Figure 7.7, which demonstrates good agreement between the static test analysis and the double torsion tests.

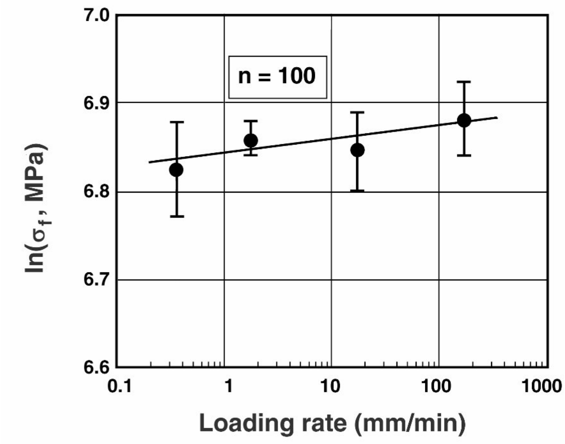

Figure 7.8. Plot of fracture strength versus loading rate of yttria-stabilized zirconia. Reprinted with permission from [6]. Copyright © 1993, Pergamon.

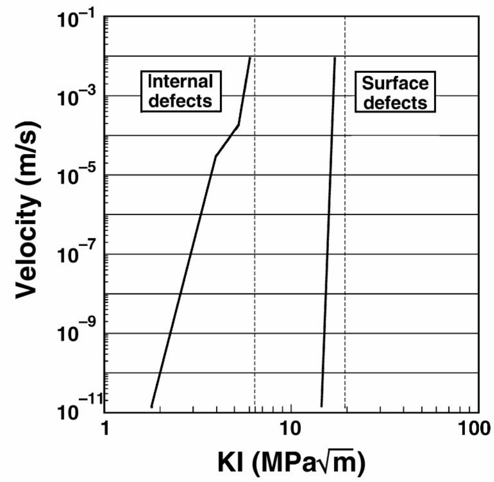

Figure 7.9. Slow crack growth behavior of bulk and surface defects. Reprinted with permission from [6]. Copyright © 1993, Pergamon.

Surface defects were characterized by a series of dynamic tests in which predetermined constant loading rates were applied. Estimated fracture strength by analysis of crack length versus loading rates is plotted in Figure 7.8, where n = 100, as obtained from Eq. (7.1). The exponent value is far larger than expected and it is speculated that there is a very high compressive stress (800 MPa) on the surface, which leads to the threshold crack propagation value. Therefore, one must be careful that the machining marks not be sources of crack initiation, which will limit fatigue strength. The subcritical type of crack growth for surface and bulk defects are shown schematically in Figure 7.9.

Example 7.1

Calculate the density of cubic zirconia and compare it with the other forms of zirconia given in Table 7.1.

Answer:

$$\text{Density} = \frac{\text{Mass}}{\text{Volume}} = \frac{(4\times 91 + 8\times 16)\,\text{g/mol}}{(5.065\times 10^{-8}\text{cm})^3\, 6.02\times 10^{23}/\text{mol}} = \underline{6.29\ \text{g/cm}^3}\ .$$

This value seems somewhat high compared to the density of the tetragonal structure — 5.86 g/cm^3. It is somewhat odd that the density increased at higher temperature since the cubic structure exists at higher temperatures than the tetragonal zirconia.

Example 7.2

Calculate exponent n for bulk- and surface-defect zirconia from the data given in Figure 7.9.

Answer:

From Eq. (7.1) and Figure 7.9, the estimated values are:

Type	K_I (MPa$\sqrt{\text{m}}$)	ν (m/s)
Bulk	2	7 × 10^{-11}
	4	3 × 10^{-5}
Surface	14	1 × 10^{-11}
	17	1 × 10^{-2}

By solving the simultaneous equations for each case, n = 18.7 and 106.7 for the bulk and surface defect cases, respectively. The result indicates that SCG is a lot more sensitive at its surface than within its bulk.

7.3. LONG-TERM STABILITY AND IMPLANT DESIGN

As mentioned before, ceramics — primarily alumina — have been used in orthopedic and dental implant fabrication. Zirconia was used to replace alumina since it can be made tougher and stronger than alumina. The tribological properties of zirconia against ultra-high-molecular-weight polyethylene (UHMWPE) is equal or better than alumina [47]. It is important that these ceramics will not degrade in vivo, and both static and dynamic tests are essential to ensure long-term service.

There have been reports of static fatigue of alumina, which is supposed to be quite inert [8,11,17,24,27,32]. Up to a 20% reduction after one year under in-vivo conditions was thought to be due to the calcium oxide content of the alumina [27]. However, it is not clear that similar fatigue or aging could take place in vivo. Similar results have been found for zirconia [15,41], while others have reported differently [5,38]. One of the problems with zirconia is variability in the amount of stabilizing oxide (Y_2O_3) and the grain size of its matrix, as shown in Figure 7.10. This diagram

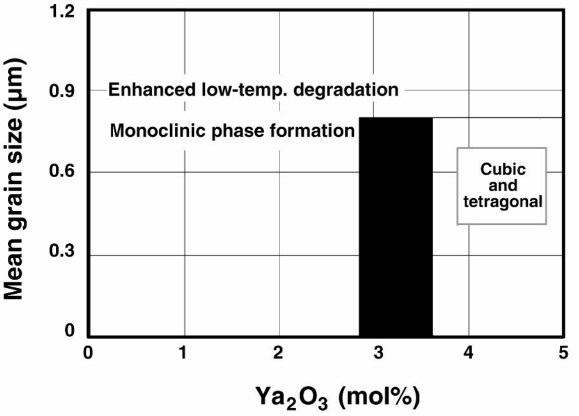

Figure 7.10. Microstructure–composition stability diagram for yttria-stabilized zirconia. The solid black area is a region of stable tetragonal structure in physiological conditions. Reprinted with permission from [5]. Copyright © 1994, Pergamon.

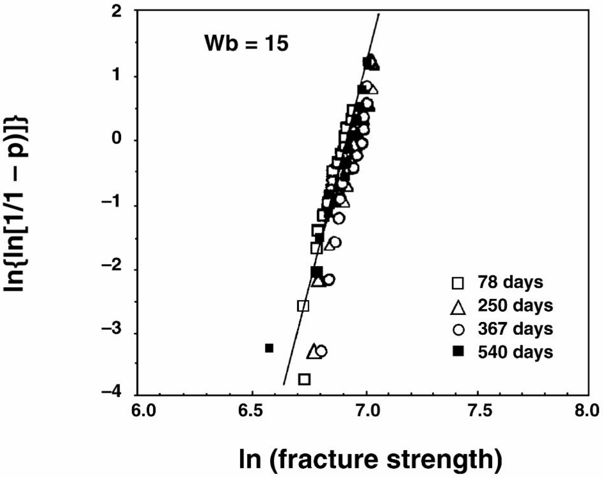

Figure 7.11. Weibull plot of zirconia. The modulus is about 15. Reprinted with permission from [5]. Copyright © 1994, Pergamon.

shows that the best result is obtained in the black rectangular region, where toughness and strength are maximized. If the yttrium oxide (yttria) is more than 3.5 mol%, a cubic structure is formed, which is detrimental for fracture strength. The concentration of yttria is less than 2.8% and its grain size is large (>1 μm), which can induce low-temperature degradation with decreased strength [5]. The Weibull plot of aged zirconia (see Fig. 7.11) shows that there is no change in mechanical properties with aging since all the aged specimens follow the slope of the plot. However, the statistical nature of the grain size and its distribution should make one extra cautious when using yttria or other stabilized zirconia for load-bearing implant fabrication (e.g., in a hip joint femoral head).

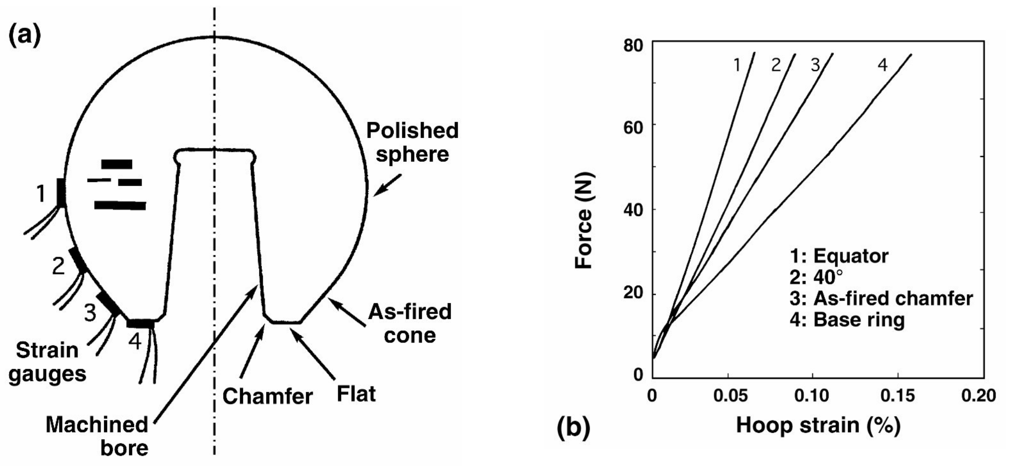

Figure 7.12. Location of strain gauges in the zirconia femoral head (a) and force versus hoop strains obtained for each location of the strain gauge. Reprinted with permission from [30]. Copyright © 1995, Pergamon.

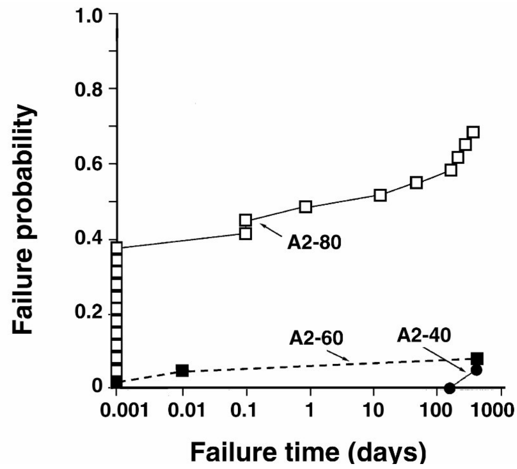

Figure 7.13. Cumulative probability of failure versus log (t_f) for A2 heads for preload levels of 40, 60, and 80% of maximum compressive strength. Reprinted with permission from [30]. Copyright © 1995, Pergamon.

The effect of stress corrosion on the zirconia femoral head of a hip joint prosthesis was evaluated after putting strain gauges on the surface, as shown in Figure 7.12. The amount of strain was measured to determine preloading levels for the extended-time experiment. This result indicates that the amount of strain on the surface of the femoral head depends on the location of the gauge. It is largest on the base and minimal at the equator. Loading of femoral heads at various levels produced the results shown in Figure 7.13. Delayed failure takes place below the fracture load, indicating

Table 7.3. Comparison of Properties of Alumina and Zirconia

Property	Alumina	Zirconia
Chemical composition	$A1_2O_3$ + MgO	ZrO_2 + MgO + Y_20_3
Purity (%)	99.9	95~97
Density (g/cm^3)	>3.97	5.74~6.0
Porosity (%)	<0.1	<0.1
Bending strength (MPa)	>500	500~1,000
Compression strength (MPa)	4,100	2,000
Young's modulus (GPa)	380	210
Poisson's ratio	0.23	0.3
Fracture toughness (MPa·m$^{1/2}$)	4	up to 10
Thermal expansion coefficient ($\times 10^{-6}$/K)	8	11
Thermal conductivity (W/m/K)	30	2
Hardness (HV0.1)	up to 2,200	1,200
Contact angle (°)	10	50

Reprinted with permission from [44]. Copyright © 1993, Pergamon.

slow crack propagation. It has not been proven that preloading strains exist to any significant extent in the femoral head after insertion into the metal stem. However, it is advisable to use less than 40% of the maximum fracture strength of the zirconia when designing an implant [30]. One could proof-test to eliminate weak implants and improve design by using a statistical analysis of service life.

As mentioned earlier, zirconia has many salient features that offer advantages over alumina (see the comparison of properties in Table 7.3). There are different types of zirconia depending largely on the types of stabilizer employed. Another difference is that zirconia can be radioactive due to impurities (mainly yttria). Although there are no reported adverse events due to radioactivity, common sense dictates that radioactive zirconia should never be used in implants [3,44]. Direct comparisons between alumina and zirconia implant ceramics have been made since the properties of zirconia are known to be affected by moisture, temperature, and time [35]. Biolox® (Cerasiv GmbH, Plochingen, Germany) zirconia is made from yttria-coated (5~5.4% by weight) zirconia powder and yttria (4.5~5%) coprecipitated powder. A stabilizing amount of yttria salt is added to the zirconium solution from which zirconia is coprecipitated, and the already calcined zirconia is coated with yttria particles. Hydrothermal treatment at 140ºC (Fig. 7.14), loading rate, and time are the variables. In addition, the type of metal stem materials are varied to measure their effect on the impact strength of the femoral head. The results for aging time are summarized in Table 7.4. The initial strength of zirconia is about twice that of alumina, but it loses strength after hydrothermal treatment, which is similar to autoclaving conditions. However, even after 120 hours aging the strength of zirconia is more than 50% higher than that of alumina. As expected, the strength of alumina is not affected by short-term treatment. The effects of loading rate on the properties of the alumina and the yttria-coated zir-

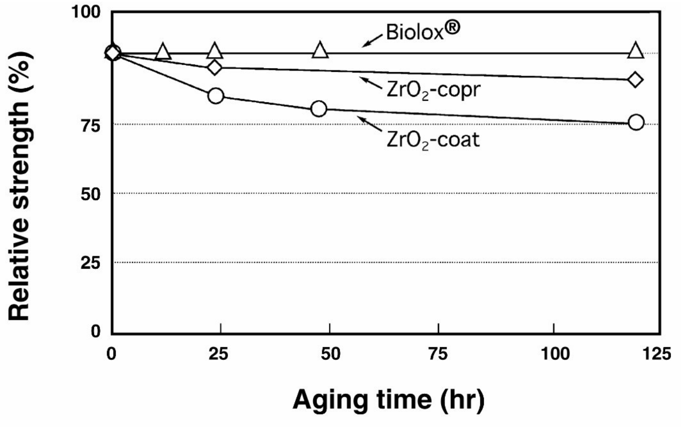

Figure 7.14. Effect of hydrothermal aging at 140°C for alumina and two types of zirconia. Reprinted with permission from [35]. Copyright © 1994, Pergamon.

Table 7.4. Four-Point-Bending Strength of Alumina and Two Types of Zirconia

	Aging time (hours)			
Material	0	24	48	120
Alumina	525	542	528	537
ZrO_2-coprecipitated	1110	942	876	836
ZrO_2-coated	986	923	922	874

Reprinted with permission from [35]. Copyright © 1994, Pergamon.

conia are given in Figure 7.15. The strength at the highest loading rate is called the "inert strength." The zirconia showed a higher susceptibility to loading rate (which can be interpreted as static fatigue). The static fatigue parameter *n* is about 40 for zirconia and 65 for alumina [35]. However, it is not known whether static fatigue behavior can be extrapolated over very long time periods (>10 years). Also, the value for zirconia is far smaller than the values given in Figure 7.8, where $n = 100$. This large variation is probably due to the different source of zirconia and the different testing conditions. The properties of zirconia depend on the phase changes during hydrothermal treatment, which can be measured by x-ray diffraction. The results of such measurements are shown in Figure 7.16, where the volume fraction of monoclinic zirconia increases rapidly to more than 80% for the yttria coprecipitated within 20 hours, but the yttria-coated zirconia showed a monotonic increase and did not reach more than 60% after 120 hr. Of course, there are no phase changes with alumina at this low temperature. The thickness of the monoclinic layer followed a similar trend, i.e., the coprecipitated zirconia increased in thickness up to 115 μm at 120 hours, but the coated zirconia showed minimal increases (see Fig. 7.17). The relationship between the material properties and the metal stem taper is given in Table 7.5. If the metal is hard

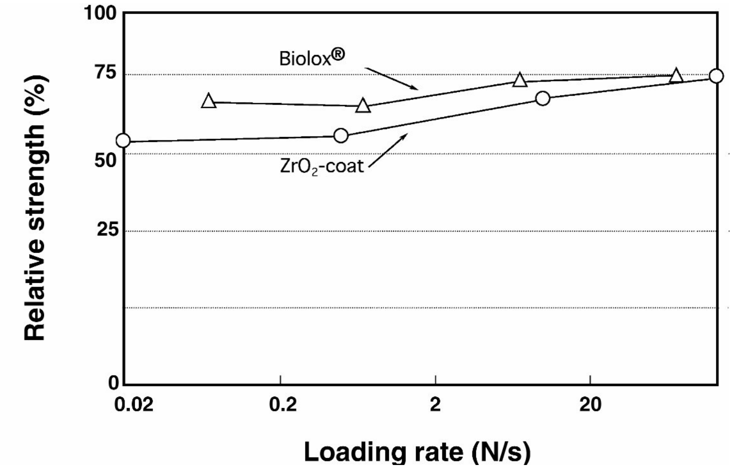

Figure 7.15. Effect of loading rate on the relative strength of alumina and two types of zirconia. Reprinted with permission from [35]. Copyright © 1994, Pergamon.

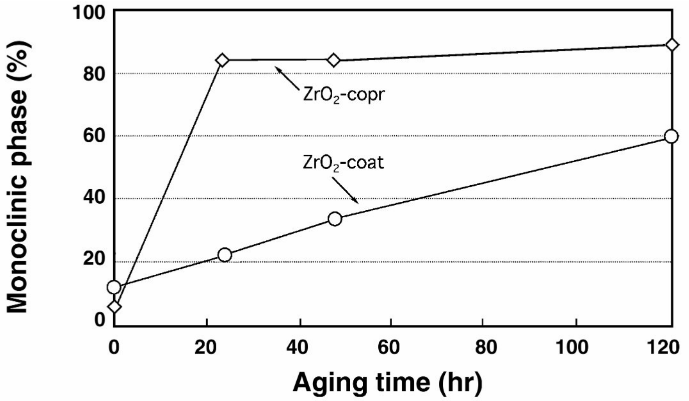

Figure 7.16. Plot of monoclinic phase changes with aging time for yttria coprecipitated and coated zirconia. Reprinted with permission from [35]. Copyright © 1994, Pergamon.

(CoCr alloy), the burst strength of the femoral head decreases compared to a softer stem (Ti alloy). In addition, surface roughness has two effects: it lowers burst strength and intensifies the stress. The smoother the surface, the less stress concentration, resulting in a more even stress distribution.

Extensive studies have been performed on the effects of temperature, time, and environment on structure and mechanical properties using animal models (rabbit) and saline solutions for up to 3 years [29]. Small (1.5 × 3.0 × 10 mm) zirconia specimens stabilized with Y_2O_3 were made and again subjected to elevated temperature and various environments. The tetragonal-to-monoclinic phase transformation was measured

Table 7.5. Burst Strength of Zirconia Femoral Head Measured on Various Metal Tapers

Taper material	Hardness (HV 10)	Surface roughness (Ra, μm)	Burst strength (kN)
Ti alloy	352	4,6	80
Ti alloy	310	48,4	93
Co–Cr alloy	435	2,7	44
Co–Cr alloy	644	2,7	47

Reprinted with permission from [35]. Copyright © 1994, Pergamon.

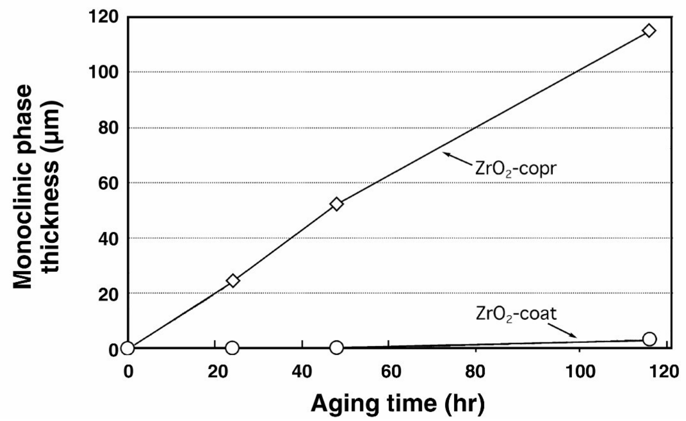

Figure 7.17. Plot of thickness of the monoclinic layer with aging time for yttria coprecipitated and coated zirconia. Reprinted with permission from [35]. Copyright © 1994, Pergamon.

with the x-ray diffraction method, as shown in Figure 7.18. A monoclinic phase could be detected at 28 and 31°. The phase transformation rate of the zirconia in vivo and in a 37°C saline solution over time is shown in Figure 7.19. As can be seen, there is no significant difference in rate for in-vitro or in-vivo conditions, indicating that in-vivo aging can be used to evaluate the effect of aging phase transformation. The same treatment conditions demonstrated minimal effect on the bending strength of zirconia, as shown in Figure 7.20. At elevated temperatures the phase transformation was faster and the effect on bending strength was higher (Fig. 7.21). The temperature dependence of the phase transformation is plotted in Figure 7.22, from which one can calculate the activation energy of the phase transformation, which in turn can be used to calculate the time to reach a certain strength at a given temperature if the conditions are equal. The calculated activation energy was 21.5 kcal/mol, and it would take 80 years to reach 800 MPa for a 30% reduction in bending strength [38]. There is a one-to-one relationship between the amount of phase transformation and the bending strength of zirconia, as shown in Figure 7.23. This indicates that only amount of phase

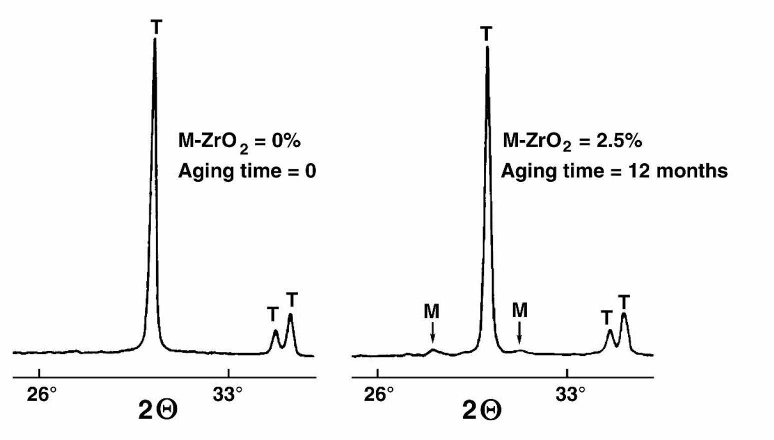

Figure 7.18. X-ray diffraction pattern changes before and after 12 months, in rabbit. Reprinted with permission from [38]. Copyright © 1993, Wiley.

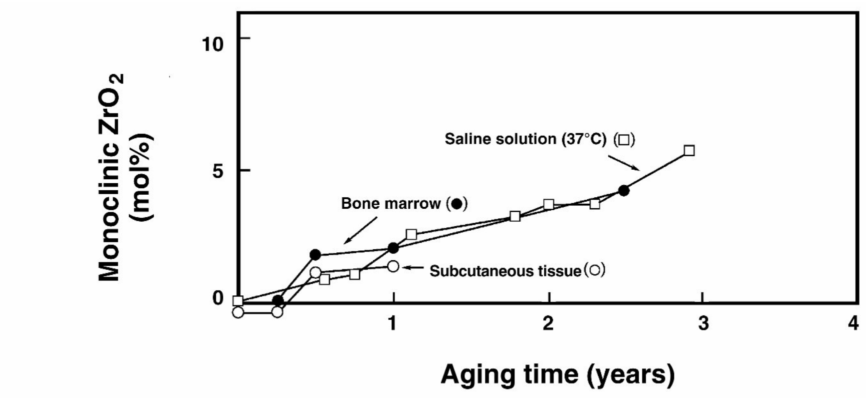

Figure 7.19. Rate of phase transformation in vitro and in vivo. Reprinted with permission from [38]. Copyright © 1993, Wiley.

transformation has an influence on the mechanical properties. Moisture has an effect on the zirconia by forming Zr–OH bonding, which precedes the phase transformation and can be detected by infrared (IR) spectroscopy (see Fig. 7.24). The study concluded that yttria-stabilized zirconia is a good candidate as a replacement for alumina ceramic in orthopedic applications since even the effect of aging on mechanical properties will make zirconia a much stronger material than alumina. In addition, the tribological properties are superior to those of alumina [25].

It has been shown that the biocompatibility of zirconia is about the same as that of alumina ceramic but that its tribological properties are quite different. In one study, the friction and wear properties of zirconia, alumina and 316L stainless steel were

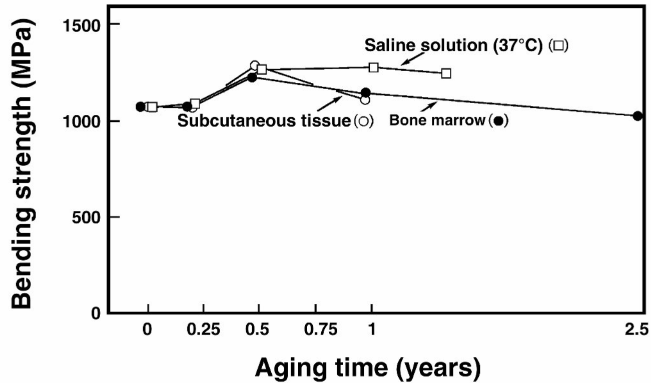

Figure 7.20. Changes in bending strength in vivo and in vitro. Reprinted with permission from [38]. Copyright © 1993, Wiley.

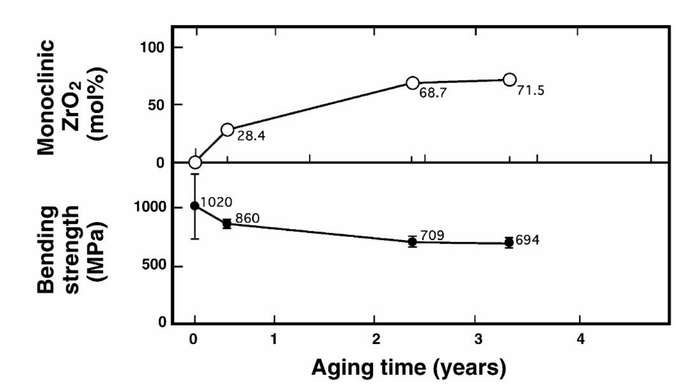

Figure 7.21. Effect of temperature on phase transformation and bending strength in zirconia. Reprinted with permission from [38]. Copyright © 1993, Wiley.

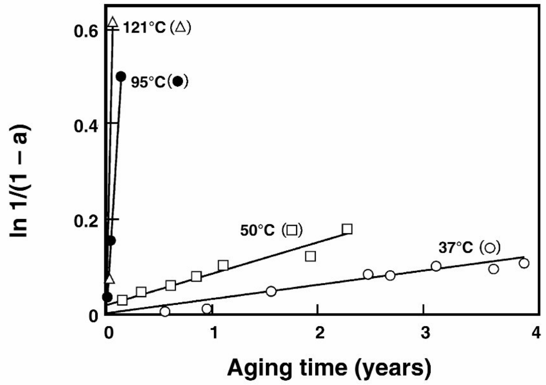

Figure 7.22. Phase transformation versus aging time for zirconia at various temperatures. Reprinted with permission from [38]. Copyright © 1993, Wiley.

compared to UHMWPE by using uni- and bidirectional wear tests in bovine serum, saline, and distilled water. Table 7.6 shows the results of UHMWPE wear. The wear factor was estimated by the following equation:

$$\text{Wear factor} = \frac{\text{Wear volume (mm}^3)}{\text{Load } (N)/\text{Sliding distnace (m)}}. \tag{7.2}$$

The wear factor for the yttrium oxide stabilized (Y–PSZ) zirconia was smaller than that of alumina and 316L stainless steel in all test conditions and modes. Also, the unidirectional wear test showed a greatly higher wear volume than the bidirectional (reciprocating) tests. The actual wear volume versus number of cycles in the unidirectional test is shown in Figure 7.25. The wear factor is the slope of the curve divided by the load or stress (3.45 MPa).

Table 7.6. Wear of UHMWPE Measured by Uni- and Bidirectional Methods

	Bovine serum		Saline		Distilled water	
Counterfaces	Unidirectional	Reciprocate	Unidirectional	Reciprocate	Unidirectional	Reciprocate
Zirconia (3)	10.7 ± 12	0.56 ± 14	7.5 ± 3	0.45 ± 5	8.61 ± 11	0.38 ± 6
Alumina (3)	18.2 ± 6	1.01 ± 8	32.7 ± 7	0.57 ± 2	11.8 ± 4	0.68 ± 4
316L SS (2)	27.7 ± 30	1.81 ± 4	90.5 ± 40	3.89 ± 8	37.1 ± 10	1.12 ± 10

Wear factor in ($mm^3/N{\cdot}m$) × 10^{-9}; number of specimens tested in parentheses.
Reprinted with permission from [25]. Copyright © 1991, Wiley.

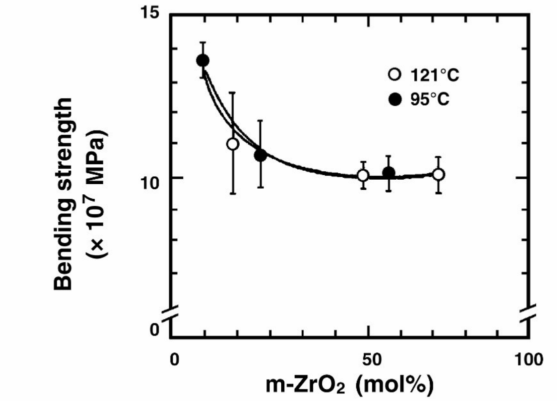

Figure 7.23. Relationship between bending strength and amount of phase transformation, aged in water at 95 and 121°C. Reprinted with permission from [38]. Copyright © 1993, Wiley.

The friction coefficient was found to be a lot lower for zirconia (0.028~0.082) than for alumina (0.044~0.115) or 316L stainless steel (0.061~0.156). The type of lubricant did not influence the friction coefficient. One reason for the excellent wear and

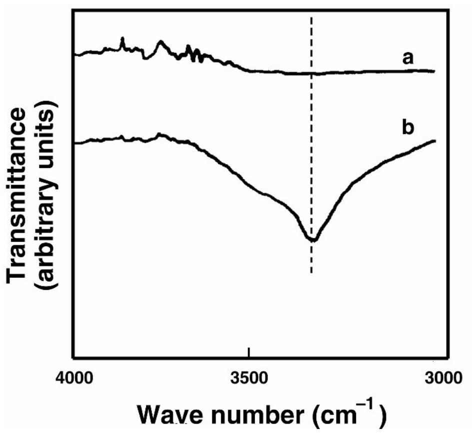

Figure 7.24. Fourier transform IR spectroscopy of zirconia before (a) and after (b) aging in water at 121°C for 960 hr. Reprinted with permission from [38]. Copyright © 1993, Wiley.

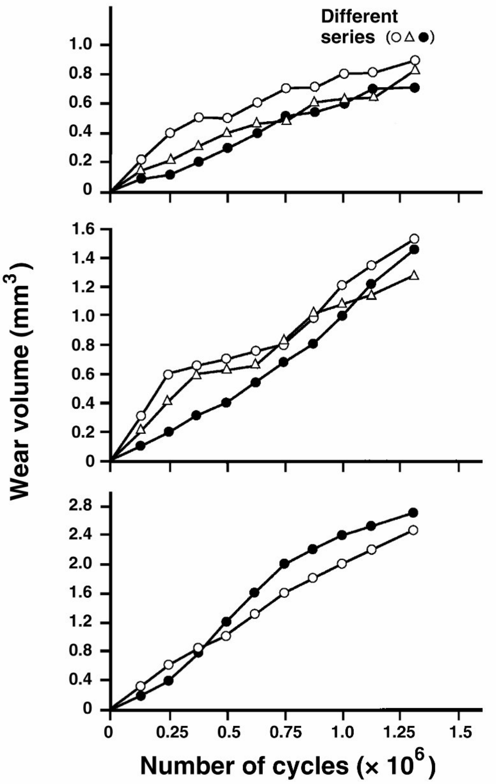

Figure 7.25. Wear volume versus number of cycles in unidirectional test (one cycle = 50 mm) for zirconia (a), alumina (b), and 316L stainless steel (c). Reprinted with permission from [25]. Copyright © 1991, Wiley.

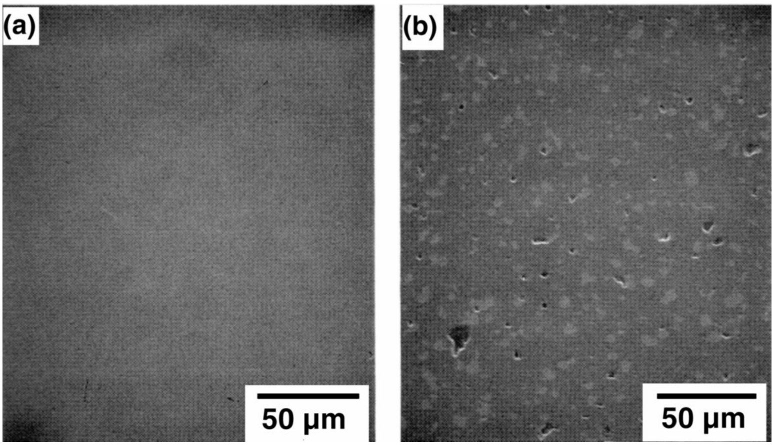

Figure 7.26. Scanning electron microscopic picture of polished surfaces of zirconia (a) and alumina (b). Note the porosity of the alumina. Reprinted with permission from [25]. Copyright © 1991, Wiley.

friction characteristics of the zirconia is attributed to its lower porosity, as shown in Figure 7.26. Additionally, the average grain size of zirconia (0.3 μm) was about one tenth that of the alumina (2.5 μm), although surface roughness was about the same for both (average Ra = 0.005~0.013 μm).

The use of zirconia as a hemiarthroplasty head implant has been studied and found to be suitable due to its low friction with articular cartilage and its excellent biocompatibility [21,33].

It is interesting that the wear properties of zirconia–zirconia couplings are quite inferior to those of alumina–alumina combinations. In one study, the wear rate was 5000 times greater (16 versus 0.033 mm^3/hr), preempting its use as a femoral head or socket, unlike alumina [29,39]. Zirconia has been tried in dental implants and found to be of adequate strength and biocompatibility, similar to alumina [42].

In order to have better tissue compatibility, one group of investigators coated zirconia with hydroxyapatite by using Na–Si–B–Ca glass as a bonding medium. HA and zirconia slurry (in a 1:1 ratio by weight) was applied to the surface of pure yttria-stabilized zirconia and sintered at 950ºC for 10 min. Successive sintering with a higher proportion of HA yielded a finished product that had an HA gradient of about 40–50 μm [46]. A much higher push-out strength was obtained after 3 months implantation in canine femur compared to the pure Ti implant (8.14 ± 1.08 vs. 3.18 ± 0.29 MPa). Due to the difference in thermal expansion, the thickness of the HA cannot exceed 500 μm. Another coating method is conversion of zirconia gel into a solid by a sol–gel thin film technique [16]. The polymeric gel film of zirconia was applied to Ti6Al4V alloy and it was found the thin (~400 nm) film could undergo large deformation (8~11%) without cracking, but pinholes could limit the use of such material. One can also sinter 50% HA/50% zirconia at very high temperature (1400ºC), which results in high porosity (50%), with pore diameters ranging from 40 to 150 μm. The material showed good biocompatibility and mechanical properties compared to HA, although no specific values were given [40].

7.4. FURTHER THOUGHTS

The development of zirconia was largely due to its application in making such jewelry as "cubic zirconia." It has also attracted intense interest for its applications in medicine and dentistry due to its unique properties of relatively low modulus and high strength, close to that of alumina [4,9,18,20,31,34,37]. On the other hand, the cubic zirconia tends to transform into a monoclinic form in vivo under high stress more rapidly than expected [1,10,19]. This has caused much concern about its use in total hip joints and similar applications. Development of a more stable zirconia that will stand up well in vivo under conditions under a high and repeated stress is a vital field of study [26]. Another drawback of this material is its high density compared to such other ceramics as alumina. It turns out that zirconia implants do not survive well in vivo. The dynamic loading and hostile physiological environment are detrimental in hip joint applications, so that the zirconia implant has been withdrawn from the market.

The use of nanotechnology for manufacturing zirconia–alumina composite ceramics may yield a better material. However, such a development may take a long time to be applied in vivo [23]. Applications in dentistry require attachment (bonding) to a metal or other substrate [2,12,28,43]. Some have tried different composites to improve its properties [28,45].

Oxidized zirconium–niobium (2.5%) has shown some promise in joint implants (e.g., Oxinium®) [13]. However, a recent recall of a porous-surfaced knee joint prosthesis for tissue ingrowth fixation illustrates the importance of studying all the aspects of a material considered for use in implants.

Example 7.3.

Calculate the wear constant of UHMWPE coupled with zirconia in an implant.

Answer:

From Figure 7.25, the average wear volume of zirconia in bovine serum is about 0.6 mm^3 after 10^5 cycles, with a sliding distance of 50 mm. Therefore, the wear constant can be calculated, since the wear constant is defined as

$$\text{Wear constant } (K) = \frac{\text{Wear volume}}{3 \times \text{Hardness} \times \text{Load} \times \text{Sliding distance}} .$$

Assume the hardness of the UHMWPE is about 100 MPa and that the load applied is 43.35 N (3.45 MPa); then,

$$\text{Wear constant } (K) = \frac{0.6 \text{ mm}^3/10^5 \times 50 \text{ mm}}{43.35 \text{ N}/3 \times 100 \text{ MPa}} = 8.3 \times 10^{-7} .$$

The wear constant for UHMWPE with 316L stainless steel would be about 3 times larger according to the wear volume at 100,000 cycles (~2 mm^3).

PROBLEMS

7.1. Zirconia (ZrO_2) stabilized with calcium is an important refractory. The basic cell is ZrO_2 with one Ca^{2+} ion present for every 10 Zr^{2+} ions. Will the vacant sites be anions or cations? What percentage of the total number of all sites will be vacant?

7.2. Calculate the density of monoclinic and tetragonal zirconia.

7.3. Calculate the amount of volume change when the zirconia changes from a monoclinic to a tetragonal structure.

7.4. Calculate the exponent *n* for bulk-defect and surface-defect zirconia from the data given in Figure7.9.

7.5. Calculate the amount of volume change by adding 3 mol% of Y_2O_3 into cubic zirconia. Make assumptions of ideal mixing.

7.6. Predict the probability of failure at 10 years for the A-2 head at a preload level of 40%.

7.7. Calculate the amount of volume change when adding 3 mol% of Y_2O_3 into cubic zirconia. Make assumptions of ideal mixing.

7.8. Predict the probability of failure at 10 years for the A-2 head at a preload level of 40% from Figure 7.13.

7.9. A bioengineer is trying to improve the mechanical properties of BME-ceram, which is made of partially stabilized ZrO_2. The Young's modulus (400 GPa), Poisson's ratio (0.3), and density (6.2 g/cm^3) are comparable to that of other ZrO_2 ceramics. The bioengineer measured rupture strength and recorded as following for the control and BME-ceram zirconia:

Stress level (MPa)	Number of broken specimens	
	Control	BME-ceram
200	0	2
190	2	8
180	6	12
170	10	12
160	12	6
150	8	0
140	2	0

a. Calculate the average strength for the control and BME-ceram zirconia.
b. Which would have a larger Weibull constant (*m*): BME-ceram or zirconia.
c. Give one probable method that the bioengineer used to enhance the mechanical properties of the BME-ceram zirconia.
d. The partially stabilized zirconia loses its strength after autoclaving. Why? How would you prevent such a problem?
e. Estimate the average surface energy of the control zirconia by assuming an elliptically shaped crack when the largest surface crack length is 1 μm.
f. Give one example of application of zirconia for making prostheses and give two advantages of using zirconia for that application.

7.10. For a 10%Y_2O_3–90%ZrO_2 solid solution, from the phase diagram in Figure 7.3 answer the following:
a. What phase(s) exist at 1000ºC?
b. What is the composition of each phase at 1000ºC?
c. What is the percentage of each phase at 1000ºC?
d. Calculate the weight percentage of the Y_2O_3 in the 10%Y_2O_3–90%ZrO_2. Atomic weights: Y, 173; Zr, 91; O, 16.

7.11. The oxidized zirconium (Oxinium®) has shown potential as a joint replacement material according to the Smith & Nephew brochure. Find and read an article on Oxinium® and discuss the pros and cons of using such an oxidized metal for such medical applications.

7.12. Can one oxidize the surface of a metal such as aluminum to make a product (e.g., Oxiluminium) that would essentially retain the properties of the metal substrate and the ceramic-like properties of the surface. Discuss the feasibility and state the pros and cons.

SYMBOLS/DEFINITIONS

Symbols

A: constant.

K_I: stress intensity factor.

n: constant, integer.

Ra: rms (root-mean square) surface roughness.

ν: crack velocity.

Definitions

Activation energy of phase transformation: Energy required to overcome phase changes, expressed as

$$\text{Rate of phase transformation} = \text{Constant} \times e^{-\frac{\Delta E}{RT}}.$$

Baddeleyite: Naturally occurring mineral ($ZrSiO_4$, zircon) used in refractory and corrosion-resistant applications such as furnace linings and muffles and as an ingredient in low-expansion ceramic bodies.

Biolox®: Zirconia made from yttria-coated (5–5.4% by weight) zirconia powder and yttria-coprecipitated (4.5–5%) powder.

Cubic zirconia: An allotropic form of ZrO_2 that exists at 2634~2953 K.

Fluorite (CaF_2) structure: Face-centered cubic structure all of whose tetragonal sites (8) are filled by F^- ions.

Inert strength: Strength at the highest loading rate.

Monoclinic structure: A crystal structure characterized by three axes of unequal length, two of which intersect obliquely and are perpendicular to the third.

Oxinium® (Smith & Nephew): Newly developed zirconium–niobium alloy. The heavily oxidized surface acts as a zirconia ceramic (ZrO_2) for good friction and wear.

Partially stabilized zirconia (PSZ): Zirconia phase with a two-phase region [$T_{SS} + C_{SS}$], which enables retention of a metastable tetragonal structure at ambient temperatures.

Phase transformation toughening process: Process in which higher fracture strength and toughness can be gained by tetragonal precipitates that strengthen the structure of the cubic zirconia matrix due to the volume difference during phase transformation.

Slow crack growth (SCG): Term that measures fatigue life, expressed as $\nu = AK_I^n$, where ν is crack velocity, K_I is the stress intensity factor, and A and n are constants.

Sol–gel thin film: Film produced or used in coating when zirconia gel is converted into a solid.

Tetragonal structure: A crystal structure in which $a = b = c$, $\alpha = \beta = \gamma = 90°$.

Wear factor: Term defined as follows: wear factor = [wear volume (mm^3)]/[load (N) × sliding distance (m)].

Weibull modulus (*m*): Term that indicates the variation in the survival probability of a Weibull distribution. When m is large, the distribution is narrow, meaning that the survival probability is low when additional strength is applied.

Weibull plot: A plot of $\ln\{\ln[1/(1 - p)]\}$ versus ln (fracture strength), where p is the failure probability.

Yttrium oxide (Y_2O_3): Used to make red phosphors for television tubes, in the production of microwave filters, and, with zirconia, in the manufacture of a special high-temperature superconductor, $YBa_2Cu_3O_7$, known as "1–2–3," to indicate the ratio of the metal constituents.

Zircon ($ZrSiO_4$): Used in porcelain enamels and glazes as an opacifier to improve color stability and crazing resistance. Also used in refractory, abrasives, grinding wheels, precision molds for casting of alloys, electrically resisting cements, and in conventional electrical and technical porcelains.

REFERENCES

1. Blaise L, Villermaux F, Cales B. 2001. Ageing of zirconia: everything you always wanted to know. *Key Eng Mater* **13**:553–556.
2. Blatz MB, Sadan A, Martin J, Lang B. 2004. In vitro evaluation of shear bond strengths of resin to densely-sintered high-purity zirconium-oxide ceramic after long-term storage and thermal cycling. *J Prosthet Dent* **91**:356–362.
3. Burger W, Willmann G. 1993. Advantages and risks of zirconia ceramics in biomedical applications. In *Bioceramics*, Vol. 6, pp. 299–304. Ed P Ducheyne, D Christiansen. Oxford: Pergamon.
4. Cales B. 2000. Zirconia as a sliding material: histologic, laboratory, and clinical data. *Clin Orthop Relat Res* **379**:94–112.
5. Cales B, Stefani Y. 1994. Long-term stability of a surgical grade zirconia ceramic. In *Bioceramics*, Vol. 7, pp. 395–400. Ed OH Andersson, R-P Happonen, A Yli-Urpo. Oxford: Pergamon.
6. Cales B, Stefani Y, Olagnon C, Fantozzi G. 1993. Mechanical characterization of a zirconia ceramic used as implant material. In *Bioceramics*, Vol. 6, pp. 259–264. Ed P Ducheyne, D Christiansen. Oxford: Pergamon.
7. Callister JWD. 1994. *Materials science and engineering: an introduction*, 3rd ed. New York: Wiley.
8. Chen C, Knapp W. 1974. Fatigue fracture of an alumina ceramic at several temperatures. In *Fracture mechanics of ceramics*, pp. 691–707. Ed RC Bradt, DPH Hasselman, FF Lange. New York: Plenum.
9. Christel P, Meunier A, Heller M, Torre JP, Peille CN. 2004. Mechanical properties and short-term in vivo evaluation of yttrium-oxide partially stabilized zirconia. *J Biomed Mater Res* **23**:45–61.
10. Clarke IC, Manaka M, Green DD, Williams P, Pezzotti G, Kim YH, Ries M, Sugano N, Sedel L, Delauney C, Nissan BB, Donaldson T, Gustafson GA. 2003. Current status of zirconia used in total hip implants. *J Bone Joint Surg* **85**:73–84.
11. Dalgeish BJ, Rawling RD. 1981. A comparison of the mechanical behavior of aluminas in air and simulated body environments. *J Biomed Mater Res* **15**:527–542.
12. Derand P, Derand T. 2000. Bond strength of luting cements to zirconium oxide ceramics. *Int J Prosthodont* **13**:131–135.
13. Orthopaedic Division. 2004. *Oxinium®, oxidized zirconium*. Memphis, TN, Smith & Nephew.
14. Drennan J, Steele BCH. 1986. Zirconia and hafnia. In *Encyclopedia of materials science and engineering*, pp. 5542–5545. Ed MB Beaver. Cambridge: MIT Press.
15. Drummond JL. 1989. In vivo aging of yttria-stabilized zirconia. *J Am Ceram Soc* **72**:675–676.
16. Filiaggi MJ, Pilliar RM. 1993. Evaluating sol-gel zirconia thin films for implant applications. In *Bioceramics*, Vol. 6, pp. 265–270. Ed P Ducheyne, D Christiansen. Oxford: Pergamon.
17. Frakes J, Brown S, Kenner G. 1974. Delayed failure and aging of porous alumina in water and physiological medium. *Am Ceram Soc Bull* **53**:193–197.
18. Hamadouche M, Sedal L. 2000. Ceramics in orthopaedics. *J Bone Joint Surg* **82**:1095–1099.
19. Haraguchi K, Sugano N, Nishii T, Miki H, Oka K, Yoshikawa H. 2001. Phase transformation of a zirconia ceramic head after total hip arthroplasty. *J Bone Joint Surg* **83**:996–1000.
20. Hernigou P, Bahrami T. 2003. Zirconia and alumina ceramics in comparison with stainless-steel heads. *J Bone Joint Surg* **85**:504–509.
21. Ishimura M, Ohgushi H, Inoue K, Simaya M, Tatnai S. 1995. Hydroxyapatite and A-W glass-ceramic spacer for knee joint surgery-Applications of bioactive ceramic spacer for patello-femoral osteoarthritis. In *Bioceramics*, Vol. 8, pp. 177–183. Ed J Wilson, LL Hench, D Greenspan. Oxford: Pergamon/Elsevier Science.
22. Kingery WD, Bowen HK, Uhlmann DR. 1976. *Introduction to ceramics*, 2nd ed, pp. 3–20. New York: Wiley.
23. Kong YM, Bae CJ, Lee SH, Kim HW, Kim HE. 2005. Related articles: improvement in biocompatibility of ZrO_2–Al_2O_3 nanocomposite by addition of HA. *Biomaterials* **26**:509–517.
24. Krainess F, Knapp W. 1978. Strength of a dense alumina ceramic after aging in vitro. *J Biomed Mater Res* **12**:241–246.

25. Kumar P, Shimizu K, Oka M. 1991. Low wear rate of UHMWPE against zirconia ceramic (Y-PSZ) in comparison to alumina ceramic and SUS 316L alloy. *J Biomed Mater Res* **25**:813–828.
26. Li J, Hermansson L, Soremark R. 1993. High-strength biofunctional zirconia: mechanical properties and static fatigue behaviour of zirconia–apatite composites. *J Mater Sci: Mater Med* **4**:50–54.
27. Mandrino AR, Eloy R, Moyen B, Lerat JL, Treheux D. 1992. Base alumina ceramics with dispersoids: mechanical behaviour and tissue response after in vivo implantation. *J Mater Sci* **3**:457–463.
28. Morita Y, Nakata K, Kim YH, Sekino T, Niihara K, Ikeuchi K. 2004. Wear properties of alumina/zirconia composite ceramics for joint prostheses measured with an end-face apparatus. *Biomed Mater Eng* **14**:263–270.
29. Murakami T, Ohtsuki N. 1989. Friction and wear characteristics of sliding pairs of bioceramics and polyethylene. In *Bioceramics*, Vol. 1, pp. 225–230. Ed H Oonishi, H Aoki, K Sawai. Tokyo: Ishiyaku EuroAmerica.
30. Murray MGS, Newman M, Morrell R, Byrne WP. 1995. Evaluation of the effect of stress corrosion on zirconia femoral heads. In *Bioceramics*, Vol. 8, pp. 151–156. Ed J Wilson, LL Hench, D Greenspan. Oxford: Pergamon.
31. Odman P, Andersson B. 2001. Procera AllCeram crowns followed for 5 to 10.5 years: a prospective clinical study. *Int J Prosthodont* **14**:504–509.
32. Osterholm HH, Day DE. 1981. Dense alumina aged in vivo. *J Biomed Mater Res* **15**:279–288.
33. Patel AM, Spector M. 1995. Oxidized zirconium for hemiarthroplasty: an in vitro assessment. In *Bioceramics*, Vol. 8, pp. 169–175. Ed J Wilson, LL Hench, D Greenspan. Oxford: Pergamon.
34. Piconi C, Maccauro G. 1999. Zirconia as ceramic biomaterial. *Biomaterials* **20**:1–25.
35. Richter HG, Burger W, Osthues F. 1994. Zirconia for medical implants: the role of strength properties. In *Bioceramics*, Vol. 7, pp. 401–406. Ed OH Andersson, R-P Happonen, A Yli-Urpo. Oxford: Pergamon.
36. Rosenberg HW. 1986. Zirconium production. In *Encyclopedia of materials science and engineering*, pp. 5545–5546. Ed MB Beaver. Cambridge: Pergamon/MIT Press.
37. Sadoun M, Perelmuter S. 1997. Alumina-zirconia machinable abutments for implant supported single tooth anterior crowns. *Pract Periodont Aesthet Dent* **9**:1047–1053.
38. Shimizu K, Oka M, Kumar P, Kotoura Y, Yamamuro T, Makinouchi K, Nakamura T. 1993. Time-dependent changes in the mechanical properties of zirconia ceramic. *J Biomed Mater Res* **27**:729–734.
39. Sudanese A, Toni A, Cattaneo GL, Ciaroni D, Greggi T, Dallari D, Galli G, Giunti A. 1989. Alumina vs zirconium oxide: a comparative wear test. In *Bioceramics*, Vol. 1, pp. 237–240. Ed H Oonishi, H Aoki, K Sawai. Tokyo: Ishiyaku EuroAmerica.
40. Takagi M, Suda A, Sato T, Ishikawa A, Osanai T, Kato H, Orui H. 1995. Osteogenic response in porous 50 vol% zirconia dispersed hydroxyapatite ceramics. In *Bioceramics*, Vol. 8, pp. 431–434. Ed J Wilson, LL Hench, D Greenspan. Oxford: Pergamon.
41. Thompson I, Rawlings RD. 1990. Mechanical behaviour of zirconia and zirconia toughened alumina in a simulated body environment. *Biomaterials* **11**:505–508.
42. Tsuji T, Enomoto T, Kuwana S, Munrshige I, Inoue J, Nagai N. 1989. Basic and clinical evaluation of zirconia ceramic dental implant system. In *Oral implantology and biomaterials*, pp. 83–91. Ed H Kawahara. Amsterdam: Elsevier Science.
43. Wegner SM, Kern M. 2000. Long-term resin bond strength to zirconia ceramic. *J Adhes Dent* **2**:139–147.
44. Willmann G. 1993. Zirconia: a medical-grade material? In *Bioceramics*, Vol. 6, pp. 271–276. Ed P Ducheyne, D Christiansen. Oxford: Pergamon.
45. Yari SA, Homaeigohar S, Khavandi AR, Javapour J. 2004. The effects of partially stabilized zirconia on the mechanical properties of the hydroxyapatite–polyethylene composites. *J Mater Sci: Mater Med* **15**:853–858.
46. Zeng S, Cao W, Liu G. 1995. ZrO_2/HAP gradient ceramic biomaterials. In *Bioceramics*, Vol. 8, pp. 461–464. Ed J Wilson, LL Hench, D Greenspan. Oxford: Pergamon.
47. Zichner LP, Wilert H-G. 1992. Comparison of alumina-polyethylene and metal-polyethylene in clinical trials. *Clin Orthop Relat Res* **292**:86–94.

8

GLASS-CERAMICS

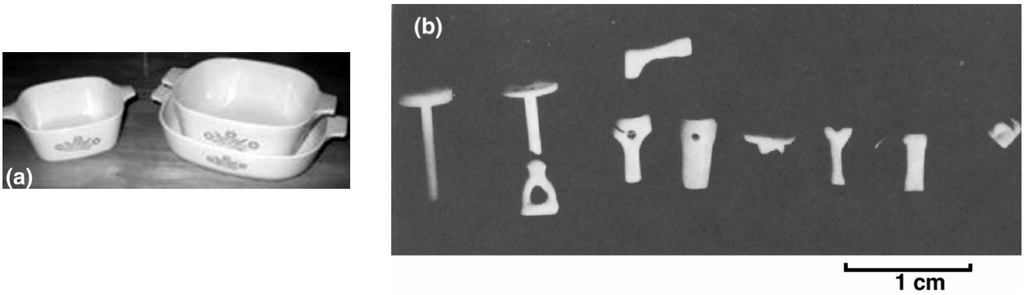

(a) Corning wares were developed in 1953 by S.D. Stookey of Corning Glass Works, as glass-ceramics that exhibit thermal shock resistance and high strength. These G-Cs can also be used as cooking tops, oven-bakable dishes, etc. A particular G-C was tailored to have a tissue reaction (via Ca/P ions) to allow intimate tissue attachment. (b) Middle ear implants shaped by a surgeon from a machinable glass-ceramic (Biovert II®). Reprinted with permission from [17]. Copyright 1993, World Scientific.

Specially formulated glass-ceramics are chemically active and react with tissues favorably, forming chemical bonds with soft and hard tissues. They are polycrystalline ceramics made by controlled crystallization of glasses, a process developed by S.D. Stookey of the Corning Glass Works in the early 1960s. Glass-ceramics were first utilized in photosensitive glasses, where small amounts of copper, silver, and gold are precipitated by irradiation with ultraviolet (UV) light. When a glass-ceramic is exposed to sunlight, the precipitates grow large enough to interfere with light waves, making the material opaque. These metallic precipitates help to nucleate and crystallize the glass into a fine-grained ceramic that possesses excellent mechanical and thermal properties and can be used in many commercial products: Corelle® wares. Bioglass®, Ceravital®, and machinable Biovert®.

8.1. FORMATION OF GLASS-CERAMICS

Important factors in forming glass-ceramics are nucleation and the growth of crystals of small (<1 μm in diameter) and uniform size [28]. It is estimated that about 10^{12} to 10^{15} nuclei per cubic centimeter are required to achieve such small crystals. In addition to the metallic agents mentioned (Cu, Ag, and Au), Pt groups, TiO_2, ZrO_2, and P_2O_5 are used as nucleating agents. The nucleation of glass is carried out at temperatures much lower than the melting or glass transition temperature, at which the melt viscosity is in the range of 10^{11} to 10^{12} Poise for at least 1 to 2 hr [21]. In order to obtain a more crystallized material, the glass is further heated to a temperature at which maximum crystal growth can be attained without deformation of product or phase transformation within the crystalline phases or redissolution of some of the phases. Crystallization is usually more than 90% complete when grain sizes are 0.1 to 1 μm, which are much smaller than in conventional ceramics. Figure 8.1 is a schematic representation of the temperature–time cycle for a glass-ceramic.

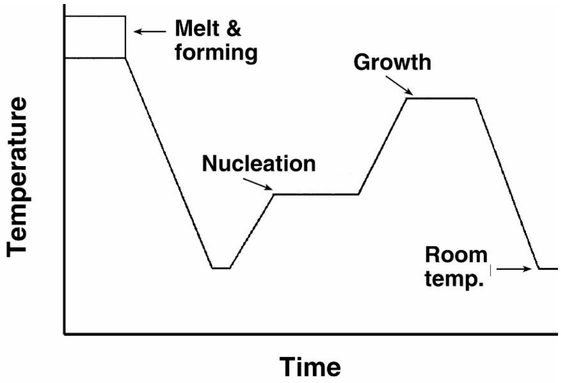

Figure 8.1. Temperature–time cycle for a glass-ceramic. Reprinted with permission from [21]. Copyright © 1976, Wiley.

Table 8.1. Compositions of Some Glass-Ceramics

Code	SiO_2	CaO	Na_2O	P_2O_5	MgO	K_2O	Al_2O_3	F	TiO_2
Bioglass®									
42S5.6	42.1	28.0	26.3	2.6	–	–	–	–	–
46S5.2(45S5)	46.1	26.9	24.4	2.6	–	–	–	–	–
49S4.9	49.1	25.3	23.0	2.6	–	–	–	–	–
52S4.6	52.1	23.8	21.5	2.6	–	–	–	–	–
55S4.3	55.1	22.2	20.1	2.6	–	–	–	–	–
60S3.8	60.1	19.6	17.7	2.6	–	–	–	–	–
Ceravital®									
Bioactive	40.0–50.0	30.0–35.0	5.0–10.0	10.0–15.0	2.5–5.0	0.5–3.0	–	–	–
Nonbioactive	30.0–35.0	25.0–30.0	3.5–7.5	7.5–12.0	1.0–2.5	0.5–2.0	–	–	–
A–W									
Bioactive	34.0	44.7	–	16.2	4.6	–	–	–	–
Biovert®									
I	29.5–50	13–28	5.5–9.5	8–18	6–28	+Na_2O	0–19.5	2.5–7	Addition
II	43–50	0.1–3	7–10.5	0.1–5	11–15	+Na_2O	26–30	3.3–4.8	–

Ceravital® and Biovert® compositions are in wt%; Bioglass® compositions are in mol%. In addition, Al_2O_3 (5.0–15.0), TiO_2 (1.0–5.0), and Ta_2O_5 (5.0–15.0) are present.
A–W has CaF_2 (0.5%) and all values are in wt%.
Data from [2,17,29,31].

Two glass-ceramics have been developed for implantation: SiO_2–CaO–Na_2O–P_2O_5 (Bioglass®) and Li_2O–ZnO–SiO_2 (Ceravital®) [2,11,31,34]. Some investigators [11,31,34] have varied the composition of the former (as given in Table 8.1) in order to obtain maximum induction of direct bonding with bone. The bonding is related to simultaneous formation of calcium phosphate and an SiO_2-rich film layer on the surface, as exhibited by the 46S5.2 system. If an SiO_2-rich layer forms first and a calcium phosphate film develops later [46–55 mol% (m/o) SiO_2] or no phosphate film is formed (60 m/o SiO_2), then no direct bonding with bone is observed [34]. The SiO_2–CaO–Na_2O (phase) diagram (Figure 8.2) shows the region (A) of reactivity, which forms bonding with tissues within 30 days; region B has too low reactivity and region C too high reactivity to form bonding; and region D does not form glass.

Machinable glass-ceramic is based on a mica–apatite glass-ceramic (SiO_2–(Al_2O_3)–MgO–Na_2O–K_2O–F–CaO–P_2O_5) and is classified as a silico-phosphate type. The chemical compositions of some glass-ceramics are given in Table 8.1. These glass-ceramics have properties similar to those of Bioglass® and can be used as a filler and for direct attachment to tissue. The illustrations on the cover of this chapter show such implants used in the ear [17].

The composition of Ceravital® is similar to Bioglass® in SiO_2 content but differs somewhat as far as the other components (Table 8.1). In addition, Al_2O_3, TiO_2, and Ta_2O_5 are present in Ceravital® in order to control the dissolution rate of the ceramic. The mixtures are melted in a (platinum) crucible at 1500ºC for 3 hr, annealed, and

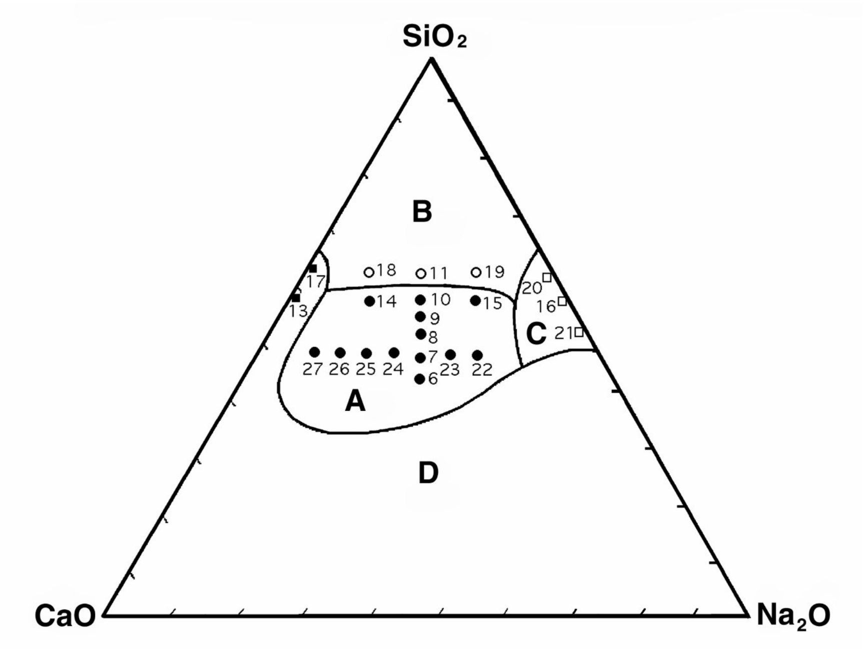

Figure 8.2. SiO_2–CaO–Na_2O (phase) diagram: (A) bonding in 30 days with bone; (B) nonbonding—too low reactivity; (C) nonbonding—too high reactivity; (D) bonding but does not form glass. Reprinted with permission from [14]. Copyright © 1982, Academic Press.

then cooled. The nucleation and crystallization temperatures are 680 and 750ºC. Both processes should proceed for 24 hr. When the crystallites are about 40 nm in size and exhibit no characteristic needle structures, the process is terminated.

The Li_2O–ZnO–SiO_2 system was originally developed for making laser crystal [12]. It was later modified to yield better x-radiopacity as well as better mechanical and thermal properties when used as filler material for restorative dental composites (see §12.2.2).

Another bioactive glass, A–W, named for its apatite and wollastonite (SiO_2·CaO) phase formation, has been developed [22,29,30]. The chemical composition of A–W glass is given in Table 8.1.

8.2. PROPERTIES OF GLASS-CERAMICS

The originally developed glass-ceramics have excellent thermal (low thermal expansion) and mechanical properties due to the controlled grain size. In addition, crystallization of the nuclei by light makes manufacture of photosensitive glass possible.

Table 8.2. Mechanical Properties of Glass-Ceramics

Properties	Bioglass®	Ceravital®	A–W
Young's modulus (GPa)	35	100–159	118
Tensile strength (MPa)	200	400	–
Compressive strength (MPa)	42	500	1080
Bending strength (MPa)	160–190	130	215
Hardness (Vickers)	458	294	680
Fracture toughness (MPa·m$^{1/2}$)	2.0	4.6	3.34

8.2.1. Mechanical Properties

Due to the controlled grain size and improved resistance to surface damage, glass-ceramics can have at least double the tensile strength (from about 100 to 200 MPa), and their resistance to scratching and abrasion are close to that of sapphire [37]. The modulus of elasticity is on the order of 100 GPa, and the compressive strength is about five times the tensile strength, as given in Table 8.2. Their mechanical properties are inferior to those of alumina or other nonbioactive ceramics, so that application of these materials is usually limited to coatings or composites — similar to hydroxyapatites.

8.2.2. Chemical Properties

Dissolution of ions into an (aqueous) medium (Fig. 8.3) is thought to be the first step in the reaction of glass-ceramics with hard or soft tissues. During this process the pH changes as shown in Figure 8.4. Auger electron spectroscopy (AES) and infrared reflection spectroscopy (IRRS) of the surface of Bioglass® has demonstrated that in-vitro formation of the calcium phosphate-rich surface film corresponds closely to the capability of the material to bond to living bone (see Figs. 8.5 and 8.6). The similarity in infrared reflectance spectra between hydroxyapatite and the glass-ceramic after dissolution is further evidence of possible direct bonding with bone. Transmission electron microscopy (Fig. 8.7) has shown a close relationship between mineralized bone and Bioglass® implanted in the femurs of rats for 6 weeks [1].

The chemical reactivity of glass-ceramics makes them bioactive with soft and hard tissues if properly selected for composition. They can thus be further subdivided into two categories (A and B) with respect to bioactivity. If a ceramic leads to "osteoproduction" (or osteoinduction), it belongs to group A, and if to "osteoconduction" group B. It was further hypothesized that osteoprodution occurs when a material elicits both an intracellular and an extracellular response at its interface with tissue [22]. Osteoconduction takes place when a material elicits only an extracellular response at its interface [12]. Figure 8.8 demonstrates the time-dependent behavior of category A and B ceramics in vivo and in vitro. The release of soluble silicon as silicic acid is due

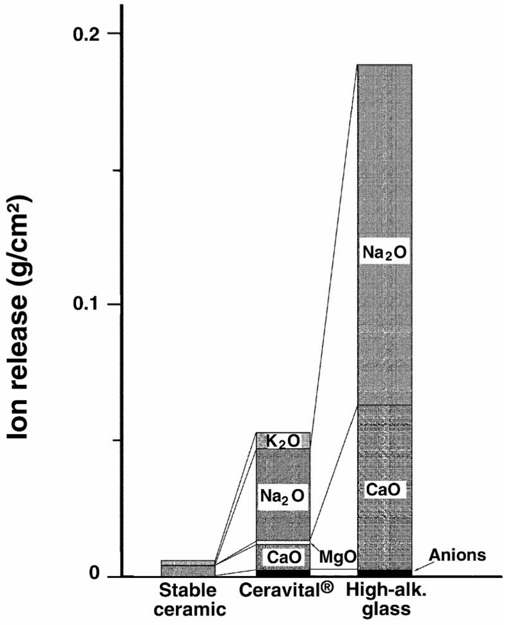

Figure 8.3. Solubility of powder samples of different bioactive glasses and ceramics in a neutral solvent at pH 7.3. Reprinted with permission from [2]. Copyright © 1978, Wiley.

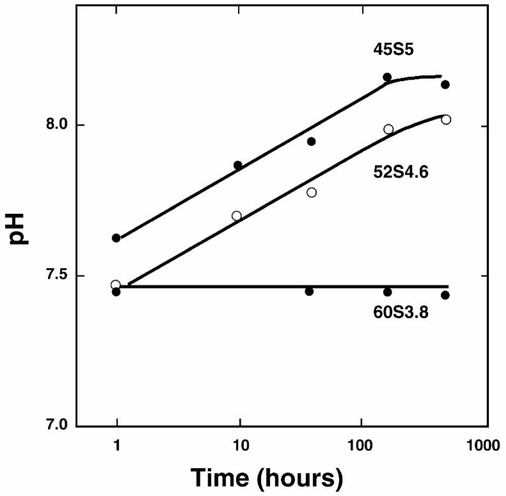

Figure 8.4. Changes in pH of a solution exposed to various glass compositions as a function of reaction time. Reprinted with permission from [31]. Copyright © 1980, Wiley.

to ion exchange with H^+ and H_3O^+, which takes place immediately (Fig. 8.8A) [23]. The rate of dissolution of silicon decreases over time due to the increased pH and precipitation of complex silicate phases near the surface. Other investigators have shown

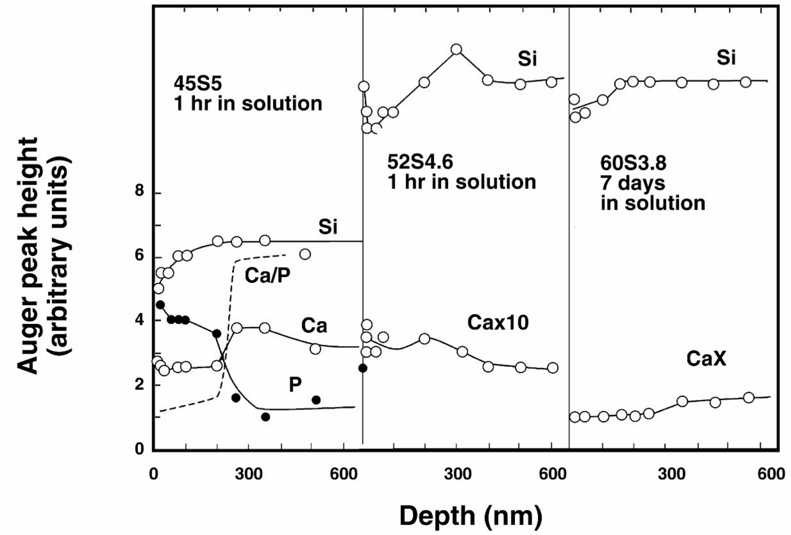

Figure 8.5. Depth profile of 45S5, 52S4.6, and 60S3.8 glasses after reactions by AES using an iron milling technique with an Ar ion beam. Reprinted with permission from [31]. Copyright © 1980, Wiley.

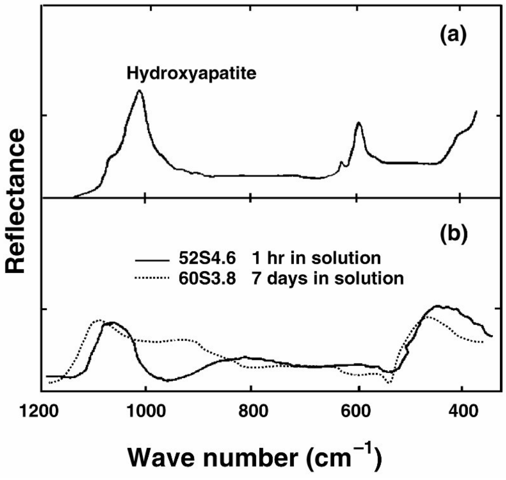

Figure 8.6. (a) IRRS spectrum of hydroxyapatite and (b) difference in IRRS spectra between 1-hr-reacted 52S4.6 and 7-day-reacted 60S3.8 glass. Reprinted with permission from [31]. Copyright © 1980, Wiley.

the importance of soluble silicon to specific metabolic role in connective tissue at the cellular level, where the silicon complexes with glycosaminoglycan proteins, which are the matrix materials for the collagen, elastin, etc. [5,39]. The marked increase in proliferation and differentiation of the cells of the osteoblast lineage may also be due to the soluble silicon, which may induce release of transforming growth factor (TGF-β_1) as shown in Figure 8.8B [20]. Similar results were seen in terms of alkaline

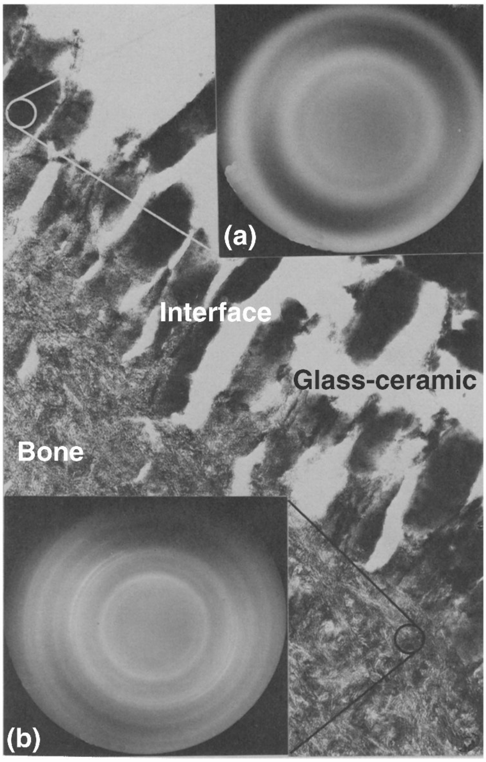

Figure 8.7. Transmission electron micrograph of well-mineralized bone juxtaposed with the glass-ceramic, which was fractured during sectioning (51,500×). Insert (a) is the diffraction pattern from the ceramic area, and (b) is from the bone area. Reprinted with permission from [1]. Copyright © 1971, Springer.

phosphatase activity (APA) and collagen production (Fig. 8.8C,D) [5,44]. The soluble silicon accelerates formation of amorphous calcium phosphate (ACP) much more in category A than in category B ceramics (Fig. 8.8E). The ACP becomes possible sites of heterogeneous nucleation of crystalline hydroxycarbonate apatite (HCA) [8,33]. (See Fig. 9.10 for a depiction of HA crystallization on the surface of Bioglass®.) In-vivo experiments have shown faster bone bonding in category A ceramics (Fig. 8.8F) due to the above-mentioned factors [13].

Clinical application of glass-ceramics is limited due to their inherent properties: brittleness, weak tensile strength, and difficulty in applying to the surface of other, stronger materials. The majority of applications is limited to the ENT, maxillofacial, and dental areas [23,25,43,46], although some load-bearing applications have been attempted [18,49].

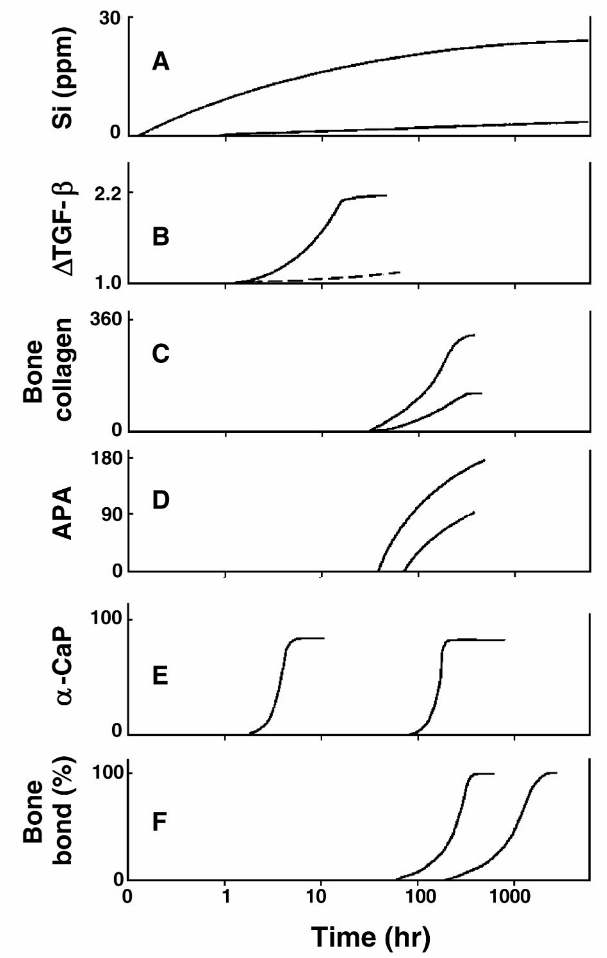

Figure 8.8. Time-dependent behavior of category A and B bioactive materials. Reprinted with permission from [12]. Copyright © 1994, Pergamon/Elsevier Science.

Example 8.1

Estimate the amount of dissolution in vitro on the surface of an implant made of 45S5 Bioglass® per year if it belongs to category A in Figure 8.8A.

Answer

From the figure one can approximate the slope between 100 and 1000 hr:

$$1 \text{ year} = 365 \text{ days} \times 24 \text{ hr/day}$$

$$\text{Dissolution rate} = \frac{28-24}{1000-100} = 4.4 \times 10^{-3} \text{ ppm/hr}$$

$$= 4.4 \times 10^{-3} \times 8760 \text{ ppm/yr} = 38.5 \text{ ppm/yr.}$$

$$1 \text{ ppm} = 1 \text{ mg/1000 g.}$$

Therefore,

$$\text{Dissolution rate} = \underline{38.5\ \text{ppm/yr}} = \underline{38.5 \times 10^{-3}\ \text{mg/g/yr}} = \underline{0.0385\ \text{mg/g/yr}}.$$

Dissolution is measured in terms of the concentration of silicon [Si]. It cannot be determined that there is a one-to-one relationship between [Si] and the matrix material. This indicates that the Bioglass® will dissolve at a rate of 0.0385 mg per year from 1 g of the Bioglass® if the conditions are the same.

8.3. COATINGS AND COMPOSITES

The main drawback of glass-ceramics, as with other glasses and ceramics, is its brittleness. Furthermore, due to the restrictions on its composition for biocompatibility (or osseo- or osteogenicity), the mechanical strength cannot be substantially improved as can be done for industrial glass-ceramics. Therefore, they cannot be used in making such major load-bearing implants as joints. Coating of bioactive glass-ceramics onto other materials is very difficult due to thermal expansion coefficient incompatibility, minimal chemical bonding, and variability of the chemical structure if the coating condition (temperature and pressure) is not properly controlled. Some have tried to coat alumina ceramic and 316L stainless steel [6,10,35]. The stainless steel was coated by sintering twice with insoluble glass (SiO_2, Al_2O_3, Na_2O, CaO, and K_2O). The third layer was applied with bioactive glass-ceramics (CaO 46.6%, P_2O_3 14.2%, MgO 4.7%, Na_2O 3.3%, CaF_2 1.2%, and SiO_2). The resulting coated implant showed similar tissue reaction to the bioactive ceramic and good enough mechanical properties (460-MPa bending strength) for such load-bearing applications as dental implants [6].

There have been many attempts to make composites from bioactive glass-ceramic powders with polyethylene [45] (see Fig. 12.12) and polysulfone [32], and glass-ceramic fibers with polysulfone to increase its strength [27]. PMMA (polymethylmethacrylate) and bis-GMA [(bisphenol-α-glycidyl methacrylate] bone cements have been formulated to test their feasibility for use in fixing implants [15,37,40]. These composites have two major drawbacks that cannot be easily overcome. One is the inherent lack of bonding between glass-ceramics and matrix materials, thus weakening their tensile/compressive strength. The other is that the bioactivity of glass-ceramics cannot be expressed at the surface due to *encapsulation* of the matrix materials over the powder or granules.

8.4. FURTHER THOUGHTS

The use of glass-ceramics in implant fabrication is quite limited.. This is mainly due to problems encountered with other glasses and ceramics, including brittleness, limited failure predictability, and difficulty in coating onto other materials [7,15,16, 19,24,38,40,42,48]. In dental applications, the glass-ceramics have shown a similar response to other hard tissues [26,41,50].

It will be a great challenge to develop a new ceramic material with the strength and toughness of the cermets now used for many years in the machine tool industry [3,9,36]. Porous glass-ceramics have also been studied and have shown properties similar to those of porous ceramics and glasses [4].

PROBLEMS

8.1. Why would one manufacture glass-ceramics by a two-step process rather than making them directly from melt?

8.2. Estimate the amount of dissolution in vitro on the surface of an implant made of 45S5 Bioglass® per year if it belongs to category A (Fig. 8.8A).

8.3. According to Figure 8.8F, the only difference in percentage of bone bonding for categories A and B is onset of time of bonding. If one is supposed to make a permanent implant from these materials, which one would you choose? State your reasons.

8.4. Bioglass® is used to make artificial bone. Propose how you would proceed to do this? Consider two possible ways of applying Bioglass® during surgery.

8.5. If the artificial bone of Problem 8.4 is made of equal proportions of the three components, calculate the tensile strength and modulus of the resulting material.

8.6. Bioglass® is used to make a composite with HDPE (high-density polyethylene) [45]. The amounts of Bioglass® are 10 and 40% by volume. They are mixed as powder, and then molded after blending, compounding, and centrifugal milling. Calculate the theoretical modulus and tensile strength of the composites if the modulus and strength of HDPE are 650 and 18 MPa, respectively. Is your estimate reasonable? If not, please explain.

8.7. Calculate the average distance between particles if the average particle size of monodispersed Bioglass® is about 45 μm. The particles constitute 10% by volume in an HDPE resin [45].

8.8. Stainless steel fibers and Bioglass® glass-ceramics are made into a composite that are 50–50% by volume.

Materials	Ultimate tensile strength (MPa)	Tensile modulus (GPa)
SS fiber	530	200
Bioglass®	40	?

a. Calculate the tensile modulus of the Bioglass® if the tensile strain of the Bioglass® is 0.1%.
b. Calculate the strength of the composite in the fiber direction.
c. Calculate the strength of the composite, in the direction *perpendicular* to the fiber.
d. Calculate the thermal shock resistance of Bioglass®, whose thermal expansion coefficient is $\alpha = 10^{-5}$/°C.
e. What is the major problem of coating stainless steel with Bioglass®? How would you overcome this?

8.9. Read: Hench LL. 1994. Bioactive ceramics: theory and clinical applications. In *Bioceramics*, Vol. 7, pp. 3–14. Ed OH Andersson, R-P Happonen, A Yli-Urpo. Oxford: Pergamon/Elsevier Science.

DEFINITIONS

ACP: Amorphous calcium phosphate that dissolves faster than crystalline form in vivo.

AES: Auger electron spectroscopy, which can identify and quantify the atoms in a material.

APA: Alkaline phosphate activity for measuring rate of glass-ceramic dissolution in vitro or in vivo.

A–W: A two-phase silica–phosphate glass-ceramic composed of apatite [$Ca_{10}(PO_4)_6(OH,F)_2$] and wollastonite [$CaO{\cdot}SiO_2$].

Bioglass®: A glass-ceramic using phosphorous pentoxide (P_2O_5) as seeding material for tissue (especially hard tissue) formation at the interface by slowly dissolving its surface.

Biovert®: A machinable glass-ceramic based on an SiO_2–(Al_2O_3)–MgO–Na_2O–K_2O–F–CaO–P_2O_5 system.

bis-GMA: Bis-phenol-α-glycidyl methacrylate — used mostly in dental adhesives and composite matrix binders.

Ceravital®: A glass-ceramic developed for implant similar to Bioglass®.

ENT: Ear, nose, and throat.

HCA: Crystalline hydroxycarbonate apatite being formed on the surface of Bioglass® when dissolved.

IRRS: Infrared reflection spectroscopy, Measures the surface properties of materials.

Osteoconduction: A material property that allows only an extracellular response at the interface .

Osteogenicity: Bone-forming capacity.

Osteoinduction: Both intracellular and extracellular affinity of bone formation.

Osteoproduction: Bone tissue formation.

Photosensitive glass: Glasses that change their light transmissivity with a change in the amount of light energy available.

TGF-β: Transforming growth factor, one of the growth factors isolated from various tissues, widely studied in hard tissue repair and regeneration.

REFERENCES

1. Beckham C, Greenlee Jr T, Crebo A. 1971. Bone formation at a ceramic implant interfacing. *Calcif Tissue Res* **8**:165–171.
2. Blencke BA, Bromer H, Deutscher KK. 1978. Compatibility and long-term stability of glass-ceramic implants. *J Biomed Mater Res* **12**:307–318.
3. Brandt AM. 1994. Cement-based composites: materials, mechanical properties and performance. Boca Raton, FL: Taylor & Francis.
4. Brovarone CV, Verne E, Appendino P. 2006. Macroporous bioactive glass-ceramic scaffolds for tissue engineering. *J Mater Sci: Mater Med* **17**:1069–1078.
5. Carlisle E. 1986. Biological silicon. In *Silicon biochemistry*, pp. 123–136. Ed D Evered. New York: Wiley.
6. Cavalheiro JJ, Bronco R, Afonso A, Vasconcerlos M. 1995. Multilayer coating of stainless steel with insoluble and bioactive glasses: "in vitro" and "in vivo" tests. In *Bioceramics*, Vol. 8, pp. 509–512. Ed J Wilson, LL Hench, D Greenspan. Oxford: Pergamon/Elsevier Science.
7. Clupper D, Hench LL. 2001. Bioactive responses of Ag-doped tape coat Bioglass® 45S5 following heat treatment. *J Mater Sci: Mater Med* **12**:917–921.
8. Damen JJM, TenCate JM. 1989. The effect of silicic acid on calcium phosphate preparation. *J Dent Res* **68**:1355–1359.
9. Evans A, San Marchi C, Mortensen A. 2003. *Metal matrix composites in industry: an introduction and a survey*. New York: Springer.
10. Griss P, Greenspan D, Heimke G, Krenpien B, Buchinger R, Hench L, Jentchura G. 1976. Evaluation of a Bioglass-coated Al_2O_3 total hip prosthesis in sheep. *J Biomed Mater Res Symp* **7**:511–518.
11. Hench L, Pachall H. 1973. Direct chemical bond of bioactive glass-ceramic materials to bone and muscle. *J Biomed Mater Res Symp* **2**:5–42.
12. Hench LL. 1994. Bioactive ceramics: theory and clinical applications. In *Bioceramics*, Vol. 7, pp. 3–14. Ed OH Andersson, R-P Happonen, A Yli-Urpo. Oxford: Pergamon/Elsevier Science.
13. Hench LL, Clark AE. 1982. Adhesion to bone. In *Biocompatibility of Orthopedic Implants*, Vol. 1, pp. 129–170. Ed DF Williams. Boca Raton, FL: CRC Press.
14. Hench LL, Ethridge EC. 1982. *Biomaterials: an interfacial approach*. New York: Academic Press.
15. Hench LL, Polak JM. 2002. Third generation biomedical materials. *Science* **295**:1014–1017.
16. Holand W, Rheinberger V, Apel E, Hoen CV, Holand M, Dommann A, Obrecht M, Mauth C, Graf-Hausner U. 2006. Clinical applications of glass-ceramics in dentistry. *J Mater Sci: Mater Med* **17**:1037–1042.
17. Holand W, Vogel W. 1993. Machinable and phosphate glass-ceramic. In *Introduction to Bioceramics*, pp. 125–137. Ed LL Hench, J Wilson. Singapore: World Scientific.
18. Ishimura M, Ohgushi H, Inoue K, Simaya M, Tatnai S. 1995. Hydroxyapatite and A-W glass-ceramic spacer for knee joint surgery-Applications of bioactive ceramic spacer for patello-femoral osteoarthritis. In *Bioceramics*, Vol. 8, pp. 177–183. Ed J Wilson, LL Hench, D Greenspan. Oxford: Pergamon/Elsevier Science.
19. Kamitakahara M, Ohtsuki C, Inada H, Tanihara M, Miyazaki T. 2006. Effect of ZnO addition on bioactive $CaO–SiO_2–P_2O_5–CaF_2$ glass-ceramics containing apatite and wollastonite. *Acta Biomater* **2**:467–71.
20. Keeting F. 1956. *Chromium-nickel autentic steels*. London: Butterworths.
21. Kingery WD, Bowen HK, Uhlmann DR. 1976. *Introduction to ceramics*, 2nd ed, pp. 3–20. New York: Wiley.
22. Kokubo T, Ito S, Shigematsu M, Sakka S, Yamamuro T. 1985. Mechanical properties of a new type of apatite-containing glass-ceramic for prosthetic applications. *J Mater Sci* **20**:2001–2004.
23. Larmas E, Sewon L, Luostarinen T, Kamgasniemi I, Yli-Urpo A. 1995. Bioactive glass in periodontal bone defects. Initial clinical findings of soft tissue and osseous repair. In *Bioceramics*, Vol. 8, pp. 279–284. Ed J Wilson, LL Hench, D Greenspan. Oxford: Pergamon/Elsevier Science.
24. Lenza RFS, Jones JR, Vasoconcelos WL, Hench LL. 2003. In vitro release kinetics of proteins from bioactive foams. *J Biomed Mater Res* **57A**:121–129.

25. Litkowski LJ, Niehaus-Rohde C. 1995. Comparison of pulpal inflammatory response using calcium hydroxide versus particulate Bioglass® in human teeth. In *Bioceramics*, Vol. 8, pp. 289–293. Ed J Wilson, LL Hench, D Greenspan. Oxford: Pergamon/Elsevier Science.
26. Low SB, King CJ, Krieger J. 1997. An evaluation of bioactive ceramic in the treatment of periodontal osseous defects. *Intern J Periodont Restor Dent* **17**:359–367.
27. Marcolongo M, Ducheyne P, Cukler J, LaCourse W. 1993. Histological evaluation of a bioactive glass fiber/polysulfone composite. In *Bioceramics*, Vol. 6, pp. 353–357. Ed P Ducheyne, D Christiansen. Oxford: Pergamon/Elsevier Science.
28. McMillan PW. 1979. *Glass-ceramics*. New York: Academic Press.
29. Nakamura T, Yamamuro T. 1993. Development of a bioactive ceramic, A-W glass-ceramic. In *Bioceramics*, Vol. 6, pp. 105–110. Ed P Ducheyne, D Christiansen. Oxford: Pergamon/Elsevier Science.
30. Nakamura T, Yamamuro T, Higashi S, Kokubo T, Ito S. 1985. A new glass-ceramic for bone replacement: evaluation of its bonding to bone tissue. *J Biomed Mater Res* **19**:685–698.
31. Ogino M, Ohuchi F, Hench L. 1980. Compositional dependence of the formation of calcium phosphate film on Bioglass. *J Biomed Mater Res* **14**:55–64.
32. Orefice RL, LaTorre GP, West JK, Hench LL. 1995. Processing and characterization of bioactive polysulfone–Bioglass® composites. In *Bioceramics*, Vol. 8, pp. 409–414. Ed J Wilson, LL Hench, D Greenspan. Oxford: Pergamon/Elsevier Science.
33. Pereira MM, Clark AE, Hench LL. 1994. Effect of texture on the rate of hydroxyapatite formation on silica gel surface. *J Am Ceram Soc* **78**:2463–2468.
34. Piotrowski G, Hench L, Allen W, Miller G. 1975. Mechanical studies of bone–Bioglass interfacial bone. *J Biomed Mater Symp* **6**:47–61.
35. Ritter Jr J, Greenspan D, Palmer R, Hench L. 1979. Use of fracture of an alumina and Bioglass-coated alumina. *J Biomed Mater Res* **13**:251–263.
36. Ryu HS, Lee JK, Seo JH, Kim H, Hong KS, Kim DJ, Lee JH, Lee DH, Chang BS, Lee CK, Chung SS. 2004. Novel bioactive and biodegradable glass ceramics with high mechanical strength in the $CaO–SiO_2–B_2O_3$ system. *J Biomed Mater Res* **68A**:79–89.
37. Saravanapavan P, Hench LL. 2000. Low-temperature synthesis, structure, and bioactivity of gel-sol derived glasses in the binary $CaO–SiO_2$ system. *J Biomed Mater Res* **54**:608–618.
38. Saravanapavan P, Jones JR, Pryce RS, Hench LL. 2003. Bioactivity of gel-glass powders in the $CaO–SiO_2$ system: a comparison with ternary ($CaO–P_2O_5–SiO_2$) and quaternary glass ($SiO_2–CaO–P_2O_5–Na_2O$). *J Biomed Mater Res* **66A**:110–119.
39. Schwartz K, Milne DB. 1972. Growth-promoting effects of silicon in rats. *Nature* **239**:333–334.
40. Sepulved P, Jones JR, Hench LL. 2002. In vitro dissolution of melt-derived 45S5 and sol-gel derived 58S bioactive glasses. *J Biomed Mater Res* **61A**:301–311.
41. Stanley HR, Hall MB, Clark AE, King CJ 3rd, Hench LL, Berte JJ. 1997. Using 45S5 bioglass cones as endosseous ridge maintenance implants to prevent alveolar ridge resorption: a 5-year evaluation. *Int J Oral Maxillofac Implants* **12**:95–105.
42. Thompson ID, Hench LL. 1998. Mechanical properties of bioactive glasses, glass-ceramics and composites. *J Eng Med* **212**:127–137.
43. Turunen T, Peltola J, Kangasniemi I, Jussila J, Uusipaikka E, Yli-Urpo A, Happonen R-P. 1995. Augmentation of the maxillary sinus wall using bioactive glass and autologous bone. In *Bioceramics*, Vol. 8, pp. 259–264. Ed J Wilson, LL Hench, D Greenspan. Oxford: Pergamon/Elsevier Science.
44. Vrouwenvelder WCA, Groot CG, de Groot K. 1993. Histological and biochemical evaluation of osteoblasts cultured on bioactive glass, hydroxylapatite, titanium alloy, and stainless steel. *J Biomed Mater Res* **27**:465–475.
45. Wang M, Bonfield W, Hench LL. 1995. Bioglass®/high density polyethylene composite as a new soft tissue bonding material. In *Bioceramics*, Vol. 8, pp. 383–388. Ed J Wilson, LL Hench, D Greenspan. Oxford: Pergamon/Elsevier Science.
46. Wilson J, Douek E, Rust K. 1995. Bioglass® middle ear devices: ten-year clinical results. In *Bioceramics*, Vol. 8, pp. 239–245. Ed J Wilson, LL Hench, D Greenspan. Oxford: Pergamon/Elsevier Science.

47. Wyatte OM, Dew-Hughes D. 1974. *Metals, ceramics, and polymers*. London: Cambridge UP.
48. Xynos ID, Edgar AJ, Buttery LDK, Hench LL, Polak JM. 2001. Gene-expression profiling of human osteoblasts following treatment with the ionic products of Bioglass® 45S5 dissolution. *J Biomed Mater Res* **55**:151–157.
49. Yamamuro T. 1995. AW glass-ceramic in spinal repair. In *Bioceramics*, Vol. 8, pp. 123–127. Ed J Wilson, LL Hench, D Greenspan. Oxford: Pergamon/Elsevier Science.
50. Zamet JS, Darbar UR, Griffiths GS, Bulman JS, Bragger U, Burgin W, Newman HN. 1997. Particulate Bioglass as a grafting material in the treatment of periodontal intrabony defects. *J Clin Periodont* **24**:410–418.

9

HYDROXYAPATITE

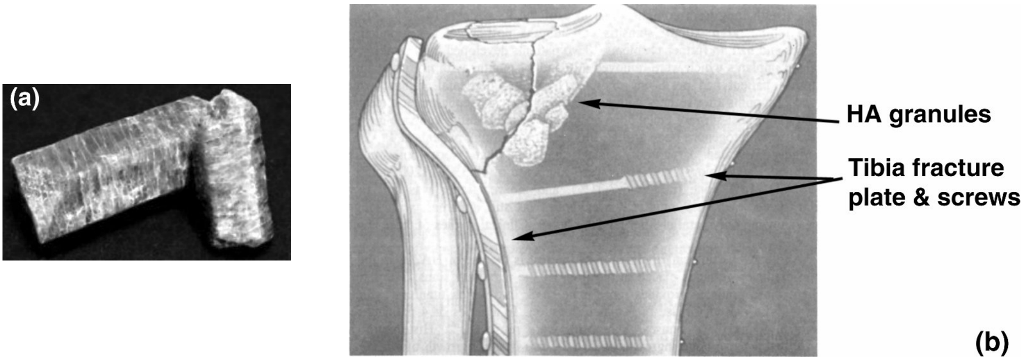
(a)
HA granules
Tibia fracture plate & screws
(b)

(a) Phosphate mineral apatites can be grouped into, hydroxy(l)apatite, fluorapatite, and chlorapatite [$Ca_5(PO_4)_3(OH,F,Cl)$]. Reprinted with permission from http://en.wikipedia.org/wiki/Apatite. (b) HAs are used extensively as bone regeneration or as substitutes in granular, porous, and solid form. Modified with permission from [57]. Copyright © 1993, World Scientific.

Hydroxyapatite (HA) is a member of the apatite group of ceramics. The term “apatite” is derived from the Greek *apatê*, which means deceit or deception. It was called such for its diversity of form and color [46]. It has been tested many times as artificial bone since it is similar to the natural bone though devoid of such organic constituents as collagen and polysaccharides [49]. HA has been synthesized and used to manufacture various forms of implants (solid and porous) and as a coating on other implants.

Table 9.1. Composition and Physical Properties of Apatites in Adult Human Enamel, Dentine, and Bone

Composition	Enamel	Dentine	Bone
Calcium, Ca^{2+}	36.5	35.1	34.10
Phosphorous, as P	17.7	16.9	15.2
(Ca/P) molar	1.63	1.61	1.71
Sodium, Na^{+}	0.5	0.6	0.9
Magnesium, Mg^{2+}	0.44	1.23	0.72
Potassium, K^{+}	0.010	0.05	0.03
Carbonate, as CO_3^{2-}	3.5	5.6	7.4
Fluoride, F^{-}	0.01	0.06	0.03
Chloride, Cl^{-}	0.30	0.01	0.13
Pyrophosphate, $P_3O_7^{4-}$	0.022	0.10	0.07
Total inorganic (mineral)	97.0	70.0	65.0
Total organic	1.5	20.0	25.0
Absorbed H_2O	1.5	10.0	10.0
Trace elements: Sr^{2+}, Pb^{2+}, Zn^{2+}, Cu^{2+}, Fe^{3+}, etc.			
Crystallographic properties			
Lattice parameters (+0.0003 nm)			
a-axis	0.9441	0.9421	0.941
c-axis	0.610100	0.610107	0.6109
“Crystallinity index”	70~75	33~37	33~37
Crystallite size (nm)	0.13 × 0.03	0.020 × 0.004	0.025 × 0.003
Ignition products (1000ºC)	β-TCMP*+HA	β-TCMP*+HA	HA + CaO

Weight analyses based on ashed samples except for CO_3, which was determined on an unashed sample using an IR method. “Crystallinity index” is determined from the ratio of coherent to incoherent scattering in mineral OH–apatite taken as 100 [37,38].

*β-TCMP = Mg-substituted β-tricalcium phosphate, or whitlockite in biological systems, β-TCP is always Mg substituted, $(Mg,Ca)_3 (PO_4)_2$.

Reprinted with permission from [36]. Copyright © 1994, CRC Press.

9.1. SOURCE, COMPOSITION, AND STRUCTURE

There are two sources of apatite: one biological and the other from mineral deposits, such as phosphate rock or phosphorite, a sedimentary rock the essential mineral components of which is carbonate fluoroapatite [46]. As mentioned in Chapter 5, bone and teeth contain a HA-like mineral component that supports the majority of load in vivo. The chemical composition, crystal structure, and other properties of enamel, dentine, and bone are summarized in Table 9.1. Deorganized bone and some sea corals

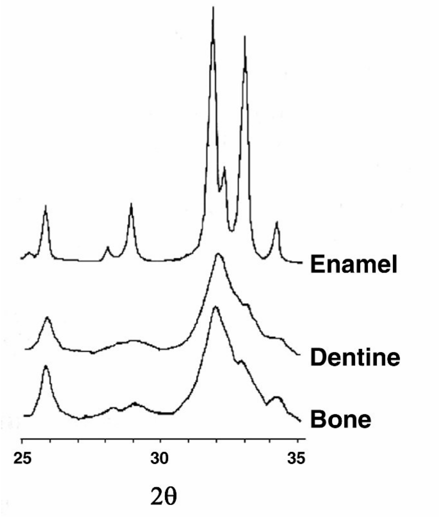

Figure 9.1. X-ray diffraction pattern of enamel, dentine, and bone. Reprinted with permission from [36]. Copyright © 1994, CRC Press.

(*porites*) are used to make implants [2,6,24,44,49]. The x-ray diffraction patterns for enamel, dentine, and bone are depicted in Figure 9.1. As can be seen, enamel has a sharp and well-defined pattern, as opposed to dentine and bone, which is due to the larger crystallites and higher crystallization of the mineral phase (see Fig. 5.6 and Table 9.1).

Table 9.2 presents the many techniques for making HA, of which the hydrothermal method is the most widely studied and commercially used. Calcium hydroxyapatite [20] ceramic is usually prepared from apatites obtained by precipitation or hydrolysis under nonacidic conditions and subsequently sintered at temperatures between 950 and 1300°C. Precipitation can be obtained by the following reactions [5,30]:

$$Ca(NO_3)_2 + (NH_4)_2HPO_4 + NH_4OH \xrightarrow[1100^\circ C]{} Ca_{10}(PO_4)_6(OH)_2, \tag{9.1}$$

$$Ca(Ac)_2 + (NH_4)_2HPO_4 + NH_4OH \xrightarrow[950\text{–}1100^\circ C]{} Ca_{10}(PO_4)_6(OH)_2, \tag{9.2}$$

or by dropwise addition of phosphoric acid to a saturated solution of calcium hydroxide, $Ca(OH)_2$:

$$Ca(OH)_2 + H_3(PO_4)_2 + NH_4OH \xrightarrow[1100^\circ C]{} Ca_{10}(PO_4)_6(OH)_2, \tag{9.3}$$

HA ceramic may also be prepared by sintering the products of hydrolysis of dicalcium phosphate dihydrate (DCPD, $CaHPO_42H_2O$), dicalcium phosphate anhydrous (DCPA, $CaHPO_4$), or octacalcium phosphate [OCP, $Ca_{10}H_2(PO_4)_65H_2O$] in basic solutions or of $CaCO_3$ in phosphate solutions [37]:

$$CaHPO_4 \text{ or } CaHPO_4 \cdot 2H_2O + NH_4OH \xrightarrow[950\text{–}1100^\circ C]{} Ca_{10}(PO_4)_6(OH)_2\,, \qquad (9.4)$$

$$CaCO_3 + (NH_4)_2HPO_4 \xrightarrow[950\text{–}1100^\circ C]{} Ca_{10}(PO_4)_6(OH)_2\,. \qquad (9.5)$$

Table 9.2. Preparation Techniques for Hydroxyapatite

Techniques	Starting materials	Synthetic conditions	Comments
Solid-state reaction	$Ca_3(PO_4)_2 + CaCO_3$ $Ca_2P_2O_7 + CaCO_3$	900~1,300ºC, usually with water vapor flowing	Ca/P = 1.67, large grain size, irregular forms, inhomogeneous
Wet chemical method	$Ca(NO_3)_2 + (NH_4)_2HPO_4$ $Ca(OH)_2 + H_3PO_4$	R.T. ~ 100ºC pH: 7~12	Ca/P < 1.67, fine irregular crystals with low crystallinity, inhomogeneous
Hydrothermal method	Wet chemically prepared HA, other calcium phosphates, seeding	100~200ºC (1~2 MPa) 300~600ºC (1~2 kbar)	Ca/P = 1.67, homogeneous, fine single crystals or large crystals
Gel growth method	Gel + Ca^{2+} + PO_4^{3-}	R.T. ~ 60ºC pH: 7~10	Large monetite, brushite, OCP, but small Hap
Melt growth method	$Ca_3(PO_4)^{2-}$ PO_4^{3-} CaF_2, $CaCl_2$	1650ºC	Large crystals with lattice strain
Flux growth method	CaF_2, $CaCl_2$ as flux $Ca(OH)_2$ as flux	1325ºC (FAp, ClAp) HA	Large crystals with little lattice strain

Sol–gel, alkoxide, and the other chemical methods have also been used. Chemical vapor deposition (CVD), the plasma spray method, and other electrochemical methods have been mainly used to form HA layers on substrate.

Reprinted with permission from [61]. Copyright © 1994, CRC Press.

It is necessary to control the pH of the reaction and the concentration of each of the reactants to obtain mainly HA, β-TCP [tricalcium phosphate, $Ca_3(PO_4)_2$], or TCP can be prepared in dense (microporous) or macroporous forms. Macroporous ceramic (pores > 500 μm) is prepared by adding foaming agents such as hydrogen peroxide or naphthalene before compacting, heating at low temperature to remove foaming agents, and then sintering at high temperatures (950–1100ºC). Dense or microporous ceramics can be obtained by sintering at high temperatures (1100–1300ºC) and pressure (140–200 MPa), by hot isotropic pressing (HIP), uniaxial pressing, or hot pressing method.

Hydrothermal processing requires an aqueous solution of carbonate and phosphate at relatively high temperatures (>100°C) and pressures (>1 atm) in a closed system. Figure 9.2 depicts the phase diagram of a $CaO–P_2O_5–H_2O$ system under hydrothermal conditions of 600°C and 2 kbar (1 bar = 0.9107 atm). At a lower temperature (200°C) and pressure (1.7 kbar), it would take longer to react and reach equilibrium [16]. Most of the products are precipitates, which have to be filtered, dried, and sintered to make usable endproducts. Some investigators have tried to fabricate single crystals and succeeded in making rods as large as 10 mm in length with a diameter of 0.5 μm by the hydrothermal method [15].

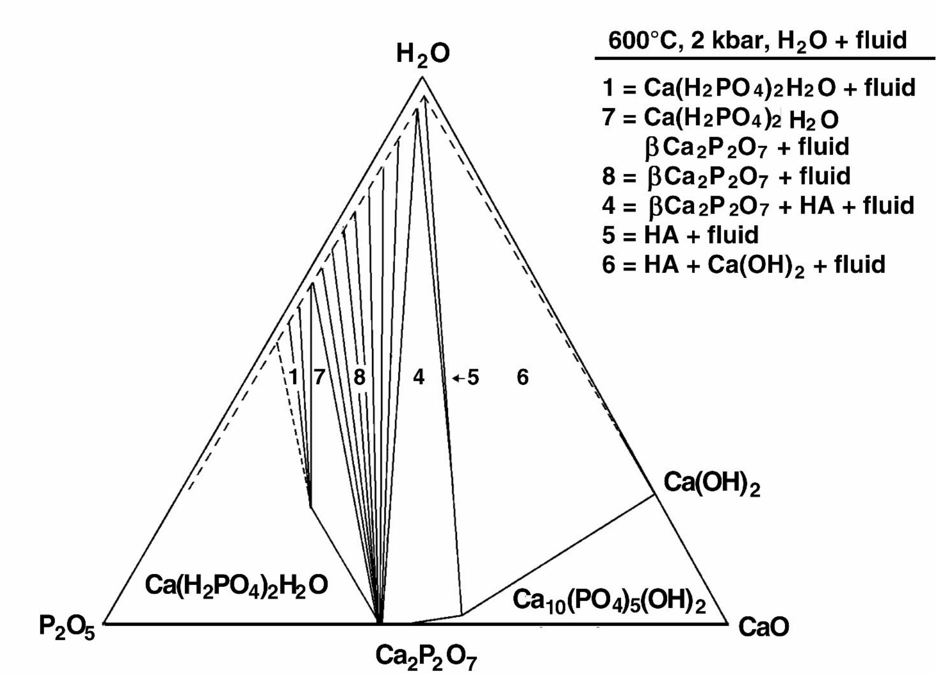
600°C, 2 kbar, H_2O + fluid
1 = $Ca(H_2PO_4)_2H_2O$ + fluid
7 = $Ca(H_2PO_4)_2$ H_2O
$\beta Ca_2P_2O_7$ + fluid
8 = $\beta Ca_2P_2O_7$ + fluid
4 = $\beta Ca_2P_2O_7$ + HA + fluid
5 = HA + fluid
6 = HA + $Ca(OH)_2$ + fluid
H_2O
1
7
8
4
5
6
$Ca(OH)_2$
$Ca(H_2PO_4)_2H_2O$
$Ca_{10}(PO_4)_5(OH)_2$
P_2O_5
CaO
$Ca_2P_2O_7$

Figure 9.2. Phase diagram of CaO–P_2O_5–H_2O system under hydrothermal conditions of 600°C and 2 kbar. Reprinted with permission from [61]. Copyright © 1993, World Scientific.

Major efforts have been expended to improve the mechanical properties of HA ceramics for use in implants. Many researchers have used filtered cake-like HA precipitates along with hot-pressing and calcination to obtain translucent HA with good mechanical properties [10,27,28,31]. The calcined powders tend to aggregate and also have some heterogeneity in their composition. In addition, the high calcination temperature (1100~1200°C) required for high densification may cause increased grain size. Therefore, the much lower temperature (200°C) and pressure (2 MPa) needed to convert precipitates of HA into near-complete crystalline form. A transmission electron microgragh of such prepared crystals is shown in Figure 9.3. The wide angle x-ray diffraction patterns showed increased crystallization of HA powders under increased temperature for prolonged times, as shown in Figure 9.4. One can see that HA may convert into β–$Ca_3(PO_4)_2$ above 350°C.

The apatite family of minerals, $A_{10}(BO_4)_6X_2$, crystallizes into a hexagonal rhombic prism. HA has unit cell dimensions of a = 0.9432 nm and c = 0.6101 nm [56]. The

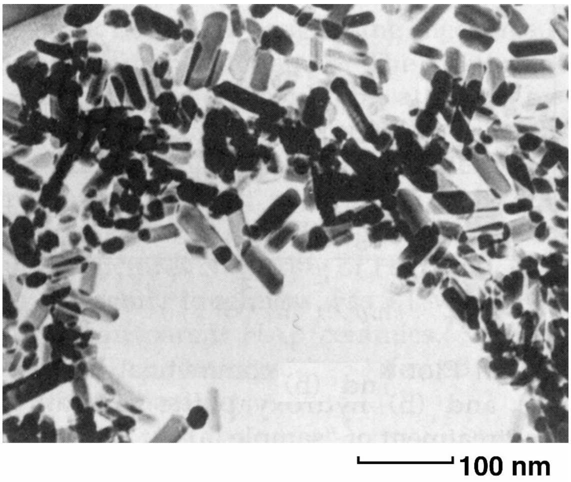

Figure 9.3. Transmission electron microgragh of hydrothermally synthesized HA at 200ºC and 2 MPa for 10 hours. Reprinted with permission from [61]. Copyright © 1993, World Scientific.

atomic structure of HA projected along the *c*-axis on the basal plane is given in Figure 9.5. Note that the hydroxyl ions lie on the corners of the projected basal plane and occur at equidistant intervals [half of the cell (0.344 nm)] along columns perpendicular to the basal plane and parallel to the *c*-axis. Six of the ten calcium ions in the unit cell are associated with the hydroxyls in these perpendicular columns, resulting in strong interactions between them. Figure 9.6 illustrates a three-dimensional view of the crystal structure of hydroxyapatite.

The ideal Ca/P ratio of HA is 10/6, and the calculated density is 3.219 g/ml [61]. It is interesting to note that substitution of OH with F gives greater structural stability, due to the closer coordination of F than the hydroxyl to the nearest calcium. This is one of the reasons why the resistance of enamel to dental caries is enhanced fluoridation. The effect of fluorine substitution on crystal structure can be seen in Figure 9.7, where the space lattice in the *a*-axis decreases with increased amounts of fluorine.

Example 9.1

Calculate the theoretical density of HA.

Answer:

$$\text{Density} = \frac{\text{Mass}}{\text{Volume}} = \frac{\left[(10\times 40) + (16\times 31) + (26\times 16) + (2\times 1)\right]}{(9.432)^2(\sqrt{3}/2)(6.881)\times 10^{-28} 6.02\times 10^{-23}} = \underline{3.15\ \text{g/cm}^3}\,.$$

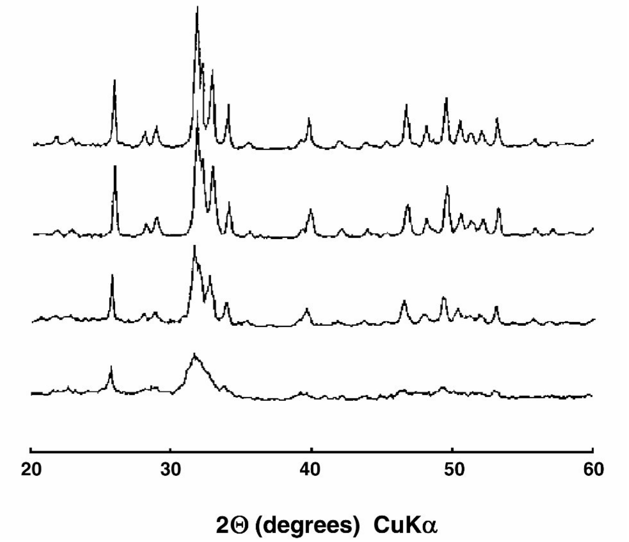

Figure 9.4. X-ray diffraction pattern of hydroxyapatite powders: (a) prepared wet chemically at room temperature for 10 hr and synthesized hydrothermally for 10 hr; (b) at 100°C, 0.1 MPa, (c) at 150°C, 0.5 MPa, and (d) at 200°C, 2 MPa. Reprinted with permission from [29]. Copyright © 1988, American Ceramic Society.

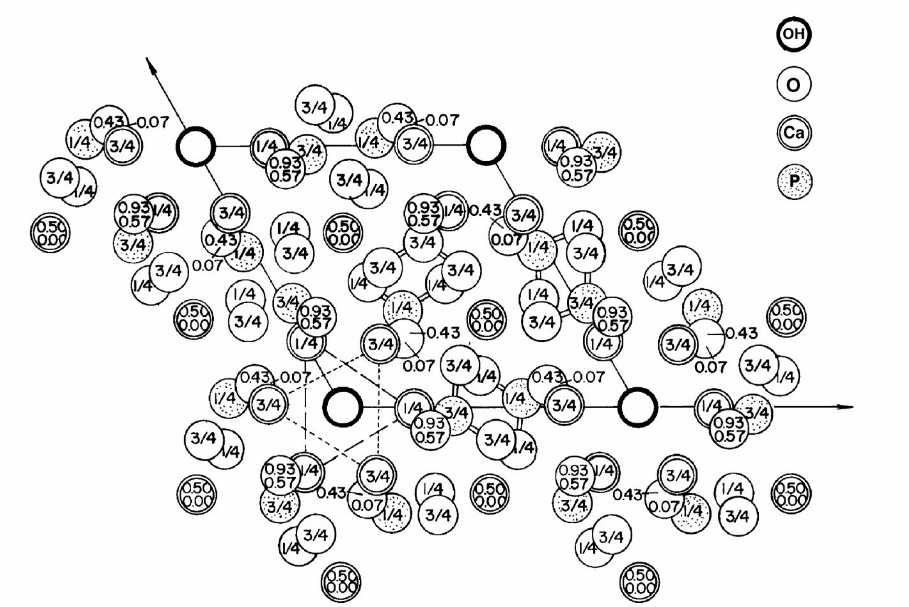

Figure 9.5. Hydroxyapatite structure projected down the *c*-axis on the basal plane. Reprinted with permission from [51]. Copyright © 1958, International Union of Crystallography.

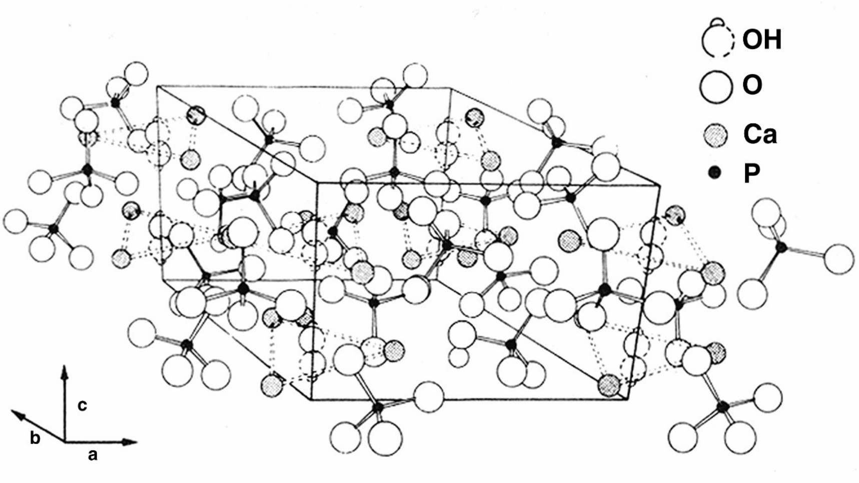

Figure 9.6. Three-dimensional view of the structure of hydroxyapatite crystal. Reprinted with permission from [32]. Copyright © 1986, Pergamon.

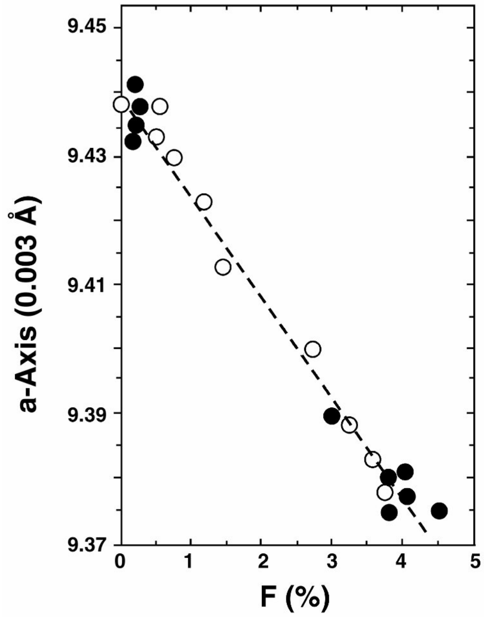

Figure 9.7. Effect of fluorine substitution on crystal structure. Synthetic apatite (o) and apatites from enameloid (●). Reprinted with permission from [42]. Copyright © 1980, Springer.

9.2. PROPERTIES OF HYDROXYAPATITE

The (bio)chemical and mechanical properties of HA are similar to those of bone and teeth. Their molecular structures are also similar, although the exact nature of the composite, the minerals and proteins, and their interactions are not fully understood.

9.2.1. Mechanical Properties

There is a wide variation in the reported mechanical properties of HA. Jarcho et al. [30] reported that fully densified polycrystalline specimens of HA synthesized by them had average compressive and tensile strengths of 917 and 196 MPa, respectively. Kato et al. [31] noted a compressive strength of 3000 kg/cm^2 (294 MPa), a bending strength of 1500 kg/cm^2 (147 MPa), and a Vickers hardness of 350 kg/mm^2 (3.43 GPa).

Table 9.3. Elastic Modulus of Hydroxyapatite and Mineralized Tissues

Test method	Material	Elastic modulus (GPa)
Ultrasonic interference technique	Hydroxyapatite (mineral)	144 [19]
	Hydroxyapatite (synthetic)	117 [19]
	Dentine	21 [18]
	Enamel	74 [18]
Destructive technique	Human cortical bone	24.6–35 [14]
Resonance frequency technique	Hydroxyapatite (synthetic)	39.4–63 [59]
	Canine cortical bone	12–14.6 [59]

The elastic modulus of HA measured by ultrasonic interference and resonance frequency techniques is given in Table 9.3. Although there are some variations in values, depending on measurement technique, it is clear that HA has a higher elastic modulus than mineralized tissues. Along this line of thought, it is interesting to note that the relatively smaller amount of organic material (mainly collagen) exists in enamel, which has a higher elastic modulus than bone and dentine. This fact is indirect evidence that the mineral portion of the hard tissue is made of HA. Poisson's ratio for the mineral or synthetic HA is about 0.27, which is somewhat close to that of bone (0.3) according to Grenoble [19].

Example 9.2

Calculate the strength of a composite of bone fully ingrown into a porous HA-coated Ti implant. Assume 50% porosity by volume with an average pore size of 150 μm. About 30% of the available pores are filled with bone.

Answer:

$$E_{\text{bone}} = 18 \text{ GPa},$$

$$E_{\mathrm{HA}} = 60 \text{ GPa (average)},$$

$$E_T = V_{\mathrm{bone}}E_{\mathrm{bone}} + V_{\mathrm{HA}}E_{\mathrm{HA}} \text{ and } \varepsilon_{\max} = \frac{\sigma_{\max}}{E}.$$

$$\text{For bone, } \varepsilon_{\max} = \frac{150 \text{ MPa}}{18 \text{ GPa}} = 0.008 \text{ ; for HA, } \varepsilon_{\max} = \frac{300 \text{ MPa}}{60 \text{ GPa}} = 0.005,$$

$$E_T = 0.5(18)0.3 + 0.5(60)$$

$$= 32.7 \text{ GPa}$$

Therefore, $\sigma_{\max} = 32.7 \text{ GPa} \times 0.005 = \underline{163.5\text{MPa}}$. This value is very high and more like 5~10% of the value for interfacial strength after full tissue ingrowth.

9.2.2. Chemical Properties

Hydroxyapatite is considered bioactive, indicating that the ceramic may undergo ionization in vivo and that the rate of dissolution may depend on many factors — including degree of crystallinity, crystallite size, processing condition (temperature, pressure, and partial water pressure), and porosity. Hydroxyapatite is soluble in an acidic solution while insoluble in an alkaline one and slightly soluble in distilled water. Solubility in distilled water increases with addition of electrolytes. Moreover, the solubility of HA changes in the presence of amino acids, proteins, enzymes, and other organic compounds. These solubility properties are closely related to the biocompatibility of HA with tissues and its chemical reactions with other compounds. However, the solubility *rate* depends on differences in shape, porosity, crystal size, crystallinity, and crystallite size. The solubility of sintered HA is very low. The rate of solubility is 0.1 mg/year in subcutaneous tissue [32]. Hydroxyapatite reacts actively with proteins, lipids, and other inorganic and organic species.

The most interesting property of HA is its excellent biocompatibility [9,24,48,50], the result of its suspected direct chemical bonding with hard tissues [31]. Hench et al. [22] reported epitaxial HA crystal growth on the surface of Bioglass® wafers (1.23 cm diam., 0.32 cm thick) after spreading a 0.254-mm thick layer of amorphous calcium orthophosphate precipitate on its surface. X-ray diffraction analysis of the crystallization of HA showed an average crystal size of approximately 20 nm, which is in the same range as the observed size for in-vivo mineral crystals [13]. A scanning electron micrograph (Figure 9.8) of a fractured section shows dendritic growth of HA crystals on a glass-ceramic surface.

9.3. APPLICATIONS

The use of HAs as implants traces back to the application of "triple calcium phosphate" powder slurry for accelerated bone healing in 1920 [1]. Other investigators have since tried to use calcium phosphate but could not find accelerated bone healing

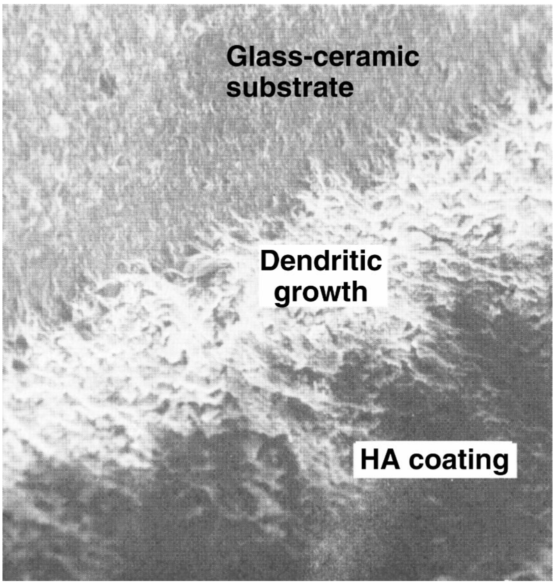

Figure 9.8. Scanning electron micrograph depicting the morphology of hydroxyapatite crystallized on Bioglass® substrate. Note the dendritic crystal growth. Reprinted with permission from [22]. Copyright © 1971, Wiley.

[21,53]. In 1961, Driskell at the Battelle Memorial Institute (Columbus, OH) developed a calcium phosphate "structural" implant and void-filling materials [11]. HA coating techniques were first used for alumina ceramic in dental implants and metals (stainless steel, Co–Cr alloys, Ti alloys, and Ta) for bone fracture plates. Later, orthopedic implants were created by dipping materials in an HA slurry solution and firing at high temperatures, and by plasma spraying. Table 9.4 summarizes the early history of HA manufacture and applications in implants.

The major problem encountered when applying HA is its relatively weak mechanical properties, thus making it necessary to apply implant devices as coatings. The most widely used technique of coating the surface of implants is plasma spraying (see Fig. 9.9). The bonding between HA and substrate is of paramount importance in any coating. In addition, the crystallinity of HA after coating may determine the dissolution rate: the higher the crystallinity, the slower the dissolution of HA. The crystallinity may be compromised due to the high temperatures used in the plasma spraying method, resulting in more amorphous calcium phosphate after spraying (see Fig. 9.10).

One method for dissolution and precipitation of CO_3–apatite on surfaces of Ca–P materials was proposed by LeGeros et al., as depicted in Figure 9.11 [41]. Dissolution of Ca–P materials depends on the type and concentration of buffered or unbuffered solution, the concentration, the time of suspension in solution, and the composition and crystallinity of the Ca–P composite. The degree of micro- and macroporosity, the

Table 9.4. Early History of HA Manufacturing and Applications for Implants

	Investigators	Comments
1920	FH Albee & HF Morrison	Triple calcium phosphate as a stimulus to osteogenesis
1934	KO Haldeman & JO Moore	Calcium phosphate on healing of fractures
1952	RD Ray & AA Ward	Tricalcium phosphate in bone replacement
1961	TD Driskell	Calcium phosphate for structural and void-filling implants, coatings on alumina and metallic implants
1971–2	Getter et al. [8]	β-TCP for porous block grafting material and coatings on dental implants
1972	Aoki et al. [3]	HA synthesis and sintering
1973	Hubbard, Hirthe, & Mueller [25]	Predominantly HA and β-TCP
1975	Chiroff et al. [6], Roy & Linnehan [56] Jarcho et al. [30]	Replamineform of coral (porite) skeletons into HA, high-density sintered HA block
Mid to late 70s	Ducheyne, Hench, & Kagan [12] Cook et al. [7]	Plasma spray coating of implants with HA; commercialization of HA and coatings

Reprinted with permission from [11]. Copyright © 1994, American Society for Testing and Materials.

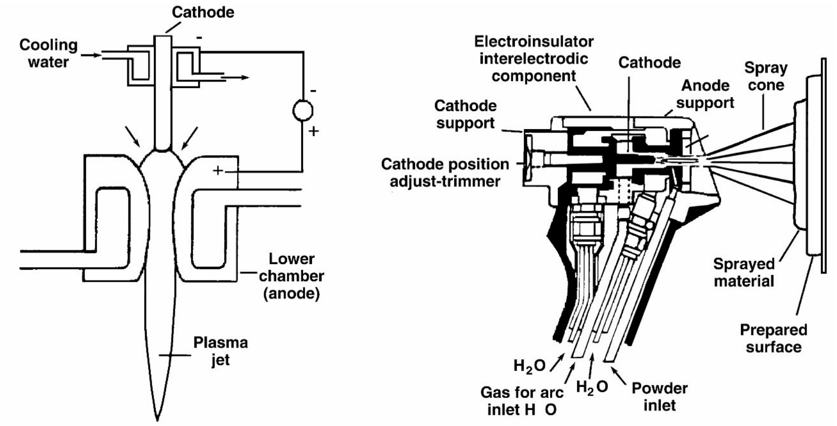
Cathode
Cooling water
-
-
+
+
Lower chamber (anode)
Plasma jet
Electroinsulator interelectrodic component
Cathode
Spray cone
Anode support
Cathode support
Cathode position adjust-trimmer
Sprayed material
Prepared surface
H_2O
Gas for arc inlet H O
H_2O
Powder inlet

Figure 9.9. Schematic illustration of plasma spraying method. Reprinted with permission from [52]. Copyright © 1992, Chapman & Hall.

presence of the defect structure, and the amount and type of other phases present also have significant effects [36]. The difference in composition and crystallographic structure of the Ca–P compound is reflected in the difference in their stability and solubility. The order of relative solubility of some of the Ca–P composites is as follows (see Fig. 9.12):

$$\text{ACP} > \alpha\text{-TCP} > \beta\text{-TCP} > \text{AP} > \text{HA}, \tag{9.6}$$

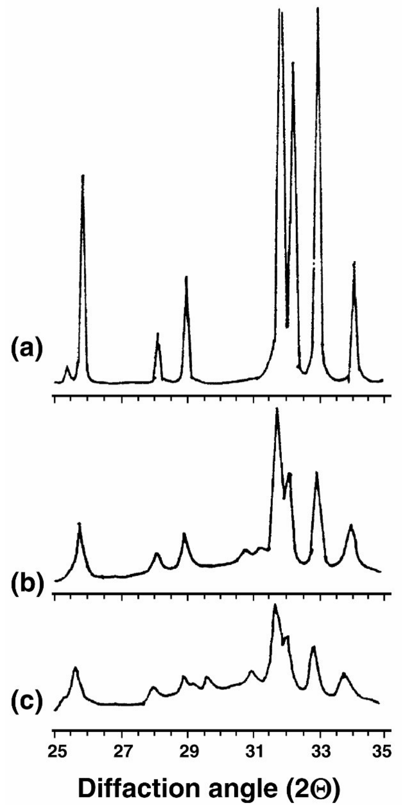

Figure 9.10. X-ray diffraction patterns of (a) hydroxyapatite, (b) coating closest to the metal implant, and (c) coating at the surface. Reprinted with permission from [37]. Copyright © 1991, Karger.

in which ACP is an amorphous calcium phosphate, TCP is tricalcium phosphate, AP is apatite, and HA is hydroxyapatite. Substitutions in the TCP or HA structure will affect their extent of dissolution. In the case of plasma-sprayed coatings — consisting principally of HA, ACP, and much smaller amounts of other Ca–P (α- and β-TCP) and sometimes CaO composites — the extent of dissolution will be affected by the type and amount of non-HA phases. Coatings with a higher ACP/HA ratio will dissolve or biodegrade faster since the ACP dissolves faster than HA.

Some have suggested that the reason for this excellent biocompatibility is that cells such as osteoblasts can attach themselves to the surface of HA through Ca^{2+} mediated by fibronectin, a glycoprotein [36]. This would favor cell anchorage, adhesion, and spreading, and hence help enhance cell growth and differentiation and deposition of bone tissue directly onto the material surface. Without the bio(re)activity of the HA, cells would not be able to attach to a substrate like alumina [45].

Many in-vivo studies have shown a direct attachment of new bone to HA without an intervening fibrous layer [4,30,31,47,54,60]. Terms such as "biointegration" and

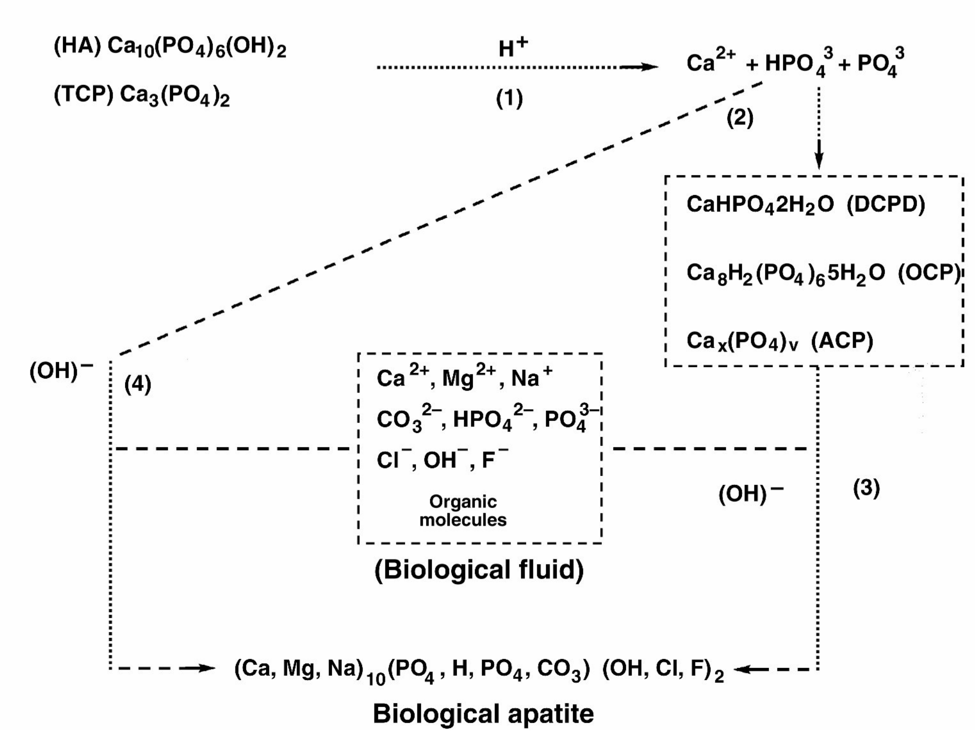
(HA) $Ca_{10}(PO_4)_6(OH)_2$
(TCP) $Ca_3(PO_4)_2$
H^+
(1)
$Ca^{2+} + HPO_4^3 + PO_4^3$
(2)
$CaHPO_42H_2O$ (DCPD)
$Ca_8H_2(PO_4)_65H_2O$ (OCP)
$Ca_x(PO_4)_v$ (ACP)
$(OH)^-$
(4)
Ca^{2+}, Mg^{2+}, Na^+
CO_3^{2-}, HPO_4^{2-}, PO_4^{3-}
Cl^-, OH^-, F^-
Organic molecules
(Biological fluid)
$(OH)^-$
(3)
$(Ca, Mg, Na)_{10}(PO_4, H, PO_4, CO_3)\ (OH, Cl, F)_2$
Biological apatite

Figure 9.11. Dissolution and precipitation processes in the formation of CO_3-apatite on surfaces of Ca–P compounds. Reprinted with permission from [41]. Copyright © 1995, Marcel Dekker.

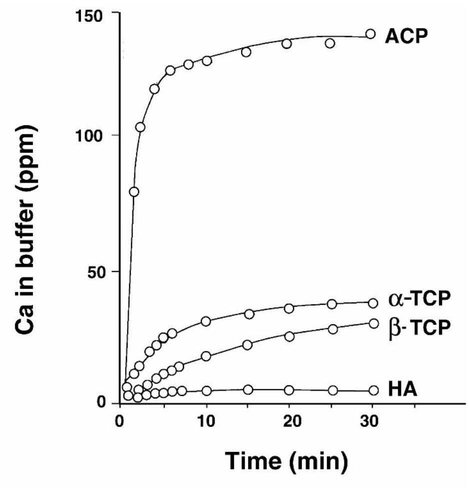

Figure 9.12. Dissolution of ACP, α- and β-TCP, and HA. Reprinted with permission from [43]. Copyright © 1994, American Society for Testing and Materials.

"osseointegration" are used to represent the bonding of new bone to HA, more precisely "a direct biochemical bond to a surface that is significant and confirmed at the electron microscopic level" [47]. It is suggested that within few hours of implantation macrophages invade the wound site and begin to phagocytize dead cell debris. Macrophages also appear to attack the surface of the HA, causing a roughened surface, which forms a chemical apatite layer seemingly indistinguishable from biological apatite. Osteoblasts then begin to lay down osteoid on the roughened HA surface. The HA and osteoid act as epitaxial nucleation sites for the formation of biologic apatite. Bone formation proceeds until the defect is bridged [34].

The HA coating has been used clinically in both dental and medical implants, as mentioned earlier. The bone–HA and HA–implant interfaces become very critical for long-term implant performance. Plasma spray coating of implants is not entirely satisfactory due to changes in HA crystallinity and the low interfacial strength between HA and the implant. When plasma spray-coated implants were tested after implantation, the interface between the metal (normally Ti or Ti6Al4V alloy) and HA failed [58]. The tensile strength between HA and Ti6Al4V was about 6.7 ± 1.5 MPa for grit-blasted specimens [17]. Another investigator used an uncoated grit-blasted titanium implant in canine cortical bone and was able to show a maximum tensile strength of 5.5 MPa; this value was increased to 12 MPa with the use of an HA coating [33]. Push-out tests on this canine cortical bone, after it was fully matured and remodeled, yielded an interfacial strength of 22–26 MPa, which is a value range close to the shear strength of cortical bone but much lower than the shear strength of a bone/implant composite. The CO_3^-–apatite microcrystals that formed on the HA surfaces in association with organic phase were made of much larger Ca–P crystals (see Fig. 9.13). Others have found that formation of CO_3^-–apatite on surfaces of HA in vitro and in vivo appears to be related to its bioactivity [10,23,26,39,40].

9.4. FURTHER THOUGHTS

One of the most difficult factors to control is the dissolution rate of implants made of semiresorbable materials like HA. Certainly, the dissolution rate depends on many factors, including surface area, which parts are exposed to body fluid, surface roughness, and particle size. Of course, such environmental conditions as local pH, variety of dissolved ions, and their concentration may be of consequence. We need to consider all these factors when designing implants using HA or any other dissolvable materials.

PROBLEMS

9.1. List the advantages and disadvantages of HA coating on the surface of implants.

9.2. Why is TCP more soluble than HA?

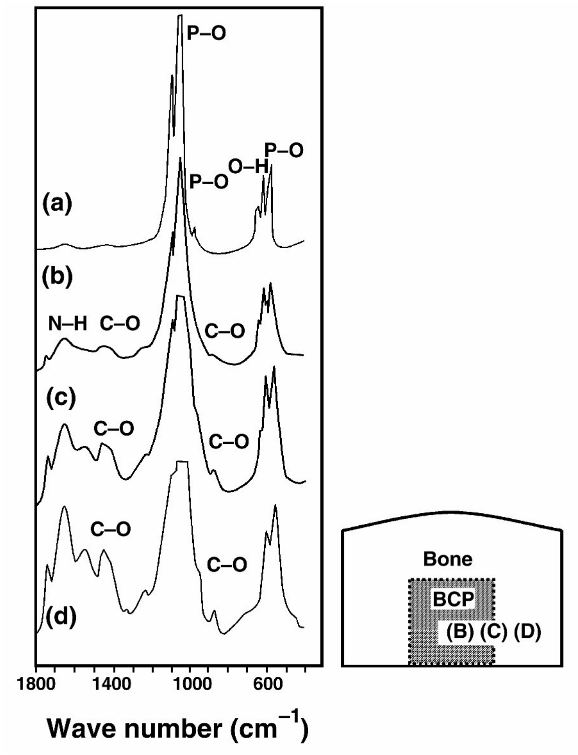

Figure 9.13. Infrared spectra of (a) HA before implantation, (b) HA from the core, (c) from the interface, (d) from bone. Organic and CO_3-apatite phases present in B–D. Reprinted with permission from [41]. Copyright © 1994, American Society for Testing and Materials.

9.3. Calculate the number of HA unit cells in one HA crystal of the bone given in the following illustration:

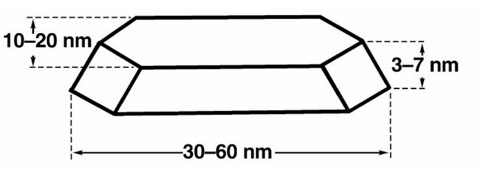

Schematic representation of a bone mineral crystal. Reprinted with permission from [55]. Copyright © 1955, New York Academy of Sciences.

9.4. The first five peaks of the x-ray diffraction pattern for tungsten (W) is shown below. (Reprinted with permission from Callister WD. 1994. *Materials science and engineering: an introduction*, 3rd ed. New York: Wiley.) Tungsten has a bcc crystal structure. Monochromatic x-radiation with a wavelength of 0.1542 nm was used.

a. Index (i.e., give indices *h*, *k*, and *l*) for each of these peaks.
b. Determine the interplanar spacing for each peak.
c. Determine the atomic radius for W for each peak and compare these with known values.

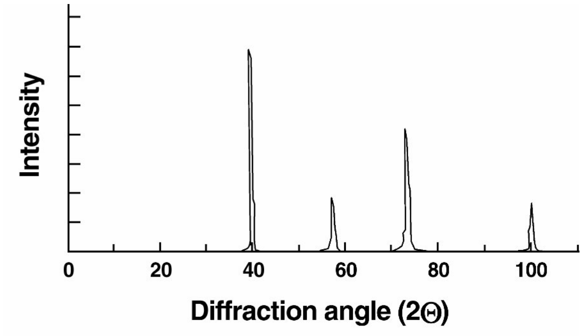

9.5. Determine the initial rate of Ca ion release into buffer solution for ACP, HA, and TCP from Figure 9.12. Also, calculate the amount of dissolved surface layer of a plasma spray-coated implant surface during one year if the ACP/HA ratio is 1/2. Give the assumptions for your calculations.

9.6. A bioengineer is trying to construct a calcium phosphate ceramic to make a dental root implant.
a. How would you make it porous (interconnected) with 100-μm diameter interconnected pores?
b. What are the Ca/P ratios for the HA and β-whitlockite?
c. The strength can be expressed as $\ln \sigma = \ln \sigma_0 - nV$. Calculate the volume fraction of porosity of a calcium phosphate if $n = 3.8$ and $\sigma/\sigma_o = 0.5$.
d. Would you expect this percentage porosity increase or decrease if the final sintering temperature was increased?
e. Which ceramic is more resorbable, HA or β-whitlockite?
f. The fatigue of calcium phosphate ceramics can be described as $\mathring{a} = \alpha_1 K_1^n$, where å is crack growth velocity and *n* and $\alpha_1 K_1^n$ are constants. What is K_1?
g. What is the approximate value of *n* for the Ca–P ceramic: 1, 10, 20, or 50?
h. Describe how you would use the Ca–P ceramic for a dental root implant. Give the reasons for your design.

9.7. If a bioengineer manufactured bone plates from the following ceramics, choose the most appropriate ceramic.

A. Single-crystal alumina
B. Calcium HA
C. Tricalcium phosphate
D. Glass ceramic (45S5)
E. Reprocessed bovine cortical bone

a. Which plate will be weakened the most due to stress concentration from the holes drilled for screws?
b. Which plate will be weakened the least due to stress concentration from the holes drilled for screws?
c. Which material would you choose for yourself? Give two reasons for your choice?
d. Which plate will lose its strength most rapidly?
e. Which plate will have the lowest Poisson's ratio?
f. Which plate will induce the least degree of osteoporosis under the plate?

9.8. TCP (30 w/o), HA (20 w/o), collagen (40 w/o), and water are used to make a composite bone substitute paste to fill bone defects. Calculate the volume percent of each phase. Would this material be as strong as cancellous bone?

9.9. List as many methods as you can for coating an implant with calcium phosphate.

9.10. List as many sources as you can of calcium phosphate from nature.

DEFINITIONS

Calcium hydroxide [$Ca(OH)_2$]: Solution that has phosphoric acid added dropwise to induce precipitation of apatites.

Dicalcium phosphorous anhydrous, [$CaHPO_4$]: One possible starting product that is combined with a basic solution of $CaCO_3$ to give a product that is sintered to produce HA.

Dicalcium phosphorous dihydrate, DCPD [$CaHPO_42H_2O$]: Hydrous calcium phosphate compound that can be made into HA.

Epitaxial nucleation: Aggregation of liquid particles onto a solid nucleus as they cool and add volume to the solid nucleus (growth). Growth on a substrate of a crystalline substance that mimics the orientation of the substrate.

Fibronectin: Substance present on epithelial and endothelial surfaces that is a major component of blood clots.

Hot isotropic pressing (HIP): Method by which dense or microporous ceramics can be obtained through use of high temperature and high pressure.

Macrophage: A large phagocytic cell found in stationary form in tissues or as a mobile white blood cell, especially at sites of infection.

Octacalcium phosphate, OCP [$Ca_6H_2(PO_4)_65H_2O$]: One possible starting product that is combined with a basic solution of $CaCO_3$ to give a product that is sintered to produce HA.

Osteoblast: Cells responsible for formation of new bone through calcification of callus into trabeculae and for synthesis and intracellular processing of type I collagen.

Osteoid: Term used to describe the organic matrix composed of osteoblasts before mineralization.

Phosphorite: A fibrous sedimentary rock containing a high proportion of calcium phosphate.

α-TCP[[$Ca_3(PO_4)_2$]: Form of tricalcium phosphate ceramic closely related to HA ceramic, with a relative solubility higher than that of β-TCP and HA.

β-TCP[[$Ca_3(PO_4)_2$]: Form of tricalcium phosphate ceramic closely related to HA ceramic, with a relative solubility less than that of α-TCP but higher than that of HA.

REFERENCES

1. Albee FH, Morrison HF. 1920. Studies in bone growth-triple calcium phosphate as a stimulus to osteogenesis. *Ann Surg* **71**:32–39.
2. Andrew C, Bassett CAL, Hurley LA, Stinchfield FE. 1962. The fate of long-term anorganic bone implants. *Transp Bull* **29**:51–55.
3. Aoki H, Kato K, Shibata M, Naganuma A. 1972. Thermal transition of calcium phosphates and observation by a scanning electron microscope [in Japanese]. *Rep Inst Med Dent Eng* **6**:50–61.
4. Block M, Kent J, Kay J. 1987. Evaluation of hydroxyapatite-coated titanium dental implants in dogs. *J Oral Maxillofac Surg* **45**:601–607.
5. Bonel G, Heughebaert JC, Heughebaert M, Lacout JL, Lebugle A. 1988. Apatitic calcium orthophosphates and related compounds for biomaterials preparation. In *Bioceramics: materials characteristics versus* in vivo *behavior*, pp. 115–130. Ed P Ducheyne, JE Lemons. New York: New York Academy of Sciences.
6. Chiroff RT, White EW, Weber JN, Roy DM. 1975. Tissue ingrowth of replamineform implants. *J Biomed Mater Res Symp* **6**:29–45.
7. Cook SD, Kay JF, Thomas KA, Jarcho M. 1987. Interface mechanics and histology of titanium and hydroxyapatite coated titanium for dental implant applications. *J Oral Maxillofac Implants* **12**:15–22.
8. Cutright DE, Bhaskar SN, Brady JM, Getter L, Posey WR. 1972. Reaction of bone to tricalcium phosphate ceramic pellets. *Oral Surg* **33**:850–856.
9. Decheyne P, de Groot K. 1981. In vivo surface activity of a hydroxyapatite alveolar bone substitute. *J Biomed Mater Res* **15**:441–445.
10. deLange GL. 1990. The bone–hydroxylapatite interface. In *Handbook of bioactive ceramics*, Vol. 1: *Calcium phosphate and hydroxylapatite ceramics*, pp. 61–75. Ed T Yamamuro, LL Hench, J Wilson. Boca Raton, FL: CRC Press.
11. Driskell TD. 1994. Early history of calcium phosphate materials and coatings. In *Characterization and performance of calcium phosphate coatings for implants*, pp. 1–8. Ed E Horowitz, J Parr. Philadelphia: American Society for Testing and Materials.
12. Ducheyne P, Hench LL, Kagan A. 1980. Effect of hydroxyapatite impregnation on skeletal bonding of porous coated implants. *J Biomed Mater Res* **14**:225–237.
13. Eanes E, Posner A. 1965. Kinetics and mechanisms of conversion of non-crystalline calcium phosphate to crystalline hydroxyapatite. *Trans NY Acad Sci* **28**:233–241.
14. Evans FG. 1973. *Mechanical properties of bones*. Springfield, IL: Thomas.
15. Eysel W, Roy DM. 1973. Hydrothermal flux growth of hydroxyapatites by temperature oscillation. *J Crystal Growth* **20**:245–250.
16. Feng SS, Rocket TJ. 1979. The system $CaO–P_2O_5–H_2O$ at 200°C. *J Am Ceram Soc* **62**:619–620.
17. Filiaggi MJ, Coombs NA, Pilliar RM. 1991. Characterization of the interface in the plasma-sprayed HA coating/Ti–6AI–4V implant system. *J Biomed Mater Res* **25**:1211–1229.
18. Gilmore R, Pollack R, Katz J. 1970. Elastic properties of bovine dentine and enamel. *Arch Oral Biol* **15**:787–796.
19. Grenoble D. 1972. The elastic properties of hard tissues and apatites. *J Biomed Mater Res* **6**:221–233.
20. Ha S-W, Mayer J, Wintermantel E. 1993. Micro-mechanical testing of hydroxyapatite coatings on carbon fiber reinforced thermoplastics. In *Bioceramics*, Vol. 6, pp. 489–493. Ed P Ducheyne, D Christiansen. Oxford: Pergamon.
21. Haldeman KO, Moore JO. 1934. Influence of a local excess of calcium and phosphate on the healing of fractures. *Arch Surg* **29**:385–396.

22. Hench L, Splinter R, Allen W. 1971. Bonding mechanisms at the interface of ceramic prosthetic materials. *J Biomed Mater Symp* **2**:117–141.
23. Heughebaert M, LeGeros RZ, Gineste M, Guilhem A, Bone G. 1988. Physico-chemical characterization of deposits associated with HA ceramics implanted in non-osseous sites. *J Biomed Mater Res* **22**:254–268.
24. Holmes R. 1979. Bone regeneration within a coralline hydroxyapatite implant. *Plast Reconstr Surg* **63**:626–633.
25. Hubbard WG, Hirthe WM, Mueller KH. 1973. Physiological calcium phosphate implants. *Proc 26th Ann Conf Eng Biol Med, Bioeng* **15**:199.
26. Hyakuna K, Yamamuro T, Kotura Y, Oka M, Nakamura T, Kitsugi T, Kokubo T, Kushitani H. 1990. Surface reactions of calcium phosphate ceramics to various solutions. *J Biomed Mater Res* **24**:471–488.
27. Ioku K, Somiya S, Yoshimura M. 1989. Dense/porous layered apatite ceramics prepared by HIP post-sintering. *J Mater Sci Lett* **8**:1203–1204.
28. Ioku K, Yoshimura M, Somiya S. 1990. Microstructure and mechanical properties of hydroxyapatite ceramics with zirconia dispersion prepared by post-sintering. *Biomaterials* **11**:57–61.
29. Ioku K, Yoshimura M, Somiya S. 1988. Post-sintering of apatite ceramics from fine powders synthesized under hydrothermal conditions [in Japanese]. *J Ceram Soc* **96**:109–110.
30. Jarcho M, Bolen C, Thomas M, Bobick J, Kay J, Doremus H. 1976. Hydroxyapatite synthesis and characterization in dense polycrystalline form. *J Mater Sci* **11**:2027–2035.
31. Kato K, Aoki H, Tabata T, Ogiso M. 1979. Biocompatibility of apatite ceramics in mandibles. *Biomater Med Devices Artif Organs* **7**:291–297.
32. Katz JL, Harper A. 1986. Calcium phosphates and Apatites. In *Encyclopedia of materials science*, pp. 474–481. Ed MB Beaver. Oxford: Pergamon Press.
33. Kay JF. 1992. Calcium phosphate coatings for dental implants: current status and future potential. *Dent Clin North Am* **36**:1–18.
34. Kitsugi T, Yamamuro T, Nakamura T, Kokubo T, Takagi M, Shibuya T, Takeuchi H, Ono M. 1987. Bonding behavior between two bioactive ceramics. *J Biomed Mater Res* **21**:1109–1123.
35. LeGeros RZ. 1981. Apatites in biological systems. *Prog Crystal Growth Charact Mater* **4**:1–45.
36. LeGeros RZ. 1994. Biological and synthetic apatites. In *Hydroxyapatite and related materials*, pp. 3–28. Ed PW Brown, B Constantz. Boca Raton, FL: CRC Press.
37. LeGeros RZ. 1991. Calcium phosphates in oral biology and medicine. In *Monographs in Oral Sciences*, Vol. 15, pp. 151–201. Ed H Myers. Basel: Karger.
38. LeGeros RZ. 1967. *Crystallographic studies of the carbonate substitution in the apatite structure*. New York: New York UP.
39. LeGeros RZ, Daculsi G. 1990. In vivo transformation of biphasic calcium phosphate ceramics: ultrastructural and physicochemical characterizations. In *Handbook of Bioactive Ceramics*, pp. 17–28. Ed T Yamamuro, LL Hench, J Wilson. Boca Raton, FL: CRC Press.
40. LeGeros RZ, Daculsi G, Orly I, Gregoire M. 1991. Substrate surface dissolution and interfacial biological mineralization. In *The bone–biomaterial interface*, pp. 76–88. Ed JE Davis. Toronto: U Toronto P.
41. LeGeros RZ, LeGeros JP, Daculsi G, Kijkowska R. 1995. Calcium phosphate biomaterials: preparation, properties, and biodegradation. In *Encyclopedic handbook of biomaterials and bioengineering*, Part A: *Materials*, pp. 1429–1463. Ed DL Wise, DJ Trantolo, DE Altobelli, MJ Yaszemski, JD Gresser, ER Schwartz. New York: Marcel Dekker.
42. LeGeros RZ, Suga S. 1980. Crystallographic nature of fluoride in the enameloids of fish. *Calcif Tissue Int* **32**:169–174.
43. LeGeros RZ, Zheng R, Kijkowska R, Fan D, LeGeros JP. 1994. Variation in composition and crystallinity of "hydroxyapatite (HA)" preparation. In *Characterization and performance of calcium phosphate coatings for implants*, pp. 43–53. Ed E Horowitz, J Parr. Philadelphia: American Society for Testing and Materials.
44. Losee FL, Hurley LA. 1956. Bone treated with ethylenediamine as a successful foundation material in cross-species bone grafts. *Nature* **177**:1032–1033.

45. Malik MA, Puleo DA, Bizios R, Doremus RH. 1992. Osteoblasts on hydroxyapatite, alumina and bone surfaces in vitro: morphology during the first 2 h of attachment. *Biomaterials* **13**:123–128.
46. McConell D. 1973. *Apatite: its crystal chemistry, mineralogy, utilization, and biologic occurrence*. Berlin: Springer-Verlag.
47. Meffert R, Block M, Kent J. 1987. What is osseointegration? *Int J Periodont Restor Dent* **7**:9–21.
48. Monroe E, Votaya W, Bass B, McMullen J. 1971. New calcium phosphate ceramic material for bone and tooth implants. *J Dent Res* **50**:860–861.
49. Muatz R, Bauermiester A. 1957. A method of bone maceration: results in animal experiments. *J Bone Joint Surg* **39A**:153–166.
50. Niwa S, Sawai K, Takahashie S, Tagai H, Ono M, Fukuda Y. 1980. Experimental studies on the implantation of hydroxyapatite in the medullary canal of rabbits. In *Transactions of the first world biomaterials congress*, p. 4.10.4. Chichester: Wiley.
51. Posner A, Perloff A, Diorio A. 1958. Refinement of the hydroxyapatite structure. *Acta Crystallogr* **11**:308–309.
52. Ravaglioli A, Krajewski A. 1992. Glasses and ceramics as coatings for massive supports. In *Bioceramics: materials, properties, applications*, pp. 198–243. Ed A Ravaglioli, A Krajewski. London: Chapman & Hall.
53. Ray RD, Ward AA. 1951. A preliminary report on studies of basic calcium and phosphate in bone replacement. *Surg Forum* **2**:429–434.
54. Ricci J, Alexander H, Parsons JR. Salsbury R, Bajpai PK. 1986. Partially resorbable hydroxylapatite interface. *J Biomed Mater Res* **18**:719–726.
55. Robinson RA, Watson ML. 1955. Crystal–collagen relationships in bone as observed in the electron microscope, III: crystal and collagen morphology as a function of age. *Ann NY Acad Sci* **60**:596–630.
56. Roy DM, Linnehan SK. 1974. Hydroxyapatite formed from coral skeletal carbonate by hydrothermal exchange. *Nature* **247**:220–222.
57. Shores EC, Holmes RE. 1993. Porous hydroxyapatite. In *Introduction to bioceramics*, pp. 181–198. Ed LL Hench, J Wilson. Singapore: World Scientific.
58. Spivak JM, Ricci JL, Logan G, Liu ST. 1986. The structure and properties of hydroxyapatite coatings on metal. In *12th meeting of the society for biomaterials*, p. 13. New York: Wiley.
59. Torgalkar A. 1979. A resonance frequency technique to determine elastic modulus of hydroxyapatite. *J Biomed Mater Res* **15**:907–920.
60. Tracy BM, Doremus BM. 1984. Direct electron microscopy studies of the bone–hydroxyapatite interface. *Dent Clin North Am* **36**:19–26.
61. Yoshimura M, Suda H. 1994. Hydrothermal processing of hydroxyapatite: past, present, and future. In *Hydroxyapatite and related materials*, pp. 45–72. Ed PW Brown, B Constantz. Boca Raton, FL: CRC Press.

10

CARBONS AND DIAMOND-LIKE CARBON COATINGS

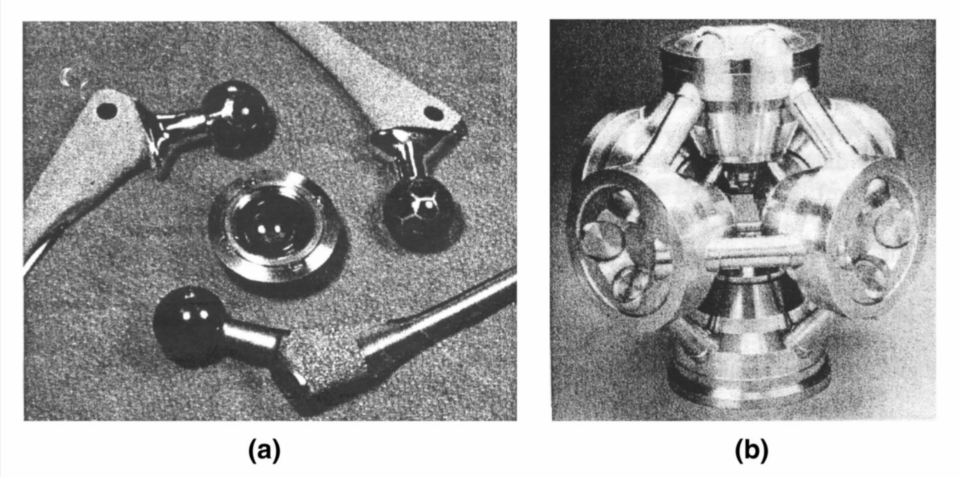

(a) Coating the surfaces of a hip joint head and an acetabular cup with diamond. (b) High temperature and pressure chamber for diamond coating shown in (a). Reprinted with permission from [40]. Copyright © 2001, Springer.

Carbons are allotropic or polymorphic and can be made into crystalline diamond and graphite, noncrystalline glassy carbons, and quasicrystalline pyrolytic carbons. Carbons can be made into blocks and fibers or coated onto the surface of other implants as thin layer of isotropic carbon or DLCs (diamond-like coatings), making them very versatile. Carbons show excellent tissue and blood compatibility, and pyrolytic carbon is widely utilized for heart valve disc fabrication. An excellent overview of carbon as a biomaterial can be found in [26].

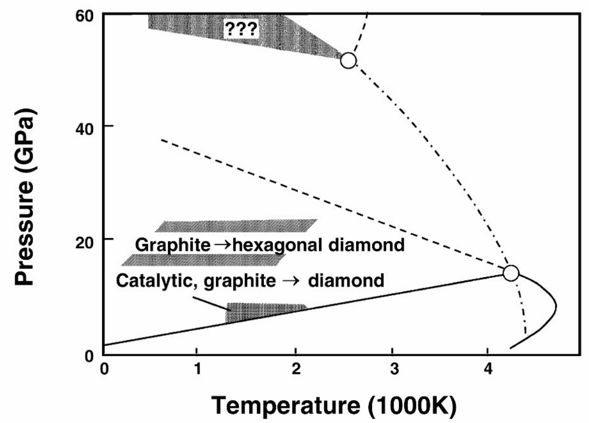

Figure 10.1. Temperature–pressure phase diagram of carbon. Reprinted with permission from [9]. Copyright © 1973, Marcel Dekker.

10.1. SOURCE AND STRUCTURE OF CARBONS

Carbons can be mined as massive lumps of anthracite or as flake graphite, and pyrolyzed as carbon black from hydrocarbons, automobile tires, or polymers. Pure carbons for engineering applications can be obtained by hot pressing at high temperatures (>2000ºC) using binders. The standard process of melting and cooling of ceramics or glasses cannot be used to obtain a large carbon mass since the melting temperature of carbon is above 4000ºC and it is stable at extremely high pressures (~15 GPa), as shown in the carbon phase diagram in Figure 10.1. Graphite is a thermodynamically stable form of carbon at ambient temperature and pressure. Graphite can be converted into diamond at very high pressure and temperature, which is very difficult to achieve under normal conditions. However, diamond can be fabricated at much lower temperatures and pressure if *catalysts* are employed. Industrial diamonds are made at pressures of 4.5–6 MPa and temperatures of 1400–1600°C using transition metals (Fe, Co, and Ni) as catalysts in a specially designed chamber, as shown on the cover page of this chapter. The high pressure can be achieved using a double-tapered piston made of tungsten carbide, while heating is done by feeding a strong electrical current through the piston [9]. At higher temperatures (>2227°C) and pressure (>13 GPa) the graphite can be crystallized into diamond within a few milliseconds. Additionally, methane can be heated above 1000°C at 0.1 MPa on the surface of diamond to form a thin layer of new diamond. The chemical vapor deposition (CVD) technique can also be used.

Glassy carbons are produced by controlled pyrolysis of polymeric materials, which eliminates volatile constituents. Products of limited thickness (<7 mm) can be obtained that often have pores, which are in turn caused by the presence of the volatiles and massive shrinkage of products (up to 50 vol%) [19]. Glassy carbons were used to make dental roots in the 1970s, but this practice was abandoned due to its inferior mechanical properties and poor quality control issues.

Carbon fibers can be made from such polymeric fibers as polyacrylonitrile (PAN) after stabilizing by heating at 220–250°C while passing through an oven with good air circulation. The fibers are subsequently pyrolyzed by passing through a series of furnaces at higher temperatures. The temperatures can reach up to 1500°C for complete elimination of such other elements as nitrogen [45].

Carbons can exist in many solid forms (see Fig. 10.2): noncrystalline glassy, crystalline diamond, and graphite. The stacking sequence of sheets of atoms (e.g., ABAB, ABCABC) can result different diamond structures. The crystalline structure of carbon

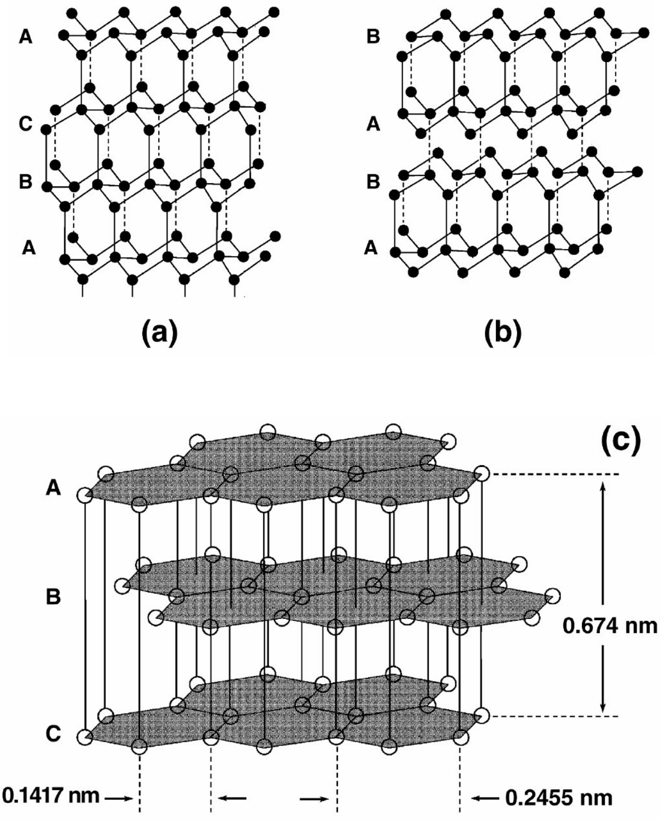

Figure 10.2. Crystalline structure of carbon: (a) cubic diamond, (b) hexagonal diamond, and (c) graphite. Reprinted with permission from [9], Copyright © 1973, Marcel Dekker, and [38], Copyright 1964, Academic Press.

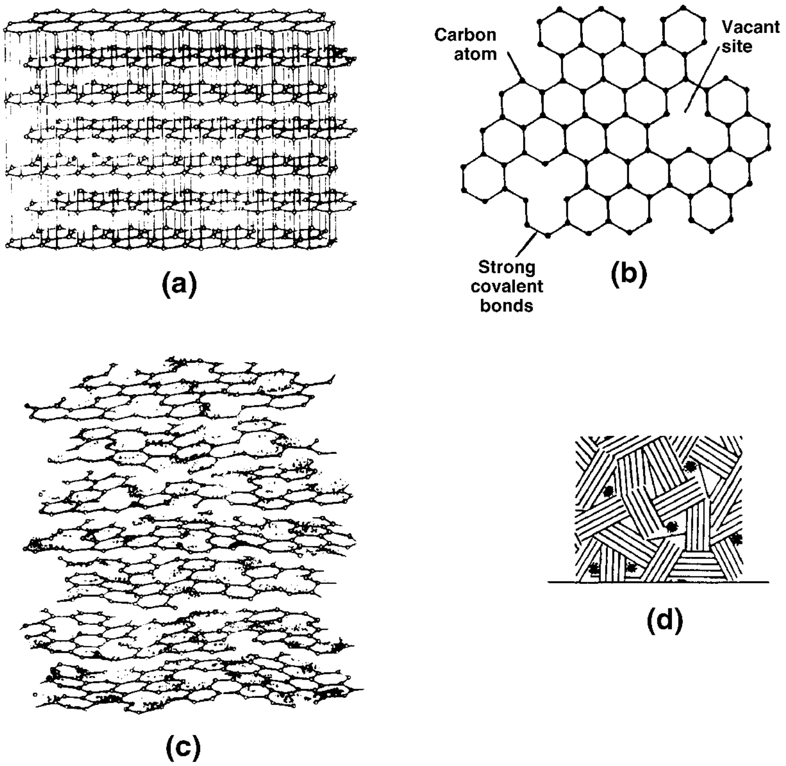

Figure 10.3. Schematic representations of carbon structures: (a) crystalline graphite; (b) single imperfect layer; (c) turbostratic structure viewed edge on; (d) aggregate of crystallites with single layers and unassociated carbon. Reprinted with permission from [19]. Copyright © 1986, Pergamon/MIT Press.

is similar to that of graphite, as shown in Figure 10.2c. The planar hexagonal structures are formed with strong covalent bonds in which one valence electron per atom is free to move, resulting in high but anisotropic electrical and thermal conductivity. Because the bonding between layers is stronger than the van der Waals force, *crosslinks* between them have been suggested [6,7]. Indeed, the remarkable lubricating property of graphite cannot be realized unless crosslinks are eliminated.

Poorly crystalline carbons are thought to contain unassociated or unoriented carbons, and their hexagonal layers are not perfectly arranged, as can be seen in Figure 10.3. The strong bonding within layers and the weaker bonding between layers cause the properties of individual crystallites to be highly anisotropic. However, if the crystallites are randomly dispersed the aggregate becomes isotropic. The turbostratic structure can be formed in glassy carbon or ultra-low-temperature isotropic (ULTI) carbon, which is deposited by the vapor deposition process shown in Figure 10.3c. Low-temperature (LTI) and ULTI deposited isotropic carbons usually have a thickness less than 1 μm, so that there would be no change in the properties of the substrate, though the properties of the carbon would be imposed upon the surface.

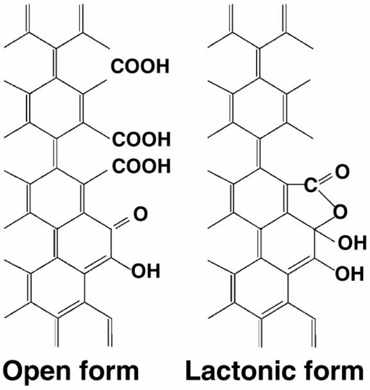

Figure 10.4. Models of oxidized carbon surfaces. Reprinted with permission from [5]. Copyright © 1966, Wiley-VCH.

The carbon surfaces have active sites. A model of an oxidized carbon is given in Figure 10.4. The four primary functional groups on the surface are carboxyl (COOH), carbonyl (C=O), hydroxyl (OH), and lactone [CH_3–CH(OH)–COOH]. It is also thought that C–H bonds exist within the mass and exposed surfaces of pyrolytic carbons when deposited below 1300°C.

10.2. PROPERTIES OF CARBONS

Structure determines the mechanical properties of any material. The covalent bond energy between carbons is very high (477 kJ/mol), resulting in the high-strength diamond structure that makes it the hardest material (10 on the Mohs scale). The weak mechanical properties of other carbons are due to the van der Waals bonds (~17 kJ/mol) that exist among the sheets of graphite, a structural arrangement that makes graphite a lubricating agent. Table 10.1 gives the physical properties of various carbons. Note that diamond exhibits the highest modulus of any material yet known. It has low density, very high thermal conductivity, and very strong semielectrical conductivity, making this material an almost ideal semiconductor material.

Poisson's ratio of the carbons is quite small, indicative of their brittleness. Some carbon materials (e.g., pyrolytic carbons) show considerable deformability (up to 5% of the original length of ULTI carbon). This is due to the turbostratic carbon structure formed by way of a hybrid vacuum process by using a catalyst to deposit carbon at high rates from a carbon-bearing gaseous precursor [38]. Consequently, the fracture toughness of the more deformable pyrolytic carbons is much higher than other carbons, as given in Table 10.1. In addition, the smaller number of flaws and unassociated carbons in the aggregate of pyrolytic carbon makes them tougher. The enhanced mechanical properties of pyrolytic carbons are largely dependent on densification, as shown in Figures 10.5 and 10.6.

Table 10.1. Properties of Various Types of Carbon

Properties	Diamond	Carbon fiber	Graphite	Glassy carbon	LTI carbon	ULTI carbon
Density (g/cm^3)	3.515	1.66–2.62	1.6–1.85	1.4–1.6	2.0–2.2	1.5–2.2
Crystallite size (nm)	Single crystal	–	–	1–4	3–4	0.8–1.5
Flexural strength (MPa)	–	2050–4500[a]	10–100	70–207	550–620	345–690
Young's modulus (GPa)	1160	250–500	10–20	24–31	28–41	14–21
Hardness	5.7–10.4 mg/mm^2 (Knoop)	– –	35–85 (Shore)	150–200 (DPH)	230–370 (DPH)	150–250 (DPH)
Poisson's ratio	0.2	–	–	–	0.2	–
Thermal expansion coefficient (10^{-6}/°C)	1	20: perpendicular to fiber axis	2.5–6 (/K)	2.0–5.8	5	–
Thermal conductivity (W/mK)	900–2600	6: perpendicular 15–90: parallel	20–100	4–25	4	–
Electrical resistivity (10^{-6} Ωm)	–	–	9–45	30–55	3–20	–
Fracture toughness (MJ/m^3)	–	–	–	0.6–1.4	5.5	9.9
Maximum strain (%)	–	0.54–1.80	–	0.8–1.3	2.0	>5.0

[a] Tensile strength.
Data from [19,45,47].

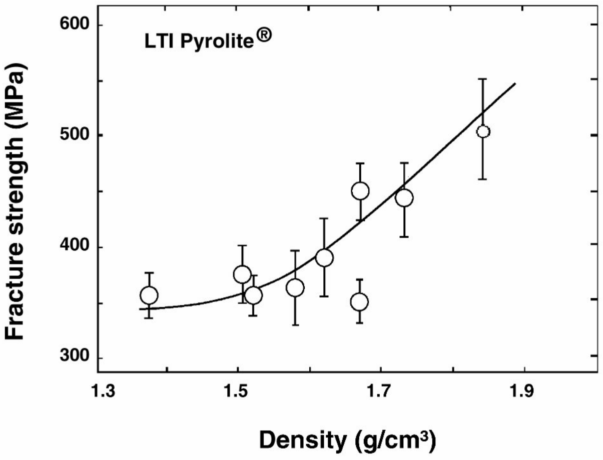

Figure 10.5. Fracture strength versus density for unalloyed LTI pyrolytic carbons. Reprinted with permission from [21]. Copyright © 1971, Elsevier.

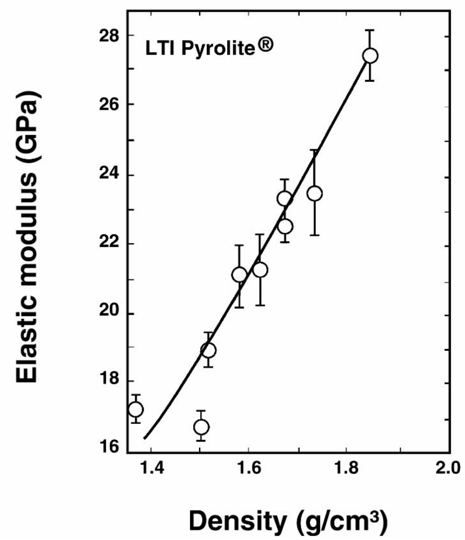

Figure 10.6. Elastic modulus versus density for unalloyed LTI pyrolytic carbons. Reprinted with permission from [21]. Copyright © 1971, Elsevier.

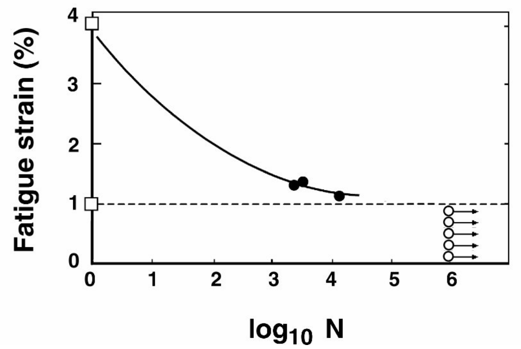

Figure 10.7. Strain versus number of cycles to failure. ○, absence of fatigue cracks in carbon film; ●, fracture of carbon film due to fatigue failure of substrate; □, data for substrate determined in single-cycle tensile test. Reprinted with permission from [37]. Copyright © 1980, Marcel Dekker.

Shim and colleagues [37] studied the fatigue behavior of a vapor-deposited pyrolytic carbon film (400–500 nm thick) onto a stainless steel substrate and showed that the film does not break until the substrate undergoes plastic deformation at a strain of 1.3% and a loading up to 10^6 cycles [37]. Therefore, fatigue behavior is closely related to the substrate, as shown in Figure 10.7.

A composite carbon reinforced with carbon fibers has been considered for implant fabrication [8,33]. Its properties are highly anisotropic, as seen from Table 10.2. Its density is in the range of 1.4–1.45 g/cm^3 and its porosity 35–38%.

Table 10.2. Mechanical Properties of Carbon Fiber-Reinforced Carbon

	Fiber lay-up	
	Unidirectional	0–90° crossply
Flexural modulus (GPa)		
Longitudinal	140	60
Transverse	7	60
Flexural strength (MPa)		
Longitudinal	1200	500
Transverse	15	500
Interlaminar shear strength (MPa)	18	18

Reprinted with permission from [1]. Copyright © 1978, Wiley.

Carbons show excellent compatibility with tissues [6,15,17,18,21,25,27]. This compatibility, especially with blood, have made the pyrolytic carbon-deposited heart valve a widely accepted part of a surgeon's armamentarium.

Example 10.1

Calculate the theoretical strength of carbon whiskers. Assume a 1-μm diameter.

Solution:

$$\sigma_{\mathrm{th}} = \sqrt{\frac{E\gamma}{c}},$$

Assuming that E = 250~500 GPa (Table 9.1) and γ = 2 N/m,

$$\sigma_{\mathrm{th}} = \sqrt{\frac{500\times10^{9}\ \mathrm{N/m^2}\times2\ \mathrm{N/m}}{1\times10^{-6}\ \mathrm{m}}} = \sqrt{1\times10^{18}}\ \mathrm{Pa} = \underline{1.0\ \mathrm{GPa}}.$$

This value is somewhat smaller than the value given in Table 3-1.

10.3. MANUFACTURE OF CARBON IMPLANTS

Carbons can be deposited onto implants from a carrier gas in a fluidized bed at a controlled temperature, as shown in Figure 10.8. The anisotropy, density, crystallite size, and structure of the deposited carbon can be controlled by varying the temperature, the composition of the fluidizing gas, the bed geometry, and the residence time of gas molecules in the bed [13]. The microstructure of deposited carbon should be particularly controlled since formation of growth features due to uneven crystallization can result in a weaker material (see Fig. 10.9). It is also possible to introduce various other elements into the fluidizing gas and codeposit them with carbon. Silicon (10–20 wt%) is usually codeposited (or *alloyed*) to increase hardness for applications that require resistance to abrasion. This may cause the struts of a heart valve disc made of Ti alloy to wear faster.

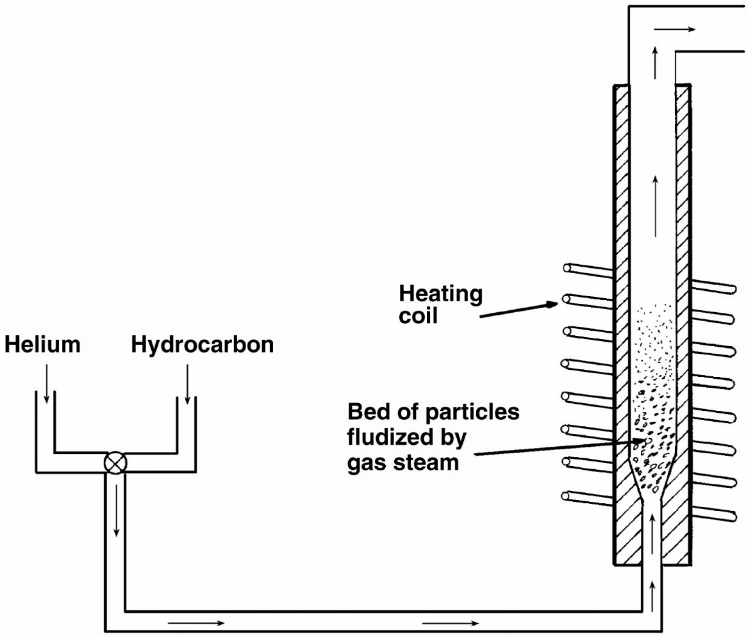

Figure 10.8. Schematic diagram showing how carbon particles are vaporized in a fluidizing bed. Reprinted with permission from [6]. Copyright © 1969, Marcel Dekker.

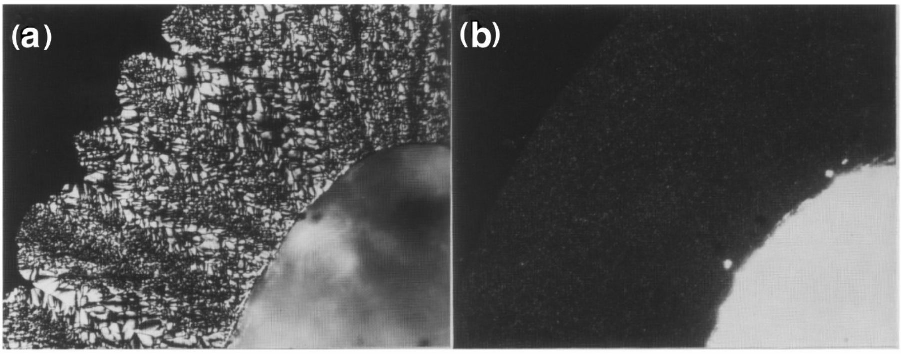

Figure 10.9. Microstructures of carbon deposited in a fluidizing bed: (a) granular carbon with distinct growth features, (b) isotropic carbon without growth features. Both under polarized light, 240×. Reprinted with permission from [7]. Copyright © 1972, Marcel Dekker.

Pyrolytic carbon has been successfully deposited onto the surface of polymeric blood vessel implants by chemical vapor deposition (CVD). This type of carbon is called ULTI carbon [18]. The deposited carbon is thin enough not to interfere with the flexibility of grafts, yet it exhibits excellent blood compatibility.

Vitreous or glassy carbon is made by controlled pyrolysis of such polymers as phenolformaldehyde (Bakelite®), rayon (cellulose), and polyacrylonitrile (PAN) at high temperature in a controlled environments [10]. This process is particularly useful for making carbon fibers and textiles that can be used by themselves or as components when making composites [15].

A composite carbon that reinforced with carbon fibers has been considered for implant fabrication (see Chapter 12 for more studies on composites) [13,15]. Its properties are highly anisotropic, as given in Table 10.2. The density is in the range of 1.4–1.45 g/cm^3 and its porosity is 35–38%. The carbons can sometimes be incorporated into an implant, such as the acetabular cup shown in Figure 10.10 [25,39]. Carbon fiber-reinforced implants have also been used for the tibial plateau of the knee joint [39]. These composite implants have higher stiffness, compressive strength, and shear strength in proportion to the amount of carbon fibers or cloth used. However, their wear properties are uneven, and in the case of the knee tibial plateau they were abandoned since the fibers were too stiff, causing wear and friction problems.

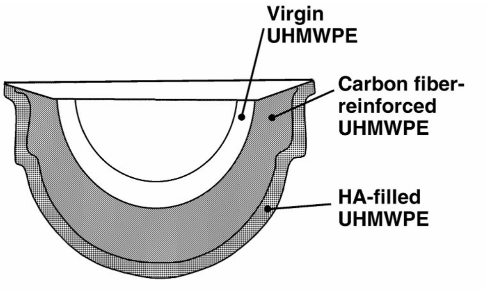

Figure 10.10. Schematic diagram of carbon fiber and carbon cloth-reinforced acetabular cup. Reprinted with permission from [39]. Copyright © 1989, Ishiyaku EuroAmerica.

The use of carbon fibers to fabricate tendon replacements has also been attempted. Up to 10,000 fine-braided carbon fibers can supply flexibility and tensile strength for such applications. However, the brittleness of each fiber can lead to breakdown into smaller particulates that cannot be easily removed by macrophages and will either be deposited into nearby tissues or into lymph nodes.

Hydroxyapatite coating by plasma spraying on the surface of carbon fiber-reinforced thermoplastic polyetheretherketone (PEEK) was then used to enhance the biocompatibility of the composite. However, the spray damaged the substrate, causing a lower flexural strength than that of the non-HA-coated controls, indicating surface microdamage [17].

10.4. DIAMOND-LIKE CARBON (DLC) COATINGS [42]

The DLC coating is an important development for many biomaterial applications. The surface properties of many implants and surgical instruments can be improved, especially the wear and lubrication properties of load-carrying implants, if the DLC coating is properly applied.

Table 10.3. Composition of Three DLC Coatings

Substrate	Thickness (nm)	Carbon	Hydrogen	Oxygen	Silicon	Nitrogen
Silicon alumina	200	66.4	14.2	6.0	6.5	<6.9
Silicon	76.4	81.2	13.4	3.4	–	<2
Nickel	76.6	76.8	13.1	4.1	–	<6

All numbers represent the atomic percentage of each element.
Reprinted with permission from [12]. Copyright © 1993, Elsevier Applied Science Publishers.

10.4.1. Composition and Structure of DLC Coatings

The structure of DLC coatings has been described as a "metastable state between graphite and diamond." In contrast to diamond, DLC coatings have an amorphous structure with no grain boundaries and contain several elements in addition to carbon. Carbon and hydrogen are the main constituents of DLC, and smaller concentrations of oxygen, silicon, and nitrogen may be present depending on the substrate and manufacturing process employed. Table 10.3 lists the composition of several DLC coatings produced by an ion beam-assisted deposition (IBAD) technique using different substrates and hydrocarbon precursors. The percentage of hydrogen for these coatings remained consistent at around 13–14%, though others have reported hydrogen concentrations as high as 36%. DLC coatings are formed by a combination of *covalent bonding* (sp^2 and sp^3) similar to that found in diamond and graphite. Layers of DLC coating are exceptionally smooth and do not require additional polishing. Initial average surface roughness values range from 0.02 to 0.03 μm.

10.4.2. Methods of Producing DLC Coatings

A number of ways of producing DLC have been developed, including iron beam-assisted deposition (IBAD), physical vapor deposition (PVD) or laser ablation, ion beam sputtering, plasma vapor deposition, and chemical vapor deposition (CVD). IBAD, laser ablation, and CVD are the most common techniques used currently. Important factors to keep in mind with these processes are the degree of adhesion achieved with the substrate, the amount of coverage (area) obtained, the coating thickness and uniformity, and the temperatures required to produce the coating.

10.4.2a. Ion Beam-Assisted Deposition (IBAD)

In this method a hydrocarbon precursor (polyphenyl ether, pentaphenyl trisiloxane) condenses on the surface of a substrate after undergoing heating to 140~150°C. Nitrogen ions are then used to bombard the surface of the substrate, which is rotated continuously to ensure an even coating. The high energy of the ions (30–80 keV) causes the carbon and hydrogen bonds to break and expels hydrogen and oxygen atoms from the surface. The remaining carbon atoms bond together with some residual hydrogen atoms to form a DLC coating. The advantages of this technique are the relatively large coverage area (<1 m^2), the fast deposition rate, and the low temperatures [2]. A diagram of the IBAD setup is provided in Figure 10.11.

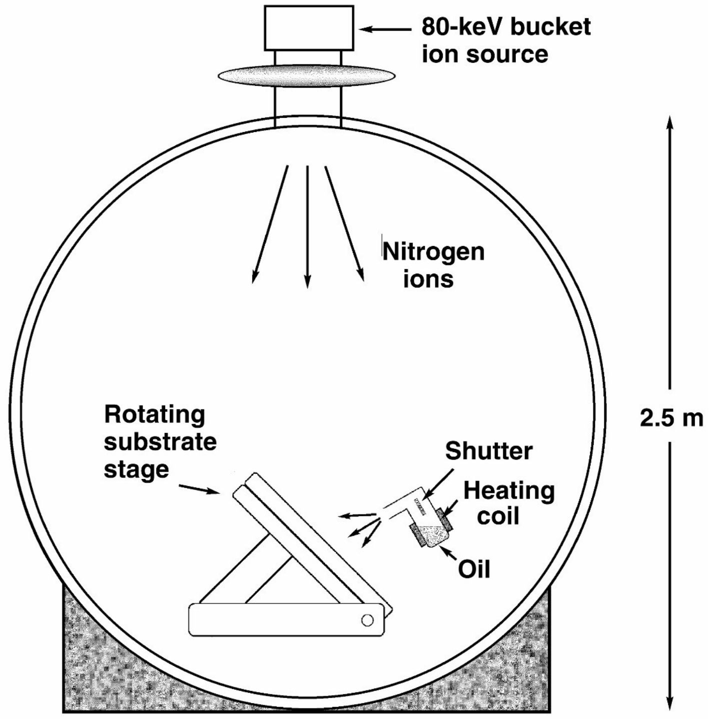

Figure 10.11. Schematic diagram for ion beam-assisted deposition (IBAD). Reprinted with permission from [12]. Copyright 1993, Elsevier Applied Science.

10.4.2b. Chemical Vapor Deposition (CVD)

DLC coating produced by CVD involves thermal decomposition of methane (CH_4) gas. The vapor of carbon and hydrogen atoms condenses on the target substrate to form a solid coating. Some elements from the substrate may diffuse into the coating, which may improve adhesion of the coating to the substrate. This method can be used to make diamonds with fewer and smaller surface flaws. This technique typically requires high temperatures (400–700°C), which may alter the mechanical properties of certain metallic substrates. Thus, its application to the coating of polymers and other biomaterials with high thermal expansion coefficients is not recommended. Another disadvantage of this technique is that it provides only a limited coating area.

10.4.2c. Physical Vapor Deposition (PVD), Laser Ablation

Laser ablation is classified as a physical vapor deposition method in which a narrow laser beam is used to bombard (ablate) a graphite target. Laser ablation releases a cloud of excited carbon atoms, which disperses and eventually condenses on the target substrate to form a diamond-like coating. A diagram of this technique is shown in Figure 10.12. The advantages of laser ablation are the cleanness of the procedure and the fact that it does not require the high temperatures essential for CVD. The drawbacks of this method include the amount of time and expense required.

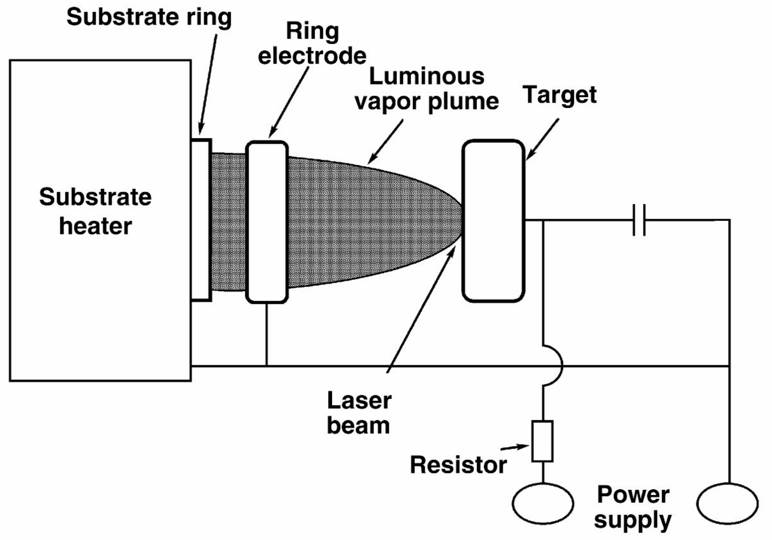

Figure 10.12. Schematic diagram for physical vapor deposition (PVD). Reprinted with permission from [12]. Copyright 1993, Elsevier Applied Science.

10.4.3. Material and Mechanical Properties of DLC Coatings

DLC has been selected as a potential coating for orthopedic implants because of its very low coefficient of friction and good wear resistance. As one would expect, DLC forms a very hard surface. Hardness values reported in the literature vary considerably, but most range from 2000 to 3000 kg/mm^2 (diamond = 5700–10,400). The hardness of DLC when in combination with polymers, ceramics, or metals increases its resistance to third-body abrasion at load-bearing surfaces as given in Table 10.4. Third-body wear may occur if particles of bone cement or polyethylene (UHMWPE) get trapped between two surfaces in an orthopedic implant.

Several authors have used pin-on-disc wear tests to compare the coefficient of friction for DLC coatings to a variety of other materials and coatings. These results along with friction values for other materials are summarized in Table 10.5. The coefficient of friction for the alumina/alumina combination is much higher than that for alumina-coated Co–Cr/UHMWPE or DLC-coated Co–Cr–Mo/DLC-coated Ti alloys.

Table 10.4. Possible Materials for Hip Joint Prostheses

Femoral component		Acetabular component	
Stem	Head	Cup	Backing
CoCr alloy[a]	CoCr alloy	UHMWPE[d]	CoCr alloy
Ti alloy[b]	Ceramics[c]	Ceramics CoCr alloy	Ceramics

[a] CoCr alloy: CoCrMo castable, CoNiCrMo wrought.

[b] Ti6Al4V.

[c] Ceramics: alumina (some zirconia).

[d] UHMWPE: Ultra-high-molecular-weight polyethylene.

Note: Fixation of components: PMMA (acrylic) bone cement, porous surfaced bone ingrowth, and direct apposition to bone surfaces.

Reprinted with permission from [29]. Copyright © 1995, CRC Press.

Table 10.5. Coefficient of Friction Values for Various Materials

Disc material	Pin material	Lubrication	Friction coefficient
CoCr w/ alumina coating	UHMWPE	Distilled water	.028
CoCrMo w/ DLC coating	UHMWPE	Distilled water	.033
CoCrMo (cast)	UHMWPE	Distilled water	.087
CoCrMo (wrought)	UHMWPE	Distilled water	.058
Ti6Al4V	UHMWPE	Bovine serum	.055
CoCrMo	UHMWPE	Bovine serum	.067
316 L S.S.	UHMWPE	Bovine serum	.056
Ti6A-4V w/ TiN coating	UHMWPE	Bovine serum	.078
Ti6Al4V w/ DLC coating	UHMWPE	Bovine serum	.056
Zr w/ ZrO_2 coating	UHMWPE	Bovine serum	.061
Alumina	Alumina	Distilled water	.09
Alumina	Alumina	Dry	.71
Alumina	UHMWPE	Distilled water	.05
Alumina	UHMWPE	Dry	.16

Data from [11,12,36,44].

DLC coatings result in faster wear initially and reach a lower steady-state value than an untreated Co–Cr–Mo/UHMWPE surface. In fact, some studies have shown an increase in the coefficient of friction of metal/UHMWPE combinations.

10.4.4. Tribology of DLC Coatings

DLC coatings are expected to provide excellent wear characteristics when one considers their hardness and low friction. Several in-vitro wear studies of DLC coatings have been performed. Wachtel et al. used a pin-on-disc wear machine with UHMWPE acting as the pin material and distilled water as lubricant [44]. Wear volume was calculated from the flattened surface of the UHMWPE pin. The wear volume was then normalized with the sliding distance to derive the wear rate. The DLC-coated Co–Cr–Mo disc produced the lowest wear rate, followed by the alumina-coated Co–Cr–Mo disc, and then untreated Co–Cr–Mo discs (Table 10.6). These results might be explained by the formation of a transfer film of UHMWPE on the untreated Co–Cr–Mo surfaces, which did not appear on coated specimens.

Table 10.6. Wear Rate of UHMWPE Compared to Several Material/Coating Combinations

Material	Wear rate (10^{-6} mm^3/m)
Alumina-coated CoCrMo	6.96 ± 1.27
DLC-coated CoCrMo	5.05 ± 1.64
CoCrMo (cast)	28.7 ± 20.9
CoCrMo (wrought)	20.2 ± 12.4

Reprinted with permission from [44]. Copyright © 1992, Institute of Metals.

Davidson et al. performed an abrasion test using a pin made of PMMA and lubricated with Ringer's solution [11]. Seven material/coating combinations were tested. The control specimen included Ti6Al4V, Co–Cr–Mo, and 316 L SS, while DLC, TiN, and ZrO_2 were chosen as coatings. The PMMA pin wore a groove in the various materials, and the authors measured the depth of the wear track to get an estimate of abrasion resistance. Zirconia demonstrated the greatest wear resistance of all the material/coating combinations tested. The wear track of the coated surfaces is much shallower than that of the untreated surfaces, indicating their excellent abrasion resistance (Table 10.7).

Dearnaley et al. [12] conducted a pin-on-disc wear test for 10,000 cycles using UHMWPE as the pin material without lubrication (dry conditions). Similar to the Wachtel et al. study, the wear volume was calculated from the flattened surface of the UHMWPE pin. Again, the coated surfaces performed better than the untreated surfaces, with the lowest wear rate exhibited by the DLC coating. The results are summarized in Table 10.8.

In each of these studies, DLC-coated metals consistently outperformed uncoated metals in terms of wear resistance. The reduced wear of DLC coatings in vitro can be attributed to its low coefficient of friction and its hard, inert surface. The results of these wear tests underscore the potential benefit of a DLC coating in minimizing wear-induced osteolysis and implant loosening. One of the unresolved questions with DLC coatings is a possible lack of interfacial strength between coating and substrate, which may be directly related to the inertness of DLC. Preliminary results have shown

Table 10.7. Wear of several material/coating combinations against PMMA

Material	Coating	Wear track depth (μm)
Ti6Al4V	–	27.5
Ti6Al4V	N_2 ion implantation	30.5
CoCrMo	–	0.80
316 L S. S.	–	48
Ti6Al4V	TiN	0.50
Ti6Al4V	DLC	0.30
Zr	ZrO_2	0
ZrO_2	–	0

Reprinted with permission from [11]. Copyright 1992, Institute of Metals.

Table 10.8. Wear Volume of UHMWPE Compared to Different Materials/Coatings

Material/coating	Wear volume (m^3)
Ti6Al4V	1.1×10^{-10}
TiN	7.4×10^{-11}
DLC	7.0×10^{-12}

Reprinted with permission from [44]. Copyright © 1992, Institute of Metals.

weak adhesion between DLC coatings and titanium and nickel, although strong adhesion was reported with Sialon (Si_3N_4 + $A1_2O_3$ + Y_2O_3) and alumina [4,12]. The formation of interlayers by diffusion of atoms from the substrate into the coating interface may promote adhesion; however, the exact cause of this is as yet not known.

10.4.5. Biocompatibility of DLC Coatings

The biocompatibility of various forms of carbons (e.g., carbon fibers, glassy carbons, and LTI carbons) with tissues and blood is already well established. Biocompatibility studies involving DLCs are not as widely reported. Some studies have surfaced that appear to confirm the biocompatibility of DLC in bulk and particulate form [13,27].

In one in-vitro study [41], a DLC coating was applied in bulk form in a cell culture dish containing mouse macrophage and fibroblast cells. The coating and cells were allowed to interact for 7 days. The authors observed no damage to the cells and no significant increase in inflammatory enzyme stimulation for the coated samples as compared to the controls. The lack of enzymes known to produce inflammatory responses suggests a mild tissue reaction in vivo.

Another in-vitro study investigated the effect of diamond, hydroxyapatite (HA), and SiC particles on enzymatic activity [28]. The cell culture contained human monocytes. All particles underwent phagocytosis; however, the diamond particles did not cause an increase in enzymatic activity. These results suggest that diamond particles are inert and can cause a milder inflammatory response than SiC and HA particles, which elicited enzyme responses comparable to that seen with PMMA particles.

In-vivo studies are not easily found in the literature. One such study involved implantation of diamond and SiC particulate in rabbits over a 3-week period [3]. A bone chamber was used during implantation to promote bone ingrowth. There is very little macrophagocytic and giant cell activity around diamond and SiC particles. The cellular response was considerably less than in similar studies of PMMA and UHMWPE particles. Additionally, diamond particles had only a slightly diminished effect on bone regeneration, and SiC particles even caused an increase in bone regeneration. In comparison, PMMA, UHMWPE, and Co–Cr particles reduced bone growth by 34–50% in a similar study.

These preliminary results appear very promising. Diamond and diamond-like carbon coatings appear to be inert in the body. They do not release ions into the body as do metallic biomaterials, and they may prevent metallic ion release when applied as a coating on orthopedic implants made of Ti6Al4V and Co–Cr alloys. More in-vivo studies are needed to confirm these preliminary results.

10.5. FURTHER THOUGHTS

DLC coatings applied to metallic substrates may overcome the limitations of orthopedic implants made entirely of ceramic or metallic components. In theory, it should be possible to combine these materials and thereby attain excellent strength and wear characteristics. In pin-on-disc wear studies, DLC has demonstrated low frictional properties and a strong resistance to abrasion and wear. The inherent inertness and biocompatibility of DLC have been reported in cell culture tests and animal studies. The strength of bonding between DLC coatings and the substrate material remains a concern, and more studies are needed to further investigate this issue.

Carbons are very attractive materials for medical and dental applications [2,4,12, 13,16,31,32,35,42,43]. DLC can be explored more since it can be utilized easily in implants or surgical tool production [4,16]. Exposure of carbons in particulate form can cause pulmonary damage, though this is not a substantial risk with carbon implants [14]. Elucidation of the fundamental structure and property relationships as well as in-vitro and in-vivo performance is key to the success of carbon and related implants [2,20,23,24,30,32,34,46]. In addition, biocompatibility may be an issue [16]. Furthermore, carbon nanotubes are being studied for delivering genes and therapeutics [22].

PROBLEMS

10.1. Consider the following mechanical properties:

Properties	Bone	Glassy carbon
Ultimate tensile strength (MPa)	100	120
Tensile modulus (GPa)	2	2.8

This comparison suggests that vitreous carbon would be an excellent material for bone replacement. Give the advantages and disadvantages of using glassy carbon for that purpose.

10.2. Give the probable explanations for the hemocompatibility of pyrolitic carbon.

10.3. Give the possible advantages and disadvantages of DLC coating of the surfaces of such joint implants as the hip and knee.

10.4. DLC has been used very successfully for coating razor blades. What other possible application can you suggest in terms of medical devices (e.g., a surgical blade).

10.5. Pyrolytic carbon has been used as a heart valve disc since the 1960s. Can one use a DLC instead of pyrolytic carbon? Propose a protocol for evaluating such disc development for commercialization.

10.6. Can one use the same DLC coating on a heart valve disc made of ruby/sapphire? Give the pros and cons of "DLC-coated ruby/sapphire."

10.7. A large number of carbon fibers are woven into a rope, which is to be used as an artificial ligament. Discuss the pros and cons for such an application. Can you make an implant like that using ceramics and/or glasses?

10.8. Carbon nanotubes can be constructed. What is a carbon nanotube? Suggest applications in medicine and dentistry. The student is directed to http://en.wikipedia.org/wiki/Nanomedicine.

DEFINITIONS

Allotropic: Ability of one substance to have more than one crystal structure.

Anthracite: Starting material from which carbons can be mined in massive lumps.

Catalyst: Substance that lowers the activation energy of a reaction without being consumed.

Crosslinks: Chemical bonds between chains of organic molecules.

CVD: Chemical vapor deposition method of surface coating. Vapors can be generated by dissolution into strong chemicals at high temperature. Mirowave energy can sometimes be used.

DLC: Diamond-like coating. Metastable state between graphite and carbon that has an amorphous structure with no grain boundaries

Fluidized bed: A furnace in which carbons are deposited onto implants via vaporization of hydrocarbon gas.

Hybrid vacuum process: Process by which turbostratic carbon structure is formed. Uses a catalyst to deposit carbon at high rates from carbon-bearing gaseous precursors.

LTI carbon deposition: Low-temperature isotropic carbon deposition.

Phenolformaldehyde: Thermosetting polymer used to make glassy carbon through controlled pyrolysis.

Polyacrylonitrile: Polymeric fiber used to make carbon fibers by heating and pyrolyzation.

Polyetheretherketone (PEEK): Biocompatible carbon fiber-reinforced thermoplastic composite that is coated with HA through plasma spraying to further enhance biocompatibility.

Polymorphic: Able to exist in more than one form or crystal structure.

Rayon: Regenerated cellulose polymer used to make glassy carbon through controlled pyrolysis.

Turbostratic structure: Structure formed in glassy carbon or ULTI carbon, which is deposited by vapor deposition processes.

ULTI carbon deposition: Ultra-low-temperature isotropic carbon deposition, such as pyrolytic carbon deposited by CVD.

Van der Waals force: Secondary interatomic force caused by adjacent dipoles. May be naturally occurring or induced.

REFERENCES

1. Adams D, Williams D. 1978. Carbon fiber-reinforced carbon as a potential implant material. *J Biomed Mater Res* **12**:35–42.
2. Agrawal CM, Micallef DM, Wirth MA, Lankford J, Dearnaley G, McCabe AR. 1993. The effects of diamond-like-carbon coatings on the friction and wear of enhanced UHMWPE-metal couples. In *19th meeting of the society for biomaterials*, p. 10. New York: Wiley.
3. Aspenberg P, Anttila A, Konttinen YT, Lappalainen R, Goodman SB, Nordsletten L, Santavirta S. 1996. Benign response to particles of diamond and SiC: Bone chamber studies of new joint replacement coating materials in rabbits. *Biomaterials* **17**:807–812.
4. Bedell CJ, Jones AM, Dearnaley G, Johnston C. 1991. Diamond-like carbon from the ion-beam decomposition of polyphenol ether. In *Applications of diamond films and related materials*, pp. 833–838. New York: Elsevier.
5. Boehm H. 1966. Funktionelle Gruppen an Festkorper-Oberflachen. *Angew Chem* **78**:617–652.
6. Bokros J. 1969. Deposition structure and properties of pyrolytic carbon. In *Chemistry and physics of carbon*, pp. 70–81. Ed P Walker. New York: Marcel Dekker.
7. Bokros J, LaGrange L, Schoen G. 1972. Control of structure of carbon for use in bioengineering. In *Chemistry and physics of carbon*, pp. 103–171. Ed P Walker. New York: Marcel Dekker.
8. Bruckmann H, Mauer HJ, Huttinger KJ, Rettig H, Weber U. 1980. New carbon materials for joint prostheses. In *Transactions of the first world biomaterials congress*, p. P1.7. Chichester: Wiley.
9. Bundy FP, Strong HM, Wentorf RH. 1973. Synthetic diamond growth. In *Chemistry and physics of carbon*, Vol. 10, pp. 213–263. Ed PL Walker. New York: Marcel Dekker.
10. Cowland F, Lewis J. 1967. Vitreous carbon: a new form of carbon. *J Mater Sci* **2**:507–512.
11. Davidson JA, Mishra AK. 1992. Surface modification issues for orthopaedic implant bearing surfaces. In *Proc. 5th international conference on surface modification technologies*, pp. 1–14. Ed TS Sudarshan, JF Braza. Birmingham, UK: Institute of Metals.
12. Dearnaley G. 1993. Diamond-like carbon: a potential means of reducing wear in total joint replacements. *Clin Mater* **12**:237–244.
13. Dion I, Roques X, Baquey C, Baudet E, Cathalinat BB, More N. 1993. Hemocompatibility of diamond-like carbon coating. *Biomed Mater Eng* **3**:51–55.

14. Donaldson K, Aitken R, Tran L, Stone V, Duffin R, Forrest G, Alexander A. 2006. Carbon nanotubes: a review of their properties in relation to pulmonary toxicology and workplace safety. *Toxicol Sci* **92**:5–22.
15. Gill R. 1972. *Carbon fibres in composite materials*. London: Butterworths.
16. Grill A. 2003. Diamond-like carbon coatings as biocompatible materials: an overview. *Diamond Relat Mater* **12**:166–170.
17. Ha S-W, Mayer J, Wintermantel E. 1993. Micro-mechanical testing of hydroxyapatite coatings on carbon fiber reinforced thermoplastics. In *Bioceramics*, Vol. 6, pp. 489–493. Ed P Ducheyne, D Christiansen. Oxford: Pergamon.
18. Haubold A, Shim H, Bokros J. 1979. Carbon cardivascular devices. In *Assisted circulation*, pp. 520–532. Ed F Unger. New York: Academic Press.
19. Haubold AD, Yapp RA, Bokros JC. 1986. Carbons for biomedical applications. In *Encyclopedia of materials science and engineering*, pp. 514–520. Ed MB Beaver. Oxford: Pergamon/MIT Press.
20. Hauert R. 2003. A review of modified DLC coatings for biological applications. *Diamond Relat Mater* **12**:583–589.
21. Kaae J. 1971. Structure and mechanical properties of isotropic pyrolytic carbon deposited below 1600°. *J Nucl Mater* **38**:42–50.
22. Klumpp C, Kostarelos K, Prato M, Bianco A. 2006. Functionalized carbon nanotubes as emerging nanovectors for the delivery of therapeutics. *Biochim Biophys Acta* **1758**:404–12.
23. Ma L, Sines G. 2000. Fatigue behavior of a pyrolytic carbon. *J Biomed Mater Res* **51**:61–68.
24. Meng WJ, Curtis TJ, Rehn LE, Blado PMV. 1998. Plasma-assisted deposition and characterization of Ti-containing diamond-like carbon coatings. *J Appl Phys* **83**:6076–6081.
25. Meunier A, Christel PS, Sedel L. 1989. Role of design and material on stress distribution of cemented hip prosthesis: Effects of low-rigidity (carbon-carbon) material. In *Bioceramics*, Vol. 1, pp. 347–352. Ed H Oonishi, H Aoki, K Sawai. Tokyo: Ishiyaku EuroAmerica.
26. More RB, Bokros JC. 2006. Biomaterials: carbon. In *Encyclopedia of medical devices and instrumentation*, pp. 296–308. Ed JG Webster. Hoboken, NJ: Wiley.
27. Narayan J, Fan WD, Narayan RJ, Tiwari P, Stadelmaier HH. 1994. Diamond, diamond-like and titanium nitride biocompatible coatings for human body parts. *Mater Sci Eng* **B25**:5–10.
28. Nordsletten L, Hogasen AKM, Konttinen YT, Santavirta S, Aspenberg P, Aasen AO. 1996. Human monocytes stimulation by particles of hydroxyapatite, silicon carbide and diamond: in vitro studies of new prosthesis coatings. *Biomaterials* **17**:1521–1527.
29. Park SH, Llinas A, Goel VK, Keller JC. 1995. Hard tissue replacements. In *The biomedical engineering handbook*, pp. 672–691. Ed JD Bronzino. Boca Raton, FL: CRC Press.
30. Polo MC, Andujar JL, Robertson J, Milne WI. 2000. Preparation of tetrahedral amorphous carbon films by filtered cathodic vacuum arc deposition. *Diamond Relat Mater* **9**:663–667.
31. Ritchie RO. 1996. Fatigue and fracture of pyrolytic carbon: a damage-tolerant approach to structural integrity and life prediction in "ceramic" heart valve prostheses. *J Heart Valve Dis* **5**(Suppl 1):S9–S31.
32. Robertson J. 2002. Diamond-like amorphous carbon. *Mater Sci Eng* **37**:129–281.
33. Rose PG, Gerstenberger F, Gruber U, Loos W, Wolter D, Neugebauer R. 1980. New aspects of the design and application of carbon fibre reinforced carbon for prosthetic devices. In *Transactions of the first world biomaterials congress*, p. P1.6. Chichester: Wiley.
34. Saikko V, Ahlroos T, Calonius O, Keränen J. 2001. Wear simulation of total hip prostheses with polyethylene against CoCr, alumina and diamond-like carbon. *Biomaterials* **22**:1507–1514.
35. Santavirta S. 2003. Compatibility of the totally replaced hip. Reduction of wear by amorphous diamond coating. *Acta Orthop Scand Suppl* **74**(310):1–19.
36. Semlitsch M, Lehmann M, Weber H, Dorre E, Willert H-G. 1977. New prospects for a prolonged functional lifespan of artificial hip joints by using the material combination polyethylene/aluminum oxide ceramic/metal. *J Biomed Mater Res* **11**:537–552.
37. Shim H, Haubold A. 1980. The fatigue behavior of vapor deposited carbon films. *Biomater Med Devices Artif Organs* **8**:333–344.
38. Shobert II E. 1964. *Carbon and graphite*. New York: Academic Press.

39. Tateishi T, Fukubayashi T. 1989. Advanced biocomposite material and application to the artificial joint. In *Bioceramics*, Vol. 1, pp. 48–53. Ed H Oonishi, H Aoki, K Sawai. Tokyo: Ishiyaku EuroAmerica.
40. Taylor JK, Pope BJ. 2001. The development of diamond as a bearing for total hip arthroplasty. In *Proceedings of the American Academy of Orthopaedic Surgery*, pp. 1–12. New York: Springer.
41. Thompson LA, Law FC, Rushton N, Franks J. 1991. Biocompatibility of diamond-like carbon coating. *Biomaterials* **22**:37–40.
42. Todd DT. 1997. Diamond-like carbon (DLC) coatings. Lecture given to an Intermediate Biomaterials (51:171) course at the University of Iowa.
43. Tran HS, Puc MM, Hewitt CW, Soll DB, Marra SW, Simonetti VA, Cilley JH, DelRossi AJ. 1999. Diamond-like carbon coating and plasma or glow discharge treatment of mechanical heart valves. *J Invest Surg* **12**:133–140.
44. Wachtel E, Villars P, Armini A, Spector M. 1992. Tribology of alumina and diamond-like coatings for orthopaedic applications. In *Proc. 5th international conference on surface modification technologies*, pp. 125–137. Ed TS Sudarshan, JF Braza. Birmingham, UK: Institute of Metals.
45. Watt W. 1986. Carbon fibers. In *Encyclopedia of materials science and engineering*, pp. 511–514. Ed MB Beaver. Oxford: Pergamon/MIT Press.
46. Weisenberg BA, Mooradian DL. 2002. Hemocompatibility of materials used in microelectromechanical system: platelet adhesion and morphology in vitro. *J Biomed Mater Res* **60**:283–291.
47. Wood AAR. 1991. Carbon and graphite. In *Concise encyclopedia of advanced ceramic materials*, pp. 57–62. Ed RJ Brook. Oxford: Pergamon.

11

SULFATES AND TITANATES

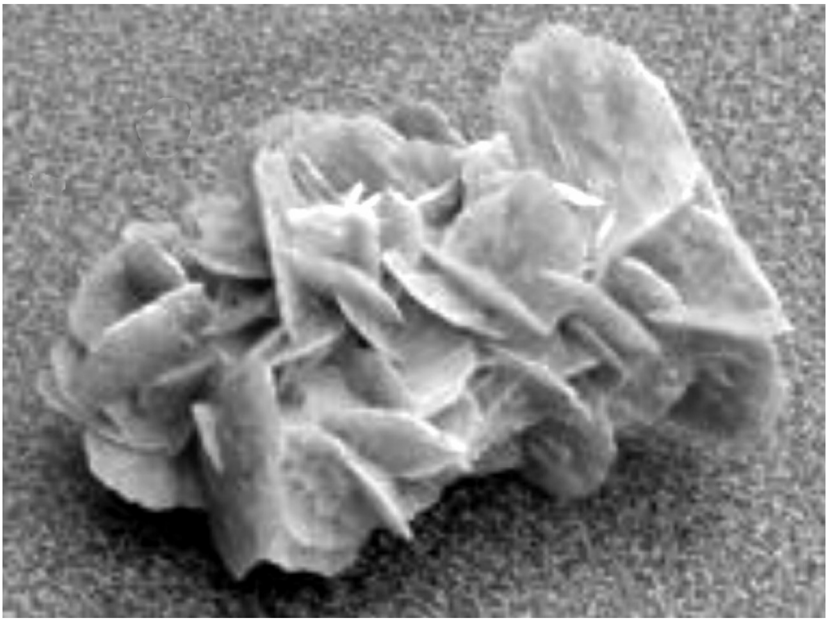

Desert rose (10 cm long) gypsum is a very soft mineral composed of calcium sulfate dihydrate ($CaSO_4 \cdot 2H_2O$).

Calcium sulfates are commonly used in the research laboratory as well as in industry. In hydrated form, they have been used to make casts and dental stones. Some investigators have tested it as a bone defect substitute [11]. It is commercially available as bone substitute (OsteoSet®, Wright Medical Technology Inc.). In its anhydrous form, it is sold as a laboratory desiccant (Drierite®). The hemihydrate is better known as *plaster of Paris*, while the dihydrate occurs naturally as gypsum. Depending on the method of calcination of calcium sulfate dihydrate, specific hemihydrates are obtained: α-hemihydrate and β-hemihydrate. The α-hemihydrate crystals are more prismatic than the β-hemihydrate ones, and when mixed with water form a much stronger and harder superstructure. Natural unrefined calcium sulfate is a translucent, crystalline white rock. After being heated and crushed into a powder, it is often used as a coagulant in soy processing to make tofu. Its most common use is in blackboard chalk and gypsum board.

Another sulfate, *barium sulfate*, has been used as an x-ray contrast medium. Barium sulfate, having a much higher molecular weight, is a superior x-ray contrast medium. It can be finely ground and suspended as a colloid and thus used as a drinkable or injectable contrast medium.

Calcium titanate can be single or polycrystalline, like alumina. Hydrothermal processing of calcium titanate by way of gel–sol transfer can be used to make implant coatings. The material itself has a perovskite structure.

Barium titanate is an electrical insulator that, when doped, can act as a semiconductor that increases the coefficient of resistivity when in polycrystalline form. This means that at a certain temperature (the Curie temperature) the material will exhibit an increased resistivity, the increase being typically several orders of magnitude. At the Curie temperature it undergoes a phase transformation from tetrahedral to cubic. It has also been reported that single crystals of barium titanate can cause a decreased coefficient of resistivity. Barium titanate also exhibits piezoelectric and ferroelectric properties. Investigators have tried to use this material to make bone substitute implants, taking advantage of its piezoelectric properties for stimulating bone ingrowth.

11.1. SOURCE, COMPOSITION, AND STRUCTURE

Sulfates and titanates are readily available commercially. Their use as biomaterials is limited at the present time. The piezoelectric properties of barium titanate need to be explored in the future.

11.1.1. Calcium Sulfate

The main source of calcium sulfate is gypsum, which is calcined as follows:

$$\mathrm{CaSO_4 \cdot 2H_2O} \xrightarrow[110\text{–}130^\circ\mathrm{C}]{} \mathrm{(CaSO_4)_2 \cdot H_2O} \xrightarrow[130\text{–}200^\circ\mathrm{C}]{} \mathrm{CaSO_4} \xrightarrow[200\text{–}1000^\circ\mathrm{C}]{} \mathrm{CaSO_4} \quad (11.1)$$

Gypsum [Calcium sulfate dihydrate]	Plaster or stone [Calcium sulfate hemihydrate]	Hexagonal anhydrite	Orthorhombic anhydrite

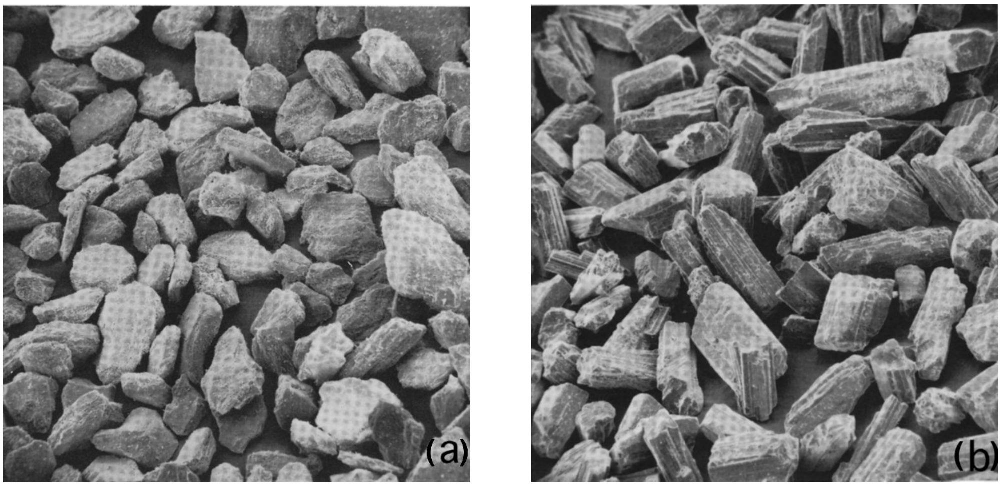

Figure 11.1. Powder particles obtained at lower (a) and higher (b) temperatures (400×). Note that the particles are sharper in (b). Reprinted with permission from [14]. Copyright © 1973, Saunders.

The resulting powders are shown in Figure 11.1. The particles obtained at low temperature are more spongy while particles obtained at higher temperatures tend to be sharper.

The anhydrites can be reacted with water:

$$(CaSO_4)_2 \cdot H_2O + 3H_2O \rightarrow 2CaSO_4 \cdot 2H_2O + \text{Heat}. \tag{11.2}$$

Orthorhombic anhydrite takes longer to react with water than the hexagonal form. The powder/water ratio, powder size and its distribution, the amount of air mixed during preparation, time, and temperature may play major roles in determining the properties of the final product. A typical change in temperature with time during setting of plaster of Paris is shown in Figure 11.2. After a rapid temperature rise due to the exothermic reaction, the growth of gypsum ($CaSO_4 \cdot 2H_2O$) from nuclei is rapid and forms needle-like crystals, as shown in Figure 11.3. Table 11.1 shows the effect of the water/particle ratio on porosity. Table 11.2 gives the molecular weight, crystal structure, and density of various calcium and barium sulfates.

11.1.2. Barium Sulfate

Another sulfate of interest is barium sulfate ($BaSO_4$), which has been used extensively as an x-ray contrast medium [14]. *Barite* (the sulfate) is a major source of barium sulfate. Some of its properties are listed in Table 11.2. The crystallographic structure is rhomboid, with unit cell dimensions of 8.89, 5.41, and 7.17 Å, containing four molecules. It is soluble in many acids — including sulfuric, hydrochloric, and hydrofluoric. It is insoluble in alkalis and water.

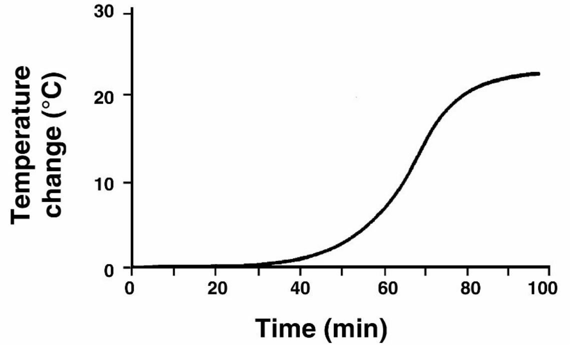

Figure 11.2. Temperature change versus time curve during setting of gypsum. Reprinted with permission from [14]. Copyright © 1973, Saunders.

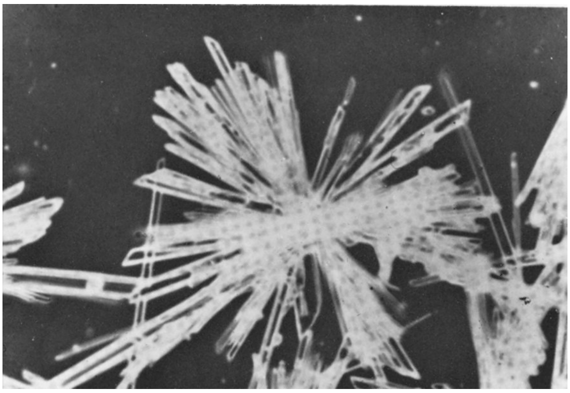

Figure 11.3. Needle-like crystal formation during setting (Eq. (6.2)). Reprinted with permission from [14]. Copyright © 1973, Saunders.

Depending on the end-use purpose, particles can be submicrometer to micrometer in size. In addition, the size distribution is carefully measured for better contrast. Colloidal barium sulfate is also suspended in water to create a medium that is easily ingested by mouth or injected intravenously [7]. This suspension is suitable for use as a contrast medium due to its high molecular weight, since x-ray absorption depends on Beer's law:

$$I = I_0 e^{-\alpha x}, \tag{11.1}$$

where I is the intensity at depth x, and α is the absorption coefficient. Absorption due to the photoelectric effect (the *Compton effect*) is proportional to the atomic number (N) and the wavelength of an x-ray:

$$\alpha = N^5 \lambda^{7/2}. \tag{11.2}$$

Table 11.1. Variations in Porosity by Water/Particle Ratios of Calcium Sulfate

Water/ particle	Porosity (%)
0.25	10.3
0.30	15.3
0.35	20.3
0.40	25.3
0.50	35.3
0.60	45.3
1.00	85.3

Reprinted with permission from [14]. Copyright © 1973, W.B. Saunders.

Table 11.2. Some Physical Constants of Various Calcium and Barium Sulfates

Material	Chemical formula	Molecular weight (g/mol)	Unit cell Structure	Density (g/cm^3)
Calcium sulfate (soluble anhydride)	$CaSO_4$	136.14	Rhombic or monoclinic	2.61
Calcium sulfate (half-hydride)	$CaSO_4 \cdot 1/2H_2O$	145.15	–	–
Calcium sulfate (dihydride)	$CaSO_4 \cdot 2H_2O$	172.17	Monoclinic	2.32
Barium sulfate	$BaSO_4$	253.37	Rhombic (monoclinic)	4.50

Data from [14,19].

Clinical x-ray diagnostic equipment operates at tube voltages of 20–200 kV. The emitted x-rays are at energies (in electron volts) equal to or less than the tube voltage. Most radiological techniques involve tube voltages between 60 and 100 kV, for which absorption by the photoelectric and Compton effects is comparably important. Since the x-ray energy can be expressed as

$$E = h\nu = \frac{hc}{\lambda}, \tag{11.3}$$

where h is Planck's constant and c is the speed of light, the x-rays have wavelengths from 100 pm (0.1 nm) at 10 keV to 5 pm at 200 keV. These wavelengths are much smaller than those of visible light: 400–700 nm.

It is clear that the heavier elements absorb x-rays strongly (see Table 11.3). Heavy metals such as lead are commonly used to shield x-ray equipment. Human soft tissue contains a great deal of the lighter elements — hydrogen, carbon, and oxygen — and is consequently relatively transparent to x-rays. Bone, by virtue of its calcium and phosphorus content, absorbs x-rays more strongly and therefore shows up well radiographic images. Metallic implants absorb strongly and are also highly visible in x-ray images. Polymers, by contrast, are relatively transparent to x-rays. Barium sulfate is incorporated in bone cement to make it visible in diagnostic x-ray images.

Table 11.3. Mass Absorption Coefficient of some Materials

Material	Atomic number	Density, ρ (g/cm^3)	Specific absorption coefficient [μ/ρ(cm^3/g)]
Al	13	2.70	48.7
P	15	1.82	73
Ca	20	1.55	172
Cr	24	7.19	259
Fe	26	7.87	324
Co	27	8.9	354
Pb	82	11.34	241

For CuKα x-rays, wavelength λ =1.54 Å or 0.154 nm.

11.2. STRUCTURE AND PROPERTIES OF TITANATES

A titanate is a salt in which the anion contains both titanium and oxygen, in particular the titanium oxide ion, TiO_3^{2-}. TiO_2 is the oxide form of titanium, which is responsible for the osteo- or osseointegration between artificial medical implants (mostly dental implants) and bone/teeth. Titanium dioxide can also be used to cleave proline from amino acids from solutions or suspensions. Aluminum, barium, calcium, and strontium titanates are used extensively in the ceramics industry, and some are summarized in Table 11.4. These ceramics can be made into nanoparticles for many applications, particularly in electronics. They can also be used to develop biomedical instruments for laparoscopy and implant coatings with better biocompatibility. Furthermore, a more active implant surface (e.g., one with a piezoelectric layer) can stimulate bone to undergo more active osseointegration. In this chapter we examine barium and calcium titanates.

Example 11.1

Calculate the density of rutile (TiO_2).

Answer:

$$\text{Density} = \frac{2\ \text{atoms/u.c.}\ (48 + 2\times16)\ \text{g/mol}}{0.4593\times0.4593\times0.2959\ \text{nm}^3 \times 6.02\times10^{23}\ \text{atoms/mol}}$$

$$= \frac{160\ \text{g}}{0.3758\times10^{23}\ \text{nm}^3} = \underline{4.26\ \text{g/cm}^3}\,.$$

Table 11.4. Properties of Some Titanates

Types	Chemical formula	Crystal structure	Density (g/cm^3)	Melting temp. (°C)	Hardness (Mohs)	Applications	Notes
Titanate	TiO_2	Tetragonal $a = 0.4593$ nm $c = 0.2959$ nm (rutile)	4.26	1870	5.5–6	Photocatalyst, paints coatings, plastics, papers inks, foods, medicines toothpastes	High n: 2.4 Proven bone com-compatibility
Barium	$BaTiO_3$	Perovskite	6.02	1650	5	Dielectric capacitors, piezoelectric transducers (replaced by lead zirconate titanate, PZT)	Possible bone stimulant, nanocomposite with a polymer
Calcium	$CaTiO_3$	Perovskite	4.1	1975	–	Dielectric capacitors	Possible coating layer for bone biocompatibility of metals
Strontium	$SrTiO_3$	Cubic	5.13	2080	6–6.5	Diamond simulant piezoelectric, superconductive material	Tausonite (natural) High n: 2.41

From various sources. n = refractive index (for diamond, $n = 2.41$).

11.2.1. Barium Titanate ($BaTiO_3$)

Barium titanate has been used as a piezoelectric material similar to quartz (SiO_2) crystal as electronic sensors and transducers. Figure 11.4 shows its perovskite structure. Perovskite is the mineral name of an oxide whose composition is $CaTiO_3$. The polymorphic nature of $BaTiO_3$ means that it is a ferroelectric. At a certain temperature, called the Curie point, the polycrystalline from of the material will exhibit increased resistivity by a few orders of magnitude. At the Curie temperature, barium titanate undergoes a phase change from tetrahedral to cubic. In the pure form, it is an electrical insulator. However, when doped with small amounts of metals (e.g., scandium, yttrium, neodymium, samarium) it becomes a semiconductor. The material also exhibits

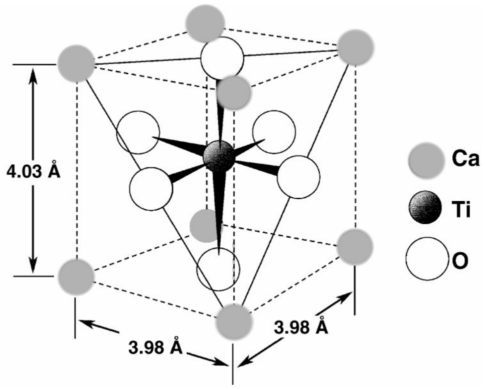

Figure 11.4. Unit cell structure of perovskite ($CaTiO_3$).

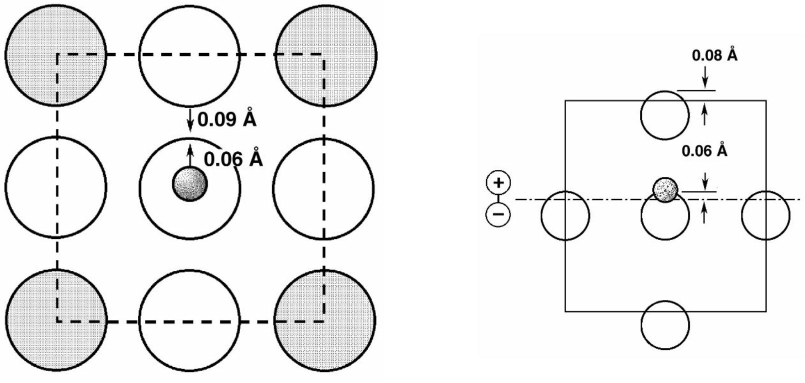

Figure 11.5. Asymmetric nature of Ti^{4+} ion, which forms dipoles with O^{2-} ions.

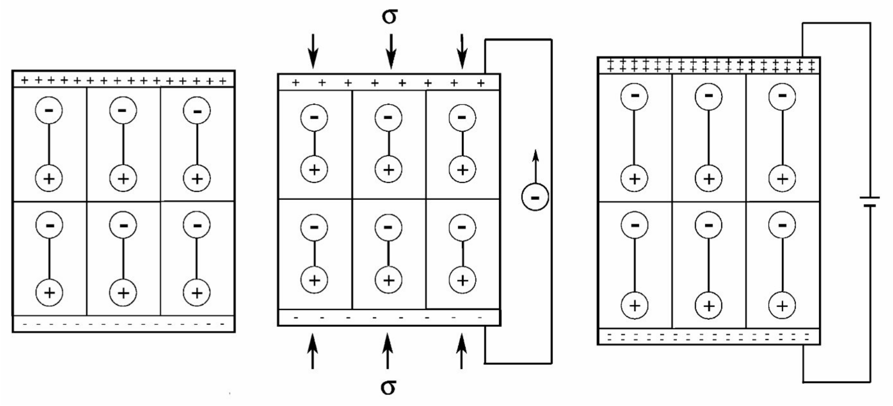

(a) (b) (c)

Figure 11.6. Piezoelectric phenomenon. The dipoles within the crystal result in a charge difference between the two ends (a). Once a stress or strain is imposed, the dipole moment and charge density changes. If shorted by an electrode, electrons will flow (b); if electric field is imposed on the crystal, it will change dimension (c). Reprinted with permission from [18]. Copyright © 1970, Addison-Wesley.

a *piezoelectric* property due to the asymmetry of the Ba^{2+} ion, as shown in Figure 11.5. Due to the spontaneous polarization arising from local fields, all cells tend to align in the same electrical direction. Positive and negative local domains will be developed within the crystal, as shown in Figure 11.6a. Under stress the dipoles are polarized and voltage develops, as shown in Figure 11.6b. A reverse phenomenon develops if voltage is applied. This electromechanical or voltage–strain behavior makes the material useful as a sensor or transducer.

Example 11.2

Calculate the density of bone cement after mixing poly(methylmethacrylate) (PMMA) powder, methylmethacrylate, and an MMA liquid monomer. The PMMA powder contains 10 g of barium sulfate. Due to air and monomer vapor, usually 2–5% porosity results.

Answer:

Assume that there are 40 grams of powder and 20 ml of liquid, and that the densities of barium sulfate and PMMA are 4.5 and 1.2 g/cm^3, respectively.

Total weight: 60 g

Total volume:

$BaSO_4$: 10 g/4.5/cm^3 = 2.222 cm^3

Monomer: 20 ml = 20 cm^3

PMMA powder: 30 g/1.2 g/cm^3 = 25 cm^3

Total volume = 47.222 cm^3

Therefore, density of bone cement = 60 g/47.222 cm^3 = 1.27 g/cm^3

If we include the pores (~3.5%), and assume the porosity measurement represents area fraction which in turn equivalent to volume fraction of the total volume,

Total volume: 47.222 cm^3(1 + 0.035) = 48.875 cm^3

Therefore, density of cement including pores = 60 g/48.875 cm^3 = 1.228 g/cm^3

The obtained values are close to the reported values for radiopacifying bone cement.

11.2.2. Calcium Titanate

Calcium titanates ($CaTiO_3$) are interesting compounds, in particular with regard to their electrical properties [13]. The phase diagram of CaO–TiO_2 is shown in Figure 11.7 [2]. Calcium titanate has a perovskite structure similar to $BaTiO_3$. Calcium titanates are normally synthesized by a solid-state reaction between $CaCO_3$ and TiO_2 at temperatures above 1300°C. Fine $CaTiO_3$ powders consisting of 0.l- to 0.5-cm crystallites can be prepared at 150–200°C by the hydrothermal method starting from hydrated titania gel and reactive calcium oxide suspended as an aqueous slurry in an autoclave [21]. The powders are sintered to high-density ceramics below 1400°C. Crystalline, phase-pure, submicrometer-sized calcium titanates have been produced by a sol–gel method at low temperatures [13].

Polycrystalline calcium titanate (up to 300 nm thick) can be coated on the surface of titanium and its alloy (Ti6Al4V) by the hydrothermal–electrochemical technique in an autoclave at 200°C. These films grown on Ti6Al4V exhibit a small aluminum content but no vanadium. All films show magnesium incorporation equivalent to a few percent of the calcium content, which can be useful for eventual use of the coating in biocompatible applications [20]. Similar to the technique of growing alumina single crystals by flame fusion, calcium titanate boules up to 25 mm in length and 12 mm in diameter were reported [6].

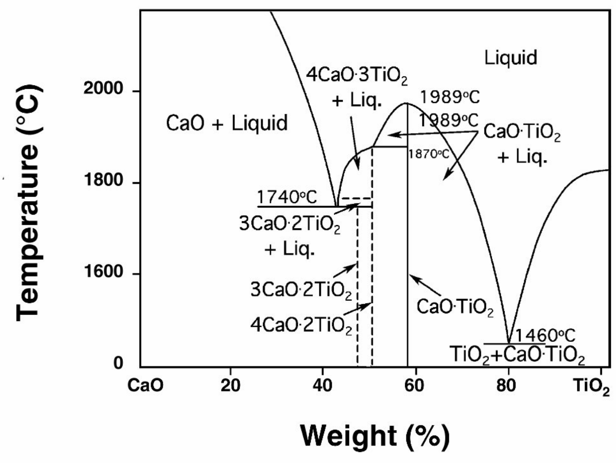

Figure 11.7. Phase diagram of CaO–TiO$_2$. Reprinted with permission from [2]. Copyright © 1970, Elsevier Science.

11.3. APPLICATIONS

Both sulfates and titanates have been used as contrast media in bone cement (barium sulfate, 10% by weight in PMMA polymer powder) and various x-ray radiograph enhancements. Barium sulfate is a white crystalline solid. It is very insoluble in water and other potential solvents. It is frequently used clinically as a contrast agent for x-ray imaging and other diagnostic procedures. It is most often used in imaging of the GI tract during what is colloquially known as a "barium meal."

It is administered, orally or by enema, as a suspension of fine particles in an aqueous solution (often with sweetening agents). Although barium is a heavy metal, and its water-soluble compounds are often highly toxic, the extremely low solubility of its sulfate protects the patient from absorbing harmful amounts of the metal. Barium sulfate is also readily removable from the body. The compound works due to barium's relatively high atomic number ($N = 56$), since large nuclei absorb x-rays much better than smaller ones, as mentioned earlier.

Calcium sulfate has been tried as a material for filling bone defects [11]. Although it has been commercialized in Europe, it is not widely accepted in the United States due to a lack of favorable clinical results. A recent prospective randomized double-blind study [3] showed no effect of calcium sulfate (Osteoset®, a bone graft substitute) on bone healing in humans. In another study on bone healing in a tibial defect in humans, 20 patients undergoing anterior cruciate ligament (ACL) reconstruction with a bone–patellar tendon–bone graft were block randomized into two groups of 10. In the treatment group, the tibial defect was filled manually with calcium sulfate pellets, while the defect was left empty in the control group. A series of CTs was taken on the first day after the operation and at 6 weeks and 3 and 6 months postoperatively. In the control group, it was found that there was about the same amount of bone within the defect at 6 weeks and 3 and 6 months. In the treatment group, the bone volume increased from at 6 weeks and 3 months, and the calcium sulfate pellets were almost completely resorbed after 6 weeks [12]. These results are somewhat contradictory to an earlier report [11], although the materials might have been refined better for the more recent study.

It was postulated in [10] that in vivo the dissolved products (e.g., SO_4^{2-}) elicit reactions by the cells. The ions unfamiliar to the cells and the changing pH surrounding the dissolving ions probably stimulate these reactions. A similar but opposite effect of PLGA dissolution has been observed, which creates an acidic environment detrimental to cells and tissues. Along this line, a porous surface coated with HA at first showed very favorable bone ingrowth; however, the interfacial strength was lower than in the control group (see Fig. 12.17), likely due to a change in the pore environment after slow dissolution of the apatite coating and concentration in the pores.

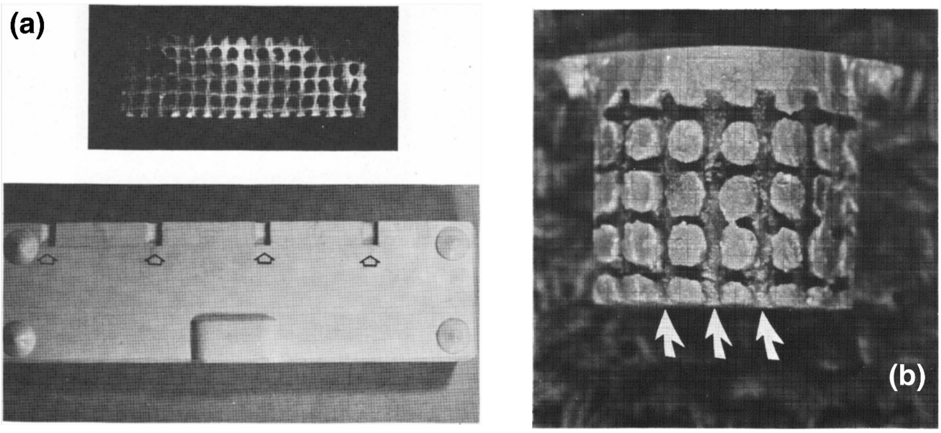

Figure 11.8. (a) Marquisette cloth (top) used to form the desired surface texture of the implant and half of the plaster of Paris mold (bottom; arrows indicate where samples were cast). (b) Final fired implant. Note the undercuts (arrows) for mechanical anchoring of implants. Reprinted with permission from [9]. Copyright © 1980, Wiley.

Barium titanate has also been investigated as a direct substitute for hard tissues [9]. Barium titanate powder was slip-cast (Fig. 11.8a,b) and fired at 1430°C for 2 hr, then made piezoelectric by polarization (Fig. 11.9). After 16 and 86 days of implantation in the cortex of canine femoral midshafts, specimens were sectioned into about 4-cm lengths (Fig. 11.10). Their voltage outputs were measured under a cyclic load at 1 Hz (Fig. 11.11a,b). The results are summarized in Tables 11.5 and 11.6. Voltage output versus distance from the implant surface for the 16-day implant is summarized in Table 11.7. The results show that the voltage gradient at the implant surface is 0.15 mV/mm for the 16-day implant, with a 445-N (100-lb) load. This in turn can give rise to about a 0.01–μA current flow in the area adjacent to the 16-day implant. The 86-

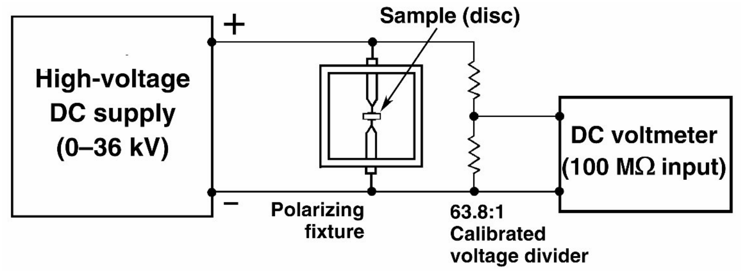
High-voltage DC supply (0–36 kV)
+
−
Sample (disc)
Polarizing fixture
63.8:1 Calibrated voltage divider
DC voltmeter (100 MΩ input)

Figure 11.9. Polarizing circuits. Reprinted with permission from [9]. Copyright © 1980, Wiley.

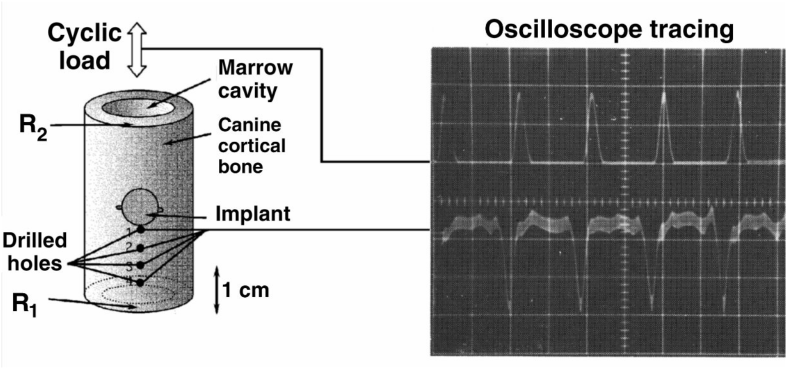
Cyclic load
Marrow cavity
Canine cortical bone
R_2
Implant
Drilled holes
1
2
3
4
R_1
1 cm
Oscilloscope tracing

Figure 11.10. Arrangement for testing voltage output using implant. A similar arrangement was used for measuring bone resistivity. Reprinted with permission from [9]. Copyright © 1980, Wiley.

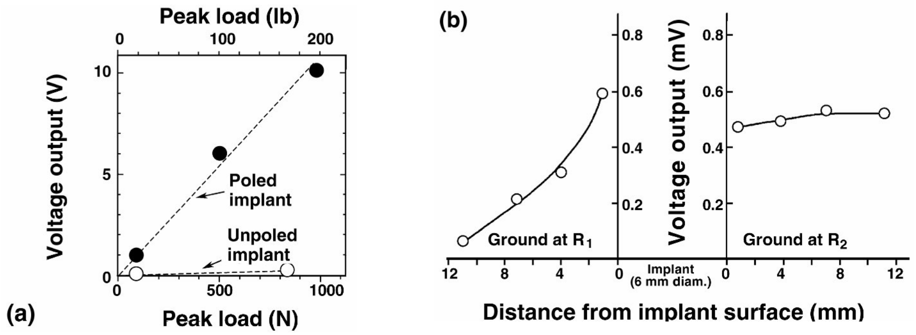

Figure 11.11. (a) Peak load versus voltage output of canine femoral bone sections containing polarized and unpolarized implants in the middle. (b) Voltage output versus distance from the implant surface (16 days after implantation). Reprinted with permission from [9]. Copyright © 1980, Wiley.

day implant showed an order of magnitude higher voltage output compared to the 16-day implant with the same magnitude of load. This is probably due to efficient load transfer, since the voltage output is directly proportional to the actual load transferred. The more bone implant interface matures, the better the load transfer through the implant, resulting in a higher voltage output. Subsequent experimentation with similar implants showed no statistical difference between polarized, stimulated, and control implants despite the initially encouraging results [8]. This is largely due to the less-than-ideal interfacial gap between the drilled hole (0.595-cm diameter) and the implant (0.55 cm) surface; therefore, there is not enough pressure to generate full potential. Another contributing factor may be autolysis of the ingrown tissue after storage in a freezer for weeks before the tests.

Table 11.5. Characteristics of Barium Titanate

Source	TAM Ceramics (a division of NL Industries)
Grade	"p" grade $BaTiO_3$
Compressive strength	486 ± 75 MPa
Density	5.7 g/cm^3 (95% of theoretical value)
Water absorption	0.00% (up to several weeks)
Coupling coefficient	0.27 (polarized at 19 kV/cm)
Voltage coefficient (g_{31})	3.6×10^{-3} V·m/N (polarized at 19 kV/cm)
Electrical resistivity	1.4–4.9 $\times 10^{11}$ Ω·cm

Reprinted with permission from [9]. Copyright © 1980, Wiley.

Table 11.6. Voltage Output vs. Peak Load from 86-Day Implant

Sample type	Peak load (N)	Output (mV)
No implant (bone)	89 (20 lhs)	0.16
	844 (190 lb)	0.25
Unpolarized implant	89 (20 lb)	0.08
Polarized implant	89 (20 lb)	0.95
	445 (100 lb)	5.50[a]
	889 (200 lb)	10.00

[a] Average of two measurements.

Reprinted with permission from [9]. Copyright © 1980, Wiley.

Example 11.3

A bioengineer is trying to construct a cochlear nerve-stimulating implant using a piezoelectric ceramic. This would possibly eliminate the use of a speech processor as well as a power source. The piezoelectric sensitivity coefficient can vary from 0.7 for

Table 11.7. Voltage Output vs. Distance from the Surface of a 16-Day Implant[a]

Position of electrodes	Distance implant surface (mm)	Output[b] (mV, peak-to-peak) with R_1	with R_2
1	0.9	0.59	0.48
2	3.7	0.32	0.50
3	6.6	0.22	0.53
4	105	0.07	0.52

[a] The loading/unloading rate was 4.45 kN/sec.

[b] Output corrected to 445-N (100-lb) peak load.

Reprinted with permission from [9]. Copyright © 1980, Wiley.

bone, 2.3 for quartz, and up to 600 pC/N for some piezoelectric ceramics ([10, pp. 84–87]). If one assumes an rms sound level of 100 dB, which produces a pressure of 2 Pa ([1, p. 86]), and a 1-mm thick ceramic implant of piezoelectric sensitivity 600 pC/N, then calculate the potential output for use for cochlear nerve cell stimulation.

Answer:

The charge density *q*/*A* is the product of the piezoelectric sensitivity coefficient and stress:

$$q/A = 600 \text{ pC/N} \times 2 \text{ Pa} = 1.2\times10^{-9} \text{ C/m}^2 . \quad (1)$$

Under the assumptions given, the implant behaves as a capacitor of capacitance *C*, for which the charge $q = CV$, where *V* is the voltage ($V = q/[ke_0A/t]$), with *k* the dielectric constant, e_0 the permittivity of space, *A* the cross-sectional area, and *t* the thickness. Using the charge density given in Eq. (1) with 1-mm thickness,

$$V = [1.2\times10^{-9} \text{ C/m}^2][10^{-3} \text{ m}]/[1000\times8.85\times10^{-12} \text{ C/V}\cdot\text{m}]$$

$$= 1.4\times10^{-4} \text{ V} = 0.14 \text{ mV} . \quad (2)$$

The amount of sound energy reduction when the sound waves hit the eardrum, pass through the tissues, and arrive at the surface of the implant can be calculated. The acoustic impedances ($Z = \rho v$, where ρ is density and *v* is the velocity of sound in the material) of air, tissue (average), and a piezoelectric ceramic such as barium titanate are 0.04, 163, and 2408 kRayl, respectively ([10, p. 92]). The amplitude reflection coefficient associated with an interface between material 1, containing the incident wave, and material 2 is given by

$$R_A = (Z_2 - Z_1)/(Z_2 + Z_1) = (163 - 0.04)/(163 + 0.04)$$

$$= 0.9995. \quad (3)$$

The percentage of sound waves reflected at the soft tissue is 99.95%, that is, only 0.05% of the waves pass through the soft tissue. For the soft tissue and implant,

$$R_B = (2408 - 163)/(2408 + 163) = 0.873\,. \tag{4}$$

The net reflection of sound waves is 87.3%, and only 12.7% is transmitted. Therefore, the net fraction of sound reaching the nerve cells would be 6.2×10^{-5}. Recalling that the potential generation in Eq. (2) is 0.14 mV, hence $0.14\ \text{mV} \times 6.2 \times 10^{-5} = 8.4 \times 10^{-9}$ V (8.4 nV). This potential is about 1/100 of the maximum potential recorded in [15, p. 257], since the amplitude of the auditory evoked potential is on the order of 1 mV in all frequency ranges. The theoretical calculations give a much smaller value than that obtained from the auditory nerve cell signals. One might consider a piezoelectric polymer, which offers a better match of acoustic impedance than the ceramic. In that case, one could stimulate the cochlear nerve cells without the use of a tuned amplifier. It is also possible to stimulate the cochlear nerve cells without the use of a tuned amplifier if one were to connect an electrode directly to the piezoelectric "implant," which would be placed outside the skin. More than enough sound energy could be delivered to the nerve tissues in that case. The electric current or voltage output may depend on the size and shape of the implant, and the angles of the incoming sound. It is also conceivable that this technique could be used to grow nerve tissues since electrical energy is known to stimulate regeneration of hard and soft tissues.

11.4. FURTHER THOUGHTS

Sulfates and titanates are useful mostly because of their inertness and high x-ray absorbability [4,16,17,20]. Some investigators have tried to make a composite for use as a bone substitute [5]. More careful studies with these ceramics are required before they can be used as implants. New nanoparticles could be coated on the surface of implants or made into transducers for medical instrument miniaturization, which could be used in such applications as laparoscopy.

PROBLEMS

11.1. Calculate the unit cell volume of gypsum (calcium sulfate, $CaSO_4 \cdot 2H_2O$), which has a monoclinic structure and a density of 2.33 g/cm^3.

11.2. Hydroxyapatites are used to make a bone substitute paste for filling defects (see Table 12.4). Propose ways of using sulfate for such an application.

11.3. A piezoelectric stimulator 1 cm^2 in cross-section and 1 mm thick is incorporated into a composite bone plate. It experiences 1% of the stress seen in a healthy leg bone during walking [8 MPa]. The material is a lead titanate zirconate ceramic for which the relevant piezoelectric coefficient is 100 pC/N and the dielectric constant 1000. Determine the peak voltage produced by the device. For the purposes of calculation, neglect the leakage of charge through the conductive pathways in the bone.

11.4. A bioengineer is trying to make a cochlear nerve-stimulating implant using a piezoelectric ceramic. This will possibly eliminate the use of speech processor as well as the power source. The piezoelectric sensitivity coefficient can vary from 0.7 for bone, 2.3 for quartz, and up to 600 pC/N for some piezoelectric ceramics [10, p. 87]. If one assumes an rms sound level of 100 dB, which produces 2 Pa pressure [1, p. 86], and a 1-mm thick ceramic implant of piezoelectric sensitivity 600 pC/N, then calculate the potential output for use in cochlear nerve cell stimulation.

11.5. Can you propose such similar ceramic implants as an active matrix liquid crystal display or an organic light-emitting diode (LED) for the optic nerve stimulation?

11.6. Hydrothermal processing of titanates can make the surface of metal implants attractive. Suggest a way to directly oxidize a titanium surface. What would be the difference between hydrothermal processing and "passivation"?

11.7. For the numbered list (1–10), choose the most appropriate lettered alternative (a–j).

a. Alumina b. Zirconia c. Hydroxyapatite
d. Diamond e. $BaSO_4$ f. Graphite
g. Pyrolytic carbon h. $CaSO_4$ i. Bioglass j. DLC

1. Amorphous carbon
2. Sialons
3. Stabilized with yttrium
4. Plaster of Paris
5. $Ca_{10}(PO_4)_6(OH)_2$
6. Glass-ceramic
7. Ruby or sapphire
8. Highest refractive index
9. Radiopacifying agent for x-rays
10. Matrix material for heart valve disc

SYMBOLS/DEFINITIONS

Symbols

c: speed of light in a vacuum, 2.998×10^8 m/s.
E: energy (x-ray).
h: Plank's constant, 6.62×10^{-34} J·s.
I: intensity (of x-rays) after passing through a material.
I_0: intensity (of x-rays) before passing through a material.
N: atomic number.
x: distance (thickness).

Definitions

Anterior cruciate ligament (ACL): Ligament connecting the tibia and femur. Often left intact during knee implant surgery due to its important role in stabilizing both the femur and tibia.

Barite: A mineral consisting of barium sulfate, typically occurring as colorless prismatic crystals or thin white flakes.

Barium meal: Radiopacifying agent (barium sulfate) to examine an upper GI series, a procedure in which radiographs of the esophagus, stomach, and duodenum are taken after barium sulfate is ingested by the patient. Barium meals are useful in the diagnosis of structural and motility abnormalities of the foregut.

Barium sulfate ($BaSO_4$): Member of the sulfate family. Used as radio contrast media for its strong absorption of x-radiation.

Barium titanate ($BaTiO_3$): Member of the titanate family. Often exhibits piezoelectric properties after polarization under a strong magnetic field. Used as a transducer of electromechanical energy.

Beer's law: Absorption of x-rays or light occurs such that the transmitted intensity decreases exponentially with distance.

Calcination: Reduce, oxidize, or desiccate by roasting.

Calcium sulfate ($CaSO_4$): Naturally occurring as gypsum mineral. Can be used as plaster of Paris, plaster board, blackboard chalk, and bone substitute.

Calcium titanate($CaTiO_3$): One of the titanate family. It has a perovskite structure and is used for its electromagnetic properties.

Compton effect: An increase in the wavelength of x-rays or gamma rays that occurs when they are scattered.

Computerized (or computed) tomography (CT or CAT scan): An x-ray image made using computerized axial tomography.

Curie temperature: The temperature above which a ferromagnetic material ceases to be ferromagnetic. For a ferroelectric material used in piezoelectric transducers, the Curie point is the temperature at which the material loses its permanent electric polarization. Control of the temperature of a magnetic metal implant is possible using electromagnetic induction and knowledge of the Curie temperature.

Drierite®: Desiccant used to remove moisture from pulmonary analyzer circuits. Drierite changes from blue to rose-red upon absorbing moisture (made by A-M Systems Inc).

Ferroelectric: Exhibiting permanent electric polarization that varies in strength with applied electric field.

Gel–sol transfer: Phase changes of from particles suspended in the liquid phase to the solid state and vice versa. This is an irreversible process if chemical bonding takes place.

Gypsum ($CaSO_4 \cdot 2H_2O$): Soft white or gray mineral consisting of hydrated calcium sulfate. It occurs chiefly in sedimentary deposits and is used to make plaster of Paris and fertilizers, as well as in the building industry. Has some use as a bone substitute (OsteoSet®).

Hemihydrate (α- and β-) ($CaSO_4H_2O$): One form of calcium sulfate. The β-crystals form at higher temperature with less porosity, and a harder material results.

OsteoSet®: Calcium sulfate-based bone graft material produced by Wright Medical Co., Memphis, TN.

Perovskite: A yellow, brown, or black mineral consisting largely of calcium titanate. the term is also used to describe a type of crystal structure.

Piezoelectricity: Electric polarization in a substance (especially certain crystals) resulting from application of mechanical stress. Piezoelectric substances are able to convert mechanical signals (such as sound waves) into electrical signals, and vice versa. They are therefore widely used in microphones, phonograph pickups, and earphones, and also to generate a spark for igniting gas.

Plaster of Paris: A soft mixture of lime with sand or cement and water for spreading on walls, ceilings, or other structures to form a smooth hard surface after drying.

Poly(lactic glycolic acid, PLGA): Resorbable polymer often used as suture and scaffold material.

Rhomboid: Having or resembling the shape of a rhombus, a parallelogram with opposite equal acute angles, opposite equal obtuse angles, and four equal sides.

REFERENCES

1. Gorga MP, Neely ST. 1994. Stimulus calibration in auditory evoked potential measurements. In *Principles and applications in auditory evoked potentials*, pp. 85–97. Ed JT Jacobson. Needham Heights, MA: Allyn and Bacon.
2. Jongejan A, Wilkins ALJ. 1970. A re-examination of the system CaO–TiO_2 at liquidus temperatures. *Less-Common Met* **20**:273–279.
3. Lee GH, Khoury JG, Bell JE, Buckwalter JA. 2002. Adverse reactions to OsteoSet bone graft substitute, the incidence in a consecutive series. *Iowa Orthop J* **22**:35–38.
4. Lei D, Wardlaw D, Hukins DWL. 2006. Mechanical properties of calcium sulphate/hydroxyapatite cement. *Biomed Mater Eng* **16**:423–428.
5. Mamidwer SS, Arena C, Kelly S, Alexander H, Ricci J. 2006. In vivo characterization of calcium sulfate/PLLA composite for use as bone graft material. *J Biomed Mater Res Appl Biomater* **81B**:57–65.
6. Merker L. 1962. Synthesis of calcium titanate single crystals by flame fusion technique. *J Am Ceram Soc* **45**:366–369.
7. Miller RE, Skucas J. 1977. *Radiographic contrast agents*. Baltimore: University Park Press.
8. Park J, Kelley B, von Recum A, Kenner G, Coffeen W, Grether M. 1981. Piezoelectric ceramic implants: in vivo results. *J Biomed Mater Res* **15**:103–110.
9. Park J, von Recum A, Kenner G, Kelley B, Coffeen W, Grether M. 1980. Piezoelectric ceramics: a feasibility study. *J Biomed Mater Res* **14**:269–277.
10. Park JB, Lakes RS. 2007. *Biomaterials: an introduction*, 3rd ed. New York: Springer.
11. Peltier LF. 1961. The use of plaster of paris to fill defects in bone. *Clin Orthop Relat Res* **21**:1–31.

12. Petruskevicius J, Nielsen S, Kaalund S, Knudsen PR, Overgaard S. 2002. No effect of Osteoset, a bone graft substitute, on bone healing in humans: a prospective randomized double-blind study. *Acta Orthop Scand* **73**(5):575–578.
13. Pfaff G. 1994. Synthesis of calcium titanate powders by the sol-gel process. *Chem Mater* **6**:58–62.
14. Phillips RW. 1973. *Skinner's science of dental materials*. Philadelphia: W.B. Saunders.
15. Stapells DR, Picton TW, Durieux-Smith A. 1994. Electrophysiologic measures of frequency-specific auditory function. In *Principles and applications in auditory evoked potentials*, pp. 251–283. Ed JT Jacobson. Needham Heights, MA: Allyn and Bacon.
16. Stubbs D, Deakin M, Chapman-Sheath P, Bruce W, Debes J, Gillies RM, Walsh WR. 2004. In vivo evaluation of resorbable bone graft substitutes in a rabbit tibial defect model. *Biomaterials* **25**:5037–5044.
17. Thomas MV, Puleo DA, Al-Sabbagh M. 2005. Calcium sulfate: a review. *J Long-Term Eff Med Implants* **15**:599–607.
18. Van Vlack LH. 1970. *Materials science for engineers*. Reading, MA: Addison-Wesley.
19. Weast RC. 1968. *Handbook of chemistry and physics*, 49th ed. Cleveland, OH: Chemical Rubber Company.
20. Wiff JP, Fuenzalida VM, Zárate RA, Arias JL, Fernández MS. 2004. Characterization of hydrothermal-electrochemical calcium titanate coatings on titanium and biomedical titanium alloy. *J Phys Condens Matter* **16**:S1345–S1350.
21. Yokokawa H, Kawada T, Dokiya MJ. 1989. Thermodynamic regularities in perovskite and K_2NiF_4 compounds. *Am Ceram Soc Bull* **72**:152–153.

12

COMPOSITES, TISSUE SUBSTITUTES, AND SCAFFOLDS

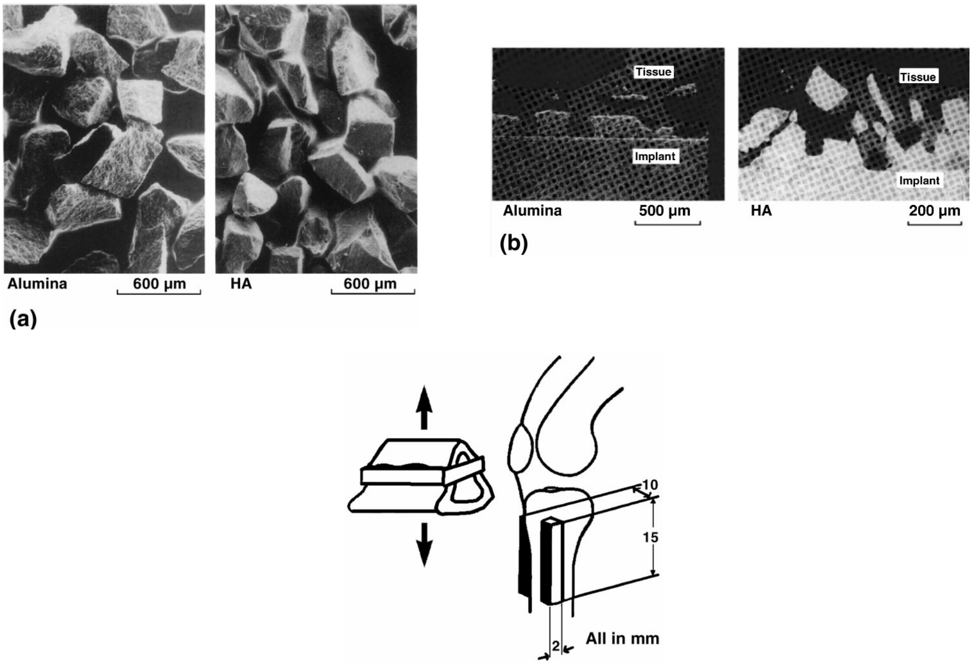
Alumina
600 μm
HA
600 μm
(a)
Tissue
Implant
Alumina
500 μm
Tissue
Implant
HA
200 μm
(b)
10
15
2
All in mm

(a) SEM pictures of alumina and HA granules. (b) After 8 weeks of implant in tibia of rabbit. (c) Study of the tissue ingrowth into the porous surfaced by alumina and hydroxyaptite granules onto the alumina, implanted in rabbit tibia [75]. After 8 and 25 weeks, the forces to separate the block were measured (see Ex. 12.5). Study results: separation load (kgf):

Materials	8 weeks	25 weeks
Alumina	6.78 ± 1.04	10.5 ± 0.84
Hydroxyapatite	3.93 ± 0.49	2.05 ± 1.22

Composites are important components of implants and such tissues as bone (see Chapter 5). Bone is made of collagen fibers that form fibrils to which hydroxyapatite (HA) crystals are discretely attached. These fibrils form lamellae wrapped around the Haversian canal using polysaccharides as a glue or adhesive, possibly forming glycosaminoglycans (GAGs). This intricate structure allows composites to have strength and toughness, and to carry out biological activity. In this chapter we discuss the fundamentals of composites.

The rapidly evolving field of tissue engineering requires characterization of the property–structure relationships of scaffolds materials. We will limit ourselves here to hard tissue engineering scaffolds. An excellent overview of tissue engineering with biomaterials can be found elsewhere [79].

12.1. FUNDAMENTALS OF COMPOSITE THEORY [7,120]

Composite materials contain two or more distinct constituent materials or phases. Accordingly, reinforced plastics like fiberglass as well as body tissues are viewed as composite materials, but such alloys as brass and steel are not. Natural biological materials tend to be composites — for example, bone, wood, dentin, cartilage, and skin. Natural biological foams include lung, cancellous bone, and wood. Natural composites often exhibit a hierarchical structure in which particulate, porous, and fibrous structural features are seen on different length scales. (See the cover illustration in Chapter 5 for the hierarchical structure of compact bone.)

12.1.1. Structure of Composites

A wide range of composite properties can be obtained through control of structure [2,37]. In particular, the properties of a composite material depend upon the shape of its inclusions, the volume fraction, and the interfacial strength among constituents. The principal shapes of inclusions are: (1) the particle, (2) the fiber, and (3) the platelet (also called the lamina) (see Fig. 12.1). The inclusions may vary in size and shape within each category. For example, particulate inclusions may be spherical, ellipsoidal, polyhedral, or irregular. Cellular solids [53] are those in which "inclusions" are voids filled with air or liquid. We distinguish between random orientation and preferred orientation in the structure of each composite.

Dental composite filling material having particulate structures are shown in Figure 12.2. The fracture surface of a fibrous material with its fibers pulled is depicted in Figure 12.3. The degree of adhesion of the reinforcing materials to the matrix is another important factor in the performance of composites.

12.1.2. Mechanics of Composites

The mechanical properties of composites depend on structure in a complex way; however, the prediction of properties is relatively simple for some structures [3]. The sim-

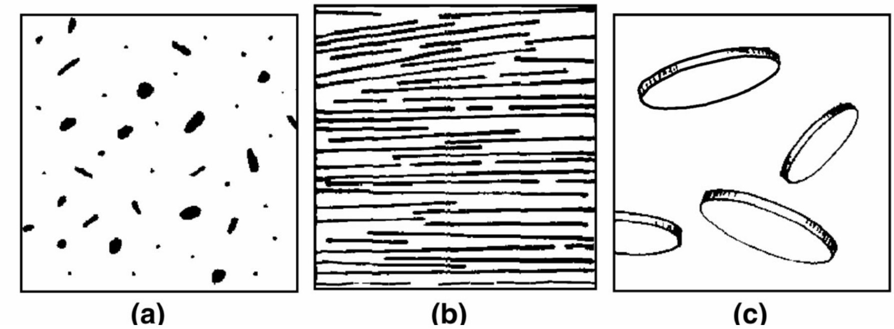

Figure 12.1. Morphology of basic composite inclusions: (a) particle, (b) fiber, and (c) platelet. Reprinted with permission from [120]. Copyright © 2007, Springer.

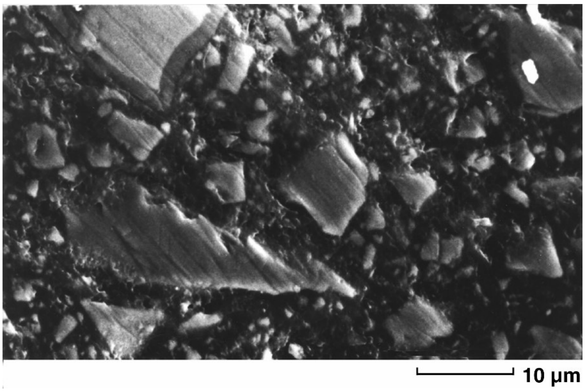

Figure 12.2. Microstructure of a dental composite. Miradapt® (Johnson & Johnson) 50% by volume filler: barium glass and colloidal silica. Reprinted with permission from [120]. Copyright © 2007, Springer.

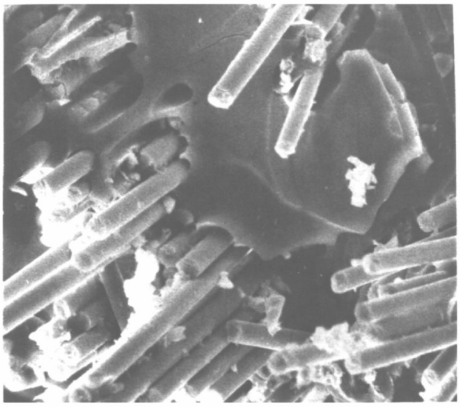

Figure 12.3. Glass–fiber–epoxy composite: fracture surface showing fiber pullout. Reprinted with permission from [2]. Copyright © 1980, Wiley.

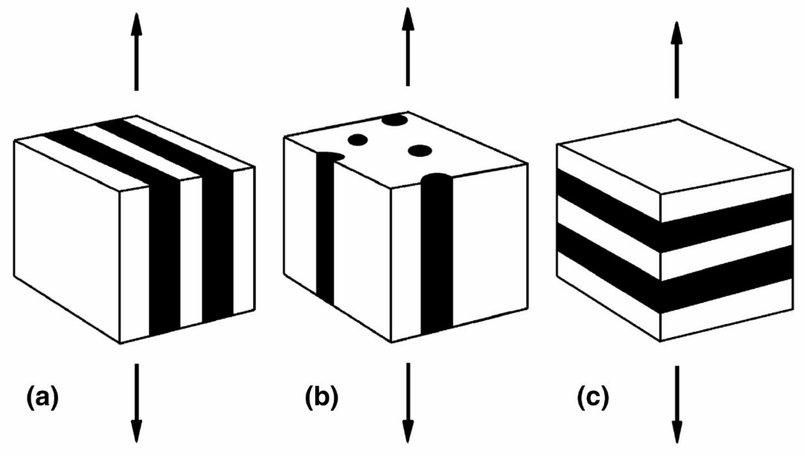

Figure 12.4. Tension force indicated by arrows, applied to Voigt (a, laminar; b, fibrous) and Reuss (c) composite models. Reprinted with permission from [120]. Copyright © 2007, Springer.

plest composite structures are the idealized Voigt and Reuss models, shown in Figure 12.4. The dark and light areas in these diagrams represent different constituent materials. In contrast to most composite structures, it is easy to calculate the stiffness of materials with the Voigt and Reuss models. Young's modulus E of a Voigt composite is (neglecting restraint due to Poisson's effect)

$$E = E_i V_i + E_m V_m, \tag{12.1}$$

where E_i is Young's modulus of the inclusions, V_i is the volume fraction of the inclusions, and E_m is Young's modulus of the matrix. The volume fraction of matrix is

$$V_m = 1 - V_i. \tag{12.2}$$

The Voigt relation for the stiffness is also called the *rule of mixtures*.

Young's modulus for the Reuss model is

$$\frac{1}{E} = \frac{V_i}{E_i} + \frac{V_m}{E_m}. \tag{12.3}$$

The Voigt and Reuss formulae constitute, respectively, the upper and lower limits of composite stiffness.

Example 12.1

Determine the Young's modulus of materials with a Reuss structure, assuming that Young's modulus is known for each constituent.

Answer:

For the Reuss model, if tension is applied as in Figure 12.4c, the inclusions (dark) and the matrix (light) deform together, with equal stress:

$$\sigma_c = \sigma_i = \sigma_m \,, \tag{1}$$

in which *c* refers to the composite, *i* to the inclusions, and *m* to the matrix. The strains are additive:

$$\sigma_c = V_i \varepsilon_i + V_m \varepsilon_m \,. \tag{2}$$

Assume linearly elastic behavior, so that

$$\sigma_c = E_c \varepsilon_c \,. \tag{3}$$

Therefore,

$$\varepsilon_c = \sigma_c / E_c = V_i \sigma_i / E_i + V_m \sigma_m / E_m \,. \tag{4}$$

Using Eq. (1), then

$$1 / E_c = V_i / E_i + V_m / E_m \,. \tag{5}$$

The stiffness under the Voigt model can be obtained in a similar manner.

This stiffness is quite different from that obtained using the Voigt model. However, the Reuss laminate is identical to the Voigt laminate, except for a rotation with respect to the direction of load. Therefore, the stiffness of the laminate is anisotropic, that is, dependent on direction.

In cubic symmetry, there are three independent elastic constants: Young's modulus *E*, shear modulus *G*, and an independent Poisson's ratio (ν). Crossweave fabrics have cubic symmetry. An isotropic, homogeneous material has the same material properties in any direction. There are only two independent elastic constants. The others are related by such equations as

$$E = 2G(1 + v) \,. \tag{12.5}$$

Random fibrous and random particulate composite materials are isotropic.

Equations for the simple theoretical stiffness of composites are given in Table 12.1, where V_i is the volume fraction [between 0 and 1] of inclusions, V_s is the solid volume fraction, *E* is Young's modulus, and *m* refers to the matrix. The strength of composites depends not only on the strength of the constituents but also on the stiffness and degree of ductility of constituents. The Voigt relation for stiffness is referred to as the rule of mixtures; related rules of mixtures are discussed elsewhere in this volume. The Voigt and Reuss models provide the upper and lower bounds of stiffness, respectively, as shown in Figure 12.5. The relations given in Table 12.1 for inclusions are valid for small volume fractions; the relations become much more complex in the case of larger volume fractions. As for particles, they are assumed to be spherical, and the matrix is assumed to have a Poisson's ratio of 0.5.

The strength of composites depends on such particulars as the brittleness or ductility of inclusions and the matrix. In fibrous composites failure may occur by fiber

Table 12.1. Equations for the Simple Theoretical Stiffness of Composites

Structure	Stiffness
Voigt model	$E = E_iV_i + E_m[1 - V_i]$
Reuss model	$E = [V_i/E_i + (1 - V_i)/E_m]^{-1}$
Isotropic, dilute:	
3D random orientation	
Particulate	$E = [5(E_i - E_m)V_i]/[3 + 2E_i/E_m] + E_m$
Fibrous	$E = E_iV_i/6 + E_m$
Platelet	$E = E_iV_i/2 + E_m$

Reprinted with permission from [2]. Copyright © 1980, Wiley.

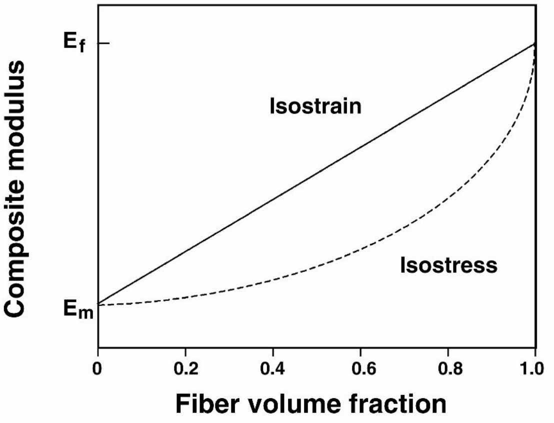

Figure 12.5. Composite modulus versus volume fraction.

breakage, buckling, or pullout; matrix cracking; or debonding of fiber from matrix. While unidirectional fiber composites can be made very strong in the longitudinal direction, they are weaker than the matrix alone when loaded transversely, as a result of stress concentration around the fibers. Short-fiber composites are used in many applications. While they are not as strong as those with continuous fibers, they can be formed economically by injection molding or by in-situ polymerization. The choice of optimal fiber length can result in improved toughness, due to the predominance of fiber pull-out as a fracture mechanism.

Example 12.2

Determine the upper and lower bounds of the Young's modulus for cortical bone composed of 69% inorganic phase and 31% organic phase. Assume the water is a part of the organic phase. Assume further that the tissue behaves as an anisotropic material so that the Voigt model can be applied. Observe that Young's modulus for mineral (HA) and collagen fibers is about 100 and 1 GPa, respectively.

Answer:

From Example 5.1 the values for the volume fraction of the inorganic and organic phases are 50%. Therefore,

$$E = 0.5 \times 100 + 0.5 \times 1 \;=\; 50.5 \text{ GPa}\,.$$

The Reuss model predicts that

$$1/E = 0.5/100 + 0.5/1, \quad E = 1.98 \text{ GPa}\,.$$

The typical compact bone modulus is 15–20 GPa. All fibers and lamellae are not fully longitudinally oriented. One could calculate the relative proportions, but the real bone may not have the mathematically predicted orientations and architect. Another important factor would be that the mineral phase is not a single crystal nor continuous polycrystals. Rather, it is a discrete phase in which the mineral particles are embedded onto collagen fibrils (see Problem 9.3). This type of arrangement will result in a much lower modulus than for the solid mineral. Other factors such as porosity due to the Haversian canal, canaliculi, and lacunae may also contribute to the much lower modulus.

12.2. APPLICATIONS OF COMPOSITES

It is very important that each constituent of the composite biomaterial be biocompatible and that the interface between constituents not be degraded within the body environment. Composites used in biomaterial applications include: (1) dental filling composites, (2) bone particle-, carbon fiber-, and ultra-high-molecular-weight polyethylene (UHMWPE)-reinforced bone cement, and (3) porous surface orthopedic implants. Rubber is usually filled with very fine particles of silica or carbon black to make it stronger and tougher.

Nanoparticle (<100 nm in diameter) composites can be created for many applications. As with other composites, the adhesion and uniform dispersion of nanoparticles are important to manufacture of useful products, as shown in Figure 12.6. New nanocomposites can be used to make scaffolds for both soft and hard tissues.

12.2.1. Orthopedic Implants

There are two types of composites employed in orthopedics: (1) those that improve the mechanical properties of existing solid homogeneous matrix materials and (2) those that incorporate other materials for improved performance of biological and nonbiological functions. The carbon fiber-reinforced carbon belongs to type 1, while bone morphogenetic proteins (BMPs) and barium sulfate-incorporated bone cement belong to type 2. The use of ceramic matrix composites (CMCs) has not been applied

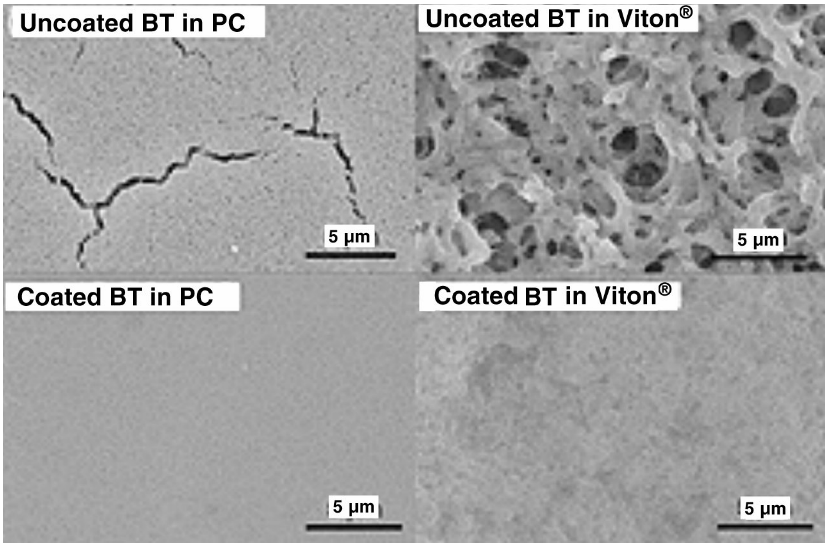

Figure 12.6. Scanning electron micrographs of barium titanate (BT, $BaTiO_3$) nanocomposites with polycarbonate (PC, left, top, and bottom) and Viton® (right, top, and bottom) polymer matrices. The uniformity through the use of phosphonic acid ($HPO(OH)_2$)-coated $BaTiO_3$ nanoparticles (bottom images) as compared to uncoated nanoparticles (top images). The higher uniformity results in greatly improved dielectric properties. Modified with permission from http://www.gatech.edu/news-room/release.php?id=1362. Copyright © 2007, Georgia Institute of Technology.

in orthopedics despite their tremendous advantages over such monolithic ceramics as alumina and zirconia. Polymer matrix composites (PMCs) have been used in such applications as self-reinforced polylactic–glycolic acid (PLGA) for bone screws and in plates used to fix small bones, as shown in Figures 12.7 and 12.8 [146]. The use of such metal matrix composites (MMCs) as cermets may be somewhat challenging since the biocompatibility of CMC or PMC is generally lower due to the probability of corrosion.

Table 12.2 lists the properties of some reinforcing fibers used commercially. Carbon fibers have been employed to make artificial tendons (personal communication), but this effort failed due to breakdown of fibers in vivo. The thought of using aramid fibers (Kevlar®) for such an application is an attractive one.

Composites have been considered for bone plates and in the femoral component of total hip replacements. Currently used implant metals (210 GPa for CoCr alloy, 110 GPa for Ti alloy) are much stiffer than bone (18 GPa). They therefore shield bone from mechanical stress, resulting in atrophy, and the bone resorbs [47]. Composite materials can be made more compliant than metal and deform elastically in response to a higher strain (to about 0.01 compared to 0.001 for "mild" steel), which is a potential advantage in this context [22,138]. Flexible composite bone plates have been found to be effective in promoting healing [73]. Hip replacement prostheses have been made with composites containing carbon fibers in a matrix of polysulfone and poly-

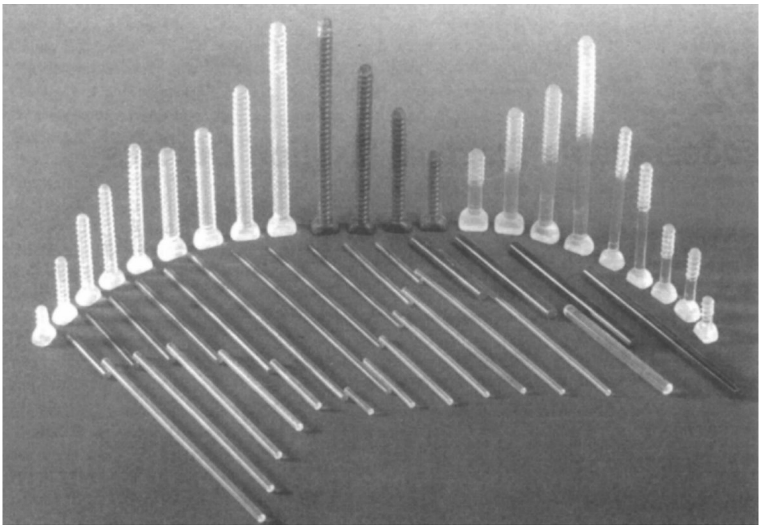

Figure 12.7. Absorbable polymers are used to make pins, screws, and rods for orthopedic applications. Reprinted with permission from [146]. Copyright © 2000, Marcel Dekker.

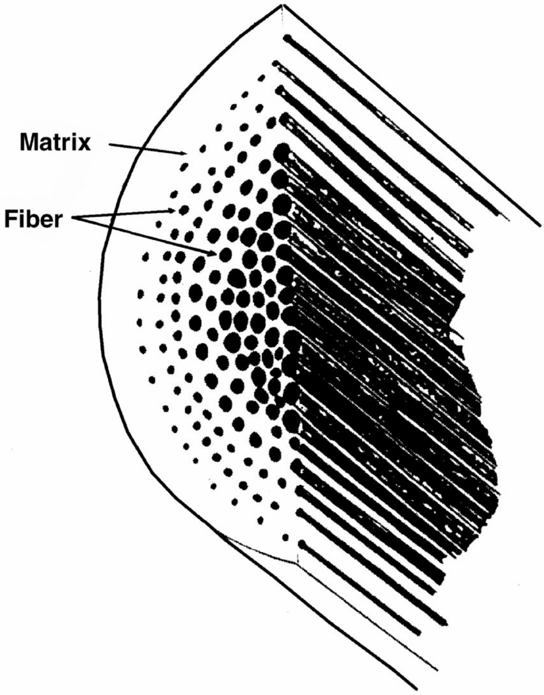

Figure 12.8. Schematic illustration of self-reinforcing biodegradable PGA, from US Pat # 4,743,257 (1988). Reprinted with permission from [146]. Copyright © 2000, Marcel Dekker.

Table 12.2. Properties of Selected Commercial Reinforcing Fibers

Fiber	Typical diameter (mm)	Density (g/cm^3)	modulus (GPa)	strength (GPa)	strain (%)	Thermal expansion coefficient (10^{-6}/°C)	Poisson's ratio
E glass	10	2.54	72.4	3.45	4.8	5	0.2
PAN carbon	7	1.76	231	3.65	1.4	–0.6, 7–12	0.2
Aramid, Kevlar® 49	11.9	1.45	131	3.62	2.8	–2, 59	0.35
PE, Spectra®-900	38	0.97	117	2.59	3.5	–	–
Boron	140	2.7	393	3.1	0.79	5	0.2
Al_2O_3	20	3.95	379	1.90	0.4	8.3	–

PAN = polyacrylonitrile; PE = polyethylene, extended chain.
Reprinted with permission from [135]. Copyright © 1997, Prentice-Hall.

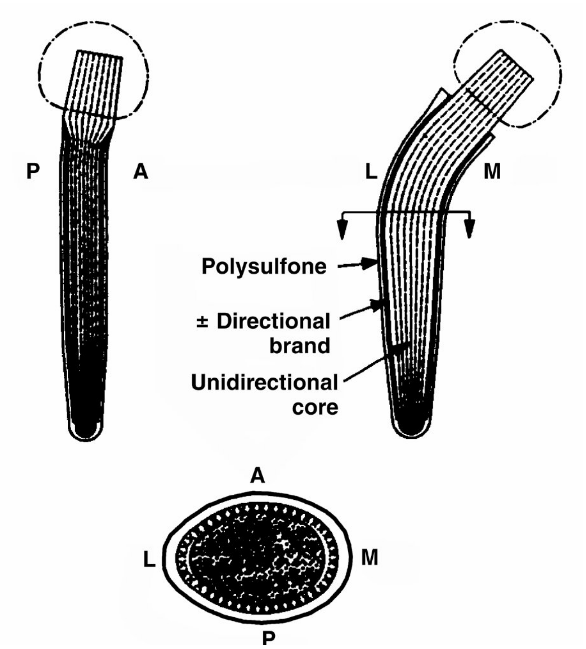

Figure 12.9. Details of carbon–polysulfone composite femoral stem construction. Reprinted with permission from [108]. Copyright © 1988, Lippincott Williams & Wilkins.

ether ether ketone (PEEK) [56]. A polysulfone–carbon composite femoral stem is shown in Figure 12.9. In polymer matrix composites, creep behavior due to the polymer component is a matter of concern. Prototype composite femoral components have exhibited creep of small magnitude limited by the fibers, which do not creep much. Creep is not expected to limit the life of an implant [109]. Figure 12.10 shows a knee prostheses with carbon fiber-reinforced polyethylene tibial components. This product is no longer available for clinical use.

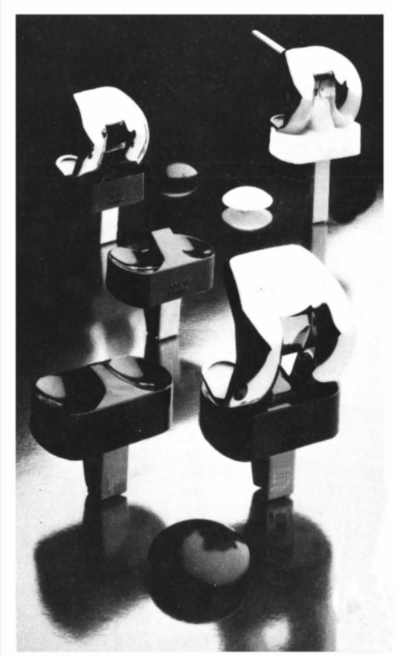

Figure 12.10. Knee prostheses with carbon fiber-reinforced polyethylene tibial components. Reprinted with permission from [120]. Copyright © 2007, Springer.

A rather complicated acetabular cup for a hip joint prosthesis is shown in Figure 10.10 [143]. The carbon fiber-reinforced UHMWPE body with HA in the cup outer surface was hoped to induce direct bonding with the acetabular bone. However, there was no bonding between the carbon and UHMWPE, resulting in eventual debonding. A more sophisticated design is shown in Figure 12.11. Some investigators [121] made the inner surface of irradiated UHMWPE to minimize wear, while the outer surface had a PMMA layer that bonds with the bone cement when implanted. This eliminates the need for grooves, which weaken the cup, to hold the cup when implanted with bone cement. However, these design concepts have not been tested clinically.

Some investigators [18] made an HA–polymer composite to be used in implants. The results of the initial study are given in Figure 12.12. They employed what they termed an “analogue composite design” that they hoped would enhance both mechanical and biological function during tissue ingrowth and regeneration. One of the problems with this type of composite is that the surface of the HA ceramic is usually completely covered with polymer, thus preventing contact between the bioactive ceramic and tissue. Similar results were obtained with bone particle-impregnated bone cement. The minimum amount of bone particles for continuous pore formation is 30–40% [106,119], similar to results obtained by Bonfield [17,18]. Bone particle-impregnated PMMA bone cement has been used for canine femoral stem fixation [60] (see Fig. 12.13 for the results). Experimental subjects experienced a maximum inter-

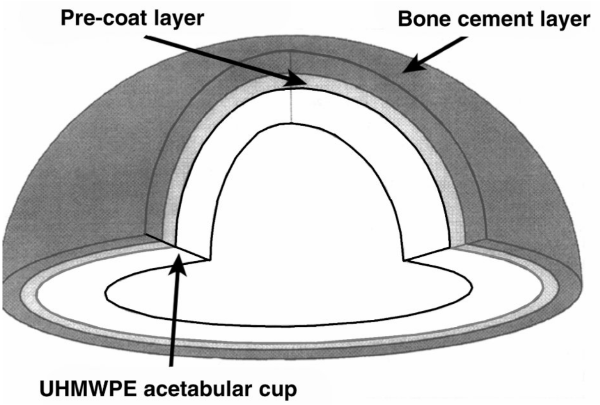

Figure 12.11. Precoating all-poly acetabular cup outer surface with bone cement layer combined with crosslinking of UHMWPE by γ-radiation. Modified with permission from [121]. Copyright © 1999, Begell House.

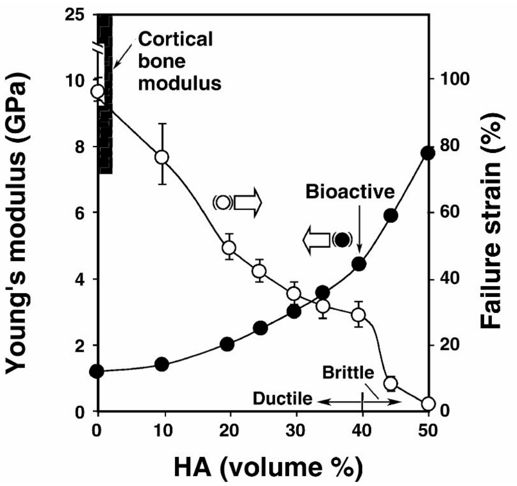

Figure 12.12. Effect of volume fraction of hydroxyapatite (HA) on Young's modulus (*E*) and strain to failure of hydroxyapatite-reinforced polyethylene composite, in comparison to cortical bone, as represented by Hench [59] based on data of Bonfield [17]. Reprinted with permission from [59], Copyright © 1993, American Ceramic Society.

facial shear strength of 7.35 MPa, while this value for controls was 2 MPa. The same investigators studied BMP particle-impregnated bone cement, and obtained similar results. However, definitive conclusions cannot be drawn due to the limited number of subjects.

Porous HA can be made into a cellular composite, as shown in Figure 12.14 [137]. The replamineform of the natural tissue cellular structure has also been used in the hope of obtaining optimal cell structure, as shown in Figure 12.15 [36].

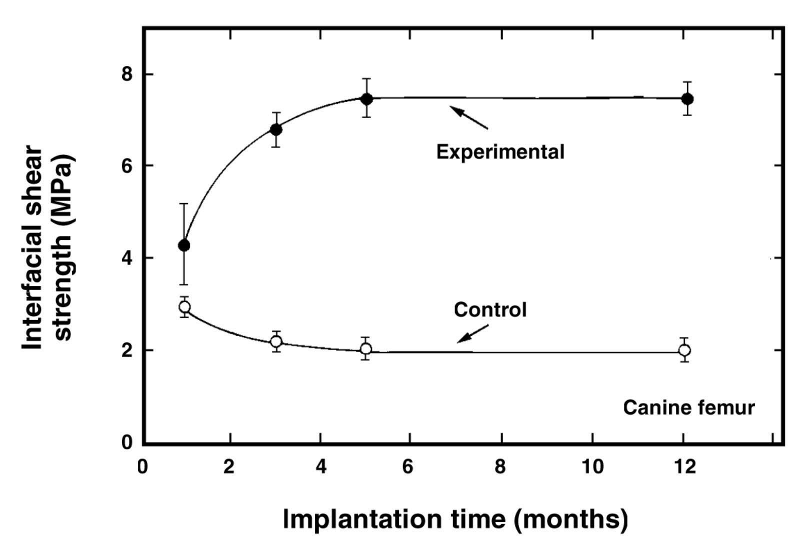

Figure 12.13. Maximum interfacial shear strength between bone and bone cement versus implant period. The femoral stems were implanted with ordinary bone cement and cement with bone particles. In both cases the interfacial strength stabilized after 5 months for this canine model. Reprinted with permission from [41]. Copyright 1991, Wiley.

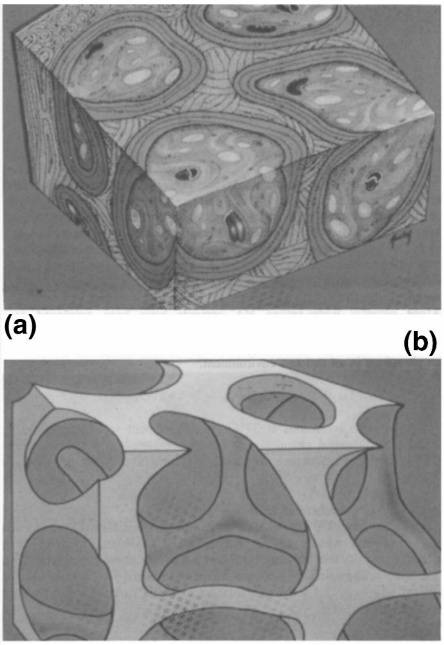

Figure 12.14. Microstructure of human cancellous bone. The osteons appear as plain lamellae with interstitial bone filling the spaces in between (a). Idealized microstructure of human cancellous bone. The large interconnected pores permit ingrowth of fibrovascular tissues, regeneration of osteons, etc. (b). Reprinted with permission from [137]. Copyright © 1993, World Scientific.

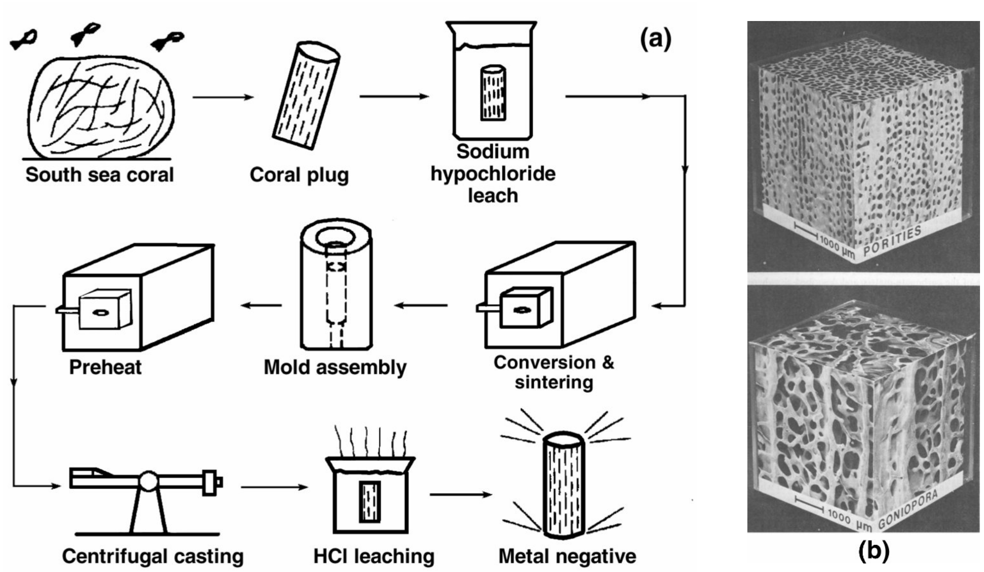

Figure 12.15. (a) Schematic representation of the replamineform process. The coral is cut and shaped for treatment to yield porous implants in a wide variety of materials. (b) Three-dimensional photographs of various corals following sodium hypochlorite leaching. (Top) genus *Porities*: virtually all pores are in the 100–200 μm range; in addition, when properly oriented, longitudinal struts of the nonporous microstructure are present. (Bottom) genus *Goniopora*: the pores here range from 200 to 1000 μm, and the complete interconnectedness of the substance is more readily appreciated. Modified with permission from [35]. Copyright 1975, Wiley.

Bioactive glass-ceramics are additionally used to make a composite using metal wires (316L stainless steel, titanium, and Co–Cr alloy) [44,58]. In-vitro and in-vivo studies have demonstrated the feasibility of using such composites for orthopedic and dental implants.

Porous-surfaced composites have also been considered for use as implants. They can be coated with bioactive ceramics, as shown in Figure 12.16. Animal experimentation has yielded mixed results [120] (see Fig. 12.17): an HA-coated porous implant at first offered higher interfacial shear strength between bone and implant; however, after 3 months the controls (without an HA coating) showed higher strength. This was mainly due to dissolution of the HA in the pores, which could not be removed fast enough for tissues to continue to grow.

Some investigators have tried to understand the role of the crystallinity of HA following coating onto a metal. Their results showed no differences in interfacial strength among low-, medium-, and high-crystallinity HA-coated Ti alloy implants and bone. The only significant difference occurred with an uncoated metal implant, again demonstrating the good bone compatibility of HA [31].

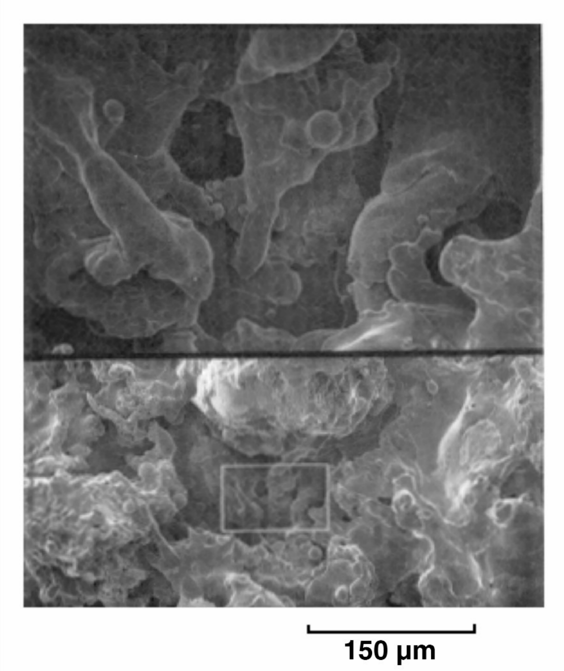

Figure 12.16. Structure of porous coating for bony ingrowth. The SEM picture is at 5× magnification of the rectangular region in the bottom picture (200×, Ti6Al4V alloy). Note the irregular pore structure. From unpublished data of J.B. Park.

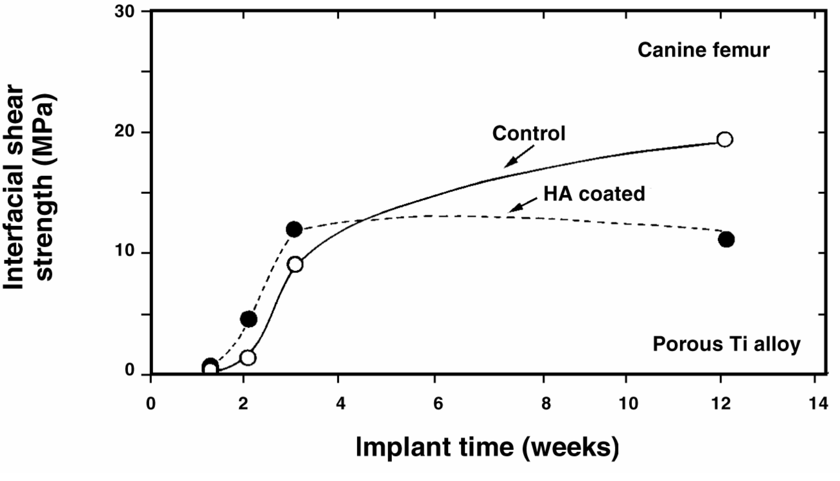

Figure 12.17. Maximum interfacial shear strength between bone and bioactive ceramic-coated porous plug implants versus implant period. Plugs with and without (control) coating were implanted in the cortices of canine femurs. Reprinted with permission from [120]. Copyright © 2007, Springer.

12.2.2. Dental Filling Composites and Cements [120]

Dental composite resins have been used for restoration in anterior teeth and have also become commonly used to restore posterior as well as anterior teeth. The composite resins consist of a polymer matrix and stiff inorganic inclusions, as shown in Figure 12.2. Note that the particles are very angular in shape. The inorganic inclusions confer relatively high stiffness and high wear resistance upon the material. Moreover, by virtue of their translucence and an index of refraction similar to that of dental enamel, they are cosmetically acceptable. The inorganic inclusions are typically barium glass or silica [quartz, SiO_2]. Inclusions, also called fillers, have a particle size from 0.04 to 13 μm, and concentrations from 33 to 78% by weight (Table 12.3). The matrix consists of bis-GMA, an additional reaction product of bis(4-hydroxyphenol), dimethylmethane, and glycidyl methacrylate. Since the material is mixed and then placed in a prepared cavity to polymerize, its viscosity must be sufficiently low and the polymerization must be controllable. Such low-viscosity liquids as triethylene glycol dimethacrylate (TEGDMA) are used to lower viscosity, and inhibitors like butylated trioxytoluene (2,4,6-tri-tert-butylphenol, BHT) are used to prevent premature polymerization. Polymerization can be initiated by a thermochemical initiator (e.g., benzoyl peroxide) or by a photochemical initiator (benzoin alkyl ether), which generates free radicals when subjected to ultraviolet light to initiate free radical polymerization.

Table 12.3. Composition and Shear Modulus of Dental Composites

Brand name	Fillers	Filler amount (w/o)	Particle size (μm)	*G* (GPa), 37°C
Adaptic	Quartz	78	13	5.3
Concise	Quartz	77	11	4.8
Nuva-fil	Barium glass	79	7	–
Isocap	Colloidal silica	33	0.05	–
Silar	Colloidal silica	50	0.04	2.3

Reprinted with permission from [118]. Copyright © 1984, Wiley.

The compositions and shear moduli of several commercial dental composite resins are given in Table 12.3. In view of the greater density of the inorganic filler phase, 77 wt% filler corresponds to a 55 vol%. The typical mechanical and physical properties of 50 vol% dental composite resins are listed in Table 12.4. Dental composites are considerably less stiff than natural enamel (which contains >97% mineral). One cannot easily obtain such high concentrations of mineral particles in synthetic composites. The particles do not pack densely. Moreover, the viscosity of unpolymerized paste increases with particle concentration. Too high a viscosity will prevent the dentist from adequately packing paste into a cavity. The use of surfactants will lessen this problem.

Table 12.4. Typical Properties of Dental Composites

Values	Property
Young's modulus, E (GPa)	10–16
Poisson's ratio, ν	0.24–0.30
Compressive strength (MPa)	170–260
Shear strength (MPa)	30–100
Porosity (vol%)	1.8–4.8
Polymerization contraction (%)	1.2–1.6
Thermal expansion, α (10^{-6}/ºC)	26–40
Thermal conductivity, k (10^{-4} cal/sec/cm^2 (ºC/cm))	25–33
Water sorption coefficient (mg/cm^2, 24 hr, room temp.)	0.6–0.8

Reprinted with permission from [28]. Copyright © 1988, Wiley.

The thermal expansion of dental composites exceeds that of teeth. There is also some contraction (up to 1.6%) during polymerization, which is thought to contribute to leakage of saliva, bacteria, among other things, at the interfacial margins. Such leakage can in some cases cause further tooth decay. For some materials this contraction is counteracted by swelling due to absorption of water in the mouth. Use of colloidal silica in so-called “microfilled” composites allows these resins to be polished, which cuts down on wear and plaque accumulation. However, it is more difficult to make these with a high fraction of filler, since the tendency for high viscosity of unpolymerized paste must be counteracted. Excessively high viscosity is problematical since it prevents the dentist from adequately packing paste into the cavity; the material will then fill crevices less effectively. All dental composites exhibit creep [118], which may result in indentation of a restoration, but wear seems to be a greater problem.

Dental composites tend to become brittle and relatively weak under tension. Moreover, they are subject to mechanical fatigue, so that they can fail at stress levels below static fracture strength [9,23]. Their use is thus restricted to certain types of dental restorations.

The “packable” or condensable dental composites have been introduced as better alternatives to amalgam in restorations of posterior teeth, and they can be packed more easily into a prepared cavity and will produce tighter contacts between restored teeth [101]. The elastic modulus of these composites ranges from about 9.5 to 21 GPa.

A variety of filled resin-based cements, with 65 to 74 wt% filler, is available to attach dental crowns to the remaining tooth structure [130]. A high modulus is considered beneficial in the ability of the cement to prevent the loss of a crown.

Dental composite resins are now established as restorative materials for both anterior and posterior teeth and as cements. The use of these materials is likely to increase as improved compositions are developed and in response to concern over the long-term toxicity of silver–mercury amalgam fillings.

Nanoparticle composites may be an attractive alternative to dental composites as fillers and adhesives. The main problem here is dispersion of nanoparticles, which can possibly be solved by treating the filler (ceramic particles) with acid (see Fig. 12.6) and surfactants.

Example 12.3

A composite is made of spherical alumina particles (20 vol%) and a polymer matrix. Calculate Young's modulus and compare with the Reuss model. Alumina and polymer have a Young's modulus of 400 and 1 GPa, respectively.

Answer:

Using the relation given in Table 12.2,

$$E = \frac{5(400-1)}{3+2\times 400/1} + 1 = \underline{3.48\text{ GPa}}\,.$$

The Reuss model gives

$$\frac{1}{E} = \frac{0.2}{400} + \frac{0.8}{1}, \quad E = \underline{1.25\text{ GPa}}.$$

The stiffness of a particulate composite is not much greater than the Reuss lower bound, while spherical inclusions increase Young's modulus only marginally.

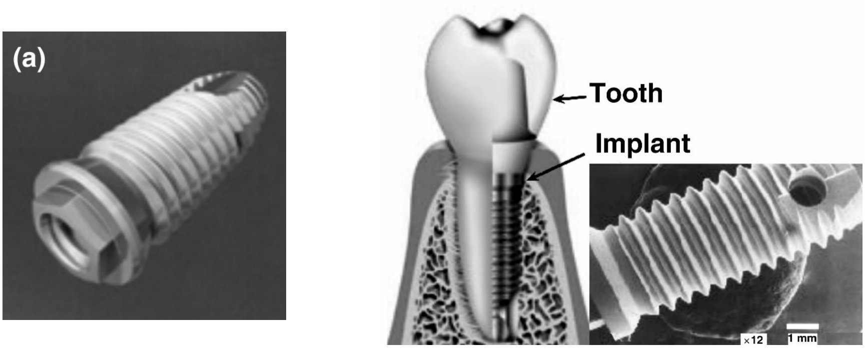

Figure 12.18. (a) Modern (Brånemark System®) dental implant. Reprinted with permission from http://www.umich.edu/~nbumictr/Implants/branemark/branemark.html. (b) Dental implant view in situ and SEM photograph of implant root. Courtesy of Pi Dental Center, Fort Washington, Pennsylvania.

12.2.3. Dental Implant and Osseointegration

Some investigators have passivated Ti and Ti alloys twice to reduce ion release, and they claim that this process yields superior osseointegration [78]. One can consider titanium oxide (TiO_2) or such other oxide ceramics as Al_2O_3 and ZrO_2 as tooth root materials, as shown in Figure 12.18. Ironically, even these "metal" implants are virtually "ceramics" coated by an oxide layer. Single-crystal alumina can also be used, as shown in Figure 12.19. The bone substitutes would have osseo- or osteointegration during the healing process. However, direct apposition of bone on the surface of an implant without intervening collagen membrane formation is termed *osseointegration* [24]. To have such a tissue–implant interface, first, there should be minimal relative motion between the two; second, there should be minimal mismatch of modulus or compliance; and, third, the implant surface material should be highly biocompatible. In orthopedics, osseointegration cannot be easily achieved due to the first two factors. Brånemark and coworkers [24,25,78,79] have championed this concept in dental implants. Figure 12.20 offers a schematic summary of the sequence of events in osseointegration.

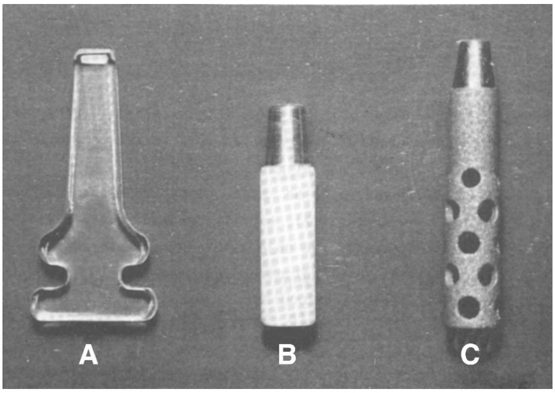

Figure 12.19. Dental implant roots: (a) single-crystal alumina; (b) HA-coated Ti alloy; and (c) through-and-through porous Ti alloy. Reprinted with permission from [141]. Copyright 1989, Elsevier Science.

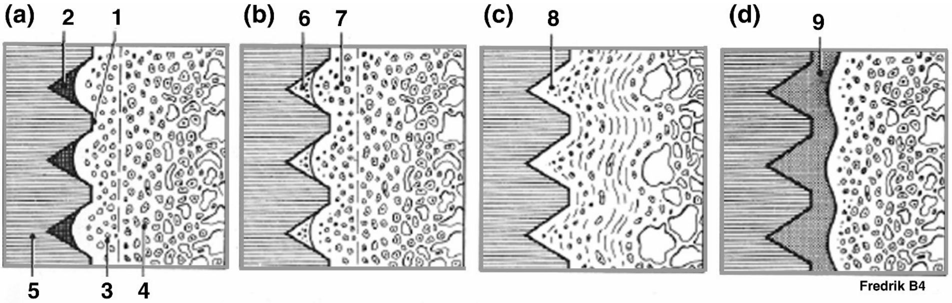

Figure 12.20. Schematic summary of the sequence of events in osseointegration. (a) The screw-thread seats cannot initially be made to be congruent with the dental implant. The importance of the threaded implant is to create immediate stability after insertion and during the initial healing phase. (1) Contact between the fixture and bone (so-called immobilization). (2) Hematoma in a confined cavity, which is bordered by the fixture and bone. (3) Bone, despite careful preparation, is thermally and mechanically damaged. (4) Unmolested bone tissue. (5) Fixture. (b) During the initial healing phase, the hematoma is transformed into new bone through in-situ bone formation. (6) Damaged bone tissue heals through revascularization, demineralization, and remineralization (7). (c) After the initial healing phase, vital bone is in direct contact with the surface of the fixture without any intermediary tissue. (8) Border zone is remodeled in response to functional loading. (d) In the case of osseointegration failure, non-mineralized connective tissue forms in the border zone in contact with the implants (9), which can be considered a form of pseudoarthrosis. Reprinted with permission from [24]. Copyright © 1977, Almqvist & Wiksell.

Other researchers have suggested that the implant–bone interface undergoes fibro-osseous integration [149,150] or biointegration [114]. Both processes describe the same collagen membrane formation at the interface. The presence of collagen membranes at the interface is key evidence of these processes. Membranes are usually formed in response to mechanical loading (relative motion) on the surface, and the presence of foreign matter. The interface can change over time, and initial osseointegration may become fibro-osseous integration due to infection, implant wear products, and overloading of implant during mastication. Moreover, a dental implant is exposed to the "exterior" of the body since the crown protrudes into the mouth. This makes it a transcutaneous or percutaneous implant, which introduces the added burden of sealing an implant to prevent invasion by foreign organisms.

The metals (Ti and Ti6Al4V) used in Brånemark-style implants have many favorable features. They are easy to machine, have high strength, toughness, and low modulus, are easily passivated, etc. However, such metals as zirconium should be explored for possible use in dental implants, as they have characteristics similar to those of titanium in terms of high oxidizability and good mechanical properties.

Example 12.4

After 12 weeks, the interfacial shear strength of HA-coated and noncoated porous-surfaced cylindrical Ti alloy implants was 10 and 18 MPa, respectively (see Fig. 11-8). Assuming the strength of compact bone as given in Table 5-4, calculate the maximum shear strength of the interface if all the pores are filled with bone. The porosity of the original implant is 35%.

Answer:

Assuming the shear strength is proportional to the tensile (compressive) strength (Table 5.4), the shear strength would be 1/2(1 + ν), where ν is Poisson's ratio. Therefore,

$$\text{Shear strength} = \frac{150\ \text{MPa}}{2(1+0.3)} \times 0.35$$

$$= \underline{20.2\ \text{MPa}}.$$

If the ingrown bone has similar properties, the control specimen will be almost fully ingrown with bone (89%). In the case of HA-coated specimens, the pores are 50% filled.

12.2.4. Hard Tissue Substitutes and Augmentation

Ceramics and polymers have been studied and employed as bone substitutes. We could classify them as bioabsorbable (biodegradable), nonabsorbable, and semiabsorbable, depending on time of degradation. Bone itself is absorbable in vivo. Table 12.5 gives a classification of ceramics according to their absorptivity. The rate of absorption depends on many factors, including size, size distribution, surface condition,

Table 12.5. Classification of Ceramics According to Their Absorption Property

Classification	Duration	Examples
Absorbable	< months	CaP compounds, $CaSO_4$,
Semiabsorbable	> years	Glass-ceramic(Bioglass®)
Nonabsorbable	> many years or permanent	Al_2O_3, ZrO_2, diamond

and porosity. Even nonabsorbable materials can be absorbed in vivo if they are made into fine particles so that macrophages can ingest them. Therefore, one must give the state of the material precisely in order to relate the material's absorbability and its rate of absorption. Most biocompatible ceramics are osteoconductive, and some absorbable ceramics are osteoinductive.

Example 12.5

Alumina is coated with granules of alumina and HA in order to increase the bone/implant interfacial strength (see the opening page of this chapter). Calculate the tensile strength of the attachments [75]. What conclusions can you draw?

Answer:

The nominal surface area is 10 × 15 mm^2. Assume that only 2/3 of the total surface area is in contact with bone. Therefore, 6.78 kgf/150 × 2/3 = 6.78 × 9.8 N/100 mm^2 = 0.664 MPa. The calculated values are given in the following table.

Tensile strength (MPa) of the interface between tissue and implant.

Coating material	8 weeks	25 weeks
Alumina	0.66 ± 0.10	1.02 ± 0.08
HA	0.39 ± 0.05	0.20 ± 0.12

Some conclusions can be drawn. These values are much lower than the typical interfacial strength for porous implants (e.g., metal) and tissue (e.g., bone): 5~10 MPa. One reason for the low values is that the ingrown tissues may not be "compact" bone, as in the experiment with a transcortical femur implant depicted in Figure 12.13. Another reason is that the interfacial strength between the alumina substrate and the coating materials is weaker than that between the bone and the porous layer. This is especially true for the HA-coated implant. The reason for the decrease in bone/HA interfacial strength after 25 weeks as compared to 8 weeks is that the HA pores experience accumulation of calcium and phosphate ions, which is detrimental to attachment of the ingrown tissue cells.

12.2.4a. Calcium Phosphate (CaP) Compounds

As mentioned in Chapter 9, CaP compounds have excellent biocompatibility. Their properties can be modified by altering the calcium-to-phosphate ratio, by incorporation of ions, by modification of crystallinity, and by changing the porosity. The dissolution or biodegradation rate depends on the stoichiometry, the crystal structure, the crystallinity, and the size of particles.

The rate of biodegradation or dissolution of different CaP compounds are given by Eq. (9.6), ACP > α-TCP > β-TCP > AP > HA, where ACP is an amorphous calcium phosphate, TCP is tricalcium phosphate, AP apatite, and HA hydroxyapatite. Figure 9.12 shows the very slow rate of dissolution of HA, which some classify as a nonbiodegradable CaP compound.

TCP is unpredictable when it comes to the biodegradation rate and the bone regeneration accompanying biodegradation. Some investigators have reported bone ingrowth (osteoconduction) through the channels (600 μm) and pores (100–150 μm) of TCP, leading to bone regeneration in critical-sized defects [65]. However, such other nonbiodegradable ceramics as alumina can behave similarly if the interconnections and porosity are similar.

Other forms of CaP are mentioned in the literature, including tetracalcium phosphate and dicalcium phosphate. The Ca/P ratio is an important indicator of the dissolution of a calcium phosphate compound. Bone minerals have a Ca/P ratio of 1.67, similar to that of HA. Other compounds would not be likely to have similar bone bonding characteristics.

Table 12.6. Classification of Bone Graft Substitutes

Class	Description	Examples
Allograft based	Allograft bone used alone or in combination with other materials	Allogro, Othroblast, Opteform, Grafton
Factor based	Natural and recombinant growth factors used alone or in combination with other materials	TGF-β, PDGF, FGF, BMP
Cell based	Cells used to generate new tissue alone or seeded onto a support matrix	Mesenchymal stem cells
Ceramic based	Includes calcium phosphate, calcium sulfate, and Bioglass® used alone or in combination	Osteograf, Norian SRS, ProOsteon, Osteoset
Polymer based	Both degradable and nondegradable polymers used alone and in combination with other materials	Cortoss, OPLA, Immix

Reprinted with permission from [97]. Copyright © 2005, WebMD.

Bone substitutes have been classified according to the source of raw materials (see Table 12.6). *Deorganized* or *anorganic bones* can be obtained from animal (bovine) or human subjects. These are HAs with very slow resorption and biodegradation. They can be made into particles or porous blocks. A *demineralized* bone matrix can be used as filler for bone regeneration. Growth factors can then be added. These are quite biodegradable.

Synthetic calcium phosphates have also been employed as bone substitutes (see Chapter 9). Tricalcium phosphate ($Ca_3(PO_4)_2$) is the most and hydroxyapatite ($Ca_{10}(PO_4)_6(OH)_2$ the least bioabsorbable. Calcium sulfate (see Chapter 11) can be used as a defect-filling material [98,122,124]. One could add such organic materials as collagen, BMPs, and TGF-β (transforming growth factor). Bioactive glass-ceramics can be used as particles or blocks. Their surfaces dissolve, creating a calcium phosphate layer between the tissue and glass-ceramic. Nonbiodegradable glass-ceramics can also be used (see Chapter 8).

Table 12.7. Classification of Bone Substitute Materials Based on Hollinger

Classification of materials	Comments
A. Bone derived	
a. Anorganic	Bovine or human bone mostly hydroxyapatite
b. Demineralized	Mostly collagen or denatured gelatin
B. Coralline derived	Nondegradable, hydrothermal treated HA
C. Calcium phosphates	
a. TCP	Synthetic, biodegradable
b. HA	Synthetic, nonbiodegradable
c. Others	Mono, di-, tri-, and tetracalcium, and sodium phosphates
d. Injectable	Easy delivery
D. Calcium sulfate	Plaster-of-Paris, biodegradable
E. Glass-ceramics	Surface-dissolving bioactive mixed with nonbioactive glass-ceramics
F. Ceramic–polymer composite	Poly(MMA–HEMA)[a] with calcium layer

[a] Poly(methylmethacrylate–hydroxy ethylmethacrylate).

Reprinted with permission from [63]. Copyright © 1996, Springer.

Non-weight-bearing *injectable* bone substitutes can also be constructed, depending on particle size and amount mixed with matrix. Again, any of the BMPs or TGF-β can be added. Such other calcium phosphates as tetra-, di-, and monocalcium phosphate have also been employed, as given in Table 12.7. These calcium phosphates can be obtained from animal or human bone. from coral, and from induced chemical reactions. However, many of their characteristics (e.g., rate of degradation, property–structure relationships) are not well known. Most bone substitute products are proprietary. They can be made into many forms — porous, nonporous, particulate, and block — and can be mixed with various BMPs, TGF-β, etc.

Clinical reports using HA- or TCP-derived bone substitutes yield favorable results [29]. Table 12.8 gives a list of FDA-approved bone substitutes.

Example 12.6

Determine the initial rate of Ca ion release into buffer solution for ACP, HA, and TCP from Figure 9.12.

Answer:

ACP:100 ppm/min
α–TCP: 5 ppm/min
β–TCP: 3 ppm/min
HA: 1 ppm/min

Table 12.8. Availability of Bone Substitutes

Name	Type	Composition	Action	Approved indications	Trials
1. ProOsteon® (Interpore International)	Bone graft substitute	Sea coral converted by hydrothermal	Acts as lattice for new bone formation	Metaphysical fractures of long bones	Being evaluated in cervical spine fusions
2. Bioglass® (US Biomaterials Corp)	Bioactive glass-ceramic implant	CaO–SiO$_2$–NaO$_2$–P$_2$O$_5$	Reacts with body fluid, causing bone-like pores to evolve on implant surface. Collagen bonds to surface and new bone forms and fills the space between the implant, collagen fibers, and bone.	Only for grafting facial bones, replacing bones in the middle ear, and repairing periodontal defects	Long bone fracture fixation, spinal fusions, and joint replacement
3. Collagraft® (Zimmer)	Synthetic bone graft substitute	HA/tricalcium phosphate and pure bovine fibrillar collagen	Mix with autogenous bone marrow to produce an osteoconductive and osteoinductive substance that acts as a matrix for repair process	Repair of diaphyseal metaphyseal fxs. Note: fx should be stabailized with skeletal fixation and recommended maximum defect site of 30 cc	Risk: immunologic risk secondary to bovine collagen (no reported serious cases)
4. Grafton® (Osteotech)	Banked human tissue	Demineralized bone matrix glycerol suspension	Elicits new bone formation by osteoconduction andn osteoinduction	As adjunctive to spinal and joint fusion, repair of osseous defects, & arthroplasties	Risk: possible disease transmission. Note: processing of Grafton has been shown to inactivate HIB, hepatitis B&C, cytomegalovirus, and polio
Experimental Products: (Awaiting FDA Approval)					
1. Norian Skeletal Repair System (SRS)	Bone mineral substitute	Mono- and tricalcium phosphate, calcium carbonate & liquid sodium phosphate	Paste that hardens to turn into the mineral phase of bone (osteoconductive). Is replaced by bone. Maximum compressive strength greater than cancellous bone		
2. Bone Source Hydroxyapatite Cement – (developmental)	HA bone substitute	Nonceramic hydroxyapatite	Initially formed into a paste that hardens over 20–30 min and converts to HA in 4 hr. Eventually replaced by new bone	Note: no human studies yet. Future applications: nonunions, bone defects, and revision implant surgery	
3. Transforming Growth Factor-β1 (TGF-β1)	Osteoinductive protein	Awaiting FDA approval on its effects on bone tissue growth and regeneration			
4. OP-1	Morphogenic protein	Currently in clinical trials	Stimulates bone formation by causing precursor stem cells to differentiate into bone-forming cells		
5. BMP-2	Bone growth protein	Human clinical trials	Induces bone growth & repair when mixed with carrier and implanted into fracture site		Trauma, AVN, boneless from tumor, & spinal reconstruction

12.2.4b. Calcium Sulfate

Calcium sulfate has many solid states (see Chapter 11). These materials are fast dissolving, even when in the form of a nonporous block. Recent clinical trials have met with mixed success. Calcium sulfate was tried as a bone defect-filling material by one investigator [122]. Though commercialized in Europe, this material is not widely accepted in the United States due to lack of favorable clinical results. A recent prospective randomized double-blind trial [98] showed no effect of calcium sulfate (Osteoset®, a bone graft substitute) on bone healing in humans. Another study [124] reported on bone healing in a tibial defect in humans. Twenty patients underwent anterior cruciate ligament (ACL) reconstruction with a bone–patellar tendon–graft and were randomized into two groups. The tibial defect in the treatment group was filled manually with calcium sulfate pellets, while it was left empty in the control subjects. Series of CTs were taken on the first day after the operation and at 6 weeks and 3 and 6 months postoperatively. The investigators found about the same amount of bone in the defect in the calcium sulfate and control groups after 6 weeks and 3 and 6 months. Bone volume increased at 6 weeks and 3 months in the control group, while there was no change in the experimental group. Calcium sulfate pellets were almost completely resorbed after 6 weeks. These results are somewhat contradictory to those of an earlier report [122], where the materials may have been better refined.

Example 12.7

Calculate the amount of dissolved surface layer of a plasma spray-coated implant surface during 1 year if the ACP/HA ratio is 1/2. Use Figure 9.12, and state the rationale for your calculations.

Answer:

Assume the ACP dissolves 100 times faster than the HA, according to Figure 9.12, and that the dissolution of each phase is independent. The dissolution rate would then be (100 + 1)/2 = 50.5 ppm/min.

1 ppm is 1 mg/1000 g; therefore,

$$\frac{50.5 \text{ mg} \times 5.256 \times 10^5 \text{ min/yr}}{1000 \text{ g}} = 26.5 \text{ g/g} \cdot \text{yr}.$$

This shows that the material will disappear well within the year. A simple calculation shows that the material will disappear after 191,000 minutes, or 13.75 days!

12.2.4c. Glass-Ceramics

As discussed in Chapter 8, these materials are made into glass first by thermal quenching and crystallized into ceramic by subsequent heat treatment. Grain size is limited to increase strength. More important, the seeding material is phosphorous pentoxide (P_2O_5), which is combined with CaO, resulting in calcium phosphate crystals among the CaO–Na_2O–SiO_2–P_2O_5 matrix. Tables 12.9 and 12.10 illustrate the reaction stages

Table 12.9. Five Stages for Surface Crystallization of Glass-Ceramics Leading to Hydroxyapatite-Like Layer

1. Leaching and formation of silanols (SiOH)
2. Loss of soluble silica and formation of silanols
3. Polycondensation of silanols to form a hydrated silica gel
4. Formation of an amorphous calcium phosphate layer
5. Crystallization of a hydroxycarbonate apatite layer

Reprinted with permission from [59]. Copyright © 1993, World Scientific.

Table 12.10. More Detailed Stages of Table 12.9

1. Rapid exchange of Na^+ or K^+ with H^+ or H_3O^+ from solution:

   $$\text{Si–O–Na}^+ + \text{H}^+ + \text{OH}^- \Rightarrow \text{Si–OH} + \text{Na (solution)} + \text{OH}^-$$

   This stage is usually controlled by diffusion and exhibits a $t^{-1/2}$ dependence.

2. Loss of soluble silica in the form of $Si(OH)_4$ to the solution, resulting from breaking of Si–O–Si bonds and formation of Si–OH (silanols) at the glass solution interface:

   $$\text{Si–O–Si} + \text{H}_2\text{O} \Rightarrow \text{Si–OH} + \text{OH–Si}$$

   This stage is usually controlled by interfacial reaction and exhibits a $t^{1.0}$ dependence.

3. Condensation and repolymerlzation of an SiO_2-rich layer on the surface depleted in alkalis and alkaline-earth cations:

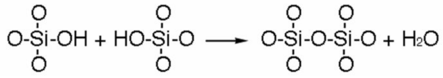

$$\text{O-}\underset{\text{O}}{\overset{\text{O}}{\text{Si}}}\text{-OH} + \text{HO-}\underset{\text{O}}{\overset{\text{O}}{\text{Si}}}\text{-O} \longrightarrow \text{O-}\underset{\text{O}}{\overset{\text{O}}{\text{Si}}}\text{-O-}\underset{\text{O}}{\overset{\text{O}}{\text{Si}}}\text{-O} + \text{H}_2\text{O}$$

4. Migration of Ca^{2+} and PO_4^{3-} groups to the surface through the SiO_2-rich layer forming a $CaO–P_2O_5$-rich film on top of the SiO_2-rich layer, followed by growth of an amorphous $CaO–P_2O_5$-rich film by incorporation of soluble calcium and phosphates from solution.

5. Crystallization of amorphous $CaO–P_2O_5$ film by incorporation of OH^-, CO_3^{2-}, or F^- anions from solution to form a mixed hydroxyl, carbonate, fluorapatite layer.

Reprinted with permission from [59]. Copyright © 1993, World Scientific.

of the glass-ceramic. Upon contact with water or tissue along with hydroxyl (OH^-), carbonate (CO_3^{2-}), or fluoride (F^-) ions, the implant reacts with the calcium and phosphate oxide to form an HA-like structure. The newly formed structure shows chemical bonding between the glass-ceramic and tissues, both soft and hard. Tissue bonding takes place through collagen molecules. Many animal and human clinical trials are summarized in [59]. A commercial product (Bioglass®) has received FDA approval and is being used for grafting of facial bones, to replace bones in the middle ear, and in repairing periodontal defects.

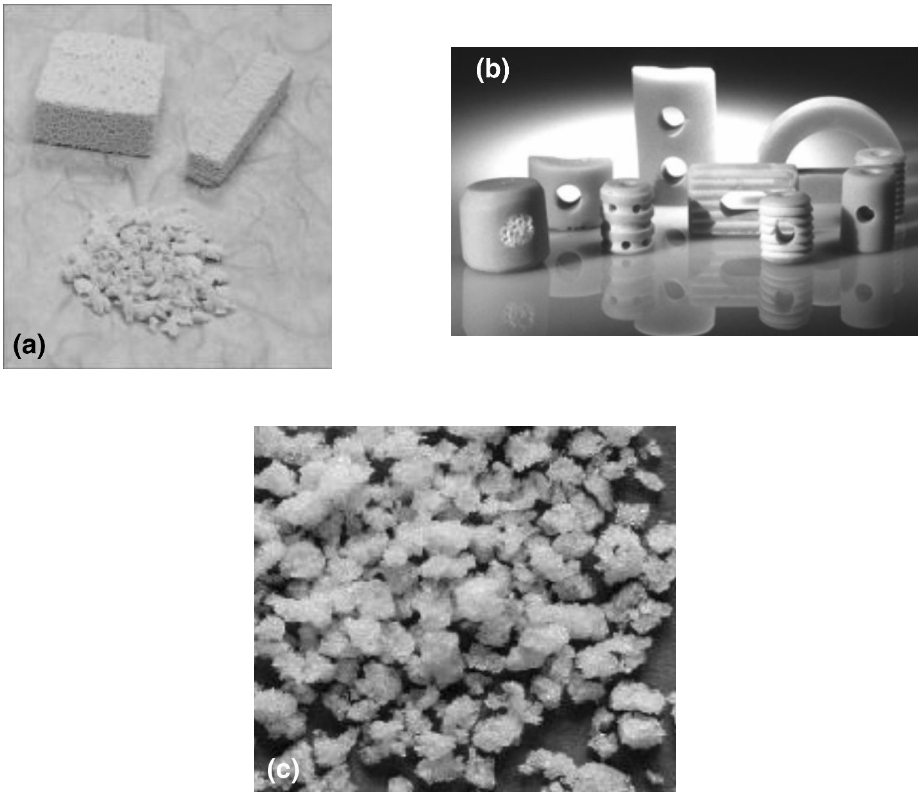

Figure 12.21. Examples of bone graft substitutes. (a) Interpore® (Cross International Inc.) is produced from hydroxyapatite in either particulate or block form by chemically treating sea coral. The product is known as ProOsteon®. Image courtesy of Interpore Cross International Inc. (b) Polymer-based bone graft substitutes include both particulate and solid forms such as Cortoss® and Rhakoss®, both produced by Orthovita Inc. (c) Degradable polymers allow for complete healing because the matrix is completely resorbed by the body. Osteobiologics Inc. has produced Immix Extenders®, a particulate polymer used as a bone graft extender. Reprinted with permission from [97]. Copyright © 2005, WebMD. http://www.emedicine.com/orthoped/topic611.htm.

Figure 12.21 depicts some commercially available bone graft substitutes. As mentioned, these can be made into particulates, porous or nonporous blocks, or injectable paste. The injectable forms are usually made in two pieces to prevent reaction or setting during storage.

It is quite natural to employ ceramics and polymers resembling HA (a calcium phosphate compound) along with proteins and polysaccharides to construct composites. These substitutes can play important roles, like filling the voids in diseased or missing bone segments and transferring loads gradually up to full capacity after healing. Many studies have demonstrated the usefulness of bone graft materials in different forms to accelerate bone regeneration [4,11,21,26,27,49,50,52,55,62,71,95,96,100,123,128,140,148]. Calcium phosphate/polymer composites have also been demonstrated to be useful in tissue engineering (see §12.4) [8,12,30,39,48,55,81,89,90, 111,125,126,142,147]. It is also noteworthy that a surface-treated (oxidized) metal (e.g., titanium and its alloys) exhibits behavior similar to that of a ceramic when its coating is on the order of a micrometer [54]. All metal implants are oxidized (passivated) in order to prevent further corrosion [120].

12.2.5. Soft Tissue Substitutes and Augmentation

Ceramics have not been considered as soft tissue replacements due to their brittleness. However, ceramics can be utilized effectively in some such applications, as can be seen in heart valve replacement with the pyrolytic carbon-coated graphite discs in a Jarvik heart (see Fig. 12.22a,b). Pyrolytic carbon is deposited by a fluidized bed for low-temperature isotropic (LTI) carbon (as discussed in §10.3). Silicon oxide (SiO_2) is codeposited (alloyed) to increase strength and wear resistance by up to 20%. Ultra-low-temperature isotropic (ULTI) pyrolytic carbon depositions onto an arterial graft surface to increase hemocompatibility are also possible. The CVD (chemical vapor deposition) technique has also been used for ULTI carbon deposition.

One group of investigators [61] created artificial blood vessels with a morphology similar to that of a living organism. Sea urchin tentacles were made into a blood vessel template, about 5 mm in diameter with a wall thickness of 1 mm. The tubes were then invested with silicone rubber resin plus a curing agent under high pressure and temperature. After curing, the original calcium phosphate matrix was dissolved with acids. The remaining replamineform porous tube was used to replace the artery. Animal experimentation yielded some success, but clinical trials have never been carried out.

Carbon (graphite) fiber and polytetrafluoroethylene (PTFE, better known as Teflon®) composites were used to make a porous composite called Proplast®. The pore size was about 10 μm. The composite can be cut at the operating table. It was acceptable as a soft tissue replacement (e.g., cartilage) but did not perform well in TMJ (temporomandibular joint) applications [68]. A porous laminated alumina/PTFE composite was also tried along with a graphite composite [68,151]. It would be interesting to use calcium phosphate nanoparticles along with a resorbable polymer (e.g., PLGA/PGA, collagen) for soft tissue replacement or augmentation. Artificial skin made of a porous collagen–mucopolysaccharide (MPS)–silastic rubber composite has been developed [154]. This is a prime candidate for incorporation of HA nanoparticles. HA nanocrystals could also be used as an adjunctive material in skin replacement (see Problem 9.3). A calcium phosphate compound (mostly HA) would have a much better biocompatibility with skin, as demonstrated in the percutaneous implants shown in Figure 12.23. The properties of carbon fiber-reinforced UHMWPE are given in Table 12.11 [136].

12.3. COMPOSITE SCAFFOLDS

Scaffolds are necessary when growing cells in vitro and in vivo for tissue engineering [64,92,107,132]. They are made of resorbable (bioabsorbable or degradable) polymers

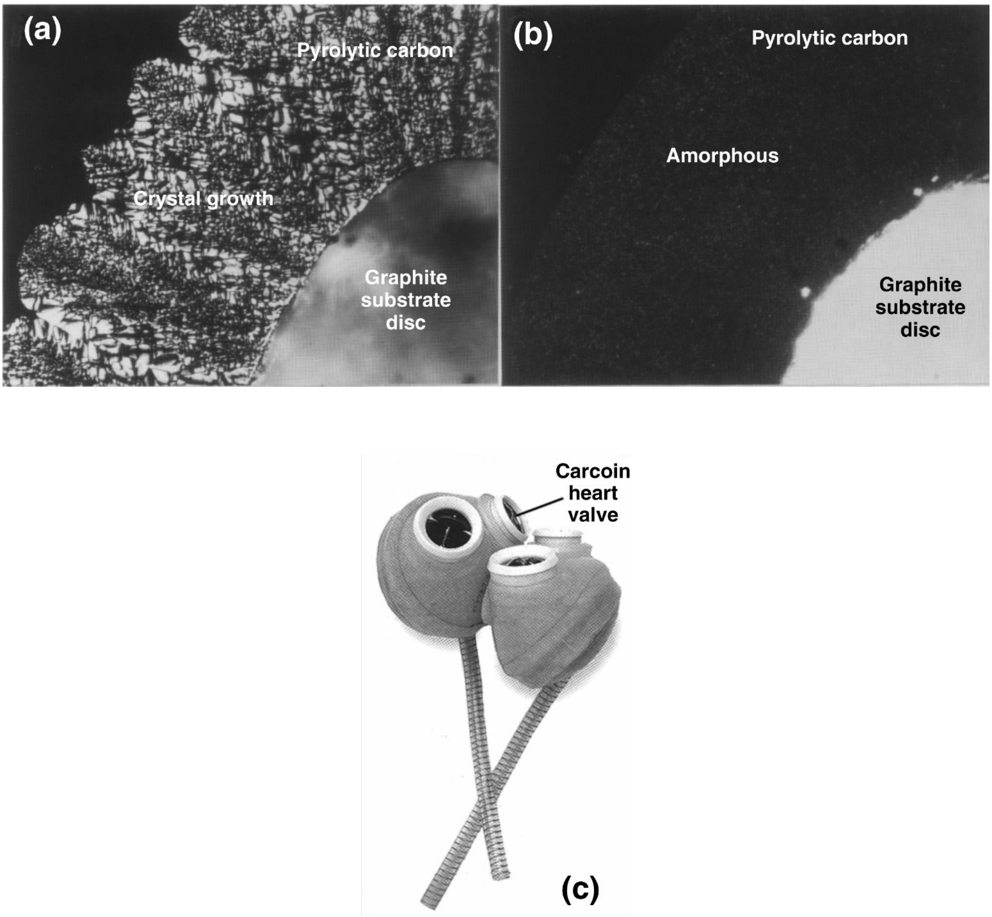

Figure 12.22. Microstructures of carbons deposited in a fluidized bed. (a) Granular carbon with distinct growth features. (b) Isotropic carbon without growth features. Both under polarized light, 240×. Reprinted with permission from [16]. Copyright 1972, Marcel Dekker. (c) Artificial heart, Robert K. Jarvik, 1982, from illustration. Modified from the Smithsonian Visual Timeline of Inventions, National Museum of American History, p. 60, Smithsonian Institute, 1994.

and their composites with ceramics (mostly HA). The scaffolds should have characteristics similar to those of cancellous bone (see Fig. 12.14): (1), they should have pores and interconnecting passageways; (2) the size of pores should be large enough to accommodate cells (osteons); (3) degradation products should not have any harmful effects on cell function and the cellular environment; and (4) the rate of degradation should match the rate of cell regeneration both in vitro and in vivo. Table 12.12 lists applications of scaffolds in tissue engineering; Table 12.13 gives examples of matrices, cells, and regulators employed in tissue engineering; and Table 12.14 presents the structural factors related to control of polymer biodegradation. The degradability of such ceramics as calcium phosphate compounds in conjunction with biodegradable

Table 12.11. Properties of Carbon Reinforced UHMWPE

Fiber amount (%)	Density (g/cm^3)	Young's modulus (GPa)	Flexural strength (MPa)
0	0.94	0.71	14
10	0.99	1.01	20
15	1.00	1.4	23
20	1.03	1.5	25

Reprinted with permission from [136]. Copyright © 1973, Wiley.

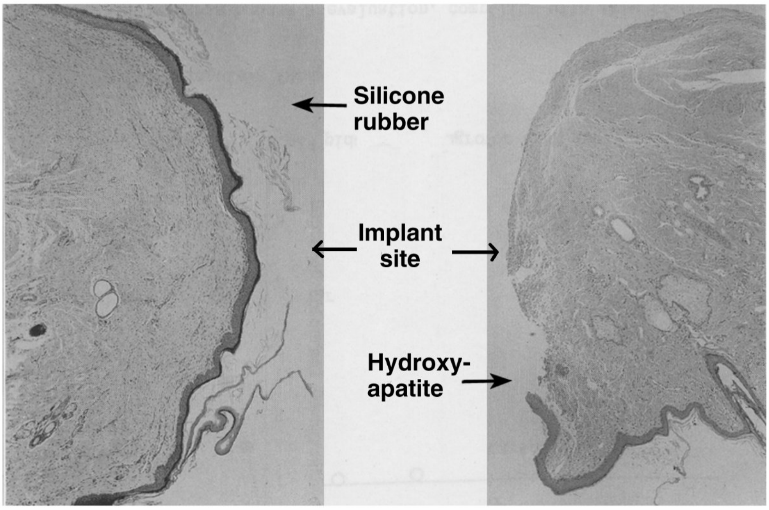

Figure 12.23. Histological view of canine dermal tissues adjacent to a percutaneous device made of hydroxyapatite and silicone rubber 3 months after implantation. Note the little epidermal layer downgrowth in the HA implant, indicating more a favorable tissue reaction (100× magnification). Reprinted with permission from [6]. Copyright © 1987, Kluwer Academic.

polymers is not well known. A better understanding of the mode, kinetics, and dynamics of the biodegradation of ceramic–polymer composites with respect to pore size and size distribution would make manufacture of better scaffolds possible. The byproducts of degradation should be studied carefully, since they may affect cell function. Readers are encouraged to refer to the chapter on tissue engineering of bone in [74]. Alvis and colleagues [5] have reported osteoinduction by a collagen mineral composite combined with autologous bone marrow in a subcutaneous rat model. Another group induced heterotopic osteogenesis in porous ceramics by marrow cells [115]. In addition, as mentioned earlier, HA has been widely used for bone regeneration [51,66,67,116,128,144,156].

Table 12.12. Some Applications of Tissue Engineering

Applications	Examples
Cell production	Bone marrow cell production in vitro
Extra corporeal devices	Artificial liver
Tissue growth and repair in situ	Nerve regeneration Artificial skin Bone and cartilage Blood vessel
Implantable devices	Endotherialized vascular graft Bone and cartilage implants Artificial pancreatic islets Skin regeneration template

Adapted with permission from [46]. Copyright © 1991, Butterworth-Heinemann in Association with the Biological Engineering Society.

The ratio between the characteristic time constant for biodegradation of an implant substrate at tissue site (t_b) and the time constant for healing by synthesis of new tissue inside the implant (t_h) is denoted as

$$O(1) = \frac{t_b}{t_h}. \tag{12.6}$$

If the ratio is close to one, the substrate material may serve its purpose properly. Another important aspect of substrate materials is the depth at which cells can receive adequate nutrition by diffusion. This can be quantified in terms of the critical path length, l_c, beyond which cell migrations away from a source of nutrition cannot take place. This calculation can be done with the aid of a cell lifeline number, S, which is a dimensionless quantity. S expresses the relative importance of reactions that consume nutrients and diffusion of nutrients. The diffusion length, l, is the distance over which nutrients diffuse in the tissue, and the rate of consumption of nutrients is r (moles/cm^3/s), the diffusivity of nutrient in the medium of implant is D (moles/cm^2/s), and the nutrient concentration at or near the surface of the implant is c_0 (moles/cm^3):

$$S = \frac{rl^2}{Dc_0}. \tag{12.7}$$

When S is on the order of 1, l is approximately l_c. Under these conditions cells can migrate from host tissue into the implanted template without a nutrient concentration greater than that supplied by diffusion. Therefore, Eq. (12.7) can be used to calculate the thickness (for half-maximum concentration of nutrient) of the implant beyond which cells require the presence of capillaries for adequate nutrient transport. Although these equations were developed to apply for skin regeneration templates, similar analysis can be made for other examples of cell migration and growth template development (e.g., nerve and knee meniscus) [92].

Table 12.13. Examples of Matrices, Cells, and Regulators Employed in Tissue Engineering

---

A. Matrices (porous structures)
  a. Absorbable
    1. Natural polymers
      Collagen (types I, II, III, IV)
      Collagen–glycosaminoglycan copolymer
      Fibrin
      Poly(hydroxybutylate), PHB
      Poly(hydroxyvaleric acid), PHV
      Sodium alginate
      Chitin and chitosan
    2. Synthetic polymers
      Polylactic acid
      Polyglycolic acid
      Poly(ε-caprolactone)
      Ployanhydrides
      Poly(ortho esters)
    3. Composites
      Bone particles/natural or synthetic polymers
    4. Natural mineral
      Anorganic bone (human and bovine)
      Reprocessed whole bone
      Anorganic mineral
      Hydroxyapatite*
  b. Nonresorbable
    1. Synthetic polymer
      Polytetrafluoroethylene
    2. Synthetic ceramics
      Hydroxyapatite (synthetic or natural)
      Calcium phosphate (mono-, di-, tri-, and tetra CaP)
      Glass-ceramic (Bioglass®)
      Calcium sulfate (plaster of Paris)
B. Cells
  a. Autologous parenchymal cells
  b. Allogeneic parenchymal cells
  c. Marrow stromal stem cells
C. Soluble Regulators
  a. Growth factors (polypeptide mitogens)
  b. Differentiation factors (e.g., bone morphogenetic protein)

Modified with permission from [139]. Copyright © 1999, Quintessence Publishing.

There are three basic mechanisms of biopolymer chemical degradation, as shown in Figure 12.24. All mechanisms involve conversion of water-insoluble constituents to a water-soluble state by cleavage of crosslinks between water-soluble polymer chains

Table 12.14. Structural Factors that Control Polymer Biodegradability

Factors		Control
Molecular structure		Chemical main chain bonds, side and functional groups,
Crystalline/aggregate state		Polymer blend, processing, copolymerization
Bulk state		Fiber, film, composite
Surface state	Area	Pore size, porosity, pore size distribution
	Hydrophilic/hydrophobic balance	Copolymerization, introduction of functional groups

Adapted with permission from [46]. Copyright © 1991, Butterworth-Heinemann in Association with the Biological Engineering Society.

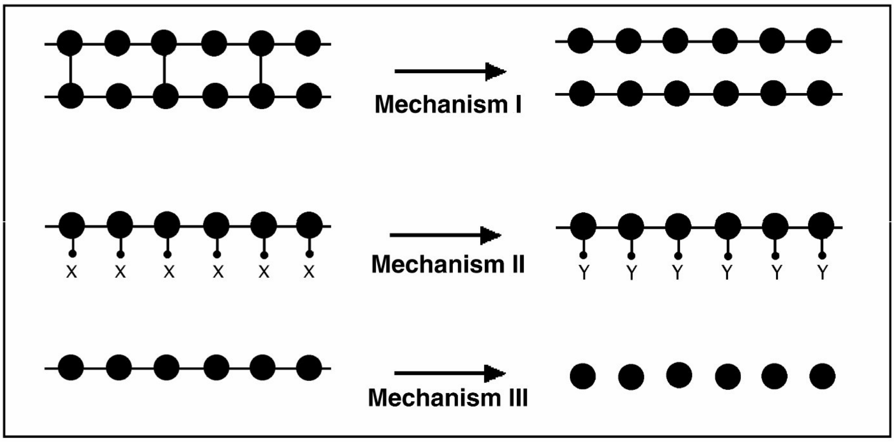

Figure 12.24. Mechanism of chemical degradation of polymers. Reprinted with permission from [83]. Copyright © 1996, Academic Press.

(mechanism I), transformation or cleavage of side groups leading to formation of polar or charged side groups (mechanism II), and cleavage of backbone chain linkages among repeating units.

Physical degradation of polymers involves surface or bulk processes and sometimes a combination of the two. Bulk degradation results from the fact that the rate of water uptake is faster than the rate of conversion of polymer into water-soluble material. Since bulk degradation takes place throughout the volume of the material, final collapse of the material can occur abruptly. Hydrophilic polymers often exhibit this behavior. Hydrophobic polymers may degrade the surface, first leaving the inner structure intact (see Fig. 12.25). It is easier to control rate of degradation in surface-degrading polymers. More detailed discussion of the types of polymers used for tissue engineering are available in the literature [83,120].

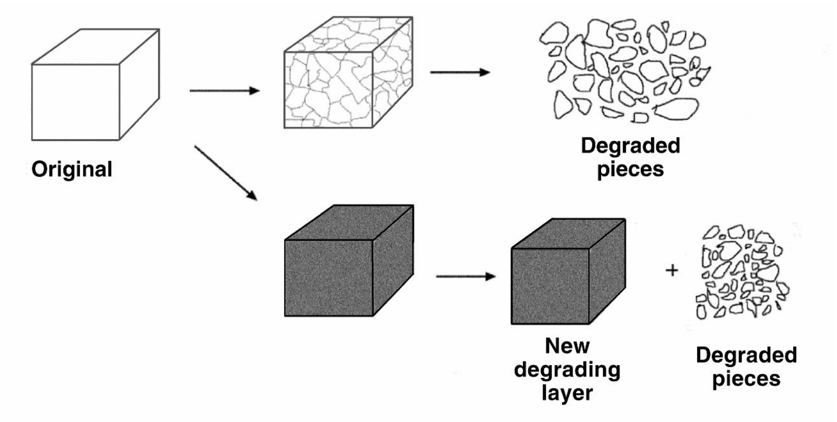
Original
Degraded pieces
+
New degrading layer
Degraded pieces

Figure 12.25. Schematic representation of two types of polymer degradation: bulk(top) and surface (bottom).

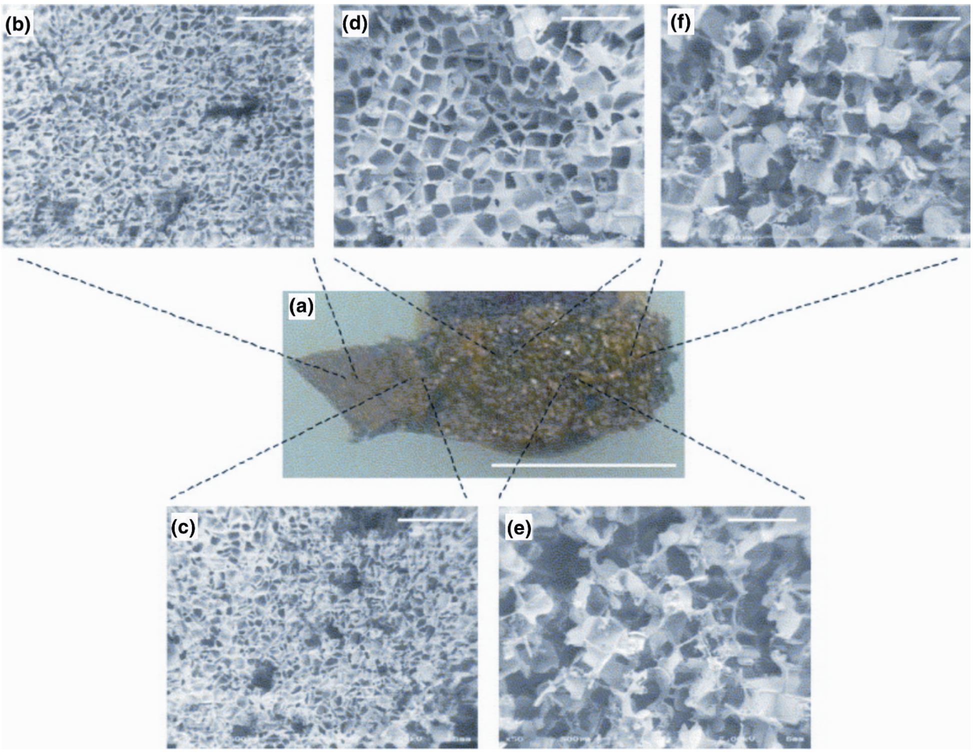

Figure 12.26. Pore size gradient across a sponge made of silk fibroin. Pore sizes are (b) 76.3 ± 16.2 μm, (c) 100.7 ± 18.2, (d) 182.0 ± 30.0, (3) 221.3 ± 40.6, (f) 260.3 ± 75.9. Bar lengths are 10 (a) and 0.5 mm (b–f). Reprinted with permission from [76]. Copyright © 2005, Butterworth-Heinemann. Please refer to the color section to view Figure 12.26a in full color.

Natural polymers like collagen are subject to enzymatic degradation. Collagen has some drawbacks as an implantable material. The structure and properties of such natural materials collagen are species- and tissue-specific, making it difficult to obtain uniform raw materials (see Fig. 12.26). As for synthetic materials, since immunogenic activities often remain even after extensive processing, it can be difficult to adequately process them to the point of obtaining raw materials with uniform properties. Methods of processing include melt extrusion, which requires elevated temperatures. Some biocompatible polymers are structurally sensitive to such elevated temperatures. By contrast, synthetic polymers such as polyglycolic acids have opposite characteristics. Their main drawback is that their degrading products are not as compatible as those of natural polymers, though there are some exceptions.

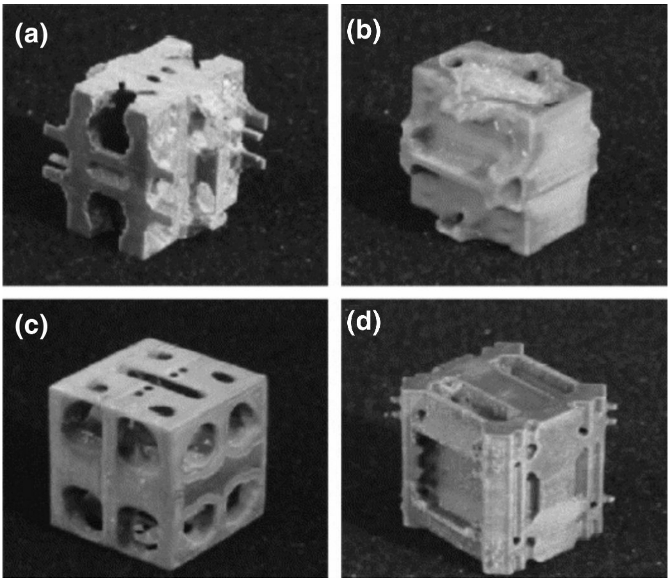

Figure 12.27. Prototypes fabricated using 3D Ink Jet Printing with different porosities [(a) 61%, (b) 49%, (c) 48%, (d) 35%], which match the porosities found in a small pig [a commonly used temporomandibular joint (TMJ) reconstruction animal model]. Size 20 × 20 × 20 mm. Reprinted with permission from [105]. Copyright © 2004, Elsevier Science.

12.4. FABRICATION OF BONE SCAFFOLDS

There are many conventional methods of fabricating bone scaffolds (see Table 12.15). The limitations of conventional techniques include labor intensiveness, time consumption, and poor reproducibility of manual processes. Additionally, inadequate porosity, low interconnectivity, and removal of solvent can result in residual toxicity or a thin scaffold wall. One newer technique of fabricating scaffolds are based largely on computer-assisted solid freeform fabrication (SFF). Other new methods are being investi-

Table 12.15. Conventional Methods of Fabricating Bone Scaffolds

Methods	Technique	Typical results	References
Solution casting	PLGA + chloroform, then adding methanol.	Porosity depends on the amount of dissolving chemical.	[134]
Solvent-casting particulate-leaching	Add salt particles in a solution to produce a uniform suspension. After the solvent evaporates, the composite is immersed in water to dissolve salt out, and produce porous structure.	Porosity depends on size of salt and its distribution.	[112]
Gas foaming	Saturated with CO_2 at high pressure, then gas solubility is decreased rapidly. Nucleation and growth of CO_2 bubbles.	100–500 μm pore size; only 10–30% interconnected pores.	[113]
Fiber-mesh/ fiber-bonding	Fiber meshes are embedded in HA, then leach or burn completely.	Woven 3D patterns: highly interconnected pores. Large surface area for cell attachment and rapid diffusion of nutrient. Difficult to control porosity.	[40]
Melt molding	Fill a mold with powder and microspheres; heat above T_g with pressure; particles are sintered together. Microspheres leached out by water immersion. Short HA fibers are incorporated.	Pore size depends on gelatin microspheres.	[145]
Emulsion freeze drying	Add water to a solution; form a water-in-oil emulsion. Quench in liquid N_2 and freeze-dry.	Porosity depends on water phase in emulsion.	[152]
Freeze drying	Dissolve in acetic acid or benzene. Freeze & freeze-dry.	Porosity depends on dispersion of frozen water.	[155]

Reprinted with permission from [131]. Copyright © 2003, European Cells & Materials.

gated, including three-dimensional printing (3DP), stereolithography (SLA), fused-deposition modeling (FDM), and 3D plotting (3DP) [131]. Some typical architectures are shown in Figure 12.27. Table 12.16 lists the ceramic–polymer composites used in bone scaffolds, and Table 12.17 presents ceramic-based scaffolds. The search for better scaffolds continues [1,82,110].

Common to all scaffolds, the effect of degradation products can be significant. The byproducts can be acids in the case of PLA or PLGA, which can significantly lower the pH of the medium. Degradation also decreases the strength of a scaffold, which may impose unfavorable stress on cells and tissues and inhibit proliferation.

Table 12.16. Ceramic–Polymer Composites for Bone Scaffolds

Materials	Methods	Pore size (μm)	Porosity (%)	References
HA/poly(ε-caprolactone)	S	150–200	87	[80]
HA/chitosan/gelatin	FD	300–500	–	[161]
HA/chitosan/β–TCP	S	300–600		[160]
HA/collagen	FD	30–100	85	[104]
	FD	30–300	49, 73, 79	[104]
β-TCP/PLA	LS	125–150	80, 87.5	[70]
β-TCP/PPF	LS	150–300	69, 74	[153]
BG/PLA	PS	50–200		[159]
Silica/ceramic	S	100–300	51, 47, 43	[45]
HA/PLGA/collagen	LS	355–425	87	[33]

HA = Hydroxyapatite; β-TCP = β-tricalcium phosphate; BG = Bioglass® glass-ceramic; PLA = poly(L-lactide); PLGA = poly(lactide-co-glycolide); S = sintering; FD = freeze dry; LS = leaching salt, PS = phase separation.
Adapted in part from [131].

Table 12.17. Ceramic-Based Scaffolds

Material	Shape	Pore size (μm)	Porosity (%)	Reference
HA	Sc/honeycomb pores	90–120, 350		[72,86,87]
	Sc	366, 444	38,44	[38]
	Sc	400, 800	60,70	[85]
	Bl	500	77	[43]
	Cy	400–600	80	[42]
	Pt	150, 230	66	[88]
	R	200, 400		[157]
TCP*	Pl	0.2, 8.7	31, 62	[10]
CMP	Bl	200		[99]
Coral	HMC	150–200	36	[32]
HA/TCP	Bl	100–150	36	[158]

All are sintered except (*) noted.
HA: Hydroxyapatite, TCP: Tricalcium phosphate, CMP: Calcium metaphosphate,
Sc: Scaffolds, Bl: Block, Cy: Cylinder, Pt: Particle, Pl: Pellet, R: Rod, HMC: Human mandibular condyle
Adapted in part from [76].

Some have addressed these concerns and are beginning to obtain preliminary results [34,77]. In addition, a better understanding of scaffold properties and structure using three-dimensional techniques can result in a better-designed scaffold [82]. More important, finding the optimal condition for cell–materials (scaffolds) interactions in terms of the surface, chemical, mechanical, and electrical properties may also accelerate development of better scaffolds [57].

Example 12.8

Calculate the percentage increase in surface areas if one changes microparticles (average 100-μm diameter) to nanoparticles (average diameter, 100 nm).

Answer:

The surface of a sphere, $A_S = 4\pi r^2$.

The volume of a sphere, $V_S = \frac{4\pi r^3}{3}$.

$$\frac{A_S}{V_S} = \frac{1}{r}.$$

The ratio of total change in surface area to volume (where *n* stands for nano and *m* for microsphere) is

$$\frac{A_{s,n} - A_{s,m}}{A_{s,m}} = \frac{r_n^{-1} - r_m^{-1}}{r_m^{-1}} = \frac{r_m - r_n}{r_n} = \frac{100\times10^{-6} - 100x10^{-9}}{100\times10^{-9}}$$

= 999 or a 99900% increase.

This 999-fold increase in surface area makes nanoparticles behave differently from microspheres. The surface energy also increases 999-fold. Indeed, a magnesium flashlight can be generated by making powders that oxidize spontaneously. Many of these nanoparticles have to be stored in an inert atmosphere or vacuum.

12.5. BIOCOMPATIBILITY OF COMPOSITE BIOMATERIALS

Each constituent of a composite must be biocompatible, and the interface between constituents must not be degraded by the body environment. As for inclusion materials, carbon itself has good compatibility and has been used successfully. Carbon fibers used in composites are known to be inert in aqueous and even seawater environments; however, they do not have a long track record as biomaterials. Substantial electrochemical activity occurs in carbon fiber composites in an aqueous environment [84]. Therefore, there is concern that composites, if placed near a metallic implant, may cause galvanic corrosion. Inclusions in dental composites are made of minerals and ceramics that have a good record of compatibility. As for the matrix material, polymers tend to absorb water when placed in a hydrated environment. Water acts as a *plasticizer* of the matrix and shifts the glass transition temperature toward lower values. This causes a reduction in stiffness and an increase in mechanical damping. Water absorption also causes swelling in polymers; this can be beneficial in dental composites since it neutralizes some of the shrinkage caused by polymerization.

The biocompatibility of the polymers (collagen, PLGA) used in tissue engineering is quite good. However, there are some concerns about PLGA, mainly due to the fact that its degradation products are acids. In the case of collagen these are natural acids, but in PLGA they are not. If the amount of acids is minute and they can be removed by the body, they are not a concern. When one attempts to use them in large quantities, as in scaffolds, this concern rises. We in fact do not know if acidity can be moderated in the PLGA/HA composites.

Many recent studies suggest the usefulness of calcium phosphates and their composites for making bone scaffolds [13,19,20,94,96,129]. However, fundamental studies — for instance, regarding the size of pores for bone ingrowth — need to be elucidated further [14,15,69,76,102,127,133].

12.6. FURTHER THOUGHTS

Nanotechnology can be utilized easily in the form of nanoceramics and glasses, which can then be made into composites [103]. This field is a work in progress. A basic understanding of cell/scaffold interactions is essential for producing better scaffolds. This does not mean we should stop developing new conventional or nanomaterials. It is hoped that a newer generation of researchers can elevate the science of bioceramics and tissue engineering to a new level.

PROBLEMS

12.1. A bone substitute (BS) is made of three natural materials — coral calcium phosphate (deorganized at high temperature), skin collagen, and MPS. The following chart gives some basic parameters of each material:

Material	Density (g/cm^3)	Wt%
Coral calcium phosphate	3	50
Skin collagen	1	30
MPS	1	10

Water (double distilled deionized) was added when making the BS.

a. Calculate the vol% of each constituent including ddd water.

b. Calculate the density of BS.

c. If a surgeon would like to use the patient's own blood to be mixed with materials instead of water, would you recommend such a practice? What would be the pros and cons?

d. Describe the course of BS paste degradation and resorption by the body.

12.2. One would like to make a porous solid BS bone substitute. A bioengineer adds hydrogen peroxide to the BS materials instead of water and pressed at high temperature to evaporate the peroxide. He finds that the weight the paste has changed from 100 g to 90 g with porosity. The density of the final "porous" product is 1 g/cm^3.

a. Calculate the porosity of the product.

b. Calculate the distance between pores. Assume a uniform interconnecting cylindrical pore (100-μm diam.) formed with the same diameter .

c. A mechanical test of the BS showed 20% of the compressive strength of cancellous bone (1.9 MPa). Assuming all the load is carried out by the mineral phase, calculate its porosity. The compressive strength of solid coral calcium phosphate is 50 MPa. Does this agree with (a)? **Hint**: $\sigma_f = \sigma_0 \exp(-np)$, $n = 4\text{~}7$.

12.3. Describe an ideal bone substitute in terms of material, bioabsorption rate, and degradation products.

12.4. Why is osseointegration so important in orthopedic and dental implants? Can you speculate about why such a phenomenon is widely accepted as a dental implant but not as an orthopedic implant?

12.5. Ti and Ti alloys can be passivated on a surface, making a surface oxide, which will prevent further corrosion of metal. Similarly, aluminum will form an oxide layer, Al_2O_3. Explain why we can use Ti and Ti alloy in implants but not Al and its alloys?

12.6. Bone cement contains barium sulfate as its radiopacifying material. $BaSiO_4$ (density, 4.5 g/cm^3) is mixed with acrylic polymer powder and a BPO (benzoyl peroxide) initiator to make a dough after adding monomer liquid (20 ml), and then inserted into the prepared cavity of a bone with an injection gun, Then a prosthesis is seated, and the "bone cement" acts as grout, as in tiles. Once the cement cures or sets, the prosthesis is mechanically fixed or secured. The strength of the bone cement is decreased by adding $BaSiO_4$ powder (10 g into 30 g of acrylic polymer powder) by 10%, contrary to the composite theory of increasing the strength of a matrix material (polymer) by adding a s-tronger ($BaSiO_4$) material.

a. Can you propose a method for minimizing this effect?

b. What would be the final density of the cement if it had 5% porosity.

c. Give some reasons for the porosity.

12.7. The precoating of a prosthesis with bone cement (without $BaSO_4$) is done to increase adhesion between the cement and prosthesis. Precoated and uncoated rods were implanted into the intramedullary cavity using bone cement. After curing, the interfacial strengths of the cement/prosthesis/bone were measured (see following illustration). The interfacial shear strength is summarized in the table below. [Reprinted with permission from Park JB, Malstrom CS, von Recum AF. 1978. Intramedullary fixation of implants pre-coated with bone cement: a preliminary study. *Biomater Med Devices Artif Organs* **6**(4):361–373. Copyright © 1978, Marcel Dekker.]

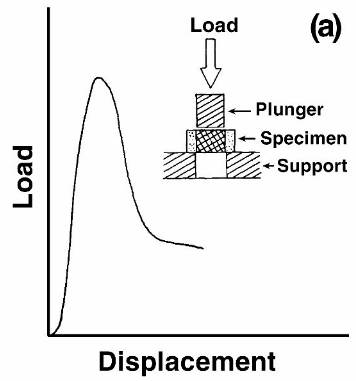
Load
(a)
Plunger
Specimen
Support
Load
Displacement

a. Push-out test arrangement and a tracing of typical load displacement curve.

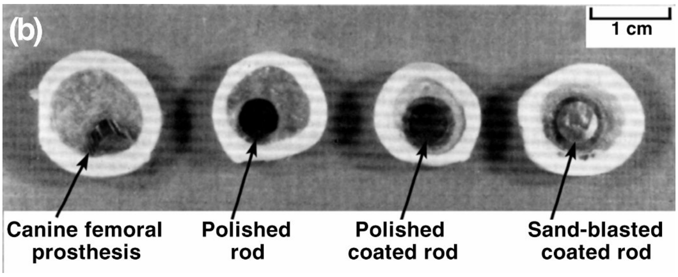
(b)
1 cm
Canine femoral prosthesis
Polished rod
Polished coated rod
Sand-blasted coated rod

b. Push-out test specimens seen cross-sectional view from left to right, canine femoral prosthesis, polished rod, polished rod coated and sand blasted rod coated. Note the darker shade of pre-coated cement layers around the rods.

Type of interface	Number of specimens	Maximum shear stress (MPa)
Bone/Cement	15	1.17 ± 0.69
Rod*/Cement	9	3.94 ± 0.78
Cement/Cement	3	23.40 ± 1.59

* Both polished and sand blasted rods are included.

a. The interfacial strength is substantially lower for the bone/cement interface than for the cement/cement interface. Why? Calculate the tensile strength of the bone cement assuming that its shear strength is the same as that at the cement/cement interface. Compare with a bone cement strength one half that solid acrylic polymer (70 MPa).
b. The shear strength between cement and an implant rod depends on surface preparation. Tests show an order of magnitude difference. Esti-

mate the surface area change after sand blasting compared to that of a polished surface.

c. Why is "autocentering of a prosthesis" important? This can be achieved by precoating?

d. Would it be better to precoat a prosthesis after precoating with such a ceramic as alumina?

e. Suggest one method of improving the prosthesis/bone cement interfacial strength.

f. Give the pros and cons of precoating prostheses.

12.8. Consider a bone plate made of a unidirectional fibrous composite, given the properties listed in the table for Problem 12.1.

a. Determine Young's modulus in the longitudinal (fiber) direction, and then in the horizontal direction. Assume 50 vol% fibers. Compare with a 316L stainless steel implant.

b. Determine the strength of the composites in both directions.

Material	Young's modulus (GPa)	Strength (GPa)
Carbon fiber (fiber direction)	≤500	≤5
PMMA	3	0.07
UHMWPE	2.2	0.25
Stainless steel (316L)	200	1 (cold-worked)

c. Compare the modulus of the composites with 316L stainless steel.

12.9. A bioengineer develops a dental composite using spherical particles of quartz and zirconia (ZrO_2). The polymer matrix is made of bis-GMA(4-hydroxyphenol), dimethylmethane, and glycidyl methacrylate. The ceramic particles have 10-μm diameter (average). Using the Properties given in the following table, answer.

Material	Young's modulus (GPa)	Density (g/cm^3)
Zirconia (ZrO_2), PSZ, cubic	210	6.1
Quartz (SiO_2)	72	2.64
Polymers	1	1

a. Determine the amount of each particles required (vol%) to make a dental composite with a modulus of 3 GPa. Use the equation given in Table 12.1.

b. Determine the wt% of each component in (a).

c. Determine the density of the composite.

d. Suggest other materials (ceramics, metals, cermets, etc.) that could be used as reinforcing material.

12.10. Calculate Young's modulus of collagen–HA composites with varying volume fractions of HA (0~100%). Plot modulus vs. percentage HA for each composite. We are trying to increase the modulus of the composite by making HA plates instead of particles. Calculate its modulus for 60% HA with the same polymer matrix.

12.11. Calculate the shear strength of dental composites with Young's moduli of 10~16 GPa. Use the relation $E = 2G(1 + \nu)$. Discuss the validity of this equation in the context of this problem. The shear modulus (G) is given as 0.17~0.26 GPa, and $\nu = 0.24\sim0.30$.

12.12. A company manufactures knee prostheses based on oxidized zirconium, essentially making the metal with a surface similar to that of zirconia (ZrO_2). Its oxidized zirconium-based knee joint replacement has been recalled, particularly the "cementless" versions. Discuss the possible problems of cementless bony tissue ingrowth fixation. Give the pros and cons of cemented fixation.

12.13. A zirconium wire 2 mm in diameter is oxidized, and the oxidized layer has a thickness of 0.1 μm. Using the following data, answer the questions.

Material	Young's modulus (GPa)	Yield strength (MPa)	Density (g/cm^3)
Zr	200	400	6.49
ZrO_2	210	–	6.0

a. What is Young's modulus of the oxidized wire in the wire direction?
b. If the wire is loaded in the longitudinal direction, what will be its yield strength?
c. How much load can the wire carry in tension without plastic deformation?
d. What is the density of the wire?

12.14. Pores are important for cells to enter and grow as well as for capillary suction of tissue fluid and blood. They also provide a very large surface area for invading cells or for interaction with the cells in place. Calculate the surface area of a collagen sponge made of spherical pores (average 50-μm diameter). How many pores are adjacent to each other in 1 cm^3.

12.15. Fifteen milligrams of PLGA is degraded in a 15-ml flask, to which is added 15 mg of phosphate buffer. The pH is monitored over time, and the results are shown in the following illustration (courtesy of Dr. J.W. Lee, University of Iowa):

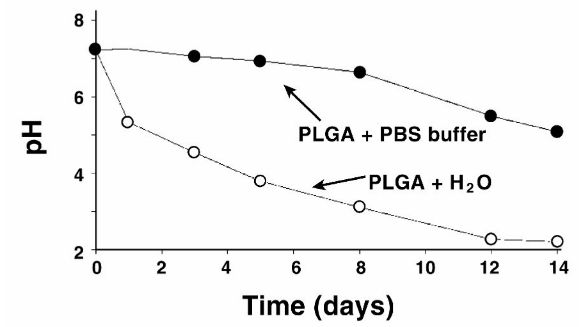

a. Calculate the concentration of acid if the pH drops from 7.0 to 2.5 for a control specimen without buffer.
b. Calculate the amount of buffer in milligrams needed to neutralize 1 mg of PLGA.
c. Propose a mechanism for how the acids are neutralized.

12.16. Investigators would like to use nanotechnology for making scaffolds.
a. Define nanotechnology.
b. Discuss what if means to make nanomaterials from the scaffold materials listed in Table 12.12.
c. Discuss the advantages and disadvantages of making nanomaterials for application in scaffolds for tissue engineering.

12.17. We would like to use nanotechnology in drug delivery.
a. Discuss the difference between conventional drug delivery by incorporating drugs into excipients and making different-sized microspheres (MSs) that release drugs at different rates dependent on surface area and surface energy.
b. Discuss the advantages and disadvantages of making nanospheres (NSs) in drug delivery.

SYMBOLS/DEFINITIONS

Greek Letters

ε: Strain.

ρ: Density.

σ: Stress.

$\sigma_{f,s}$: Fracture strength of a solid,

Roman Letters

C_{ijkl}: Elastic modulus tensor.

c_0: Nutrient concentration at or near the surface of an implant (mol/cm^3).

D: Diffusivity of nutrient in the medium of an implant (moles/cm^2/s).

E: Young's modulus.

l: Diffusion path length.

l_c: Critical cell path length in porous scaffold or the depth of diffusion of cells.

$O(1)$: t_b/t_h ratio.

r: Rate of consumption of nutrient by cells (moles/cm^3/s).

S: Cell lifeline number.

t_b: Time constant for biodegradation of implant substrate at a tissue site.

t_h: Time constant for healing by synthesis of new tissue inside an implant.

V: Volume fraction of a constituent.

Definitions

ACP: Amorphous calcium phosphate.

Aldehyde: Any one of a group of organic chemical compounds having the radical CHO, derived from primary alcohols by oxidation, and yielding acids upon further oxidation. Formaldehyde is an aldehyde produced by oxidation of methanol, CH_3CHO.

Allogro® (Wright Medical Technologies): Demineralized bone matrix bone substitute.

Allomatrix® (Wright Medical Technologies Inc.): Combination of calcium sulfate and demineralized bone matrix (DBM) that forms an injectable paste or a formable putty.

Anisotropic: Dependent upon direction, referring to the material properties of composites.

AP: Apatite.

Autograft: A transplant from one part of the body to another.

Autologous: Derived from a person's own tissue.

Benzoin alkyl ether: Photochemical initiator for free radical polymerization reaction.

Benzoyl peroxide: An initiator of a free radical polymerization reaction.

BHT (butylated trioxytoluene, or 2,4,6-tri-tert-butylphenol): An initiator for free radical polymerization reaction.

Bioabsorbable (biodegradable): Capable of being absorbed or decomposed by bacteria or other living organisms.

Bioabsorption: Absorption by blood or tissue.

Biodegradation: Decomposition by bacterial or enzymatic action.

Bioglass®: Commercially available type of bioactive glass, composed of SiO_2, Na_2O, CaO, and P_2O_5. Professor Larry Hench developed Bioglass® during the late 1960s. He was challenged by a MASH army officer to develop a material to help regenerate bone, as many Vietnam veterans suffered from severe bone damage, to the point that most of them injured in this way lost their limbs.

bis-GMA: An additional reaction product of bis(4-hydroxyphenol), dimethylmethane, and glycidyl methacrylate.

Bone morphogenetic proteins (BMPs): Group of growth factors known for their ability to induce formation of bone and cartilage. Originally, seven such proteins were discovered. Six of them (BMP2–BMP7) belong to the TGF-β (transforming growth factor-β) superfamily of proteins. Several more BMPs have since been discovered. There are now 16 reported BMPs. Some are termed cartilage-derived morphogenetic proteins (CDMPs) and growth differentiation factors (GDFs). BMP1 has a novel protein structure.

Bone Source® (Stryker Inc.): Self-setting hydroxyapatite (HA) cement.

Ca/P ratio: Calcium phosphate compound ratio, an indicator of chemical composition. TCP, 1.5; HA, 1.67.

Chemical degradation: Erosion of materials by breakage of main bonds or crosslinks.

Chitin: A horny substance forming the hard outer covering of lobsters, crabs, beetles, crickets, and some fungi. Closely related to cellulose.

Chitosan: A derivative of chitin by N-deacetylation.

Closed cell: A type of cellular solid in which a cell wall isolates adjacent pores.

Collagen: Protein substance in the fibers of the connective tissues, bone, and cartilage of vertebrates. Boiling with water converts collagen to gelatin.

Collagen–glycosaminoglycan copolymer: Two natural polymers made into a copolymer, one a protein (collagen) and the other a polysaccharide, which yields good mechanical, chemical, and biological properties for such applications as scaffolding.

Collagraft® (Zimmer and Collagen Corporation): Mixture of porous beads composed of 60% HA and 40% tricalcium phosphate ceramic and fibrillar collagen. When mixed with autogenous bone marrow, it serves as an effective bone graft substitute.

Composite: Composite materials are those that contain two or more distinct constituent materials or phases.

Cortoss® (Orthovita Inc.): Polymer-based bone graft substitutes, including both particulate and solid forms. Also available as injectable paste.

Cubic: A type of anisotropic symmetry in which the unit cells are cube shaped. There are three independent elastic constants.

CVD (chemical vapor deposition): Chemical process used to produce high-purity, high-performance solid materials. The substrate is exposed to one or more volatile precursors, which react and/or decompose on the surface to produce the desired deposit. Silicon, SiO_2, carbon (fibers of various size, nanotubes, graphite, synthetic diamond), etc. can be deposited.

Dynagraft® (GenSci Regeneration Technologies Inc.): Mixture of demineralized bone matrix (DBM) and a reverse phase polymer and forms a solid matrix, putty, or injectable paste.

FGF-2 (fibroblast growth factor 2): Promotes acquisition of epidermal growth factor (EGF) precursor cells: identification of neural precursors responding to both EGF and FGF-2.

Fibrin: An insoluble protein formed from fibrinogen during the clotting of blood. It forms a fibrous mesh that impedes blood flow.

Fused deposition modeling (FDM): Type of rapid prototyping or rapid manufacturing (RP) technology developed by S. Scott Crump in the late 1980s and commercialized by Stratasys Inc. in 1990. Like most other RP processes (3D printing and stereolithography), FDM works on an "additive" principle by laying down material in layers.

Gelatin: Denatured collagen obtained by boiling bones and cartilage.

Glutaraldehyde ($C_5H_8O_2$): Chemical made from cyclohexene in an atmospheric reaction, and used to preserve and sterilize tissues.

Grafton® (Osteotech Inc.): Mixture of demineralized bone matrix with an inactive carrier that is rapidly cleared from the body.

HA: Hydroxyapatite.

Immix Extenders® (Osteobiologics Inc.): Biodegradable particulate polymer used as a bone graft extender.

Immunogenicity: The property of causing immunity (antigenicity) to a disease.

Inclusion: Embedded phase of a composite.

Isotropic: Independent of direction, referring to material properties.

LTI (low-temperature isotropic) carbon: Pyrolytic carbon deposited onto a graphite heart valve disc by fluidized bed at relatively low temperatures (a few hundred ºC), resulting in an amorphous isotropic carbon layer.

Matrix: The portion of the composite in which inclusions are embedded. The matrix is usually less stiff than the inclusions.

Mesenchymal stem cells (MSCs): Along with marrow stromal cells, these are multipotent stem cells that can differentiate into a variety of cell types: osteoblasts, chondrocytes, myocytes, adipocytes, neuronal cells, and, as recently described, into β-pancreatic islet cells. MSCs can be obtained from bone marrow. However, this term now encompasses multipotent cells derived from other tissues, such as adult muscle or the Wharton's jelly present in the umbilical cord.

MPS (mucopolysaccharide): Class of polysaccharide molecules, known as glycosaminoglycans, composed of amino sugars chemically linked into repeating units that form a linear unbranched polymeric compound.

Nanotechnology: Applied science and technology dealing with atomic to molecular scale (1~100 nm) matter and fabrication of devices within that size range.

Neointima: New lining of a blood vessel. Its formation is stimulated by fabric-type blood vessel replacements.

Norian SRS ® (Synthes): Injectable, fast-setting carbonated apatite cement used to fill defects in areas of compromised cancellous bone during restoration or augmentation of the skeleton.

OP-1® (Stryker Biotech Inc.): Osteogenic protein-1, known as BMP-7, and used to induce new bone formation in both developing and mature skeletal systems.

Open cell: A type of cellular solid in which there is no barrier between adjacent pores.

Opteform® (Exactech Inc.): Demineralized bone matrix (DBM) obtained from bone banks.

Orthoblast® (GenSci Regeneration Technologies Inc.): Reverse-phase polymer mixed with cancellous bone chips and DBM to create a formable paste.

Orthotropic: A type of anisotropic symmetry in which unit cells are shaped like rectangular parallelepipeds. In crystallography this is called orthorhombic. There are nine independent elastic constants.

Osteoconductive: Supports ingrowth of capillaries, perivascular tissues, and osteoprogenitor cells from a host into an implant or graft, and limited to extracellular activities.

Osteograf® (Dentsply Inc.): Pure, natural, bovine-derived HA xenograft.

Osteoinduction: Elicits mesenchymal stem cells (MSCs) from the surrounding area that differentiate into osteoblasts, and involves intra- and extracellular activity.

Osteoset® (Wright Medical Technologies Inc.): Calcium sulfate tablet used for bone defect filling material.

PDGF (platelet-derived growth factor): One of the numerous proteins that regulate cell growth and division.

PGA (polyglycolic acid): One of the synthetic polymers, poly-α-hydroxyesters, used to make biodegradable scaffolds.

Physical degradation: Erosion of materials at the surface or within the bulk.

PLA (polylactic acid): A synthetic polymer, poly-α-hydroxyester, used to make biodegradable scaffolds.

Porous ingrowth: Growth of tissue into the pores of an implanted porous biomaterial.

ProOsteon (Interpore Cross International Inc.): HA in either a particulate or block form by chemically treating sea coral.

Proplast®: Carbon (graphite) fiber composite with PTFE matrix polymer. Used in soft tissue replacement. The composite showed pores 10 μm in diameter for tissue ingrowth.

PTFE (polytetrafluoroethylene): A linear thermoplastic having excellent heat resistance, found to be useful as a thermal insulator after drawing/expanding, and having a very low surface energy, which makes it nonsticking. Goretex® (W.L. Gore & Associates) has been used to make arterial grafts. Teflon® is a DuPont brand.

Replamineform: Cellular solid made using a biological material as a mold.

Resorption: Absorption of a material, typically a polymer or ceramic.

Rhakoss® (Orthovita Inc.): A polymer-based bone graft substitute that includes both particulate and solid forms.

Solid freeform fabrication (SFF): A technique for manufacturing solid objects by sequential delivery of materials to specified points in space to produce a final product. Rapid prototyping, rapid manufacturing, layered manufacturing, and additive fabrication are a few other terms synonymous with SFF.

Stem cells: Undifferentiated cells capable of proliferation, self-renewal, and differentiation into at least one type of specialized cell.

Stereolithography (SLA): Rapid prototyping, automatic construction of physical objects using solid freeform fabrication.

TCP: Tricalcium phosphate.

Three-dimensional printing (3DP): Computer-controlled layer-by-layer deposition of material powder until desired objects are constructed. Can be used to make scaffolds in tissue engineering.

Tissue engineering: An interdisciplinary field for development of biological substitutes containing living cells, with the aim of restoring, maintaining, and improving cells, tissues, and organs in the body.

Transforming growth factor (TGF): There are two types of polypeptide growth factors: TGFα and TGFβ. Application of TGF to normal rat kidney fibroblasts stimulates cultured cells to proliferate and overgrow, no longer subject to the normal inhibition caused by contact between cells.

Triethylene glycol dimethacrylate (TEGDMA): A compound used to lower the viscosity of dental filling resin.

ULTI (ultra-low-temperature isotropic) carbon: CVD-deposited pyrolytic carbon showing isotropic, amorphous structure.

REFERENCES

1. Adachi T, Osako Y, Tanaka M, Hojo M, Hollister SJ. 2006. Framework for optimal design of porous scaffold microstructures by computational simulation of bone regeneration. *Biomaterials* **27**:3964–3972.
2. Agarwal BD, Broutman LJ. 1980. *Analysis and performance of fiber composites*. New York: Wiley.
3. Agarwal BD, Broutman LJ. 2006. *Analysis and performance of fiber composites*, 2nd ed. New York: Wiley.
4. Albee F. 1920. Studies in bone growth: triple CaP as a stimulus to osteogenesis. *J Ann Surg* **71**:32–36.
5. Alvis M, Lalor P, Brown MK, Thorn MR, Block JE, Hornby S, Berg R, Reddi AH. 2003. Osteoinduction by a collagen mineral composite combined with isologous bone marrow in a subcutaneous rat model. *Orthopedics* **26**(1):77–80.
6. Aoki H, Akao M, Shin Y, Tsuki T, Togawa T. 1987. Sintered hydroxyapatite for a percutaneous device and its clinical applications. *Med Prog Technol* **12**:213–220.
7. ASM. 1987. Composites. In *Engineered materials handbook*. Metal Park, OH: ASM International.
8. Babis GC, Soucacos PN. 2005. Bone scaffolds: the role of mechanical stability and instrumentation. *Injury* **36**(Suppl 4):S38–S44.
9. Ban S, Anusavice KJ. 1990. Influence of test method on failure stress of brittle dental materials. *J Dent Res* **69**:1791–1799.
10. Barralet JE, Grover L, Gaunt T, Wright AJ, Gibson JR. 2002. Preparation of macroporous calcium phosphate cement tissue engineering scaffold. *Biomaterials* **23**:3063–3072.
11. Bauer TW, Smith ST. 2002. Bioactive materials in orthopaedic surgery: overview and regulatory considerations. *J Clin Orthop* **395**:11–22.
12. Beruto DT, Mezzasalma SA, Capurro M, Botter R, Cirillo P. 2000. Use of alpha-tricalcium phosphate (TCP) as powders and as an aqueous dispersion to modify processing, microstructure, and mechanical properties of polymethylmethacrylate (PMMA) bone cements and to produce bone-substitute compounds. *J Biomed Mater Res* **49**:498–505.
13. Boccaccini AR, Blaker JJ. 2005. Bioactive composite materials for tissue engineering scaffolds. *Expert Rev Med Devices* **2**:303–317.
14. Bohner M, Baumgart F. 2004. Effects of geometrical factors on the resorption of calcium phosphate bone substitutes. *Biomaterials* **25**:3569–3582.
15. Bohner M, van Lenthe GH, Gruenenfelder S, Hirsiger W, Evison R, Müller R. 2005. Synthesis and characterization of porous alpha-tricalcium phosphate blocks. *Biomaterials* **26**:6099–6105.
16. Bokros J, LaGrange L, Schoen G. 1972. Control of structure of carbon for use in bioengineering. In *Chemistry and physics of carbon*, pp. 103–171. Ed P Walker. New York: Marcel Dekker.
17. Bonfield W. 1988. Hydroxyapatite reinforced polyethylene as an analogous material for bone replacement. In *Bioceramics: materials characterization versus in vivo behavior*, pp. 173–177. Ed P Ducheyne, JE Lemons. New York: New York Academy of Sciences.
18. Bonfield W, Grynpas MD, Tully AE, Bowman J, Abram J. 1981. Hydroxyapatite reinforced polyethylene: a mechanically compatible implant. *Biomaterials* **2**:185–186.
19. Borden M, Attawia M, Khan Y, Laurencin CT. 2002. Tissue engineered microsphere-based matrices for bone repair: design and evaluation. *Biomaterials* **23**:551–559.
20. Borden M, Attawia M, Laurencin CT. 2002. The sintered microsphere matrix for bone tissue engineering: in vitro osteoconductivity studies. *J Biomed Mater Res* **61**:421–429.
21. Bostrom MP, Saleh KJ, Einhorn TA. 1999. Osteoinductive growth factors in preclinical fracture and long bone defects models. *Orthop Clin North Am* **30**:647–58.
22. Bradley JS, Hastings GW, Johnson-Hurse C. 1980. Carbon fibre reinforced epoxy as a high strength, low modulus material for internal fixation plates. *Biomaterials* **1**:38–40.
23. Braem M, Davidson CL, Lambrechts P, Vanherle G. 1994. In vitro flexural fatigue limits of dental composites. *J Biomed Mater Res* **28**:1397–1402.

24. Brånemark P-I, Hansson BO, Adell R, Breine U, Lidstrom J, Hallen O, Ohman A. 1977. *Osseous integrated implants in the treatment of the edentulous jaw, experience from a 10-year period*. Stockholm: Almqvist & Wiksell International.
25. Brånemark P-T. 1992. Osseointegration: a method of anchoring prostheses. *The Swedish Society of Medicine*, pp. 7–15.
26. Breitbart AS, Staffenberg DA, Thorne CH, Glat PM, Cunningham NS, Reddi AH, Ricci J, Steiner G. 1995. Tricalcium phosphate and osteogenin: a bioactive onlay bone graft substitute. *J Plast Reconstr Surg* **96**:699–708.
27. Bucholz RW. 2002. Nonallograft osteoconductive bone graft substitutes. *Clin Orthop Relat Res* **395**:44–52.
28. Cannon ML. 1988. Composite resins. In *Encyclopedia of medical devices and instrumentation*. Ed JG Webster. New York: Wiley.
29. Cassidy C, Jupiter JB, Cohen M, Delli-Santi M, Fennell C, Leinberry C, Husband J, Ladd A, Seitz WR, Constanz B. 2003. Norian SRS cement compared with conventional fixation in distal radial fractures: a randomized study. *J Bone Joint Surg* **85**:2127–2137.
30. Chang B-S, Lee CK, Hong K-S, Youn H-J, Ryu H-S, Chung S-S, Park K-W. 2000. Osteoconduction at porous hydroxyapatite with various pore configurations. *Biomaterials* **21**:1291–1298.
31. Chang Y-L, Lew D, Park JB, Keller JC. 1999. Biomechanical and mophometric analysis of hydroxyapatite-coated implants with varying crystallinity. *J Oral Maxillofac Surg* **57**:1096–1108.
32. Chen F, Mao T, Tao K, Chen L, Ding M, Cu X. 2002. Bone graft in the shape of human mandibular condyle reconstruction via seeding marrow-derived osteoblasts into porous coral in a nude mice model. *J Oral Maxillofac Surg* **60**:1155–1159.
33. Chen G, Ushida T, Tateishi T. 2001. Poly(DL-lactic-co-glycolic acid) sponge hybridized with collagen microsponges and deposited apatite particulates. *J Biomed Mater Res* **57**:8–14.
34. Chim H, Hutmacher DW, Chou AM, Reis RL, Lim TC, Schantz J-T. 2006. A comparative analysis of scaffold material modifications for load-bearing applications in bone tissue engineering. *Int J Oral Maxillofac Surg* **35**:928–934.
35. Chiroff RT, White EW, Weber JN, Roy DM. 1975. Tissue ingrowth of replamineform implants. *J Biomed Mater Res Symp* **6**:29–45.
36. Chiroff RT, White RA, White EW, Weber JE, Roy DM. 1977. The restoration of articular surfaces overlying replamineform porous biomaterials. *J Biomed Mater Res* **11**:168–178.
37. Christensen RM. 1979. *Mechanics of composite materials*. New York: Wiley.
38. Chu TM, Orton DO, Hollister SJ, Feinberg SE, Halloran JW. 2002. Mechanical and in vivo performance of hydroxyapatite implants with controlled architectures. *Biomaterials* **23**:1283–1293.
39. Chu TMG, Orton DG, Hollister SJ, Feinberg SE, Halloran JW. 2002. Mechanical and in vivo performance of hydroxyapatite implants with controlled architectures. *Biomaterials* **23**:1283–1293.
40. Cima LG, Vacanti JP, Vacanti C, Inger D, Mooney DJ, Langer R. 1991. Tissue engineering by cell transplantation using degradable polymer substrates. *J Biomech Eng-T ASTM* **113**:143–151.
41. Dai KR, Liu YK, Park JB, Clark CR, Nishiyama K, Zheng ZK. 1991. Bone-particle-impregnated bone cement: An in vivo weight-bearing study. *J Biomed Mater Res* **25**:141–156.
42. Dong J, Kojima H, Uemura T, Kikuchi M, Tateishi T, Tanaka J. 2001. In vivo evaluation of a novel porous hydroxyapatite to sustain osteogenesis of transplanted bone marrow-derived osteoblastic cells. *J Biomed Mater Res* **57**:208–211.
43. Dong J, Kojima H, Uemura TM, Tateishi T, Tanaka J. 2001. In vivo evaluation of a novel porous hydroxyapatite to sustain osteogenesis of transplanted bone marrow-derived osteoblastic cells. *J Biomed Mater Res* **57**:208–216.
44. Ducheyne P, Marcolongo M, Schepers E. 1993. Bioceramic composites. In *Introduction to bioceramics*, pp. 281–297. Ed LL Hench, J Wilson. Singapore: World Scientific.
45. El-Ghannam AR. 2004. Advanced bioceramic composite for bone tissue engineering: design principles and structure–bioactivity relationship. *J Biomed Mater Res* **69**:490–501.
46. Engelberg I, Kohn J. 1991. Physicomechanical properties of degradable polymers used in medical applications: a comparative study. *Biomaterials* **12**:292–304.
47. Engh CA, Bobyn JD. 1988. Results of porous coated hip replacement using the AML prosthesis. In *Non-cemented total hip arthroplasty*, p. 393. Ed RJ Fitzgerald. New York: Raven Press.

48. Fini M, Giavaresi G, Aldini NN, Torricelli P, Botter R, Beruto D, Giardino R, 2002. A bone substitute composed of polymethylmethacrylate and alpha-tricalcium phosphate: results in terms of osteoblast function and bone tissue formation. *Biomaterials* **23**:4523–4531.
49. Fisher J. 1996. New ways to heal fractures enter market in the works. *Orthop Today* **16**(1):24–26.
50. Flautre B, Descamps M, Delecourt C, Blary MC, Hardouin P. 2001. Porous HA ceramic for bone replacement: role of the pores and interconnections: experimental study in the rabbit. *J Mater Sci: Mater Med* **12**:679–682.
51. Friedman C, Costantino PD, Takagi S, Chow LC. 1998. BoneSource hydroxyapatite cement: a novel biomaterial for craniofacial skeletal tissue engineering and reconstruction. *J Biomed Mater Res* **43**:428–432.
52. Galois L, Mainard D. 2004. Bone ingrowth into two porous ceramics with different pore sizes: an experimental study. *Acta Orthop Belg* **70**:598–603.
53. Gibson LJ, Ashby MF. 1997. *Cellular solids*, 2nd ed. Oxford: Pergamon.
54. Götz HE, Müller M, Emmel A, Holzwarth U, Erben RG, Stangl R. 2004. Effect of surface finish on the osseointegration of laser-treated titanium alloy implants. *Biomaterials* **25**:4057–4064.
55. Grynpas MD, Pilliar RM, Kandel RA, Renlund R, Filiaggi M, Dumitriu M. 2002. Porous calcium polyphosphate scaffolds for bone substitute applications in vivo studies. *Biomaterials* **23**:2063–2070.
56. Guyer DW, Wiltse LL, Peek RD. 1988. The Wiltse pedicle screw system. *Orthopedics* **11**:1455–1460.
57. Harbers GM, Grainger DW. 2006. Cell-materials interactions: Fundamental design issues for tissue engineering and clinical consideration. In *An introduction to biomaterials*, pp. 15–45. Ed SA Guelcher. Boca Raton, FL: CRC Press, Taylor & Francis Group.
58. Hench LL, Andersson O. 1993. Bioactive glass coatings. In *Introduction to bioceramics*, pp. 239–259. Ed LL Hench, J Wilson. Singapore: World Scientific.
59. Hench LL, Wilson J. 1993. *An Introduction to Bioceramics*, pp. 1–24. Singapore: World Scientific.
60. Henrich DE, Cram AE, Park JB, Liu YK, Reddi H. 1993. Inorganic bone and bone morphogenetic protein impregnated bone cement: a preliminary in vivo study. *J Biomed Mater Res* **27**:277–280.
61. Hiratzka LF, Goeken JA, White RA, Wright CB. 1979. In vivo comparison of replamineform silastic and bioelastic polyurethane arterial grafts. *Arch Surg* **114**:698–702.
62. Hoexter DL. 2002. Bone regeneration graft materials. *J Oral Implantol* **28**:290–204.
63. Hollinger JO, Brekke J, Gruskin E, Lee D. 1996. Role of bone substitutes. *Clin OrthopRelat Res* **324**:55–65.
64. Hollinger JO, Einhorn TA, Doll B, Sfeir C. 2004. *Bone tissue engineering*. Boca Raton, FL: CRC Press.
65. Hollinger JO, Schmitz JP, Mizgala JW, Hassler C. 1989. An evaluation of two configurations of tricalcium phosphate for treating craniotomies. *J Biomed Mater Res* **23**:17–29.
66. Holmes R, Mooney V, Bucholz R, Tencer A. 1984. A coralline hydroxyapatite bone graft substitute: preliminary report. *Clin Orthop Relat Res* **188**:252–284.
67. Holmes RE, Bucholz RW, Mooney V. 1987. Porous hydroxyapatite as a bone graft substitute in diaphyseal defects: a histometric study. *J Orthop Res* **5**:114–121.
68. Homsy CA, Prewitt III JM, Kessler FB, Andeson MS. 1978. Observation of traumatically induced articular surface defects using a porous implant material. In *Transactions of the 4th annual meeting of the society for biomaterials*, p. 85. New York: Wiley.
69. Itälä AI, Ylänen HO, Ekholm C, Karlsson KH, Aro HT. 2001. Pore diameter of more than 100 mm is not requisite for bone ingrowth in rabbits. *J Biomed Mater Res* (*Appl Biomater*) **58**:679–683.
70. Itch M, Shimazu A, Hirata I, Yoshida Y, Shintani H, Okazaki M. 2004. Characterization of CO3Ap-collagen sponges using x-ray high-resolution microtomography. *Biomaterials* **25**:2577–2583.
71. Jarcho M. 1981. Calcium phosphate ceramics as hard tissue prosthetics. *Clin Orthop Relat Res* **157**:259–278.
72. Jin QM, Takita H, Kohgo TK, A. Itoh H, Kuboki Y. 2000. Effects of geometry of hydroxyapatite as a cell substratum in BMP-induced ectopic bone formation. *J Biomed Mater Res* **51**:491–499.
73. Jockisch KA, Brown SA, Bauer TW, Merritt K. 1992. Biological response to chopped-carbon-fiber-reinforced PEEK. *J Biomed Mater Res* **26**:133–146.

74. Kakar S, Einhorn TA. 2005. Tissue engineering of bone. In *An introduction to biomaterials*, pp. 417–440. Ed SA Guelcher, JO Hollinger. Boca Raton, FL: CRC Press, Taylor & Francis Group.
75. Kakutani Y, Yamamuro T, Kotoura Y, Kitsugi T, Hyyakuna K, Saito T, Kitaoji M, Noda I, Makinouchi K. 1988. Granular ceramic coating on alumina. In *Orthopedic ceramic implants*. Ed H Ooonishi, Y Obi. Kyoto: Japanese Society of Orthopedic Ceramic Implants.
76. Karageorgiou V, Kaplan D. 2005. Porosity of 3D biomaterial scaffolds and osteogenesis. *Biomaterials* **26**:5474–5491.
77. Keller DJ, Prendergast PJ. 2006. Prediction of the optimal mechanical properties for a scaffold used in osteochondral defect repair. *Tissue Eng* **12**:2509–2519.
78. Keller JC. 1995. Dental implants: the relationship of materials characteristic to biologic properties. In *The biomedical engineering handbook*, pp. 691–703. Ed JD Bronzino. Boca Raton, FL: CRC Press.
79. Khang G. 2006. Biomaterials: tissue engineering and scaffolds. In *Encyclopedia of medical devices and instrumentation*, pp. 366–383. Ed JG Webster. Hoboken, NJ: Wiley.
80. Kim HW, Knowles JC, Kim HE. 2004. Hydroxyapatite/poly(epsilon-caprolactone) composite coatings on hydroxyapatite porous bone scaffold for drug delivery. *Biomaterials* **25**:1279–1287.
81. Kim SS, Ahn KM, Park MS, Lee JH, Choi CY, Kim BS. 2007. A poly(lactide-co-glycolide)/hydroxyapatite composite scaffold with enhanced osteoconductivity. *J Biomed Mater Res* **80A**:206–215.
82. Knackstedt MA, Arns CH, Senden TJ, Gross K. 2006. Structure and properties of clinical coralline implant measured via 3D imaging and analysis. *Biomaterials* **27**:2776–2786.
83. Kohn J, Langer R. 1996. Bioresorbable and bioerodible materials. In *Biomaterials science: an introduction to materials in medicine*, pp. 64–73. Ed BD Ratner, AS Hoffman, FJ Schoen, JE Lemons. San Diego: Academic Press.
84. Kovacs P. 1993. In vitro studies of the electrochemical behavior of carbon-fiber composites. In *Composite materials for implant applications in the human body: characterization and testing*, pp. 41–52. Ed RD Jamison, LN Gilbertson. Philadelphia: American Society for Testing and Materials.
85. Kruyt MC, de Bruijn JD, Wilson CE, Oner FC, van Blitterswijk CA, Verbout AJ, Dhert WJA. 2003. Viable osteogenic cells are obligatory for tissue-engineered ectopic bone formation in goats. *Tissue Eng* **9**:327–336.
86. Kuboki Y, Jin Q, Kikuchi MJ, Takita H. 2002. Geometry of artificial ECM: sizes of pores controlling phenotype expression in BMP-induced osteogenesis and chondrogenesis. *Connect Tissue Res* **43**:529–534.
87. Kuboki Y, Jin Q, Takita H. 2001. Geometry of carriers controlling phenotypic expression in BMP-induced osteogenesis and chondrogenesis. *J Bone Joint Surg Am* **83A** (Suppl 1, Pt 2):S105–S115.
88. Kuboki Y, Takita H, Kobayashi D, Tsuruga E, Inoue M, Murata M, Nagai N, Dohi Y, Ohgushi H. 1998. BMP-induced osteogenesis on the surface of hydroxyapatite with geometrically feasible and nonfeasible structures: topology of osteogenesis. *J Biomed Mater Res* **39**:190–199.
89. Landi E, Celotti G, Logroscino G, Tampieri A. 2003. Carbonated hydroxyapatite as bone substitute. *J Eur Ceram Soc* **23**:2931–2937.
90. Landi E, Tampieri A, Celotti G, Sprio S. 2000. Densification behaviour and mechanisms of synthetic hydroxyapatites. *J Eur Ceram Soc* **20**:2377–2387.
91. Laney WR, Tolman DE. 1990. Tissue integration in oral and maxillofacial reconstruction. Chicago: Quintessence.
92. Lanza R, Langer R, Vacanti J. 2007. *Principles of tissue engineering*, 3rd ed. San Diego: Academic Press.
93. Laurencin C, Khan Y, El-Amin SF. 2006. Bone graft substitutes. *Expert Rev Med Devices* **3**:49–57.
94. Laurencin CT, Ambrosio AA, Borden MD, Cooper J., 1999. Tissue engineering: orthopaedic applications. *Annu Rev Biomed Eng* **19**:19–46.
95. Laurencin CT, Attawia MA, Lu LQ. 2001. Poly(lactide-co-glycolide)/hydroxyapatite delivery of BMP-2-producing cells: a regional gene therapy approach to bone regeneration. *Biomaterials* **22**:1271–1277.

96. Laurencin CT, Khan Y, Kofron M, El-Amin S, Botchwey E, Yu X, Cooper JAJ. 2006. The ABJS Nicolas Andry award: tissue engineering of bone and ligament: a 15-year perspective. *Clin Orthop Relat Res* **447**:221–236.
97. Laurencin CT, Yusuf Khan Y. 2005. Bone graft substitute materials. http://www.emedicine.com/orthoped/topic611.htm, eMedicine from WebMD.
98. Lee GH, Khoury JG, Bell JE, Buckwalter JA. 2002. Adverse reactions to OsteoSet bone graft substitute, the incidence in a consecutive series. *Iowa Orthop J* **22**:35–38.
99. Lee YM, Seol YJ, Lim YT, Kim S, Han SB, Rhyu IC, Baek SH, Heo SJ, Choi JY, Klokkevold PR, Chung CP. 2001. Tissue-engineered growth of bone by marrow cell transplantation using porous calcium metaphosphate matrices. *J Biomed Mater Res* **54**:216–23.
100. LeGeros RZ. 1993. Biodegradation and bioresorption of calcium phosphate ceramics. *J Clin Mater* **14**:65–88.
101. Leinfelder KF, Bayne SC, Swift Jr EJ. 1999. Packable composites: overview and technical considerations. *J Esthet Dent* **11**:234–249.
102. Li S, De Wijn JR, Li J, Layrolle P, De Groot K. 2003. Macroporous biphasic calcium phosphate scaffold with high permeability/porosity ratio. *Tissue Eng* **9**:535–548.
103. Liao S, Watari F, Zhu Y, Uo M, Akasaka T, Wang W, Xu G, Cui F. 2007. The degradation of the three layered nano-carbonated hydroxyapatite/collagen/PLGA composite membrane in vitro. *Dent Mater* **23**:1120–1128.
104. Lickorish D, Ramshaw JA, Werkmeister JA, Glattauer V, Howlett CR. 2004. Collagen–hydroxyapatite composite prepared by biomimetic process. *J Biomed Mater Res* **68**:19–27.
105. Lin CY, Kikuchi N, Hollister SJ. 2004. A novel method for biomaterial scaffold internal architect design to match bone elastic properties with desired porosity. *J Biomech* **37**:623–636.
106. Liu YK, Park JB, Njus GO, Stienstra D. 1987. Bone particle impregnated bone cement, I: in vitro study. *J Biomed Mater Res* **21**:247–261.
107. Ma PX, Elisseeff J. 2005. *Scaffolding in tissue engineering*. Boca Raton, FL: CRC Press.
108. Magee FP, Weinstein AM, Longo JA, Koeneman JB, Yarp RA. 1988. A canine composite femoral stem: an in vivo study. *Clin Orthop Relat Res* **235**:237–252.
109. Maharaj GR, Jamison RD. 1993. Creep testing of a composite material human hip prosthesis. In *Composite materials for implant applications in the human body: characterization and testing*. Ed RD Jamison, LN Gilbertson. Philadelphia: American Society for Testing and Materials.
110. Mastrogiacomo M, Muraglia A, Komlev V, Rustichelli F, Crovace A, Cancedda R. 2005. Tissue engineering of bone: search for a better scaffolds. *Orthod Craniofac Res* **8**:277–284.
111. Miki T, Masaka K, Imai Y, Enomoto S. 2000. Experience with freeze-dried PGLA/HA/rhBMP-2 as bone graft substitute. *J Craniomaxillofac Surg* **28**:294–299.
112. Mikos AG, Sarakinos G, Leite SM, Vacanti JP, Langer R. 1993. Laminated three-dimensional biodegradable foams for use in tissue engineering. *Biomaterials* **14**(5):323–330.
113. Mooney DJ, Baldwin DF, Suh NP, Vacanti JP, Langer R. 1996. Novel approach to fabricate porous sponges of poly(D,L-lactic co-glycolic acid) without the use of organic solvents. *Biomaterials* **17**:1417–1422.
114. Niznick GA. 1987. Osseointegration vs fibro-osseous integration. *J Oral Implantol* **13**:10–19.
115. Ohgushi H, Goldberg VM, Caplan A. 1989. Heterotopic osteogenesis in porous ceramics induced by marrow cells. *J Orthop Res* **7**:568–578.
116. Okamura M, Ohgushi H, Dohi Y, Katuda T, Tamai S, Koerten HK, Tabata S. 1997. Osteoblastic phenotype expression on the surface of hydroxyapatite ceramics. *J Biomed Mater Res* **37**:122–129.
117. Olsson J, Stearns N. 2006. Osseointegration of immediately loaded dental implants in the edentulous jaws: a study of the literature. www.ki.se/odont/cariologi_endodonti/99B/JohanOlssonNathonStearns.pdf.
118. Papadogianis Y, Boyer DB, Lakes RS. 1984. Creep of conventional and microfilled dental composites. *J Biomed Mater Res* **18**:15–24.
119. Park JB, Choi WW, Liu YK, Haugen TW. 1986. Bone particle-impregnated polymethylmethacrylate: an in vivo study. In *Tissue integration in oral and maxillofacial reconstruction*, pp. 118–124. Ed DV Steenberghe. Amsterdam, Excerpta Medica.
120. Park JB, Lakes RS. 2007. *Biomaterials: an introduction*, 3rd ed. New York: Springer.

121. Park KD, Kang YH, Park JB. 1999. Interfacial strength between molded and UHMWPE-MMA monomer treated UHMWPE powder. *J Long-Term Eff Med Implants* **9**:303–318.
122. Peltier LF. 1961. The use of plaster of paris to fill defects in bone. *Clin Orthop Relat Res* **21**:1–31.
123. Perry CR. 1999. Bone repair techniques, bone graft, and bone graft substitutes. *Clin Orthop Relat Res* **360**:71–86.
124. Petruskevicius J, Nielsen S, Kaalund S, Knudsen PR, Overgaard S. 2002. No effect of Osteoset, a bone graft substitute, on bone healing in humans: a prospective randomized double-blind study. *Acta Orthop Scand* **73**(5):575–578.
125. Pillar RM, Filiaqqi MJ, Wells JD, Grynpas MD, Kandel RA. 2001. Porous calcium polyphosphate scaffolds for bone substitute applications: in vitro characterization. *Biomaterials* **22**:963–972.
126. Redey SA, Nardin M, Bernache-Assolant D, Rey C, Delannoy P, Sedel L, Marie PJ. 2000. Behavior of human osteoblastic cells on stoichiometric hydroxyapatite and type A carbonate apatite: role of surface energy. *J Biomed Mater Res* **50**:353–364.
127. Richart O, Descamps M, Liebetrau A. 2001. Macroporous calcium phosphate ceramics: optimization of the porous structure and its effect on the bone ingrowth in a sheep model. *Key Eng Mater* **192–195**:425–428.
128. Ripamonti U. 1996. Osteoinduction in porous hydroxyapatite implanted in heterotopic sites of different animal models. *Biomaterials* **17**:31–35.
129. Rose FR, Cyster LA, Grant DM, Scotchford CA, Howdle SM, Shakesheff KM. 2004. In vitro assessment of cell penetration into porous hydroxyapatite scaffolds with a central aligned channel. *Biomaterials* **25**:5507–5514.
130. Rosenstiel SF, Land MF, Crispin BJ. 1998. Dental luting agents: a review of the current literature. *J Prosthet Dent* **80**:280–301.
131. Sachlos E, Czernuszka JT. 2003. Making tissue engineering scaffolds work: review on the application of solid freeform fabrication technology to the production of tissue engineering scaffolds. *Eur Cells Mater* **5**:29–40.
132. Saltzman WM. 2004. Tissue engineering: engineering principles for the design of replacement organs and tissues. Oxford: Oxford UP.
133. Sarkar MR, Wachter N, Patka P, Kinzl L. 2001. First histological observations on the incorporation of a novel calcium phosphate bone substitute material in human cancellous bone. *J Biomed Mater Res* **58**:329–334.
134. Schmitz JP, Hollinger JO. 1988. A preliminary study of the osteogenic potential of biodegradable alloplastic osteoinductive alloimplant. *Clin Orthop Relat Res* **237**:245–255.
135. Schwartz MM. 1997. Composite materials: properties, nondestructive testing, and repair. Upper Saddle River, NJ: Prentice-Hall.
136. Sclippa E, Piekarski K. 1973. Carbon fiber reinforced polyethylene for possible orthopaedic usage. *J Biomed Mater Res* **7**:59–70.
137. Shores EC, Holmes RE. 1993. Porous hydroxyapatite. In *Introduction to bioceramics*, pp. 181–198. Ed LL Hench, J Wilson. Singapore: World Scientific.
138. Skinner HB. 1988. Composite technology for total hip arthroplasty. *Clin Orthop Relat Res* **235**:224–236.
139. Spector M. 1999. Basic principles of tissue engineering. In *Tissue engineering: application in maxillofacial surgery and periodontics*, pp. 3–16. Ed SE Lynch, RJ Genco, RE Marx. Chicago: Quintessence.
140. Steffen T, Stoll T, Arvinte T, Schenck RK. 2001. Porous tricalcium phosphate and transforming growth factor used for anterior spine surgery. *Eur Spine J* **10**:132–140.
141. Takuma M, Tstsumi S, Fukunaga S, Takamori Y, Harada S, Kurokawa F, Takashima F, Maruyama T. 1989. Study on the functional bone adaptation around dental implants: animal experimentations and stress analysis. In *Oral implantology and biomaterials*, pp. 251–256. Ed H Kawahara: Amsterdam: Elsevier Science.
142. Tampieri A, Celotti G, Sprio S, Delcogliano A, Franzese S. 2001. Porosity-graded hydroxyapatite ceramics to replace natural bone. *Biomaterials* **22**:1365–1370.

143. Tateishi T, Fukubayashi T. 1989. Advanced biocomposite material and application to the artificial joint. In *Bioceramics*, Vol. 1, pp. 48–53. Ed H Oonishi, H Aoki, K Sawai. Tokyo: Ishiyaku EuroAmerica.
144. Thalgott JS, Klezl Z, Timlin M, Giuffre JM. 2002. Anterior lumbar interbody fusion with processed sea coral (coralline hydroxyapatite) as part of a circumferential fusion. *Spine* **27**:E518–E525.
145. Thompson JI, Czernuszka JT. 1995. Fabrication of biodegradable polymer scaffolds to engineering trabecular bone. *J Biomater Sci—Polym Ed* **7**:23–38.
146. van der Elst M, Klein CPAT, Patka P, Haarman HJTM. 2000. Biodegradable fracture fixation devices. In *Biomaterials and bioengineering handbook*, pp. 509–524. Ed DL Wise. New York: Marcel Dekker.
147. Von Doernberg MC, von Rechenberg B, Bohner M, Grönenfelder S, van Lenthe GH, Müller R, Gasser B, Mathys R, Baroud G, Auer J. 2006. In vivo behavior of calcium phosphate scaffolds with four different pore sizes. *Biomaterials* **30**:5186–5198.
148. Wahl DA, Czernuszka JT. 2006. Collagen–hydroxyapatite composites for hard tissue repair. *Eur Cell Mater* **11**:43–56.
149. Weiss CM. 1987. A comparative analysis of fibro-osteal and osteal integration and other variables that affect long term bone maintenance around dental implants. *J Oral Implantol* **13**:467–487.
150. Weiss CM. 1986. Tissue integration of dental endosseous implants: descriptive and comparative analysis of fiber-osseous and osseointegration system. *J Oral Implantol* **12**:169–187.
151. Westfall R, Kent J, Homsy C. 1980. A comparison of porous composite PTFE/Al_2O_3 and PTFE/Graphite microporous facial implants in primates. In *Transactions of the first world biomaterials congress*, p. 3.8.3. Chichester: Wiley.
152. Whang K, Thomas CH, Healy KE, Nuber G. 1995. A novel method to fabricate bioabsorbable scaffolds. *Polymer* **36**:837–842.
153. Wolfe MS, Dean D, Chen JE, Fisher JP, Han S, Rimnac CM, Mikos AG. 2002. In vitro degradation and fracture toughness of multilayered porous poly(propylene fumarate)/beta-tricalcium phosphate scaffolds. *J Biomed Mater Res* **61**:159–164.
154. Yannas IV. 1995. Regeneration templates. In *The biomedical engineering handbook*, pp. 1619–1635. Ed JD Bronzino. Boca Raton, FL: CRC Press.
155. Yannas IV, Burke JF, Gordon PL, Huang C, Rubenstein RH. 1980. Design of an artificial skin, Part II: control of chemical composition. *Biomaterials* **14**:107–131.
156. Yoshikawa T, Ohgushi H, Tamai S. 1996. Immediate bone forming capability of prefabricated osteogenic hydroxyapatite. *J Biomed Mater Res* **32**:481–492.
157. Yuan H, Kurashina K, de Bruijn JD, Li Y, de Groot K, Zhang X, 1999. A preliminary study on osteoinduction of two kinds of calcium phosphate ceramics. *Biomaterials* **20**:1799–1806.
158. Zhang C, Wang J, Feng H, Lu B, Song Z, Zhang X. 2001. Replacement of segmental bone defects using porous bioceramic cylinders: a biomechanical and x-ray diffraction study. *J Biomed Mater Res* **54**:407–411.
159. Zhang K, Wang Y, Hillmyer MA, Francis LF. 2004. Processing and properties of porous poly(L-lactide)/bioactive glass composites. *Biomaterials* **25**:2489–2500.
160. Zhang Y, Zhang M. 2002. Three-dimensional macroporous calcium phosphate bioceramics with nested chitosan sponges for load-bearing bone implants. *J Biomed Mater Res* **61**:1–8.
161. Zhao F, Yi Y, Lu WW, Leong JC, Zhang W, Zhang J, Zhang M, Yao K. 2002. Preparation and histological evaluation of biomimetic three-dimensional hydroxyapatite/chitosan-gelatin network composite scaffolds. *Biomaterials* **23**:3227–3234.

Appendix I

PHYSICAL CONSTANTS AND CONVERSIONS

Physical Constants

Name	Symbol	Units
Atomic mass unit	amu	1.66×10^{-24} g
Avogadro's number	N	6.023×10^{23}/mol (or molecules/g·mol)
Boltzmann's constant	k	1.381×10^{-23} J/K or 8.63×10^{-5} eV/K
Permittivity (vacuum)	ε	8.85×10^{-12} C/V·m
Electron charge	q	1.602×10^{-19} C
Electron volt	eV	1.60×10^{-19} J
Faraday's constant	F	0.649×10^{4} C/mol
Gas constant	R	8.314 J/mol K or 1.987 cal/mol·K
Planck's constant	h	6.62×10^{-34} J·s
Standard gravity	g	9.807 m/s^2
Velocity of light	c	3×10^{6} m/s

Conversions

1 Angstrom (Å) =	10^{-10} m
1 Ampere (A) =	1 Coul/s
1 Inch (in) =	0.0254 m
1 Calorie (cal) =	4.1868 J
1 Erg =	10^{-7} J
1 Dyne =	10^{-5} N
1 Joule (J) =	1 N·m
1 kg force (kgf) =	9.807 N
1 Pound force (lb) =	4.448 N
1 Pound (mass) =	0.4536 kg
1 atmosphere (standard) =	0.1 MPa
1 mmHg (60ºF) =	1.329×10^{2} Pa
1 inch of Hg (60ºF) =	3.37685×10^{3} Pa
1 dyne/cm^2 =	0.1 Pa
1 kgf/mm^2 =	9.807×10^{6} Pa
1 lb/in^2 (psi) =	6.895×10^{3} Pa
1 MPa =	145 psi
1 Poise =	0.1 Pa·s
1 Rad =	0.01 Gy

Appendix II

SI UNITS

The International System of Units of SI (Le Système Internationale d'Unités) define the base units as following:

Base Units

Quantity	Unit	Symbol
Length	meter	m
Mass	kilogram	kg
Time	second	s
Electric current	Ampere	A
Temperature	Kelvin	K
Amount of substance	mole	mol

Derived Units

Quantity	Unit	Symbol	Formula
Frequency	Hertz	Hz	1/s
Force	Newton	N	kg m/s^2
Pressure, stress	Pascal	Pa	N/m^2
Energy, work, heat	Joule	J	N m
Power	Watt	W	J/s
Absorbed dose	gray	Gy	J/kg

Appendix III

COMMON PREFIXES

Multiplication factor	Prefix	Symbol
10^{18}	peta	P
10^{12}	tera	T
10^{9}	giga	G
10^{6}	mega	M
10^{3}	kilo	k
10^{-2}	centi	c
10^{-3}	milli	m
10^{-6}	micro	μ
10^{-9}	nano	n
10^{-12}	pico	p
10^{-15}	femto	f
10^{-18}	atto	a

Appendix IV

PROPERTIES OF SELECTED ELEMENTS

Element	Symbol	Atomic no.	Weight (amu)	T_m (°C)	Density[a] (g/cm^3)	Crystal struc.	Atomic rad. (Å[b])	Ionic rad. (nm)	Common valence
Hydrogen	H	1	1.008	–259.14	9×10^{-5}	hcp	0.46	1.54	–1
Lithium	Li	3	6.94	180	0.534	bcc	1.519	0.78	+1
Beryllium	Be	4	9.01	1289	1.85	hcp	1.14	0.54	+2
Boron	B	5	10.81	2103	2.34	ortho.	0.97	0.2	+3
Carbon	C	6	12.011	>3500	2.25	hex	0.77	<0.2	+4
Nitrogen	N	7	14.007	–210	1.25×10^{-3}	cubic	0.71	0.1~0.2	+5
Oxygen	O	8	15.999	–218.4	1.43×10^{-3}	ortho.	0.60	1.32	–2
Fluorine	F	9	19.0	–220	1.70×10^{-3}	–	0.6	1.33	–1
Neon	Ne	10	20.18	–248.7	0.90×10^{-3}	fcc	1.60	–	–
Sodium	Na	11	22.99	97.8	0.97	bcc	1.857	0.98	+1
Magnesium	Mg	12	24.31	649	1.74	hcp	1.61	0.78	+2
Aluminum	Al	11	26.98	660.4	2.70	fcc	1.43	0.57	+3
Silicon	Si	14	28.09	1414	2.33	diamond	1.176	0.39	+4
Phosphorus	P	15	30.97	1.8	1.83	ortho.	0.11	0.3~0.4	+5
Sulfur	S	16	32.06	112.8	2.07	ortho.	1.06	1.74	–2
Chlorine	Cl	17	35.45	–101	3.21×10^{-3}	ortho.	1.07	1.81	–1
Argon	Ar	18	39.95	–189.2	1.78×10^{-3}	fcc	1.92	–	–
Potassium	K	19	39.10	63	0.86	bcc	2.312	1.33	+1
Calcium	Ca	20	40.08	840	1.54	fcc	1.969	1.06	+2
Titanium	Ti	22	47.90	1672	4.51	hcp	1.46	0.64	+4
Vanadium	V	23	50.94	1910	6.09	bcc	1.32	0.61	+4
Chromium	Cr	24	52.00	1863	7.20	bcc	1.249	0.64	+3
Manganese	Mn	25	54.94	1246	7.43	hcp	1.12	0.91	+2
Iron	Fe	26	55.85	1538	7.88	bcc	1.241	0.87	+2
Cobalt	Co	27	58.93	1494	8.9	hcp	1.25	0.82	+2
Nickel	Ni	28	58.71	1455	8.90	fcc	1.246	0.78	+2
Copper	Cu	29	63.54	1084.5	8.92	fcc	1.278	0.96	+1
Zinc	Zn	30	65.37	419.6	7.14	hcp	1.33	0.83	+2
Yttrium	Y	39	88.9	1522	4.47	hcp	2.12	1.62	+3
Zirconium	Zr	40	91.22	1852	6.51	hcp	1.59	0.87	+4
Molybdenum	Mo	42	95.94	2617	10.22	bcc	1.36	0.68	+4
Silver	Ag	47	107.87	961.9	10.5	fcc	1.444	1.13	+1
Tin	Sn	50	118.69	232	7.3	bct	1.509	0.74	+4
Antimony	Sb	51	121.75	630.7	6.7	rhomb.	1.452	1.38	+3
Cesium	Cs	55	132.9	28.4	1.9	bcc	2.62	1.65	+1
Tungsten	W	74	183.9	3387	19.4	bcc	1.367	0.65	+4
Gold	Au	79	197.0	1064.4	19.32	bcc	1.441	1.37	+1
Mercury	Hg	80	200.6	–38.86	13.55	rhomb.	1.50	1.12	+2
Lead	Pb	82	207.2	327.5	11.34	fcc	1.75	1.32	+2

[a] Most densities are for solids, some for liquids. Gas densities are much lower (<<1 g/cm^3).

[b] 1 nm = 10 Å.

BIBLIOGRAPHY

Adachi T, Osako Y, Tanaka M, Hojo M, Hollister SJ. 2006. Framework for optimal design of porous scaffold microstructures by computational simulation of bone regeneration. *Biomaterials* **27**:3964–3972.

Adams D, Williams D. 1978. Carbon fiber-reinforced carbon as a potential implant material. *J Biomed Mater Res* **12**:35–42.

Agarwal BD, Broutman LJ. 1980. *Analysis and performance of fiber composites*. New York: Wiley.

Agarwal BD, Broutman LJ. 2006. *Analysis and performance of fiber composites*, 2nd ed. New York: Wiley.

Agrawal CM, Micallef DM, Wirth MA, Lankford J, Dearnaley G, McCabe AR. 1993. The effects of diamond-like-carbon coatings on the friction and wear of enhanced UHMWPE-metal couples. In *19th meeting of the society for biomaterials*, p. 10. New York: Wiley.

Albee FH, Morrison HF. 1920. Studies in bone growth: triple calcium phosphate as a stimulus to osteogenesis. *Ann Surg* **71**:32–39.

Alvis M, Lalor P, Brown MK, Thorn MR, Block JE, Hornby S, Berg R, Reddi AH. 2003. Osteoinduction by a collagen mineral composite combined with isologous bone marrow in a subcutaneous rat model. *Orthopedics* **26**(1):77–80.

Andrew C, Bassett CAL, Hurley LA, Stinchfield FE. 1962. The fate of long-term anorganic bone implants. *Transp Bull* **29**:51–55.

Aoki H, Akao M, Shin Y, Tsuki T, Togawa T. 1987. Sintered hydroxyapatite for a percutaneous device and its clinical applications. *Med Prog Technol* **12**:213–220.

Aoki H, Kato K, Shibata M, Naganuma A. 1972. Thermal transition of calcium phosphates and observation by a scanning electron microscope [in Japanese]. *Rep Inst Med Dent Eng* **6**:50–61.

Ashby MF, Jones DR. 1985. *Engineering materials 2: an introduction to microstructures, processing and design*, pp. 147–152, Oxford: Pergamon.

ASM. 1987. Composites. In *Engineered materials handbook*. Metal Park, OH: ASM International.

ASM. 1987. *Engineered materials handbook*, Vol. 4: *Ceramics and glasses*. Metal Park, OH: ASM International.

Aspenberg P, Anttila A, Konttinen YT, Lappalainen R, Goodman SB, Nordsletten L, Santavirta S. 1996. Benign response to particles of diamond and SiC: Bone chamber studies of new joint replacement coating materials in rabbits. *Biomaterials* **17**:807–812.

Babis GC, Soucacos PN. 2005. Bone scaffolds: the role of mechanical stability and instrumentation. *Injury* **36**(Suppl 4):S38–S44.

Baier R. 1980. Guidelines for physicochemical characterization of biomaterials. In *Devices and technology branch, National Heart, Lung and Blood Institute*, pp. 97–104. Washington, DC: NIH Publication.

Ban S, Anusavice KJ. 1990. Influence of test method on failure stress of brittle dental materials. *J Dent Res* **69**:1791–1799.

Barralet JE, Gaunt T, Wright AJ, Gibson IR, Knowles JC. 2002. Effect of porosity reduction by compaction on compressive strength and microstructure of calcium phosphate cement. *J Biomed Mater Res* **63**:1–9.

Barralet JE, Grover L, Gaunt T, Wright AJ, Gibson JR. 2002. Preparation of macroporous calcium phosphate cement tissue engineering scaffold. *Biomaterials* **23**:3063–3072.

Bauer TW, Smith ST. 2002. Bioactive materials in orthopaedic surgery: overview and regulatory considerations. *J Clin Orthop* **395**:11–22.

Beckham C, Greenlee Jr T, Crebo A. 1971. Bone formation at a ceramic implant interfacing. *Calcif Tissue Res* **8**:165–171.

Bedell CJ, Jones AM, Dearnaley G, Johnston C. 1991. Diamond-like carbon from the ion-beam decomposition of polyphenol ether. In *Applications of diamond films and related materials*, pp. 833–838. New York: Elsevier.

Bell ET. 1986. The prince of mathematicians: Gauss. In *Men of mathematics: the lives and achievements of the great mathematicians from Zeno to Poincaré*, pp. 218–269. New York: Simon and Schuster.

Beruto DT, Mezzasalma SA, Capurro M, Botter R, Cirillo P. 2000. Use of alpha-tricalcium phosphate (TCP) as powders and as an aqueous dispersion to modify processing, microstructure, and mechanical properties of polymethylmethacrylate (PMMA) bone cements and to produce bone-substitute compounds. *J Biomed Mater Res* **49**:498–505.

Billmeyer Jr FW. 1984. *Textbook of polymer science*. New York: Wiley.

Bizot P, Nizard R, Lerouge S, Prudhommeaux F, Sedel L. 2000. Ceramic/ceramic total hip arthroplasty. *J Orthop Sci* **5**:622–627.

Black J. 1981. *Biological performance of materials: fundamentals of biocompatibility*. New York: Marcel Dekker.

Blaise L, Villermaux F, Cales B. 2001. Ageing of zirconia: everything you always wanted to know. *Key Eng Mater* **13**:553–556.

Blatz MB, Sadan A, Martin J, Lang B. 2004. In vitro evaluation of shear bond strengths of resin to densely-sintered high-purity zirconium-oxide ceramic after long-term storage and thermal cycling. *J Prosthet Dent* **91**:356–362.

Blencke BA, Bromer H, Deutscher KK. 1978. Compatibility and long-term stability of glass-ceramic implants. *J Biomed Mater Res* **12**:307–318.

Block M, Kent J, Kay J. 1987. Evaluation of hydroxyapatite-coated titanium dental implants in dogs. *J Oral Maxillofac Surg* **45**:601–607.

Bloom W, Fawcett DW. 1968. *A Textbook of Histology*, 9th ed. Philadelphia: Saunders.

Boccaccini AR, Blaker JJ. 2005. Bioactive composite materials for tissue engineering scaffolds. *Expert Rev Med Devices* **2**:303–317.

Boehm H. 1966. Funktionelle Gruppen an Festkorper-Oberflachen. *Angew Chem* **78**:617–652.

Bohner M, Baumgart F. 2004. Effects of geometrical factors on the resorption of calcium phosphate bone substitutes. *Biomaterials* **25**:3569–3582.

Bohner M, van Lenthe GH, Gruenenfelder S, Hirsiger W, Evison R, Müller R. 2005. Synthesis and characterization of porous alpha-tricalcium phosphate blocks. *Biomaterials* **26**:6099–6105.

Bokros J. 1969. Deposition structure and properties of pyrolytic carbon. In *Chemistry and physics of carbon*, pp. 70–81. Ed P Walker. New York: Marcel Dekker.

Bokros J, LaGrange L, Schoen G. 1972. Control of structure of carbon for use in bioengineering. In *Chemistry and physics of carbon*, pp. 103–171. Ed P Walker. New York: Marcel Dekker.

Bonel G, Heughebaert JC, Heughebaert M, Lacout JL, Lebugle A. 1988. Apatitic calcium orthophosphates and related compounds for biomaterials preparation. In *Bioceramics: materials characteristics versus* in vivo *behavior*, pp. 115–130. Ed P Ducheyne, JE Lemons. New York: New York Academy of Sciences.

Bonfield W. 1988. Hydroxyapatite reinforced polyethylene as an analogous material for bone replacement. In *Bioceramics: materials characterization versus in vivo behavior*, pp. 173–177. Ed P Ducheyne, JE Lemons. New York: New York Academy of Sciences.

Bonfield W, Grynpas MD, Tully AE, Bowman J, Abram J. 1981. Hydroxyapatite reinforced polyethylene: a mechanically compatible implant. *Biomaterials* **2**:185–186.

Borden M, Attawia M, Khan Y, Laurencin CT. 2002. Tissue engineered microsphere-based matrices for bone repair: design and evaluation. *Biomaterials* **23**:551–559.

Borden M, Attawia M, Laurencin CT. 2002. The sintered microsphere matrix for bone tissue engineering: in vitro osteoconductivity studies. *J Biomed Mater Res* **61**:421–429.

Bostrom MP, Saleh KJ, Einhorn TA. 1999. Osteoinductive growth factors in preclinical fracture and long bone defects models. *Orthop Clin North Am* **30**:647–58.

Bradley JS, Hastings GW, Johnson-Hurse C. 1980. Carbon fibre reinforced epoxy as a high strength, low modulus material for internal fixation plates. *Biomaterials* **1**:38–40.

Braem M, Davidson CL, Lambrechts P, Vanherle G. 1994. In vitro flexural fatigue limits of dental composites. *J Biomed Mater Res* **28**:1397–1402.

Brandt AM. 1994. Cement-based composites: materials, mechanical properties and performance. Boca Raton, FL: Taylor & Francis.

Brånemark P-T. 1992. Osseointegration: a method of anchoring prostheses. *The Swedish Society of Medicine*, pp. 7–15.

Brånemark P-I, Hansson BO, Adell R, Breine U, Lidstrom J, Hallen O, Ohman A. 1977. *Osseous integrated implants in the treatment of the edentulous jaw, experience from a 10-year period*. Stockholm: Almqvist & Wiksell International.

Breitbart AS, Staffenberg DA, Thorne CH, Glat PM, Cunningham NS, Reddi AH, Ricci J, Steiner G. 1995. Tricalcium phosphate and osteogenin: a bioactive onlay bone graft substitute. *J Plast Reconstr Surg* **96**:699–708.

Brighton C, Friedenberg Z, Black J. 1979. Evaluation of the use of constant direct current in treatment of nonunion. In *Electrical properties of bone and cartilage*, pp. 519–545, Ed C Brighton, J Black, S Pollack. New York: Grune & Stratton.

Brovarone CV, Verne E, Appendino P. 2006. Macroporous bioactive glass-ceramic scaffolds for tissue engineering. *J Mater Sci: Mater Med* **17**:1069–1078.

Bruce RH. 1965. Science of ceramics. *Sci Ceram* **2**:359–381.

Bruckmann H, Mauer HJ, Huttinger KJ, Rettig H, Weber U. 1980. New carbon materials for joint prostheses. In *Transactions of the first world biomaterials congress*, p. P1.7. Chichester: Wiley.

Bucholz RW. 2002. Nonallograft osteoconductive bone graft substitutes. *Clin Orthop Relat Res* **395**:44–52.

Bundy FP, Strong HM, Wentorf RH. 1973. Synthetic diamond growth. In *Chemistry and physics of carbon*, Vol. 10, pp. 213–263. Ed PL Walker. New York: Marcel Dekker.

Burger W, Willmann G. 1993. Advantages and risks of zirconia ceramics in biomedical applications. In *Bioceramics*, Vol. 6, pp. 299–304. Ed P Ducheyne, D Christiansen. Oxford: Pergamon.

Cales B. 2000. Zirconia as a sliding material: histologic, laboratory, and clinical data. *Clin Orthop Relat Res* **379**:94–112.

Cales B, Stefani Y. 1994. Long-term stability of a surgical grade zirconia ceramic. In *Bioceramics*, Vol. 7, pp. 395–400. Ed OH Andersson, R-P Happonen, A Yli-Urpo. Oxford: Pergamon.

Cales B, Stefani Y, Olagnon C, Fantozzi G. 1993. Mechanical characterization of a zirconia ceramic used as implant material. In *Bioceramics*, Vol. 6, pp. 259–264. Ed P Ducheyne, D Christiansen. Oxford: Pergamon.

Callister JWD. 1994. *Materials science and engineering: an introduction*, 3rd ed. New York: Wiley.

Carlisle E. 1986. Biological silicon. In *Silicon biochemistry*, pp. 123–136. Ed D Evered. New York: Wiley.

Cannon ML. 1988. Composite resins. In *Encyclopedia of medical devices and instrumentation*. Ed JG Webster. New York: Wiley.

Cassidy C, Jupiter JB, Cohen M, Delli-Santi M, Fennell C, Leinberry C, Husband J, Ladd A, Seitz WR, Constanz B. 2003. Norian SRS cement compared with conventional fixation in distal radial fractures: a randomized study. *J Bone Joint Surg* **85**:2127–2137.

Cavalheiro JJ, Bronco R, Afonso A, Vasconcerlos M. 1995. Multilayer coating of stainless steel with insoluble and bioactive glasses: "in vitro" and "in vivo" tests. In *Bioceramics*, Vol. 8, pp. 509–512. Ed J Wilson, LL Hench, D Greenspan. Oxford: Pergamon/Elsevier Science.

Chang B-S, Lee CK, Hong K-S, Youn H-J, Ryu H-S, Chung S-S, Park K-W. 2000. Osteoconduction at porous hydroxyapatite with various pore configurations. *Biomaterials* **21**:1291–1298.

Chang Y-L, Lew D, Park JB, Keller JC. 1999. Biomechanical and mophometric analysis of hydroxyapatite-coated implants with varying crystallinity. *J Oral Maxillofac Surg* **57**:1096–1108.

Chen C, Knapp W. 1974. Fatigue fracture of a alumina ceramic at several temperatures. In *Fracture mechanics of ceramics*, pp. 691–707. Ed RC Bradt, DPH Hasselman, FF Lange. New York: Plenum.

Chen F, Mao T, Tao K, Chen L, Ding M, Cu X. 2002. Bone graft in the shape of human mandibular condyle reconstruction via seeding marrow-derived osteoblasts into porous coral in a nude mice model. *J Oral Maxillofac Surg* **60**:1155–1159.

Chen G, Ushida T, Tateishi T. 2001. Poly(DL-lactic-co-glycolic acid) sponge hybridized with collagen microsponges and deposited apatite particulates. *J Biomed Mater Res* **57**:8–14.

Chim H, Hutmacher DW, Chou AM, Reis RL, Lim TC, Schantz J-T. 2006. A comparative analysis of scaffold material modifications for load-bearing applications in bone tissue engineering. *Int J Oral Maxillofac Surg* **35**:928–934.

Chiroff RT, White EW, Weber JN, Roy DM. 1975. Tissue ingrowth of replamineform implants. *J Biomed Mater Res Symp* **6**:29–45.

Chiroff RT, White RA, White EW, Weber JE, Roy DM. 1977. The restoration of articular surfaces overlying replamineform porous biomaterials. *J Biomed Mater Res* **11**:168–178.

Christel P, Meunier A, Heller M, Torre JP, Peille CN. 2004. Mechanical properties and short-term in vivo evaluation of yttrium-oxide partially stabilized zirconia. *J Biomed Mater Res* **23**:45–61.

Christensen RM. 1979. *Mechanics of composite materials*. New York: Wiley.

Chu TM, Orton DO, Hollister SJ, Feinberg SE, Halloran JW. 2002. Mechanical and in vivo performance of hydroxyapatite implants with controlled architectures. *Biomaterials* **23**:1283–1293.

Chvapil M. 1967. *Physiology of connective tissue*. London: Butterworths.

Cima LG, Vacanti JP, Vacanti C, Inger D, Mooney DJ, Langer R. 1991. Tissue engineering by cell transplantation using degradable polymer substrates. *J Biomech Eng-T ASTM* **113**:143–151.

Clarke IC, Manaka M, Green DD, Williams P, Pezzotti G, Kim YH, Ries M, Sugano N, Sedel L, Delauney C, Nissan BB, Donaldson T, Gustafson GA. 2003. Current status of zirconia used in total hip implants. *J Bone Joint Surg* **85**:73–84.

Clupper D, Hench LL. 2001. Bioactive responses of Ag-doped tape coat Bioglass® 45S5 following heat treatment. *J Mater Sci: Mater Med* **12**:917–921.

Coble RL, Kingery WD. 1956. Effect of porosity on physical properties of sintered alumina. *J Am Ceram Soc* **39**:377–385.

Cook SD, Kay JF, Thomas KA, Jarcho M. 1987. Interface mechanics and histology of titanium and hydroxyapatite coated titanium for dental implant applications. *J Oral Maxillofac Implants* **12**:15–22.

Cowin S. 1981. *Mechanical properties of bone*. New York: ASME.

Cowland F, Lewis J. 1967. Vitreous carbon: a new form of carbon. *J Mater Sci* **2**:507–512.

Currey JD. 1981. What is bone for? property–function relationships in bone. In *Mechanical properties of bone*, pp. 13–26. Ed SC Cowin. New York: ASME.

Cutright DE, Bhaskar SN, Brady JM, Getter L, Posey WR. 1972. Reaction of bone to tricalcium phosphate ceramic pellets. *Oral Surg* **33**:850–856.

Dai KR, Liu YK, Park JB, Clark CR, Nishiyama K, Zheng ZK. 1991. Bone-particle-impregnated bone cement: An in vivo weight-bearing study. *J Biomed Mater Res* **25**:141–156.

Dalgeish BJ, Rawling RD. 1981. A comparison of the mechanical behavior of aluminas in air and simulated body environments. *J Biomed Mater Res* **15**:527–542.

Damen JJM, TenCate JM. 1989. The effect of silicic acid on calcium phosphate preparation. *J Dent Res* **68**:1355–1359.

Davidson JA, Mishra AK. 1992. Surface modification issues for orthopaedic implant bearing surfaces. In *Proc. 5th international conference on surface modification technologies*, pp. 1–14. Ed TS Sudarshan, JF Braza. Birmingham, UK: Institute of Metals.

Day DE, Day TE. 1993. Radiotherapy glasses. In *An introduction to bioceramics*, pp. 305–317. Ed LL Hench, J Wilson. Singapore: World Scientific.

Dearnaley G. 1993. Diamond-like carbon: a potential means of reducing wear in total joint replacements. *Clin Mater* **12**:237–244.

De Aza AH, Chevalier J, Fantozzi G, Schehl M, Torrecillas R. 2002. Crack growth resistance of alumina, zirconia and zirconia toughened alumina ceramics for joint prostheses. *Biomaterials* **23**:937–945.

Decheyne P, de Groot K. 1981. In vivo surface activity of a hydroxyapatite alveolar bone substitute. *J Biomed Mater Res* **15**:441–445.

deLange GL. 1990. The bone–hydroxylapatite interface. In *Handbook of bioactive ceramics*, Vol. 1: *Calcium phosphate and hydroxylapatite ceramics*, pp. 61–75. Ed T Yamamuro, LL Hench, J Wilson. Boca Raton, FL: CRC Press.

Dempster WT, Coleman RF. 1961. Tensile strength of bone along and across the grain. *J Appl Physiol* **16**:355.

Dempster WT, Liddicoat RT. 1952. Compact bone as a nonisotropic material. *Am J Anat* **91**:331–362.

Derand P, Derand T. 2000. Bond strength of luting cements to zirconium oxide ceramics. *Int J Prosthodont* **13**:131–135.

Dion I, Roques X, Baquey C, Baudet E, Cathalinat BB, More N. 1993. Hemocompatibility of diamond-like carbon coating. *Biomed Mater Eng* **3**:51–55.

Donaldson K, Aitken R, Tran L, Stone V, Duffin R, Forrest G, Alexander A. 2006. Carbon nanotubes: a review of their properties in relation to pulmonary toxicology and workplace safety. *Toxicol Sci* **92**:5–22.

Dong J, Kojima H, Uemura T, Kikuchi M, Tateishi T, Tanaka J. 2001. In vivo evaluation of a novel porous hydroxyapatite to sustain osteogenesis of transplanted bone marrow-derived osteoblastic cells. *J Biomed Mater Res* **57**:208–211.

Doremus RH. 1973. *Glass science*. New York: Wiley.

Dorre E, Dawihl W. 1980. Ceramic hip endoprostheses. In *Mechanical properties of biomaterials*, pp. 113–127. Ed GW Hastings, DF Williams. New York: Wiley.

Dorre E, Hubner H. 1984. *Alumina*. Berlin: Springer-Verlag.

Drennan J, Steele BCH. 1986. Zirconia and hafnia. In *Encyclopedia of materials science and engineering*, pp. 5542–5545. Ed MB Beaver. Cambridge: MIT Press.

Driskell TD. 1994. Early history of calcium phosphate materials and coatings. In *Characterization and performance of calcium phosphate coatings for implants*, pp. 1–8. Ed E Horowitz, J Parr. Philadelphia: American Society for Testing and Materials.

Drummond JL. 1989. In vivo aging of yttria-stabilized zirconia. *J Am Ceram Soc* **72**:675–676.

Ducheyne P, Hench LL, Kagan A. 1980. Effect of hydroxyapatite impregnation on skeletal bonding of porous coated implants. *J Biomed Mater Res* **14**:225–237.

Ducheyne P, Marcolongo M, Schepers E. 1993. Bioceramic composites. In *Introduction to bioceramics*, pp. 281–297. Ed LL Hench, J Wilson. Singapore: World Scientific.

Eanes E, Posner A. 1965. Kinetics and mechanisms of conversion of non-crystalline calcium phosphate to crystalline hydroxyapatite. *Trans NY Acad Sci* **28**:233–241.

El-Ghannam AR. 2004. Advanced bioceramic composite for bone tissue engineering: design principles and structure–bioactivity relationship. *J Biomed Mater Res* **69**:490–501.

Engelberg I, Kohn J. 1991. Physicomechanical properties of degradable polymers used in medical applications: a comparative study. *Biomaterials* **12**:292–304.

Engh CA, Bobyn JD. 1988. Results of porous coated hip replacement using the AML prosthesis. In *Noncemented total hip arthroplasty*, p. 393. Ed RJ Fitzgerald. New York: Raven Press.

Eriksson C. 1974. Streaming potentials and other water-dependent effects in mineralized tissue. *Ann NY Acad Sci* **238**:321–338.

Ernst CP, Cohen U, Stender E, Willershausen B. 2005. In vitro retentive strength of zirconium oxide ceramic crowns using different luting agents. *J Prosthet Dent* **93**:551–558.

Evans A, San Marchi C, Mortensen A. 2003. *Metal matrix composites in industry: an introduction and a survey*. New York: Springer.

Evans FG. 1973. *Mechanical properties of bones*. Springfield, IL: Thomas.

Evans FG, Lebow M. 1952. The strength of human compact bone as revealed by engineering technics. *Am J Surg* **83**:326–331.

Eysel W, Roy DM. 1973. Hydrothermal flux growth of hydroxyapatites by temperature oscillation. *J Crystal Growth* **20**:245–250.

Feng SS, Rocket TJ. 1979. The system CaO–P_2O_5–H_2O at 200°C. *J Am Ceram Soc* **62**:619–620.

Filiaggi MJ, Pilliar RM. 1993. Evaluating sol-gel zirconia thin films for implant applications. In *Bioceramics*, Vol. 6, pp. 265–270. Ed P Ducheyne, D Christiansen. Oxford: Pergamon.

Filiaggi MJ, Coombs NA, Pilliar RM. 1991. Characterization of the interface in the plasma-sprayed HA coating/Ti–6AI–4V implant system. *J Biomed Mater Res* **25**:1211–1229.

Fini M, Giavaresi G, Aldini NN, Torricelli P, Botter R, Beruto D, Giardino R, 2002. A bone substitute composed of polymethylmethacrylate and alpha-tricalcium phosphate: results in terms of osteoblast function and bone tissue formation. *Biomaterials* **23**:4523–4531.

Fisher J. 1996. New ways to heal fractures enter market in the works. *Orthop Today* **16**(1):24–26.

Flautre B, Descamps M, Delecourt C, Blary MC, Hardouin P. 2001. Porous HA ceramic for bone replacement: role of the pores and interconnections: experimental study in the rabbit. *J Mater Sci: Mater Med* **12**:679–682.

Frakes J, Brown S, Kenner G. 1974. Delayed failure and aging of porous alumina in water and physiological medium. *Am Ceram Soc Bull* **53**:193–197.

Friedenberg Z, Brighton C. 1966. Bioelectric potential in bone. *J Bone Joint Surg* **48A**:915–923.

Friedman C, Costantino PD, Takagi S, Chow LC. 1998. BoneSource hydroxyapatite cement: a novel biomaterial for craniofacial skeletal tissue engineering and reconstruction. *J Biomed Mater Res* **43**:428–432.

Fung YC. 1981. *Biomechanics: mechanical properties of living tissues*. Berlin: Springer-Verlag.

Galois L, Mainard D. 2004. Bone ingrowth into two porous ceramics with different pore sizes: an experimental study. *Acta Orthop Belg* **70**:598–603.

Geduldig D, Lade R, Prussner P, Willert H-G, Zichner L, Dorre E. 1976. Experimental investigations of dense alumina ceramic for hip and knee joint replacements. In *Advances in artificial hip and knee joint technology*, *Engineering in medicine*, Vol. 2, pp. 434–445. Ed M Schaldach, D Hohmann. Berlin: Springer-Verlag.

Gibson LJ, Ashby MF. 1997. *Cellular solids*, 2nd ed. Oxford: Pergamon.

Gill R. 1972. *Carbon fibres in composite materials*. London: Butterworths.

Gilmore R, Pollack R, Katz J. 1970. Elastic properties of bovine dentine and enamel. *Arch Oral Biol* **15**:787–796.

Gitzen WH. 1970. *Alumina as a ceramic material*. Columbus, OH: American Ceramic Society.

Gorga MP, Neely ST. 1994. Stimulus calibration in auditory evoked potential measurements. In *Principles and applications in auditory evoked potentials*, pp. 85–97. Ed JT Jacobson. Needham Heights, MA: Allyn and Bacon.

Götz HE, Müller M, Emmel A, Holzwarth U, Erben RG, Stangl R. 2004. Effect of surface finish on the osseointegration of laser-treated titanium alloy implants. *Biomaterials* **25**:4057–4064.

Grenoble D. 1972. The elastic properties of hard tissues and apatites. *J Biomed Mater Res* **6**:221–233.

Griffith A. 1920. The phenomena of rupture and flow in solids. *Philos Trans Roy Soc London Ser A* **221**:163–198.

Grill A. 2003. Diamond-like carbon coatings as biocompatible materials: an overview. *Diamond Relat Mater* **12**:166–170.

Griss P, Greenspan D, Heimke G, Krenpien B, Buchinger R, Hench L, Jentchura G. 1976. Evaluation of a Bioglass-coated Al_2O_3 total hip prosthesis in sheep. *J Biomed Mater Res Symp* **7**:511–518.

Gross J. 1961. Collagen. *Sci Am* **204**:121–130.

Grynpas MD, Pilliar RM, Kandel RA, Renlund R, Filiaggi M, Dumitriu M. 2002. Porous calcium polyphosphate scaffolds for bone substitute applications in vivo studies. *Biomaterials* **23**:2063–2070.

Guyer DW, Wiltse LL, Peek RD. 1988. The Wiltse pedicle screw system. *Orthopedics* **11**:1455–1460.

Ha S-W, Mayer J, Wintermantel E. 1993. Micro-mechanical testing of hydroxyapatite coatings on carbon fiber reinforced thermoplastics. In *Bioceramics*, Vol. 6, pp. 489–493. Ed P Ducheyne, D Christiansen. Oxford: Pergamon.

Haldeman KO, Moore JO. 1934. Influence of a local excess of calcium and phosphate on the healing of fractures. *Arch Surg* **29**:385–396.

Ham A, Harris W. 1971. Repair and transplantation of bone. In *The biochemistry and physiology of bone*, pp. 337–399. Ed G Bourne. New York: Academic Press.

Hamadouche M, Sedal L. 2000. Ceramics in orthopaedics. *J Bone Joint Surg* **82**:1095–1099.

Hannouche D, Hamadouche M, Nizard R, Bizot P, Meunier A, Sedel L. 2005. Ceramics in total hip replacement. *Clin Orthop Relat Res* **430**:62–71.

Haraguchi K, Sugano N, Nishii T, Miki H, Oka K, Yoshikawa H. 2001. Phase transformation of a zirconia ceramic head after total hip arthroplasty. *J Bone Joint Surg* **83**:996–1000.

Harbers GM, Grainger DW. 2006. Cell-materials interactions: Fundamental design issues for tissue engineering and clinical consideration. In *An introduction to biomaterials*, pp. 15–45. Ed SA Guelcher. Boca Raton, FL: CRC Press, Taylor & Francis Group.

Harris B, Bunsell A. 1977. *Structure and properties of engineering materials*. London: Longmans.

Haubold A, Shim H, Bokros J. 1979. Carbon cardivascular devices. In *Assisted circulation*, pp. 520–532. Ed F Unger. New York: Academic Press.

Haubold AD, Yapp RA, Bokros JC. 1986. Carbons for biomedical applications. In *Encyclopedia of materials science and engineering*, pp. 514–520. Ed MB Beaver. Oxford: Pergamon/MIT Press.

Hauert R. 2003. A review of modified DLC coatings for biological applications. *Diamond Relat Mater* **12**:583–589.

Hench LL. 1994. Bioactive ceramics: theory and clinical applications. In *Bioceramics*, Vol. 7, pp. 3–14. Ed OH Andersson, R-P Happonen, A Yli-Urpo. Oxford: Pergamon/Elsevier Science.

Hench LL, Andersson O. 1993. Bioactive glass coatings. In *Introduction to bioceramics*, pp. 239–259. Ed LL Hench, J Wilson. Singapore: World Scientific.

Hench LL, Clark AE. 1982. Adhesion to bone. In *Biocompatibility of Orthopedic Implants*, Vol. 1, pp. 129–170. Ed DF Williams. Boca Raton, FL: CRC Press.

Hench L, Ethridge E. 1975. Biomaterials: the interfacial problem. *Adv Biomed Eng* **5**:35–150.

Hench LL, Ethridge EC. 1982. *Biomaterials: an interfacial approach*. New York: Academic Press.

Hench L, Pachall H. 1973. Direct chemical bond of bioactive glass-ceramic materials to bone and muscle. *J Biomed Mater Res Symp* **2**:5–42.

Hench LL, Polak JM. 2002. Third generation biomedical materials. *Science* **295**:1014–1017.

Hench LL, Wilson J, eds. 1993. *An Introduction to bioceramics*, pp. 1–24. Singapore: World Scientific.

Hench L, Splinter R, Allen W. 1971. Bonding mechanisms at the interface of ceramic prosthetic materials. *J Biomed Mater Symp* **2**:117–141.

Henrich DE, Cram AE, Park JB, Liu YK, Reddi H. 1993. Inorganic bone and bone morphogenetic protein impregnated bone cement: a preliminary in vivo study. *J Biomed Mater Res* **27**:277–280.

Hernigou P, Bahrami T. 2003. Zirconia and alumina ceramics in comparison with stainless-steel heads. *J Bone Joint Surg* **85**:504–509.

Heughebaert M, LeGeros RZ, Gineste M, Guilhem A, Bone G. 1988. Physico-chemical characterization of deposits associated with HA ceramics implanted in non-osseous sites. *J Biomed Mater Res* **22**:254–268.

Hill D. 1998. *Design engineering of biomaterials for medical devices*. New York: Wiley.

Hiratzka LF, Goeken JA, White RA, Wright CB. 1979. In vivo comparison of replamineform silastic and bioelastic polyurethane arterial grafts. *Arch Surg* **114**:698–702.

Hoexter DL. 2002. Bone regeneration graft materials. *J Oral Implantol* **28**:290–204.

Hohling H, Ashton B, Koster H. 1974. Quantitative electron microscope investigation of mineral nucleation in collagen. *Cell Tissue Res* **148**:11–26.

Hohling HJ, Barckhaus RH, Krefting ER, Althoff J, Quint P. 1990. Collagen mineralization: aspects of the structural relationship between collagen and apatite crystallites. In *Ultrastructure of skeletal tissues: bone and cartilage in health and disease*, pp. 41–62. Ed E Bonucci, PM Morra. Boston: Kluwer Academic Publishers.

Holand W, Rheinberger V, Apel E, Hoen CV, Holand M, Dommann A, Obrecht M, Mauth C, Graf-Hausner U. 2006. Clinical applications of glass-ceramics in dentistry. *J Mater Sci: Mater Med* **17**:1037–1042.

Holand W, Vogel W. 1993. Machinable and phosphate glass-ceramic. In *Introduction to Bioceramics*, pp. 125–137. Ed LL Hench, J Wilson. Singapore: World Scientific.

Hollinger JO, Buck DC, Bruder SP. 1999. Biology of bone healing: its impact on clinical therapy. In *Tissue engineering: applications in maxillofacial surgery and periodontics*, pp. 17–53. Ed SF Lynch, RJ Genco, RE Marx. Chicago: Quintessence.

Hollinger JO, Brekke J, Gruskin E, Lee D. 1996. Role of bone substitutes. *Clin OrthopRelat Res* **324**:55–65.

Hollinger JO, Einhorn TA, Doll B, Sfeir C. 2004. *Bone tissue engineering*. Boca Raton, FL: CRC Press.

Hollinger JO, Schmitz JP, Mizgala JW, Hassler C. 1989. An evaluation of two configurations of tricalcium phosphate for treating craniotomies. *J Biomed Mater Res* **23**:17–29.

Holmes R. 1979. Bone regeneration within a coralline hydroxyapatite implant. *Plast Reconstr Surg* **63**:626–633.

Holmes RE, Bucholz RW, Mooney V. 1987. Porous hydroxyapatite as a bone graft substitute in diaphyseal defects: a histometric study. *J Orthop Res* **5**:114–121.

Holmes R, Mooney V, Bucholz R, Tencer A. 1984. A coralline hydroxyapatite bone graft substitute: preliminary report. *Clin Orthop Relat Res* **188**:252–284.

Homsy CA, Prewitt III JM, Kessler FB, Andeson MS. 1978. Observation of traumatically induced articular surface defects using a porous implant material. In *Transactions of the 4th annual meeting of the society for biomaterials*, p. 85. New York: Wiley.

Hubbard WG, Hirthe WM, Mueller KH. 1973. Physiological calcium phosphate implants. *Proc 26th Ann Conf Eng Biol Med, Bioeng* **15**:199.

Hulbert SF, Klawitter JJ. 1976. Ceramics as a new approach to the improvement of artificial joints. In *Advances in artificial hip and knee joint technology*, Engineering in Medicine Vol. 2, pp. 287–293. Ed M Schaldach, D Hohmann. Berlin: Springer-Verlag.

Hyakuna K, Yamamuro T, Kotura Y, Oka M, Nakamura T, Kitsugi T, Kokubo T, Kushitani H. 1990. Surface reactions of calcium phosphate ceramics to various solutions. *J Biomed Mater Res* **24**:471–488.

Inglis C. 1913. Stress in a plate due to the pressure of cracks and sharp corners. *Trans Inst Naval Arch* **55**:219–230.

Ioku K, Somiya S, Yoshimura M. 1989. Dense/porous layered apatite ceramics prepared by HIP post-sintering. *J Mater Sci Lett* **8**:1203–1204.

Ioku K, Yoshimura M, Somiya S. 1988. Post-sintering of apatite ceramics from fine powders synthesized under hydrothermal conditions [in Japanese]. *J Ceram Soc* **96**:109–110.

Ioku K, Yoshimura M, Somiya S. 1990. Microstructure and mechanical properties of hydroxyapatite ceramics with zirconia dispersion prepared by post-sintering. *Biomaterials* **11**:57–61.

Ishimura M, Ohgushi H, Inoue K, Simaya M, Tatnai S. 1995. Hydroxyapatite and A-W glass-ceramic spacer for knee joint surgery-Applications of bioactive ceramic spacer for patello-femoral osteoarthritis. In *Bioceramics*, Vol. 8, pp. 177–183. Ed J Wilson, LL Hench, D Greenspan. Oxford: Pergamon/Elsevier Science.

Itälä AI, Ylänen HO, Ekholm C, Karlsson KH, Aro HT. 2001. Pore diameter of more than 100 mm is not requisite for bone ingrowth in rabbits. *J Biomed Mater Res* (*Appl Biomater*) **58**:679–683.

Itch M, Shimazu A, Hirata I, Yoshida Y, Shintani H, Okazaki M. 2004. Characterization of CO3Ap-collagen sponges using x-ray high-resolution microtomography. *Biomaterials* **25**:2577–2583.

Jaglinski T, Kochman D, Stone D, Lakes RS. 2007. Composite materials with viscoelastic stiffness greater than diamond. *Science* **315**:620–622.

Jarcho M. 1981. Calcium phosphate ceramics as hard tissue prosthetics. *Clin Orthop Relat Res* **157**:259–278.

Jarcho M, Bolen C, Thomas M, Bobick J, Kay J, Doremus H. 1976. Hydroxyapatite synthesis and characterization in dense polycrystalline form. *J Mater Sci* **11**:2027–2035.

Jin QM, Takita H, Kohgo TK, A. Itoh H, Kuboki Y. 2000. Effects of geometry of hydroxyapatite as a cell substratum in BMP-induced ectopic bone formation. *J Biomed Mater Res* **51**:491–499.

Jockisch KA, Brown SA, Bauer TW, Merritt K. 1992. Biological response to chopped-carbon-fiber-reinforced PEEK. *J Biomed Mater Res* **26**:133–146.

Jones JJ. 2006. Biomaterials: bioceramics. In *Encyclopedia of medical devices and instrumentation*, pp. 283–296. Ed JG Webster. Hoboken, NJ: Wiley.

Jongejan A, Wilkins ALJ. 1970. A re-examination of the system CaO–TiO_2 at liquidus temperatures. *Less-Common Met* **20**:273–279.

Kaae J. 1971. Structure and mechanical properties of isotropic pyrolytic carbon deposited below 1600°. *J Nucl Mater* **38**:42–50.

Kakar S, Einhorn TA. 2005. Tissue engineering of bone. In *An introduction to biomaterials*, pp. 417–440. Ed SA Guelcher, JO Hollinger. Boca Raton, FL: CRC Press, Taylor & Francis Group.

Kakutani Y, Yamamuro T, Kotoura Y, Kitsugi T, Hyyakuna K, Saito T, Kitaoji M, Noda I, Makinouchi K. 1988. Granular ceramic coating on alumina. In *Orthopedic ceramic implants*. Ed H Oonishi, Y Obi. Kyoto: Japanese Society of Orthopedic Ceramic Implants.

Kamitakahara M, Ohtsuki C, Inada H, Tanihara M, Miyazaki T. 2006. Effect of ZnO addition on bioactive CaO–SiO_2–P_2O_5–CaF_2 glass-ceramics containing apatite and wollastonite. *Acta Biomater* **2**:467–71.

Karageorgiou V, Kaplan D. 2005. Porosity of 3D biomaterial scaffolds and osteogenesis. *Biomaterials* **26**:5474–5491.

Kato K, Aoki H, Tabata T, Ogiso M. 1979. Biocompatibility of apatite ceramics in mandibles. *Biomater Med Devices Artif Organs* **7**:291–297.

Katz JL, Harper A. 1986. Calcium phosphates and Apatites. In *Encyclopedia of materials science*, pp. 474–481. Ed MB Beaver. Oxford: Pergamon Press.

Kawahara H, Hirabayashi M, Shikita T. 1980. Single crystal alumina for dental implants and bone screws. *J Biomed Mater Res* **14**:597–606.

Kay JF. 1992. Calcium phosphate coatings for dental implants: current status and future potential. *Dent Clin North Am* **36**:1–18.

Keeting F. 1956. *Chromium-nickel autentic steels*. London: Butterworths.

Keller DJ, Prendergast PJ. 2006. Prediction of the optimal mechanical properties for a scaffold used in osteochondral defect repair. *Tissue Eng* **12**:2509–2519.

Keller JC. 1995. Dental implants: the relationship of materials characteristic to biologic properties. In *The biomedical engineering handbook*, pp. 691–703. Ed JD Bronzino. Boca Raton, FL: CRC Press.

Ketenjian A, Arsenis C. 1975. Morphological and biochemical studies during differentiation and calcification of fracture callus cartilage. *Clin Orthop Relat Res* **107**:266–273.

Khang G. 2006. Biomaterials: tissue engineering and scaffolds. In *Encyclopedia of medical devices and instrumentation*, pp. 366–383. Ed JG Webster. Hoboken, NJ: Wiley.

Kim HW, Knowles JC, Kim HE. 2004. Hydroxyapatite/poly(epsilon-caprolactone) composite coatings on hydroxyapatite porous bone scaffold for drug delivery. *Biomaterials* **25**:1279–1287.

Kim SS, Ahn KM, Park MS, Lee JH, Choi CY, Kim BS. 2007. A poly(lactide-co-glycolide)/hydroxyapatite composite scaffold with enhanced osteoconductivity. *J Biomed Mater Res* **80A**:206–215.

King BG, Showers MJ. 1963. *Human anatomy and physiology*. Philadelphia: Saunders.

Kingery WD, Bowen HK, Uhlmann DR. 1976. *Introduction to ceramics*, 2nd ed, pp. 3–20. New York: Wiley.

Kitsugi T, Yamamuro T, Nakamura T, Kokubo T, Takagi M, Shibuya T, Takeuchi H, Ono M. 1987. Bonding behavior between two bioactive ceramics. *J Biomed Mater Res* **21**:1109–1123.

Klumpp C, Kostarelos K, Prato M, Bianco A. 2006. Functionalized carbon nanotubes as emerging nanovectors for the delivery of therapeutics. *Biochim Biophys Acta* **1758**:404–12.

Knackstedt MA, Arns CH, Senden TJ, Gross K. 2006. Structure and properties of clinical coralline implant measured via 3D imaging and analysis. *Biomaterials* **27**:2776–2786.

Kohn J, Langer R. 1996. Bioresorbable and bioerodible materials. In *Biomaterials science: an introduction to materials in medicine*, pp. 64–73. Ed BD Ratner, AS Hoffman, FJ Schoen, JE Lemons. San Diego: Academic Press.

Kokubo T, Ito S, Shigematsu M, Sakka S, Yamamuro T. 1985. Mechanical properties of a new type of apatite-containing glass-ceramic for prosthetic applications. *J Mater Sci* **20**:2001–2004.

Kong YM, Bae CJ, Lee SH, Kim HW, Kim HE. 2005. Related articles: improvement in biocompatibility of ZrO_2–Al_2O_3 nanocomposite by addition of HA. *Biomaterials* **26**:509–517.

Kovacs P. 1993. In vitro studies of the electrochemical behavior of carbon-fiber composites. In *Composite materials for implant applications in the human body: characterization and testing*, pp. 41–52. Ed RD Jamison, LN Gilbertson. Philadelphia: American Society for Testing and Materials.

Krainess F, Knapp W. 1978. Strength of a dense alumina ceramic after aging in vitro. *J Biomed Mater Res* **12**:241–246.

Kruyt MC, de Bruijn JD, Wilson CE, Oner FC, van Blitterswijk CA, Verbout AJ, Dhert WJA. 2003. Viable osteogenic cells are obligatory for tissue-engineered ectopic bone formation in goats. *Tissue Eng* **9**:327–336.

Kuboki Y, Jin Q, Kikuchi MJ, Takita H. 2002. Geometry of artificial ECM: sizes of pores controlling phenotype expression in BMP-induced osteogenesis and chondrogenesis. *Connect Tissue Res* **43**:529–534.

Kuboki Y, Jin Q, Takita H. 2001. Geometry of carriers controlling phenotypic expression in BMP-induced osteogenesis and chondrogenesis. *J Bone Joint Surg Am* **83A** (Suppl 1, Pt 2):S105–S115.

Kuboki Y, Takita H, Kobayashi D, Tsuruga E, Inoue M, Murata M, Nagai N, Dohi Y, Ohgushi H. 1998. BMP-induced osteogenesis on the surface of hydroxyapatite with geometrically feasible and nonfeasible structures: topology of osteogenesis. *J Biomed Mater Res* **39**:190–199.

Kumar P, Shimizu K, Oka M. 1991. Low wear rate of UHMWPE against zirconia ceramic (Y-PSZ) in comparison to alumina ceramic and SUS 316L alloy. *J Biomed Mater Res* **25**:813–828.

Lakes RS. 1993. Materials with structural hierarchy. *Nature* **361**:511–515.

Lakes RS. 2006. Properties of bone and teeth. In *Encyclopedia of medical devices and instrumentation*, pp. 523–540. Ed JG Webster. Hoboken, NJ: Wiley.

Landi E, Celotti G, Logroscino G, Tampieri A. 2003. Carbonated hydroxyapatite as bone substitute. *J Eur Ceram Soc* **23**:2931–2937.

Landi E, Tampieri A, Celotti G, Sprio S. 2000. Densification behaviour and mechanisms of synthetic hydroxyapatites. *J Eur Ceram Soc* **20**:2377–2387.

Laney WR, Tolman DE. 1990. Tissue integration in oral and maxillofacial reconstruction. Chicago: Quintessence.

Lanza R, Langer R, Vacanti J. 2007. *Principles of tissue engineering*, 3rd ed. San Diego: Academic Press.

Larmas E, Sewon L, Luostarinen T, Kamgasniemi I, Yli-Urpo A. 1995. Bioactive glass in periodontal bone defects. Initial clinical findings of soft tissue and osseous repair. In *Bioceramics*, Vol. 8, pp. 279–284. Ed J Wilson, LL Hench, D Greenspan. Oxford: Pergamon/Elsevier Science.

Laurencin CT, Yusuf Khan Y. 2005. Bone graft substitute materials. http://www.emedicine.com/orthoped/topic611.htm, eMedicine from WebMD.

Laurencin CT, Ambrosio AA, Borden MD, Cooper J., 1999. Tissue engineering: orthopaedic applications. *Annu Rev Biomed Eng* **19**:19–46.

Laurencin CT, Attawia MA, Lu LQ. 2001. Poly(lactide-co-glycolide)/hydroxyapatite delivery of BMP-2-producing cells: a regional gene therapy approach to bone regeneration. *Biomaterials* **22**:1271–1277.

Laurencin C, Khan Y, El-Amin SF. 2006. Bone graft substitutes. *Expert Rev Med Devices* **3**:49–57.

Laurencin CT, Khan Y, Kofron M, El-Amin S, Botchwey E, Yu X, Cooper JAJ. 2006. The ABJS Nicolas Andry award: tissue engineering of bone and ligament: a 15-year perspective. *Clin Orthop Relat Res* **447**:221–236.

Lee GH, Khoury JG, Bell JE, Buckwalter JA. 2002. Adverse reactions to OsteoSet bone graft substitute, the incidence in a consecutive series. *Iowa Orthop J* **22**:35–38.

Lee YM, Seol YJ, Lim YT, Kim S, Han SB, Rhyu IC, Baek SH, Heo SJ, Choi JY, Klokkevold PR, Chung CP. 2001. Tissue-engineered growth of bone by marrow cell transplantation using porous calcium metaphosphate matrices. *J Biomed Mater Res* **54**:216–23.

Lei D, Wardlaw D, Hukins DWL. 2006. Mechanical properties of calcium sulphate/hydroxyapatite cement. *Biomed Mater Eng* **16**:423–428.

LeGeros RZ. 1967. *Crystallographic studies of the carbonate substitution in the apatite structure*. New York: New York UP.

LeGeros RZ. 1981. Apatites in biological systems. *Prog Crystal Growth Charact Mater* **4**:1–45.

LeGeros RZ. 1991. Calcium phosphates in oral biology and medicine. In *Monographs in Oral Sciences*, Vol. 15, pp. 151–201. Ed H Myers. Basel: Karger.

LeGeros RZ. 1993. Biodegradation and bioresorption of calcium phosphate ceramics. *J Clin Mater* **14**:65–88.

LeGeros RZ. 1994. Biological and synthetic apatites. In *Hydroxyapatite and related materials*, pp. 3–28. Ed PW Brown, B Constantz. Boca Raton, FL: CRC Press.

LeGeros RZ, Daculsi G. 1990. In vivo transformation of biphasic calcium phosphate ceramics: ultrastructural and physicochemical characterizations. In *Handbook of Bioactive Ceramics*, pp. 17–28. Ed T Yamamuro, LL Hench, J Wilson. Boca Raton, FL: CRC Press.

LeGeros RZ, Suga S. 1980. Crystallographic nature of fluoride in the enameloids of fish. *Calcif Tissue Int* **32**:169–174.

LeGeros RZ, Daculsi G, Orly I, Gregoire M. 1991. Substrate surface dissolution and interfacial biological mineralization. In *The bone–biomaterial interface*, pp. 76–88. Ed JE Davis. Toronto: U Toronto P.

LeGeros RZ, LeGeros JP, Daculsi G, Kijkowska R. 1995. Calcium phosphate biomaterials: preparation, properties, and biodegradation. In *Encyclopedic handbook of biomaterials and bioengineering*, Part A: *Materials*, pp. 1429–1463. Ed DL Wise, DJ Trantolo, DE Altobelli, MJ Yaszemski, JD Gresser, ER Schwartz. New York: Marcel Dekker.

LeGeros RZ, Zheng R, Kijkowska R, Fan D, LeGeros JP. 1994. Variation in composition and crystallinity of "hydroxyapatite (HA)" preparation. In *Characterization and performance of calcium phosphate coatings for implants*, pp. 43–53. Ed E Horowitz, J Parr. Philadelphia: American Society for Testing and Materials.

Leinfelder KF, Bayne SC, Swift Jr EJ. 1999. Packable composites: overview and technical considerations. *J Esthet Dent* **11**:234–249.

Lenza RFS, Jones JR, Vasoconcelos WL, Hench LL. 2003. In vitro release kinetics of proteins from bioactive foams. *J Biomed Mater Res* **57A**:121–129.

Li J, Hermansson L, Soremark R. 1993. High-strength biofunctional zirconia: mechanical properties and static fatigue behaviour of zirconia–apatite composites. *J Mater Sci: Mater Med* **4**:50–54.

Li S, De Wijn JR, Li J, Layrolle P, De Groot K. 2003. Macroporous biphasic calcium phosphate scaffold with high permeability/porosity ratio. *Tissue Eng* **9**:535–548.

Liao S, Watari F, Zhu Y, Uo M, Akasaka T, Wang W, Xu G, Cui F. 2007. The degradation of the three layered nano-carbonated hydroxyapatite/collagen/PLGA composite membrane in vitro. *Dent Mater* **23**:1120–1128.

Liboff AB. 2006. Electrical treatment of bone-united fracture and spinal fusion. In *Encyclopedia of medical devices and instrumentation*, pp. 558–571. Ed JG Webster. Hoboken, NJ: Wiley.

Lickorish D, Ramshaw JA, Werkmeister JA, Glattauer V, Howlett CR. 2004. Collagen–hydroxyapatite composite prepared by biomimetic process. *J Biomed Mater Res* **68**:19–27.

Lin CY, Kikuchi N, Hollister SJ. 2004. A novel method for biomaterial scaffold internal architect design to match bone elastic properties with desired porosity. *J Biomech* **37**:623–636.

Litkowski LJ, Niehaus-Rohde C. 1995. Comparison of pulpal inflammatory response using calcium hydroxide versus particulate Bioglass® in human teeth. In *Bioceramics*, Vol. 8, pp. 289–293. Ed J Wilson, LL Hench, D Greenspan. Oxford: Pergamon/Elsevier Science.

Liu YK, Park JB, Njus GO, Stienstra D. 1987. Bone particle impregnated bone cement, I: in vitro study. *J Biomed Mater Res* **21**:247–261.

Losee FL, Hurley LA. 1956. Bone treated with ethylenediamine as a successful foundation material in cross-species bone grafts. *Nature* **177**:1032–1033.

Low SB, King CJ, Krieger J. 1997. An evaluation of bioactive ceramic in the treatment of periodontal osseous defects. *Intern J Periodont Restor Dent* **17**:359–367.

Ma L, Sines G. 2000. Fatigue behavior of a pyrolytic carbon. *J Biomed Mater Res* **51**:61–68.

Ma PX, Elisseeff J. 2005. *Scaffolding in tissue engineering*. Boca Raton, FL: CRC Press.

Magee FP, Weinstein AM, Longo JA, Koeneman JB, Yarp RA. 1988. A canine composite femoral stem: an in vivo study. *Clin Orthop Relat Res* **235**:237–252.

Maharaj GR, Jamison RD. 1993. Creep testing of a composite material human hip prosthesis. In *Composite materials for implant applications in the human body: characterization and testing*. Ed RD Jamison, LN Gilbertson. Philadelphia: American Society for Testing and Materials.

Maier HR, Stark N, Krauth A. 1980. Reliability of ceramic-metallic hip joints based on strength analysis, proof, and structural testing, In *Mechanical properties of biomaterials*, pp. 177–194. Ed GW Hastings, DF Williams. New York: Wiley.

Malchau H, Garellick G, Eisler T, Karrholm J, Herberts P. 2005. The Swedish hip registry, increasing the sensitivity by patient outcome data. *Clin Orthop Relat Res* **441**:19–29.

Malik MA, Puleo DA, Bizios R, Doremus RH. 1992. Osteoblasts on hydroxyapatite, alumina and bone surfaces in vitro: morphology during the first 2 h of attachment. *Biomaterials* **13**:123–128.

Mamidwer SS, Arena C, Kelly S, Alexander H, Ricci J. 2006. In vivo characterization of calcium sulfate/PLLA composite for use as bone graft material. *J Biomed Mater Res Appl Biomater* **81B**:57–65.

Mandrino AR, Eloy R, Moyen B, Lerat JL, Treheux D. 1992. Base alumina ceramics with dispersoids: mechanical behaviour and tissue response after in vivo implantation. *J Mater Sci* **3**:457–463.

Marcolongo M, Ducheyne P, Cukler J, LaCourse W. 1993. Histological evaluation of a bioactive glass fiber/polysulfone composite. In *Bioceramics*, Vol. 6, pp. 353–357. Ed P Ducheyne, D Christiansen. Oxford: Pergamon/Elsevier Science.

Mastrogiacomo M, Muraglia A, Komlev V, Rustichelli F, Crovace A, Cancedda R. 2005. Tissue engineering of bone: search for a better scaffolds. *Orthod Craniofac Res* **8**:277–284.

Marti A. 2000. Inert bioceramics (Al_2O_3, ZrO_2) for medical application. *Injury* (Suppl) **4**:33–36.

McArthur SL. 2006. Surface properties of biomaterials. In *Encyclopedia of medical devices and instrumentation*, pp. 342–354. Ed JG Webster. Hoboken, NJ: Wiley.

McClintock F, Argon A. 1966. *Mechanical behavior of materials*. Reading, MA: Addison-Wesley.

McConell D. 1973. *Apatite: its crystal chemistry, mineralogy, utilization, and biologic occurrence*. Berlin: Springer-Verlag.

McElhaney J. 1966. Dynamic response of bone and muscle tissue. *J Appl Physiol* **21**:1231–1236.

McMillan PW. 1979. *Glass-ceramics*. New York: Academic Press.

Meffert R, Block M, Kent J. 1987. What is osseointegration? *Int J Periodont Restor Dent* **7**:9–21.

Meng WJ, Curtis TJ, Rehn LE, Blado PMV. 1998. Plasma-assisted deposition and characterization of Ti-containing diamond-like carbon coatings. *J Appl Phys* **83**:6076–6081.

Merker L. 1962. Synthesis of calcium titanate single crystals by flame fusion technique. *J Am Ceram Soc* **45**:366–369.

Meunier A, Christel PS, Sedel L. 1989. Role of design and material on stress distribution of cemented hip prosthesis: Effects of low-rigidity (carbon-carbon) material. In *Bioceramics*, Vol. 1, pp. 347–352. Ed H Oonishi, H Aoki, K Sawai. Tokyo: Ishiyaku EuroAmerica.

Miki T, Masaka K, Imai Y, Enomoto S. 2000. Experience with freeze-dried PGLA/HA/rhBMP-2 as bone graft substitute. *J Craniomaxillofac Surg* **28**:294–299.

Mikos AG, Sarakinos G, Leite SM, Vacanti JP, Langer R. 1993. Laminated three-dimensional biodegradable foams for use in tissue engineering. *Biomaterials* **14**(5):323–330.

Miller RE, Skucas J. 1977. *Radiographic contrast agents*. Baltimore: University Park Press.

Monroe E, Votaya W, Bass B, McMullen J. 1971. New calcium phosphate ceramic material for bone and tooth implants. *J Dent Res* **50**:860–861.

Mooney DJ, Baldwin DF, Suh NP, Vacanti JP, Langer R. 1996. Novel approach to fabricate porous sponges of poly(D,L-lactic co-glycolic acid) without the use of organic solvents. *Biomaterials* **17**:1417–1422.

Moore WJ. 1962. *Physical chemistry*, 3rd ed. Englewood Cliffs, NJ: Prentice-Hall.

More RB, Bokros JC. 2006. Biomaterials: carbon. In *Encyclopedia of medical devices and instrumentation*, pp. 296–308. Ed JG Webster. Hoboken, NJ: Wiley.

Morita Y, Nakata K, Kim YH, Sekino T, Niihara K, Ikeuchi K. 2004. Wear properties of alumina/zirconia composite ceramics for joint prostheses measured with an end-face apparatus. *Biomed Mater Eng* **14**:263–270.

Muatz R, Bauermiester A. 1957. A method of bone maceration: results in animal experiments. *J Bone Joint Surg* **39A**:153–166.

Murakami T, Ohtsuki N. 1989. Friction and wear characteristics of sliding pairs of bioceramics and polyethylene. In *Bioceramics*, Vol. 1, pp. 225–230. Ed H Oonishi, H Aoki, K Sawai. Tokyo: Ishiyaku EuroAmerica.

Murphy S. 2002. Alumina ceramic–ceramic bearings in THA: the new gold standard. *Orthopedics* **25**:2–3.

Murray MGS, Newman M, Morrell R, Byrne WP. 1995. Evaluation of the effect of stress corrosion on zirconia femoral heads. In *Bioceramics*, Vol. 8, pp. 151–156. Ed J Wilson, LL Hench, D Greenspan. Oxford: Pergamon.

Nakamura T, Yamamuro T. 1993. Development of a bioactive ceramic, A-W glass-ceramic. In *Bioceramics*, Vol. 6, pp. 105–110. Ed P Ducheyne, D Christiansen. Oxford: Pergamon/Elsevier Science.

Nakamura T, Yamamuro T, Higashi S, Kokubo T, Ito S. 1985. A new glass-ceramic for bone replacement: evaluation of its bonding to bone tissue. *J Biomed Mater Res* **19**:685–698.

Narayan J, Fan WD, Narayan RJ, Tiwari P, Stadelmaier HH. 1994. Diamond, diamond-like and titanium nitride biocompatible coatings for human body parts. *Mater Sci Eng* **B25**:5–10.

Niwa S, Sawai K, Takahashie S, Tagai H, Ono M, Fukuda Y. 1980. Experimental studies on the implantation of hydroxyapatite in the medullary canal of rabbits. In *Transactions of the first world biomaterials congress*, p. 4.10.4. Chichester: Wiley.

Nizard R, Sedel L, Hannouche D, Hamadouche M, Bizot P. 2005. Alumina pairing in total hip replacement. *J Bone Joint Surg Br* **87**:755–758.

Niznick GA. 1987. Osseointegration vs fibro-osseous integration. *J Oral Implantol* **13**:10–19.

Nordsletten L, Hogasen AKM, Konttinen YT, Santavirta S, Aspenberg P, Aasen AO. 1996. Human monocytes stimulation by particles of hydroxyapatite, silicon carbide and diamond: in vitro studies of new prosthesis coatings. *Biomaterials* **17**:1521–1527.

Odman P, Andersson B. 2001. Procera AllCeram crowns followed for 5 to 10.5 years: a prospective clinical study. *Int J Prosthodont* **14**:504–509.

Ogino M, Ohuchi F, Hench L. 1980. Compositional dependence of the formation of calcium phosphate film on Bioglass. *J Biomed Mater Res* **14**:55–64.

Ohgushi H, Goldberg VM, Caplan A. 1989. Heterotopic osteogenesis in porous ceramics induced by marrow cells. *J Orthop Res* **7**:568–578.

Ohura K, Nakamura T, Yamamuro T, Ebisawa Y, Kokubo Y, Oka M. 1991. A heat-generating bioactive glass-ceramic for hyperthermia. *J Appl Biomed* **2**:153–159.

Okamura M, Ohgushi H, Dohi Y, Katuda T, Tamai S, Koerten HK, Tabata S. 1997. Osteoblastic phenotype expression on the surface of hydroxyapatite ceramics. *J Biomed Mater Res* **37**:122–129.

Olsson J, Stearns N. 2006. Osseointegration of immediately loaded dental implants in the edentulous jaws: a study of the literature. www.ki.se/odont/cariologi_endodonti/99B/JohanOlssonNathon Stearns.pdf.

Oosterbos CJM, Rahmy AIA, Tonino AJ, Witpeerd W. 2004. High survival rate of hydroxyapatite-coated hip prostheses: 100 consecutive hips followed for 10 years. *Acta Orthop Scand* **75**:127–133.

Orefice RL, LaTorre GP, West JK, Hench LL. 1995. Processing and characterization of bioactive polysulfone–Bioglass® composites. In *Bioceramics*, Vol. 8, pp. 409–414. Ed J Wilson, LL Hench, D Greenspan. Oxford: Pergamon/Elsevier Science.

Orowan E. 1934. Die mechanischen Festigkeitseigenschaften und die Realstruktur der Kristalle. *Z Kristallogr* **A89**:327–343.

Osterholm HH, Day DE. 1981. Dense alumina aged in vivo. *J Biomed Mater Res* **15**:279–288.

Oxinium®, oxidized zirconium. 2004. Memphis, TN, Smith & Nephew, Orthopaedic Division.

Papadogianis Y, Boyer DB, Lakes RS. 1984. Creep of conventional and microfilled dental composites. *J Biomed Mater Res* **18**:15–24.

Park JB. 1984. *Biomaterials science and engineering*. New York: Plenum.

Park JB. 1992. Orthopedic prosthesis fixation. *Ann Biomed Eng* **20**(1):583–594.

Park JB, Lakes RS. 2007. *Biomaterials: an introduction*, 3rd ed. New York: Springer.

Park JB, Choi WW, Liu YK, Haugen TW. 1986. Bone particle-impregnated polymethylmethacrylate: an in vivo study. In *Tissue integration in oral and maxillofacial reconstruction*, pp. 118–124. Ed DV Steenberghe. Amsterdam, Excerpta Medica.

Park JB, Kelley BJ, von Recum AF, Kenner GH, Coffeen WW, Grether MF. 1981. Piezoelectric ceramic implants: in vivo results. *J Biomed Mater Res* **15**:103–110.

Park JB, Malstrom CS, von Recum AF. 1978. Intramedullary fixation of implants pre-coated with bone cement: a preliminary study. *Biomater Med Devices Artif Organs* **6**(4):361–373.

Park JB, von Recum AF, Kenner GH, Kelley BJ, Coffeen WW, Grether MF. 1980. Piezoelectric ceramics: a feasibility study. *J Biomed Mater Res* **14**:269–277.

Park KD, Kang YH, Park JB. 1999. Interfacial strength between molded and UHMWPE-MMA monomer treated UHMWPE powder. *J Long-Term Eff Med Implants* **9**:303–318.

Park SH, Llinas A, Goel VK, Keller JC. 1995. Hard tissue replacements. In *The biomedical engineering handbook*, pp. 672–691. Ed JD Bronzino. Boca Raton, FL: CRC Press.

Patel AM, Spector M. 1995. Oxidized zirconium for hemiarthroplasty: an in vitro assessment. In *Bioceramics*, Vol. 8, pp. 169–175. Ed J Wilson, LL Hench, D Greenspan. Oxford: Pergamon.

Paulus JA, Richardson JS, Tucker RD, Park JB. 1996. Evaluation of inductively heated ferromagnetic alloy implants for therapeutic interstitial hyperthermia. *IEEE Trans Biomed Eng* **43**:406–413.

Peltier LF. 1961. The use of plaster of paris to fill defects in bone. *Clin Orthop Relat Res* **21**:1–31.

Pereira MM, Clark AE, Hench LL. 1994. Effect of texture on the rate of hydroxyapatite formation on silica gel surface. *J Am Ceram Soc* **78**:2463–2468.

Perry CR. 1999. Bone repair techniques, bone graft, and bone graft substitutes. *Clin Orthop Relat Res* **360**:71–86.

Petruskevicius J, Nielsen S, Kaalund S, Knudsen PR, Overgaard S. 2002. No effect of Osteoset, a bone graft substitute, on bone healing in humans: a prospective randomized double-blind study. *Acta Orthop Scand* **73**(5):575–578.

Pfaff G. 1994. Synthesis of calcium titanate powders by the sol-gel process. *Chem Mater* **6**:58–62.

Phillips RW. 1973. *Skinner's science of dental materials*. Philadelphia: W.B. Saunders.

Piconi C, Maccauro G. 1999. Zirconia as ceramic biomaterial. *Biomaterials* **20**:1–25.

Piekarski K. 1978. Structure, properties and rheology of bone. In *Orthopaedic mechanics: procedures and devices*. Ed D Ghista, R Roaf. New York: Academic Press.

Pillar RM, Filiaqqi MJ, Wells JD, Grynpas MD, Kandel RA. 2001. Porous calcium polyphosphate scaffolds for bone substitute applications: in vitro characterization. *Biomaterials* **22**:963–972.

Piotrowski G, Hench L, Allen W, Miller G. 1975. Mechanical studies of bone–Bioglass interfacial bone. *J Biomed Mater Symp* **6**:47–61.

Platt R. 1994. *Smithsonian visual timeline of inventions*. New York: Dorling Kindersley.

Polo MC, Andujar JL, Robertson J, Milne WI. 2000. Preparation of tetrahedral amorphous carbon films by filtered cathodic vacuum arc deposition. *Diamond Relat Mater* **9**:663–667.

Posner A, Perloff A, Diorio A. 1958. Refinement of the hydroxyapatite structure. *Acta Crystallogr* **11**:308–309.

Ravaglioli A, Krajewski A. 1992. Glasses and ceramics as coatings for massive supports. In *Bioceramics: materials, properties, applications*, pp. 198–243. Ed A Ravaglioli, A Krajewski. London: Chapman & Hall.

Ray RD, Ward AA. 1951. A preliminary report on studies of basic calcium and phosphate in bone replacement. *Surg Forum* **2**:429–434.

Redey SA, Nardin M, Bernache-Assolant D, Rey C, Delannoy P, Sedel L, Marie PJ. 2000. Behavior of human osteoblastic cells on stoichiometric hydroxyapatite and type A carbonate apatite: role of surface energy. *J Biomed Mater Res* **50**:353–364.

Ricci J, Alexander H, Parsons JR. Salsbury R, Bajpai PK. 1986. Partially resorbable hydroxylapatite interface. *J Biomed Mater Res* **18**:719–726.

Richart O, Descamps M, Liebetrau A. 2001. Macroporous calcium phosphate ceramics: optimization of the porous structure and its effect on the bone ingrowth in a sheep model. *Key Eng Mater* **192–195**:425–428.

Richter HG, Burger W, Osthues F. 1994. Zirconia for medical implants: the role of strength properties. In *Bioceramics*, Vol. 7, pp. 401–406. Ed OH Andersson, R-P Happonen, A Yli-Urpo. Oxford: Pergamon.

Rieker C, Konrad R, Schon R. 2001. In vitro comparison of the two hard-hard articulations for total hip replacements. *J Eng Med* **215**:153–160.

Ripamonti U. 1996. Osteoinduction in porous hydroxyapatite implanted in heterotopic sites of different animal models. *Biomaterials* **17**:31–35.

Ritchie RO. 1996. Fatigue and fracture of pyrolytic carbon: a damage-tolerant approach to structural integrity and life prediction in "ceramic" heart valve prostheses. *J Heart Valve Dis* **5**(Suppl 1):S9–S31.

Ritter Jr J, Greenspan D, Palmer R, Hench L. 1979. Use of fracture of an alumina and Bioglass-coated alumina. *J Biomed Mater Res* **13**:251–263.

Robertson J. 2002. Diamond-like amorphous carbon. *Mater Sci Eng* **37**:129–281.

Robinson RA, Watson ML. 1955. Crystal–collagen relationships in bone as observed in the electron microscope, III: crystal and collagen morphology as a function of age. *Ann NY Acad Sci* **60**:596–630.

Rose FR, Cyster LA, Grant DM, Scotchford CA, Howdle SM, Shakesheff KM. 2004. In vitro assessment of cell penetration into porous hydroxyapatite scaffolds with a central aligned channel. *Biomaterials* **25**:5507–5514.

Rose PG, Gerstenberger F, Gruber U, Loos W, Wolter D, Neugebauer R. 1980. New aspects of the design and application of carbon fibre reinforced carbon for prosthetic devices. In *Transactions of the first world biomaterials congress*, p. P1.6. Chichester: Wiley.

Rosenberg HW. 1986. Zirconium production. In *Encyclopedia of materials science and engineering*, pp. 5545–5546. Ed MB Beaver. Cambridge: Pergamon/MIT Press.

Rosenstiel SF, Land MF, Crispin BJ. 1998. Dental luting agents: a review of the current literature. *J Prosthet Dent* **80**:280–301.

Roy DM, Linnehan SK. 1974. Hydroxyapatite formed from coral skeletal carbonate by hydrothermal exchange. *Nature* **247**:220–222.

Ryu HS, Lee JK, Seo JH, Kim H, Hong KS, Kim DJ, Lee JH, Lee DH, Chang BS, Lee CK, Chung SS. 2004. Novel bioactive and biodegradable glass ceramics with high mechanical strength in the CaO–SiO_2–B_2O_3 system. *J Biomed Mater Res* **68A**:79–89.

Sachlos E, Czernuszka JT. 2003. Making tissue engineering scaffolds work: review on the application of solid freeform fabrication technology to the production of tissue engineering scaffolds. *Eur Cells Mater* **5**:29–40.

Sadoun M, Perelmuter S. 1997. Alumina-zirconia machinable abutments for implant supported single tooth anterior crowns. *Pract Periodont Aesthet Dent* **9**:1047–1053.

Saikko V, Ahlroos T, Calonius O, Keränen J. 2001. Wear simulation of total hip prostheses with polyethylene against CoCr, alumina and diamond-like carbon. *Biomaterials* **22**:1507–1514.

Saltzman WM. 2004. Tissue engineering: engineering principles for the design of replacement organs and tissues. Oxford: Oxford UP.

Santavirta S. 2003. Compatibility of the totally replaced hip. Reduction of wear by amorphous diamond coating. *Acta Orthop Scand Suppl* **74**(310):1–19.

Saravanapavan P, Hench LL. 2000. Low-temperature synthesis, structure, and bioactivity of gel-sol derived glasses in the binary CaO–SiO_2 system. *J Biomed Mater Res* **54**:608–618.

Saravanapavan P, Jones JR, Pryce RS, Hench LL. 2003. Bioactivity of gel-glass powders in the CaO–SiO_2 system: a comparison with ternary (CaO–P_2O_5–SiO_2) and quaternary glass (SiO_2–CaO–P_2O_5–Na_2O). *J Biomed Mater Res* **66A**:110–119.

Sarkar MR, Wachter N, Patka P, Kinzl L. 2001. First histological observations on the incorporation of a novel calcium phosphate bone substitute material in human cancellous bone. *J Biomed Mater Res* **58**:329–334.

Schmitz JP, Hollinger JO. 1988. A preliminary study of the osteogenic potential of biodegradable alloplastic osteoinductive alloimplant. *Clin Orthop Relat Res* **237**:245–255.

Schnittgrund G, Kenner G, Brown S. 1973. In vivo and in vitro changes in strength of orthopedic calcium aluminate. *J Biomed Mater Res Symp* **4**:435–452.

Schwartz K, Milne DB. 1972. Growth-promoting effects of silicon in rats. *Nature* **239**:333–334.

Schwartz MM. 1997. Composite materials: properties, nondestructive testing, and repair. Upper Saddle River, NJ: Prentice-Hall.

Sclippa E, Piekarski K. 1973. Carbon fiber reinforced polyethylene for possible orthopaedic usage. *J Biomed Mater Res* **7**:59–70.

Sedel L. 1992. Symposium: alumina ceramic arthroplasty. *Clin Orthop Relat Res* **282**:2–94.

Sedel L. 2000. Evolution of alumina-on-alumina implants: a review. *Clin Orthop Relat Res* **379**:48–454.

Semlitsch M, Lehmann M, Weber H, Dorre E, Willert H-G. 1977. New prospects for a prolonged functional lifespan of artificial hip joints by using the material combination polyethylene/aluminum oxide ceramic/metal. *J Biomed Mater Res* **11**:537–552.

Sepulved P, Jones JR, Hench LL. 2002. In vitro dissolution of melt-derived 45S5 and sol-gel derived 58S bioactive glasses. *J Biomed Mater Res* **61A**:301–311.

Shi D. 2006. Testing and structural properties of biomaterials. In *Encyclopedia of medical devices and instrumentation*, pp. 354–365. Ed JG Webster. Hoboken, NJ: Wiley.

Shim H, Haubold A. 1980. The fatigue behavior of vapor deposited carbon films. *Biomater Med Devices Artif Organs* **8**:333–344.

Shimizu K, Oka M, Kumar P, Kotoura Y, Yamamuro T, Makinouchi K, Nakamura T. 1993. Time-dependent changes in the mechanical properties of zirconia ceramic. *J Biomed Mater Res* **27**:729–734.

Shobert II E. 1964. *Carbon and graphite*. New York: Academic Press.

Shores EC, Holmes RE. 1993. Porous hydroxyapatite. In *Introduction to bioceramics*, pp. 181–198. Ed LL Hench, J Wilson. Singapore: World Scientific.

Skinner HB. 1988. Composite technology for total hip arthroplasty. *Clin Orthop Relat Res* **235**:224–236.

Simpson LA. 1974. Microstructural considerations for the application of fracture mechanics techniques. In *Fracture mechanics of ceramics*, pp. 567–577. Ed RC Bradt, DPH Hasselman, FF Lange. New York: Plenum.

Spector M. 1999. Basic principles of tissue engineering. In *Tissue engineering: application in maxillofacial surgery and periodontics*, pp. 3–16. Ed SE Lynch, RJ Genco, RE Marx. Chicago: Quintessence.

Spivak JM, Ricci JL, Logan G, Liu ST. 1986. The structure and properties of hydroxyapatite coatings on metal. In *12th meeting of the society for biomaterials*, p. 13. New York: Wiley.

Spraggs M, Vasilos T. 1963. Effect of grain size on transverse bend strength of alumina and magnesia. *J Am Ceram Soc* **46**:224–228.

Stanley HR, Hall MB, Clark AE, King CJ 3rd, Hench LL, Berte JJ. 1997. Using 45S5 bioglass cones as endosseous ridge maintenance implants to prevent alveolar ridge resorption: a 5-year evaluation. *Int J Oral Maxillofac Implants* **12**:95–105.

Stapells DR, Picton TW, Durieux-Smith A. 1994. Electrophysiologic measures of frequency-specific auditory function. In *Principles and applications in auditory evoked potentials*, pp. 251–283. Ed JT Jacobson. Needham Heights, MA: Allyn and Bacon.

Starkebaum W, Pollack S, Korostoff E. 1979. Microelectric studies of stress-generated potential in four-point bending of bone. *J Biomed Mater Res* **3**:729–751.

Steffen T, Stoll T, Arvinte T, Schenck RK. 2001. Porous tricalcium phosphate and transforming growth factor used for anterior spine surgery. *Eur Spine J* **10**:132–140.

Stubbs D, Deakin M, Chapman-Sheath P, Bruce W, Debes J, Gillies RM, Walsh WR. 2004. In vivo evaluation of resorbable bone graft substitutes in a rabbit tibial defect model. *Biomaterials* **25**:5037–5044.

Sudanese A, Toni A, Cattaneo GL, Ciaroni D, Greggi T, Dallari D, Galli G, Giunti A. 1989. Alumina vs zirconium oxide: a comparative wear test. In *Bioceramics*, Vol. 1, pp. 237–240. Ed H Oonishi, H Aoki, K Sawai. Tokyo: Ishiyaku EuroAmerica.

Takagi M, Suda A, Sato T, Ishikawa A, Osanai T, Kato H, Orui H. 1995. Osteogenic response in porous 50 vol% zirconia dispersed hydroxyapatite ceramics. In *Bioceramics*, Vol. 8, pp. 431–434. Ed J Wilson, LL Hench, D Greenspan. Oxford: Pergamon.

Takuma M, Tstsumi S, Fukunaga S, Takamori Y, Harada S, Kurokawa F, Takashima F, Maruyama T. 1989. Study on the functional bone adaptation around dental implants: animal experimentations and stress analysis. In *Oral implantology and biomaterials*, pp. 251–256. Ed H Kawahara: Amsterdam: Elsevier Science.

Tampieri A, Celotti G, Sprio S, Delcogliano A, Franzese S. 2001. Porosity-graded hydroxyapatite ceramics to replace natural bone. *Biomaterials* **22**:1365–1370.

Tateishi T, Fukubayashi T. 1989. Advanced biocomposite material and application to the artificial joint. In *Bioceramics*, Vol. 1, pp. 48–53. Ed H Oonishi, H Aoki, K Sawai. Tokyo: Ishiyaku EuroAmerica.

Tamura J, Kawanabe K, Yamamuro T, Nakamura T, Kokubo T, Yoshihara S, Shibuya T. 1993. Bioactive bone cement: effect of amount of glass powder on its bioactivity and mechanical properties. In *Bioceramics*, Vol. 6, pp. 463–468. Ed P Ducheyne D Christiansen. Oxford: Pergamon/Elsevier Science.

Taylor JK, Pope BJ. 2001. The development of diamond as a bearing for total hip arthroplasty. In *Proceedings of the American Academy of Orthopaedic Surgery*, pp. 1–12. New York: Springer.

Thalgott JS, Klezl Z, Timlin M, Giuffre JM. 2002. Anterior lumbar interbody fusion with processed sea coral (coralline hydroxyapatite) as part of a circumferential fusion. *Spine* **27**:E518–E525.

Thomas MV, Puleo DA, Al-Sabbagh M. 2005. Calcium sulfate: a review. *J Long-Term Eff Med Implants* **15**:599–607.

Thompson ID, Hench LL. 1998. Mechanical properties of bioactive glasses, glass-ceramics and composites. *J Eng Med* **212**:127–137.

Thompson I, Rawlings RD. 1990. Mechanical behaviour of zirconia and zirconia toughened alumina in a simulated body environment. *Biomaterials* **11**:505–508.

Thompson JI, Czernuszka JT. 1995. Fabrication of biodegradable polymer scaffolds to engineering trabecular bone. *J Biomater Sci—Polym Ed* **7**:23–38.

Thompson LA, Law FC, Rushton N, Franks J. 1991. Biocompatibility of diamond-like carbon coating. *Biomaterials* **22**:37–40.

Todd DT. 1997. Diamond-like carbon (DLC) coatings. Lecture given to an Intermediate Biomaterials (51:171) course at the University of Iowa.

Torgalkar A. 1979. A resonance frequency technique to determine elastic modulus of hydroxyapatite. *J Biomed Mater Res* **15**:907–920.

Tracy BM, Doremus BM. 1984. Direct electron microscopy studies of the bone–hydroxyapatite interface. *Dent Clin North Am* **36**:19–26.

Tran HS, Puc MM, Hewitt CW, Soll DB, Marra SW, Simonetti VA, Cilley JH, DelRossi AJ. 1999. Diamond-like carbon coating and plasma or glow discharge treatment of mechanical heart valves. *J Invest Surg* **12**:133–140.

Trantina C. 1977. Brittle fracture and subcritical crack growth in a ceramic structure. In *Fracture*, pp. 921–927. Ed D Taplin. Waterloo, Canada: University of Waterloo.

Triffit JT. 1980. The organic matrix of bone tissue. In *Fundamental and clinical bone physiology*, pp. 45–82. Ed MR Urist. Philadelphia: Lippincott.

Tsuji T, Enomoto T, Kuwana S, Munrshige I, Inoue J, Nagai N. 1989. Basic and clinical evaluation of zirconia ceramic dental implant system. In *Oral implantology and biomaterials*, pp. 83–91. Ed H Kawahara. Amsterdam: Elsevier Science.

Turunen T, Peltola J, Kangasniemi I, Jussila J, Uusipaikka E, Yli-Urpo A, Happonen R-P. 1995. Augmentation of the maxillary sinus wall using bioactive glass and autologous bone. In *Bioceramics*, Vol. 8, pp. 259–264. Ed J Wilson, LL Hench, D Greenspan. Oxford: Pergamon/Elsevier Science.

Uhlman DR. 1972. A kinetic treatment of glass formation. *J Noncryst Solids* **7**:337–348.

van der Elst M, Klein CPAT, Patka P, Haarman HJTM. 2000. Biodegradable fracture fixation devices. In *Biomaterials and bioengineering handbook*, pp. 509–524. Ed DL Wise. New York: Marcel Dekker.

Van Vlack LH. 1970. *Materials science for engineers*. Reading, MA: Addison-Wesley.

Von Doernberg MC, von Rechenberg B, Bohner M, Grönenfelder S, van Lenthe GH, Müller R, Gasser B, Mathys R, Baroud G, Auer J. 2006. In vivo behavior of calcium phosphate scaffolds with four different pore sizes. *Biomaterials* **30**:5186–5198.

Vrouwenvelder WCA, Groot CG, de Groot K. 1993. Histological and biochemical evaluation of osteoblasts cultured on bioactive glass, hydroxylapatite, titanium alloy, and stainless steel. *J Biomed Mater Res* **27**:465–475.

Wachtel E, Villars P, Armini A, Spector M. 1992. Tribology of alumina and diamond-like coatings for orthopaedic applications. In *Proc. 5th international conference on surface modification technologies*, pp. 125–137. Ed TS Sudarshan, JF Braza. Birmingham, UK: Institute of Metals.

Wahl DA, Czernuszka JT. 2006. Collagen–hydroxyapatite composites for hard tissue repair. *Eur Cell Mater* **11**:43–56.

Wang M, Bonfield W, Hench LL. 1995. Bioglass®/high density polyethylene composite as a new soft tissue bonding material. In *Bioceramics*, Vol. 8, pp. 383–388. Ed J Wilson, LL Hench, D Greenspan. Oxford: Pergamon/Elsevier Science.

Watt W. 1986. Carbon fibers. In *Encyclopedia of materials science and engineering*, pp. 511–514. Ed MB Beaver. Oxford: Pergamon/MIT Press.

Watzek G, Watejka M, Lill W, Mailath G. 1989. Efficiency of different clinical procedures regarding optimal implant integration. In *Oral implantology and biomaterials*, pp. 287–293. Ed H Kawhara. Amsterdam: Elsevier.

Weast RC. 1968. *Handbook of chemistry and physics*, 49th ed. Cleveland, OH: Chemical Rubber Company.

Wegner SM, Kern M. 2000. Long-term resin bond strength to zirconia ceramic. *J Adhes Dent* **2**:139–147.

Weibull W. 1939. Statistical theory of the strength of materials. *Proc Roy Swedish Inst Eng Res* **151**:1–45.

Weibull W. 1951. A statistical distribution function of wide applicability. *J Appl Mech* **18**:293–297.

Weisenberg BA, Mooradian DL. 2002. Hemocompatibility of materials used in microelectromechanical system: platelet adhesion and morphology in vitro. *J Biomed Mater Res* **60**:283–291.

Weiss CM. 1986. Tissue integration of dental endosseous implants: descriptive and comparative analysis of fiber-osseous and osseointegration system. *J Oral Implantol* **12**:169–187.

Weiss CM. 1987. A comparative analysis of fibro-osteal and osteal integration and other variables that affect long term bone maintenance around dental implants. *J Oral Implantol* **13**:467–487.

Westfall R, Kent J, Homsy C. 1980. A comparison of porous composite PTFE/Al_2O_3 and PTFE/Graphite microporous facial implants in primates. In *Transactions of the first world biomaterials congress*, p. 3.8.3. Chichester: Wiley.

Whang K, Thomas CH, Healy KE, Nuber G. 1995. A novel method to fabricate bioabsorbable scaffolds. *Polymer* **36**:837–842.

Wiff JP, Fuenzalida VM, Zárate RA, Arias JL, Fernández MS. 2004. Characterization of hydrothermal-electrochemical calcium titanate coatings on titanium and biomedical titanium alloy. *J Phys Condens Matter* **16**:S1345–S1350.

Willmann G. 1993. Zirconia: a medical-grade material? In *Bioceramics*, Vol. 6, pp. 271–276. Ed P Ducheyne, D Christiansen. Oxford: Pergamon.

Willmann G. 1994. Medical-grade alumina during the past two decades. In *Bioceramics*, Vol. 7, pp. 359–363. Ed OH Andersson, R-P Happonen, A Yli-Urpo. Oxford: Pergamon.

Wilson J, Douek E, Rust K. 1995. Bioglass® middle ear devices: ten-year clinical results. In *Bioceramics*, Vol. 8, pp. 239–245. Ed J Wilson, LL Hench, D Greenspan. Oxford: Pergamon/Elsevier Science.

Wolfe MS, Dean D, Chen JE, Fisher JP, Han S, Rimnac CM, Mikos AG. 2002. In vitro degradation and fracture toughness of multilayered porous poly(propylene fumarate)/beta-tricalcium phosphate scaffolds. *J Biomed Mater Res* **61**:159–164.

Wolff J. 1892. *Das Gesetz der Transformation der Krochen*. Berlin: Hirchwild.

Woo S-Y, Akeson W, Coutts R, Rutherford L, Doty D, Jemmott G, Amiel D. 1976. A comparison of cortical bone atrophy secondary to fixation with plates with large differences in bending stiffness. *J Bone Joint Surg* **58A**:190–195.

Wood AAR. 1991. Carbon and graphite. In *Concise encyclopedia of advanced ceramic materials*, pp. 57–62. Ed RJ Brook. Oxford: Pergamon.

Wozney JM. 1999. Biology and clinical application of rhBMP-2. In *Tissue engineering: application in maxillofacial surgery and periodontics*, pp. 103–123. Ed SE Lynch, RJ Genco, RE Marx. Chicago: Quintessence.

Wyatte OM, Dew-Hughes D. 1974. *Metals, ceramics, and polymers*. London: Cambridge UP.

Xynos ID, Edgar AJ, Buttery LDK, Hench LL, Polak JM. 2001. Gene-expression profiling of human osteoblasts following treatment with the ionic products of Bioglass® 45S5 dissolution. *J Biomed Mater Res* **55**:151–157.

Yamada H. 1970. *Strength of biological materials*. Baltimore: Williams & Wilkins.

Yamamuro T. 1995. AW glass-ceramic in spinal repair. In *Bioceramics*, Vol. 8, pp. 123–127. Ed J Wilson, LL Hench, D Greenspan. Oxford: Pergamon/Elsevier Science.

Yannas IV. 1995. Regeneration templates. In *The biomedical engineering handbook*, pp. 1619–1635. Ed JD Bronzino. Boca Raton, FL: CRC Press.

Yannas IV, Burke JF, Gordon PL, Huang C, Rubenstein RH. 1980. Design of an artificial skin, Part II: control of chemical composition. *Biomaterials* **14**:107–131.

Yari SA, Homaeigohar S, Khavandi AR, Javapour J. 2004. The effects of partially stabilized zirconia on the mechanical properties of the hydroxyapatite–polyethylene composites. *J Mater Sci: Mater Med* **15**:853–858.

Yokokawa H, Kawada T, Dokiya MJ. 1989. Thermodynamic regularities in perovskite and K_2NiF_4 compounds. *Am Ceram Soc Bull* **72**:152–153.

Yoshikawa T, Ohgushi H, Tamai S. 1996. Immediate bone forming capability of prefabricated osteogenic hydroxyapatite. *J Biomed Mater Res* **32**:481–492.

Yoshimura M, Suda H. 1994. Hydrothermal processing of hydroxyapatite: past, present, and future. In *Hydroxyapatite and related materials*, pp. 45–72. Ed PW Brown, B Constantz. Boca Raton, FL: CRC Press.

Yuan H, Kurashina K, de Bruijn JD, Li Y, de Groot K, Zhang X, 1999. A preliminary study on osteoinduction of two kinds of calcium phosphate ceramics. *Biomaterials* **20**:1799–1806.

Zamet JS, Darbar UR, Griffiths GS, Bulman JS, Bragger U, Burgin W, Newman HN. 1997. Particulate Bioglass as a grafting material in the treatment of periodontal intrabony defects. *J Clin Periodont* **24**:410–418.

Zeng S, Cao W, Liu G. 1995. ZrO_2/HAP gradient ceramic biomaterials. In *Bioceramics*, Vol. 8, pp. 461–464. Ed J Wilson, LL Hench, D Greenspan. Oxford: Pergamon.

Zhang C, Wang J, Feng H, Lu B, Song Z, Zhang X. 2001. Replacement of segmental bone defects using porous bioceramic cylinders: a biomechanical and x-ray diffraction study. *J Biomed Mater Res* **54**:407–411.

Zhang K, Wang Y, Hillmyer MA, Francis LF. 2004. Processing and properties of porous poly(L-lactide)/bioactive glass composites. *Biomaterials* **25**:2489–2500.

Zhang Y, Zhang M. 2002. Three-dimensional macroporous calcium phosphate bioceramics with nested chitosan sponges for load-bearing bone implants. *J Biomed Mater Res* **61**:1–8.

Zhao F, Yi Y, Lu WW, Leong JC, Zhang W, Zhang J, Zhang M, Yao K. 2002. Preparation and histological evaluation of biomimetic three-dimensional hydroxyapatite/chitosan-gelatin network composite scaffolds. *Biomaterials* **23**:3227–3234.

Zichner LP, Wilert H-G. 1992. Comparison of alumina-polyethylene and metal-polyethylene in clinical trials. *Clin Orthop Relat Res* **292**:86–94.

NAME INDEX

A

Aasen, A.O., 224
Abram, J., 295
Adachi, T., 295
Adams, D., 223
Adell, R., 138, 296
Afonso, A., 179
Agarwal, B.D., 295
Agrawal, C.M., 223
Ahlroos, T., 224
Ahn, K.M., 298
Aitken, R., 224
Akao, M., 295
Akasaka, T., 299
Akeson, W., 115
Albee, F.H., 201, 295
Aldini, N.N., 297
Alexander, A., 224
Alexander, H., 203, 244
Allen, W., 180, 202
Al-Sabbagh, M., 245
Alvis, M., 295
Ambrosio, A.A., 298
Amiel, D., 115
Andersson, B., 166
Andersson, O., 297
Andeson, M.S., 297
Andrew, C., 201
Andujar, J.L., 224
Anttila, A., 223
Anusavice, K.J., 295
Aoki, H., 201, 202, 295
Apel, E., 179
Appendino, P., 179
Arena, C., 244
Argon, A., 68
Arias, J.L., 245
Armini, A., 225
Arns, C.H., 298
Aro, H.T., 297
Arsenis, C., 115
Arvinte, T., 300
Ashby, M.F., 8, 68, 81, 297
Ashton, B., 115
Aspenberg, P., 223, 224
Attawia, M.A., 295, 298
Auer, J., 301

B

Babis, G.C., 295
Bae, C.J., 165
Baek, S.H., 299
Bahrami, T., 165
Baier, R., 68
Bajpai, P.K., 203
Baldwin, D.F., 299
Ban, S., 295
Baquey, C., 223
Baroud, G., 301
Barralet, J.E., 138, 295
Bass, B., 203
Bassett, C.A.L., 201
Bauer, T.W., 295, 297
Bauermiester, A., 203
Baumgart, F., 295
Bayne, S.C., 299
Beckham, C., 179
Bedell, C.J., 223
Bell, E.T., 81
Bell, J.E., 244, 299
Berg, R., 295
Bernache-Assolant, D., 300
Berte, J.J., 180
Beruto, D.T., 295, 297
Bhaskar, S.N., 201
Bianco, A., 224
Billmeyer Jr., F.W., 81
Bizios, R., 203
Bizot, P., 138, 139
Black, J., 114
Blado, P.M.V., 224
Blaise, L., 165
Blaker, J.J., 95
Blary, M.C., 297
Blatz, M.B., 165
Blencke, B.A., 179
Block, J.E., 295
Block, M., 201, 203
Bloom, W., 114

Bobick, J., 202
Bobyn, J.D., 296
Boccaccini, A.R., 295
Boehm, H., 223
Bohner, M., 295, 301
Bokros, J.C, 223–224, 295
Bolen, C., 202
Bone, G., 202
Bonel, G., 201
Bonfield, W., 180, 295
Borden, M.D., 295, 298
Bostrom, M.P., 295
Botchway, E., 299
Botter, R., 295, 297
Bowen, H.K., 9, 27, 165, 179
Bowman, J., 295
Boyer, D.B., 299
Bradley, J.S., 295
Brady, J.M., 201
Braem, M., 295
Bragger, U., 181
Brandt, A.M., 179
Brånemark, P.-I., 138, 296
Brånemark, P.-T., 296
Breine, U., 138, 296
Breitbart, A.S., 296
Brekke, J., 297
Brighton, C., 114
Bromer, H., 179
Bronco, R., 179
Broutman, L.J., 295
Brovarone, C.V., 179
Brown, M.K., 295
Brown, S., 68, 138, 165
Brown, S.A., 297
Bruce, R.H., 68
Bruce, W., 245
Bruckmann, H., 223
Bruder, S.P., 115
Buchinger, R., 179
Bucholz, R.W., 297
Buck, D.C., 115
Buckwalter, J.A., 244, 299
Bulman, J.S., 181
Bundy, F.P., 223
Bunsell, A., 68
Burger, W., 165, 166
Burgin, W., 181
Burke, J.F., 301
Buttery, L.D.K., 181
Byrne, W.P., 166

C

Cales, B., 165
Callister, J.W.D., 68, 165
Calonius, O., 224
Cancedda, R., 299
Cannon, M.L., 296
Cao, W., 166
Caplan, A., 299
Capurro, M., 295
Carlisle, E., 179
Cassidy, C., 296
Cathalinat, B.B., 223
Cattaneo, G.L., 166
Cavalheiro, J.J., 179
Celotti, G., 298, 300
Chang, B.-S., 296
Chang, B.S., 180
Chang, Y.-L., 296
Chapman-Sheath, P., 245
Chen, C., 138, 165
Chen, F., 296
Chen, G., 296
Chen, J.E., 301
Chen, L., 296
Chevalier, J., 138
Chim, H., 296
Chiroff, R.T., 201, 296
Choi, C.Y., 298
Choi, J.Y., 299
Choi, W.W., 299
Chou, A.M., 296
Chow, L.C., 297
Christel, P.S., 165, 224
Christensen, R.M., 296
Chu, T.M.G., 296
Chung, C.P., 299
Chung, S.-S., 296
Chung, S.S., 180
Chvapil, M., 114
Ciaroni, D., 166
Cilley, J.H., 225
Cima, L.G., 296
Cirillo, P., 295
Clark, A.E., 179, 180
Clark, C.R., 296
Clarke, I.C., 165
Clupper, D., 179
Coble, R.L., 138
Coffeen, W.W., 68, 244
Cohen, M., 296
Cohen, U., 138
Coleman, R.F., 114
Constanz, B., 296
Cook, S.D., 201
Coombs, N.A., 201
Cooper, J.A.J., 298, 299
Costantino, P.D., 297
Coutts, R., 115
Cowin, S., 114
Cowland, F., 223
Cram, A.E., 297
Crebo, A., 179
Crispin, B.J., 300
Crovace, A., 299
Cu, X., 296

Cui, F., 299
Cukler, J., 180
Cunningham, N.S., 296
Currey, J.D., 114
Curtis, T.J., 224
Cutright, D.E., 201
Cyster, L.A., 300
Czernuszka, J.T., 300, 301

D

Daculsi, G., 202
Dai, K.R., 296
Dalgeish, B.J., 165
Dallari, D., 166
Damen, J.J.M., 179
Darbar, U.R., 181
Davidson, C.L., 295
Davidson, J.A., 223
Dawihl, W., 138
Day, D.E., 8, 166
Day, T.E., 8
Deakin, M., 245
Dean, D., 301
Dearnaley, G., 223
De Aza, A.H., 138
Debes, J., 245
de Bruijn, J.D., 298, 301
Decheyne, P., 201
de Groot, K., 180, 201, 299, 301
deLange, G.L., 201
Delannoy, P., 300
Delauney, C., 165
Delcogliano, A., 300
Delecourt, C., 297
Delli-Santi, M., 296
DelRossi, A.J., 225
Dempster, W.T., 114
Derand, P., 165
Derand, T., 165
Descamps, M., 297, 300
Deutscher, K.K., 179
Dew-Hughes, D., 181
De Wijn, J.R., 299
Dhert, W.J.A., 298
Ding, M., 296
Dion, I., 223
Diorio, A., 203
Dohi, Y., 298, 299
Dokiya, M.J., 245
Doll, B., 297
Dommann, A., 179
Donaldson, K., 224
Donaldson, T., 165
Dong, J., 296
Doremus, B.M., 203
Doremus, H., 202
Doremus, R.H., 68, 81, 203
Dorre, E., 138, 139, 224
Doty, D., 115
Douek, E., 180
Drennan, J., 165
Driskell, T.D., 201
Drummond, J.L., 165
Ducheyne, P., 180, 201, 296
Duffin, R., 224
Dumitriu, M., 297
Durieux-Smith, A., 245

E

Eanes, E., 201
Ebisawa, Y., 9
Edgar, A.J., 181
Einhorn, T.A., 295, 297, 298
Eisler, T., 68
Ekholm, C., 297
El-Amin, S., 299
El-Ghannam, A.R., 296
Elisseeff, J., 299
Eloy, R., 166
Emmel, A., 297
Engelberg, I., 296
Engh, C.A., 296
Enomoto, S., 299
Enomoto, T., 166
Erben, R.G., 297
Eriksson, C., 114
Ernst, C.P., 138
Ethridge, E.C., 115, 179
Evans, A., 179
Evans, F.G., 114, 201
Evison, R., 295
Eysel, W., 201

F

Fan, D., 202
Fan, W.D., 224
Fantozzi, G., 138, 165
Fawcett, D.W., 114
Feinberg, S.E., 296
Feng, H., 301
Feng, S.S., 201
Fennell, C., 296
Fernández, M.S., 245
Filiaggi, M.J., 165, 201, 297, 300
Fini, M., 297
Fisher, J., 297
Fisher, J.P., 301
Flautre, B., 297
Forrest, G., 224
Frakes, J., 138, 165
Francis, L.F., 301
Franks, J., 225
Franzese, S., 300
Friedenberg, Z., 114
Friedman, C., 297

Fuenzalida, V.M., 245
Fukubayashi, T., 225, 301
Fukuda, Y., 203
Fukunaga, S., 300
Fung, Y.C., 115

G

Galli, G., 166
Galois, L., 297
Garellick, G., 68
Gaunt, T., 138, 295
Geduldig, D., 138
Gerstenberger, F., 224
Getter, L., 201
Giardino, R., 297
Giavaresi, G., 297
Gibson, I.R., 138
Gibson, J.R., 295
Gibson, L.J., 297
Gill, R., 224
Gillies, R.M., 245
Gilmore, R., 201
Gineste, M., 202
Gitzen, W.H., 138
Giuffre, J.M., 301
Giunti, A., 166
Glasser, B., 301
Glat, P.M., 296
Glattauer, V., 299
Goeken, J.A., 297
Goel, V.K., 224
Goldberg, V.M., 299
Goodman, S.B., 223
Gordon, P.L., 301
Gorga, M.P., 244
Götz, H.E., 297
Graf-Hausner, U., 179
Grainger, D.W., 297
Grant, D.M., 300
Green, D.D., 65
Greenlee Jr., T., 179
Greenspan, D., 139, 179, 180
Greggi, T., 166
Gregoire, M., 202
Grenoble, D., 201
Grether, M.F., 68, 244
Griffith, A., 68
Griffiths, G.S., 181
Grill, A., 224
Griss, P., 179
Grönenfelder, S., 301
Groot, C.G., 180
Gross, J., 115
Gross, K., 298
Grover, L., 295
Gruber, U., 224
Gruenefelder, S., 295
Gruskin, E., 297
Grynpas, M.D., 295, 297, 300
Guilhem, A., 202
Gustafson, G.A., 165
Guyer, D.W., 297

H

Ha, S.-W., 201, 224
Haarman, H.J.T.M., 301
Haldeman, K.O., 201
Hall, M.B., 180
Hallen, O., 138, 296
Halloran, J.W., 296
Ham, Z., 115
Hamadouche, M., 138, 165
Han, S.B., 299, 301
Hannouche, D., 138
Hannouche, M., 139
Hansson, B.O., 138, 296
Happonen, R.-P., 180
Harada, S., 300
Haraguchi, K., 165
Harbers, G.M., 297
Hardouin, P., 297
Harper, A., 202
Harris, B., 68
Harris, W., 115
Hassler, C., 297
Hastings, G.W., 295
Haubold, A., 224
Hauert, R., 224
Haugen, T.W., 299
Healy, K.E., 301
Heimke, G., 179
Heller, M., 165
Hench, L.L., 9, 115, 139, 179, 180, 181, 201–202, 297
Henrich, D.E., 297
Heo, S.J., 299
Herberts, P., 68
Hermansson, L., 166
Hernigou, P., 165
Heughebaert, J.C., 201
Heughebaert, M., 201, 202
Hewitt, C.W., 225
Higashi, S., 180
Hill, D., 115
Hillmyer, M.A., 301
Hirabayashi, M., 138
Hirata, I, 297
Hiratzka, L.F., 297
Hirsiger, W., 295
Hirthe, W.M., 202
Hoen, C.V., 179
Hoexter, D.L., 297
Hogasen, A.K.M., 224
Hohling, H., 115
Hojo, M., 295
Holand, M., 179

Holand, W., 179
Hollinger, J.O., 115, 297, 300
Hollister, S.J., 295, 296, 299
Holmes, R.A., 202, 297
Holmes, R.E., 203, 300
Holzwarth, U., 297
Homaeigohar, S., 166
Homsy, C.A., 297, 301
Hong, K.S., 180, 296
Hornby, S., 295
Howdle, S.M., 300
Howlett, C.R., 299
Huang, C., 301
Hubbard, W.G., 202
Hubner, H., 138
Hukins, D.W.L., 244
Hurley, L.A., 201, 202
Husband, J., 296
Hutmacher, D.W., 296
Huttinger, K.J., 223
Hyakuna, K., 202
Hyyakuna, K., 298

I

Ikeuchi, K., 138, 166
Imai, Y., 299
Inada, H., 179
Inger, D., 296
Inglis, C., 68
Inoue, J., 166
Inoue, K., 165, 179
Inoue, M., 298
Ioku, K., 202
Ishikawa, A., 166
Ishimura, M., 165, 179
Itälä, A.I., 297
Itch, M., 297
Ito, S., 179, 180
Itoh, H., 297

J

Jaglinski, T., 9
Jamison, R.D., 299
Jarcho, M., 201, 202, 297
Javapour, J., 166
Jemmott, G., 115
Jentchura, G., 179
Jin, Q.M, 197, 298
Jockisch, K.A., 297
Johnson-Hurse, C., 295
Johnston, C., 223
Jones, A.M., 223
Jones, D.R., 8, 68, 81
Jones, J.J., 9
Jones, J.R., 179, 180
Jongejan, A., 244
Jupiter, J.B., 296
Jussila, J., 180

K

Kaae, J., 224
Kaalund, S., 245, 300
Kagan, A., 201
Kakar, S., 298
Kakutani, Y., 298
Kamgasniemi, I., 179
Kamitakahara, M., 179
Kandel, R.A., 297, 300
Kang, Y.H., 300
Kangasniemi, I., 180
Kaplan, D., 298
Karageorgiou, V., 298
Karlsson, K.H., 297
Karrholm, J., 68
Kato, H., 166
Kato, K., 201, 202
Katuda, T., 299
Katz, J.L., 201, 202
Kawada, T., 245
Kawahara, H., 138
Kawanabe, K., 139
Kay, J.F., 201, 202
Keeting, F., 179
Keller, D.J., 298
Keller, J.C., 224, 296, 298
Kelley, B., 244
Kelley, B.J., 68
Kelly, S., 244
Kenner, G.H., 68, 138, 165, 244
Kent, J., 201, 203, 301
Keränen, J., 224
Kern, M., 166
Kessler, F.B., 297
Ketenjian, A., 115
Khan, Y., 295, 298, 299
Khang, G., 298
Khavandi, A.R., 166
Khoury, J.G., 244, 299
Kijkowska, R., 202
Kikuchi, M.J., 296, 298
Kikuchi, N., 299
Kim, B.S., 298
Kim, D.J., 180
Kim, H., 180
Kim, H.E., 165, 298
Kim, H.W., 165, 298
Kim, S.S., 298, 299
Kim, Y.H., 138, 165, 166
Kindersley, D., 69
King, B.G., 115
King, C.J., 180
Kingery, W.D., 9, 27, 138, 165, 179
Kinzl, L., 300

Kitaoji, M., 298
Kitsugi, T., 68, 202, 298
Klein, C.P.A.T., 301
Klezl, Z., 301
Klokkevold, P.R., 299
Klumpp, C., 224
Knacksteadt, M.A., 298
Knapp, W., 138, 165
Knowles, J.C., 138, 298
Knudsen, P.R., 245, 300
Kobayashi, D., 298
Kochman, D., 9
Koeneman, J.B., 299
Koerten, H.K., 299
Kofron, M., 299
Kohgo, T.K., 297
Kohn, J., 296, 298
Kojima, H., 296
Kokubo, T., 68, 139, 179, 180, 202
Kokubo, Y., 9
Komlev, V., 299
Kong, Y.M., 165
Konrad, R., 139
Konttinen, Y.T., 223, 224
Korostoff, E., 115
Kostarelos, K., 224
Koster, H., 115
Kotoura, Y., 166, 298
Kotura, Y., 202
Kovacs, P., 298
Krainess, F., 138, 165
Krajewski, A., 203
Krauth, A., 138
Krenpien, B., 179
Krieger, J., 180
Kruyt, M.C., 298
Kuboki, Y., 297, 298
Kumar, P., 166
Kurashina, K., 301
Kurokawa, F., 300
Kushitani, H., 202
Kuwana, S., 166

L

LaCourse, W., 180
Lacout, J.L., 201
Ladd, A., 296
Lade, R., 138
LaGrange, L., 223, 295
Lakes, R.S., 9, 115, 244, 299
Lalor, P., 295
Lambrechts, P., 295
Land, M.F., 300
Landi, E., 298
Laney, W.R., 298
Lang, B., 165
Langer, R., 296, 298, 299
Lankford, J., 223
Lanza, R., 298
Lappalainen, R., 223
Larmas, E., 179
LaTorre, G.P., 180
Laurencin, C.T., 295, 298, 299
Law, F.C., 225
Layrolle, P., 299
Lebow, M., 114
Lebugle, A., 201
Lee, C.K., 180, 296
Lee, D., 297
Lee, D.H., 180
Lee, G.H., 244, 299
Lee, J.H., 180, 298
Lee, J.K., 180
Lee, S.H., 165
Lee, Y.M., 299
LeGeros, J.P., 202
LeGeros, R.Z., 202, 299
Lehmann, M., 139, 224
Lei, D., 244
Leinberry, C., 296
Leinfelder, K.F., 299
Leite, S.M., 299
Lenza, R.F.S., 179
Leong, J.C., 301
Lerat, J.L., 166
Lerouge, S., 138
Lew, D., 296
Lewis, J., 223
Li, J., 166, 299
Li, S., 299
Li, Y., 301
Liao, S., 299
Liboff, A.B., 115
Lickoish, D., 299
Liddicoat, R.T., 114
Lidstrom, J., 138, 296
Liebetrau, A., 300
Lill, W., 139
Lim, T.C., 296
Lim, Y.T., 299
Lin, C.Y., 299
Linnehan, S.K., 203
Litkowski, L.J., 180
Liu, G., 166
Liu, S.T., 203
Liu, Y.K., 296, 297, 299
Llinas, A., 224
Logan, G., 203
Logroscino, G., 298
Longo, J.A., 299
Loos, W., 224
Losee, F.L., 202
Low, S.B., 180
Lu, B., 301
Lu, L.Q., 298
Lu, W.W., 301
Luostarinen, T., 179

M

Ma, L., 224
Ma, P.X., 299
Maccauro, G., 166
Magee, F.P., 299
Maharaj, G.R., 299
Maier, H.R., 138
Mailath, G., 139
Mainard, D., 297
Makinouchi, K., 166, 298
Malchau, H., 68
Malik, M.A., 203
Mamidwer, S.S., 244
Manaka, M., 165
Mandrino, A.R., 166
Mao, T., 296
Marcolongo, M., 180, 296
Marie, P.J., 300
Marra, S.W., 225
Marti, A., 138
Martin, J., 165
Maruyama, T., 300
Masaka, K., 299
Mastrogiacomo, M., 299
Mathys, R., 301
Mauer, H.J., 223
Mauth, C., 179
Mayer, J., 201, 224
McArthur, S.L., 68
McCabe, A.R., 223
McClintock, F., 68
McConell, D., 203
McElhaney, J., 115
McMillan, P.W., 180
McMullen, J., 203
Meffert, R., 203
Meng, W.J., 224
Merker, L., 244
Merritt, K., 297
Meunier, A., 138, 165, 224
Mezzasalma, S.A., 295
Micallef, D.M., 223
Miki, H., 165
Miki, T., 299
Mikos, A.G., 299, 301
Miller, G., 180
Miller, R.E., 244
Milne, D.B., 180
Milne, W.I., 224
Mishra, A.K., 223
Miyazaki, T., 179
Mizgala, J.W., 297
Monroe, E., 203
Mooney, D.J., 296, 299
Mooney, V., 297
Mooradian, D.L., 225
Moore, J.O., 201
Moore, W.J., 68
More, N., 223
More, R.B., 224
Morita, Y., 138, 166
Morrell, R., 166
Morrison, H.F., 201
Mortensen, A., 179
Moyen, B., 166
Muatz, R., 203
Mueller, K.H., 202
Müller, M., 297
Müller, R., 295, 301
Munrshige, I., 166
Muraglia, A., 299
Murakami, T., 166
Murata, M., 298
Murphy, S., 138
Murray, M.G.S., 166

N

Nagai, N., 166, 298
Naganuma, A., 201
Nakamura, T., 9, 68, 139, 166, 180, 202
Nakata, K., 138, 166
Narayan, J., 224
Narayan, R.J., 224
Nardin, M., 300
Neely, S.T., 244
Neugebauer, R., 224
Newman, H.N., 181
Newman, M., 166
Niehaus-Rohde, C., 180
Nielsen, S., 245, 300
Niihara, K., 138, 166
Nishii, T., 165
Nishiyama, K., 296
Nissan, B.B., 165
Niwa, S., 203
Nizard, R., 138, 139
Niznick, G.A., 299
Njus, G.O., 299
Noda, I., 287
Nordsletten, L., 223, 224
Nuber, G., 301

O

Obrecht, M., 179
Odman, P., 166
Ogino, M., 180
Ogiso, M., 202
Ohgushi, H., 165, 179, 298, 299, 301
Ohman, A., 138, 296
Ohtsuki, C., 179
Ohtsuki, N., 166
Ohuchi, F., 180
Ohura, K., 9
Oka, K., 165
Oka, M., 9, 166, 202
Okamura, M., 299

Okazaki, M., 297
Olagnon, C., 165
Olsson, J., 299
Oner, F.C., 298
Ono, M., 68, 202, 203
Oosterbos, C.J.M., 68
Orefice, R.L., 180
Orly, I., 202
Orowan, E., 68
Orton, D.G., 296
Orton, D.O., 296
Orui, H., 166
Osako, Y., 295
Osanai, T., 166
Osterholm, H.H., 166
Osthues, F., 166
Overgaard, S., 245, 300

P

Pachall, H., 179
Palmer, R., 139, 180
Papadogianis, Y., 299
Park, J.B., 9, 68, 115, 139, 244, 296, 297, 299, 300
Park, K.D., 300
Park, K.-W., 296
Park, M.S., 298
Park, S.H., 224
Parsons, J.R., 203
Patel, A.M., 166
Patka, P., 300, 301
Paulus, J.A., 9
Peek, R.D., 297
Peille, C.N., 165
Peltier, L.F., 244, 300
Peltola, J., 180
Pereira, M.M., 180
Perelmuter, S., 166
Perloff, A., 203
Perry, C.R., 300
Petruskevicius, J., 245, 300
Pezzotti, G., 165
Pfaff, G., 245
Phillips, R.W., 245
Piconi, C., 166
Picton, T.W., 245
Piekarski, K., 115, 300
Pillar, R.M., 300
Pilliar, R.M., 165, 201, 297
Piotrowski, G., 180
Platt, R., 81
Polak, J.M., 179, 181
Pollack, R., 201
Pollack, S., 115
Polo, M.C., 224
Pope, B.J., 225
Posey, W.R., 201
Posner, A., 201, 203
Prato, M., 224
Prendergast, P.J., 298
Prewitt III, J.M., 297
Prudhommeaux, F., 138
Prussner, P., 138
Pryce, R.S., 180
Puc, M.M., 225
Puleo, D.A., 203, 245

R

Rahmy, A.I.A., 68
Ramshaw, J.A., 299
Ravaglioli, A., 203
Rawling, R.D., 165
Rawlings, R.D., 166
Ray, R.D., 203
Reddi, A.H., 295, 296
Reddi, H., 297
Redey, S.A., 300
Rehn, L.E., 224
Reis, R.L., 296
Renlund, R., 297
Rettig, H., 223
Rey, C., 300
Rheinberger, V., 179
Rhyu, I.C., 299
Ricci, J.L., 203, 244, 296
Richardson, J.S., 9
Richart, O., 300
Richter, H.G., 166
Rieker, C., 139
Ries, M., 165
Rimnac, C.M., 301
Ripamonti, U., 300
Ritchie, R.O., 224
Ritter Jr., J., 139, 180
Robertson, J., 224
Robinson, R.A., 203
Rocket, T.J., 201
Roques, X., 223
Rose, F.R., 300
Rose, P.G., 224
Rosenberg, H.W., 166
Rosenstiel, S.F., 300
Roy, D.M., 201, 203, 296
Rubenstein, R.H., 301
Rushton, N., 224
Rust, K., 180
Rustichelli, F., 299
Rutherford, L., 115
Ryu, H.S., 180, 296

S

Sachlos, E., 300
Sadan, A., 165
Sadoun, M., 166
Saikko, V., 224

Saito, T., 298
Sakka, S., 179
Saleh, K.J., 295
Salsbury, R., 203
Saltzman, W.M., 300
San Marchi, C., 179
Santavirta, S., 223, 224
Sarakinos, G., 299
Saravanapavan, P., 180
Sarkar, M.R., 300
Sato, T., 166
Sawai, K., 203
Schantz, J.-T., 296
Schehl, M., 138
Schenck, R.K., 300
Schepers, E., 296
Schmitz, J.P., 297, 300
Schnittgrund, G., 68
Schoen, G., 223, 295
Schon, R., 139
Schwartz, K., 180
Schwartz, M.M., 300
Sclippa, E., 300
Scotchford, C.A., 300
Sedel, L., 138, 139, 165, 224, 300
Seitz, W.R., 296
Sekino, T., 138, 166
Semlitsch, M., 139, 224
Senden, T.J., 298
Seo, J.H., 180
Seol, Y.J., 299
Sepulved, P., 180
Sewon, L., 179
Sfeir, C., 297
Shakesheff, K.M., 300
Shi, D., 68
Shibata, M., 201
Shibuya, T., 68, 139, 202
Shigematsu, M., 179
Shikita, T., 138
Shim, H., 224
Shimazu, A., 297
Shimizu, K., 166
Shin, Y., 295
Shintani, H., 297
Shobert II, E., 224
Shores, E.C., 203, 300
Showers, M.J., 115
Simaya, M., 165, 179
Simonetti, V.A., 225
Simpson, L.A., 68
Sines, G., 224
Skinner, H.B., 300
Skucas, J., 244
Smith, S.T., 295
Soll, D.B., 225
Somiya, S., 202
Song, Z., 301
Soremark, R., 166
Soucacos, P.N., 295
Spector, M., 166, 225, 300
Spivak, J.M., 203
Splinter, R., 202
Spraggs, M., 68, 139
Sprio, S., 298, 300
Stadelmaier, H.H., 224
Staffenberg, D.A., 296
Stangl, R., 297
Stanley, H.R., 180
Stapells, D.R., 245
Stark, N., 138
Starkebaum, W., 115
Stearns, N., 299
Steele, B.C.H., 165
Stefani, Y., 165
Steffen, T., 300
Steiner, G., 296
Stender, E., 138
Stienstra, D., 299
Stinchfild, F.E., 201
Stoll, T., 300
Stone, D., 9
Stone, V., 224
Strong, H.M., 223
Stubbs, D., 245
Suda, A., 166
Suda, H., 203
Sudanese, A., 166
Suga, S., 202
Sugano, N., 165
Suh, N.P., 299
Swift, Jr., E.J., 299

T

Tabata, S., 299
Tabata, T., 202
Tagai, H., 203
Takagi, M., 68, 166, 202
Takagi, S., 297
Takahashie, S., 203
Takamori, Y., 300
Takashima, F., 300
Takeuchi, H., 68, 202
Takita, H., 297, 298
Takuma, M., 300
Tamai, S., 299, 301
Tampieri, A., 298, 300
Tamura, J., 139
Tanaka, J., 296
Tanaka, M., 295
Tanihara, M., 179
Tao, K., 296
Tateishi, T., 225, 296, 301
Tatnai, S., 165, 179
Taylor, J.K., 225
TenCate, J.M., 179
Tencer, A., 297

Thalgott, J.S., 301
Thomas, C.H., 301
Thomas, K.A., 201
Thomas, M., 202
Thomas, M.V., 245
Thompson, I., 166
Thompson, I.D., 180
Thompson, J.I., 301
Thompson, L.A., 225
Thorn, M.R., 295
Thorne, C.H., 296
Timlin, M., 301
Tiwari, P., 224
Todd, D.T., 225
Togawa, T., 295
Tolman, D.E., 298
Toni, A., 166
Tonino, A.J., 68
Torgalkar, A., 203
Torre, J.P., 165
Torrecillas, R., 138
Torricelli, P., 297
Tracy, B.M., 203
Tran, H.S., 225
Tran, L., 224
Trantina, C., 139
Treheux, D., 166
Triffit, J.T., 115
Tstsumi, S., 300
Tsuji, T., 166
Tsuki, T., 295
Tsuruga, E., 298
Tucker, R.D., 9
Tully, A.E., 295
Turunen, T., 180

U

Uemura, T.M., 296
Uhlmann, D.R., 9, 27, 81, 165, 179
Uo, M., 299
Ushida, T., 296
Uusipaikka, E., 180

V

Vacanti, C., 296
Vacanti, J.P., 296, 298, 299
van Blitterswijk, C.A., 298
van der Elst, M., 301
Vanherle, G., 295
van Lenthe, G.H., 295, 301
Van Vlack, L.H., 27, 68, 245
Vasconcerlos, M., 179
Vasilos, T., 68, 139
Vasoconcelos, W.L., 179
Verbout, A.J., 298
Verne, E., 179
Villars, P., 225
Villermaux, F., 165
Vogel, W., 179
Von Doernberg, M.C., 301
von Rechenberg, B., 301
von Recum, A.F., 68, 244
Votaya, W., 203
Vrouwenvelder, W.C.A., 180

W

Wachtel, E., 225
Wachter, N., 300
Wahl, D.A., 301
Walsh, W.R., 245
Wang, J., 301
Wang, M., 180
Wang, W., 299
Wang, Y., 301
Ward, A.A., 203
Wardlaw, D., 244
Watari, F., 299
Watejka, M., 139
Watson, M.L., 203
Watt, W., 225
Watzek, G., 139
Weast, R.C., 245
Weber, H., 139, 224
Weber, J.E., 296
Weber, J.N., 201, 296
Weber, U., 223
Wegner, S.M., 166
Weibull, W.A., 68
Weilbull, W., 68
Weinstein, A.M., 299
Weisenberg, B.A., 225
Weiss, C.M., 301
Wekmeister, J.A., 299
Wells, J.D., 300
Wentorf, R.H., 223
West, J.K., 180
Westfall, R., 301
Whang, K., 301
White, E.W., 201, 296
White, R.A., 296, 297
Wiff, J.P., 245
Wilert, H.-G., 166
Wilkins, A.L.J., 244
Willerhausen, B., 138
Willert, H.-G., 138, 139, 224
Williams, D., 223
Williams, P., 165
Willmann, G., 139, 165, 166
Wilson, C.E., 298
Wilson, J., 9, 180, 297
Wiltse, L.L., 297
Wintermantel, E., 201, 224
Wirth, M.A., 223
Witpeerd, W., 68
Wolfe, M.S., 301

Wolff, J., 115
Wolter, D., 224
Woo, S.-Y., 115
Wood, A.A.R., 225
Wozney, J.M., 115
Wright, A.J., 138, 295
Wright, C.B., 297
Wyatte, O.M., 181

X

Xu, G., 299
Xynos, I.D., 181

Y

Yamada, H., 115
Yamamuro, T., 9, 68, 139, 166, 179, 180, 181, 202, 298
Yannas, I.V., 301
Yao, K., 301
Yapp, R.A., 224
Yari, S.A., 166
Yarp, R.A., 299
Yi, Y., 301
Ylänen, H.O., 297
Yli-Urpo, A., 179, 180
Yokokawa, H., 245
Yoshida, Y., 297
Yoshihara, S., 139
Yoshikawa, H., 165
Yoshikawa, T., 301
Yoshimura, M., 202, 203
Youn, H.-J., 296
Yu, X., 299
Yuan, H., 301
Yusuf Khan, Y., 299

Z

Zamet, J.S., 181
Zárate, R.A., 245
Zeng, S., 166
Zhang, C., 301
Zhang, J., 301
Zhang, K., 301
Zhang, M., 301
Zhang, W., 301
Zhang, X., 301
Zhang, Y., 301
Zhao, F., 301
Zheng, R., 202
Zheng, Z.K., 296
Zhu, Y., 299
Zichner, L.P., 138, 166

SUBJECT INDEX

A

$A_{10}(BO_4)_6X_2$ family of minerals, 187
Abrasions on slide glass, **74**
Abrasives, 2
Acetabular back, *1*
Acetabular cup, 2, 129
  composite carbon in, *214*
  with diamond coating, *205*
  for hip joint prosthesis, 257
  inserts, *29*
  precoating in composite, *258*
  zirconia-based, *141*
ACP, 178, 291
Activation energy of phase transformation
  definition, 164
Acupuncture, 112
Adaptic® dental composite, **262**
Adhesive friction, 44
Adhesive wear, 46
AES, 178
Ag as nucleating agent, 168
Aging time for zirconia, 155–156, *157*
Alanine, **86**
Aldehyde, 291
Alkali oxides in alumina, 119
Alkaline phosphatase activity (APA), 173–174
Allogro® bone graft, **268**, 291
Allomatrix®, 291
Allotropic, 47–49, 222
Alloys
  shape memory, 55
  solidification, 15
AlP, atomic bonding and arrangement, **14**
α-alumina, 118
  crystal structure, 119
α-helix, 87
α-hemihydrate, 228
Alternative medicine in bone diseases, 112
Alumina (Al_2O_3) (aluminum oxide), 2, 4, 63–65, 79, 264
  adhesion with diamond-like carbon (DLC) coatings, 220
  atomic bonding and arrangement, **14**
  basal plane of crystal structure, *119*
  bending strength, *60*, **120**
  bioinert nature, 5
  biomedical applications, 128–132
  brittleness, 34
  calcined, 118
  chemical composition, grain size, and density, **118**
  coefficient of friction, *122*, **123**, 217
  compressive strength, **120**
  crack initiation stress, 36
  density, 120
  in dental composites, 264
  elastic modulus, 30
  entropy, **50**
  fatigue life, 126, *127*
  fatigue properties, 124–128
  flexural strength, *125*
  four-point-bending strength, *153*
  fracture strength, 36
  fracture toughness (K_{IC}), *129*, *130*
  friction, *122*
  friction and wear, 156, 158
  friction coefficient, 158
  grain size, 120–121, *121*, 133
  hardness, 121
  in hip prosthesis, *1*
  impact fatigue property, 124, *125*
  in implants, 4
  in joint replacements, 129–131
  in knee joints, 131
  loading rate, *154*
  mechanical properties, **31**, **36**, **120**, 120–124
  microstructure, 121, *122*
  model of ceramic, *13*
  modulus of elasticity, **120**
  modulus of rupture, **120**
  Poisson's ratio, **120**
  porosity, 135, *160*
  proof testing, *128*
  proof-test stress, 127–128, 133
  properties, **6–7**, **39**, **152**
  properties of composite reinforcing fibers, **256**
  purity, 119
  scanning electron microscopy of, *247*
  single crystals, *117*
  solidification, 15
  static fatigue, 133, 149
  surface adsorption, *124*
  surface energy, 59, *60*, 61
  surface roughness, *122*
  tensile strength, **120**, 267
  theoretical strength, 33, **34**

- time to fracture, *126*
- total hip joint implant, *129*
- transparency, 80
- tribological properties, 121, *122*
- unit cell representation, *14*
- wear, *122*
- whiskers, **40**

Alumina–alumina pairing in ceramics, 132
Alumina/PTFE composite, 274
Alumina–UHMWPE, tribological properties, **123**
Alumina–zirconia pairing, 132
Aluminum ions, atomic bonding and arrangement, 1, 3
Aluminum oxides, 117–139
- *see also* Alumina
- corundum, 118
- source, composition, and structure, 118–120

Aluminum silicates, 2
Alveolar P_{CO2}, **84**
Alveolar ridge augmentation, *3*
American Society for Testing and Materials (ASTM), 22, **23**, 119
Amino acid, 85
- in collagen, **87**
- sequence, 87
- sequence in bone morphogenetic proteins (BMPs), *106*
- sequence in TGF superfamily, *107*
- types, **86**

Amino group of amino acids, 85
Ammonium alum, 119, 137
Amorphous calcium phosphate (ACP), 174
A_mX_n type structure, 12
- properties, **13**

Analogue composite design, 257
Anhydrites, 229
Anhydrous silica (SiO_2), 2, 7
Anisotropic, 291
Anisotropy of bone, 97
Ankylosis integration with bone, 132
Annealing, 4
Anorganic bones, 268
Anterior cruciate ligament (ACL)
- and calcium sulfate, 236
- definition, 243
- reconstruction with bone substitute, 271

Anthracite, 206, 222
AO_2, 72
A_2O_3, 72
AP, 291
APA, 178
Apatite, 184
- composition and physical properties, **184**
- crystals, 93
- in glass-ceramics, 170

Apparent porosity, 20, 26
Applied stress in alumina, 127
Appositional growth, 104
Aramid properties of composite reinforcing fibers, 254, **256**
Area of contact between two materials, 44–45
Arginine, **86**
Arterial P_{O2}, **84**
Artificial
- blood vessels, 274
- bone, 177
- heart valve discs, 4
- heart valves, 3
- joint prostheses, 118
- ligaments, *3*
- skin, 274
- teeth, 118
- tendon, 3, 5

Aseptic loosening of implant, 130
As_2O_3, formation into glass, **70**
Aspartic acid, **86**
As_2S_3, formation into glass, **70**
ASTM, 80
Atmospheric P_{O2}, **84**
Atomic bonding, 12–17
Atomic number (N), 230
Atomic radius, **13**
Auger electronic spectroscopy (AES), 171
Au_4Si, **70**
Autograft, 291
Autologous, 291
A–W, 170
- composition, **169**
- definition, 178

AX structure, 12
A_2X_3 type structure, 12

B

Baddeleyite, 142, 164
Bakelite®, 213
- on bakelite wear constant, **47**

Ball mill, 4
BaO, rock salt structure, 12
Barite, 239, 243
Barium glass inclusions, 262
Barium meal, 236, 243
Barium sulfate, 2, 228–232
- applications of, 236
- as cochlear nerve-stimulating implant, 239–242
- definition, 243
- density, 235
- physical constants of, **231**
- properties, **233**
- unit cell dimensions, 230
- x-ray absorption, 230

Barium sulfate-incorporated bone cement, 253
Barium titanate, 228, 233–235, 243
- acoustic impedances, 240
- characteristics of, **239**
- composites, *254*
- ferroelectric properties, 233
- as hard tissues substitute, 237–239
- phase transformation, 55

  properties, **6–7**
  surface textured implant, *237*
  voltage output, 237–239
  voltage output vs. peak load, **239**
Barium titanate–tin ($BaTiO_3$–Sn) composite
  definition, 7
  microstructure, *5*
Basic metabolic rate, **84**
Bauxite, 2, 118, 137
Bayer process, 118, 137
Bayerite, 118, 137
Beer's law, 230, 243
Bending strength
  of alumina, **120**, 121
  of alumina and zirconia, **152**
  of bone, **100**
  of glass ceramics, **171**
  of hydroxyapatite, 191
  of zirconia, 155, *157*, *158*
Benzene, surface tension, **62**
Benzoin alkyl ether, 262, 291
Benzoyl peroxide, 262, 291
β-hemihydrate, 228
β-silicon carbide (SiC)
  atomic bonding and arrangement, **14**
  surface energy, **61**
BHT, 291
Binder, 2
Bioabsorbable, 291
Bioabsorption, 291
Bioactive bioceramics, 5
  glass ceramics, 176, 260
  as bone substitutes, 269
Bioactive materials, time-dependent behavior, *175*
Bioceramics
  bioactive, 5
  bioinert, 5
  classification, 5
Biocompatibility
  assessment guidelines, **111**
  of ceramics and glasses, 109–111
  schematic illustration, *111*
  of titanate in implants, 232
Biodegradation, 291
Bioglass®, 4, 65, 168, 171, 177–178, *193*, **270**, 272
  composition, 169, **169**
  definition, 137, 178, 291
  dissolution, 175–176
  fatigue life, 126, *127*
  properties, **6–7**
Biointegration, 266
  of hydroxyapatite, 195
Biolox®, **118**, 152, 164
Biopolymer chemical degradation, 278–279, **279**
Biopotential in bone, 104
Biovert®, 168
  composition, **169**
  definition, 178
Biovert II®, *167*
bis-GMA, 176, 178, 262, 291
Bivariant equilibrium, 47
Blackboard chalk, 228
Blood
  distribution in human tissue, **84**
  effect on static loading, *43*
  pH, **84**
Blowing glass products, 4
BMP-2, 104, *106*, **270**
BMP-4, 104, *106*
B_2O_3, formation into glass, 70, **70**
Body-centered cubic (bcc) structure, 12
Body-centered tetragonal (bct) structure, 54
Boltzmann's constant, 50
Bond density of silica glass, **73**
Bond distance of silica glass, **73**
Bonding dental implants, 132
Bone, 248
  bonding, 171
  bonding with glass ceramics, 169, 171
  bounds for Young's modulus, 252–253
  cancellous structure, *108*
  compact, 92
  as a composite, 248
  composition and physical properties, **184**
  composition and structure, 90–92
  cortical, 90, *91*, 96
  distribution in human tissue, **84**
  drying, 97, *98*
  fibrils, 87
  mineral content, 98
  mineral phase, 98
  modeling of mechanical properties, 98–102
  organic phase, 98
  organization, *90*
  properties, **97**, **100**
  ratios of properties, **98**
  rheological properties, 101
  spongy, 92, 104
  three-element viscoelastic model, *101*
  x-ray diffraction pattern, 185, *185*
Bone, compact, *83*
Bone cement, 2, 286
  density, 235
  hyperthermia, 5
  methacrylate, 176
Bone fracture, sequence of events, *103*
Bone graft substitutes, **268**, 272–274
Bone healing and use of hydroxyapatite, 192–193
Bone ingrowth stimulation by barium titanate, 228
Bone matrix, *89*
Bone mineral deposition, 108
Bone morphogenetic proteins (BMPs), 104, 253
  amino acid sequence, *106*
  as bone substitutes, **268**, 269
  definition, 292
  particle-impregnated bone cement, 257–258
Bone particle reinforced composites, 253

Bone particle-impregnated bone cement, 257–258
Bone plates, 288
  use of composites, 254
Bone remodeling, 105–109
Bone scaffolds
  ceramic–polymer composites for, **283**
  fabrication, 281–284
  methods of fabricating, **282**
Bone Source®, **270**, 292
Bone substitutes, 228, 266, 285–286
  availability of, **270**
  classification of materials, **269**
Bone-integrating dental implants, 132
Boron glass fiber, properties for composite materials, **40**
Boron properties of composite reinforcing fibers, **256**
Boron whisker, properties for composite materials, **40**
Borosilicate glass
  mechanical properties, **31**
  properties, **6–7**
Boundary lubrication, 47
Brain, **84**
Brånemark System®, *264*
Brinell hardness number (BHN), 44
Brittle failure, 38–43
Brittle fracture, 30
Brittleness, 18, 33–34, 37
  of glass ceramics, 176
Bulk degradation of polymers, 279, *280*
Bulk density, 20, 26
Bulk modulus, 30, 67
Bulk soda glass, properties, **39**
Butylated trioxytoluene (2,4,6-tri-tert-butylphenol, BHT), 262

C

Calcination
  definition, 243
  of hydroxyapatite, 187
Calcine, 137
Calcined alumina, 118
Calcium, ion release, 269
Calcium hydroxide ($Ca(OH)_2$), 200
Calcium hydroxyapatite, 185
Calcium oxide. *See* CaO
Calcium phosphate compounds
  biodegradation, 268
  as hard tissue substitutes, 267–270
Calcium phosphate/polymer composites, 273
Calcium phosphate-rich film in glass ceramics, 171
Calcium phosphates, 2
  in bonding tissues, 5
  for bone scaffolds, 285
  use in bone healing, 192–193
Calcium sulfate, 228, 243, 268–269
  applications of, 236–237
  as bone substitute, 4, 271
  β-hemihydrate, 228
  physical constants of, **231**
  porosity by water/particle ratios, **231**
  powder particles, *229*
  properties, **233**
  source, composition, and structure, 228–229
Calcium sulfate dihydrate, *227*
Calcium titanate, 228, 235–236, 243
Calcium/phosphorus ratio
  in calcium phosphate dissolution, 268
  definition, 292
  in hydroxyapatite, 188
Callus, 104
  metabolic interrelationships, *110*
Canaliculi, 92, 113
Cancellous bone, 92, 105
  as a composite, 248
  microstructure, *259*
  structure, *108*
CaO
  in alumina, 149
  chemical composition, **118**
  glass transition temperature (T_g), 15
  phase transition of zirconia, 142
  rock salt structure, 12
$CaO–P_2O_5–H_2O$ system, phase diagram, *187*
$CaO–TiO_2$, phase diagram of, *236*
Capacitors, 2
$(Ca_{10}PO_4)_6(OH)_2$. *See* Hydroxyapatite
Carbides, 2
  brittleness, 31
  elastic modulus, 30
Carbon, 2
  bonds between, 209
  carbon fiber-reinforced, 211–212, **212**
  codeposited with silicon, 212
  compatibility with tissues, 212
  covalent bonds, 208
  crosslinks, 208
  crystalline structure of, *207*, *208*
  crystallite size, **210**
  density, **210**
  elastic modulus vs. density, *211*
  electrical resistivity, **210**
  fatigue behavior, *211*
  flexural strength, **210**
  fluidized bed, *213*
  fracture toughness, **210**
  hardness, **210**
  maximum strain, **210**
  microstructure, fluidized bed, *275*
  microstructures of deposited, *213*
  oxidized surfaces, *209*
  phase diagram of, *206*
  Poisson's ratio, **210**
  properties of, 209–212
  pyrolytic, 206, 209
  source and structure of, 206–209
  theoretical strength, 212
  thermal conductivity, **210**

  thermal expansion coefficient, **210**
  turbostratic structure, 208
  Young's modulus, **210**
Carbon black, 206
  in composites, 253
Carbon dioxide, in alumina processing, 118
Carbon fiber composites, 284
Carbon fiber-reinforced carbon, 253
Carbon fibers, 207
  for artificial tendons, 254
  properties, **210**
Carbon implants, manufacture, 212–214
Carbon nanotubes, 222
Carbon reinforced UHMWPE, **276**
Carbon steel wire, properties for composite materials, **40**
Carbon tetrachloride, surface tension, **62**
Carbonate, 90
Carbonate fluoroapatite, 184
Carbonates, formation into glass, 70
Carbon–polysulfone composite, *256*
Carbonyl group in carbon, 209
Carboxyl group
  of amino acids, 85
  in carbon, 209
Carboxylic acid
  absorption on alumina, 121
  definition, 137
Cartilage, 104
  as a composite, 248
$CaSO_4 2H_2O$. *See* Calcium sulfate
Casting glass products, 4
Catalyst
  definition, 222
  use in diamond fabrication, 206
CdO, rock salt structure, 12
CdS, atomic bonding and arrangement, **14**
Cell lifeline number in scaffolds, 277
Cells in tissue engineering, **278**
Cement, portland, mechanical properties, **31**
Cementing line, 92
Cements, 2
Cementum, 96, 113
Ceramic crowns, 132
Ceramic head, reliability, 129
Ceramic matrix composites (CMCs), 253–254
Ceramic nitrides, in implants, 4
Ceramic-based scaffolds, **283**
Ceramics
  absorption property, **267**
  A_mX_n type structure, 12
  biocompatibility, 109–111
  forming and firing of, 3–4
  glass, 2, 167–181
  inertness, 2
  mechanical properties, 30–36
  monolithic, 254
  osteoconductive, 267
  osteoinductive, 267
  packing of, 324
  processing, 2
  properties, 2, **6–7**
  strength, 20
  strengthening, 36–38
  thermal properties, 47–59
  uses in the body, *3*
Ceravital®, 168
  composition, 169, **169**
  definition, 178
Cermets, 254
  bioinert nature, 5
  as cutting tools, 4
  definition, 7
Cesium chloride (CsCl), 2, *12*
  atomic bonding and arrangement, **13–14**
Chemical degradation, 292
Chemical etching, 37, **38**
Chemical vapor deposition (CVD), 4
  for carbon, 274
  for carbon deposition on implants, 213
  definition, 8
  for diamond fabrication, 207
  producing diamond-like carbon (DLC) coatings, 216
Chemisorption, 137
Chitin, 292
Chitosan, 292
Chlorapatite, 183
Chlorine bonding and arrangement, 12–13
Chondroblasts, 104
Citrate, 90
Clay minerals, 2
Clay products, 2
Clay ware in implants, 4
Closed cell, 292
Closed pores, 20, 26
Cobalt–chromium alloys
  as acetabular cup inserts, *29*
  in hip joint prostheses, **218**
  as hip prosthesis, *1*
Cochlear nerve-stimulating implant, 239–242
CoCrMo alloy
  disc wear rate, **219**
  in joint replacements, 129
  wear, 219
Coefficient of friction
  of alumina, *122*, **123**
  of alumina-UHMWPE, **123**
  in diamond-like carbon (DLC) coatings, 217
  for various materials, **218**
Coefficient of resistivity, of barium titanate, 228
Coefficient of sliding friction, 45–46
Coefficient of thermal expansion of teeth, **102**
Collagen, 84, 87–88
  amino acid content, **87**
  as bone substitute, 269
  definition, 292
  enzymatic degradation, 281

  formation, *88*
  for soft tissue replacement, 274
  structure, *91*
Collagen fibrils, 87
  in dentin, 96
Collagen membrane in dental implants, 132
Collagen–glycosaminoglycan copolymer, 292
Collagen–mucopolysaccharide (MPS)–silastic rubber composite, 274
Collagraft®, **270**, 292
Compact bone, 92, *93*
  compression tests, **99**
  strength of strain rate, *99*
Composite biomaterials, biocompatibility, 284–285
Composite models, tension force, *250*
Composite scaffolds, 274–281
  degradation, 275–276
  ratio between characteristic time constant, 277
Composites. *See also* Specific types of composites
  applications, 253–274
  in the body, *3*
  composite carbon in, *214*
  definition, 292
  fundamentals of, 248–253
  hierarchical structure of, 248
  mechanics of, 248–250
  modulus vs. volume fraction, *252*
  properties, **256**
  stiffness, 250–251, **252**
  strength, 251–252
  structure of, 248
Compression tests on compact bone, **99**
Compressive strength, **6**, 36
  of alumina, **120**
  of alumina and zirconia, **152**
  of bone, **97**
  of glass ceramics, **171**
  of hydroxyapatite, 191
  of teeth, **102**
Compton effect, 230, 243
Computerized tomography (CT), 243
Concise® dental composites, **262**
Concrete
  mechanical properties, **36**
  properties, **6–7**
Conductivity and porosity, 20–21
Contact angle, 62, *62*
  of alumina and zirconia, **152**
CoO, rock salt structure, 12
Coordination number (CN), 12
  definition, 26, 80
  in glass formation, 72
Copper
  on copper wear constant, **47**
  ductile, 34
  on low-carbon steel wear constant, **47**
  as nucleating agent, 168
  surface tension, **62**
  theoretical strength, **34**
Coral in composites, *260*
Corelle® wares, 168
Corning® 7052, 75
Corning Glass Works, *167*
Corning ware, *167*
Corrosive wear, 46
Cortical bone, 90, 96
  constituents, *91*
Cortoss®, *273*
  as bone graft substitute, **268**
  definition, 292
Corundum
  entropy, **50**
  native, 118
Covalent bonds, 2, 13
  and brittleness, 31
Crack
  around stress tip, 34–35
  elliptic, 34–35
  growth, 42, *42*
  growth and delayed effect on fatigue strength, 124
  initiation stress (K_{IC}), 36
  propagation, 146–147, *147*
  size and fracture strength of glass, **74**
  tips, 37
Cranial repair, *3*
Creep
  in composites, 256, 263
  in dental composites, 263
Cristobalite, 15, 26
  crystallization rate, 70, *71*
  phase transformation, 58
Critical nucleus, 71
Critical path length in scaffolds, 277
Critical stress of fracture (σ_c), 129
Cr_2O_3, 63
  in alumina implants, 119
  atomic bonding and arrangement, 13, **14**
  surface energy, **61**
Crosslinks, 87, 222
  in carbon, 208
Crown
  ceramic, 132
  definition, 113
Crystallite size, types of carbon, **210**
Crystallization
  in glass ceramics, 168
  of hydroxyapatite, 187
  rate in glass, 70–71, **72**
Crystallography, zirconia, **143**
Crystals, growth of, *11*
CsBr, 12
Cubic, 292
Cubic silica, unit cell representation, *14*
Cubic zirconia, 142, 149, 161
  atomic bonding and arrangement, 13
  definition, 164
  phase transformation, 57–58
  unit cell representation, *14*

Culmann's crane, *108*
Cumulative fatigue probability, 125–126, *126*
Cumulative probability of failure, 77
Curie temperature, 228, 233, 243
Cusp, diagram of, *94*
Cuspid, 92
Cutting tools, 4
CVD, 222, 292
Cysteine methionine, **86**
Cystine, **86**
Czochralski process, 4, 8

D

$D^6$3 space group, 137
$D^6$3d space group of alumina, 119
Decalcified bovine dental enamel, *95*, 96
Deciduous teeth, 92
Demineralized bone matrix, 268
Demineralized bone strength, 100
Densification, 209
Density, **39**
  of alumina, **118**, 120
  of alumina and zirconia, **152**
  of bone, **100**
  calculation, 15–16
  of ceramics, **31**
  of porous materials, 20
  of teeth, **102**
  of types of carbon, **210**
  of zirconia, **143**, **145**
Dental cements, 262–264
Dental composites, 253, 262–264, 284
  composition and shear modulus, **262**
  decalcified bovine dental enamel, *95*, 96
  filling material, 248
  microstructure, *249*
  properties, **263**
Dental implants, *3*, 5, 132, 176
  factors affecting outcome, *131*
  interfacial shear strength, 266
  and osseointegration, 264–266
  roots, *265*
  scanning electron microscopy of, *264*
  use of zirconia, 160
Dentin(e), 96
  as a composite, 248
  composition and physical properties, **184**
  definition, 113
  physical properties, **102**
  x-ray diffraction pattern, *185*
Dentinal tubules, 96
Dentinoenamel junction, 92, *94*
Deorganized bones, 268
Desert rose, *227*
Diamond, 2
  atomic bonding and arrangement, 13
  brittleness, 31, 34
  coating implant surfaces, *205*
  cubic, *207*
  density, 15–16
  entropy, **50**
  on enzymatic activity, 221–222
  fabrication, 206
  hexagonal, *207*, 207–208
  properties, **6–7**, 209, **210**
  theoretical strength, 33, **34**
  transparency, 80
  unit cell representation, *14*
Diamond-like carbon (DLC) coatings, 214–221
  abrasion, **220**
  biocompatibility of, 220–221
  composition, **215**
  in-vivo studies, 221
  material and mechanical properties, 217–218
  producing, 215–217
  tribology, 218–220
Diaphysis, 92
Dicalcium phosphate, 268, 269
Dicalcium phosphate anhydrous, 185
Dicalcium phosphate dihydrate, 185, 200
Die forming, 4
Diffusion length in scaffolds, 277
Diffusion-controlled nucleation and growth, 54–55
Diffusionless transformation, 54–55
Diffusivity of nutrient in scaffolds, 277
Direct biochemical bond in hydroxyapatite, 197
Disaccharides, 89
Dislocation, 67
Dislocation motion, *31*, 36
Dislocations in bonds, 31
Dissolution rate, 175–176
DLC, 222
DLC coatings. *See* Diamond-like carbon (DLC) coatings
DNA microassays, *69*
Drawn silica fiber, properties for composite materials, **40**
Drierite®, 228, 243
Drug delivery, 5
Dry pressing, 4
Drying bone, 97, *98*
Ductile materials, 33–34
  wear properties, 44
Dynagraft®, 292
Dynamic (cyclic) load, 43
Dynamic fatigue of alumina, 125–126

E

Ectopic bone formation in implants, 130
E glass fiber, properties, **39**, **256**
Elastic modulus, 30, **31**
  of compact bone, **99**
Elastic strain energy, 51
Elastin, 87, 89, 113
Electric arc use in implants, 119
Electric callus, 106–107

Electric conductivity, 19
Electrical potentials, 107
  in bone, 104
Electrical resistivity, types of carbon, **210**
Electron diffraction, 18
Electron microprobe, 18
Electronegative potential
  of rabbit limb, *108*
Electronegativity, 2, 106–107
  in bone, 104–105
  definition, 8
Elemental analysis, 18
Elliptic crack, 34–35
Emulsion freeze drying of bone scaffolds, **282**
Enamel, 2,, 96
  composition and physical properties, **184**
  physical properties, **102**
  prism, 92
  ultra-structure, *95*
  undecalcified, *95*
  x-ray diffraction pattern, 185, *185*
Encapsulation of matrix in glass ceramics, 176
Endosteal surfaces, 109
Endosteum, 92
Energy absorption capacity of compact bone, **99**
Energy to fracture, 34–35
ENT, 178
Enthalpy, 48, 51
Entropic energy, *52*
Entropy, 48
  of common substances, **50**
  of mixing (S_{mix}), 49–50, *51*
Epiphysis, 92, 105
Epitaxial nucleation
  definition, 200
  sites in hydroxyapatite, 197
E rods, etched in hydrofluoric acid (HF), **39**
Ethanol, formation into glass, 70
Ethyl mercaptan, surface tension, **62**
Eutectic reaction, 53–54

F

46S5.2 system, glass-ceramics, 169
Face-centered cubic (fcc) structure, 12–13, *14*, 26
Failure probability, femoral head of hip joint prosthesis, *151*
Failure strength in ceramics, 30
Fatigue fracture, 42
Fatigue life
  of alumina, 126, *127*
  of zirconia, 146
Fatigue strength of alumina, 124–125
Fatigue tests, 43
FDA guidelines for toxicity tests, *111*
Fe^{3+} in alumina implants, 119
Feldspar, *11*
Femoral head, 2
  zirconia-based, *141*
Femoral head sphere, 129
Femoral stem fixation and interfacial shear strength, *259*
Femur, 92
FeO, rock salt structure, 12
Fe_2O_3
  in alumina, 119
  atomic bonding and arrangement, 13, **14**
  chemical composition, **118**
Ferroelectric, 2, 244
Ferroelectric properties of barium titanate, 228
Fiber inclusion, *249*
Fiber pull-out, 252
Fiberglass as a composite, 248
Fiber-mesh/fiber-bonding of bone scaffolds, **282**
Fibers in composites, properties, **40**
Fibrin, 292
Fibroblast growth factor 2 (FGF-2), 292
Fibroblast growth factor (FGF)
  as bone graft substitute, **268**
  definition, 113
Fibroblasts, 103–104
Fibronectin, 200
  in hydroxyapatite, 195
Fibrosseous integration, 266
Fibrous composites, 251–252
Filaments of alumina, mechanical properties, **120**
Fire polishing, 37, **38**, 67
Flake graphite, 206
Flat sheet structure of protein, *85*
Flexural modulus, of carbon fiber-reinforced carbon, **212**
Flexural strength
  of alumina, *125*
  of carbon fiber-reinforced carbon, **212**
  of types of carbon, **210**
  of zirconia, **145**
Fluid lubrication, 46–47
Fluidized bed, 8, 222
Fluoride, 90
Fluorine, in hydroxyapatite, 188, *190*
Fluorite structure, 164
  of zirconia, 142, *143*
Fluoroapatite, 183
Flux growth method for hydroxyapatite, **186**
FN borosilicate glass, 75, *76*
Force of cohesion, 32
Force vs. interatomic separation, *32*
Forming and firing, 3–4
Four-point-bending strength, *153*
Fraction of porosity, 20
Fracture
  electronegative potential, *108*
  healing, 102–105
Fracture strength, 30, 38–39
  of alumina, 36
  of glass, **74**

Fracture toughness, **7**, 35–36, **36**, 137
  of alumina, 129, *130*
  of alumina and zirconia, **152**
  of glass ceramics, **171**
  of types of carbon, **210**
  of zirconia, 145, **145**, *146*
Free energy, 48–49, *49*
  vs. composition, *53*
  of mixing, 51–52, *52*
  of nucleation, 55–57
Freeze drying of bone scaffolds, **282**
Friction, 44–47
  adhesive, 44
  of alumina, *122*
Friction and wear
  of alumina, 156–157
  of 316L stainless steel, 156–157
  of zirconia, 156–157
Friction coefficient, 158, 160
Fully dense Al_2O_3 (bulk polycrystalline body), properties, **39**
Functional adaptation of bone, 105
Fused deposition modeling (FDM), 292
  of bone scaffolds, 282
Fused silica, *71*
  mechanical properties, **31**

G

Ga_2O_3, atomic bonding and arrangement, 13
Garnet, 4
Gas foaming of bone scaffolds, **282**
Gastric contents pH, **84**
Gaussian distribution, 75, 80
Gel growth method for hydroxyapatite, **186**
Gelatin, 292
Gel–sol transfer
  definition, 244
  for processing calcium titanate, 228
GeO_2
  formation into glass, 70, **70**
  viscosity, **72**
Gibbs free energy (G), 48–49
Gingiva, 92
Glass(es), 2, 70
  biocompatibility, 109–111
  formation, **70**, 70–72
  fracture strength, **74**
  mechanical properties, 30–36
  properties, 2, **6–7**, **39**
  static fatigue, 74–77
  strength, 72–74
  strengthening, 36–38
  surface compression, *37*
  theoretical strength, 33
  thermal properties, 47–59
  transition temperature, 14–15, 26
  uses in the body, *3*
  uses of, *69*
Glass ceramics, 2, 167–181
  apatites in, 170
  bioactive, 176
  bonding to bone, 169, 171
  in bonding tissues, 5
  as bone substitutes, 271–272
  changes in pH, *172*
  chemical properties, 171–176
  coatings and composites, 176
  compositions, **169**
  crystallization, 38
  definition, 8
  dental applications, 174
  depth profile, *173*
  ENT applications, 174
  formation, 168–170
  maxillofacial applications, 174
  mechanical properties, 171, **171**
  nucleation, 168
  properties, **6–7**, 170–176
  solubility, *172*
  special processing of, 4
  surface crystallization, **272**
  temperature–time cycle, *168*
  transmission electron micrograph, *174*
Glass-fiber-epoxy composite, *249*
Glass products, 2
  processing of, 4
Glass structures, *16*
Glass transition temperature, 14–15, 26
Glassy carbon, 207
  properties, **210**
Glazes, 2
Glutamic acid (Glu), **86**, 113
Glutaraldehyde, 293
Glycerol, viscosity, **72**
Glycine (Gly), 85, **86**, 113
Glycoproteins, 96
Glycosaminoglycans (GAGs), 89, 173, 248
Gold
  surface tension, **62**
  theoretical strength, **34**
  transparency, 80
Goniopora coral in composites, *260*
Grafton®, **270**
  as bone graft substitute, **268**
  definition, 293
Grain size
  of alumina, **118**, 120–121, *121*, 123
  in crystalline solids, 22–24, *23*
  influence on tensile strength, 59–60, *60*
  of Lucalox®, 24
  ranges, **23**
Grain size index, 22
  alumina, 133
Grain size number
  alumina, 123, 133
Granulation tissue, 102

Graphite, 2
  properties, **6–7**, **210**
  theoretical strength, **34**
Graphite whisker
  properties for composite materials, **40**
Green in ceramics, 4
Griffith crack length, 76
Griffith flaws, 37, 63, 129, 137
Griffith law, average depth, 134
Griffith theory, 67
Griffith-Orowan-Irwin approach, 34
Griffith's theory of fracture, 38, 72, 112
Growth plate, 105
Gum, 92
Gypsum, 228–229, 244
  crystal formation, *230*
  setting of, *230*
  unit cell volume, 241

H

HA, 293. *See* Hydroxyapatite
Halides, formation into glass, 70
Hard tissue engineering scaffolds, 248
Hard tissue substitutes, 266–274
Hard tissues, 84
  healing and remodeling, 102–109
Hardness, 44
  of alumina and zirconia, **152**
  for diamond-like carbon (DLC) coatings, 217
  of glass ceramics, **171**
  test, *44*
  of types of carbon, **210**
  of zirconia, **145**
Hardness scales, *45*
Haversian canal, 91, 107, 248
Haversian system, 91, 92
  definition, 113
  lamellae, *93*
HCA, 178
HDPE (high-density polyethylene), 177
Heart, distribution in human tissue, **84**
Heart valve
  implantation, 5
  replacement, 274
Heart valve disc
  from alumina, 136
  made with pyrolytic carbon, 206
Heat of formation, zirconia, **143**
Heat of fusion, 72
Helical arrangement of a protein, *85*
Hematoma, 102–103
Hemihydrate
  of calcium sulfate, 228
  definition, 244
Heterotopic osteogenesis, 276
Hexagonal close-packed (hcp) structure, 12–13, *14*
  of alumina, 119
  definition, 26
n-hexane
  surface tension, **62**
High-density nylon 66 fiber, properties for composite materials, **40**
Hip joint head, with diamond coating, *205*
Hip joint implant, *129*
Hip joint prostheses, *29*, 257
  materials for, **218**
  stress corrosion on, 151
Hip joint structure, testing, *131*
Histidine, **86**
Homogeneous nucleation, 55–57, *56*, 71
Hooke's law, 30, 67
Hoop strain, *151*
Hot isotropic pressing (HIP)
  definition, 200
  of hydroxyapatite, 186
Hot pressing method of hydroxyapatite, 186
Hybrid vacuum process, 223
Hydrides, 2
Hydrofluoric (HF) acid, 37
Hydrophilic polymers, 279
Hydrophobic amino acids, 88
Hydrophobic polymers, 279
Hydrostatic molding, 4
Hydrothermal method for hydroxyapatite, **186**, *188*
Hydrothermal treatment of zirconia, 152, *153*
Hydroxides, precipitation of zirconium, 142
Hydroxyapatite, 2, 90, 102, 171, 183–203
  applications for implants, 192–197
  attachment to bone, 248
  bending strength, 191
  biocompatibility, 192
  biointegration and osseointegration, 195, 197
  for bone regeneration, 276
  calcium/phosphorus ratio, 188
  chemical properties, 192
  coating, 192–193
  coating by plasma spraying, 214
  coating zirconia, 160
  compressive strength, 191
  crystallinity of, 260
  definition, 113
  dense (microporous) form, 186
  dissolution and precipitation, 193–195, *196*
  early history of manufacturing, **194**
  elastic modulus, **191**
  on enzymatic activity, 221–222
  formation of artificial, 272
  hydrothermally synthesized, *188*
  infrared reflection spectroscopy (IRRS), *173*
  initial rate of calcium ion release, 199
  macroporous form, 186
  mechanical properties, 191–192
  morphology, *193*
  nanoparticles, 274
  plasma spraying, 193, *194*, 197
  Poisson's ratio, 191
  porosity in implants, 260

  precipitates, 187
  preparation techniques, **186**
  properties, **6–7**
  scanning electron microscopy of, *247*
  solubility, 192
  strength of composite, 191–192
  substitution of OH with fluorine, 188, *190*
  tensile strength, 267
  three-dimensional view of structure, *190*
  unit cell dimensions, *189*
  unit cells in, 198
  Vickers hardness, 191
  x-ray diffraction pattern, *189*, *195*
  Young's modulus, 289
Hydroxyapatite implant, histology of, *276*
Hydroxyapatite–polymer composite, 257
  effect of volume fraction, *258*
Hydroxycarbonate apatite (HCA), 174
Hydroxyl group in carbon, 209
Hydroxyl ions, 87, 90
Hydroxyproline (Hypro), **86**, 87, 113
Hyperthermia
  in bone cement formulation, 5
  definition, 8

I

Ideal gas, 49
Iliac crest repair, *3*
Immix® as bone graft substitute, **268**
Immix Extenders®, *273*, 293
Immunogenicity, 293
Impact fatigue
  in alumina, 124
  definition, 137
Impact strength, 43, 67
Implants. *See also* Specific types of implants
  aseptic loosening, 130
  coating, 193
  dental, *131*, 132
  fabrication with alumina, 118
  fixation, 130, 132
  load-bearing, 30, 176
  middle ear, 167
  pain in, 130
  strength, 151–154
  study of tissue ingrowth, *247*
  surface textured, *237*
  thickness of, 277
  use of alumina crystals, 119
  voltage output vs. distance from the surface, **240**
  voltage output vs. peak load, **239**
  voltage outputs, *238*
Inclusion, 293
  principle shapes of, 248, *249*
Incongruency
  definition, 137
  in knee joints, 131
Industrial diamond, 206
Inert strength
  definition, 164
  of zirconia, 153
Infection in implants, 130
Infrared reflection spectroscopy (IRRS), 171
  of hydroxyapatite, *173*
Injectable bone substitutes, 269
In_2O_3, formation into glass, 70, **70**
Insulin-like growth factor (IGF), 113
Interatomic separation vs. force, *32*
Interatomic spacing, 35
Interchain crosslinks, 87
Interfacial shear strength
  in composites, 257–258
  of dental implants, 266
Interlaminar shear of carbon fiber-reinforced carbon, **212**
Internal bone remodeling, 109
Internal energy
  of mixing, 51
  variation, *51*, *52*
Interpore®, *273*
Interstitial P_{O2}, **84**
Intracellular fluid pH, **84**
Intraocular lenses (IOLs), 79
Invariant point in allotropy, 47
In-vitro aging of collagen, 88
Ion beam-assisted deposition (IBAD), 215–216
  schematic diagram for, *216*
Ion exchange, 37, **38**
Ionic bond, 87
  and brittleness, 31
  definition, 67
Ionic compounds, bonding and arrangement, 12–17
Ionic radius, **13**
Iron
  entropy, **50**
  mechanical properties, 34
  phase transformations, *49*
  theoretical strength, **34**
Iron whisker, properties for composite materials, **40**
Irreversible process of mixing, 49
IRRS, 178
ISO (International Standard Organization) guidelines, *111*
Isocap® composition of dental composites, **262**
Isopentane, surface tension, **62**
Isotropic, 293

J

Jarvik artificial heart, 274
Joint replacements with alumina, 129–131

K

Kaolinite ($Al_2(Si_2O_5)(OH)_4$), 2, 8
K_2CO_3–$MgCO_3$, formation into glass, **70**
Keratoprostheses, 3

Kevlar®, 254
  of composite reinforcing fibers, **256**
Kidneys, distribution in human tissue, **84**
Knee joint implants, 131
Knee joint prosthesis, *141*
Knoop test, 44

L

Lactone group in carbon, 209
Lacuna, 92, 114
Lamellae, 248
Lamellar bone, 103
Laparoscopy and use of titanate, 232
Laser, 137
Laser ablation, 217
Laser crystals, 119, 170
Lattice straining, 38
Laughing gas (N_2O), **50**
Law of bone transformation, 105
Lead, entropy, **50**
Leucine, **86**
Lever rule, 52, 58
LiF, atomic bonding and arrangement, **14**
Ligament replacement, 5
Li_2O–ZnO–SiO_2, 169, 170
Liquid metal, 79
Liquids, wetting characteristics, 62
Liquid–vapor interface, *61*
Liver, distribution in human tissue, **84**
Load carrying function of hard tissues, 90
Load transmission function of hard tissues, 90
Load-bearing implants, 30, 176
Loading rate of zirconia, 153, *154*
Low-carbon steel on copper wear constant, **47**
Low-temperature isotropic (LTI) carbon, 208
  definition, 293
  properties, **210**
Low-temperature isotropic (LTI) carbon deposition, 223
Lubricant, 2
Lubrication, 46–47
  boundary, 47
  fluid, 46–47
Lucalox®, *18*, 121
  definition, 137
  grain size, 24
Lungs
  as a composite, 248
  distribution in human tissue, **84**
Lyophilization of collagen, 88
Lysine, **86**, 87

M

Machinable glass-ceramics, *167*, 169
Macrophage, 200
Magnetic materials (nonmetallic), 2
Mandibular (lower) bone, 92
Manufactured single crystals, 2
Marrow cavity, 104
Martensitic phase transformation, 54–55
Master curve, 80
Matrices in tissue engineering, **278**
Matrix, 293
Maxillary (upper) bone, 92
Maxillofacial reconstruction, *3*
Maximum strain, types of carbon, **210**
Maximum strain to failure of compact bone, **99**
Maximum velocity of glass forming liquids, **72**
Maximum velocity temperature of glass forming liquids, **72**
Mean absorption coefficient, **232**
Mean free distance between particle centers, 22, 27
Mean free distance between particles, 22, 26
Mean intercept length, 21, 27
Measured strengths of silica glass, **73**
Melt extrusion of scaffolds, 281
Melt growth method for hydroxyapatite, **186**
Melt molding of bone scaffolds, **282**
Melting temperature, **7**
Mercury, entropy, **50**
Mesenchymal stem cells (MSCs)
  as bone graft substitute, **268**
  definition, 293
Metal head taper in implants, 153–154, *154*
Metal implants, 274
Metal ions, in alumina implants, 119
Metal matrix composites (MMCs), 254
Metallic bond, 31, 67
Metallic oxides, 2
Metals
  in bone regeneration, 274
  brittle, 34
Methane
  for diamond fabrication, 206–207
  in producing diamond-like carbon (DLC) coatings, 216
Methanol, formation into glass, 70
MgO
  atomic bonding and arrangement, 13
  effect on grain size in alumina, 121
  mechanical properties, **31**
  rock salt structure, 12
  stabilizing zirconia, 145
  surface energy, **61**
  use with aluminum oxides, 118
MgO–CaO, phase diagram, *54*
MgP, atomic bonding and arrangement, **14**
Microcracks in implants, 132
Microfilled composites, 263
Microstructure
  characterization, 18–21
  determination, 22–24
  statistical analysis, 21–22
Middle ear implants, *167*
Mineral content of bone, 98, **100**
Minimum radius ratio (r/R), 12, 27

Minimum service life (t_{min}), 127
Miradapt®, *249*
Mixing
  contribution to energy, 51
  entropy of, 49
Mixture rule, 114
MnO, rock salt structure, 12
MnS, atomic bonding and arrangement, **14**
Modulus of elasticity, 112
  of alumina, **120**
  of bone, **97**
  of teeth, **102**
Modulus of rupture, **6**, 59
  of alumina, **120**, 135–136
Modulus of rupture tests, 77–78
Mohs hardness, *11*
  in alumina, 121
  zirconia, **143**
Mohs number, 137
Moisture, affecting zirconia, 156
Molar, diagram of, *94*
Molybdenum wire, properties for composite materials, **40**
Monocalcium phosphate, 269
Monoclinic phase changes, zirconia, *154*, *155*
Monoclinic strength, 164
Monoclinic structure, 47
Monolithic ceramics, 254
MPS (mucopolysaccharide), 293
Mucopolysaccharide–protein complexes, 88, 89
Mullite, 15
  definition, 27
  phase transformation, 58
Muscle
  and bone, 90
  distribution in human tissue, **84**

N

NaBr, surface tension, **62**
NaF, surface tension, **62**
Nanoparticle composites, 253, *254*, 263
Nanoparticles, 232
  in scaffolds, 284
Nanotechnology
  in bone scaffolds, 285
  definition, 293
  for manufacturing zirconia–alumina composites, 161
  for scaffolds, 290
Na_2O
  in alumina, 119
  chemical composition, **118**
  glass transition temperature (T_g), 15
$Na_2O–2SiO_2$, viscosity, **72**
Native corundum (aluminum oxide mineral), 118
Neodymium-doped glass, 69, 80
Neointima, 293
NiO, rock salt structure, 12
Niobium oxidized with zirconium, 161
Nitinol®, 55
Nitrides, formation into glass, 70
Norian SRS®, **270**
  as bone graft substitute, **268**
  definition, 293
Nucleation
  of glass ceramic, 168
  and glass formation, 71–72
Nucleation energy, 55–56
Nucleation rate vs. temperature, *57*
Nutrient concentration at implant, 277
Nuva-fil® dental composites, **262**

O

Octacalcium phosphate (OCP), 185, 200
Octagonal space, 12, *14*
Octahedral site, 12–13
  of alumina, 119
  definition, 27
OP-1, 270, 293
Open cell, 293
Open pores, 20, 27
OPLA as bone graft substitute, **268**
Opteform®
  as bone graft substitute, **268**
  definition, 293
Ordinary-quality glass fiber (E glass), properties, **39**
Orthoblast®
  as bone graft substitute, **268**
  definition, 293
Orthopedic fixation devices, *3*
Orthopedic implants, 253–261
  use of polymers, *255*
Orthopedic load-bearing applications, *3*
Orthotropic, 293
Osseoinduction, 293
Osseointegration, 232
  with bone, 132
  in dental implants, 132, 264–266
  of hydroxyapatite, 197
  sequence of, *265*
Osteoblast, 104, 173, 200
Osteoconduction, 171, 178
Osteoconductive, 293
Osteoconductive ceramics, 267
Osteogenic cells, 103–104
Osteogenicity, 178
Osteograf®
  as bone graft substitute, **268**
  definition, 93
Osteoid, 200
Osteoinduction, 171
  by collagen mineral composite, 276
  definition, 178
Osteoinductive ceramics, 267
Osteon lamillae, mineral portion, *92*

Osteons, 85, 89, 91–92, 109, 275
  definition, 114
  tension and compression data, *109*
Osteoporosis, 109
Osteoproduction, 178
OsteoSet®, 228, 236
  as bone graft substitute, **268**
  definition, 244, 294
Otolaryngological implants, *3*
Oxides, 2
  in glass formation, 70, 72
Oxinium®, 161, 163, 164
Oxygen ion (O^{2-}), radius, 12
Oxygen polyhedra in glass formation, 72
Oxyhydrogen flame, 119

P

Packable dental composites, 263
Packing of ceramics, 3–4
Pain in implants, 130
PAN carbon properties of composite reinforcing fibers, **256**
Partially stabilized zirconia (PSZ), 164
Particle or fiber diameter, **39**
Particulate inclusions, 248, *249*
PbO_2, formation into glass, 70, **70**
$PbO–2B_2O_5$, viscosity, **72**
PdCo alloy
  in cancer treatment, 5
  definition, 8
PDGF (platelet-derived growth factor)
  as bone graft substitute, **268**
  definition, 294
Pd_4Si, formation into glass, **70**
Peptides, 85
Percutaneous access devices, *3*
Percutaneous implant, 266
Periodontal membrane, 96
Periodontal pocket obliteration, *3*
Periosteal callus, 104
Periosteal surfaces, 109
Periosteum, 92, 103–104
Perovskite, 233
  definition, 244
  unit cell structure, *233*
PGA (polyglycolic acid), 294
pH, **84**
Phase, 47
Phase changes, 47–59
  composition and stability, 49–54
Phase diagram, *48*
  of $CaO–P_2O_5–H_2O$ system, *187*
  of carbon, *206*
  MgO–CaO, *54*
  of $SiO_2–Al_2O_3$, *17*, 133–134
Phase rule, 15, 27
Phase separation phenomena, 17
Phase transformation
  bending strength, **158**
  mechanism, 54–59
  rate, *55*
  of zirconia, 145, 154–156, *156*, *157*
Phase transformation toughening process, 164
Phenolformaldehyde, 213, 223
Phenylalanine, **86**
Phosphate mineral apatites, 183
Phosphate rock, 184
Phosphorite, 184, 200
Phosphorus, formation into glass, **70**
Phosphorus pentoxide (P_2O_5), 271
Photoelectric effect, 230
Photosensitive glass, 178
Physical degradation, 294
Physical vapor deposition (PVD), 217
  schematic diagram, *217*
Piezoelectric ceramic, 55
Piezoelectric layer of titanate, 232
Piezoelectric properties, 107
  of barium titanate, 228
Piezoelectric sensitivity coefficient, 239–240
Piezoelectric stimulator, 241
Piezoelectricity, 106, 114, 244
Pin-on-disc wear tests, 217, 219
Planck's constant, 231
Plasma spraying of hydroxyapatite, 193, *194*, 197
Plaster of Paris, 228
  as bone substitute, 5
  definition, 244
  porosity, *20*
Plastic deformation, 37, 44, 67
Plastic junctions, 44, *46*
Plastic work, 35
Platelet inclusions, *249*
Platelet-derived growth factor (PDGF), 114
Platinum, entropy, **50**
Plexiglas®, 70
PLGA/PGA polymer, 274
Plug implants
  interfacial shear strength, *261*
PMMA. *See also* Polymethylmethacrylate (PMMA), 80
P_{O2}, **84**
P_2O_3, formation into glass, 70, **70**
P_2O_5
  as nucleating agent, 168
  viscosity, **72**
Poise, 81
Poisson's ratio, 30, **31**
  of alumina, **120**
  of alumina and zirconia, **152**
  of carbon, 209
  of composites, 251
  definition, 67
  of hydroxyapatite, 191
  of types of carbon, **210**
Polar amino acids, 87

Polarizing circuits, *238*
Polyacrylonitrile (PAN), 207, 213, 223
Polyamides, 85
Polycrystalline alumina, *117*
  mechanical properties, **120**
Polycrystalline calcium titanate, 235
Polycrystalline ceramics, 59
Polycrystalline fiber, properties, **39**
Polyetheretherketone (PEEK)
  in carbon fiber composites, 254, 256
  coating hydroxyapatite, 214
  definition, 223
Polyethylene
  in glass ceramics, 176
  properties of composite reinforcing fibers, **256**
  theoretical strength, **34**
Polyglycine, 87
Polylactic glycolic acid (PLGA), 281
  as byproduct of scaffold degradation, 282
  definition, 244, 294
  degradation, 290
  in tissue engineering, 285
Polylactic glycolic acid (PLGA) composites, 254
  schematic illustration, **255**
Polymer matrix composites (PMCs), 254
Polymeric fibers for carbon fabrication, 207
Polymeric phase transformation, 47
Polymers
  biocompatibility, 285
  chemical degradation, *279*
  in orthopedic implants, *255*
Polymethylmethacrylate (PMMA), 70, **70**, 79, 27
  in glass ceramics, 176
  mechanical properties, **36**
  properties, **6–7**
  strength, 20
  wear of coating combinations against, **220**
Polymorphic, 223
Polymorphism, zirconia, **143**
Polyphenol ether, pentaphenyl trisiloxane, 215
Polysaccharides, 85, 89, 114, 248
Polystyrene, properties, **6–7**
Polysulfone in glass ceramics, 176
Polysulfone matrix in carbon fiber composites, 254
Porcelain, 2, **6–7**
  enamels, 2
Pore size gradient across a sponge, *280*
Pores
  closed, 20
  formation, 18–19, *19*
  open, 20
Porities coral in composites, *260*
Porosity, *18*, 18–20, *20*
  of alumina, 135–136
  of alumina and zirconia, **152**
  apparent, 20
  distribution in alumina, 121
  fraction, 20
  model of bone, 101
Porous ingrowth, 294
Porous-surfaced composites, 260
Porous-surfaced implant
  structure of, *261*
Portland cement in implants, 4
Pottery, 2
Pressing glass products, 4
Probability of failure, 127
Proline (Pro), **86**, 87, 114
Proof-test stress, *41*
  of alumina, 127–128, 133
Proof-testing of ceramic heads, 129–130
ProOsteon®, **270**, *273*
  as bone graft substitute, **268**
  definition, 294
Proplast®, 274, 294
Prostate cancer, 5
Prosthesis. *See also* specific types
  hip, *1*
  precoating with bone cement, 286–287
Proteins, structure, *85*, 85–89
Proteoglycans, 89
PS, **70**, 81
Pt groups as nucleating agents, 168
PTFE (polytetrafluoroethylene), 274, 294
Pulp, 114
Purification of materials, 17
Purity of alumina and zirconia, **152**
Push-out test, 287
PVC, formation into glass, **70**
Pyrex®, 79
Pyrolidine, 87
Pyrolytic carbon, 4, 206, 209, 274
  deposited on implants, 213
  fracture strength vs. density, *210*
Pyrolyzed carbon, 2

Q

Quartz, 2, *11*
  definition, 8
  properties, **6–7**
Quenching, 37, *37*, **38**, 67

R

Radiation, therapeutic, 5
Radioactive materials in implants, 152
Radius ratio, 2, 8
Range of motion in joints, 131
Rate of consumption of nutrients in scaffolds, 277
Rate of crystallization, 70–71, *71*, **72**
Rate of loading on bone, 97
Rayon, 213, 223
Refractive index, zirconia, **143**
Refractory materials, 2
Reinforcing fiber composites, properties, **256**
Remodeling of bone. *See* Bone remodeling
Remodeling process, 104

Replamineform, 274, 294
  porous tube, 274
Replamineform process, 258, *260*
Residual stresses, 4
Resistors, 2
Resorption, 294
Reuss model, 19, *19*, 100–101, 112
  for composite structures, *250*, 250–251
  definition, 27, 114
Rhakoss®, *273*, 294
Rheological properties of bone, 101
Rhomboid, 244
Rib, fractured, *105*
Ringer's solution, 137
Rock salt structure, 12
Rockwell test, 44
Rolling glass products, 4
Rubber in composites, 253
Ruby, 2, 118
  mechanical properties, **120**
Rule of mixtures, 250
Rutile, density of, 232

S

S glass fiber
  properties, **39**
Sapphire, 2, 75, 118
  alumina production, 119
  mechanical properties, **120**
Sb_2O_3, formation into glass, 70, **70**
Sb_2S_3, formation into glass, **70**
Scaffolds
  cell lifeline number in scaffolds, 277
  cell materials interaction, 283–284
  ceramic-based, **283**
  prototypes, *281*
  surface area percentage increase, 284
Scanning electronic microscopy (SEM), 18
Sea corals (porites), 184–185
Sea urchin tentacles, 274
Second crystalline phase in strengthening, 38
Second-phase particles, **38**
Selenides, 2
SeO_2, formation into glass, 70
Serine, **86**
Shape memory alloys, 55
Shear modulus, 30, **31**, 33, **34**, 67
  of composites, 251
  of dental composites, **262**
Shear strength, 33, 44
Short-fiber composites, 252
Shrinkage of ceramics, 3–4
SI (International System) unit, 61
Sialon
  adhesion with diamond-like carbon (DLC) coatings, 220
  bioinert nature, 5
  properties, **6–7**
SiC. *See* Silicon carbide (SiC)
Silar® dental composites, **262**
Silica
  atomic bonding and arrangement, 13
  in composites, 253
  fatigue strength, 124
  tetrahedron, *11*, 13
  theoretical strength, **34**
Silica fiber, properties, **39**
Silica glass, properties, **73**
Silica inclusions, 262
Silicate glasses, 73
  atomic bonding and arrangement, 13
Silicates, 2
  in implants, 4
  structures, *15*
Silicic acid, 171–172
Silicon
  brittle, 34
  codeposited for carbon implants, 212
  theoretical strength, **34**
Silicon carbide (SiC)
  atomic bonding and arrangement, 13
  bond energy of silica glass, **73**
  on enzymatic activity, 221–222
  mechanical properties, **31**
  properties, **6–7**
  unit cell representation, *14*
Silicon carbide whisker, properties for composite materials, **40**
Silicon dissolution in glass ceramics, 171–173
Silicon nitride, 77
  definition, 8
  in implants, 4
  mechanical properties, **31**
  properties, **6–7**
Silicone oil, 79
Silicone rubber resin, 274
Silico-phosphate type of glass ceramics, 169
Silver
  surface tension, **62**
  theoretical strength, **34**
Simple cubic structure (CsCl), 12, 27
Si_3N_4 whisker, properties for composite materials, **40**
Single-crystal Al_2O_3, in implants, 4
Single-crystal Al_2O_3 rod, flame-polished, **39**
Single-crystal Al_2O_3 rod, surface-ground, **39**
Single-crystal ceramics, 4
Sintered Al_2O_3 (bulk polycrystalline body), properties, **39**
Sintered alumina, 134
Sintering, 137
SiO_2
  in alumina, 119
  chemical composition, **118**
  formation into glass, 70, **70**
  solidification, 15
  surface energy, **61**
  viscosity, **72**

Si–O bond distance, 72
SiO_2 fiber, properties, **39**
SiO_4 tetrahedron, 13, *15*
SiO_2–Al_2O_3, phase diagram, *17*, 64, 133–134
SiO_2–(Al_2O_3)–MgO–Na_2O–K_2O–F–CaO–P_2O_5 in glass ceramics, 169
SiO_2–CaO–Na_2O phase diagram in glass ceramics, 169, *170*
SiO_2–CaO–Na_2O–P_2O_5, 169
SiO_2-rich film layer in glass ceramics, 169
Skin
  as a composite, 248
  distribution in human tissue, **84**
  fibrils, 87
  regeneration, 277
  replacement, 274
Slide glass, mechanical properties, **74**
Sliding force, 44
Slip, 37
Slip system, 31, 67
Slow crack growth, *42*, 146, *147*, *148*, 164
SnO_2, formation into glass, 70, **70**
Soda–lime glass
  in implants, 4
  mechanical properties, **31**, **36**
  properties, **6–7**
  transparency, 80
Soda–lime glass slide, **75**
Sodium, bonding and arrangement, 12–13
Sodium chloride (NaCl), 2, 12, *12*
  atomic bonding and arrangement, **13**
  brittle, 34
  density, 16
  strengthening, 37
  surface tension, **62**
  theoretical strength, **34**
Sodium hydroxide (NaOH), 118, 138
Sodium silicate, 70
Soft tissue substitutes, 274
Softening temperature, **7**
Sol–gel thin film, 160, 164
Solid freeform fabrication (SFF)
  of bone scaffolds, 281
  definition, 294
Solid-state reaction for hydroxyapatite, **186**
Soluble regulators in tissue engineering, **278**
Solution casting of bone scaffolds, **282**
Solvent-casting particulate leaching of bone scaffolds, **282**
Spark plug insulators, 2
Specific gravity, **6**
Specific heat, **7**
Specific modulus, 30, **31**
Spectra®-900 properties of composite reinforcing fibers, **256**
Speed of light, 231
Spinal surgery, *3*
Spinel ($MgAl_2O_4$)
  mechanical properties, **31**
Spleen, distribution in human tissue, **84**
Spongy bone, 104
SrO, rock salt structure, 12
Stainless steel
  porosity, *20*
  on stainless steel wear constant, **47**
  316L stainless steel, 156, 158, 176, 219
Static fatigue
  of alumina, 124–126, 133, 149
  of glass, 74–77
  of zirconia, 153
Static fracture strength in dental composites, 263
Static loading, *43*
Steel
  elastic modulus, 30
  fracture strength, 39
Stem cells, 294
Step-reaction polymerization, 85
Stereolithography (SLA)
  of bone scaffolds, 282
  definition, 294
Steric rigidity, 87
Stiffness of composites, 250–251, **252**
Stirling's approximation, 50
Strain, 30
Strain gauges in femoral head of hip joint prosthesis, *151*
Strain rate of compact bone, **99**
Strain-generated potentials (SGPs), 107
Streaming potentials of ions, 107
Strength curve, 32
Strength for fibers in composites, **40**
Strength of ceramics, 20
Strengthening, **38**
Stress, 30
  on alumina implant, *127*, 127–128
  around crack tip, 34–35
  increase in, 18
  residual, 4
  true, 30
Stress corrosion
  on alumina, 126
  on femoral head of hip joint prosthesis, 151
Stress intensity factor in zirconia, 146
Stress shielding effect in bone, 105
Stress trajectories of bone, 105
Stress–strain curve, 35
Stretch ratio, 30
Strontium titanate, properties, **233**
Sublimation energy, 59
Sulfates
  as coagulant in tofu, 228
  precipitation of zirconium, 142
Sulfides, 2
  formation into glass, 70
Sulfur, formation into glass, **70**
Supersaturated sodium aluminate, 118

Surface area
  of grains, 24
  of single-phase microstructure, 21
  in surface free energy, 60
Surface bone remodeling, 109
Surface compression, *37*, 37–38
Surface crystallization, 37, **38**, 67
Surface defects, 148
  and slow crack growth, *148*
Surface degradation of polymers, 279, *280*
Surface energy, 67
  of single-crystal ceramics, **61**
  varying with grain size, *60*
Surface energy of silica glass, **73**
Surface fatigue wear, 46
Surface free energy, 59–60
Surface properties, 59–63
Surface roughness
  of alumina, *122*
  of implant, 153–154
Surface tension, 60, **62**
Survival probability, 40, *41*
Synovial fluid, 89
Synthodont®, 132

T

316L stainless steel, 176
  friction and wear, 156, 158
  friction coefficient, 158
  wear, 219
3D plotting of bone scaffolds, 282
Talc ($Mg_3(Si_2O_5)_2(OH)_2$), 2, 8
TCP, 294
  α-TCP [[$Ca_3(PO_4)_2$]], 200
  β-TCP (tricalcium phosphate) [[$Ca_3(PO_4)_2$]], 186, 201
Teeth
  composition and structure, 92–96
  physical properties, **102**
  types, 92
Teflon®, *63*, 274
Temperature
  affecting phase transformation of zirconia, 155, *157*
  vs. composition, *53*
  dependence by free energy, 49, *49*
  vs. nucleation rate, *56*
Temperature–time cycle for glass ceramic, 168, *168*
Temporomandibular joint (TMJ) applications, 274
Tendon fibrils, 87
Tendon replacement, 214
Tendons, and bone, 90
Tensile loading applications, 5
Tensile modulus, for fibers in composites, **40**
Tensile strength, 36, **39**, 59–60, *60*
  of alumina, **120**
  of bone, **97**
  of coated alumina, 267
  of glass ceramics, **171**
Tensile stress, 44
Tension force, *250*
Tension in brittle materials, 34
Tetracalcium phosphate, 268, 269
Tetragonal space, 12, *14*
Tetragonal structure, 164
  of zirconia, 145
Tetragonal-to-monoclinic phase transformation, 154–155
Tetrahedra, in glass formation, 72
Tetrahedron, 27
TGF (transforming growth factor), 294
TGF-β (transforming growth factor β), 104–106, 178
  as bone graft substitute, **268**
  as bone substitute, 269
TGF-β_1 (transforming growth factor β_1), 173, **270**
TGF superfamily, 104
  amino acid sequence, *107*
Theoretical strength, 32–33, **34**
  of glass, 79
  of silica glass, **73**
Thermal conductivity, **7**, 19, *19*
  of alumina and zirconia, **152**
  of teeth, **102**
  of types of carbon, **210**
  zirconia, **143**
Thermal expansion coefficient, **7**, 57, 59
  of alumina and zirconia, **152**
  of types of carbon, **210**
  zirconia, **143**
Thermal expansion of dental composites, 263
Thermal seeds in cancer treatment, 5
Thermal shock, 79
  of alumina, 135
  resistance, **7**, 57, 59, 64, 76
Third-body wear in diamond-like carbon (DLC) coatings, 217
Three-dimensional networks in glass formation, 72
Three-dimensional printing (3DP), 294
  of bone scaffolds, 282
Threonine, **86**
Ti^{3+} in alumina implants, 119
Ti6Al4V, 235
  in hydroxyapatite implants, 197
  mechanical properties, **36**
  polymeric gel film with zirconia, 160
  wear, 219
Ti alloys, 132
  in dental implants, 264
  in hip joint prostheses, **218**
Tibial defect and calcium sulfate, 236
Time exponent, **6**
TiN wear, 219
Ti_2O_3, atomic bonding and arrangement, 13
Tissue engineering
  applications, **277**
  definition, 294
  examples of matrices, cells, regulators employed, **278**

- Tissue ingrowth fixation, *1*
- Tissue ingrowth into implants, 132
- Tissues
  - mechanical properties, 97–98
  - structure–property relationships, 90–102
- Titanates, *233*
  - asymmetric nature, *234*
  - density, 232, 235
  - electromechanical/voltage–strain behavior, 234
  - hydrothermal processing, 242
  - piezoelectric phenomenon, *234*
  - structure and properties of, 232–236
- Titanium alloy, in hip prosthesis, *1*
- Titanium carbide (TiC), mechanical properties, **31**
- Titanium oxide (TiO_2), 232
- Titanium oxide (TiO_2), in dental implants, 264
- Titanium oxide (TiO_2), as nucleating agent, 168
- Tl_2O_3, formation into glass, 70, **70**
- Total hip joint prostheses, use of zirconia, 145
- Total hip joint replacement, 2
  - use of composites, 254
- Total hip joint structure, testing, *131*
- Toughness, 35, 67
- Toxicity tests, *111*
- Trabeculae, 104, 109
- Transcutaneous implant, 266
- Transition metals, 206
  - mechanical properties, 34
- Transition temperature (T_g), 37
- Transmission electron microscopy, 18, 171, *174*
- Tribological properties of alumina, 121, *122*
- Tricalcium phosphate, 268
- Tridymite, 15
  - definition, 27
  - phase transformation, 58
- Triethylene glycol dimethacrylate (TEGDMA), 262, 294
- Triple superhelix, 87
- Tropocollagen, 87, 114
- True density, 27
- True stress, 30
- Tryptophan, **86**
- Tungsten
  - mechanical properties, 34
  - theoretical strength, **34**
- Tungsten wire, properties for composite materials, **40**
- Turbostratic structure, 223
- Tyrosine, **86**

U

- UHMWPE (ultrahigh-molecular-weight polyethylene), *9*, 129, 149
  - coefficient of friction, 218–219
  - in composites, 257
  - friction and wear, 158, 158
  - wear constant with zirconia, 161
  - wear rate, **219**
  - wear volume of, 220
- UHMWPE (ultrahigh-molecular-weight polyethylene)-reinforced composites, 253
- ULTI carbon deposition, 223
- ULTI (ultra low-temperature isotropic) pyrolytic carbon, 274
- ULTI (ultra-low-temperature isotropic) carbon, 208
  - definition, 294
  - on implants, 213
  - properties, **210**
- Ultimate compressive strength
  - of bone, 97
  - of compact bone, **99**
- Ultrahigh-molecular-weight polyethylene. *See* UHMWPE
- Ultraviolet (UV) light irradiation of glass ceramics, 168
- Undecalcified bovine embryonic dental enamel, *95*
- Uniaxial pressing of hydroxyapatite, 186
- Unit cell representation, *14*
- Univarient equilibrium, 47
- Urea, 88
- Urine pH, **84**

V

- Valence electrons, 12
- Valine, 86
- Van der Waals force, 208, 223
- Velocity of glass-forming liquids, **72**
- Venous P_{O2}, **84**
- Verneuil process, 4, 8
- Vickers hardness, of hydroxyapatite, 191
- Vickers test, 44
- Viscera, distribution in human tissue, **84**
- Viscoelastic gels, 89
- Viscosity
  - definition, 81
  - of glass, 70
  - of glass forming liquids, **72**
  - at $T_m(P)$ of glass forming liquids, **72**
- Viscous state in ceramics, 4
- V_2O_3, atomic bonding and arrangement, 13
- Voigt model, 19, *19*, 100, 112
  - for composite structures, *250*, 250–251
  - definition, 27, 114
- Volkmann's canal, 92, 114
- Voltage output of implants, *238*

W

- Water
  - distribution in human tissue, **84**
  - effect on static loading, 43
  - entropy, **50**
  - phase diagram, *48*
  - as plasticizer in dental composites, 284
  - and stability of collagen, 88
- Water absorption on alumina, 121
- Wavelength of x-ray, 230–231

Wear constant, 46, **47**
  of zirconia with UHMWPE, 161
Wear factor
  definition, 164
  of zirconia, 158
Wear properties, 44–47
Wear rate
  of alumina, *122*, **123**
  of alumina–UHMWPE, **123**
  of UHMWPE, **219**
Wear volume vs. number of cycles, *159*
Weibull distribution, 39, *41*, 67
Weibull exponent, **6**
Weibull modulus, 39, 164
  in alumina, 126
  of zirconia, 145, **145**
Weibull plot
  definition, 164
  of zirconia, *150*
Weibull relationship, 127, 138
Weibull statistics, 38–43
Wet chemical method for hydroxyapatite, **186**
Wetting characteristics of liquids and solids, 62
Whisker
  definition, 67
  properties, **39**
White wares, 2
WLF equation, 74, 81
Wohler graph of stress, 124, 138
Wollastonite in glass ceramics, 170
Wood as a composite, 248
Work in surface free energy, 60
Work of fracture of bone, **100**
Wound healing, 102–105
Woven bone, 103

X

X-ray contrast medium, 228
X-ray diffraction patterns of bone, *185*
X-ray energy, 231

Y

YAS (yttrium aluminosilicate), 5, 8
Yield strength, **36**
  of bone, 97
Young's modulus, **6**, 30, 33, **34**, **39**, 59, 72, 97, 112
  of alumina and zirconia, **152**
  of bone, 100, **100**
  bounds for cortical bone, 252–253
  of composites, 251
  definition, 67
  of dental composites, 264
  of glass ceramics, **171**
  of hydroxyapatite, 289
  of silica glass, **73**
  of types of carbon, **210**
  of zirconia, **145**
Yttria, stabilizing zirconia, 152–153, *155*
Yttrium aluminosilicate. *See* YAS (yttrium aluminosilicate)
Yttrium magnesium oxide-stabilized zirconia (Y–Mg–PSZ), 145
Yttrium oxide, 145
  affecting stability of zirconia, 150
  definition, 164

Z

Zinc on zinc wear constant, **47**
Zinc sulfide (ZnS), 2
Zircon ($ZrSiO_4$), 142, 164
Zirconia (ZrO_2), 2, 141–166
  aging in water, *159*
  allotropic phase transformation, 47
  bending strength, *157*, *158*
  biocompatibility, 156
  bioinert nature, 5
  Biolox®, 152
  boiling point, **143**
  burst strength of femoral head, 153–154, *155*
  coated with hydroxyapatite, 160
  crystallography, **143**
  cubic structure, *143*
  density, **143**, **145**, 161
  in dental implants, 132, 160, 266
  effect of stress corrosion on, 151–152
  fatigue life, 146
  fatigue tests, *147*
  flexural strength, **145**
  fluorite structure, 142, *143*
  four-point-bending strength, *153*
  fracture strength and loading rate, 148, *148*
  fracture toughness, **145**, *146*
  friction and wear, 156, 158
  friction coefficient, 158
  hardness, **145**
  heat of formation, **143**
  as hemiarthroplasty head implant, 160
  hydrothermal treatment, 152, *153*
  in implants, 4
  inert strength, 153
  load-bearing implants, 130, 176
  loading rate, 153, *154*
  microstructure-composition stability, *150*
  Mohs hardness, **143**
  moisture effects, 166
  monoclinic, 161
  monoclinic phase changes, *154*, *155*
  monoclinic to tetragonal phase transition, 142, *144*
  as nucleating agent, 168
  partial phase diagram, *144*
  partially stabilized (PSZ), 142
  phase diagram, *48*
  phase transformation, 154–156, *156*, *157*
  physical properties, **143**
  polymeric gel film onto Ti6Al4V alloy, 160

  polymorphism, **143**
  porosity, *160*
  properties, **6–7**, **145**, **152**
  refractive index, **143**
  single crystal, 142
  source and manufacturing, 142
  stability, 149–161
  static fatigue, 153
  stress intensity factor, 146
  structure and properties, 142–149
  subcritical type of crack growth, 148, *148*
  surface roughness, 160
  tetragonal to cubic phase transition, 142, *144*
  thermal conductivity, **143**
  thermal expansion coefficient, **143**
  tribological properties, 149
  wear constant with UHMWPE, 161
  wear factor, 158
  wear volume vs. number of cycles, *159*
  of Weibull modulus, **145**
  Weibull plot, *150*
  x-ray diffraction, 155, *156*
  Young's modulus, **145**
  yttrium- and magnesium-stabilized, *145*, 145–146
  yttrium magnesium oxide-stabilized, 145
  zintering, 160
Zirconia (ZrO_2), cubic, mechanical properties, **31**
Zirconia–alumina composite, 161
Zirconia–zirconia couplings, 160
Zirconium, 142
  oxidized with niobium, 161
Zirconium oxides, 141–166
  in dental implants, 132
Zirconium–niobium alloy, *141*, 142
Zisman plot, 62, *63*
ZnS, *12*
  atomic bonding and arrangement, **14**
Zone melting and solidification process, 17
$ZrCl_4$, 142
ZrO_2 wear, 219
ZrO_2–CaO
  binary phase, 54
  partial phase diagram, *144*
Zr–OH bonding, 156
ZrO_2–Y_2O_3
  phase diagram, *144*

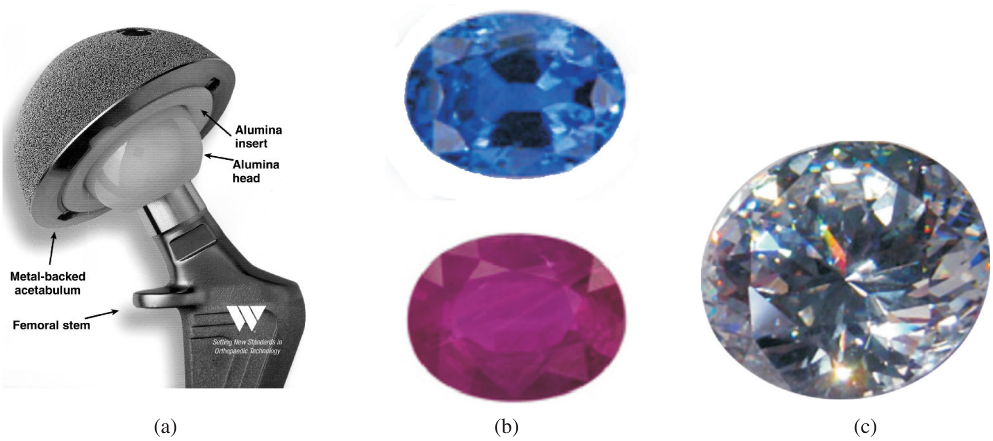
Alumina insert
Alumina head
Metal-backed acetabulum
Femoral stem
Setting New Standards in Orthopaedic Technology
(a)
(b)
(c)

Chapter 1 cover: (a) Use of alumina as bearing surfaces for a hip prosthesis. The metal (likely CoCr alloy, not specified) acetabular back is coated with Ti alloy beads to create porosity for tissue ingrowth fixation. Courtesy of Wright Medical Technology Inc., Arlington, TN. (b) Single-crystal alumina can be grown and cut as sapphire (top) and ruby (bottom) depending on the impurities (see Chapter 6). (c) Single-crystal cubic zirconia as a jewelry stone (see Chapter 7).

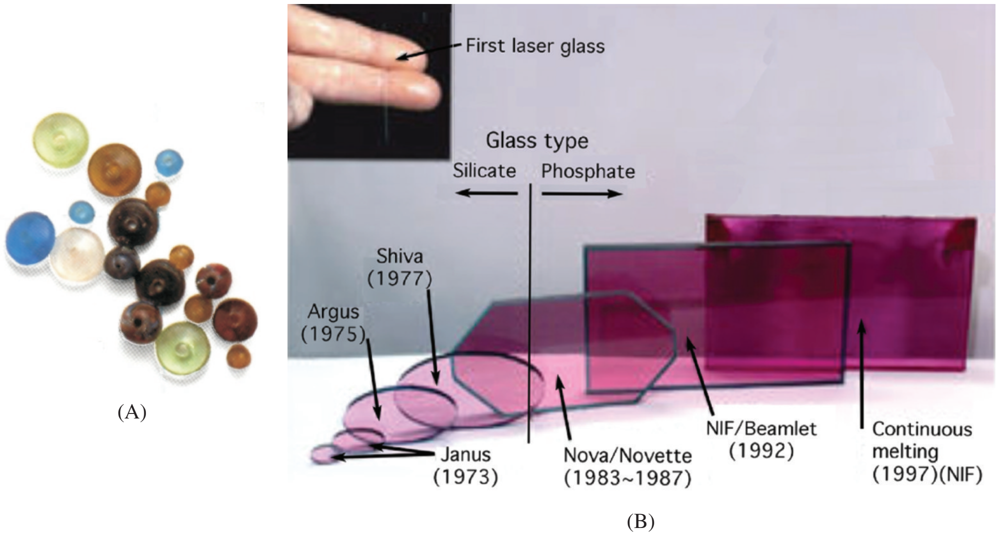
First laser glass
Glass type
Silicate
Phosphate
Shiva (1977)
Argus (1975)
Janus (1973)
Nova/Novette (1983~1987)
NIF/Beamlet (1992)
Continuous melting (1997)(NIF)
(A)
(B)

Chapter 4 cover: (A) Egyptian glass beads (ca. 3,000–2,500 BCE. Modified with permission from [5]. Copyright © 1994, Dorling Kindersley. (B) The types and uses of glass for scientific and technical purposes are myriad, and range from applications involving the smallest of devices, such as DNA microarrays, to football field-sized, enormously powerful neodymium-doped glass lasers used in laser fusion. Modified with permission from http://en.wikipedia.org/wiki/Glass.

Chapter 6 cover: Many-colored alumina single crystals. These can be grown artificially. Polycrystalline alumina has been used for many years as spark plug insulators, high-voltage insulators, and implants. See Figures 6.11 and 6.15. Reprinted with permission from http://en.wikipedia.org/wiki/Image: Sapphire01.jpg.

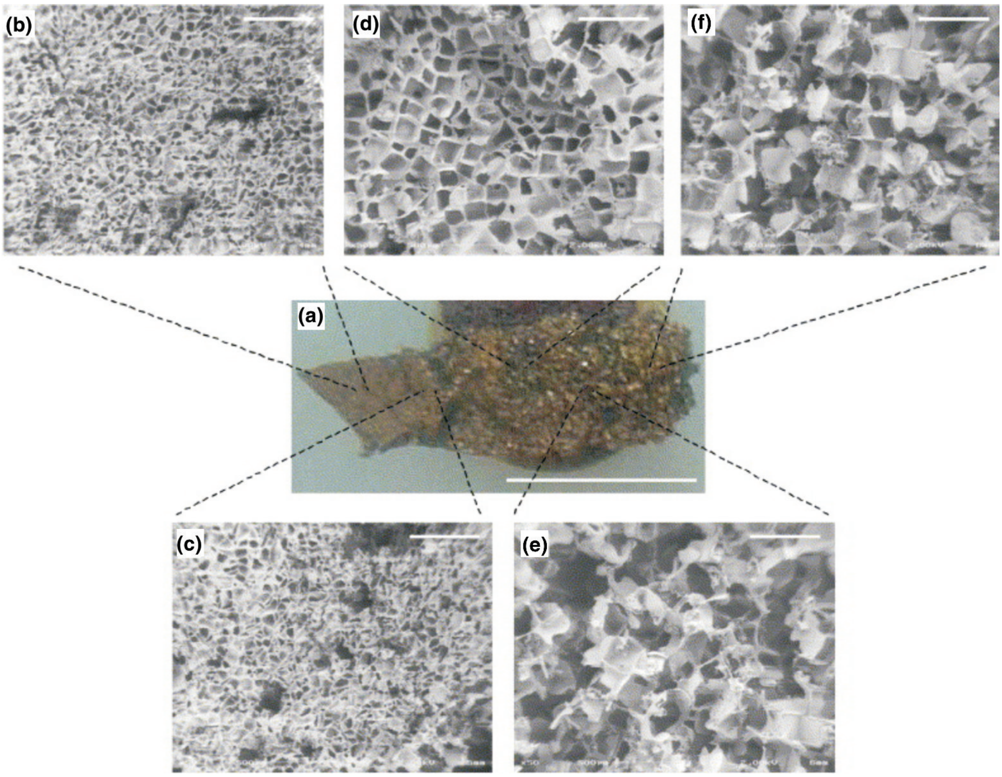

Figure 12.26. Pore size gradient across a sponge made of silk fibroin. Pore sizes are (b) 76.3 ± 16.2 μm, (c) 100.7 ± 18.2, (d) 182.0 ± 30.0, (3) 221.3 ± 40.6, (f) 260.3 ± 75.9. Bar lengths are 10 (a) and 0.5 mm (b–f). Reprinted with permission from [76]. Copyright © 2005, Butterworth-Heinemann.